QA: QA

ANL-WIS-MD-000010 REV 05

July 2005

Dissolved Concentration Limits of Radioactive Elements

NOTICE OF OPEN CHANGE DOCUMENTS - THIS DOCUMENT IS IMPACTED BY THE LISTED CHANGE DOCUMENT AND CANNOT BE USED WITHOUT IT.

----

1) ACN-001, DATED 10/06/2005

Prepared for:

U.S. Department of Energy
Office of Civilian Radioactive Waste Management
Office of Repository Development
1551 Hillshire Drive
Las Vegas, Nevada 89134-6321

Prepared by:

Bechtel SAIC Company, LLC
1180 Town Center Drive
Las Vegas, Nevada 89144

Under Contract Number
DE-AC28-01RW12101

DISCLAIMER

This report was prepared as an account of work sponsored by an agency of the United States Government. Neither the United States Government nor any agency thereof, nor any of their employees, nor any of their contractors, subcontractors or their employees, makes any warranty, express or implied, or assumes any legal liability or responsibility for the accuracy, completeness, or any third party's use or the results of such use of any information, apparatus, product, or process disclosed, or represents that its use would not infringe privately owned rights. Reference herein to any specific commercial product, process, or service by trade name, trademark, manufacturer, or otherwise, does not necessarily constitute or imply its endorsement, recommendation, or favoring by the United States Government or any agency thereof or its contractors or subcontractors. The views and opinions of authors expressed herein do not necessarily state or reflect those of the United States Government or any agency thereof.

QA: QA

Dissolved Concentration Limits of Radioactive Elements

ANL-WIS-MD-000010 REV 05

July 2005

Complete only applicable items.

2. Type of Mathematical Model

☒ Process Model ☐ Abstraction Model ☐ System Model

Describe Intended Use of Model

The model reports solubility limits for use in TSPA-LA calculations of radionuclide transport.

3. Title

Dissolved Concentration Limits of Radioactive Elements

4. DI (including Rev. No.):

ANL-WIS-MD-000010 REV 05

	Printed Name	Signature	Date
5. Originator	Patricia Bernot		7/12/05
6. Independent Technical Reviewer	Laura Price	Laura Price	7/13/05
7. Checker	Emma R. Thomas	E Thomas	7/13/05
8. QER	Judith Gebhart	J E Gebhart	7/13/05
9. Responsible Manager/Lead	Jim Cunnane	Christi Stockman	7/13/05
10. Responsible Manager	Paul Dixon	Paul	7-13-05

11. Remarks

Appendix I – One (1) CD-ROM.

Change History

12. Revision No.	13. Description of Change
00	Initial Issue.
01	Revised the response surfaces of Np and Pu solubility limits; revised the distribution of Ni solubility. Addressed model validation deficiency (LVM0-00-D-119) found in REV 00. Removed text regarding Cm, Sm, Ni, Sn, Cl, Nb, and Zr solubility. This entire document was revised due to extensive changes.

01/01	Interim Change Notice (ICN) to remove a to be verified (TBV). Pages 14 and 15 are affected. Removed Unresolved Reference Number (URN) from DTN: MO0009THRMODYN.001 on p. 64. Vertical bars in the right margin of the document identify changes made to the text.
02	Extensive revision. Solubility limits for all the elements have been revised using the newly qualified thermodynamic database *data0.ymp.R2* (DTN: MO0302SPATHDYN.000 [DIRS 161756]).
03	A new Pu-solubility model – the adjusted-Eh model was developed in this revision. A new U-solubility model that is applicable to CDSP WPs in all three scenarios and to CSNF waste packages in igneous intrusion scenario was also developed in this revision. The applicable pH range of the base-case Np-solubility model was expanded. The following CRs were also resolved in this revision: CR 167C (Section 6.4.2.5, second paragraph); CR 168C (TER-03-0037 – Steinborn et al. 2003 is corroborative information only); CR 1936D (Table 6.5.2 and Section 9.3), and CR 79B (DIRS 101876, 109205, and 109206 are verified, direct input. Note however that 109205 and 109206 are no longer used as direct input to the document). The entire document was revised, and changes were too extensive to use change bars.
04	Updates to this model include updates to the Np-solubility model. The model is now split between in-package dissolved concentrations and ex-package (invert) dissolved concentrations. The base-case fluoride uncertainty for Th and Am has been made consistent with Pu, Np, and U. An independent technical review has been performed for the new Np models and redone for Pu (although the Pu model has not been revised). CR 4961 is resolved through changes, additions, and rewrites of Section 7. Changes made to this document were too extensive to use change bars. Portions of this model that were not updated were not re-checked. The changes are too numerous to list here. Refer to the record package for details of all changes to the document.
05	Limited text changes made to document to enhance clarity. Sections affected include Sections 1, 6.3.3.3, 6.4.4, 6.5.3.2, 6.6.2, 6.6.3.1, 6.6.3.2.1, 6.6.3.3.1, 6.6.4.1, 6.8.4.1, 6.9.4.1, 6.11.1, 6.11.2, 6.11.4, 7.2, 7.2.2, 7.2.3, 7.2.4, 7.2.5, 7.2.6, 7.2.9, 8.2, and Appendices II and IV. Changes are indicated by vertical bars in the margins.

This model report was developed through the contributions of the following individuals, listed in alphabetical order:

- Steve Alcorn, ISSI. Contributing author to the final REV 03.
- Sara Arthur, Framatome-ANP. Major contributing author to REV 04.
- Patricia Bernot, BSC. Lead author on Rev 05. Lead author on REV 04. Lead author on REV 03 starting from REV 03C. Major contributor to final REV 03 and responsible for incorporation of Regulatory Integration Team comments and items in the RIT Action Item Database.
- Yueting Chen, BSC. Lead author REV 03 up to REV 03B and major contributor to the final REV 03.
- Jim Cunnane, ANL. Contributing author to REV 04 and 05.
- Bill Downs, Frankie Friend and Associates Inc. Contributing author to the final REV 03.
- Louis Kovach, IDT. Contributing author to REV 04.
- Susan LeStrange, BSC. Contributing author to the final REV 03.
- F. Joe Pearson, IDT. Contributing author to REV 05. Major contributing author on REV 04. Major contributing author of final REV 03 and responsible for incorporation of Regulatory Integration Team comments and items in the RIT Action Item Database.
- Christine Stockman, SNL. Contributing author to REV 04.

INTENTIONALLY LEFT BLANK

EXECUTIVE SUMMARY

The purpose of this study is to evaluate dissolved concentration limits (also referred to as solubility limits) of elements with radioactive isotopes under probable repository conditions, based on geochemical modeling calculations using geochemical modeling tools, thermodynamic databases, field measurements, and laboratory experiments.

The scope of this activity is to predict dissolved concentrations or solubility limits for elements with radioactive isotopes (actinium, americium, carbon, cesium, iodine, lead, neptunium, plutonium, protactinium, radium, strontium, technetium, thorium, and uranium) relevant to calculated dose. Model outputs for uranium, plutonium, neptunium, thorium, americium, and protactinium are provided in the form of tabulated functions with pH and log fCO_2 as independent variables, plus one or more uncertainty terms. The solubility limits for the remaining elements are either in the form of distributions or single values. Even though selection of an appropriate set of radionuclides documented in *Radionuclide Screening* (BSC 2002 [DIRS 160059]) includes actinium, transport of Ac is not modeled in the total system performance assessment for the license application (TSPA-LA) model because of its extremely short half-life. Actinium dose is calculated in the TSPA-LA by assuming secular equilibrium with ^{231}Pa (Section 6.10); therefore, Ac is not analyzed in this report.

The output data from this report are fundamental inputs for TSPA-LA used to determine the estimated release of these elements from waste packages and the engineered barrier system.

Consistent modeling approaches and environmental conditions were used to develop solubility models for the actinides discussed in this report. These models cover broad ranges of environmental conditions so they are applicable to both waste packages and the invert. Uncertainties from thermodynamic data, water chemistry, temperature variation, and activity coefficients have been quantified or otherwise addressed.

INTENTIONALLY LEFT BLANK

CONTENTS

Page

CONTENTS (Continued)

Page

CONTENTS (Continued)

Page

INTENTIONALLY LEFT BLANK

FIGURES

Page

FIGURES (Continued)

Page

FIGURES (Continued)

Page

INTENTIONALLY LEFT BLANK

TABLES

Page

TABLES (Continued)

Page

TABLES (Continued)

Page

TABLES (Continued)

Page

ACRONYMS AND ABBREVIATIONS

ANL	Argonne National Laboratory
ATM	approved testing material
CDNR	codisposal N Reactor spent fuel
CDSP	codisposal spent fuel package
CSNF	commercial spent nuclear fuel
$\Delta_f G^0$	standard-state Gibbs free energy of formation
$\Delta_f H^0$	standard-state enthalpy of formation
$\Delta_r G^0$	standard-state Gibbs free energy of reaction
$\Delta_r H^0$	standard-state enthalpy of reaction
DOE	U.S. Department of Energy
EBS	Engineered Barrier System
EELS	Electron Energy Loss Spectroscopy
EXAFS	Extended X-Ray Absorption Fine Structure
F_c	concentrating factor
FEPs	features, events, and processes
HDR	high drip rate
LANL	Los Alamos National Laboratory
LDR	low drip rate
NEA	Nuclear Energy Agency
PNNL	Pacific Northwest National Laboratory
OECD	Organisation for Economic Co-operation and Development
QA	quality assurance
SHE	Standard Hydrogen Electrode
SIT	Specific Ion Interaction Theory
TBV	to be verified
TSPA-LA	total system performance assessment for license application
VA	validation activity
WP	waste package
YMP	Yucca Mountain Project

Elemental Symbols

Ac	actinium
Am	americium
C	carbon
Cs	cesium
F	fluorine
H	hydrogen
I	iodine
Pb	lead
Na	sodium
Np	neptunium
O	oxygen
Pu	plutonium
Pa	protactinium
Ra	radium
Sr	strontium
Tc	technetium
Th	thorium
U	uranium

Chemistry Abbreviations

aged	aged from fresh precipitate
am	amorphous solid
aq	aqueous
cr, c	crystalline
e	electron
hyd	hydrated
s	solid
f	fugacity

1. PURPOSE

The purpose of this study is to determine dissolved concentration limits (also referred to as solubility limits) of elements with radioactive isotopes under probable repository conditions via geochemical modeling calculations using equilibrium geochemical simulators, thermodynamic databases, and field measurements and laboratory experiments. This report was prepared in accordance with *Technical Work Plan for Postclosure Waste Form Modeling* (BSC 2005 [DIRS 173246]) and LP-SIII.10Q-BSC, *Models.*

The scope of this modeling activity is to predict dissolved concentrations or solubility limits as a function of environmental conditions (i.e., fCO_2 (f = fugacity) and pH) for all elements with radioactive isotopes relevant to the performance of the repository. The output of this report provides fundamental inputs for the total system performance assessment for the license application (TSPA-LA).

The selection of an appropriate set of radionuclides for TSPA-LA evaluation is documented in *Radionuclide Screening* (BSC 2002 [DIRS 160059]). With a 0.95 screening-product cutoff and a regulatory period of 10,000 years after waste emplacement, the following 14 elements with radioactive isotopes have been identified to be relevant to total dose calculations: actinium (Ac), americium (Am), carbon (C), cesium (Cs), iodine (I), lead (Pb), neptunium (Np), plutonium (Pu), protactinium (Pa), radium (Ra), strontium (Sr), technetium (Tc), thorium (Th), and uranium (U). Transport of Ac is not modeled in the TSPA-LA model because of its extremely short half-life. Actinium dose is calculated in TSPA-LA by assuming secular equilibrium with ^{231}Pa (Section 6.10); therefore, Ac is not analyzed in this report.

The output of this report may be applied to different repository locations and to different scenarios (nominal, seismic, and igneous intrusion) by the TSPA-LA model under different environmental physicochemical conditions. The TSPA-LA requires solubilities of elements with radioactive isotopes be presented as functions of environmental conditions. The environmental conditions at different locations and scenarios are not defined by this report, but by several other reports. The TSPA-LA model uses the solubility models generated by this report and environmental conditions provided by other reports (BSC 2004 [DIRS 167621]; BSC 2004 [DIRS 170028]; BSC 2004 [DIRS 169860]) to generate solubilities for each element with radioactive isotopes at different locations and in different scenarios. As pH and fCO_2 conditions for these different locations and scenarios could be very diverse, it is necessary for solubility models developed in this report to cover broad pH and fCO_2 ranges.

Technical Work Plan for Postclosure Waste Form Modeling (BSC 2005 [DIRS 173246]) requires that neptunium- and plutonium-solubility models developed in this report must be validated at a medium level of confidence (Level II). All other modeled elements (U, Th, Am, Pa, and Ra) are validated at a low level (Level I) of confidence. Analyses are carried out for Pb, Tc, C, I, Cs, and Sr. As these are analyses, they do not need to be validated. Additionally, TSPA-LA does not require dissolved concentrations for Ac, so Ac dissolved concentrations are not considered in the technical work plan (BSC 2005 [DIRS 173246], Table 2-3).

The solubility models developed in this report are valid for broad ranges of water composition (Table 8-4) and they may be applied inside and outside waste packages. However, as specified

in Section 6.4.4, they are subject to three restrictions. First, because the B-dot equation was used in model calculations, the solubilities are restricted to ionic strengths no greater than 1 molal. Inclusion of an additional uncertainty factor to the solubility allows application of the solubility model to an ionic strength of 3 molal. Second, for calculations that did not converge or gave an ionic strength higher than 1 molal, the value "500" was used to indicate that no equilibrium solubilities were estimated for those conditions. This value is intended as a flag to indicate that, rather than concentration limits, the dissolution rate of individual waste forms, water volume, and solubility caps presented in Table 8-3 (instead of the flag itself) should be used for these physicochemical conditions in the TSPA-LA modeling. Third, for any conditions outside the pH range of 3.0 to 11.0, the log fCO_2 range of -1.5 to -5.0, or for an ionic strength greater than 3 molal (Table 8-4), the inventory concentrations will be calculated using the dissolution rate of individual waste forms, water volume, and the solubility caps presented in Table 8-3.

2. QUALITY ASSURANCE

2.1 QA PROGRAM APPLICABILITY

Development of this report is subject to the YMP quality assurance program (BSC 2005 [DIRS 173246], Section 8) because it will be used to support TSPA-LA. Approved quality assurance procedures identified in the technical work plan (BSC 2005 [DIRS 173246], Section 4) have been used to conduct and document the activities described in this model report. The report does not address any items in *Q-List* (BSC 2005 [DIRS 171190]).

2.2 ELECTRONIC MANAGEMENT OF DATA

The technical work plan contains the process control evaluation used to evaluate the control of electronic management of data (BSC 2005 [DIRS 173246], Section 8 and Attachment I) during modeling and documentation activities. This evaluation determined that the methods in the implementing procedures are adequate and, as such, there are no deviations from these methods.

INTENTIONALLY LEFT BLANK

3. USE OF SOFTWARE

The computer software used to carry out the calculations in this model is summarized in Table 3-1.

Table 3-1. Computer Software Used

Software Name	Version	Software Tracking Number (Qualification Status)	Description and Components Used	Input and Output Files [a] (Included in Appendix I)
EQ3/6	7.2b	UCRL-MA-110662 (LSCR198) (Qualified on Windows 95 and HP-UX 10.20 B)	EQ3NR: a FORTRAN speciation-solubility code	input: *.3i output: *.3o
			EQPT: a data file preprocessor in FORTRAN	input: data0.* output: data1.*
EQ6	7.2bLV	10075-7.2bLV-02 (Qualified on Windows 2000 and NT 4.0)	EQ6: a reaction-path code that models water–rock interaction or fluid mixing in either a pure reaction progress mode or a time mode	input: *.6i pickup: *.6p output: *.6o *.elem_aqu.txt *.elem_min.txt *.elem_tot.txt *.min_info.txt *.bin
GetEQData	1.0.1	10809-1.0.1-00 (Qualified on Windows NT 4.0 and Windows 2000)	A Microsoft Excel macro. It is used to postprocess EQ3/6 output information.	input: *.3o output: *.xls
BUILDEQ3.BAS	1.00	10365-1.00-00 (DOS Emulation)	A QBASIC code used to generate EQ3 input files	input. *.bas output: *.3i
Microsoft Excel	97 SR-2 and 2000 SR-1	Used only as a worksheet, not as a software routine. In accordance with LP-SI.11Q-BSC, it is not required to be qualified or documented.	Used in this document for graphical representation and arithmetical manipulations	input: *.3o output: *.xls
Sigma Plot	4.0	Used only as a worksheet, not as a software routine. In accordance with LP-SI.11Q-BSC, *Software Management*, it is not required to be qualified or documented	Used in this document for graphical representation and arithmetical manipulations	Input: *.3o *.6o Output: *.jnb

NOTE: [a]Files are explained in more detail in Appendix II.

All applicable products were obtained from Software Configuration Management and have been verified appropriate for the application. No macros were developed for either Microsoft Excel or SigmaPlot; thus, additional qualification was not necessary. Only the functions that are part of the off-the-shelf codes were used to make arithmetical manipulations. The software was run on standard personal computers and the Hewlett Packard workstation using operating system HP-UX 10.20 B listed in Table 3-2.

Table 3-2. Computers Used

Computer Make	CPU #	Operating System	Software Used
Dell PowerEdge 2200	112378	Windows NT 4.0	BUILDEQ3.BAS (run through DOS emulation), GetEQData, Microsoft Excel 97 SR-2, Sigma Plot
Dell Optiplex GX400	151295	Windows NT 4.0	BUILDEQ3.BAS (run through DOS emulation), GetEQData, Microsoft Excel 97 SR-2, EQ6 V7.2bLV
Dell Optiplex GX260	152392	Windows 2000	GetEQData, Microsoft Excel 97 SR-2, Sigma Plot
Dell Optiplex GX260	152383	Windows 2000	GetEQData, Microsoft Excel 97 SR-2
Dell Optiplex GX300	117728	Windows 95	EQ3/6 V7.2b
Dell Optiplex GX260	152393	Windows 2000	GetEQData, Microsoft Excel 97 SR-2
Dell Optiplex GX260	152381	Windows 2000	GetEQData, Microsoft Excel 97 SR-2
Hewlett-Packard workstation	112515	HP-UX 10.20 B	EQ3/6 V7.2b
Dell Latitude C610	Framatome ANP Tag #: H22MT11	Windows 2000	GetEQData, Microsoft Excel 2000 SR-1

NOTE: CPU = central processing unit.

3.1 QUALIFIED SOFTWARE

The EQ3/6 package consists of several components: EQ3NR, EQ6, EQPT, and EQLIB (the supporting library, which was not necessary for this report and not used). EQ3NR, the main component used in the solubility calculations, computes the thermodynamic static state of an aqueous solution by determining the distribution of chemical species using a thermodynamic database. The input to the code describes the aqueous solution in terms of total concentrations of dissolved components and other parameters, such as pH and Eh. The input for this report also includes a desired electrical balancing adjustment and constraints that impose equilibrium with specified pure minerals and gases. EQ3NR evaluates the degree of disequilibrium in terms of saturation index and the thermodynamic affinity for mineral dissolution and precipitation; EQ6 is for reaction path simulations; EQPT is a database preprocessor. BUILDEQ3.BAS (a preprocessor) and GetEQData (a postprocessor) are designed for use with the EQ3/6 package. The EQ3/6 software and its pre- and postprocessors were selected for this model because they were developed to simulate equilibrium conditions in groundwater. The thermodynamic database was compiled for the YMP. The use of the software listed in Table 3-1 is consistent with its intended use. There are no limitations on the output of this model due to the use of any of the software listed in this section. The software are appropriate for their use in this model and were not used outside the range of parameters for which they were validated.

3.2 EXEMPT SOFTWARE

Microsoft Excel (Versions 2000 SR-1 and 97 SR-2) and SigmaPlot (Version 4.0) are problem-solving environments used in calculations and analyses. They are also used to tabulate and chart results. The user-defined expressions, inputs, and results are documented in sufficient detail to allow an independent repetition of computations. Thus, Microsoft Excel and SigmaPlot

are used as worksheets, not as software routines. The formulae, including the inputs and outputs, are provided in Appendix I.

Microsoft Excel (Versions 2000 SR-1 and 97 SR-2) and SigmaPlot (Version 4.0) are exempt software in accordance with LP-SI.11Q-BSC, Section 2.1.6.

INTENTIONALLY LEFT BLANK

4. INPUTS

4.1 DIRECT INPUTS

Sources of direct inputs used to develop solubility models are summarized in Table 4-1. Data used in the direct development of this model ("direct inputs") are not used to validate the model in Section 7.

A key input for this study is the thermodynamic database (*Data0.ymp.R2*) used for EQ3NR and EQ6 calculations. *Data0.ymp.R2* (DTN: MO0302SPATHDYN.000 [DIRS 161756]) was developed specifically for the YMP for use with the EQ3/6 software and contains the best available thermodynamic data. It is appropriate for this use and maintains consistency among models. For this report, the *Data0.ymp.R2* database was modified slightly (called *Data0.yc3.R1*) to incorporate the equilibrium constant for sodium boltwoodite ($NaUO_2SiO_3OH \bullet 1.5H_2O$) recommended as a solubility-controlling phase by the NEA Thermodynamic Database Project in *Update on the Chemical Thermodynamics of Uranium, Neptunium, Americium and Technetium* (Guillaumont et al. 2003 [DIRS 168382]). *Update on the Chemical Thermodynamics of Uranium, Neptunium, Americium and Technetium* (Guillaumont et al. 2003 [DIRS 168382]) is one in a series of publications from the NEA that are widely used and well accepted by the nuclear waste management community as handbooks; therefore, their data are considered established fact.

The *Data0.ymp.R2* database contains the information necessary for extrapolations to 200°C. The B-dot equation used in *Data0.ymp.R2* and *Data0.yc3.R1* is considered valid up to ionic strengths of 1 molal (Steinborn et al. 2003 [DIRS 161956], p. 60). As discussed in Section 6.3.3.4, this limitation can be relaxed by adding an additional uncertainty term and the estimations can be extended to ionic strengths between 1 and 3 molal. (DTN: SN0410T0510404.001 [DIRS 172759] indicates that several transcription errors were made from the references sources for DTN: MO0302SPATHDYN.000 [DIRS 161756] to the calculation spreadsheets where the log K values were computed. These errors occurred in the high temperature data and not in the 25°C data. As all model calculations in this report were made at 25°C, there is no impact.)

The majority of the sources of direct input data (Table 4-1) are handbooks (Lide 1995 [DIRS 101876], Guillaumont et al. 2003 [DIRS 168382], OECD 2001 [DIRS 159027], Silva et al. 1995 [DIRS 102087], Grenthe et al. 1992 [DIRS 101671], Hummel et al. 2002 [DIRS 161904], and Lide 2002 [DIRS 160832]), and, as such, their contents are considered established fact and the data are qualified. These sources are generally accepted by the scientific community and are, thus, considered appropriate for use in the model.

One source, the original source for the coefficients used in the extended Debye-Huckel equation for calculating single-ion activity coefficients, is a U.S. Geological Survey report (Truesdell and Jones 1974 [DIRS 170136]) qualified here for its intended use in this report by the following factors: reliability of data source, qualification of personnel or organizations generating the data, and prior uses of data (LP-SIII.10Q-BSC, Section 5.2.1). All equilibrium geochemistry numerical simulators use single-ion activity coefficients in their calculations. These data are integral to the EQ3/6 simulations used to estimate the equilibrium solubility of the various elements with radioactive isotopes. The authors (Truesdell and Jones) are recognized senior

scientists with the U.S. Geological Survey and are eminently qualified to make these calculations. The senior author has many peer-reviewed papers concerning geochemical thermodynamics and estimation of geochemical parameters. These data have been included in virtually all equilibrium geochemistry simulation codes (e.g., PHREEQC, MINTEQA2, etc.) since they were originally published and have been accepted by the scientific community as "established fact."

Section 6.3.3.4 compares the values of single-ion activity coefficients (γ_i) that Truesdell and Jones (1974 [DIRS 170136]) calculated using WATEQ with those previously calculated using other methods and demonstrated that the agreement was within a few percent. Therefore, their work by is qualified for its intended use.

The initial water composition used as the base case, summarized in Table 4-1 with details given in Table 4-2, was intended to be generically representative of water present in the repository host rock. The composition chosen, J-13 well water (DTN: MO0006J13WTRCM.000 [DIRS 151029]), was used as a starting point to develop the solubility models. Although it is not expected to enter the repository, the use of J-13 well water composition maintains continuity between the current work and past dissolved concentrations analyses and is also consistent with *In-Package Chemistry Abstraction* (BSC 2004 [DIRS 167621]). Also, as indicated in *In-Package Chemistry Abstraction* (BSC 2004 [DIRS 167621]), the composition of the incoming water has little effect on chemistry within the package. As shown in Section 6.4, most of the constituents in the fluid, even at high concentration, have little to no effect on the dissolved concentration limits modeled in this report. The only aqueous ion of concern is fluoride, which can greatly impact the dissolved concentrations. Uncertainty in fluoride composition is taken into account for the dissolved concentrations of radioelements through an uncertainty term as indicated in Section 6.3.3.2. The applicable ranges for the solubility models developed in this report are much wider than the conditions listed in Table 4-2 (Section 6.4.4). While initial values of pH, T (°C), and fCO_2 were direct input to the code, these parameters were varied over a set range during the simulation. DTN: MO0302SPATHDYN.000 [DIRS 161756] is a thermodynamic database developed specifically for speciation calculations on the YMP. Therefore, its use in this model is appropriate.

Table 4-1. Direct Inputs for Solubility Models

Data Description	Data Source [a]	Data Tracking Number	Parameters Used	Used in
Data0.ymp.R2 (thermodynamic database for EQ3NR calculations)	BSC 2004 [DIRS 171916]	MO0302SPATHDYN.000 [DIRS 161756]	All parameters pertinent to the EQ3NR calculations	Sections 6.5.3, 6.5.4, 6.6.3, 6.7 to 6.9, 6.11, and 6.12 for solubility calculations
Groundwater composition of Well J-13	CRWMS M&O 2000 [DIRS 152507]	MO0006J13WTRCM.000 [DIRS 151029]	See Table 4-2	Section 6.4 for solubility model configuration
Atomic weight	Lide 1995 [DIRS 101876], inside cover	N/A	All pertinent elements	Throughout this report
Equilibrium constant of sodium boltwoodite	Guillaumont et al. 2003 [DIRS 168382], p. 256	N/A	Equilibrium constant of sodium boltwoodite	Incorporated into *Data0.yc3.R1* based on *Data0.ymp.R2*, used in Section 6.7 to develop the U-solubility model
Uncertainties in Thermodynamic Data	OECD 2001 [DIRS 159027], Tables 3.1, 3.2, 4.1, and 4.2	N/A	Uncertainties in Thermodynamic Data for Np and Pu	Sections 6.5.3.4, 6.6.3.2.2, and 6.6.3.2.3 for uncertainties in plutonium-, Np_2O_5-, and NpO_2-solubility models
Uncertainties in Thermodynamic Data	Silva et al. 1995 [DIRS 102087], Table III-2	N/A	Uncertainties in Thermodynamic Data for Am	Section 6.9.4.2 for uncertainties in americium-solubility model
Uncertainties in Thermodynamic Data	Grenthe et al. 1992 [DIRS 101671], Tables III.1, III.2	N/A	Uncertainties in Thermodynamic Data for U	Sections 6.3.3.1 and 6.7.5 for uncertainties in uranium-solubility model
Uncertainties in Thermodynamic Data	Hummel et al. 2002 [DIRS 161904], p. 284, Table 5.21.1	N/A	Uncertainties in Thermodynamic Data for Pu and Th	Section 6.5.3.4 for uncertainties in plutonium-solubility model. Section 6.8.4.2 for uncertainties in thorium-solubility model
Density of actinides	Lide 2002 [DIRS 160832]	N/A	All pertinent elements	Section 8.2
Fluoride Concentration Range	BSC 2004 [DIRS 167621], Table 8-6	N/A	Maximum F^- concentrations in the waste package	For uncertainties associated with fluoride concentrations
Ionic Strength Uncertainty	Truesdell and Jones 1974 [DIRS 170136]	N/A	a-zero and b parameters of Truesdell-Jones activity coefficient expression	Section 6.3.3.4 for additional uncertainties at ionic strength from 1 to 3 molal

NOTE: [a] Where data sources have associated DTNs, the DTNs are the direct input and the reports are indirect input.

Table 4-2. Chemical Composition of Reference Water (J-13 Well Water)

Component	Abundance (mg/L)	Uncertainty (mg/L)
Na^+	45.8	±2.29
K^+	5.04	±0.61
Ca^{2+}	13.0	±0.99
Mg^{2+}	2.01	±0.21
Si (SiO_2 (aq))	28.5 (60.97)[a]	±1.85
Cl^-	7.14	±0.61
F^-	2.18	±0.29
NO_3^-	8.78	±1.03
SO_4^{2-}	18.4	±1.03
pH	7.41	±0.44
Alkalinity (HCO_3^-)	128.9	±8.6

Source: DTN: MO0006J13WTRCM.000 [DIRS 151029] contains recommended mean values of major constituents in J-13 well water.

NOTE: [a]The conversion from Si to SiO_2 is 1 mg/L Si = 2.14 mg/L SiO_2.

4.2 CRITERIA

Projects Requirements Document (Canori and Leitner 2003 [DIRS 166275]) identifies the high-level requirements for the YMP. The requirements pertaining to this report, and their link to 10 CFR 63 [DIRS 173164], are shown in Table 4-3.

Table 4-3. Applicable Project Requirements Criteria

Requirement Number	Title	10 CFR 63 Link
PRD-002/T-014	Performance Objectives for the Geologic Repository After Permanent Closure	10 CFR 63.113 [DIRS 173164]
PRD-002/T-015	Requirements for Performance Assessment	10 CFR 63.114 [DIRS 173164]
PRD-002/T-016	Requirements for Multiple Barriers	10 CFR 63.115 [DIRS 173164]

Work described in this document will support the following criteria from *Yucca Mountain Review Plan, Final Report* (NRC 2003 [DIRS 163274]) as described in Table 3-1 of *Technical Work Plan for Postclosure Waste Form Modeling* (BSC 2005 [DIRS 173246]). Applicable Yucca Mountain Review Plan acceptance criteria are presented below. The full text of these criteria is quoted in Section 8.3 along with a detailed explanation of how this document addresses those criteria and the location where the appropriate information can be found.

Radionuclide Release Rates and Solubility Limits Acceptance Criteria (NRC 2003 [DIRS 163274], Section 2.2.1.3.4.3)

- Acceptance Criterion 1 – System Description and Model Integration Are Adequate
- Acceptance Criterion 2 – Data Are Sufficient for Model Justification

- Acceptance Criterion 3 – Data Uncertainty Is Characterized and Propagated Through the Model Abstraction

- Acceptance Criterion 4 – Model Uncertainty Is Characterized and Propagated Through the Model Abstraction

- Acceptance Criterion 5 – Model Abstraction Output Is Supported by Objective Comparisons.

Section 8.3 quotes the full text of the applicable acceptance criteria with pointers to the information within this report that pertains to the criteria.

4.3 CODES, STANDARDS, AND REGULATIONS

10 CFR 63. [DIRS 173164] Energy: Disposal of High-Level Radioactive Wastes in a Geologic Repository at Yucca Mountain, Nevada

Standard Practice for Prediction of the Long-Term Behavior of Materials, Including Waste Forms, Used in Engineered Barrier Systems (EBS) for Geological Disposal of High-Level Radioactive Waste (ASTM C 1174-97 [DIRS 105725]) is used to support the model development methodology, categorize the models developed with respect to their usage for long-term TSPA-LA, and to relate the information and data used to develop the model to the requirements of the standard.

INTENTIONALLY LEFT BLANK

5. ASSUMPTIONS

5.1 OXIDIZING CONDITIONS

Assumption: The repository is in an oxidizing condition and oxygen fugacity equals 0.2 bars (the atmospheric value).

Rationale: The existence of reducing conditions in the repository has not been proven, except for transient and localized conditions. Also, as the repository is in the unsaturated zone, it is connected to the atmosphere. Therefore, atmospheric oxygen fugacity is used.

Confirmation Status: Many of the radionuclides critical to dose are less soluble under reducing conditions (Langmuir 1997 [DIRS 100051], Chapter 13). Therefore, it is a conservative assumption because radionuclides are either more soluble under atmospheric oxygen fugacity or insensitive to oxygen fugacity. Thus, it does not need further confirmation.

Use in the Model: This assumption is used throughout Section 6, with an exception for Section 6.5 (Pu-solubility model), and Section 6.6 (Np-solubility model), where slightly different redox conditions are used and a detailed rationale is given.

5.2 INVENTORY VALUES

Assumption: The abundance of ^{238}U and ^{237}Np in the ATM-103 and ATM-106 samples used in the Argonne National Laboratory (ANL) drip tests can be represented by the inventory values given by Guenther et al. (1988 [DIRS 109205]; 1988 [DIRS 109206]) for fuels out of reactors for 15 years.

Rationale: The abundance of ^{238}U does not change with the out-of-reactor time, and ^{237}Np abundance changes less than 1.5 percent over a period of 5 years (Guenther et al. 1988 [DIRS 109205], Table F.2.d, p. F.23).

Confirmation Status: This assumption is reasonable because the uncertainty it introduces is small. Therefore, no confirmation is required.

Use in the Model: This assumption is used in Section 6.6.4.3.

INTENTIONALLY LEFT BLANK

6. MODEL DISCUSSION

6.1 MODELING OBJECTIVES

The objective of this modeling effort is to evaluate and abstract dissolved concentration limits of certain elements with radioactive isotopes in the environments expected in the repository. Fourteen elements with radioactive isotopes (actinium, americium, carbon, cesium, iodine, neptunium, protactinium, lead, plutonium, radium, strontium, technetium, thorium, and uranium) are considered based on *Radionuclide Screening* (BSC 2002 [DIRS 160059]).

Dissolved concentration limits for plutonium, neptunium, uranium, thorium, americium, and protactinium are presented as tabulated functions of environmental conditions (namely, pH and fCO_2) with one or more uncertainty terms or distributions. The presentation of other radionuclides (carbon, cesium, iodine, lead, radium, strontium, and technetium) is discussed in Sections 6.12 through 6.18. Even though selection of an appropriate set of radionuclides documented in *Radionuclide Screening* (BSC 2002 [DIRS 160059]) includes actinium, transport of Ac is not modeled in the TSPA-LA model because of its extremely short half-life. Actinium dose is calculated in TSPA-LA by assuming secular equilibrium with ^{231}Pa (Section 6.10); therefore, Ac is not analyzed in this report. The results of this report are inputs for TSPA-LA.

The corroborating and supporting data used in this section are summarized below.

6.1.1 Indirect Inputs

Many of the indirect inputs are summarized in Table 6.1-1 (the remaining indirect inputs are summarized in Tables 6.5-6 and 7.1). These indirect inputs provide additional information to support, validate, or invalidate solubility models, or to establish the ranges of environmental conditions for solubility calculations.

Table 6.1-1 Summary of Indirect Inputs

Input	Source	Used In
pH Ranges	BSC 2004 [DIRS 167621], BSC 2004 [DIRS 169860], and BSC 2004 [DIRS 170028]	Section 6.4 for pH ranges used for EQ3NR calculations[a]
fCO_2 Range	BSC 2004 [DIRS 169860], Section 6.7.2.2	Section 6.4 for fCO_2 ranges used for EQ3NR calculations[a]
Pa(IV) Radii and Equilibrium Constants	Shannon 1976 [DIRS 153587], Table 1	Section 6.11 for protactinium solubility analogues
log K of Protactinium Species	Baes and Mesmer 1986 [DIRS 100702]; Table 9.1	Section 6.11 for protactinium solubility analogues
log K of Protactinium Species	Yui et al. 1999 [DIRS 162664]	Section 6.11 for protactinium solubility analogues
Lead Concentrations in Environments	Hem 1985 [DIRS 115670], p. 144	Section 6.13 for lead solubility corroboration
Plutonium Solubility	Efurd et al. 1998 [DIRS 108015], Table 4	Section 6.5 to compare with model results
Pu Solubility and Pu Oxidation States Distribution	Nitsche et al. 1993 [DIRS 155218], Tables XVI and XVII	Section 6.5 to compare with model results
Pu Solubility and Pu Oxidation States Distribution	Nitsche et al. 1994 [DIRS 144515], Tables II and XVII	Section 6.5 to compare with model results
Pu Solubility and Oxidation States Distribution	Rai 1984 [DIRS 122768]	Section 6.5 to compare with model results
Pu Solubility	Rai et al. 2001 [DIRS 168392], Tables A.1 and A.2	Section 6.5 to compare with model results
Mean Salt Activity Coefficients	Robinson and Stokes 1965 [DIRS 108567], Appendix 8.10	Section 6.3.3.4 to corroborate the Truesdell-Jones equation for activity coefficients. Used in workbooks *1-1 Salts data & calc* and *1-2 Salts data & calc* in spreadsheet *gamma comp calcs.xls*.
Spent Nuclear Fuel Characterizations	Guenther et al. 1988 [DIRS 109205], Table F.2.d, p. F.23; Guenther et al. 1988 [DIRS 109206], Table F.2.f, p. F.31	Section 6.6.4.3 to develop the alternative secondary-phase neptunium-solubility model

NOTES: [a]The values for pH and fCO_2 only serve to determine the range over which the solubility calculations in this report must be performed.

6.2 FEATURES, EVENTS, AND PROCESSES INCLUDED IN MODEL

Table 6.2-1 provides the FEPs included in the TSPA-LA submodels described in this model document.

Table 6.2-1 Included FEPs

FEP Name	FEP Number	Section Where Disposition is Discussed
Radionuclide Solubility, Solubility Limits, and Speciation in the Waste Form and EBS	2.1.09.04.0A	6.3.1 and 6.5 to 6.18
Reduction-Oxidation Potential in Waste Package	2.1.09.06.0A	6.5 and 6.6
Reaction Kinetics in Waste Package	2.1.09.07.0A	6.3

Source: DTN: MO0407SEPFEPLA.000 [DIRS 170760].

6.3 TECHNICAL ISSUES IN SOLUBILITY EVALUATION

There are two prerequisites to solubility evaluations based on geochemical modeling: 1) a thermodynamic database and compatible geochemical modeling tool and 2) environmental conditions for which solubility must be evaluated. With these prerequisites, a model can be constructed based on environmental information and the chemical properties of radionuclides. Solubility limits are based on the model results.

The first prerequisite is input to this analysis and is discussed in Section 4.1. The second prerequisite is discussed in Section 6.4. The discussion in this section focuses on several technical issues common to solubility evaluation, such as the selection of solubility-controlling solids and uncertainty treatment. Specific issues related to certain elements are discussed in relevant sections.

6.3.1 Definition of Solubility

From the viewpoint of laboratory chemistry, solubility is defined as the concentration of a substance when the solution is saturated with that substance (Atkins 1994 [DIRS 134303], p. 312). This definition implies: 1) solubility is defined in terms of thermodynamics, and 2) solubility is the maximum concentration (with a certain degree of uncertainty) the substance can reach in solution at equilibrium for a given set of environmental conditions. In other words, solubility is the concentration of a substance when the substance is at equilibrium with the solution. For this case, the substance is a radionuclide-bearing solid called the solubility-controlling solid.

Performance assessments are more interested in the solubility of specific elements in water than the solubility of a substance. Except for colloidal and kinetically transient phenomena such as oversaturation, solubility is the maximum concentration that an element can reach under the conditions of interest. The phrase “maximum concentration” reflects a key requirement for solubility evaluation (i.e., it is bounding).

Solubility limits are input for TSPA-LA analyses as one of two possible constraints on the maximum radionuclide concentrations. The other constraint is calculated within the TSPA-LA model based on the dissolution rate of individual waste forms, water volume, and the solubility caps presented in Table 8-3.

A solubility-controlling solid can be either a pure radionuclide-bearing solid or a solid solution of two (or more) end members. In practice, pure radionuclide-bearing solids are nearly always used to evaluate solubility principally because proof of the formation of solid solutions is a more demanding task than demonstration of the formation of pure solids. In addition, values for parameters required for solubility models based on solid-solution control are commonly not available. Use of a pure solubility-controlling phase over the use of a solid solution is acceptable because it yields higher (conservative) solubility limits.

Sorption is another mechanism that controls radionuclide concentrations in solution. The net effect of sorption is to lower radionuclide concentrations in solutions. This study excludes sorption from current consideration, as it is conservative for maintaining the highest concentration in solution.

Concentrations in aqueous solutions may be given in several different units. The standard unit for chemical computations is moles of solute per kilogram of solvent (molality). For dilute solutions, this differs only slightly from moles per liter (molarity). Another common expression of units is mg/L (milligrams/liter).

6.3.2 Identification of the Controlling Solid

As discussed previously, element solubility is defined with respect to a solid. To evaluate solubility within a repository, the controlling solid or solids must be identified. Since solubility depends strongly on the solid phase, the outcome varies (orders of magnitude) depending on the solids chosen.

Laboratory experiments and observations of natural systems provide the basis for choosing the controlling phase. For example, in experiments from oversaturation conducted at Los Alamos National Laboratory (LANL) (Efurd et al. 1998 [DIRS 108015]; Runde et al. 2002 [DIRS 168432]; CRWMS M&O 2001 [DIRS 154629]) solids precipitated have a dark green color, which is characteristic of Pu(IV) solid phases. Diffuse reflectance infrared spectra of the precipitated solid indicate the presence of Pu(IV) and the X-ray diffraction pattern matched that of PuO_2(s). The diffuse and broad X-ray diffraction peaks suggest poorly crystalline structures (Efurd et al. 1998 [DIRS 108015]; Runde et al. 2002 [DIRS 168432]; CRWMS M&O 2001 [DIRS 154629]). It is concluded that plutonium hydroxides, colloids, or both aging toward $PuO_2 \cdot xH_2O$ are, therefore, interpreted to be the solubility-controlling solids in these experiments. Unfortunately, laboratory evidence and field observations are not available for all the radionuclides at the environmental conditions and time scales of interest. Moreover, the identity of the controlling solid may change with environment conditions. Choice of solubility-controlling phases used in models is outlined in Sections 6.5.3.1 (for Pu), 6.6.3.1 (for Np), 6.7.2 (for U), 6.8.2 (for Th), 6.9.1 and 6.9.2 (for Am), and 6.12 (for Ra). Solubility of Pa is done through analogy to other actinides, which is outlined in Sections 6.11.1 and 6.11.2.

Thermodynamic data on actinide solids are derived from laboratory solubility measurements and from direct thermochemical measurements such as calorimetry (Nordstrom and Munoz 1986 [DIRS 153965], Chapter 11). The thermodynamic properties of the minerals uraninite (UO_2), thorianite (ThO_2), and analogous phases have been well defined using thermochemical techniques. However, other phases such as NpO_2 and PuO_2 have not. Solubility studies of actinide dioxide (Grenthe et al. 1992 [DIRS 101671], Section v3.2.3.3; Guillaumont et al. 2003 [DIRS 168382], Section 9.3.2.2; Hummel et al. 2002 [DIRS 161904]; Neck and Kim 2001 [DIRS 168258]), using over- and under-saturation tests at pH greater than 3 to 5 (depending on reference) indicate that the dissolved actinide concentrations are not controlled by high-temperature crystalline phases, but solids (such as hydrated or amorphous phases) that are considerably more soluble. Hummel et al. (2002 [DIRS 161904], Figure 3.2.2) clearly show the solubility calculated from the thermodynamic properties of the high-temperature mineral form of ThO_2 is nine orders of magnitude lower than concentrations measured in laboratory experiments at pH values above about 6. Similarly, Figure 3.2.3 of the report by Hummel et al. (2002 [DIRS 161904]) shows calculated solubility of the high-temperature mineral form of UO_2 is six orders of magnitude lower than concentrations measured in laboratory experiments at pH values above about 3. The more soluble phases leading to the higher, laboratory-measured concentrations are not well defined crystallographically. However, solubility values are reproducible and these solubility values do not change over a period of several years (time scale of laboratory experiments). Thus, critically compiled thermodynamic databases, such as those of the NEA (Grenthe et al. 1992 [DIRS 101671]; Silva et al. 1995 [DIRS 102087]; OECD 2001 [DIRS 159027]; Guillaumont et al. 2003 [DIRS 168382]); NAGRA/PSI (Hummel et al. 2002 [DIRS 161904]), include several actinide dioxide solids for Th, U, Np, and Pu. One such actinide dioxide solid variety is high-temperature, crystalline (example, PuO_2 or PuO_2(cr) (cr = crystalline)), or referred to by its mineral name (i.e., plutonium dioxide). Other varieties include solids that control laboratory solubilities (examples, written as PuO_2(am) (am = amorphous), PuO_2 (am,hyd) (hyd = hydrated), PuO_2(hyd,aged), and $Pu(OH)_4$(am)). These types of solids are included in the thermodynamic database supporting the modeling described in this report (Section 4.1) and are listed in Table 6.3-1. The one exception to this is NpO_2. The formation of this mineral at low temperatures is described in Appendix IV.

Table 6.3-1. Solid Phases of Four Valent Actinides Included in Project Thermodynamic Database *Data0.ymp.R2*

Element	Highly Crystalline Solid	Observed Solids that Control Experimental Studies
Thorium	Thorianite (ThO_2)	ThO_2(am)
Uranium	Uraninite (UO_2)	See Table 6.7-1
Neptunium	Neptunium Dioxide (NpO_2)	NpO_2(am,hyd), $Np(OH)_4$(am), NpO_2
Plutonium	Plutonium Dioxide (PuO_2)	PuO_2(hyd,aged)

From the viewpoint of thermodynamics, the most-stable solid would be selected as the controlling phase because thermodynamically less-stable phases would ultimately be replaced by the most-stable phase. However, it cannot be demonstrated that the thermodynamically most-stable solid appears during the regulatory period under the expected repository conditions. This fact makes identification of the controlling solid purely from thermodynamic considerations unreliable.

The Ostwald Step Rule provides a useful guide for such situations. This rule says that unstable or metastable minerals form first, followed by progressively more-stable minerals (Langmuir 1997 [DIRS 100051], p. 324). The formation of $PuO_2 \cdot xH_2O$ in plutonium experiments is an example of the Ostwald Step Rule. The thermodynamically more-stable phase, PuO_2(s) (s denotes solid), is sufficiently more stable than the PuO_2 (hyd,aged) under atmospheric oxygen (Efurd et al. 1998 [DIRS 108015], Figure 5). Precipitation kinetics is the governing factor for the Ostwald Step Rule. In other words, during the process of waste corrosion, more-stable minerals are prevented from precipitating because less-stable minerals are kinetically favored. Another good example of the Ostwald Step Rule is the formation of secondary uranyl minerals during spent nuclear fuel dissolution. Less-stable schoepite precipitates first, and is then replaced by more-stable uranyl silicates (Wronkiewicz et al. 1992 [DIRS 100493], Section 4.2).

The Ostwald Step Rule has significant implications for choosing the controlling phase. To use a more-stable phase (rather than the first formed, less-stable phase) as the controlling phase for solubility calculations, it is necessary to demonstrate that the less-stable mineral(s) is replaced by the more-stable mineral(s) in a shorter period than the characteristic time scale of the problem. Specifically, since the time scale of repository performance is 10^4 years, the time scale for more-stable mineral(s) to form should be less than 10^2 to 10^3 years. Additionally, because several fuel types are modeled in TSPA-LA with instantaneous degradation, the majority of the fuel in these categories (such as DOE spent nuclear fuels) can be degraded in one TSPA-LA time step. The smallest time step used in TSPA-LA is 10 years. Therefore, arguments for the formation of stable minerals must also account for time periods as small as 10 years. Arguments that the thermodynamically more-stable phase ultimately replaces less-stable kinetically precipitated minerals are not convincing because, under certain conditions, it may take a very long time for thermodynamic phases to replace a kinetic phase through aging or other processes. For example, the mixture of hydrogen and oxygen gases at room temperature is thermodynamically unstable with respect to water, but water never forms from the mixture unless the mixture is ignited by flame or other means. A good geologic example is the persistence of oxygen and nitrogen gas in the atmosphere in the presence of moisture and liquid water in spite of the fact that equilibrium for these substances is nitric acid.

For some elements, the identification of controlling solids for the repository by experiments has yet to be reported (e.g., protactinium), or experimental observations are not conclusive (e.g., plutonium). For situations like this, a conservative approach is, as suggested by Bruno et al. (1997 [DIRS 111794], p. 81), to choose the amorphous solids (oxide or hydroxide) as their controlling solids. The Ostwald Step Rule is the main reason for choosing an amorphous phase. Another reason is that radiation associated with spent nuclear fuel could damage the lattice structure of solids and make it less crystalline (Rai and Ryan 1982 [DIRS 112060], p. 216). It is well known that radioactive decay, especially α-decay, can damage the crystal structure of plutonium solids. Rai and Ryan (1982 [DIRS 112060]) reported in an experiment lasting 1,266 days that $^{238}PuO_2$(c) (c = crystalline) was found to convert to an amorphous form of PuO_2, which has higher solubility than PuO_2(c). In waste forms, the fraction of isotope ^{238}Pu in the total plutonium inventory is small (BSC 2004 [DIRS 170022], Table 7-1), so crystal structure damage is not expected to occur rapidly enough to be significant. However, over the regulatory time period, it is reasonable to expect that PuO_2(c) would gradually convert to a PuO_2(am).

Therefore, this phenomenon is recognized, and the uncertainty it introduces to radionuclide solubility is addressed.

Freshly precipitated solids tend to be fine particles with a large specific surface area. The extra surface energy given by the large surface area makes fresh precipitates more soluble. However, with time, the freshly precipitated fine particles go through a process called aging in which particle size increases. As a result, an aged precipitate has a lower solubility than the freshly precipitated solid. Aging could be a long-lasting process. For example, in a study lasting 1,266 days, Rai and Ryan (1982 [DIRS 112060]) observed continuous aging of $PuO_2 \cdot xH_2O$ (amorphous). As solubility experiments usually last less than a year, it is reasonable to expect that the measured solubility is actually an upper limit. Therefore, because of aging, a solid's real solubility could be lower than its measured solubility.

In fact, aging and decay effects (radiation damage) have opposite effects on solubility. Aging could make a radionuclide less soluble if the starting material is an amorphous solid. Decay effects could make a radionuclide more soluble, provided the initial material is a crystalline solid. Therefore, it is reasonable to speculate that the real controlling material may contain both amorphous and crystalline phases. Indeed, Rai and Ryan (1982 [DIRS 112060], p. 214) found that "the solubility of $^{239}PuO_2$ and $^{239}PuO_2 \cdot xH_2O$ tend to merge; most, if not all, of the effect is due to decreased solubility of $PuO_2 \cdot xH_2O$ with time." While there is not enough information to define the thermodynamic properties of this intermediate solid quantitatively and, consequently, to calculate solubility controlled by it, the uncertainty can be bounded by use of the amorphous and crystalline phases.

For some very soluble elements (i.e., Tc), solids are not expected to precipitate from solution under the repository conditions. The transport of those elements may not be solubility controlled. An arbitrary large number is assigned to their solubility so their release is controlled by the dissolution rate of individual waste forms and water volume as indicated in Section 8-2. This is a conservative approach and no further validation is needed.

For some elements, there is more than one mineral with overlapping stability fields within the range of environmental conditions. For these, a multiple controlling-mineral model has been adopted to derive solubility limits. For uranium, three solids are used (Sections 6.7.1 and 6.7.2) and for neptunium, two different phases control the in-package solubility versus the solubility of Np in the invert (Section 6.6.3.1).

6.3.3 Treatment of Variation and Uncertainty

In general, the solubility of an element under repository-relevant conditions changes as a function of environmental variables. As chemical conditions change over time, solubility changes as well. Knowledge of the solubility is also subject to uncertainty, because of the chemical conditions and the parameter values used to calculate it. Although variation of chemical conditions with time and uncertainty have similar effects on solubility limits, distinguishing between them is beneficial.

As repository-relevant conditions change or vary, so does radionuclide solubility. A meaningful solubility evaluation should account for the variation in solubility caused by the changes in environmental conditions. As long as the environmental condition ranges are known (as inputs to the analysis), the range of solubility variation can be calculated. It is useful to understand the

effects of changes in environmental conditions on solubility limits. For example, how a repository design feature would affect solubility limits and, ultimately, the repository performance could be predicted by analyzing its effects on environmental conditions.

This report has three output types, each with its own treatments of variation of chemical conditions and uncertainty. Solubilities of actinides (i.e., americium, neptunium, protactinium, plutonium, thorium, and uranium) are tabulated for certain ranges of pH and fCO_2 values with several uncertainty terms. For radium and lead, stochastic distributions are given. For those elements for which no solubility-controlling solids are expected to form under repository conditions (carbon, cesium, iodine, strontium, and technetium), a constant of "500" is assigned to their solubility. This number should not be taken literally. Rather, it is meant to indicate, for these elements and conditions, the TSPA-LA calculation should use concentrations based on the dissolution rate of individual waste forms and water volume as indicated in Section 8-2. The functional relations (tabulated) between solubilities and those conditions developed in Sections 6.5 through 6.18 account for effects of variations in relevant environmental conditions (namely, pH and $\log fCO_2$).

Uncertainty is associated with all of the steps in solubility evaluations. For example, it can be associated with the thermodynamic data used for the calculation. Another source is uncertainty in environmental conditions. Distinguishing uncertainty from temporal variability and understanding the major sources of uncertainty are prerequisites to estimating the uncertainty in the solubility values presented.

The uncertainties discussed in this section apply only to those dissolved concentrations tabulated in this report. For those elements flagged by the value of "500," because they are merely flags for the TSPA-LA model to use waste form dissolution rates or mass balance considerations to constrain their releases, the uncertainties should be based on those of the release rates.

Four types of uncertainty are associated with the output of this report: 1) in the thermodynamic data supporting the EQ3NR calculations, 2) due to variations in the chemistry of the water into which dissolution is occurring, 3) in the temperature, and 4) in activity coefficients. For some elements, the identities of the solubility-controlling phases existing over the repository lifetime are also uncertain. No uncertainty term is presented as output from this model for this uncertainty because calculated base-case model solubilities have been shown to be realistic (matching experimental data) or conservative. The model for Pa introduces a different type of uncertainty as those indicated above. Very little reliable information is available concerning the aqueous chemistry of Pa. Therefore, the model is developed based on chemical analogues, rather than experimental data. The uncertainty for Pa is concerned with the differences in the solubilities of the analogue elements.

Uncertainties in solubilities due to uncertainties in thermodynamic data and in the chemistry of the water into which dissolution occurs are included as variables in the solubility expressions given for the actinide elements. Temperature uncertainties are treated as bounding or limiting conditions on the solubilities given. Activity coefficient uncertainties are also treated as bounding conditions when the ionic strength of the solutions does not exceed 1 molal (the nominal limit of applicability of the EQ3NR modeling code) (Wolery 1992 [DIRS 100836], p. 38) and the supporting database *Data0.ymp.R2* (DTN: MO0302SPATHDYN.000 [DIRS 161756]). Additional activity coefficient uncertainty in solutions with ionic strengths

from 1 molal to 3 molal is treated by augmenting the uncertainty applied to the solubility to account for thermodynamic data uncertainty (Section 6.3.3.4).

It is possible that the thermodynamic databases (*Data0.ymp.R2* (DTN: MO0302SPATHDYN.000 [DIRS 161756]) and *Data0.yc3.R1*) used for solubility calculations do not include all the species that may occur for the system of interest. The extensive review and data compilation efforts required to ensure relevant species are present are examined by Steinborn et al. (2003 [DIRS 161956]). Because of the extensive reviews conducted by the NEA (Grenthe et al. 1992 [DIRS 101671]; Silva et al. 1995 [DIRS 102087]; OECD 2001 [DIRS 159027]) and others (e.g., Hummel et al. 2002 [DIRS 161904]), the most relevant or abundant species controlling the system chemistry for actinides are included in the databases. Therefore, there is no reason to expect other than small uncertainty from this source.

The NEA published an update on thermodynamic data for U, Np, Pu, Am, and Tc (Guillaumont et al. 2003 [DIRS 168382]). Table 6.3-2 compares the new results (Guillaumont et al. 2003 [DIRS 168382]) to those used in the creation of *Data0.ymp.R2* (DTN: MO0302SPATHDYN.000 [DIRS 161756]) for the most prevalent Am, Np, Pu, and U species modeled in EQ3. Inspection of the data suggests that its effect on this report is minimal.

Table 6.3-2. Comparison of $\Delta_f G^0$ Values for Major Aqueous Species

	Species	*Data0.ymp.R2* Values[a] (kJ/mol)	Updated Value[b] (kJ/mol)
Major Am Species (Figure 6.9-2)	$AmSO_4^+$	-1,364.678 ± 4.776	-1,361.538 ± 4.89
	$AmCO_3^+$	-1,171.120 ± 5.069	-1,172.262 ± 5.289
	$Am(CO_3)_2^-$	-1,724.706 ± 5.332	-1,728.131 ± 5.911
	$Am(CO_3)_3^{3-}$	-2,269.159 ± 5.976	-2,268.018 ± 7.521
Major Np Species (Figure 6.6-4)	NpO_2^+	-907.765 ± 5.652	-907.765 ± 5.628
	$NpO_2CO_3^-$	-1,463.988 ± 5.652	-1,463.988 ± 5.652
	$NpO_2(CO_3)_3^{4-}$	-2,185.949 ± 15.451	-2,185.949 ± 15.451
Major Pu Species (Figures 6.5-3 and 6.5-5)	PuO_2SO_4 (aq)	-1,525.650 ± 3.072	-1,525.650 ± 3.072
	PuO_2^+	-852.646 ± 2.868	-852.646 ± 2.868
	PuO_2CO_3 (aq)	-1,356.466 ± 17.359	-1,344.479 ± 4.180
	$PuO_2(CO_3)_3^{4-}$	-2,447.085 ± 5.977	-2,448.797 ± 4.180
	$PuO_2CO_3^-$	-1,409.771 ± 3.002	-1,263.527 ± 1.911
Major U Species (Figure 6.7-4)	UO_2SO_4 (aq)	-1,714.535 ± 2.021	-1,714.535 ± 1.800
	UO_2F^+	-1,263.128 ± 2.021	-1,263.527 ± 1.911
	$*UO_3$ (aq)	-1,368.038 ± N/A	-1,357.479 ± 1.794
	$(UO_2)_2CO_3(OH)_3^-$	-3,139.525 ± 4.517	-3,139.526 ± 4.517

Table 6.3-2. Comparison of $\Delta_f G^0$ Values for Major Aqueous Species (Continued)

	Species	*Data0.ymp.R2* Values (kJ/mol)	Updated Value (kJ/mol)
Major U Species (Figure 6.7-4)	$UO_2(CO_3)_3^{4-}$	-2,659.543 ± 2.123	-2,660.914 ± 2.116
	$UO_2(CO_3)_2^{2-}$	-2,105.044 ± 2.033	-2,103.161 ± 1.982

Source: [a](DTN: MO0302SPATHDYN.000 [DIRS 161756]).

[b](Guillaumont et al. 2003 [DIRS 168382]).

NOTE: *UO_3(aq) (as indicated in DTN: MO0302SPATHDYN.000 [DIRS 161756]) is the nonconventional equivalent of $UO_2(OH)_2$(aq); the $\Delta_f G^0$ value adopted for UO_3(aq) is consistent with those for $UO_2(OH)_2$(aq).

In determining the radionuclide concentration limits to be used in the recent safety analysis of a proposed geologic repository in Switzerland (NAGRA 2002 [DIRS 170922]), an analysis was made of the completeness of thermodynamic data available for modeling the solubilities of selected actinide elements (Berner 2002 [DIRS 162000]; Hummel and Berner 2002 [DIRS 170921]). The authors developed a list of aqueous species and solids for which data were available for actinide(III) species (Np^{3+}, Pu^{3+}, and Am^{3+}) and actinide(IV) species (Th^{4+}, U^{4+}, Np^{4+}, and Pu^{4+}). Because of the close chemical similarity of the members of these two groups of ions, there should be analogous aqueous species and solids for each member of each group with similar stability constants. Berner (2002 [DIRS 162000]) and Hummel and Berner (2002 [DIRS 170921]) found that for some elements, data were not available for one or more species. For these cases, they estimated the missing data and calculated solubilities. When these solubilities were compared with solubilities calculated using the incomplete data sets made up of only measured data, the results of the two sets of calculations were virtually identical for most elements, indicating the missing data had no effect on the calculated solubilities. However, for Pu, including the estimated species increased the calculated solubilities by a factor of 3 to 6. The extent of this possible effect is discussed below.

The NAGRA (2002 [DIRS 170922]) studies are directly relevant only to the solubilities of these elements under the reducing conditions of the proposed Swiss repository where the actinide(III) and actinide(IV) oxidation states of these elements dominate in solution. They are applicable in this report only to Am and Th, which are present as Am^{+3} and Th^{+4}, even in the oxidizing conditions of the Yucca Mountain repository. Under these same oxidizing conditions, oxidation states of U, Np, and Pu dissolved from waste forms is dominated by actinide(V) and actinide(VI) species. Therefore, the conclusions of the Swiss studies cannot be extended to include U, Np, and Pu dissolved from waste forms. Hummel et al. (2002 [DIRS 161904], Table 3) compared the data available in the NAGRA/PSI database for complexes and solids of actinide(VI) species, UO_2^{+2}, NpO_2^{+2}, and PuO_2^{+2}. Data are available for all UO_2^{+2} species, fewer NpO_2^{+2} species, and still fewer PuO_2^{+2} species. This suggests that missing data could have a larger effect on calculated Pu solubilities than on U solubilities. However, the extent of this possible effect cannot be estimated with the data at hand.

The remainder of this section provides a general discussion of these four types of uncertainty including their sources and the general procedure used in their evaluation. The discussions of

each element in Section 6 include element-specific information for evaluating the uncertainty in their concentrations. Element-specific uncertainties are summarized in Table 8-2.

6.3.3.1 Uncertainties in the log K Values of Controlling Solid(s) and Aqueous Species

There are uncertainties in the thermodynamic data used to make the solubility calculations. Because of the complexity of the solubility modeling code, EQ3NR (Wolery 1992 [DIRS 100836]), uncertainties in the entire suite of supporting thermodynamic data were not propagated rigorously through the solubility calculations. Rather, uncertainties in the solubilities of the elements modeled considered uncertainties in the thermodynamic properties of the solubility-controlling solid and of the aqueous species that dominate the dissolved concentration of each element.

Uncertainties in the thermodynamic properties, specifically $\Delta_f G^0$ values, of the controlling solids and relevant aqueous species and the log K values of reactions connecting them are treated explicitly. Uncertainties in these values propagate directly to uncertainties in log(solubilities). The log K values used in the modeling are those in *Data0.ymp.R2* (DTN: MO0302SPATHDYN.000 [DIRS 161756]), which do not include uncertainties. Uncertainties of $\Delta_f G^0$ values for americium, neptunium, plutonium, and uranium are those recommended in the NEA compilations (Grenthe et al. 1992 [DIRS 101671]; Silva et al. 1995 [DIRS 102087]; OECD 2001 [DIRS 159027]; Guillaumont et al. 2003 [DIRS 168382]), from which the log K values in *Data0.ymp.R2* (DTN: MO0302SPATHDYN.000 [DIRS 161756]) were derived. The uncertainties of log K values for thorium species are based on the review of thorium data made to support the NAGRA/PSI database as documented by Hummel et al. (2002 [DIRS 161904]).

Guillaumont et al. (2003 [DIRS 168382], Appendix C) describe the technique used to develop the uncertainties given in the NEA and NAGRA/PSI database compilations (Grenthe et al. 1992 [DIRS 101671]; Silva et al. 1995 [DIRS 102087]; OECD 2001 [DIRS 159027]; Hummel et al. 2002 [DIRS 161904]; Guillaumont et al. 2003 [DIRS 168382]). These uncertainties are based on least squares analyses of the underlying solution equilibrium data and are characterized in the captions for the data tables in each of the NEA volumes as "total uncertainties and correspond, in principle, to the statistically defined 95 percent confidence interval" (e.g., Guillaumont et al. 2003 [DIRS 168382], Tables 3-1, 3-2, 4-1, 4-2, 5-1, 5-2, 6-1, 6-2, 7-1, 7-2, 8-1, and 8-2). In this report, uncertainties in solubility based on uncertainties in the underlying thermodynamic data are considered to be total uncertainties. This is the manner in which these uncertainties are treated in other nuclear waste management programs (e.g., Berner 2002 [DIRS 162000]). The "95 percent confidence interval" is interpreted to mean tabulated values on data uncertainty representing two standard deviations (2σ) in a normal distribution. The uncertainties in the solubility values given in this report are reported as 1σ values for normal distributions. Because the uncertainties of the underlying thermodynamic data are considered to be total uncertainties, the distributions of solubilities should be truncated at $\pm 2\sigma$.

The log K values in *Data0.ymp.R2* (DTN: MO0302SPATHDYN.000 [DIRS 161756]) are related to the standard thermodynamic properties by the expression $\Delta_r G^0 = -RT\ln K$. $\Delta_r G^0$ is derived from the $\Delta_f G^0$ values of reactants and species by the expression $\Delta_r G^0 = \Sigma \Delta_f G^0_{products} - \Sigma \Delta_f G^0_{reactants}$. Thus, uncertainties in $\Delta_f G^0$ values propagate directly to

uncertainties in log K values. These, in turn, propagate directly to uncertainties in log solubilities. The solubility data provided in this report are given as log solubility values. The uncertainties in them are expressed as normal distributions of the log solubility values because they are derived from uncertainties in the standard thermodynamic properties, which are given as normal distributions.

The solubility of a substance depends not only on the properties of its controlling solid, but also on the properties of the aqueous species that contribute to its total solution concentration. Thus, the uncertainty of the solubility includes that of the controlling solid and those of the dominant aqueous species. The uncertainty attributable to the controlling solid is constant, but the uncertainty attributable to aqueous species varies because solubilities are reported for a range of chemical conditions over which the identity and relative importance of aqueous species differ widely. The uncertainty due to aqueous species is evaluated by examining the solution speciation indicated by the EQ3NR runs at selected chemical conditions. The process by which this uncertainty is evaluated can best be illustrated by specific examples (as described here for uranium and thorium). The calculations for the other elements to which this process was applied (plutonium, neptunium, and americium) are described in Sections 6.5, 6.6, and 6.9.

Figures 6.3-1 and 6.3-2 show concentrations of total dissolved U and of aqueous species contributing to that concentration calculated at $fCO_2 = 10^{-3.0}$ bars, and expressed as molalities and percents total U, respectively. The figures span the pH range from 3.5 to 9.5. As discussed in Section 6.7, these calculations are based on solubility control by three solids: the minerals schoepite ($UO_3 \cdot 2H_2O$) and Na-boltwoodite ($NaUO_2SiO_3OH \cdot 1.5H_2O$), which prevail at low and intermediate pH values, respectively, and the solid $Na_4UO_2(CO_3)_3$, which is found in laboratory experiments under conditions of high pH and fCO_2. The cusps in Figure 6.3-1 represent the point at which solubility control by one solid gives way to control by another.

Figure 6.3-2 shows the following species constitute more than 10 percent of the dissolved uranium under the range of conditions modeled: $UO_2(CO_3)_3^{4-}$, $UO_2(CO_3)_2^{2-}$, $(UO_2)_2CO_3(OH)_3^-$, $UO_3(aq)$, UO_2F^+, $UO_2F_2(aq)$, UO_2^{2+}, $UO_2SO_4(aq)$, and $(UO_2)_2(OH)_2^{2+}$.

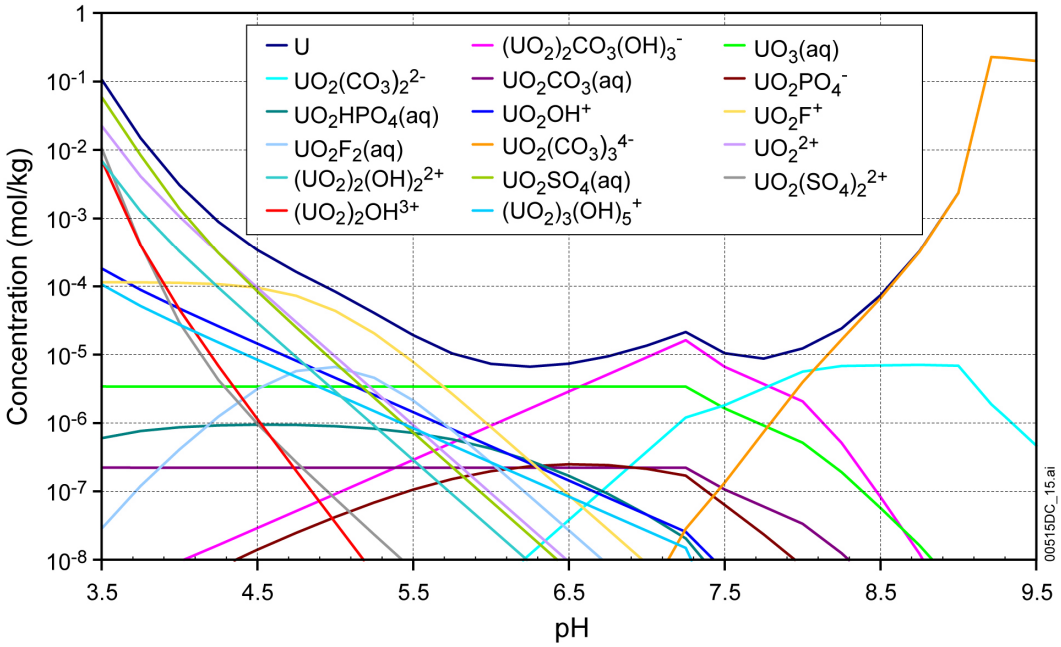

Source: Workbook *U chart highest*, spreadsheet *U species plot.xls* (Appendix I).

NOTE: $UO_3(aq)$ (as indicated in DTN: MO0302SPATHDYN.000 [DIRS 161756]) is the nonconventional equivalent of $UO_2(OH)_2(aq)$; the $\Delta_f G^0$ value adopted for $UO_3(aq)$ is consistent with those for $UO_2(OH)_2(aq)$.

Figure 6.3-1. Total Uranium Concentration and Speciation Diagram in moles U/kg H_2O Calculated at $fCO_2 = 10^{-3.0}$ Bars

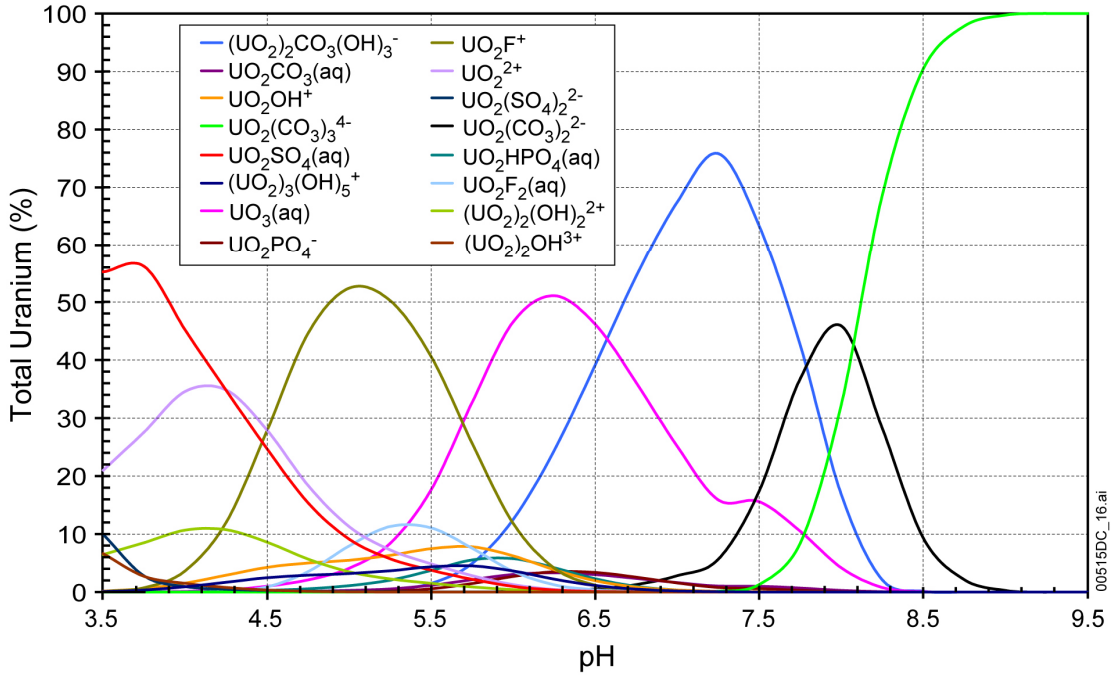

Source: Workbook *Chart percent*, spreadsheet *U species plot.xls* (Appendix I).

NOTE: $UO_3(aq)$ (as indicated in DTN: MO0302SPATHDYN.000 [DIRS 161756]) is the nonconventional equivalent of $UO_2(OH)_2(aq)$; the $\Delta_f G^0$ value adopted for $UO_3(aq)$ is consistent with those for $UO_2(OH)_2(aq)$.

Figure 6.3-2. Uranium-Speciation Diagram in Percent Total Uranium Calculated at $fCO_2 = 10^{-3.0}$ Bars

Consider the reaction describing the dissolution of the controlling solid, $UO_3 \cdot 2H_2O$, to one of the dominant species, $UO_2(CO_3)_2^{2-}$:

$$UO_3 \cdot 2H_2O + 2\ HCO_3^- = UO_2(CO_3)_2^{2-} + 3\ H_2O \qquad \text{(Eq. 6.3-1)}$$

This reaction is written in terms of HCO_3^-, rather than CO_3^{2-}, because under the pH range expected, the concentration of bicarbonate exceeds that of carbonate.

The standard-state Gibbs free energy of the reaction ($\Delta_r G^0$) is the value needed to calculate its log K using $\Delta_r G^0 = -RT\ln K$. This equals:

$$\Delta_r G^0(UO_2(CO_3)_2^{2-}) = \Delta_f G^0(UO_2(CO_3)_2^{2-}) + 3 \cdot \Delta_f G^0(H_2O) - \Delta_f G^0(UO_3 \cdot 2H_2O) - 2 \cdot \Delta_f G^0(HCO_3^-) \qquad \text{(Eq. 6.3-2)}$$

Because this expression is a simple algebraic sum, the uncertainties of the $\Delta_f G^0$ terms can be combined to give the uncertainty of $\Delta_r G^0(UO_2(CO_3)_2^{2-})$ by the square root of the mean (Bevington 1969 [DIRS 146304], Section 4-2). This procedure gives ±2.703 kJ/mol for $2\sigma\Delta_r G^0(UO_2(CO_3)_2^{2-})$. Dividing this by -RTln(10) (= -5.708 kJ/mol at 298.15K) gives $2\sigma \log K = \pm 0.47$ (*log K Uncertainties_040624.xls* in Appendix I). When this procedure is followed for all dominant aqueous species, the largest uncertainty is for $(UO_2)_2CO_3(OH)_3^-$ at $2\sigma \log K = \pm 0.99$ for pH values above about 6.5 (for $fCO_2 = 10^{-3.0}$ bars as used in the calculation illustrated), where the dominant species are carbonate and hydroxycarbonate complexes. At lower pH values, where fluoride and sulfate complexes and UO_2^{2+} dominate, the largest uncertainties are for the two fluoride complexes, $UO_2F_2(aq)$ and UO_2F^+ at ±0.55 and ±0.48, respectively, and for $UO_2SO_4(aq)$ at ±0.44. The largest $2\sigma \log K$ value of ±0.99 leads to a 1σ standard deviation for the solubility value of ±0.5, which is applied in a normal distribution truncated at ±2σ for all uranium concentrations.

A different approach must be taken to estimate the uncertainty of thorium solubilities because the source of the uncertainty data (Hummel et al. 2002 [DIRS 161904]) gives uncertainties for log K values rather than for $\Delta_f G^0$ values. The NEA compilations (Grenthe et al. 1992 [DIRS 101671]; Silva et al. 1995 [DIRS 102087]; OECD 2001 [DIRS 159027]; Guillaumont et al. 2003 [DIRS 168382]), from which uncertainty data for uranium, americium, plutonium, and neptunium were taken, also give uncertainty data for some, but not all, necessary log K values. Uncertainties based on $\Delta_f G^0$ values were used for these elements unless only uncertainties for log K values were available.

The principal dissolved thorium species accounting for more than 10 percent of the total dissolved thorium ($Th(SO_4)_2(aq)$, ThF_2^{2+}, ThF_3^+, $ThF_4(aq)$, $Th(OH)_3CO_3^-$, $Th(OH)_4(aq)$, and $Th(CO_3)_5^{6-}$) were taken from the Th-speciation diagram (Figure 6.4-13).

As an example of the approach taken for thorium, consider the reaction for the dissolution of the controlling solid, $ThO_2(am)$ (am = amorphous), to one of the principal species, $Th(OH)_4(aq)$:

$$ThO_2(am) + 2\ H_2O = Th(OH)_4(aq) \qquad \text{(Eq. 6.3-3)}$$

The uncertainty of this reaction is not given by Hummel et al. (2002 [DIRS 161904]). However, this reaction can be taken as the sum of two other reactions for which Hummel et al. (2002 [DIRS 161904]) provide uncertainty data. These are:

$$ThO_2(s) + 4\ H^+ = Th^{4+} + 2\ H_2O,\ 2\sigma \log K = \pm 0.8$$

$$Th^{4+} + 4\ H_2O = Th(OH)_4(aq) + 4\ H^+,\ 2\sigma \log K = \pm 0.6 \qquad \text{(Eq. 6.3-4)}$$

These reactions sum to the overall dissolution reaction. Combining their uncertainties using the square root of the mean gives $2\sigma \log K = \pm 1.0$ (*Th Uncertainty.xls* in Appendix I). When this procedure is followed for all dominant aqueous species, the uncertainties in $2\sigma \log K$ for the carbonate complexes are ±1.3 for $Th(OH)_3CO_3^-$ and ±1.4 for $Th(CO_3)_5^{6-}$, which dominate at pH values above about 6. At lower pH values where $Th(SO_4)_2(aq)$, ThF_2^{2+}, ThF_3^+ and $ThF_4(aq)$ dominate, the uncertainties range from $2\sigma \log K$ values of ±0.8 for $Th(SO_4)_2(aq)$ to ±1.3 for ThF_3^+, and $ThF_4(aq)$. These lead to a 1σ standard deviation for Th solubility of ±0.7, which is used in a normal distribution truncated at ±2σ for all thorium concentrations.

$ThO_2(s)$ appears in the first of the two subreactions rather than $ThO_2(am)$, which is the designation of the controlling phase in *Data0.ymp.R2* (DTN: MO0302SPATHDYN.000 [DIRS 161756]) used for the modeling. The terminology of ThO_2 solids is discussed in Section 5.21.2 of *NAGRA/PSI Chemical Thermodynamic Data Base 01/01* (Hummel et al. 2002 [DIRS 161904]). The solid they refer to as $ThO_2(s)$ is also known as $ThO_2(am)$.

The approach taken here is to apply the largest uncertainty associated with any aqueous species representing >10 percent of the total concentration at any pH and fCO_2 to concentrations at all pH and fCO_2 values. This leads to maximum uncertainties because it is likely that other aqueous species with lower uncertainties dominate at different pH and fCO_2 values. While it would be possible in principle to examine the results of the aqueous speciation calculations and derive uncertainty values for each pH and fCO_2, the additional interpretive effort required would be extensive. This was not deemed necessary because the adopted approach led to the highest and, therefore, most conservative uncertainty estimates.

6.3.3.2 Uncertainties in Water Chemistry

The selection of the chemical characteristics of the water used for the solubility calculations is discussed in Section 6.4. The effects of uncertainties on the composition of that water on the modeled solubilities are examined here.

As shown in Section 6.4.2.5.1, aqueous carbonate and hydroxycarbonate complex species are the principal contributors to actinide solubilities at high pH values, while sulfate complexes are the principal contributors at low pH values. Under moderately acid conditions, solubilities are also very sensitive to fluoride because of the formation of fluoride aqueous complex species. Carbonate and hydroxide concentrations depend on pH and fCO_2. The solubilities are tabulated in terms of pH and fCO_2, so the sensitivities to variations in these ligands are considered explicitly. As discussed in Section 6.4.3.5, sulfate concentrations are varied in the modeling to maintain charge balance at lower pH values in order to simulate the occurrence of H_2SO_4 in the in-package environment from the possible oxidation of sulfur during steel degradation. In this way, sulfate variations are also considered explicitly in this report. Variations in fluoride

concentrations are not treated explicitly in this report so their effects must be included as uncertainties in the total actinide concentrations.

Solubilities of the actinides are sensitive to the fluoride contents of the water because of the strength of actinide ion-fluoride solution complexes (Section 6.4.2.5.1). Analyses of the sensitivity of actinide concentrations to solution F^- concentrations were carried out for three cases, which correspond to the three abstractions from *In-Package Chemistry Abstraction* (BSC 2004 [DIRS 167621]): 1) CSNF waste package breached under normal conditions or by seismic activity (CSNF water-influx model), 2) codisposal waste package with alteration by water from condensation only (codisposal vapor-influx model), and 3) codisposal waste package with alteration by seepage water and CSNF waste package breached by igneous activity (codisposal water-influx model). The maximum fluoride concentrations in each environment are given in Table 6.3-3. Except for the first case (1), the F^- contents used for each analysis are the maximum values provided in *In-Package Chemistry Abstraction* (BSC 2004 [DIRS 167621], Table 8-6). For case (1), the modeling supporting the sensitivity analysis was carried out using 10× the J-13 well water F^- content before the results of the abstractions were available. Because 10× the J-13 well water F^- content is slightly higher than the results of the abstractions and, thus, would lead to higher conservative actinide concentrations, the analysis was not rerun with the *In-Package Chemistry Abstraction* (BSC 2004 [DIRS 167621]) values.

Table 6.3-3. Fluoride Concentrations from the In-Package Chemistry Abstraction Report Used in Uncertainty Analyses

Situation	Maximum F^-		Source	F^- Used for Sensitivity Analysis (mg/L)	Multiplication Factor from Base Case
	Mol/kg	mg/l			
Base Case	1.15E-04	2.18	J-13 Well Water (Table 4-2)	2.18	1×
CSNF Water Influx	9.8E-04	18.6	BSC 2004 [DIRS 167621], Table 8-6	21.8	10×
Codisposal (Vapor Influx)	1.1E-02	209.0	BSC 2004 [DIRS 167621], Table 8-6	209	95×
Codisposal (Water Influx)	3.1E-03	58.90	BSC 2004 [DIRS 167621], Table 8-6	58.89	27×

Source: *F_Cons* in *sens runs_a.xls* (Appendix I).

Tables showing the effects of varying fluoride concentrations on the solubilities of Pu, Np, U, Th, and Am are given in Sections 6.5 through 6.9. They show fluoride effect varies with pH. To capture this variation, uncertainties applied to the Pu, Np, U, Th, and Am concentrations to account for uncertainties in the F^- concentrations are expressed as functions of pH. These are given in uncertainty tables for each actinide listed. The values in the uncertainty tables (presented in Sections 6.5 through 6.9) are the differences between solubilities calculated using the F^- values for sensitivity analyses and the base-case solubility values.

The effects of fluoride on the solubility of Pa are given in Section 6.11. For this actinide, since solubilities are based on natural analogues, only the maximum uncertainty associated with fluoride uncertainty is used in the model with no pH dependence (Section 6.11.5).

For Pu, Np, U, Th, and Am the uncertainties due to varying fluoride uncertainties are given as functions of pH. However, it is difficult for the TSPA-LA model to implement uncertainty as a function of fCO_2. Thus, uncertainty associated with fluoride is based on calculations made at a single fCO_2 value ($10^{-3.0}$ bars).

The uncertainties due to fluoride are treated as a right-angled triangular distribution with the minimum (designated "a"), the most probable (designated "b") (those of the base-case), and the maximum concentrations (designated "c") calculated with adjusted fluoride concentration (see individual uncertainty sections for more information). As the name suggests, the probability density function of a triangular distribution has the shape of triangle. A triangular distribution is defined by the three vertices of a triangle (the minimum, a; the most probable, b; and the maximum, c). The area under the triangle equals 1. For the uncertainties due to fluoride, a = b = 0, and c = maximum uncertainty (creating a right triangle). The maximum concentrations in each of the three environments considered are given as functions of pH for Pu, Np, U, Th, and Am and as single values for Pa (tables in Sections 6.5 through 6.9 and Section 6.11).

6.3.3.3 Uncertainties in Temperature

All calculations were made at 25°C, although liquid water can exist at temperatures up to 100°C or more. To estimate the effects of changing temperature on solubilities, calculations were made at 100°C for a range of pH values at a single fCO_2. These results are summarized in Table 6.3-4.

Because differences vary with pH, the maximum and minimum differences for each element are given. In all cases, solubilities at 100°C are lower than those at 25°C because, for each mineral listed in Table 6.3-4, the log K for the dissolution reaction in the thermodynamic database (DTN: MO0302SPATHDYN.000 [DIRS 161756]) is lower at higher temperatures. For example, the log K values for schoepite dissolution at 25°C and 60°C are 4.8443 and 3.9389, respectively. The minimum differences in the logs of the solubilities in Table 6.3-4 range from −0.27 to −2.06, and the maximum differences from −1.77 to −4.88.

Solubilities given in this report are for 25°C. This is a conservative approach because the higher solubilities at lower temperatures allow for maximum dissolved concentrations of radionuclides in solution. For example, as indicated in Figure 6.3-3, the modeled neptunium concentrations (using NpO_2) at 100°C are lower than those for 25°C. The 100°C values may represent a more realistic model for higher temperatures than those for 25°C. TSPA-LA implements only one temperature for solubilities. Therefore, it is necessary to present a model that will include pertinent solubilities for all possible repository temperatures. Due to the retrograde solubilities of actinides, 25°C was chosen as the base-case temperature for modeling.

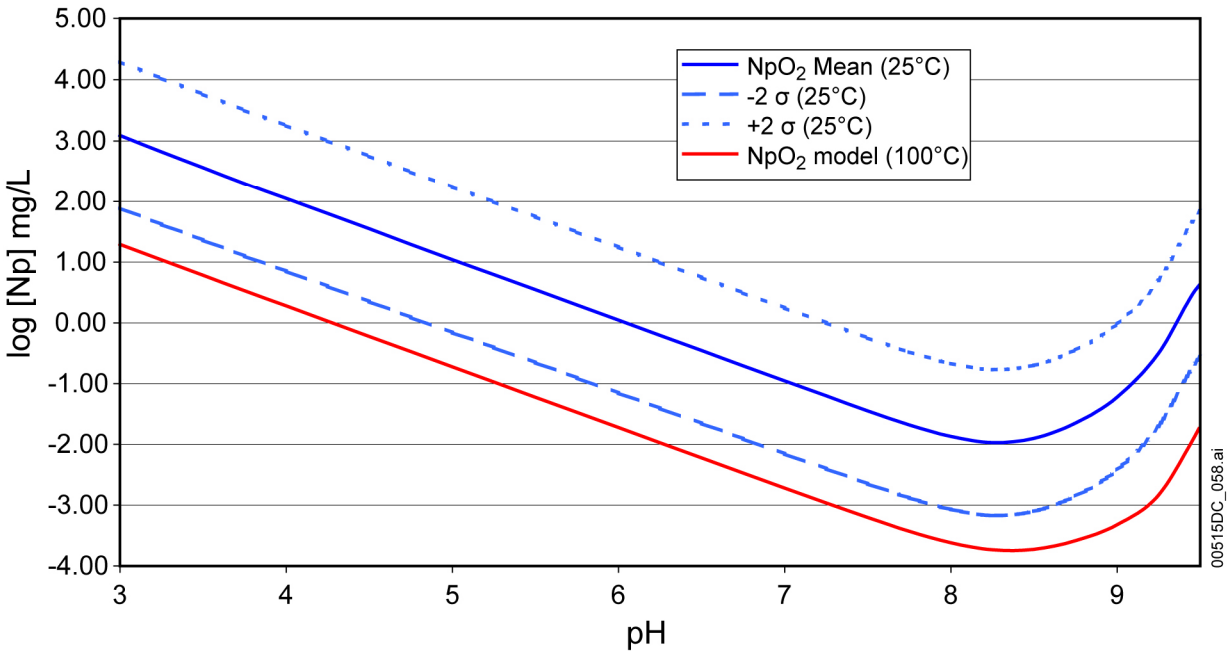

Figure 6.3-3. Comparison of NpO_2 Model at 25°C and 100°C

Table 6.3-4. Differences in Solubility of Solids Modeled at 25°C and 100°C

	Solid	PuO_2	Np_2O_5	NpO_2	Schoepite ($UO_3 \cdot 2H_2O$)	$AmOHCO_3$
Minimum Difference	$\log[C]_{100C} - \log[C]_{25C}$	–0.79	–1.48	–1.76	–0.27	-2.06
Maximum Difference	$\log[C]_{100C} - \log[C]_{25C}$	–3.74	–4.11	–4.88	–1.77	-3.85

Source: Appendix I: *PuO2 Solubility.xls*, *Np2O5 Solubility for Pa.xls*, *NpO2 Solubility for Pa.xls*, *U Solubility.xls*, and *Am Solubility.xls*.

NOTE: Calculations were made at $\log(fCO_2$ bars) = –3.00 for range of pH values. Maximum and minimum differences occur at different pH values.

Because retrograde solubilities are unusual, the results in Table 6.3-4 merit further scrutiny. Inspection of the source files for the table shows that the maximum decrease in solubility at the higher temperature occurs at high pH values. As the speciation diagrams in Sections 6.4 through 6.9 illustrate, the aqueous species that contribute most to actinide solubilities at high pH values are carbonate complexes. The solubility modeling is carried out at a series of fixed values of fCO_2. As temperature increases, the solubility of gases, including CO_2, decreases. Thus, higher temperatures lead to lower dissolved-carbonate concentrations that generate lower concentrations of carbonate complexes leading to lower actinide solubilities.

6.3.3.4 Uncertainties of Activity Coefficients

Electrolyte solutions differ substantially from ideal solutions. Nevertheless, thermodynamic calculations for solutes are based on the equations for ideal solutions with the use of approximate corrections, known as activity coefficients. Activity coefficients are multiplied by

concentrations, specifically molalities, to obtain the activities needed in calculations of solubilities (i.e., γ_i m_i = a_i; where γ_i is the activity coefficient; m_i, the molality (such as the solubility of a solid); and a_i, the activity for the ion, i). The smaller the value of γ for a given activity calculated, for example, from a solubility product, the larger the molality or solubility. Activity coefficients for molecular solutes tend to increase with solution ionic strength ("salting out" effect) while those for ionic solutes tend to decrease with ionic strength ("salting in" effect) (Langmuir 1997 [DIRS 100051], Section 4.4).

An equation generally used for calculating single ion activity coefficients was developed by Hückel (Langmuir 1997 [DIRS 100051], p. 133). It consists of the conventional extended Debye-Hückel equation with a second term linear in ionic strength:

$$\log \gamma_i = \frac{-\mathrm{A} \times z_i^2 \times \sqrt{\mu}}{1 + B \times a_i \times \sqrt{\mu}} + b \times \mu \qquad \text{(Eq. 6.3-5)}$$

where

γ_i = activity coefficient of ion, i

z_i = charge of ion, i

A, B = temperature-dependent properties of the solvent (Langmuir 1997 [DIRS 100051], p. 128)

M = ionic strength = $0.5\sum_j m_j z_j^2$

m_j, z_j = molality and charge of each ion j in the solution

a_i = ion-specific parameter

b = ion-specific or temperature-dependent parameter.

Two variants of this equation are included in widely used aqueous speciation modeling codes. One, referred to as the B-dot equation (Wolery 1992 [DIRS 100836], Chapter 3), is used in version 7.2b and 7.2bLV of EQ3NR and EQ6. In the equation, a_i is the effective diameter or ion-size parameter, values of which, for virtually all solute ions, are available in the literature (Kielland 1937 [DIRS 151237]) and handbooks (Langmuir 1997 [DIRS 100051], Table 4.1), or can be estimated by analogy to ions whose values are listed (Steinborn et al. 2003 [DIRS 161956], Section 9.2.2). The B-dot parameter (b) is a function of temperature only. Values for B-dot, as well as for the solvent parameters A and B, at various temperatures are given in the "miscellaneous parameters" block of *Data0.ymp.R2* (DTN: MO0302SPATHDYN.000 [DIRS 161756]). Values of a_i for each ion included in the database are given in the "B-dot parameters" block.

In the second variant of the Hückel equation, the a_i and b parameters are ion-specific with values based on fits to ion activity data derived from measured mean salt-activity coefficients of electrolyte solutions. In this form, it is known as the WATEQ or Truesdell-Jones equation and is employed in geochemical modeling codes (e.g., PHREEQC) (Nordstrom and Munoz 1986 [DIRS 153965], Section 7.6; Parkhurst and Appelo 1999 [DIRS 159511], p. 11).

The Truesdell-Jones equation reproduces mean salt activity coefficients to ionic strengths of several molal, but because parameters are available only for major ions, its use is limited. Calculations made using the Truesdell-Jones equation are included in the comparison given here. Parameter values used are from Table 7.6 of *Geochemical Thermodynamics* (Nordstrom and Munoz 1986 [DIRS 153965]).

The effects of the formation of ion pairs and other complex solute species are incorporated in the activity coefficient corrections through the ionic strength term. Total, or stoichiometric, ionic strength is calculated using the total concentration of dissolved salts ignoring the formation of solute complexes. The effective, or true, ionic strength is calculated from the free and complexed ions actually present in the solution and is in all cases lower than the stoichiometric ionic strength. This is because the formation of solution complexes removes charged species from the ionic strength calculation and the complex always has a lower charge than its component ions.

All known activity coefficient models have limitations, which introduce increasing uncertainty into the calculations as ionic strength increases. The B-dot equation used in *Data0.ymp.R2* (DTN: MO0302SPATHDYN.000 [DIRS 161756]) and *Data0.yc3.R1* is considered valid up to ionic strengths of 1 molal (Steinborn et al. 2003 [DIRS 161956], p. 60). Accordingly, no uncertainty related to activity coefficients is introduced into the solubility results for solutions of ionic strengths below 1 molal. Some of the solutions modeled in the course of calculating the concentrations given in this report exceeded 1 molal. The concentration results from such solutions were rejected, with one exception: uranium concentrations at high pH and fCO_2 values are associated with ionic strengths to 2.5 molal. As discussed in Section 6.7.5.2, the concentration uncertainty associated with log K (Section 6.3.3.1) was augmented to account for the increased uncertainty in activity coefficients in these solutions.

The remainder of this section develops the additional uncertainty associated with concentrations in solutions of ionic strengths above 1 molal. This is done by comparing ion activity coefficients calculated using the two forms of the Hückel equation with values derived from measurements of solution properties. The conclusions are corroborated by reference to other YMP documents in which activity coefficient values calculated with the B-dot form of the Hückel equation are compared with values calculated with other activity coefficient expressions.

Measured activity coefficients of electrolyte solutions found in handbooks (e.g., Robinson and Stokes 1965 [DIRS 108567]) are not those of individual ions, but mean activity coefficients of all ions comprising the dissolved salt. Mean salt activity coefficients are related to individual ion activity coefficients by the expression:

$$\gamma_{\pm} = \left(\gamma_{+}^{\nu_{+}} \gamma_{-}^{\nu_{-}}\right)^{1/(\nu_{+}+\nu_{-})} \qquad \text{(Eq. 6.3-6)}$$

where

$\gamma_{\pm}$ = mean salt coefficient of the electrolyte
γ_{+}, ν_{+} = activity coefficient and stoichiometric coefficient of the cation
γ_{-}, ν_{-} = activity coefficient and stoichiometric coefficient of the anion.

To extract individual ion activities from mean salt activity coefficient data using this expression the activity coefficient of at least one ion must be found. This is done using the MacInnes convention (Nordstrom and Munoz 1986 [DIRS 153965], Section 7.6) that $\gamma_{K+} = \gamma_{Cl-}$. Thus, from the mean salt activity coefficients of KCl, the activities of the K^+ and Cl^- ion are calculated:

$$\gamma_{KCl} = \left(\gamma_{K^+}\gamma_{Cl^-}\right)^{1/2}$$
$$\gamma_{K^+} = \gamma_{Cl^-} = \gamma_{KCl}$$

With γ_{K+} and γ_{Cl-} available, activities of other ions can be calculated from mean salt data of other electrolytes. For example:

$$\gamma_{Na^+} = \frac{\gamma^2_{NaCl}}{\gamma_{Cl^-}}$$
$$\gamma_{Ca^{2+}} = \frac{\gamma^3_{CaCl_2}}{\gamma^2_{Cl^-}}$$

γ_{SO4}^{2-} could be calculated from handbook data for K_2SO_4 or Na_2SO_4 solutions except for the formation of KSO_4^- and $NaSO_4^-$ ion pairs. To minimize the disturbing effects of SO_4^{2-} ion pairs, γ_{SO4}^{2-} is better calculated using:

$$\gamma_{Cs^+} = \frac{\gamma^2_{CsCl}}{\gamma_{Cl^-}}$$
$$\gamma_{SO_4^{2-}} = \frac{\gamma^3_{Cs_2SO_4}}{\gamma^2_{Cs^+}}$$

Activity coefficients for the cations Na^+ and Ca^{2+} and the anions Cl^- and SO_4^{2-} were calculated up to ionic strengths of 3 molal using the B-dot equation of version 7.2b of EQ3NR and EQ6 and compared with values calculated from handbook mean salt data and values calculated using the Truesdell-Jones equation. The calculations, supporting data, and results are in *gamma comp calcs.xls* in Appendix I. Contents of the individual worksheets within the spreadsheet are as follows. The values for the B-dot parameters used in the calculations were taken from *Data0.ymp.R2* (DTN: MO0302SPATHDYN.000 [DIRS 161756]) and are given in the workbook *D-H parameters*. The values for the parameters of the Truesdell-Jones equation are also given in *D-H parameters*. The calculations of individual ion activities from handbook mean salt data (Robinson and Stokes 1965 [DIRS 108567], Appendix 8.10) are given in *1-1 Salts data & calc* and *1-2 Salts data & calc*.

The results are summarized in Figures 6.3-3 and 6.3-4 and Table 6.3-5. Mean salt values are available only at the higher ionic strengths, but the Truesdell-Jones values, which are based on fits to mean salt data, overlap the mean salt values and extend to lower ionic strengths.

Figure 6.3-4 compares the results for the anions Cl^- and SO_4^{2-}. For Cl^-, the B-dot values are indistinguishable from the others up to an ionic strength of 1 molal. They begin to diverge at

higher ionic strengths with the B-dot value about 0.04 units higher than the mean salt value at 3 molal. For SO_4^{2-}, the B-dot values are within 0.03 units of the mean salt and Truesdell-Jones values to an ionic strength of about 2 molal. At 3 molal, the B-dot values are about 0.1 units less negative than the mean salt value.

Figure 6.3-5 compares the results for the cations Na^+ and Ca^{2+}. For Na^+, the B-dot values are indistinguishable from the mean salt-based Truesdell-Jones values to an ionic strength of about 0.2 molal. They then diverge and are 0.03 units more negative at 1 molal and 0.1 units more negative at 3 molal. For Ca^{2+}, the B-dot values are within 0.01 units to an ionic strength of about 0.6 molal. They diverge at higher ionic strengths to 0.05 units at 1 molal and 0.3 units at 3 molal.

Uncertainties of activity coefficients are discussed in two other YMP documents:

- Appendix D of *Degraded Mode Criticality Analysis of Immobilized Plutonium Waste Forms in a Geologic Repository* (CRWMS M&O 1997 [DIRS 100222]) provides examples comparing activity coefficients derived from experimental measurements with those calculated by EQ3/6 using the B-dot form of the Hückel equation. These comparisons are based on mean salt rather than single ion activity coefficients. Because the latter are used in the modeling described here, these comparisons are not considered further.

- Section 5.1.2 of *In-Drift Accumulation of Fissile Material from Waste Packages Containing Plutonium Disposition Waste Forms* (CRWMS M&O 2000 [DIRS 135790]) includes computations made using the B-dot equation and compares them with those obtained from the Specific Ion Interaction Theory (SIT) (Grenthe et al. 1992 [DIRS 101671], Appendix B). For tetravalent ions, such as Th^{4+} and Pu^{4+}, at ionic strength 1.0, the SIT value for γ is about twice the "B-dot" value. The difference of a factor of two in γ at 1-molal ionic strength quoted for these ions corresponds to a difference of 0.3 in log γ. Considering the increasing deviations with ion charge, this is consistent with the difference of 0.3 in log γ for Ca^{2+} at an ionic strength of 3 molal.

This factor of two (0.3 in log units) between the B-dot and SIT values would translate to a doubling of the solubility as calculated using the "B-dot" equation as compared to using the SIT approach, if the dominant solution species were the Th^{4+}, Pu^{4+}, or some other tetravalent ion, such as $UO_2(CO_3)_3^{4-}$. This would occur only at very low pH for $Th^{4+}$and Pu^{4+} or very high pH for $UO_2(CO_3)_3^{4-}$. However, examination of the outputs of the EQ3NR solubility calculations shows that such high charges for the most important dissolved species seldom occur. Specifically, this is found only for plutonium and neptunium, in the form of the $PuO_2(CO_3)_3^{4-}$ and $NpO_2(CO_3)_3^{4-}$, respectively, above a pH of about 8. The corresponding species for uranium also is reported in the output for some neutral-to-high pH calculations, but only as a minor species. Because the use of the "B-dot" equation, as compared to the SIT or similar approaches, results in higher solubilities, it is conservative, and may be used at sufficiently small concentrations without incorporating its uncertainty into the overall solubility uncertainty.

No uncertainties based on ionic strength calculations are presently included in the results of EQ3NR and EQ6 modeling at ionic strengths up to 1 molal. As shown in Table 6.3-5, the

uncertainties in log γ values at this ionic strength are no more than 0.05 for divalent ions, although other calculations suggest they could be up to 0.3 for more highly charged ions.

Table 6.3-5 shows in addition that uncertainties in log γ values approach ±0.3 for divalent ions at an ionic strength of 3. More highly charged ions would presumably have larger differences, but because such ions occur only at extreme pH values, they can be disregarded.

As mentioned previously, the database used in EQ3/6 calculations is qualified up to an ionic strength of 1 molal. In solutions with ionic strengths from 1 to 3, the uncertainty in the solubility should be increased. This can be done simply by increasing the uncertainty term applied to the solubility values to account for the uncertainty in the log K values (Section 6.3.3.1). Because uncertainties in log K values and uncertainties due to high ionic strengths have different causes, the two uncertainties should be combined by the square root of the mean by the following equation:

$$((\text{log K uncertainty})^2 + \pm 0.3^2)^{1/2} \qquad \text{(Eq. 6.3-7)}$$

For uranium, for example, the log K uncertainty is ±0.5 (Section 6.3.3.1). In solutions of ionic strengths from 1 molal to 3 molal, this value should be increased to $(\pm 0.5^2 + \pm 0.3^2)^{1/2} = \pm 0.6$.

Table 6.3-5. Comparison of Ion Activity Coefficients Based on Mean Salt Data and Calculated from the B-dot Equation

Ion	Ionic Strength, μ (molal)	Log γ			Difference in Gamma
		B-dot	Mean Salt	Difference	
Cl^-	1.0	–0.216	–0.219	0.003	–1%
	2.0	–0.220	–0.241	0.021	–5%
	3.0	–0.204	–0.245	0.041	–10%
SO_4^{2-}	1.0	–0.843	–0.806	–0.037	8%
	2.0	–0.930	–0.967	0.037	–9%
	3.0	–0.958	–1.070	0.113	–30%
Na^+	1.0	–0.180	–0.146	–0.034	8%
	2.0	–0.171	–0.108	–0.063	13%
	3.0	–0.147	–0.048	–0.100	20%
Ca^{2+}	1.0	–0.647	–0.595	–0.052	11%
	2.0	–0.681	–0.535	–0.146	29%
	3.0	–0.679	–0.413	–0.266	46%

Source: *gamma comp calcs.xls*.

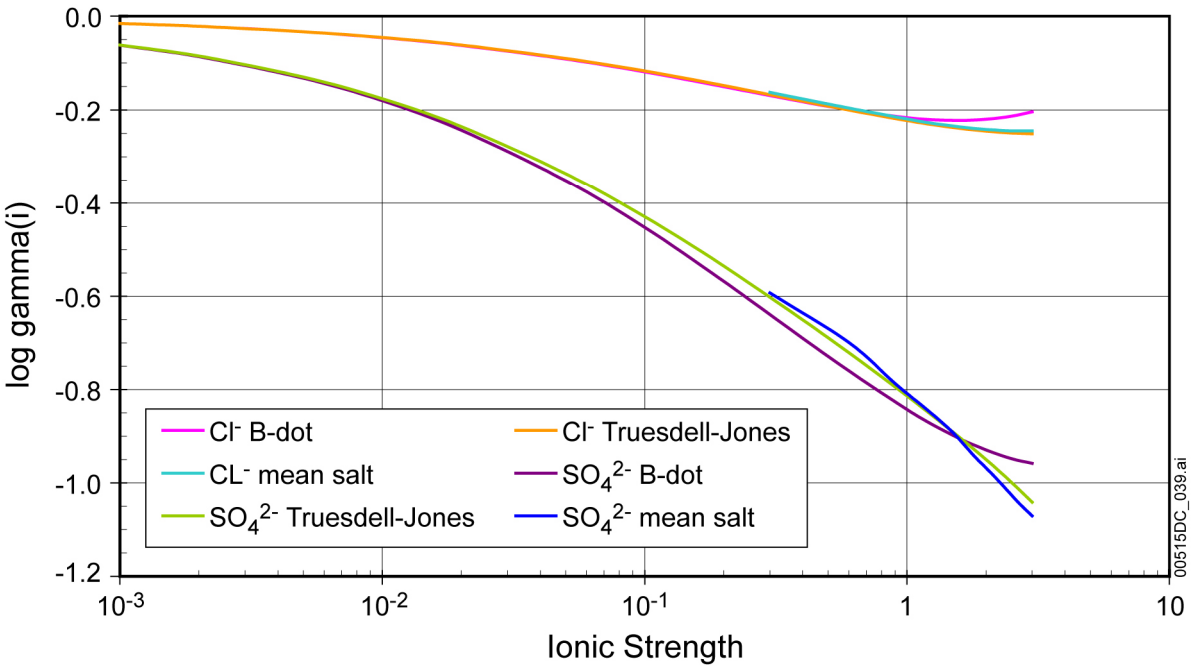

Source: *gamma comp calcs.xls*.

Figure 6.3-4. Comparison of Activity Coefficients of Anions Calculated from Mean Salt Data and the B-dot and Truesdell-Jones Equations

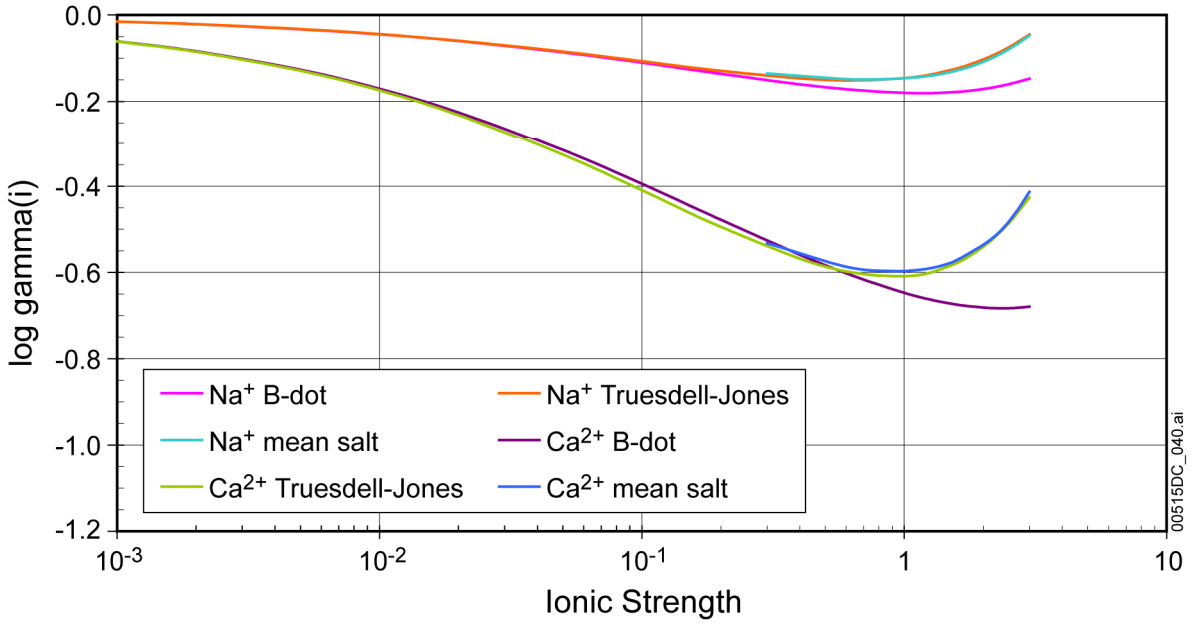

Source: *gamma comp calcs.xls*.

Figure 6.3-5. Comparison of Activity Coefficients of Cations Calculated from Mean Salt Data and the B-dot and Truesdell-Jones Equations

6.4 CHEMICAL CONDITIONS FOR SOLUBILITY CALCULATIONS

The solubility of an element depends on the nature of the solubility-controlling phase and the physical and chemical properties of the solution and its environment. In theory, the solubility of a phase can be calculated for a given solution. However, the interactions among solute species are too complicated for their modeling to be included directly in TSPA-LA. Simplifying solubility calculations by focusing on the most relevant controlling factors allows a feasible, yet realistic model to be included in TSPA-LA. To achieve the most representative simplification, the chemical conditions must be ranked by their importance. The simplification process consists of three parts: 1) simplifications based on knowledge of actinide properties and behavior, 2) simplifications to the site-specific water composition information, and 3) how these simplifications can be incorporated into the model.

6.4.1. Actinide Properties

The chemical and physical conditions most relevant to determining the solubilities of actinide elements are oxidation potential, pH, temperature, and concentrations of ligands that form strong solution complexes (including ion pairs) with dissolved actinide species.

In general, the oxidation potential has the strongest single effect on the solubility of all actinides except thorium and americium, which are relatively redox insensitive. In the case of Yucca Mountain, however, the oxidation state of uranium does not change over a range of oxidizing conditions. Only plutonium and neptunium (and Pa, by analogue with Np) are sensitive to the specific value chosen for the oxidation potential. Plutonium is discussed and illustrated in detail in Sections 6.5.3 and 6.5.4.

pH affects solubility in two ways. Typically, in acidic solutions, hydrogen ions react with solids to release cations to solution (e.g., by combining with oxide in the solid to form water). In basic (high pH) solutions OH^- may act as a ligand that forms complexes with the cations in the solid, thereby increasing the solubility. Temperature changes may raise or lower solubilities depending on the element and the specific conditions being considered. As discussed in Sections 6.3.3.3 and 6.4.2.2, only solubilities at 25°C are provided in this report as solubilities of actinides decrease with increasing temperature.

For the most common ligands in the environment, the trend in strengths of complexation is (Silva and Nitsche 1995 [DIRS 112092]):

$$OH^-, CO_3^{2-} \quad > F^-, HPO_4^{2-}, SO_4^{2-} \quad > Cl^-, NO_3^-$$

(Primary) (Secondary) (Tertiary)

Primary Ligands: Actinide solubilities increase with decreasing pH. Because of the strength of OH– complexes, solubilities also increase with pH values under alkaline conditions. The concentration of CO_3^{2-} increases with fCO_2 and pH, which also increases actinide solubility because of the strength of CO_3^{2-} complexes.

Secondary Ligands: The ligands F^-, HPO_4^{2-}, and SO_4^{2-} could affect actinide solubilities if present in high enough concentrations. The effects of these ligands are considered in Sections 6.4.2.5.1 and 6.4.3.6.

Tertiary Ligands and Cations: Cl^- and NO_3^- are weakly complexing ligands and do not occur in high enough concentrations to be considered in the modeling. Generally speaking, the effect of cation concentrations on actinide solubility is weak because they do not form complexes with actinides. They influence actinide solubility through their effects on ionic strengths and as ligands competing with actinides for complex-forming anions. Because the most common cations in the repository environments (Na^+, K^+, Ca^{2+}, and Mg^{2+}) form complexes with carbonate, bicarbonate, or sulfate accounting for only a few percent of their total dissolved concentrations, only their ionic strength effects are important.

Based on this discussion, fO_2, pH, fCO_2, temperature, and concentration of ligands in water are considered in this report to calculate the actinide solubilities.

The impacts of elements other than those listed in Table 4-2, or considered specifically in Sections 6.5 through 6.18, relate either to complexes that these ions may form with radionuclides, their effect on pH, or their effect on ionic strength. Other elements expected to be present in potentially significant amounts within the waste package or the invert are lithium, boron, aluminum, titanium, chromium, manganese, iron, nickel, zirconium, hafnium, and possibly vanadium, cobalt, niobium, molybdenum, and tungsten. None of these is shown to form significant complexes with any of the radionuclides considered in this report, as shown for the actinides by examination of Table III.1 in *Chemical Thermodynamics of Uranium* (Grenthe et al. 1992 [DIRS 101671]), Table III.1 in *Chemical Thermodynamics of Americium* (Silva et al. 1995 [DIRS 102087]), and Tables 3.1 and 4.1 in *Chemical Thermodynamics of Neptunium and Plutonium* (OECD 2001 [DIRS 159027]). Therefore, they are not included in model calculations in this report. Other ligands not considered in this report are organic complexes produced by microbial activity. In *Waste-Form Features, Events, and Processes* (BSC 2004 [DIRS 170020], Section 6.2.25), organic complexation is screened out based on the argument that microbial populations are not sufficient to generate significant concentrations of radionuclide-chelating organics.

The previous discussion considers the relative importance of various chemical conditions to actinide solubility. In order to choose the right variables to be accounted for in solubility evaluations, site-specific information, such as the levels and ranges of common cations and anions, must also be considered.

6.4.2 Site-Specific Chemical Conditions

The chemical conditions controlling dissolved concentrations may vary widely from place to place and at different periods of repository evolution. Thus, the solubility calculations have been made over a range of conditions that are expected to include the actual conditions. This section discusses how the countless possibilities are simplified, based on site-specific characteristics.

This study considers two waste package types consistent with TSPA-LA models. One contains commercial spent nuclear fuel (CSNF) and the other, called codisposal spent nuclear fuel packages (CDSP), contains defense spent nuclear fuel and high-level radioactive waste glass.

6.4.2.1 Oxidation Potential

The repository is designed so the waste is under atmospheric conditions except in isolated, local situations. Thus, oxidizing conditions are assumed (Section 5.1), and all solubilities are calculated with a theoretical fO_2 of 0.2 bars (the atmospheric value). The solubilities of all elements considered here except plutonium and neptunium are, within limits, insensitive to the oxidation potential. The details of the selection of the oxidation potential used in modeling plutonium and neptunium are discussed in Sections 6.5 and 6.6.

6.4.2.2 Temperature

Due to decay heat from the waste, the temperature within waste packages is increased from the ambient temperature. Immediately after the emplacement of waste packages, the temperature can rise to nearly 200°C. The temperature in the repository relevant to this model is between 25°C and 100°C, since any temperature above boiling is not relevant for solubility considerations because liquid water will not exist in the waste package. Only solubilities at 25°C are given as solubilities decrease at higher temperatures (Section 6.3.3.3). As discussed in Section 6.3.3.3, solubilities of actinides decrease with increasing temperature, so the use of 25°C solubilities is conservative.

6.4.2.3 pH

According to *In-Package Chemistry* (BSC 2004 [DIRS 167621], Table 8-2), the pH value range for fluids reacting with CSNF is 4.5 to 8.1, while the range for fluids reacting with codisposal materials is from 4.5 to 8. The physical and chemical environment model (BSC 2004 [DIRS 169860]) documents the response surface for pH values in the invert ranges from 3.5 to 10.5. *Dike/Drift Interactions* (BSC 2004 [DIRS 170028]) reports pH values ranging from 8.1 to 9.9 for fluids reacting with basalt.

To cover the full range of conditions, the target pH for the modeling was set to a range of 3 to 11. As discussed below, for some elements, the controlling phases are not stable over the entire pH range, or the ionic strengths of the resulting solutions are beyond the limit for which the EQ3NR program and supporting database are applicable. In these cases, results are given for a more limited range of pH values. For example, the sensitivity runs for plutonium solubility presented in Section 6.4.2.5.1 cover the pH range of 3 to 9.75. The higher pH value range, from 9.75 to 11, is not covered because PuO_2(hyd,aged) is not stable (does not form) under those conditions.

6.4.2.4 CO_2 Fugacity

The atmospheric value of CO_2 partial pressure is $10^{-3.5}$ bars. Section 6.7.2.2 of *Engineered Barrier System: Physical and Chemical Environment Model* (BSC 2004 [DIRS 169860], Section 6.7.2.2) gives the range of fCO_2 as 1.75E-02 bars (maximum) to 2.29E-05 bars (minimum). This document considers a broader range of $10^{-5.0}$ bars to $10^{-1.5}$ bars for the

plutonium-, neptunium-, uranium-, thorium-, americium-, and protactinium-solubility models to cover its likely range.

6.4.2.5 Water Composition

Table 4-2 gives the composition of the base-case water used in the solubility calculations. A water of this composition has been used as the reference water composition for the Yucca Mountain site for many years. A detailed rationale for using water of this composition as a reference water for the repository has been thoroughly investigated (Harrar et al. 1990 [DIRS 100814]).

The compositions of 25 different pore waters collected from 15 ECRB-SYS-SERIES boreholes of the Yucca Mountain site (USW SD-9 and USW NRG-7/7A) were reported in DTN: GS020408312272.003 [DIRS 160899]. For the nine components (Na, K, Ca, Mg, SiO_2(aq), Cl, F, NO_3, and SO_4) listed in Table 4-2, these pore waters are similar to the composition of the base-case water. The ratios of the average pore water values to the base-case values of those nine components range from 0.83 (for SiO_2(aq)) to 8.51 (for Ca), and the ratios of the maximum values of those nine components to the base-case values range from 1.07 to 18.46 (*Pore Water.xls* in Appendix I). As the sensitivity analysis described below covers the range up to 1,000× the base-case values for those nine components, the results and conclusions reached in this section are considered applicable to the pore waters that might become infiltrating waters.

6.4.2.5.1 Sensitivity Analysis

Two approaches are used to assess the effects of varying ligand concentrations on actinide solubilities. The first is a series of sensitivity calculations conducted over a range of pH values at a fixed fCO_2 ($10^{-3.0}$ bars). This analysis examines the solubility of plutonium calculated using the base-case adjusted-Eh model (Section 6.5.3) with PuO_2(hyd,aged) as the controlling solid. Pu was chosen rather than another actinide for the sensitivity studies because (1) Pu is one of the most important actinides, (2) it simplifies the process, as only one solid controls the Pu solubility over the entire pH range, unlike U and Np, which have a change in the controlling mineral at higher pH values, and (3) the results for Pu would be expected to represent the results for the group of actinides as a whole, as all actinides have similar chemical properties.

Initial calculations are run with the base-case J-13 water composition given in Table 4-2. Additional sets are run with concentrations of all constituents increased up to 100 times their original values (1× (base case), 10×, and 100×), with the results shown in Figure 6.4-1. Then, separate sets of runs are conducted that varied selected solutes individually at 10×, 100×, and 1,000× the base-case concentration. These files are located in Appendix I in *Sens Eq3 files.zip*. The results of these calculations are shown in Figures 6.4-2 through 6.4-11. All plotted results represent solutions with an ionic strength less than one. The Na sensitivity at 1,000× was not plotted because the ionic strength was greater than one. See Section 6.3.3.4 for a discussion of ionic strength and activity coefficient calculations.

The objective of the sensitivity calculations is to analyze the effects of a single factor on solubility. Often, it is not possible to isolate the effects of one factor, because when that factor is changed, it causes something else to change. For example, as the specified pH is varied, anions

or cations are mathematically added to the solution for charge balance. The effect of adding these ions is minimized by selecting the most innocuous ions for the charge-balance feature in EQ3NR. More acidic solutions are balanced by adding Cl^-, while more basic solutions by adding Cs^+. These reactants are chosen because actinide chloride and cesium species are not likely to form in large quantities under any pH condition, as discussed later in this section. For the specific Cl^- sensitivities (Figure 6.4-8) the anion Br is used so as not to interfere with the actual subject of the sensitivity. All of the plutonium solubility plots (Figures 6.4-1 through 6.4-10) have similar shapes. Solubilities are high at the low and high pH values and decrease to minimum values at pH values around 8.

The sensitivity analyses show that increases in both F^- and SO_4^{2-} concentrations lead to higher solubilities under neutral and moderately acid conditions (Figures 6.4-2 and 6.4-3). The effect of F^- is treated explicitly as discussed in Section 6.4.3.6. SO_4^{2-} concentrations are not considered to be uncertain, as also discussed in Section 6.4.3.6.

The concentrations of the four cations (Na^+, K^+, Ca^{2+}, Mg^{2+}, Figures 6.4-4 through 6.4-7) affect plutonium solubility very little at low to circum-neutral pH values. Around pH 9, the 1,000× levels, especially of Ca^{2+} and Mg^{2+}, increase the solubilities by more than a factor of ten. However, Ca^{2+} and Mg^{2+} concentrations at these levels are physically unreasonable because of the low solubility of calcium-carbonate and magnesium-carbonate minerals (e.g., calcite and dolomite) at such high pH values. Solubility controls on Ca^{2+} and Mg^{2+} concentrations by such minerals are not considered in the sensitivity analysis modeling.

The concentrations of Cl^-, NO_3^-, and SiO_2(aq) show little effect on Pu solubility as seen in Figures 6.4-8 through 6.4-10, although at the 1,000× level, SiO_2(aq) appears to increase the solubility by more than a factor of ten around pH 9. SiO_2(aq) concentrations at these high levels are physically unreasonable because of the low solubility of SiO_2 minerals. Solubility controls on SiO_2(aq) concentrations are not considered in the sensitivity analysis modeling.

In some of the solutions, once a large quantity of an element is added, the solution becomes supersaturated with a mineral containing that element. For example, in the case of high F^- concentrations, the EQ3NR output file indicates that a solution at low pH is supersaturated with respect to fluorite (CaF_2) and sellaite (MgF_2). These minerals are not allowed to precipitate because the objective is to examine the effects of increased F^- on solubility. Section 6.4.3.7 further discusses supersaturation of minerals.

The effects of changing phosphate concentrations are examined using a different procedure. Because there are relatively few data available for plutonium–phosphate solids and aqueous species, the sensitivity analysis is performed using uranium, for which there is much more data. The uranium solubilities in this report are based on schoepite ($UO_3 \cdot 2H_2O$), Na-boltwoodite ($NaUO_2SiO_3OH \cdot 1.5H_2O$), and $Na_4UO_2(CO_3)_3$. At low-to-moderate pH values, when schoepite is the uranium-controlling solid, the uranium-phosphate minerals, $(UO_2)_3(PO_4)_2 \cdot 4H_2O$ and $(UO_2)_3(PO_4)_2 \cdot 6H_2O$, are also likely to form, as evidenced by the EQ3 solubility calculations that indicate supersaturation of these phosphate minerals. If the phosphate minerals form along with the formation of schoepite, then the phosphate minerals would control the phosphate level. However, this mineral is not allowed to precipitate since the objective is to examine the effects of increased phosphate on solubility.

A sensitivity exercise is performed to examine whether the dissolved uranium concentration in the base-case solution would increase if the phosphate concentrations are controlled by $(UO_2)_3(PO_4)_2 \cdot 4H_2O$. As discussed in Section 6.4.3.6, the phosphate concentration of the base-case water is chosen as 0.1 mg/L. This value is based on the phosphate analyses of the water chosen as the reference water (Table 4-2), which vary from less than 0.01 mg/L to more than 0.1 mg/L (Harrar et al. 1990 [DIRS 100814]). The base-case value is plotted as the horizontal line in Figure 6.4-11.

In the sensitivity cases, the uranium concentration is fixed by schoepite saturation and the total phosphate concentration by saturation with $(UO_2)_3(PO_4)_2 \cdot 4H_2O$. The cases are run for a range of pH values at a fixed fCO_2 of $10^{-3.5}$ bars. The line on the bottom in Figure 6.4-11 shows the phosphate concentration in equilibrium with $(UO_2)(PO_4)_2 \cdot 4H_2O$ (ranging from 10^{-3} to 1 mg/L). A comparison of the two phosphate concentrations shows that concentrations controlled by $(UO_2)_3(PO_4)_2 \cdot 4H_2O$ are below the base-case water concentration for pH values less than about 7.5 and above it at higher pH values. As the figure shows, the uranium concentrations are virtually identical whether modeled using the base-case water phosphate concentration (dotted line), or with phosphate concentrations controlled by $(UO_2)_3(PO_4)_2 \cdot 4H_2O$ saturation (solid line). This also means that should phosphate be added to the system from the degradation of waste glass (e.g., the dissolved phosphate), solution concentration does not rise because it is fixed by the precipitation of a uranium-phosphate solid.

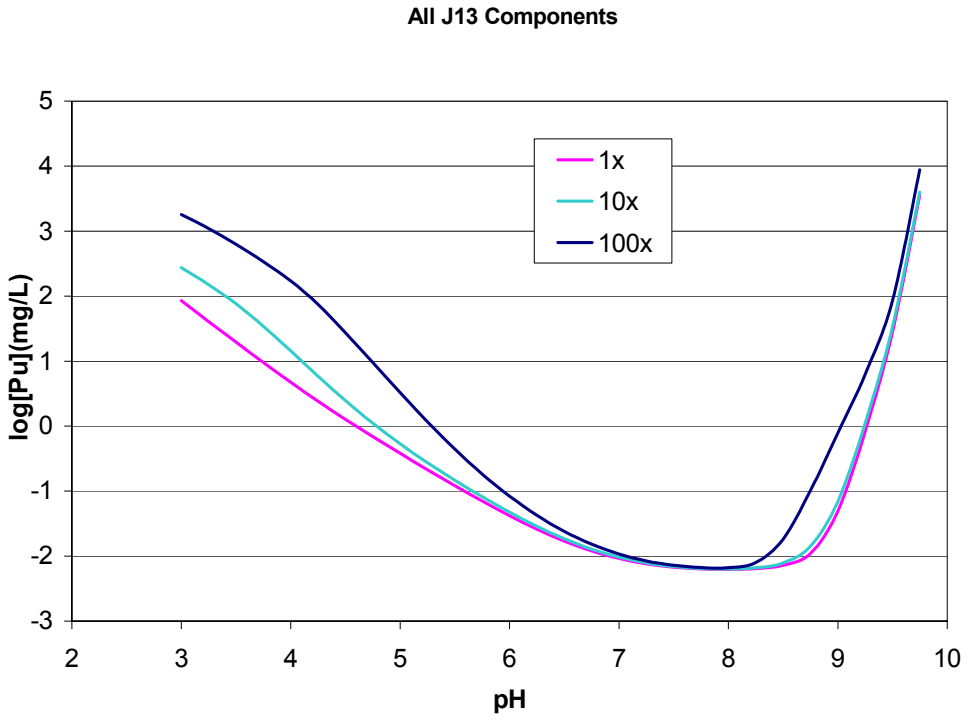

Source: *Sensitivies.xls* (Appendix I).

Figure 6.4-1. Sensitivity to Variation in the Total Concentration of the Base-Case Water

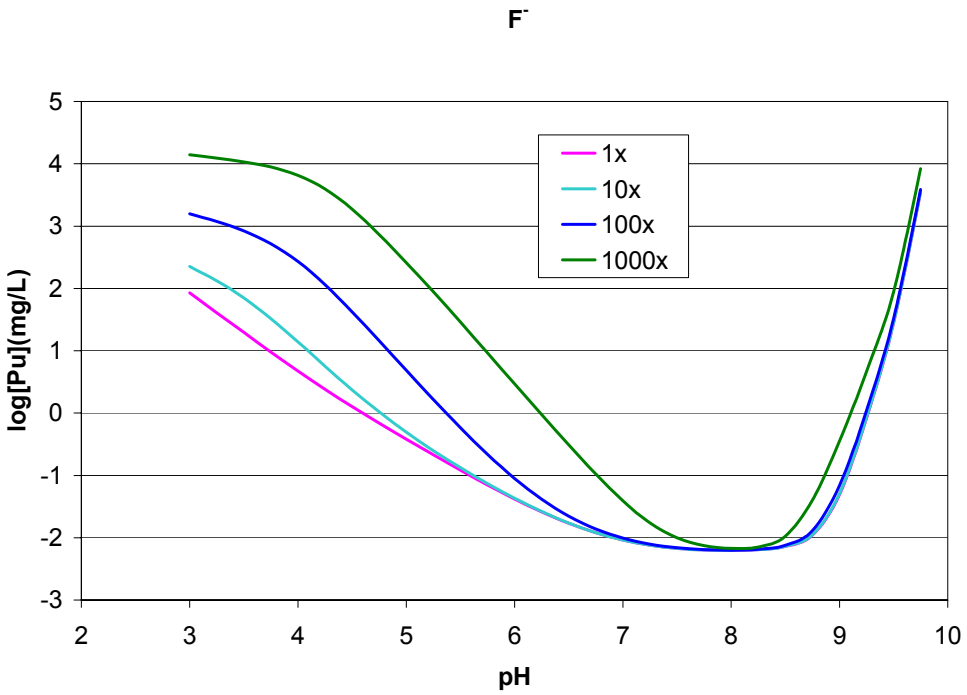

Source: *Sensitivies.xls* (Appendix I).

Figure 6.4-2. F^- Sensitivity

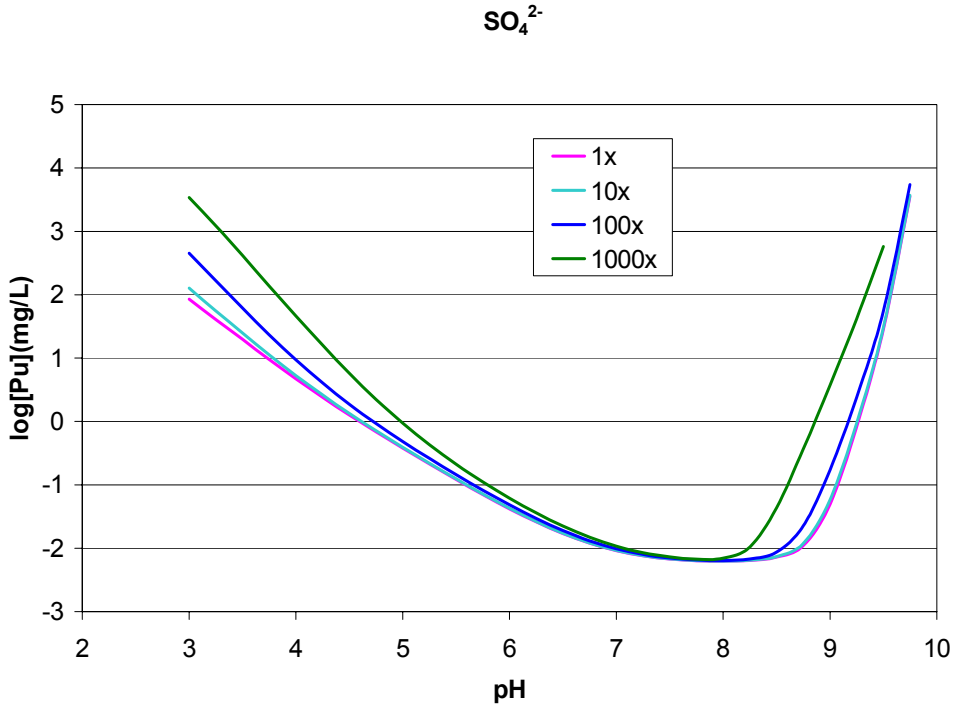

Source: *Sensitivies.xls* (Appendix I).

Figure 6.4-3. SO_4^{2-} Sensitivity

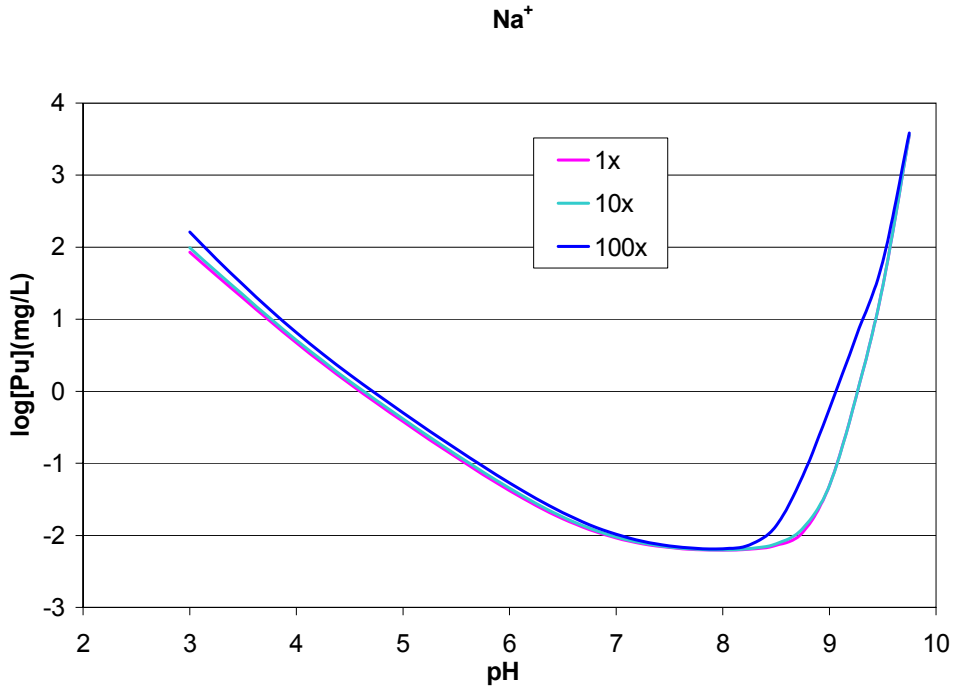

Source: *Sensitivies.xls* (Appendix I).

Figure 6.4-4. Na^+ Sensitivity

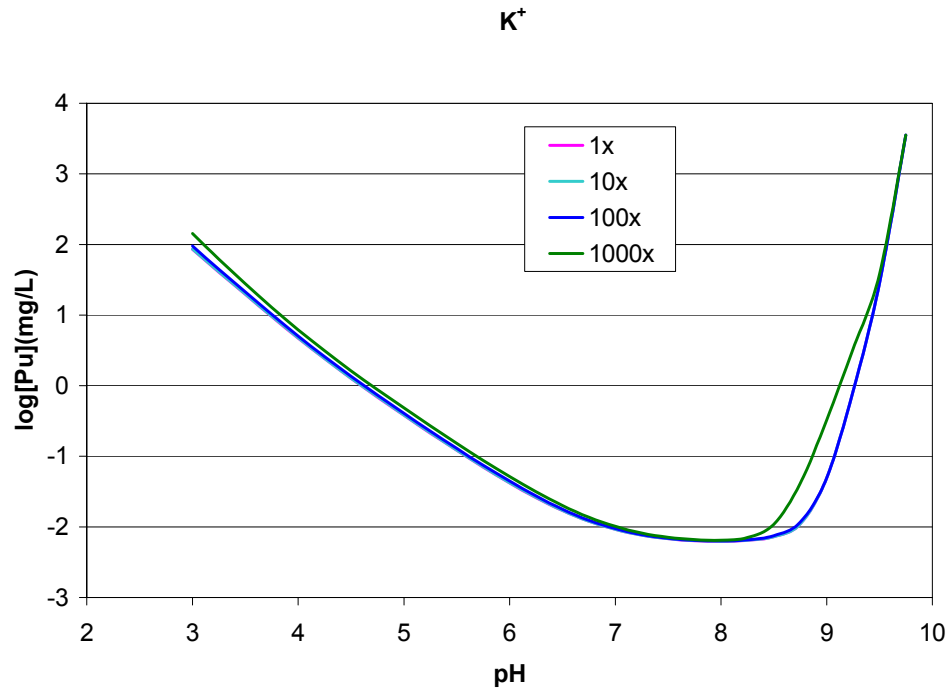

Source: *Sensitivies.xls* (Appendix I).

Figure 6.4-5. K^+ Sensitivity

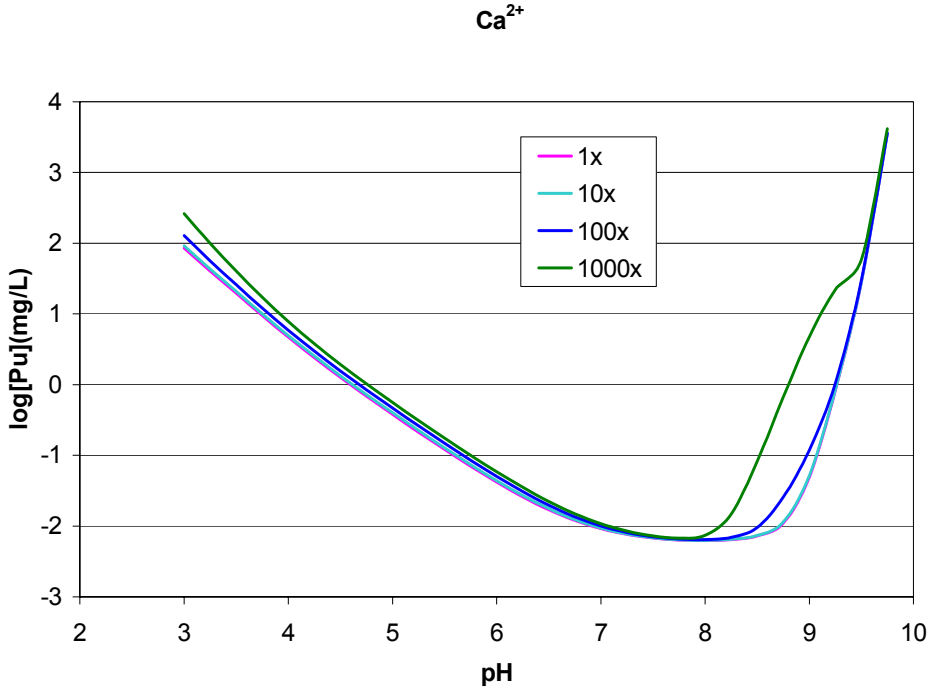

Source: *Sensitivies.xls* (Appendix I).

Figure 6.4-6. Ca^{2+} Sensitivity

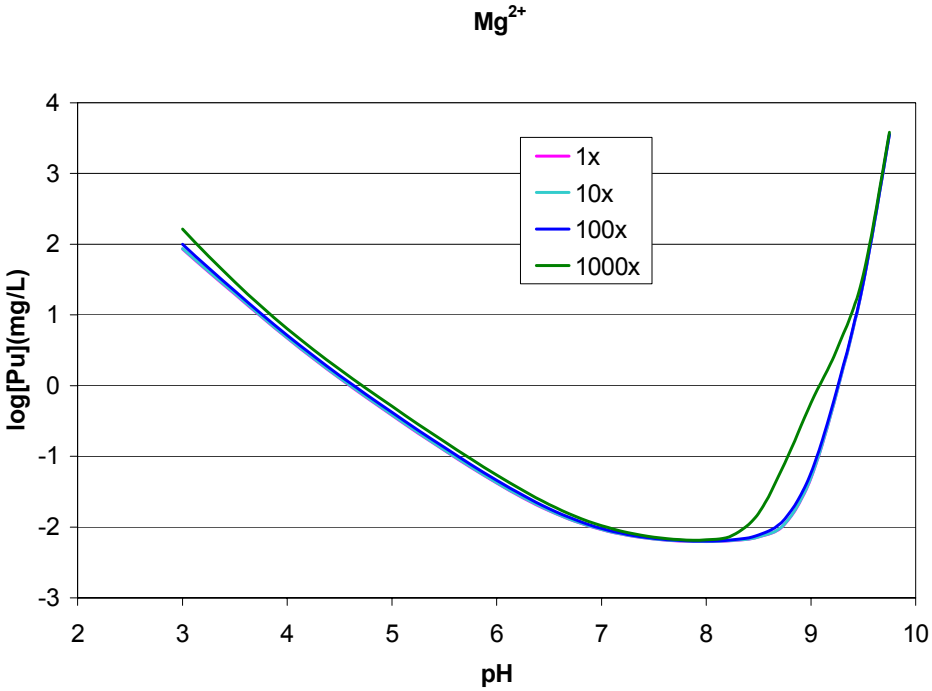

Source: *Sensitivies.xls* (Appendix I).

Figure 6.4-7. Mg^{2+} Sensitivity

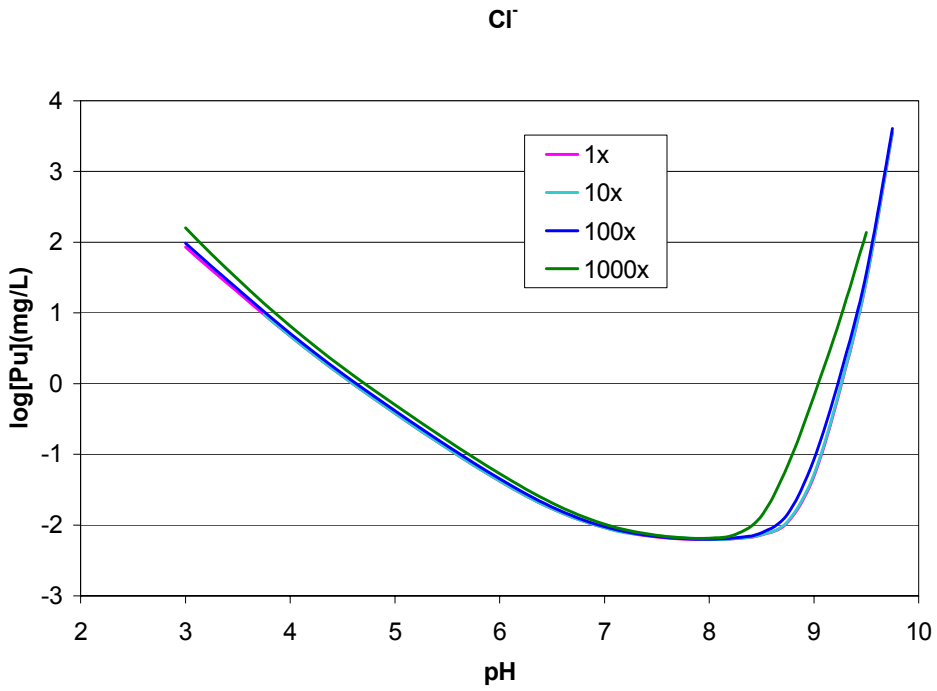

Source: *Sensitivies.xls* (Appendix I).

Figure 6.4-8. Cl^- Sensitivity

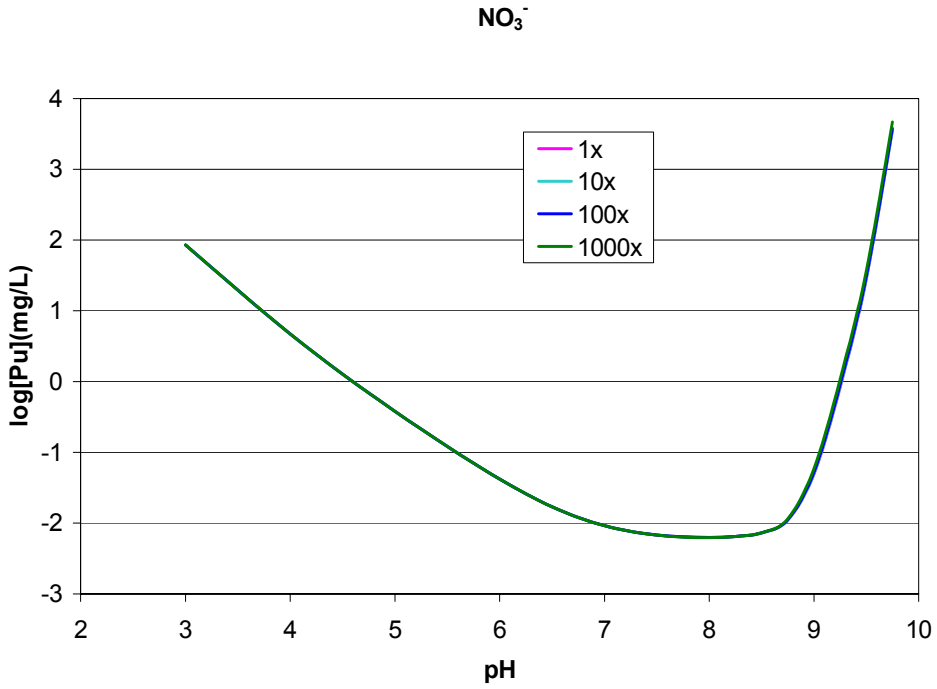

Source: *Sensitivies.xls* (Appendix I).

Figure 6.4-9. NO_3^- Sensitivity

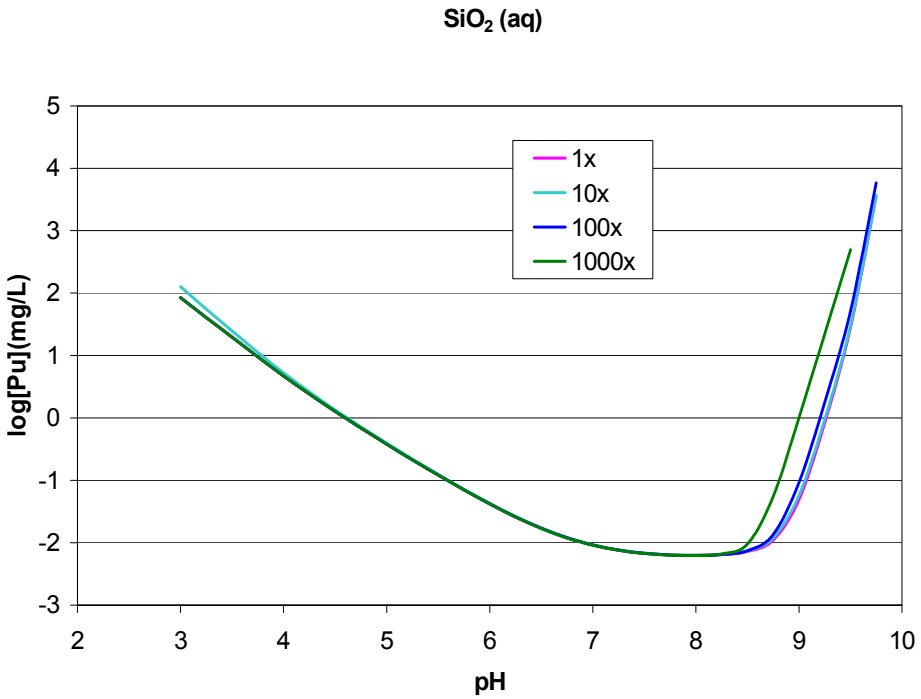

Source: *Sensitivies.xls* (Appendix I).

Figure 6.4-10. SiO_2(aq) Sensitivity

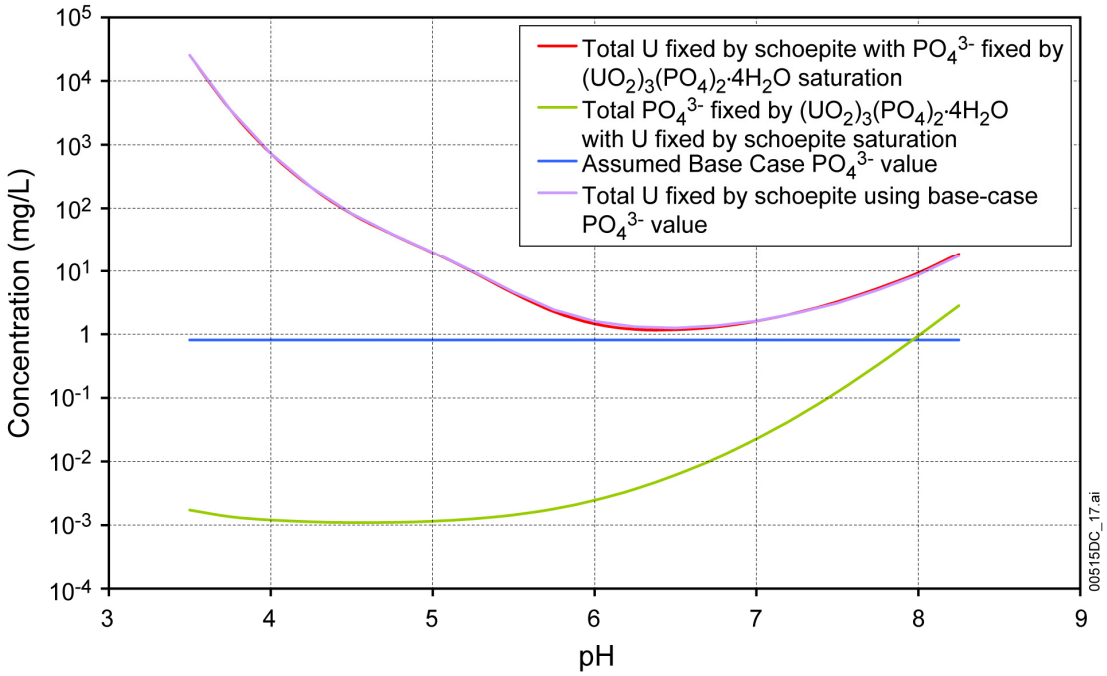

Source: *PO4sensitivity.xls* (Appendix I).

Figure 6.4-11. Effect of $(UO_2)_3(PO_4)_2 \cdot 4H_2O$ Saturation on Uranium Solubility

The second approach to sensitivity analysis examines the concentrations of the various aqueous complexes and species that compose the total solubility of each of the actinides. The solubilities are most sensitive to varying concentrations of those ligands that form the solution complexes contributing most to the total dissolved concentrations of the elements. Th- and Pu-speciation diagrams are discussed in this section as examples of this approach to sensitivity analysis. Similar diagrams for Np, U, and Am are given in the sections below devoted to those elements.

Figures 6.4-12 and 6.4-13 are speciation diagrams for Th from pH values 3.25 to 9.5. The former displays the molar concentration of total Th and its solution complexes; the latter displays the complex concentrations in percent of total Th. The diagrams represent a system at equilibrium with the solid ThO_2(am) at log fCO_2 (bars) = –3.0. The choice of this controlling solid is discussed in Section 6.8.2. Th occurs only in the Th(IV) oxidation state in aqueous solution.

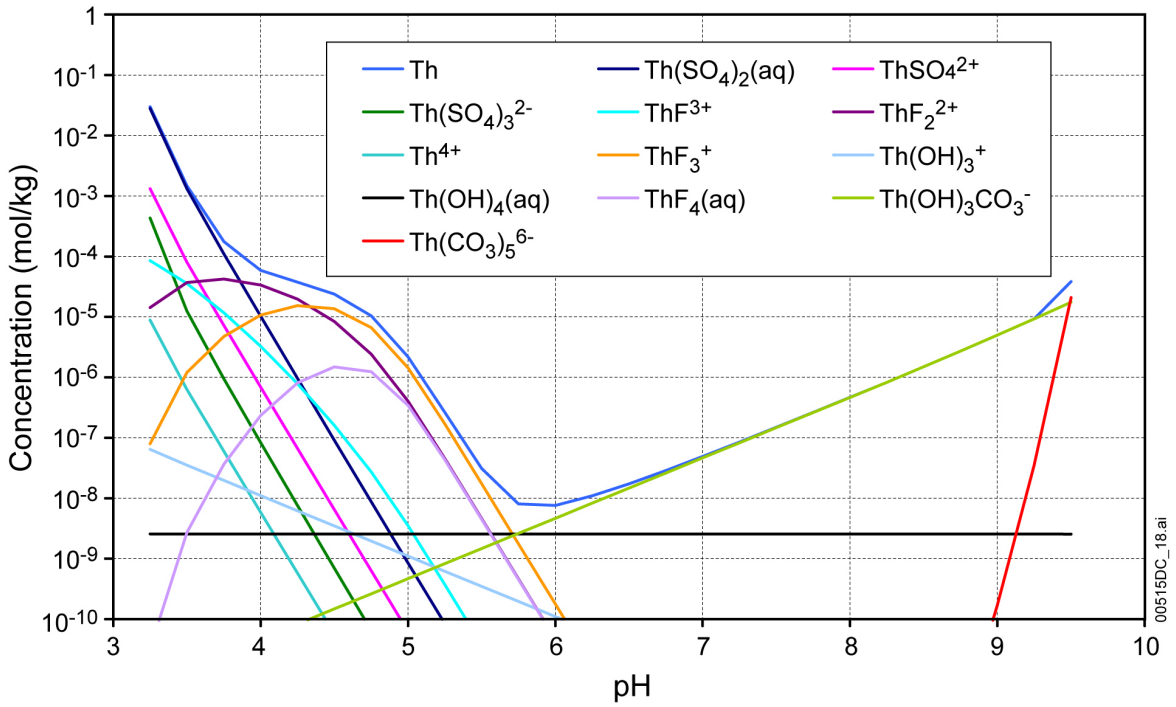

Source: *Th species plot.xls* (Appendix I).

Figure 6.4-12. Total Th Concentration and Speciation Diagram at log fCO_2 (bars) = –3.0 in mol/kg H_2O

The calculated total Th concentration ranges from nearly 0.1 mol at pH 3.25 to a minimum of less than 10^{-8} mol at pH 6.0 and increases again to nearly 10^{-4} mol at pH 9.5. At the lowest pH, over 90 percent of the total Th consists of the $Th(SO_4)_2$(aq) complex, with the $ThSO_4^{2+}$ complex contributing less than 10 percent of the total. At pH values from below 4.0 to above 5.5, F^--bearing complexes dominate the total Th. The principal complex at pH 4.0 is ThF_2^{2+} while ThF_3^+ dominates from pH 4.5 to 5.5. From pH 5 to 5.5, ThF_4(aq) also contributes about 15 percent of the total, as does ThF_2^{2+}. At higher pH values, the importance of F^- complexes diminishes and the principal contributors to total Th become the CO_3^{2-} complexes, $Th(OH)_3CO_3^-$ and, at pH 9.5, $Th(CO_3)_5^{6-}$. At around pH 6.0, $Th(OH)_4$(aq) also contributes over 30 percent of the total Th.

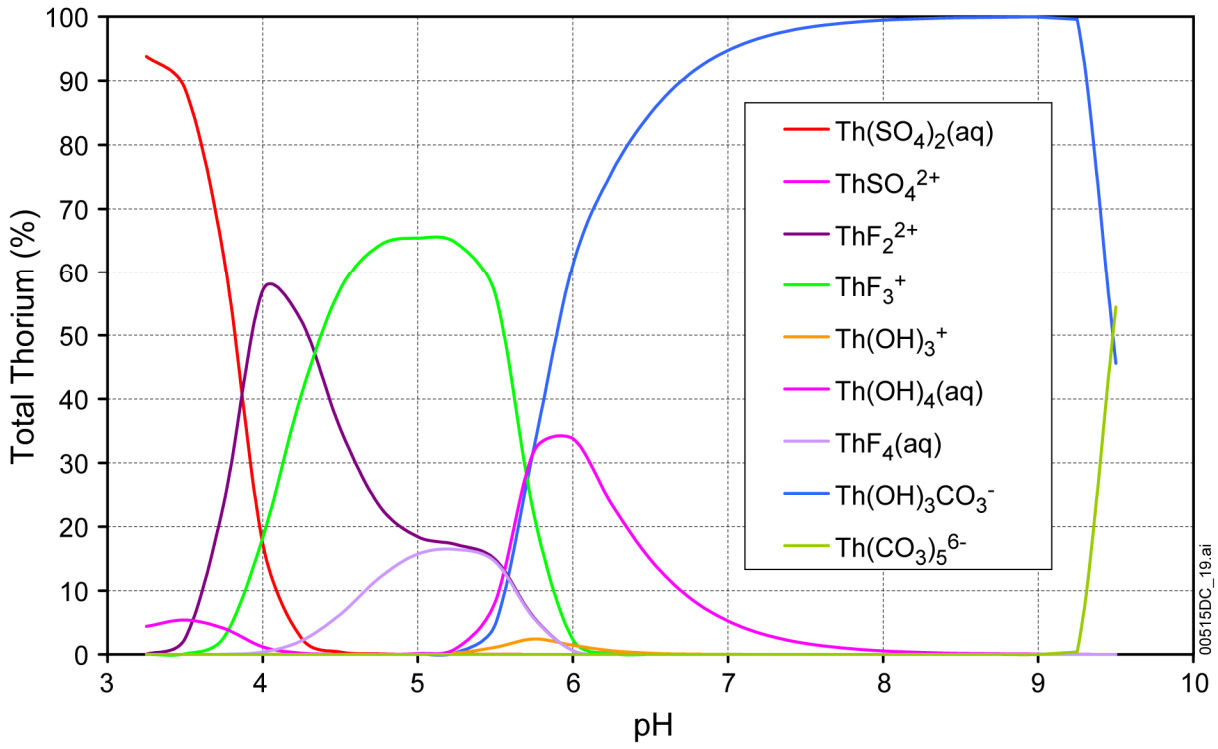

Source: *Th species plot.xls*.

Figure 6.4-13. Th-Speciation Diagram at log fCO_2 (bars) = –3.0 in Percent Total Dissolved Th

$Th(CO_3)_5^{6-}$ is formed by the reaction:

$$Th^{4+} + 5\ HCO_3^- = Th(CO_3)_5^{6-} + 5\ H^+$$

where $Th(CO_3)_5^{6-}$ dominates, the total Th concentration increases by 10^5 for each unit increase in the pH. The extreme nonlinearity of the variation of total Th with pH where this complex dominates is why the EQ3NR program does not converge in the high pH–high fCO_2 range.

Figures 6.4-12 and 6.4-13 show total Th concentration is sensitive to SO_4^{2-} concentrations at low pH values, to F^- concentrations under moderately acid conditions and to OH^- and CO_3^{2-} concentrations under circumneutral and basic conditions. The OH^- concentrations depend on the pH, and CO_3^{2-} concentrations on pH and fCO_2. The solubilities are tabulated in terms of pH and fCO_2 so the sensitivities to OH^- and CO_3^{2-} variations are considered explicitly. As discussed in Section 6.4.3.5, SO_4^{2-} concentrations are varied in the modeling to maintain charge balance in order to simulate the occurrence of H_2SO_4 in the in-package environment from the oxidation of sulfur during steel degradation. In this way, SO_4^{2-} variations are also considered explicitly. Variations in F^- concentrations are not treated explicitly, rather as uncertainties in the total Th concentrations.

Figures 6.4-14 and 6.4-15 are speciation diagrams for Pu calculated using the adjusted-Eh model for Pu solubility (Section 6.5.3). The figures are from pH 2 to 9.75 at log fCO_2 (bars) = –3.0. The former displays the molar concentration of total Pu and its solution complexes; the latter

displays the complex concentrations in percent of total Pu. The oxidation state of the Pu species influences the complexes that form and is discussed in Section 6.5.4.3

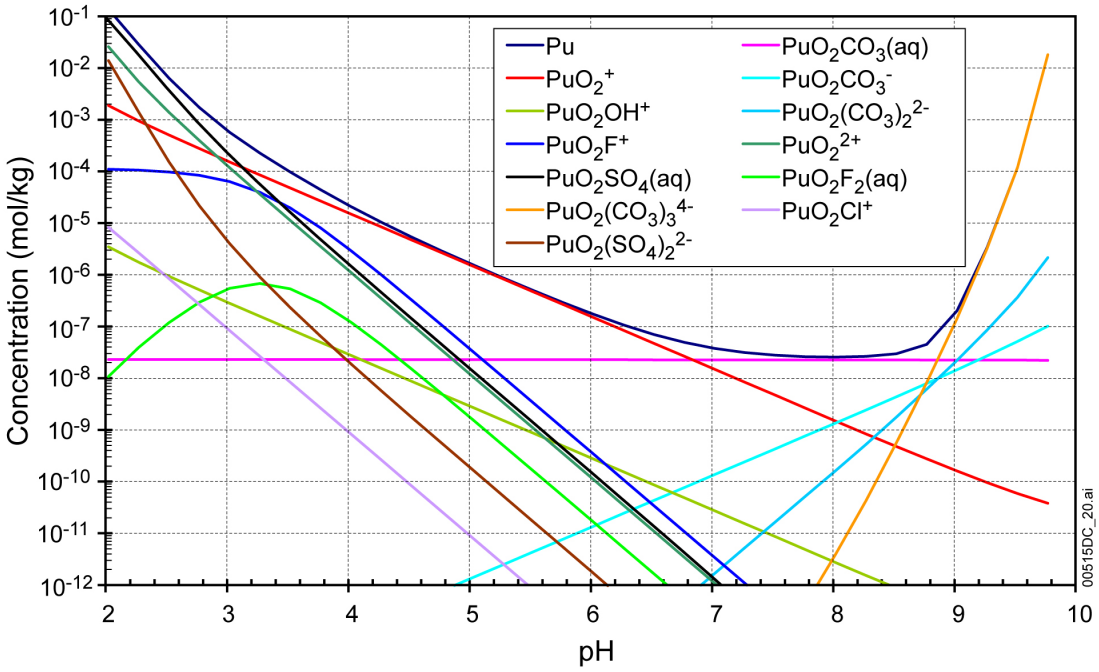

Source: *Pu species plot_2.xls*.

Figure 6.4-14. Total Pu Concentration and Speciation Diagram at log fCO_2 (bars) = –3.0 in mol/kg H_2O

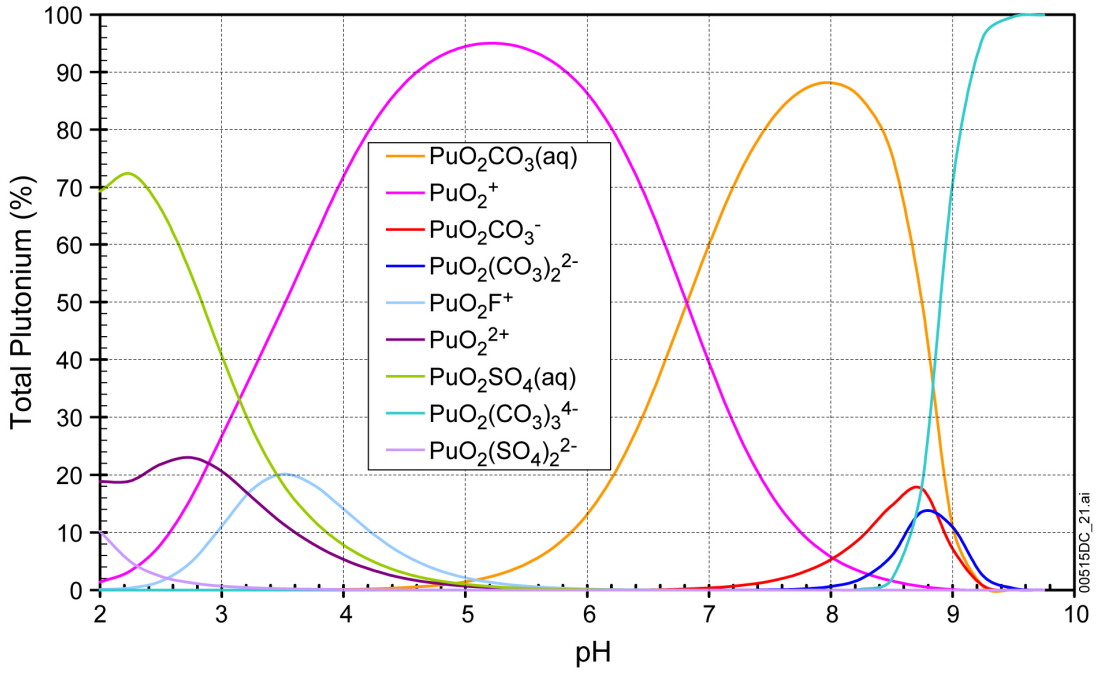

Source: *Pu species plot_2.xls*.

Figure 6.4-15. Pu-Speciation Diagram at log fCO_2 (bars) = –3.0 in Percent Total Pu

These figures show Pu(V) is the dominant oxidation state from about pH 3.5 to 6.8, and is represented by the species PuO_2^+. At lower and higher pH values, aqueous complex species of SO_4^{2-}, F^-, and CO_3^{2-} become important. These are Pu(VI) species so, with their increasing importance, Pu(VI) becomes the dominant oxidation state. Pu speciation is described in detail in Section 6.5.3.2, which focuses on information provided by these speciation diagrams concerning the sensitivity of Pu solubility to other species in solution.

As Figures 6.4-14 and 6.4-15 show, from below pH 7 to the highest values modeled, PuO_2^{2+}–CO_3^{2-} complex species dominate, while at pH values lower than just above 3, $PuO_2SO_4(aq)$ dominates and $PuO_2(SO_4)^{2-}$ becomes significant. The importance of PuO_2^{2+}–SO_4^{2-} complexes accounts for the sensitivity of total Pu to SO_4^{2-} at low pH values shown in Figure 6.4-3.

Around pH 3.5, PuO_2F^+ contributes 20 percent of the total Pu. At higher F^- concentrations, this and other PuO_2^{2+}–F^- complexes contribute more strongly and even dominate the total Pu concentration. For example, from Figure 6.4-14, it can be concluded that at 10× F^- the PuO_2F^+ concentration exceeds that of PuO_2^+, thus approximately doubling the total Pu; while at higher F^- concentrations, PuO_2F^+ and $PuO_2F_2(aq)$ become dominant and together increase the total Pu concentration by orders of magnitude. This accounts for the strong effect of increasing F^- on Pu concentrations shown in Figure 6.4-2.

To summarize, the speciation diagrams in Figures 6.4-12 through 6.4-15 show that at high pH values, CO_3^{2-} aqueous complex species are the principal contributors to actinide solubilities. These diagrams, together with the results of the sensitivity calculations shown in Figures 6.4-2 and 6.4-3, show that at low pH values, SO_4^{2-} complexes are the principal contributors to total solubilities, while under moderately acid conditions, solubilities are also very sensitive to F^- because of the formation of F^- aqueous complex species. CO_3^{2-} concentrations depend on pH and fCO_2. The solubilities are tabulated in terms of pH and fCO_2, so the sensitivities to CO_3^{2-} variations are considered explicitly. As discussed in Section 6.4.3.5, SO_4^{2-} concentrations are varied in the modeling to maintain charge balance at lower pH values in order to simulate the occurrence of H_2SO_4 in the in-package environment from the oxidation of sulfur during steel degradation. In this way, SO_4^{2-} variations are also considered explicitly. Variations in F^- concentrations are not treated explicitly, rather as uncertainties in the total actinide concentrations. As Figures 6.4-2 and 6.4-3 illustrate, the effect of F^- varies with the pH. To capture this, the uncertainty factors applied to the solubilities to account for F^- uncertainty are expressed as functions of pH (Section 6.5.3.4)

6.4.3 Model Configuration

In the previous discussion, it was concluded that the important physical and chemical conditions for solubility evaluation are oxidation potential, pH, *f*CO2, water chemistry (particularly concentrations of ligands such as F^-), and temperature. This section explains how each parameter is accounted for in geochemical model calculations, whether they are treated as an independent variable or as an uncertainty term, and how each parameter is varied. This section also discusses charge-balancing species SO_4^{2-} and Na^+.

6.4.3.1 Oxidation Potential

This model assumes that the atmosphere controls the oxidation state (Section 5.1). To achieve this, the value of fO_2 is set to 0.2 bars. However, this assumption was modified for Pu and Np solubility calculations. Sections 6.5 and 6.6 discuss reasons and details of the selection of the oxidation potential used in modeling Pu and Np solubility.

6.4.3.2 Temperature

Solubility is calculated at 25°C. As shown in Section 6.3.3.3, the solubility of plutonium, neptunium, uranium, and americium decreases with temperature. By analogy, thorium should behave similarly to other actinide elements. Thus, it is reasonable that thorium should have retrograde solubility as well. Therefore, using actinide solubilities at 25°C is conservative for temperatures higher than 25°C.

6.4.3.3 pH

Because of its strong effect on actinide solubility, pH is selected as an independent variable in solubility calculations. In other words, solubility calculations are carried out for different pH values. The pH range for fluids reacting with CSNF is 4.5 to 8.1, while the range for fluids reacting with codisposal materials is from 4.5 to 8 (BSC 2004 [DIRS 167621], Table 8-2). According to *Engineered Barrier System: Physical and Chemical Environment* (BSC 2004 [DIRS 169860), the response surface for pH in the invert ranges from 3.5 to 10.5. *Dike/Drift Interactions* (BSC 2004 [DIRS 170028]) reports pH values ranging from 8.1 to 9.9 for fluids reacting with basalt. To cover the full range of conditions, the target pH range for the modeling was set at 3 to 11. The pH values varied in 0.25 increments.

6.4.3.4 CO_2 Fugacity

As discussed earlier, fCO_2 is another important independent variable in actinide-solubility models because of the strong tendency for actinides to form complexes with CO_3^{2-}. The atmospheric value of CO_2 partial pressure is $10^{-3.5}$ bars. Section 6.7.2.2 of *Engineered Barrier System: Physical and Chemical Environment Model* (BSC 2004 [DIRS 169860]) gives the range of fCO_2 from 1.75E-02 bars (maximum) to 2.29E-05 bars (minimum). The range of applicability of *In-Package Chemistry Abstraction* (BSC 2004 [DIRS 167621]) is from 10^{-5} to $10^{-1.5}$ bars (Table 8-1). The fCO_2 range used for actinide solubility calculations in this report is from 10^{-5} to $10^{-1.5}$ bars. It is varied in increments of 0.5 log units.

6.4.3.5 Charge Balance Species: SO_4^{2-} and Na^+

In the EQ3NR modeling performed to calculate solubilities, assigning a pH value different from that of the initial base-case water leads to solutions not electrically neutral (charge balanced). To maintain charge balance in the solution modeled, a charge-balancing cation or anion was added during the modeling. The in-package chemistry study indicates that the major driving force for lowering pH is the oxidation of Carbon Steel Type A516 (which contains sulfur), while the major driving force for pH increase is the release of alkali and alkaline earth metals from waste glass dissolution (BSC 2004 [DIRS 167621]). In accordance with these studies, SO_4^{2-} is

specified as the anion added to balance low pH solutions and Na^+ as the cation to balance high pH solutions. This is achieved by specifying one of them in EQ3NR calculations as the species to be adjusted for charge balance. For runs near neutral, the choice of whether to balance on SO_4^{2-} or Na^+ is made by determining whether the code is balancing by adding or subtracting the charge-balancing ion. If the balancing ion is subtracted, the resulting solution has a lower concentration of the balancing ion than the input water composition. Only runs balanced by adding the charge-balancing ion are used. SO_4^{2-}, one of the balancing ions, accounts for the effects of changing concentration on solubility.

In solutions at high and low pH, a significant increase in the charge-balancing ion concentration is required to achieve charge balance. For example, in the case of PuO_2(hyd,aged) adjusted-Eh model at a pH of 2, the total sulfate in the system (expressed as SO_4^{2-}) increased from 18.4 mg/L to 14,195 mg/L (0.148 molality) (directory Pu Eq3 *runs.zip*, file *pu410401.3o*). At a pH of 9.75, the total sodium (expressed as Na^+) increased from 45.8 mg/L to 11,875 mg/L (0.518 molality) in order to achieve charge balancing (path Pu Eq3 runs.zip, file *pu420432.3o*). Table 6.4-1 lists the top aqueous species for both the low and high pH solutions. At the low pH, a significant portion of the sulfur goes to Pu complexes, whereas at the high pH, the Na does not form many complexes, but mainly balances charges on the carbonate and bicarbonate species.

Table 6.4-1. Major Aqueous Species at pH Extremes

Species Present After Charge Balancing for PuO_2 (hyd,aged) Adjusted-Eh Model, Molality Greater than 1×10^{-2}			
pH=2 (balance with SO_4^{2-})		pH=9.75 (balance with Na^+)	
Species	**Molality**	**Species**	**Molality**
PuO_2SO_4(aq)	9.52E-02	Na^+	4.51E-01
PuO_2^{2+}	2.58E-02	HCO_3^-	1.23E-01
SO_4^{2-}	1.68E-02	CO_3^{2-}	1.12E-01
$PuO_2(SO_4)_2^{2-}$	1.40E-02	$NaHCO_3$(aq)	3.54E-02
H^+	1.24E-02	$NaCO_3^-$	3.08E-02
		$PuO_2(CO_3)_3^{4-}$	1.81E-02

6.4.3.6 Concentration of Secondary Ligands (F^-, HPO_4^{2-}, and SO_4^{2-})

TSPA-LA models two groups of waste packages. CSNF waste packages (which include naval waste packages because of their robustness) comprise more than 90 percent of the waste inventory, while codisposal waste packages comprise the remainder. The concentration range of fluorides in CSNF waste packages is provided in *In-Package Chemistry Abstraction* (BSC 2004 [DIRS 167621], Table 8-6). The maximum value at 25°C is 9.8E-4 mol/kg (18.6 mg/L), which is about 8.5 times that of the base-case value. The minimum value is 3.0E-05 mol/kg (0.57 mg/L), which is less than the base-case value (BSC 2004 [DIRS 167621], Figure 6-71). A range from the base-case value (2.18 mg/L) to 10 times the base-case value (21.8 mg/L) is assigned to fluoride concentration in the CSNF waste packages.

In-Package Chemistry Abstraction (BSC 2004 [DIRS 167621], Table 8-6) also provides fluoride concentrations for codisposal waste packages under vapor-influx and water-influx conditions of

water flow. The highest fluoride concentration is 1.1E-02 mol/kg (209 mg/L) for the vapor-influx case, which is 95 times higher than the base-case value. The lowest concentration is many times lower than the base-case value (BSC 2004 [DIRS 167621], Figure 6-72), but a lower fluoride concentration yields a lower solubility, so it is conservative to set the minimum fluoride concentration to the base-case value. There are no known sources of fluorine in the invert other than that coming from the high-level radioactive waste glass contained in the codisposal waste packages; therefore, the maximum fluoride concentration should not be greater than that in the solution in the codisposal waste packages. Thus, the same range of fluoride concentration (from the base-case value to 95 times the base-case value) is assigned to the invert.

Because of the existence of large quantities of uranium in the repository and the low solubility of uranium-phosphate minerals, Section 6.4.2.5 concludes that the influence of phosphate concentration on actinide solubility is negligible. Nonetheless, phosphate as a component is included in the model calculation and a base-case value is elected based on Table 4.2 of *Report of the Committee to Review the Use of J-13 Well Water in Nevada Nuclear Waste Storage Investigations* (Harrar et al. 1990 [DIRS 100814]), which provides nine measurements of PO_4^{3-} for the reference water. Four of them are listed as less than 10 μg/L, two as less than 100 μg/L, and the remaining three are 120 μg/L, 100 μg/L, and 2,800 μg/L, respectively. However, the latter two are marked as "probably erroneous" and, thus, are excluded from consideration. Because the majority of the remaining seven measurements are less than 100 μg/L, this report assigns the value of 100 μg/L (0.1 mg/L) to HPO_4^{2-}.

SO_4^{2-} concentrations also have an influence on actinide solubilities. As discussed in Section 6.4.3.5, this ligand is associated with the acidity of waste package solutions and is treated as the charge-balancing species in the EQ3NR solubility calculations. Since a major source of SO_4^{2-} in corroding waste packages is structural steel, the effect of SO_4^{2-} concentration on actinide solubilities is accounted for by linking its variation with pH changes.

6.4.3.7 Concentration of Tertiary Ligands (Cl^- and NO_3^-) and Cations

Based on the discussion in Sections 6.4.1 and 6.4.2.5.1, the effects of the tertiary ligands (Cl^- and NO_3^-) and the four common cations (K^+, Na^+, Ca^{2+}, and Mg^{2+}) are very minor; thus, using their base-case values is justified. In addition, Na^+ is used to balance charge in the solution (Section 6.4.3.5), which accounts for the potential variation in common cation concentrations.

Depending on the fugacity of CO_2, when pH increases sufficiently, some cations are expected to precipitate. This is because the solution is set to be in equilibrium with CO_2(g) at a set fugacity, which could result in the formation of carbonate solids. For example, the EQ3NR runs show that the solution becomes supersaturated with calcite at pH between 8.0 and 8.25 when log fCO_2 (bars) = −3.0. Similarly, the EQ3NR outputs commonly show fluorapatite ($Ca_5F(PO_4)_3$) supersaturation at high pH owing to the conversion of protonated phosphate anions, such as HPO_4^{2-}, to PO_4^{3-}. If precipitation does not occur, the ionic strength remains relatively high, thereby maintaining a somewhat higher solubility of radionuclides as a consequence of the salting-in effect (i.e., activity coefficients stay relatively low). However, the main effect of the supersaturation in carbonate and fluoride is to leave these ions in solution and, thereby, increase the concentrations of carbonate and fluoride complexes with actinides. Thus, actinide solubilities calculated by EQ3NR without precipitation are conservatively high.

The discussion on model configuration is summarized in Table 6.4-2.

Table 6.4-2. Summary of EQ3NR Model Configuration

Variable	Treatment in Model	Value or Range
pH	Independent variable	3.0 to 11.0
log fCO_2 (bars)	Independent variable	–5.0 to –1.5
Temperature	Conservatively using 25°C value	25°C to 100°C
log fO_2 (bars)	Constant	–0.7 (except for Pu and Np; see Sections 6.5 and 6.6 for details)
F^- concentration	Uncertainty term	(for Pu, Np, U, Th, Am, and Pa) 1 to 10 times the base-case value for CSNF waste packages; 1 to 27 times the base-case value for water-influx codisposal waste packages; and 1 to 95 times the base-case value for vapor-influx codisposal waste packages and for the invert
SO_4^{2-} concentration	Charge balance species	Base-case (J-13 well water) concentration or as automatically determined by the code, whichever is higher
Na^+ concentration	Charge balance species	Base-case (J-13 well water) concentration or as automatically determined by the code, whichever is higher
PO_4^{3-}, NO_3^-, and Cl^-	Constant	The base-case (J-13 well water) value
K^+, Ca^{2+}, and Mg^{2+}	Constant	The base-case (J-13 well water) value

6.4.4 Valid Ranges of Solubility Models

As discussed in the previous section, the solubility models developed in this report are valid for broad ranges of water composition as listed in Table 6.4-2. However, three exceptions are noted.

The first exception arises from the limitations in activity coefficient corrections. As discussed in Section 6.3.3.4, the nominal range of applicability of activity coefficients calculated by the B-dot equation (used in EQ3NR with parameter values given in *Data0.ymp.R2* (DTN: MO0302SPATHDYN.000 [DIRS 161756])) is to solutions with ionic strengths up to 1 molal. Thus, no uncertainties related to activity coefficients are included in the solubilities given in this report for modeled solutions with ionic strengths of 1 molal or less. However, for some elements, certain pH and fCO_2 conditions lead to modeled solutions with ionic strengths exceeding 1 molal. In most cases when this occurs, the solubility tables for these pH and fCO_2 conditions show the "500" placeholder. In other cases, when the modeled solution exceeds 1 molal by a factor of 3 or less and it was important to provide a solubility value to TSPA-LA, the calculated values given in the solubility tables must take into account additional uncertainty, which is added to the solubility of the actinides by the square root of the mean described in Section 6.3.3.4.

The second exception occurs under conditions of low pH or of high pH and high fCO_2, where the EQ3NR calculations do not converge. Mathematically, this unstable condition occurs at low pH values largely due to rapid increases in total actinide and SO_4^{2-} concentrations. As discussed in Section 6.4.3.6, the rapid increases are due to the strength of actinide–SO_4^{2-} solution

complexes such as $AmSO_4^+$ and $Th(SO_4)_2(aq)$ and the addition of SO_4^{2-} as the charge-balancing anion. Instability from this condition occurs in calculations for thorium and has a particularly strong effect on the calculations of americium solubilities (Section 6.9.4). In the high fCO_2 and pH region, increasing CO_3^{2-} concentrations favor the formation of actinide-carbonate complexes such as $Am(CO_3)_3^{3-}$, $Th(CO_3)_5^{6-}$, and $Th(OH)_3CO_3^-$. The fCO_2 is fixed in the modeling, so CO_3^{2-} concentrations are sensitive to pH changes. This produces rapid changes in total actinide concentrations with pH changes and leads to the nonconvergence noted for all actinides under these modeling conditions. In the low pH and high pH–high fCO_2 regions, calculation results may be invalid, even if the EQ3NR modeling converges, because the total solute concentrations in these regions may exceed 1-molal ionic strength. As discussed previously in this section, EQ3NR solubility models should not be used above this ionic strength without adding allowance for the increased uncertainty.

Physically, the nonconvergence at low pH due to sulfate complexing is conceptually different from that at high pH due to carbonate complexing. In the latter, the reason for modeling at increasing pH and fCO_2 values is to investigate the compositional dependence of the solubility on these variables. At high levels, actinide carbonate complexes become the dominant form of dissolved actinides and the dominant form of dissolved carbonate. Both dissolved carbonate and actinide masses are constrained only by mass action relations (e.g., by equilibrium with the various controlling solids and fixed fCO_2 values) and not by constraints on the total masses in the system being modeled. This leads to increasing amounts of carbonate being added as dissolved actinide concentrations increase and the calculation becomes unbounded. This cannot happen in real systems because there will be other active constraints that limit either the dissolved carbonate (calcite precipitation, CO_2 gas depletion, etc.) or dissolved actinide (entire mass of material available dissolved), or both. However, for the compositional space being modeled, nonconvergence occurs where the solubility curve becomes nearly vertical in terms of these parameters. For the low-pH case, the sulfate interactions are driving the same sort of computational problem. However, sulfate is only a secondary part of the compositional space being investigated. The primary change being explored is the decrease in pH with sulfate added for charge balance. It is through this latter constraint that the sulfate causes the calculation to become unbounded. From this point of view, nonconvergence at low pH values can be considered a modeling artifact indicating sulfate is a poor choice for charge-balance constraint under those conditions. This might be avoided by using chloride as the charge-balancing anion because actinide-chloride complexes are less strong than actinide-sulfate complexes. However, this would be less representative of the physical system being modeled because low pH values within degrading waste packages result from sulfate produced by the oxidation of sulfur in the steels of the waste package (Section 6.4.3.5).

When these two exceptions are observed, no solubility values are reported in the tables of calculated results. Tabulated log solubilities are flagged by "500." For TSPA-LA modeling, when values of "500" are encountered they are considered flags that concentrations should be established by its release rate, rather than from a solubility control.

A third exception arises from the assigned fluoride concentration ranges in waste packages and in the invert (Sections 6.3.3.2 and 6.4.3.6). These ranges are based on modeling results of in-package chemistry for certain scenarios. The fluoride uncertainty term is modeled separately for each of the elements.

6.4.4.1 EQ3 Input Files

The EQ3 input file names follow the convention, Pu010203.3i:

- The first two characters are the element name.
- The next two numbers are the fO_2 step (since fO_2 was not varied, this value is always 01).
- The next two numbers give the fCO_2 step (01 to 08: varying the fCO_2 from $10^{-1.5}$ to $10^{-5.0}$ bars in $10^{-0.5}$ bar increments).
- The last two numbers represent the pH step (01 to 37: varying the pH from 3.0 to 12.0 in 0.25 pH increments).

The input files are located in Appendix I, with the directory structure given in Appendix II. The runs balanced on different elements (Section 6.4.3.5) are stored in directories named for the balancing element. For example, all of the runs for the Am solubility balanced on Na^+ are in the "na" directory under Am.

6.5 PLUTONIUM SOLUBILITY

6.5.1 Introduction

Plutonium has a complex chemistry. Despite numerous studies, the understanding of Pu solubility remains uncertain. In Section 6.5.3, the base-case Pu-solubility model is presented. Section 6.5.4 describes the basis for using an adjusted-Eh solubility model for Pu.

In natural environments, Pu exists primarily as colloids (Rai and Swanson 1981 [DIRS 144599]; Choppin 1983 [DIRS 168395]; Toth et al. 1983 [DIRS 168394]; Choppin and Stout 1989 [DIRS 168379]; Silva and Nitsche 1995 [DIRS 112092]). Colloids are defined as particles with at least one dimension between 1 nm to 1 µm (Lide 2002 [DIRS 160832], p. 2-42). Often, particularly in reporting of experimental results, the upper end of the colloid size range is 450 nm and the lower limit is >2 nm, due to conventional dimensions of laboratory equipment (primarily filters) (BSC 2004 [DIRS 170025]). Table 6.5-2 indicates the filter size used to separate colloids from solution used in experimental determination of aqueous Pu. This report deals only with dissolved Pu as defined by the largest of these sieve sizes (4.1 nm). Thus, the Pu-solubility product in solubility model calculations represents Pu solubility controlled by dual equilibrium as discussed in Section 6.5.3.1. Pu transport by colloids is discussed in a separate report, as directed in *Technical Work Plan for Postclosure Waste Form Modeling* (BSC 2005 [DIRS 173246]).

Data0.ymp.R2 (DTN: MO0302SPATHDYN.000 [DIRS 161756]) incorporates plutonium thermodynamic data compiled by the Chemical Thermodynamics project of the NEA (OECD 2001 [DIRS 159027]). This database was used for plutonium solubility calculations. A correction was made to the log K value and formula in *Data0.ymp.R2* (DTN: MO0302SPATHDYN.000 [DIRS 161756]) of the phase $PuO_2(OH)_2 \cdot H_2O$ when creating the *Data0.yc3.R1* database. As this solid was not used as a solubility-controlling phase in this report, this correction has no impact on its output.

6.5.2 Chemical Conditions

Table 6.4-2 presents the chemical conditions used for the plutonium calculations. For the base-case adjusted-Eh model, different redox conditions were used, as discussed in Section 6.5.3.2.

6.5.3 The Adjusted-Eh Pu-Solubility Model (Base-Case Pu-Solubility Model)

6.5.3.1 Selection of Solubility-Controlling Phases

The most studied plutonium solid for its solution behavior is a hydrated-plutonium dioxide variously written as $Pu(OH)_4$(am), $PuO_2 \cdot xH_2O$, or PuO_2(hyd,aged), where "am" stands for amorphous, "hyd" for hydrated, and "aged" for aged from fresh precipitate. The NEA data compilation (OECD 2001 [DIRS 159027]) uses PuO_2(hyd,aged) and $Pu(OH)_4$(hyd,aged) to denote the same Pu(IV) hydrated oxide/hydroxide "aged for several months near room temperature." The solubility constant of PuO_2(hyd,aged), recommended by the NEA (OECD 2001 [DIRS 159027]) and used in this study, is based on solubility experiments conducted by Rai (1984 [DIRS 122768]) and Kim and Kanellakopulos (1989 [DIRS 122387]).

The NEA updated the Pu data set (Guillaumont et al. 2003 [DIRS 168382]). The revised value of PuO_2(hyd,aged) equilibrium constant given in this update does not differ much from the value used in this report (only 0.33 in log K). This is well within the uncertainty associated with the calculated Pu concentrations (±2.0, see Section 6.5.3.4.1), so not adopting the new value does not change the calculated concentrations beyond the uncertainty already associated with them.

In experiments from oversaturation conducted at Los Alamos National Laboratory (LANL) (Efurd et al. 1998 [DIRS 108015]; Runde et al. 2002 [DIRS 168432]; CRWMS M&O 2001 [DIRS 154629]), solids precipitated have a dark green color, which is characteristic of Pu(IV) solid phases. Diffuse reflectance infrared spectra of the precipitated solid indicates that the presence of Pu(IV) and the X-ray diffraction pattern matched that of PuO_2(s). The diffuse and broad X-ray diffraction peaks suggest poor crystalline structures (Efurd et al. 1998 [DIRS 108015]; Runde et al. 2002 [DIRS 168432]; CRWMS M&O 2001 [DIRS 154629]). It is concluded that "plutonium hydroxides and/or colloids, aging toward $PuO_2 \cdot xH_2O$ are, therefore, interpreted to be the solubility-controlling solids in these experiments."

Similar results were obtained in another plutonium solubility experiment with Yucca Mountain waters (Nitsche et al. 1993 [DIRS 155218]; Nitsche et al. 1994 [DIRS 144515]). In that study, at least two solid phases were observed for experiments at 90°C. One is a yellow-green powdery phase, probably noncrystalline. The other consists of darker green clumps. Nitsche et al. (1993 [DIRS 155218], p. 63) concluded, "such a combination of crystalline and amorphous materials in this solid can explain the observed powder [X-ray diffraction] pattern, which is composed of both very sharp and diffuse lines."

In addition to Pu(IV) hydrous precipitates, Pu(IV) hydrolysis forms polymer suspensions (colloids) (Rai and Swanson 1981 [DIRS 144599]; Choppin 1983 [DIRS 168395]; Kim and Kanellakopulos 1989 [DIRS 122387]). The measured Pu solubility can also be measured by Pu colloids. In other words, a dual equilibrium is established among dissolved Pu, $Pu(OH)_4$(am) precipitates, and Pu colloids or polymers, as shown in Figure 6.5-1.

As pointed out by Kim and Kanellakopulos (1989 [DIRS 122387]), "the experimental differentiation of the two equilibrium reactions is practically impossible." Thus, the Pu-solubility product measured in experiments actually reflects the dual equilibrium and using the measured Pu-solubility product in solubility model calculations also represents Pu solubility controlled by the dual equilibrium. The following discussion states that PuO_2(hyd,aged) is used as the solubility-controlling phase for Pu and no distinction between PuO_2(hyd,aged) precipitates control and PuO_2(hyd,aged) colloids control is made.

Aging has been widely observed in Pu precipitates or polymers in solubility experiments. For example, Rai and Ryan (1982 [DIRS 112060]) observed $PuO_2 \cdot xH_2O$ (amorphous) continuously aging over a period of 1,266 days by dehydration. The dehydration process of Pu(IV) hydrous involves the conversion of hydroxy bridge into oxygen bridge (Choppin 1983 [DIRS 168395]). This aging process is irreversible (i.e., once aged, the solid becomes kinetically stable (Choppin 2003 [DIRS 168308]) and difficult to redissolve).

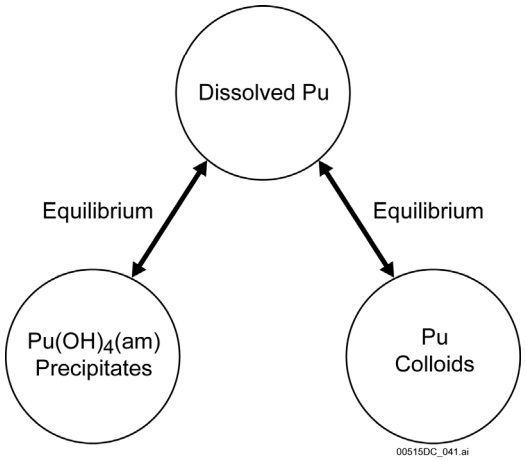

Figure 6.5-1. Dual Equilibrium Among Dissolved Pu, Pu Precipitates, and Pu Colloids

Radiolytic processes limit the extent to which dehydration of amorphous PuO_2 hydrates can cause them to revert to more-crystalline, less-soluble forms. The Organisation for Economic Co-operation and Development (OECD) (2001 [DIRS 159027], Section 17.2.2.3) reports $^{239}PuO_2$ is slowly converted to (or becomes coated with) a less- crystalline form when in contact with water. This form is similar to the PuO_2(hyd,aged) form produced by the dehydration of amorphous, hydrated PuO_2. The OECD (2001 [DIRS 159027], Section 17.2.2.3) also notes $^{238}PuO_2$ is converted to the amorphous solid in water.

Plutonium is present in PuO_2(hyd,aged) in the Pu(IV) oxidation state. Under reducing conditions where Pu(IV) is the stable oxidation state, the solid dissolves directly to Pu(IV) aqueous species. However, under the oxidizing conditions of Yucca Mountain, the dissolved Pu is present dominantly as Pu(V) and Pu(VI), depending on the Eh, pH, and concentrations of complex-forming ligands in the solution. The following sections explore the effect of the choice of Eh (the value of which most closely reproduces laboratory experimental data). The distribution of dissolved species and of oxidation states of dissolved Pu are discussed in more detail below.

Recently, a solid with the general formula PuO_{2+x} that forms from PuO_2 in the presence of water vapor was described by Haschke et al. (2000 [DIRS 150367]), Haschke and Oversby (2002 [DIRS 161911]), and Haschke and Allen (2002 [DIRS 162001]). Based on a review of these papers, the update to the NEA compilation of chemical thermodynamic data (Guillaumont et al. 2003 [DIRS 168382], Section 11.2.2.1) concludes that "the evidence for the formation of a thermodynamically stable bulk phase with O/Pu>2 is far from conclusive." For this reason and others discussed in Section 6.5.6, this solid was not considered in selecting the Pu-controlling solids.

6.5.3.2 Calculated Pu Solubility and Speciation Using the Adjusted-Eh Model

The adjusted-Eh model sets Eh conditions using Equation 6.5-7, as described in Section 6.5.4.3, for pH values between 3.0 and 10.75. Table 6.4-2 provides other model calculation conditions.

Table 6.5-1 provides the calculated-Pu solubility (log [Pu] (mg/L)) with pH and log fCO_2 as independent variables. Because the independent variables are in log scales, and Table 6.5-1 may need to be interpolated between calculated values, the logarithm of Pu solubility is given.

Table 6.5-1. Calculated Pu Solubility (Adjusted-Eh Model) (log [Pu] mg/L)

	log fCO_2 (bars)							
pH	–1.50	–2.00	–2.50	–3.00	–3.50	–4.00	–4.50	–5.00
2.00	4.53E+00	4.53E+00	4.53E+00	4.53E+00	4.53E+00	4.53E+00	4.53E+00	4.53E+00
2.25	3.84E+00	3.84E+00	3.84E+00	3.84E+00	3.84E+00	3.84E+00	3.84E+00	3.84E+00
2.50	3.19E+00	3.19E+00	3.19E+00	3.19E+00	3.19E+00	3.19E+00	3.19E+00	3.19E+00
2.75	2.62E+00	2.62E+00	2.62E+00	2.62E+00	2.62E+00	2.62E+00	2.62E+00	2.62E+00
3.00	2.14E+00	2.14E+00	2.14E+00	2.14E+00	2.14E+00	2.14E+00	2.14E+00	2.14E+00
3.25	1.74E+00	1.74E+00	1.74E+00	1.74E+00	1.74E+00	1.74E+00	1.74E+00	1.74E+00
3.50	1.38E+00	1.38E+00	1.38E+00	1.38E+00	1.38E+00	1.38E+00	1.38E+00	1.38E+00
3.75	1.04E+00	1.03E+00	1.03E+00	1.03E+00	1.03E+00	1.03E+00	1.03E+00	1.03E+00
4.00	7.22E-01	7.12E-01	7.09E-01	7.08E-01	7.07E-01	7.07E-01	7.07E-01	7.07E-01
4.25	4.32E-01	4.12E-01	4.06E-01	4.04E-01	4.03E-01	4.03E-01	4.03E-01	4.03E-01
4.50	1.72E-01	1.35E-01	1.23E-01	1.19E-01	1.18E-01	1.17E-01	1.17E-01	1.17E-01
4.75	-5.78E-02	-1.22E-01	-1.45E-01	-1.52E-01	-1.54E-01	-1.55E-01	-1.55E-01	-1.55E-01
5.00	-2.54E-01	-3.60E-01	-3.99E-01	-4.12E-01	-4.17E-01	-4.18E-01	-4.19E-01	-4.19E-01
5.25	-4.13E-01	-5.75E-01	-6.42E-01	-6.65E-01	-6.73E-01	-6.75E-01	-6.76E-01	-6.76E-01
5.50	-5.33E-01	-7.62E-01	-8.70E-01	-9.11E-01	-9.25E-01	-9.29E-01	-9.30E-01	-9.31E-01
5.75	-6.17E-01	-9.17E-01	-1.08E+00	-1.15E+00	-1.17E+00	-1.18E+00	-1.18E+00	-1.18E+00
6.00	-6.73E-01	-1.03E+00	-1.27E+00	-1.37E+00	-1.41E+00	-1.43E+00	-1.43E+00	-1.43E+00
6.25	-7.07E-01	-1.12E+00	-1.42E+00	-1.58E+00	-1.65E+00	-1.67E+00	-1.68E+00	-1.69E+00
6.50	-7.28E-01	-1.17E+00	-1.54E+00	-1.77E+00	-1.88E+00	-1.92E+00	-1.93E+00	-1.93E+00
6.75	-7.39E-01	-1.21E+00	-1.62E+00	-1.92E+00	-2.08E+00	-2.15E+00	-2.18E+00	-2.18E+00
7.00	-7.44E-01	-1.23E+00	-1.67E+00	-2.04E+00	-2.27E+00	-2.38E+00	-2.42E+00	-2.43E+00
7.25	-7.44E-01	-1.24E+00	-1.70E+00	-2.12E+00	-2.42E+00	-2.58E+00	-2.65E+00	-2.67E+00
7.50	-7.32E-01	-1.24E+00	-1.72E+00	-2.17E+00	-2.53E+00	-2.76E+00	-2.87E+00	-2.91E+00
7.75	-6.64E-01	-1.23E+00	-1.72E+00	-2.20E+00	-2.61E+00	-2.91E+00	-3.08E+00	-3.15E+00
8.00	-2.26E-01	-1.17E+00	-1.71E+00	-2.20E+00	-2.65E+00	-3.02E+00	-3.25E+00	-3.37E+00
8.25	9.33E-01	-8.71E-01	-1.66E+00	-2.19E+00	-2.67E+00	-3.08E+00	-3.39E+00	-3.56E+00
8.50	2.39E+00	1.11E-01	-1.44E+00	-2.14E+00	-2.65E+00	-3.11E+00	-3.48E+00	-3.73E+00
8.75	500	1.50E+00	-6.37E-01	-1.96E+00	-2.59E+00	-3.09E+00	-3.51E+00	-3.84E+00

Table 6.5-1. Calculated Pu Solubility (Adjusted-Eh Model) (log [Pu] mg/L) (Continued)

	log fCO_2 (bars)							
pH	**–1.50**	**–2.00**	**–2.50**	**–3.00**	**–3.50**	**–4.00**	**–4.50**	**–5.00**
9.00	500	3.20E+00	6.73E-01	-1.31E+00	-2.43E+00	-3.01E+00	-3.49E+00	-3.88E+00
9.25	500	500	2.25E+00	-8.16E-02	-1.90E+00	-2.85E+00	-3.40E+00	-3.84E+00
9.50	500	500	500	1.46E+00	-7.69E-01	-2.41E+00	-3.22E+00	-3.74E+00
9.75	500	500	500	3.65E+00	7.62E-01	-1.39E+00	-2.86E+00	-3.56E+00
10.00	500	500	500	500	2.74E+00	1.24E-01	-1.96E+00	-3.24E+00
10.25	500	500	500	500	500	2.10E+00	-4.65E-01	-2.47E+00
10.50	500	500	500	500	500	500	1.52E+00	-1.02E+00
10.75	500	500	500	500	500	500	500	9.86E-01

Source: *puehadjustmodel.xls* (Appendix I).

NOTE: Cells with no valid data, because the EQ3NR calculations do not converge, are reported as "500."

For those calculations that do not converge or are not valid, a large number ("500") is entered to indicate that under such pH and fCO_2 conditions, solubility of plutonium is not defined or the calculation results are outside the valid range of the computing tool. When the flag ("500") is encountered or for conditions between a valid solubility and a flag of "500," concentrations should be calculated according to the dissolution rate of individual waste forms, water volume, and the solubility caps presented in Table 8-3 instead of the flag itself. In addition, for conditions outside of the 3.0 to 11.0 pH range, or the fCO_2 range from $10^{-1.5}$ to $10^{-5.0}$ bars, the concentrations should be calculated according to the dissolution rate of individual waste forms, water volume, and the solubility caps presented in Table 8-3.

Figures 6.5-2 and 6.5-4 illustrate the total Pu concentration and the concentrations of Pu aqueous complex species composing the total Pu calculated at fCO_2 values of $10^{-3.0}$ and $10^{-5.0}$ bars, respectively. Figures 6.5-3 and 6.5-5 show the same aqueous Pu speciation results plotted as percent of total Pu. These calculations were made at redox conditions of the adjusted-Eh model as specified by Equation 6.5-7.

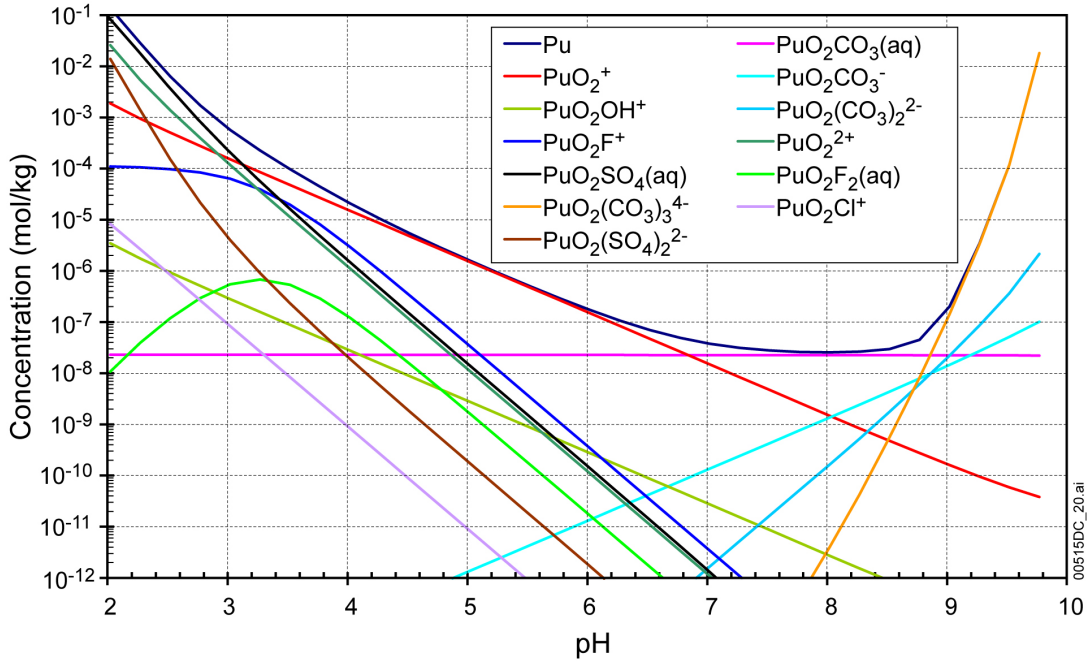

Source: *Pu species plot_2.xls* (Appendix I).

Figure 6.5-2. Molal Concentrations of Total Pu and Pu Aqueous Complex Species at log fCO_2 (bars) = –3.0

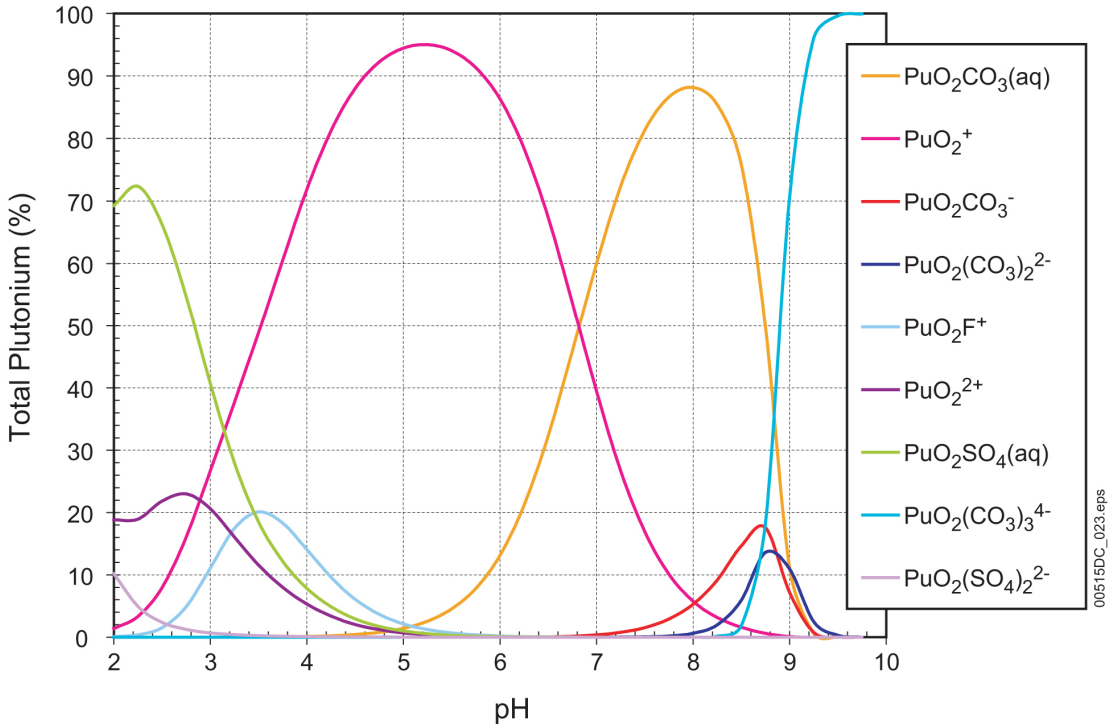

Source: *Pu species plot_2.xls* (Appendix I).

Figure 6.5-3. Relative Concentrations of Pu Aqueous Complex Species as Percent of Total Dissolved Pu at log fCO_2 (bars) = –3.0

At log fCO_2 = -3, Pu is principally in the +5 oxidation state for pH values from just above 3 to 7. At log fCO_2 = -5, Pu(V) is the dominate oxidation state between pH values of 3 and 10. As Figures 6.5-2 through 6.5-5 show, Pu(V) is the dominant oxidation state. At lower pH values, Pu(VI) becomes the dominant oxidation state as the PuO_2SO_4(aq) complex becomes the chief contributor to the total dissolved Pu concentration. However, at low SO_4^{2-} concentrations, the PuO_2SO_4(aq) complex will contribute less to the total dissolved Pu, so the range of Pu(V) dominance as PuO_2^+ would extend to lower pH values.

At higher pH values, the dominant redox state also shifts from Pu(V) to Pu(VI), and the principal species become Pu(VI) carbonate complexes. As Figures 6.5-2 and 6.5-3 illustrate, at log fCO_2 = –3.0 bars, Pu(V) complex gives way to Pu(VI) complex at a pH just below 7. From pH 7 to just below 9, PuO_2CO_3(aq) dominates while at higher pH values, $PuO_2(CO_3)_3^{4-}$ contributes virtually all the dissolved Pu. In solutions at $fCO_2 = 10^{-5.0}$ bars (Figures 6.5-4 and 6.5-5), the pH range in which Pu(V) dominates extends above pH 10. At pH 9, the Pu(VI) species PuO_2CO_3 (aq) is the most prevalent, but it is still less than the sum of the Pu(V) species PuO_2^+ and $PuO_2CO_3^-$. $PuO_2(CO_3)_3^{4-}$ dominates at the highest pH values.

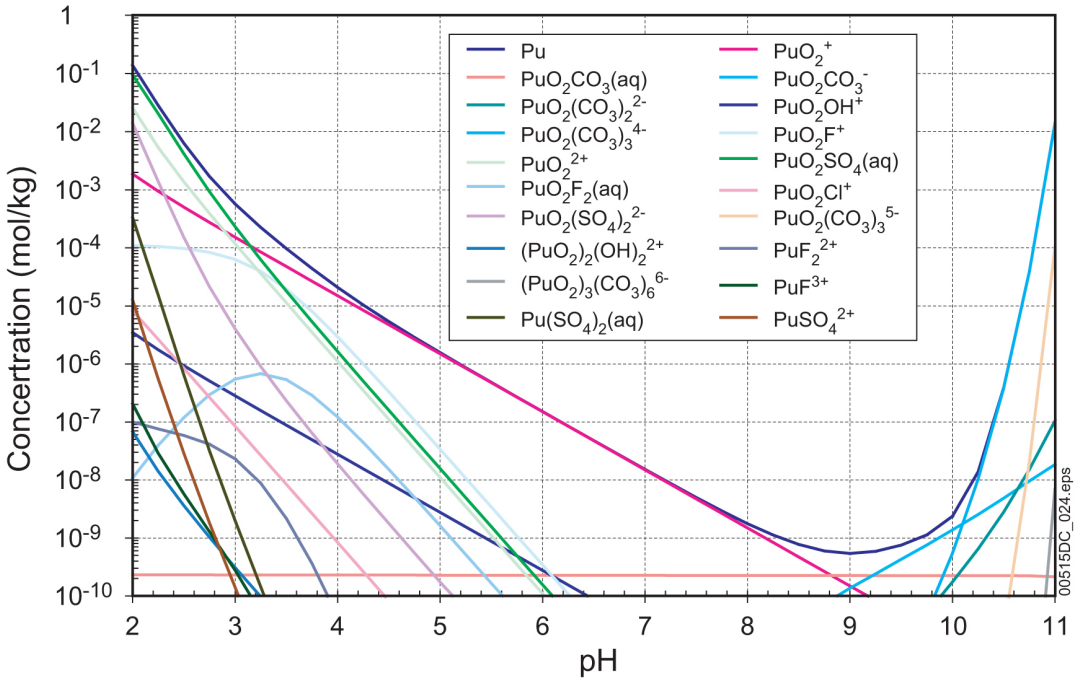

Source: *Pu species plot_2.xls* (Appendix I).

Figure 6.5-4. Molal Concentrations of Total Pu and Pu Aqueous Complex Species at log fCO_2 (bars) = –5.0

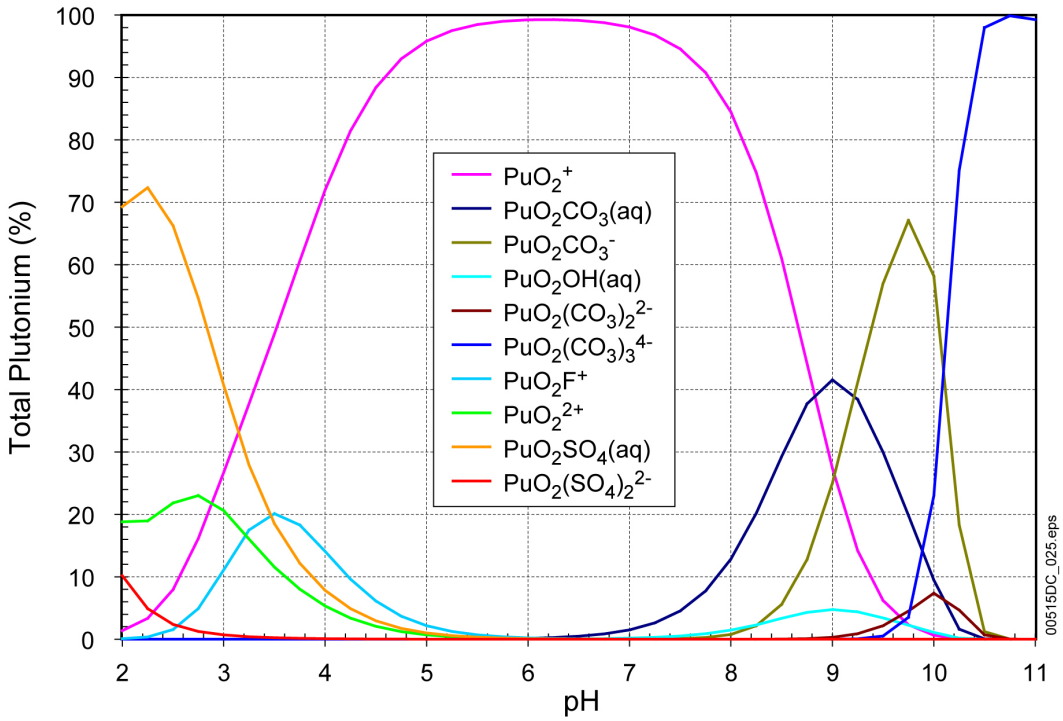

Source: *Pu species plot_2.xls* (Appendix I).

Figure 6.5-5. Relative Concentrations of Pu Aqueous Complex Species as Percent of Total Dissolved Pu at log fCO_2 (bars) = –5.0

The modeled speciation shown in Figures 6.5-2 through 6.5-5 is consistent only in part with the distribution of Pu(V) and Pu(VI) reported by Nitsche et al. (1993 [DIRS 155218]; 1994 [DIRS 144515]) and illustrated in Figure 6.5-9. At pH = 6, the experimental data and model results agree that Pu(V) dominates. At pH = 7, Pu(V) is the dominant redox state in the experiments and in the model results at $fCO_2 = 10^{-5.0}$ bars, but the modeling at $fCO_2 = 10^{-3.0}$ bars shows Pu(V) and Pu(VI) at about equal concentrations. At pH = 8.5, Pu(V) continues to dominate the experimental results, and the model results at $fCO_2 = 10^{-5.0}$ bars, but at $fCO_2 = 10^{-3.0}$ bars Pu(VI) clearly dominates the modeling. As indicated in the caption to Figure 6.5-9, the CO_2 partial pressures ($\approx fCO_2$) in the Ar/CO_2 mixtures in which the experiments were carried out are greater than $10^{-3.0}$ bars, except for one that equaled $10^{-3.2}$ bars. Thus, the persistence of Pu(V) dominance in the high pH experimental solutions presented by Nitsche et al. (1993 [DIRS 155218]; 1994 [DIRS 144515]) is inconsistent with the modeling. The fact that the NEA, in its review of experimental data supporting its chemical thermodynamic database, does not include the experimental studies by Nitsche et al. (1993 [DIRS 155218]; 1994 [DIRS 144515]) supports the conclusion that these results are not reliable. The reliability of the experiments conducted by Rai (1984 [DIRS 122768]), with which the modeled results agree, is used to compare to the model as described in the following section.

6.5.3.3 Comparison with Experimental Results

Figure 6.5-6 presents the adjusted-Eh plutonium-solubility model for log $fCO_2 = -3.5$ bars. The solid line represents the mean values of log[Pu]; the dotted line and the dashed lines represent

upper and lower thermodynamic uncertainty ranges at the 95 percent confidence interval, respectively. Eight sets of experimental data are also plotted in Figure 6.5-6. These data are relevant to the repository and are directly applicable for comparison to the calculations presented in this report.

Experiments conducted by Rai (1984 [DIRS 122768]) and Rai et al. (2001 [DIRS 168392]) were open to air while experiments conducted by Nitsche et al. (1993 [DIRS 155218], Nitsche et al. 1994 [DIRS 144515]), and Efurd et al. (1998 [DIRS 108015]) were conducted in argon/CO_2 atmospheres of various CO_2 contents. Other conditions are also comparable to the modeled conditions. Four different types of solutions were used in the experiments conducted by Rai et al. (2001 [DIRS 168392]): 1) 0.403-m NaCl solution, 2) 0.408-m $NaClO_4$ solution, 3) 4.36-m NaCl solution, and 4) 4.92-m $NaClO_4$ solution. Since the thermodynamic database used in this report is invalid for high ionic strength solutions, only the results of Types 1 and 2 solutions reported by Rai et al. (2001 [DIRS 168392]) are discussed in this report. The solutions were filtered before measuring Pu concentration. Table 6.5-2 lists the calculated pore sizes of filters used for filtration. Colloids are defined as particles with at least one dimension between 1 nm to 1 µm (or 0.45 µm) (BSC 2004 [DIRS 170025]). Nitsche et al. (1993 [DIRS 155218]; 1994 [DIRS 144515]) reported in their 25°C experiments that Pu colloids consist of only 3 percent to 5 percent of total Pu in the solution. Therefore, the measured Pu solubility is considered as true dissolved Pu concentration (since only a small amount of Pu will be in colloidal form).

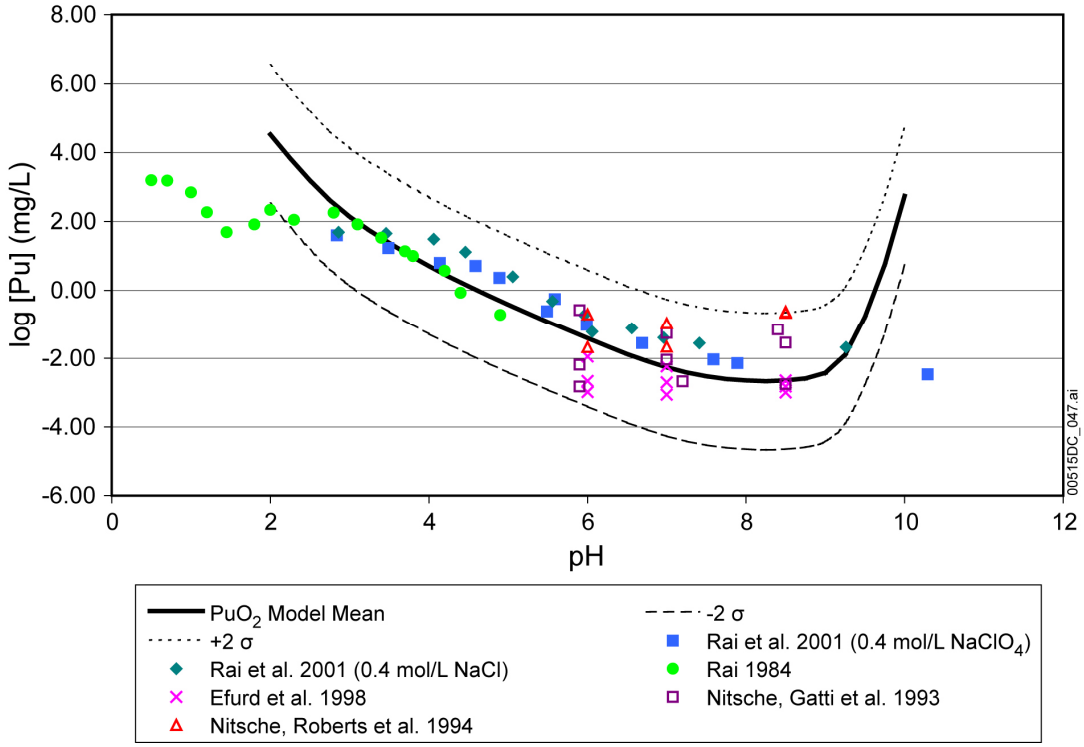

Source: *Pu model-lab.xls* (Appendix I).

NOTE: Modeled results are for log fCO_2 = -3.5

Figure 6.5-6. Comparison of Experimental Data with the Predictions of the Plutonium-Solubility Model

Table 6.5-2. Pore Size of Filters Used in Experiments

Experiment	Pore Size of Filter (nm)
Rai 1984 [DIRS 122768]	1.8
Rai et al. 2001 [DIRS 168392]	1.8
Efurd et al. 1998 [DIRS 108015]	4.1
Nitsche et al. 1993 [DIRS 155218]	4.1
Nitsche et al. 1994 [DIRS 144515]	4.1

Most of the data points from these five solubility experiments fall within the uncertainty range of the model. More importantly, no data points are above the upper bound of the model. The good match between model prediction and experimental measurement indicates this is a good model to represent Pu behavior. Model validation is further discussed in Section 7.2.2.

6.5.3.4 Uncertainties

This section discusses uncertainties of the adjusted-Eh Pu-solubility model.

6.5.3.4.1 Uncertainty in log K of the Solubility-Controlling Solids and Aqueous Species

The uncertainty in log K includes uncertainties in the thermodynamic properties of the controlling solid and significant dissolved species. The rationale behind the evaluation and combination of these uncertainties is discussed in some detail in Section 6.3.3.1. The total uncertainties applied to the solubility values correspond to that for log K of the dissolution reaction. This, in turn, includes the uncertainties in both the controlling solid species and the aqueous species.

The aqueous plutonium species accounting for more than 10 percent of the dissolved plutonium in the adjusted-Eh model adopted in Section 6.5.3.2 are evident by inspection of Figures 6.5-2 and 6.5-4. They are $PuO_2SO_4(aq)$, PuO_2^{+}, PuO_2F^{+}, PuO_2^{2+}, $PuO_2CO_3(aq)$, $PuO_2CO_3^{-}$, $PuO_2(CO_3)_2^{2-}$, and $PuO_2(CO_3)_3^{4-}$. The total uncertainties in log K given for these species by the NEA (OECD 2001 [DIRS 159027], Table 4.2) range, with two exceptions, from ±0.1 to ±0.9. The exceptions are $PuO_2CO_3(aq)$ and $PuO_2(CO_3)_2^{-}$ to which the OECD (2001 [DIRS 159027], Table 4.2) assigns uncertainties of ±3.0 and ±2.6. Hummel et al. (2002 [DIRS 161904], p. 284) disagree with the assignment of such large errors. They derive their log K values differently from the OECD (2001 [DIRS 159027]) and assign them uncertainties of ±0.5 and ±0.9. The updated NEA data set (Guillaumont et al. 2003 [DIRS 168382]) also assigned uncertainties of ±0.5 to both these species. In calculating the uncertainty of the dissolution reactions to these species, the log K uncertainties given by the NEA (OECD 2001 [DIRS 159027], Table 4.2) were used for all aqueous species except $PuO_2CO_3(aq)$ and $PuO_2(CO_3)_2^{2-}$, for which values of ±0.5 were used.

The extensive review of the OECD's (2001 [DIRS 159027]) report recommends −963.654 ± 6.324 kJ/mol for Gibbs free energies of formation for PuO_2(hyd,aged). Dissolution reactions for this solid to each of the eight dissolved plutonium species identified earlier were

evaluated in *log K uncertainties_a.xls*, included in Appendix I. The two greatest uncertainties were for the reactions to $PuO_2CO_3^-$ and $PuO_2(CO_3)_3^{4-}$. These are significant only at high pH. For $PuO_2CO_3^-$ the total uncertainty in log K for PuO_2(hyd,aged) is ±1.2. Corresponding uncertainties for $PuO_2(CO_3)_3^{4-}$ are ±1.5. Uncertainties for other dissolved species range from ±0.5 to ±1.3.

Therefore, the maximum uncertainty in log [Pu] values due to uncertainty in log K values is given the rounded value ±2.0. These total uncertainties are treated as normal distributions truncated at 2σ values (Section 6.3.3.1) so 1σ values are passed to TSPA-LA. The 1σ-uncertainty assigned to log[Pu] values is ±1.0.

6.5.3.4.2 Uncertainty from Fluoride Concentration

Table 6.5-3 lists the calculated logarithm of plutonium solubilities using the adjusted-Eh model using the fluoride levels indicated in Table 6.3-3 (10 times base case for CSNF waste packages and 27 and 95 times for codisposal waste packages and the invert). The three right-hand columns are the differences between the respective elevated F^- cases and the base case. The fugacity of CO_2 is set to $10^{-3.0}$.

Equation 6.5-1 summarizes the Pu-solubility model:

$$\log[Pu] = S(pH, \log fCO_2) + \varepsilon_1 + (\varepsilon_2 \times N) \qquad \text{(Eq. 6.5-1)}$$

The values for the parameters in this equation depend on the waste package type. Parameter $S\left(pH, \log f_{CO_2}\right)$ is the base solubility and is taken from Table 6.5-1. Parameter ε_1 is associated with the uncertainties in the log K data. Parameter ε_2 is associated with the uncertainties in the fluoride concentrations. Table 6.5-5 gives the values for the parameters ε_1 and ε_2.

Table 6.5-3 shows that the uncertainty terms $\varepsilon_2^{\text{CSNF}}$, $\varepsilon_2^{\text{CDSP-water influx}}$, and $\varepsilon_2^{\text{CDSP-vapor influx}}$ vary with pH. This pH dependence is implemented into the TSPA-LA model through the use of a multiplication factor (N) that is a function of pH. Values for N(pH) for both fuel types are given in Table 6.5-4. This modification requires that $\varepsilon_2^{\text{CSNF}}$, $\varepsilon_2^{\text{CDSP-water influx}}$, and $\varepsilon_2^{\text{CDSP-vapor influx}}$ values be fixed at the maximum value given in Table 6.5-3. For each realization in the TSPA-LA model the uncertainty parameters are sampled at the beginning of the realization. This sample value is then multiplied by 'N' at each time step to produce a modified ε_2, which is then added to the base solubility value.

Table 6.5-3. The Effect of Variations in Fluoride Concentration on Plutonium Solubility

	Base Case	CSNF	CDSP – Water-Influx Scenario	CDSP – Vapor-Influx Scenario	CSNF	CDSP – Water-Influx Scenario	CDSP – Vapor-Influx Scenario
pH	log[Pu] mg/L				Difference		
2.25	3.84E+00	3.87E+00	3.95E+00	4.13E+00	2.78E-02	1.10E-01	2.89E-01
2.50	3.19E+00	3.27E+00	3.43E+00	3.73E+00	7.76E-02	2.43E-01	5.41E-01
2.75	2.62E+00	2.80E+00	3.05E+00	3.44E+00	1.76E-01	4.27E-01	8.23E-01

Table 6.5-3. The Effect of Variations in Fluoride Concentration on Plutonium Solubility (Continued)

pH	**Base Case**	**CSNF**	**CDSP – Water-Influx Scenario**	**CDSP – Vapor-Influx Scenario**	CSNF	CDSP – Water-Influx Scenario	CDSP – Vapor-Influx Scenario
	log[Pu] mg/L				**Difference**		
3.00	2.14E+00	2.45E+00	2.77E+00	3.24E+00	3.086E-01	6.28E-01	1.10E+00
3.25	1.74E+00	2.17E+00	2.54E+00	3.08E+00	4.264E-01	7.99E-01	1.34E+00
3.50	1.38E+00	1.87E+00	2.29E+00	2.91E+00	4.931E-01	9.15E-01	1.53E+00
3.75	1.03E+00	1.53E+00	1.99E+00	2.69E+00	4.962E-01	9.57E-01	1.66E+00
4.00	7.08E-01	1.15E+00	1.62E+00	2.40E+00	4.421E-01	9.15E-01	1.69E+00
4.25	4.04E-01	7.58E-01	1.21E+00	2.02E+00	3.539E-01	8.05E-01	1.62E+00
4.50	1.19E-01	3.77E-01	7.77E-01	1.58E+00	2.581E-01	6.58E-01	1.47E+00
4.75	-1.52E-01	2.18E-02	3.51E-01	1.12E+00	1.737E-01	5.03E-01	1.27E+00
5.00	-4.12E-01	-3.03E-01	-5.22E-02	6.50E-01	1.093E-01	3.60E-01	1.06E+00
5.25	-6.65E-01	-6.00E-01	-4.23E-01	1.84E-01	6.512E-02	2.42E-01	8.49E-01
5.50	-9.11E-01	-8.74E-01	-7.57E-01	-2.65E-01	3.701E-02	1.54E-01	6.46E-01
5.75	-1.15E+00	-1.13E+00	-1.05E+00	-6.86E-01	2.004E-02	9.41E-02	4.62E-01
6.00	-1.37E+00	-1.36E+00	-1.32E+00	-1.07E+00	1.019E-02	5.56E-02	3.08E-01
6.25	-1.58E+00	-1.58E+00	-1.55E+00	-1.39E+00	4.708E-03	3.22E-02	1.90E-01
6.50	-1.77E+00	-1.76E+00	-1.75E+00	-1.66E+00	1.797E-03	1.84E-02	1.08E-01
6.75	-1.92E+00	-1.92E+00	-1.91E+00	-1.86E+00	4.319E-04	1.05E-02	5.69E-02
7.00	-2.04E+00	-2.04E+00	-2.03E+00	-2.01E+00	-1.083E-04	5.93E-03	2.86E-02
7.25	-2.12E+00	-2.12E+00	-2.11E+00	-2.10E+00	-2.442E-04	3.39E-03	1.41E-02
7.50	-2.17E+00	-2.17E+00	-2.17E+00	-2.16E+00	-2.366E-04	2.00E-03	7.20E-03
7.75	-2.20E+00	-2.20E+00	-2.19E+00	-2.19E+00	-2.044E-04	1.35E-03	4.22E-03
8.00	-2.20E+00	-2.20E+00	-2.20E+00	-2.20E+00	1.388E-04	1.28E-03	3.65E-03
8.25	-2.19E+00	-2.19E+00	-2.19E+00	-2.18E+00	7.128E-04	1.90E-03	5.64E-03
8.50	-2.14E+00	-2.14E+00	-2.13E+00	-2.12E+00	1.736E-03	4.86E-03	1.62E-02
8.75	-1.96E+00	-1.95E+00	-1.94E+00	-1.89E+00	6.765E-03	1.93E-02	6.75E-02
9.00	-1.31E+00	-1.29E+00	-1.26E+00	-1.16E+00	1.487E-02	4.21E-02	1.42E-01
9.25	-8.16E-02	-6.96E-02	-4.75E-02	3.49E-02	1.205E-02	3.41E-02	1.16E-01
9.50	1.46E+00	1.47E+00	1.48E+00	1.53E+00	6.534E-03	1.83E-02	6.45E-02
9.75	3.65E+00	3.65E+00	3.66E+00	3.68E+00	3.715E-03	1.00E-02	3.64E-02
Maximum					4.96E-01	9.57E-01	1.68E+00

Source: *puehadj f uncert.xls* and *Pu F Uncertainty.xls* in Appendix I.

Table 6.5-4. Multiplication Factor, (N), Used to Modify F^- Uncertainty Terms for Plutonium

pH	Multiplication Factor for F^- Uncertainty		
	CSNF	CDSP – Water-Influx Scenario	CDSP – Vapor-Influx Scenario
2.25	5.60E-02	1.15E-01	1.71E-01
2.50	1.56E-01	2.54E-01	3.21E-01
2.75	3.54E-01	4.46E-01	4.87E-01
3.00	6.22E-01	6.56E-01	6.50E-01
3.25	8.59E-01	8.35E-01	7.91E-01
3.50	9.94E-01	9.56E-01	9.06E-01
3.75	1.00E+00	1.00E+00	9.81E-01
4.00	8.91E-01	9.56E-01	1.00E+00
4.25	7.13E-01	8.41E-01	9.57E-01
4.50	5.20E-01	6.88E-01	8.68E-01
4.75	3.50E-01	5.26E-01	7.54E-01
5.00	2.20E-01	3.76E-01	6.29E-01
5.25	1.31E-01	2.53E-01	5.03E-01
5.50	7.46E-02	1.61E-01	3.83E-01
5.75	4.04E-02	9.83E-02	2.74E-01
6.00	2.05E-02	5.81E-02	1.83E-01
6.25	9.49E-03	3.37E-02	1.12E-01
6.50	3.62E-03	1.92E-02	6.38E-02
6.75	8.70E-04	1.09E-02	3.37E-02
7.00	-2.18E-04	6.20E-03	1.69E-02
7.25	-4.92E-04	3.54E-03	8.35E-03
7.50	-4.77E-04	2.09E-03	4.26E-03
7.75	-4.12E-04	1.41E-03	2.50E-03
8.00	2.80E-04	1.34E-03	2.16E-03
8.25	1.44E-03	1.99E-03	3.34E-03
8.50	3.50E-03	5.07E-03	9.60E-03
8.75	1.36E-02	2.01E-02	4.00E-02
9.00	3.00E-02	4.39E-02	8.39E-02
9.25	2.43E-02	3.56E-02	6.90E-02
9.50	1.32E-02	1.91E-02	3.82E-02
9.75	7.49E-03	1.04E-02	2.16E-02

Source: *Pu F Uncertainty.xls* in Appendix I.

6.5.3.4.3 Summary of Pu-Solubility Model Uncertainty

The Pu concentrations used in the TSPA-LA modeling are selected from a distribution of values defined by the concentrations given in Table 6.5-1 plus or minus the uncertainties in

concentrations due to uncertainties in the log K values and resulting from uncertainties in the fluoride concentrations (Sections 6.5.3.4.1 and 6.5.3.4.2).

These are described by the following equation:

$$\log[\mathrm{Pu}] = S(\mathrm{pH}, \log fCO_2) + \varepsilon_1 + (\varepsilon_2 \times N) \qquad \text{(Eq. 6.5-2)}$$

where

$S(pH, \log f_{CO_2})$ is log of the modeled Pu concentration as a function of pH and $\log f_{CO2}$ given by Table 6.5-1

ε_1 is the uncertainty term associated with uncertainty in log K values. As discussed in Section 6.5.3.4.1, this term has a normal distribution with $\sigma = 1.0$, truncated at 2σ. The value used during a given run is chosen from within this distribution by the TSPA-LA model.

ε_2 is the uncertainty term associated with variations in fluoride concentration. As discussed in Section 6.5.3.4.2, the range of fluoride uncertainty for a given TSPA-LA run depends on the type of waste package being considered and the pH. This term has a right-angled triangular distribution with the minimum (a) and most probable (b) values equal to one another and the maximum (c) value corresponding to the maximum value in the appropriate column of Table 6.5-3.

N is the factor by which the maximum uncertainty ε_2 is normalized for pH. Values of N are given by Table 6.5-4 and are ≤ 1.0.

The distribution properties of these uncertainty terms are summarized in Table 6.5-5.

Table 6.5-5. Uncertainty Terms of log[Pu]

Uncertainty Term	Associated With	Distribution Type	Distribution Parameter	Applicable To
ε_1	Uncertainties in log K	Normal Truncated at $\pm 2\sigma$	$\mu = 0$, $\sigma = 1.0$[a]	Values in Table 6.5-1
$\varepsilon_2^{\mathrm{CSNF}}$	Fluoride concentration in CSNF waste packages	Triangular	a = b = 0, c = 0.50	CSNF waste packages
$\varepsilon_2^{\mathrm{CDSP\text{-}Water\ Influx}}$	Fluoride concentration in codisposal waste packages (water-influx scenario)	Triangular	a = b = 0, c = 0.96	Codisposal waste packages and the invert
$\varepsilon_2^{\mathrm{CDSP\text{-}Vapor\ Influx}}$	Fluoride concentration In CDNR waste package (vapor-influx scenario)	Triangular	a = b = 0, c = 1.69	Codisposal waste packages and the invert

NOTE: [a] For ionic strength values between 1 and 3, Log K uncertainty should be treated as a normal distribution truncated at $\pm 2\sigma$ with distribution parameters $\mu = 0$, $\sigma = 1.04$ (Section 6.3.3.4, Equation 6.3-7).

6.5.3.5 Redox Conditions Within Waste Packages

No direct measurements of redox conditions within breached waste packages are available. Nonetheless, since (1) corrosion of waste package materials and waste forms consumes oxygen and, thus, it lowers redox conditions within waste packages; and (2) breached waste packages are not totally open to air, and transport of oxygen gas into the waste package is limited by waste package cracks or holes that can be plugged by corrosion products of waste package materials and waste forms; (3) redox conditions within waste packages cannot be higher than that given by Equation 6.5-5. Therefore, the adjusted-Eh Pu-solubility model, which uses Equation 6.5-7 to set redox conditions, is conservative.

6.5.4 Logic Basis for Adjusted-Eh Pu-Solubility Model

6.5.4.1 Theoretical fO_2 Model

The calculations for this model are carried out with the solution redox conditions controlled by theoretical equilibrium between the solution and the atmosphere with an oxygen fugacity (fO_2) of 0.2 bars.

6.5.4.1.1 Modeling Results

The plutonium solubility for a range of pH and fCO_2 values calculated using PuO_2(hyd,aged) as the controlling solid with fO_2 = 0.2 bars is shown in Figure 6.5-7. The variation of solubility with pH and fCO_2 results from the presence in solution of Pu(V) and Pu(VI) species including PuO_2^{2+} and Pu(V) and(VI) aqueous complexes with CO_3^{2-}, F^- and SO_4^{2-}. The stability constants used in the modeling were those of the NEA compilation of chemical thermodynamic data (OECD 2001 [DIRS 159027]) included in the project databases *Data0.ymp.R2* ((DTN: MO0302SPATHDYN.000 [DIRS 161756]); Section 4.1 and Table 4-1). At each fCO_2, plutonium solubility increases with pH under alkaline conditions, while under acidic conditions it increases conversely to pH. This U-shape (or V-shape) curve is typical for actinides.

When modeling with fO_2 = 0.2 bars at pH < 3.75, the EQ3NR calculations do not converge. Neither do EQ3NR calculations when pH is greater than 7.5 to 10.5, depending on fCO_2. The lack of convergence is because the modeling code is unable to reach a mathematical solution at these conditions. For example, at high pH values, and especially at high fCO_2 values, formation of the strong $PuO_2(CO_3)_3^{4-}$ complex may require the code to add very large amounts of CO_2 or Pu, or both, to form the complex, or to add a very large amount of Na^+ to balance the charge of large quantities of this complex. At low pH values, PuO_2SO_4(aq) dominates. Under the relatively high oxidation state represented by fO_2 = 0.2 bars and with the use of SO_4^{2-} as the charge-balancing anion at low pH values, EQ3NR is also unable to reach a mathematical solution at low pH values (Section 6.4.4).

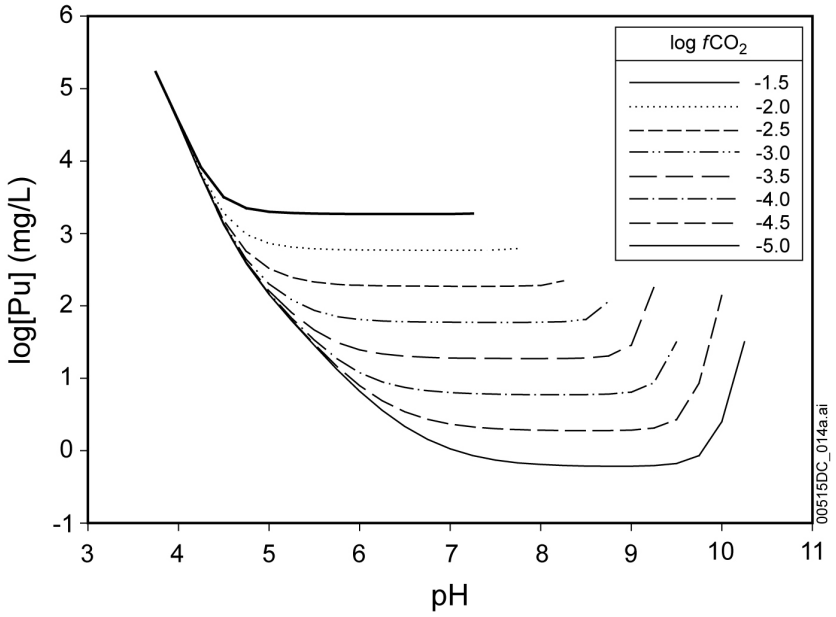

Source: *PuO2_hyd_aged_sol.jnb* in Appendix I.

Figure 6.5-7. PuO_2(hyd,aged) Solubility Modeled with Theoretical fO_2 as a Function of pH and log fCO_2

6.5.4.1.2 Comparison with Experimental Measurements

Figure 6.5-8 presents the modeling results at log fCO_2 = -3.5 (bars) along with Pu-solubility measurements from five experiments (Rai 1984 [DIRS 122768]; Nitsche et al. 1993 [DIRS 155218]; Nitsche et al. 1994 [DIRS 144515]; Efurd et al. 1998 [DIRS 108015]; Rai et al. 2001 [DIRS 168392]). These five experiments have been discussed in Section 6.5.3.3.

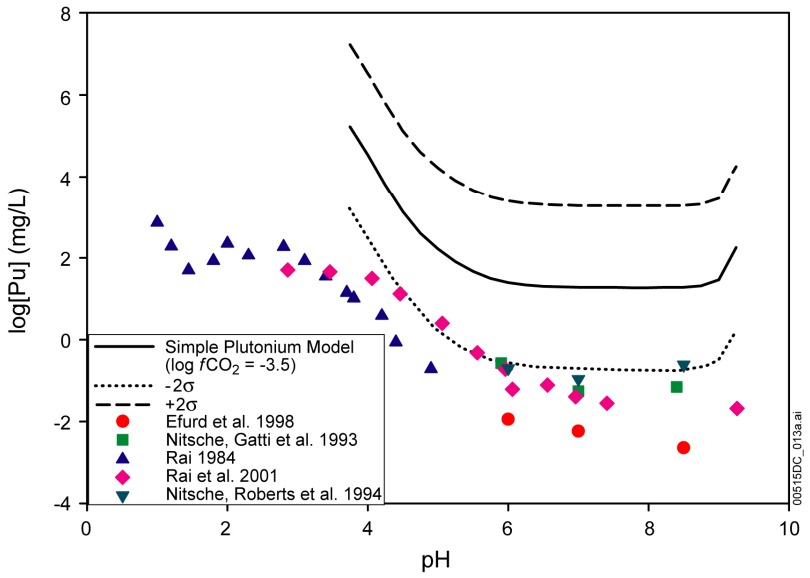

Source: *simple pu solb.jnb* in Appendix I.

Figure 6.5-8. Comparison of the Theoretical fCO_2, PuO_2(hyd,aged) Model with Pu Solubility Measurements

The inconsistency and the large difference between the experimental and modeling results strongly suggest that this model using a redox potential calculated from fO_2 = 0.2 bars does not represent Pu-solubility behavior. Furthermore, the high Pu concentrations predicted by the theoretical fO_2 model are unrealistic because it does not take into account the formation of Pu colloids. It is well known that when the total concentration of plutonium is higher than 1.0E-6 mol/L, plutonium polymers (colloids) form (Choppin 1983 [DIRS 168395]). The formation of Pu colloids is quite rapid and its rate is third order in Pu concentration. Colloids remove Pu from the aqueous phase and, thus, reduce the dissolved Pu concentration. The predicted Pu concentration by the theoretical fO_2 model ranges from 2.54E-6 mol/L to 2.25 mol/L, which is above the threshold for colloids. Thus, it is reasonable to expect that these high concentrations of Pu in aqueous phase cannot be sustained. In other words, because of colloids, such a high Pu solubility predicted by the theoretical fO_2 model is unrealistic.

6.5.4.1.3 Determining the Cause of the Discrepancy

The discussion in Section 6.5.4.1.2 concluded that the theoretical fO_2 model with redox potential calculated from fO_2 = 0.2 bars does not correctly represent Pu behavior in solution. Therefore, a more-sophisticated Pu-solubility model is needed to correctly represent Pu behavior in water. The first step in developing such a model is to examine in more detail the cause of the discrepancy between this model and experimental results.

One of the properties of Pu is that species of different oxidation states (from III to VII) can coexist in equilibrium in many aqueous systems (Choppin 1983 [DIRS 168395]; 2003 [DIRS 168308]), although for natural aqueous environments, Pu(VII) is not important (Silva and Nitsche 1995 [DIRS 112092]). The oxidation state has a large impact on the geochemical behavior of Pu in aqueous environments.

Figure 6.5-9 shows the distribution of different oxidation states in experiments reported by Nitsche et al. (1993 [DIRS 155218]; 1994 [DIRS 144515]). For pH from 6 to 8.5, the dominant Pu species is Pu(V).

Pu(V) is also the dominant species in the experiments conducted by Rai (1984 [DIRS 122768]) for pH from 3.5 to 5, as shown in Figure 6.5-10.

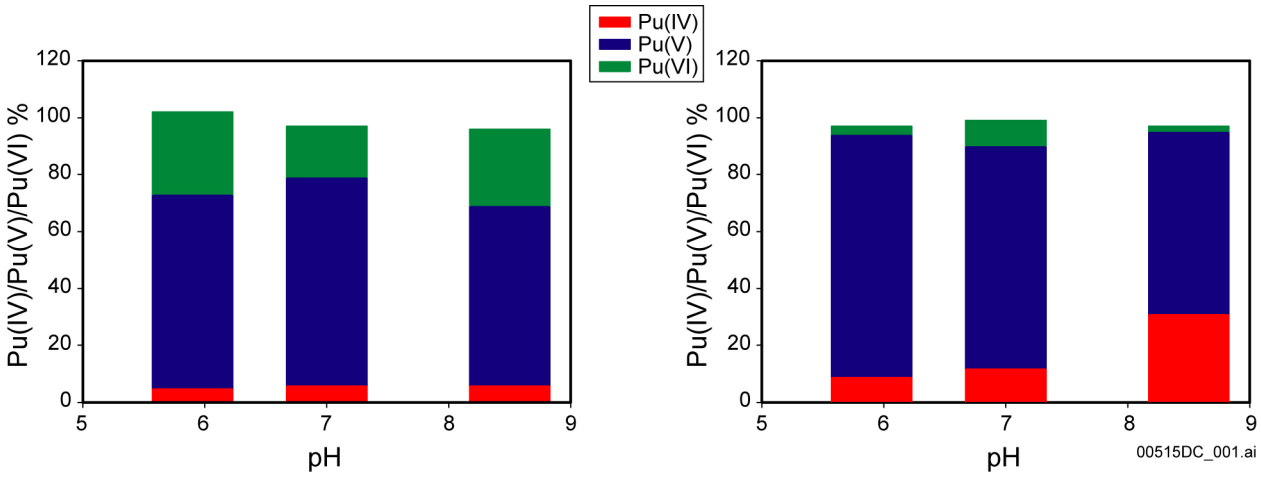

Source: *Nitsche93aSDist.jnb* and *Nitsche94SDist.jnb* in Appendix I

NOTE: Data in the left figure are from Nitsche et al. (1993 [DIRS 155218]), while data in the right figure are from Nitsche et al. 1994 [DIRS 144515]. The fCO_2 values used in these experiments were $10^{-1.2}$, $10^{-1.8}$, and $10^{-3.2}$ bars for the left figure and $10^{-0.5}$ bars, $10^{-1.2}$ bars, and $10^{-2.6}$ bars in the right figure for pH values of 6, 7, and 8.5, respectively.

Figure 6.5-9. Pu-Oxidation States Distribution in Pu-Solubility Experiments

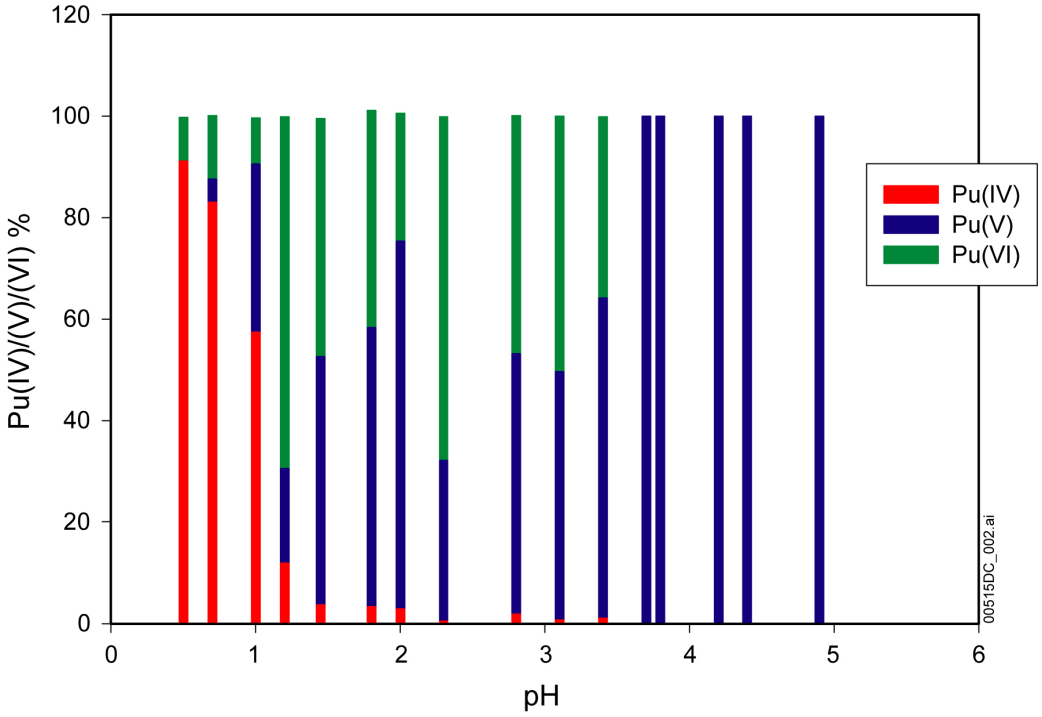

Source: *Rai84SpecDistr.jnb* in Appendix I.

NOTE: Data is from Rai 1984 [DIRS 122768].

Figure 6.5-10. Pu-Oxidation States Distribution in Pu-Solubility Experiments

In natural waters, Pu(V) is observed to be the dominant dissolved species (Choppin et al. 1986 [DIRS 168377]; Choppin and Stout 1989 [DIRS 168379]; Choppin 2003 [DIRS 168308]; Murphy and Shock 1999 [DIRS 168433]). However, the oxidation state distribution in the EQ3 results using the theoretical fO_2 model with fO_2 = 0.2 bars shows that Pu(VI) is the dominant species over the entire pH range modeled (Appendix I, Spreadsheet *PuO2_hyd_aged Solubility.xls*).

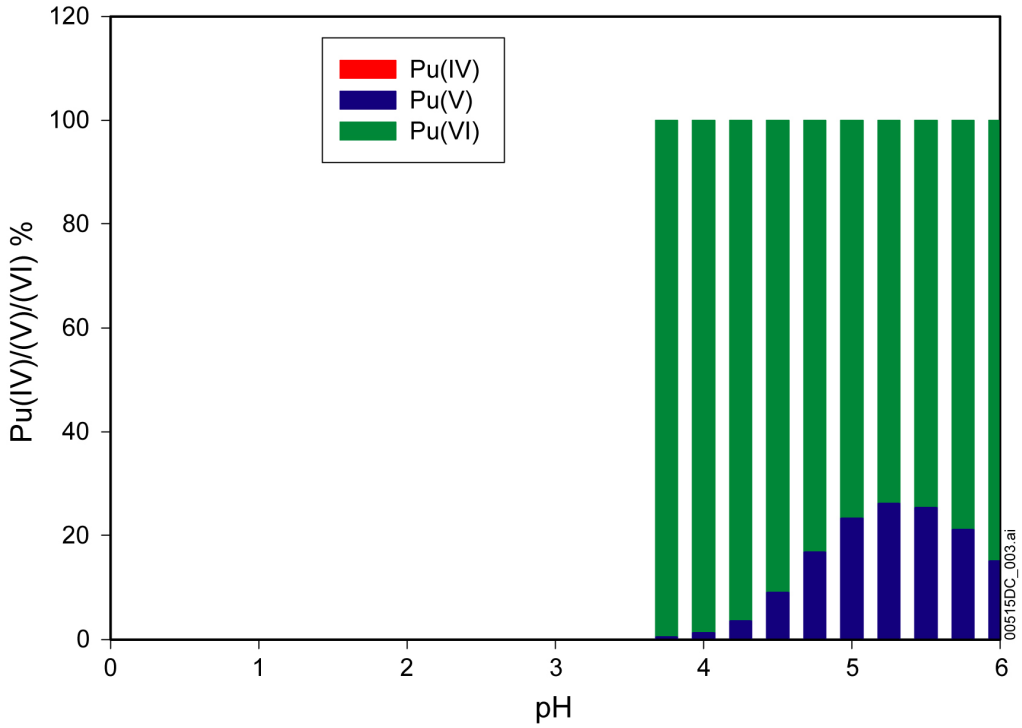

Source: *simplespecdistr.jnb* in Appendix I.

Figure 6.5-11. Pu-Oxidation States Distribution Given by the Simple PuO_2(hyd,aged) Model

Since the distribution of different oxidation states is mainly controlled by redox reactions, the discrepancy between the theoretical fO_2 model results and solubility experiments as well as observations in natural waters strongly suggests that the redox potential, based on fO_2 = 0.2 bars, causes the discrepancy.

6.5.4.2 Redox Potential

6.5.4.2.1 Redox Potentials in Natural Waters

There are several different ways to represent redox potential. Oxygen fugacity is convenient and commonly used in geochemistry. In many systems, the oxygen fugacity is approximately equal to its partial pressure, so when a system is open to air, it is assumed that fO_2 = 0.2 bars. As already pointed out, this convention was used in the theoretical fO_2 model described earlier.

Other parameters used to represent redox conditions are Eh and pe (Eh = 0.0592pe at 25°C). Assuming fO_2 = 0.2 bars is equivalent to assuming (Wolery 1992 [DIRS 100836]; Krauskopf and Bird 1995 [DIRS 101702]; Langmuir 1997 [DIRS 100051]):

$$Eh(volt.) = 1.22 - 0.0592\,pH \quad \text{(Eq. 6.5-3)}$$

Equation 6.5-3 is given by the Nernst equation for reaction:

$$2H_2O = O_2 + 4H^+ + 4e^- \quad \text{(Eq. 6.5-4)}$$

when fO_2 = 0.2 bars. This is the upper bound of the water stability field in an Eh–pH diagram. Because water is unstable above this line, natural aqueous systems do not exist.

However, by analyzing 6,200 Eh and pH measurements in natural waters, Baas Becking et al. (1960 [DIRS 168371]) found that for pH between 3.2 and 12.6 there is an upper boundary for Eh–pH conditions in natural waters, that is:

$$Eh(volt.) = 1.04 - 0.0592\,pH \quad \text{(Eq. 6.5-5)}$$

In other words, in these 6,200 samples, not one measurement exceeded the limit set by Equation 6.5-5. This equation is a more-realistic boundary of redox conditions in natural waters that are in contact with the atmosphere (Krauskopf and Bird 1995 [DIRS 101702]). However, "none of the likely inorganic reactions yielded characteristics remotely resembling" Equation 6.5-5 (Baas Becking et al. 1960 [DIRS 168371]). Thus, this upper limit is empirical.

There are several plausible explanations for the discrepancy between the theoretical upper boundaries given by Equations 6.5-3 and 6.5-5. One is that the noble metal electrodes commonly used to measure solution Eh values do not respond to the couple defined by Equation 6.5-4 (Langmuir 1997 [DIRS 100051], Section 11.1.4). Other researchers attribute it to the slow kinetics of redox reactions involving O_2 (Krauskopf and Bird 1995 [DIRS 101702]; Stumm and Morgan 1996 [DIRS 125332]; Langmuir 1997 [DIRS 100051]). It has been accepted that "dissolved oxygen does not exert the potential expected if it is functioning at equilibrium" (Garrels and Christ 1990 [DIRS 144877]).

For pH values between –0.6 to 3.2, the upper limit of Eh follows (Baas Becking et al. 1960 [DIRS 168371]):

$$Eh(volt.) = 0.860 \quad \text{(Eq. 6.5-6)}$$

6.5.4.2.2 Redox Potential Measurements at Yucca Mountain

Figure 6.5-12 presents measured Eh–pH values for waters obtained from wells at or near Yucca Mountain. Table 6.5-6 lists the data sources. Most of these measurements were made in situ, either downhole or using a flow-through cell. Some samples are bailed samples. The in situ samples provide more accurate Eh measurements since equilibration with the atmosphere at the wellhead does not occur as may happen in bailed samples taken in open containers.

Equations 6.5-3 and 6.5-5 are also plotted in Figure 6.5-12 for comparison with measured Eh–pH values. Figure 6.5-12 shows that all the Eh-pH measurements made at Yucca Mountain are below Equation 6.5-5.

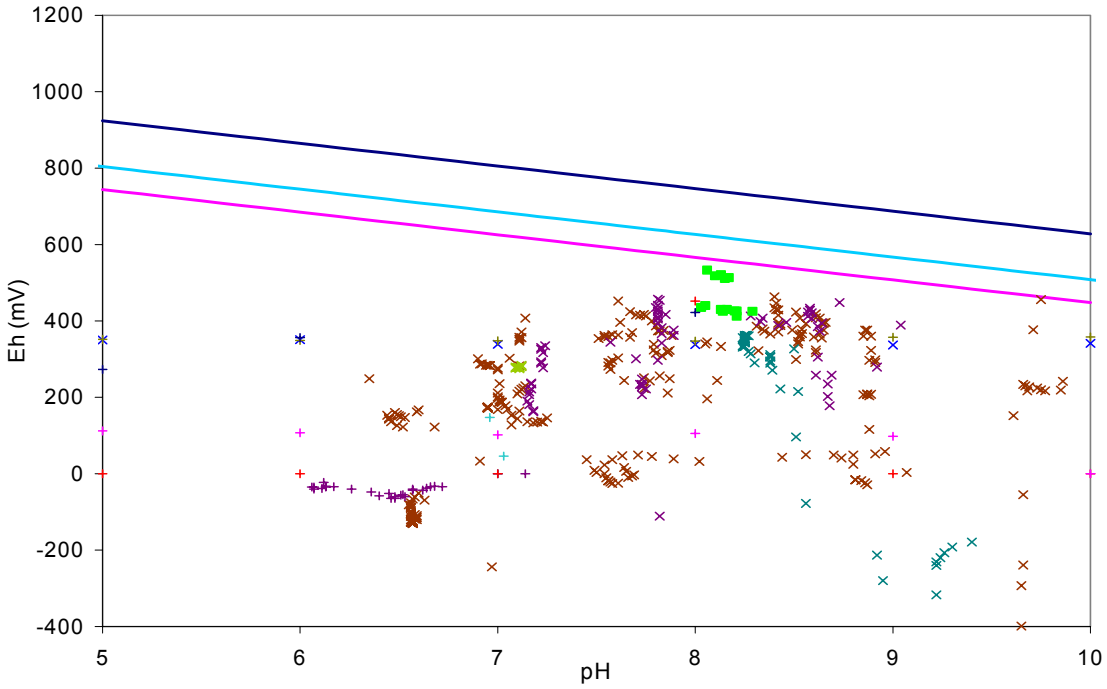

■	USW SD-6ST1 Flow-through	+	UE-25 WT #3 Downhole
x	NC- '99 to '01 Flow-through	+	UE-25 WT #3 Flow-through
x	NC-EWDP-01S Flow-through	+	UE-25 WT #17 Downhole
x	NC-EWDP-03S Downhole	+	UE-25 WT #17 Pumped
x	NC-EWDP-01DX Downhole	+	UE-25 WT #17 Bailed
x	NC-EWDP-01,3,9S(X) Flow-through	+	UE-25 WT #17 Flow-through Pumped

Source: Table 6.5-6.

NOTE: The upper line shows the theoretical oxidation potential at fO_2 = 0.2 bars (Equation 6.5-3) and the lower line shows the upper limit for empirical Eh measurements in natural waters (Equation 6.5-5). The middle line shows the adjusted Eh (Equation 6.5-7) discussed in Section 6.5.4.3.

Figure 6.5-12. Eh–pH Measurements at Yucca Mountain

Table 6.5-6. Data Sources for Figure 6.5-12

	Sample	Source	Details
■	USW SD-6ST1	LA9907AM831234.010 [DIRS 149210]	Flow-through cell measurements for well water USW SD-6ST1. Depth is pump depth. No casing in this well below the water table.
x	NC- '99 to '01	LA0206AM831234.001 [DIRS 160051]	Flow-through cell measurements from Nye County EWDP wells, Nevada
x	NC-EWDP-01S	LA0004AM831234.001 [DIRS 149202]	Flow-through cell measurements from well NC-EWDP-O1S in Amargosa Valley, Nevada
x	NC-EWDP-03S	LA0004AM831234.002 [DIRS 149213]	Downhole probe measurements from well NC-EWDP-03S, in Amargosa Valley, Nevada

Table 6.5-6. Data Sources for Figure 6.5-12 (Continued)

	Sample	Source	Details
x	NC-EWDP-01DX	LA9907AM831234.003 [DIRS 149196]	Downhole measurements from well NC-EWDP-01DX in Amargosa Valley, Nevada
x	NC-EWDP-01,3,9S (X)	LA9907AM831234.009 [DIRS 149209]	Flow-through cell measurements from wells NC-EWDP-01S, NC-EWDP-03S and NC-EWDP-09SX in Amargosa Valley, Nevada
+	UE-25 WT #3 Downhole	LAAM831311AQ98.004 [DIRS 168346]	Eh data of downhole measurements from well UE-25 WT #3
+	UE-25 WT #3 Flow-through	LAAM831311AQ98.007 [DIRS 149520]	Flow-through cell and static measurements of water from UE-25 WT #3. Analysis made on flow-through samples as they flowed directly from pump outlet through a cell, to avoid contact with air.
+	UE-25 WT #17 Downhole	LAAM831311AQ98.003 [DIRS 168347]	Eh data of downhole measurements from well UE-25 WT #17
+	UE-25 WT #17 Pumped	LAAM831311AQ98.005 [DIRS 149181]	Field measurements of pumped water samples from well UE-25 WT #17. Static measurements obtained in containers open to the atmosphere during analysis.
+	UE-25 WT #17 Bailed	LAAM831311AQ98.008 [DIRS 149521]	Analysis of bailed samples from well UE-25 WT #17. Data values are static field measurements in an open beaker.
+	UE-25 WT #17 F-t Pumped	LAAM831311AQ98.009 [DIRS 168348]	Eh data from flow-through cell measurements of pumped water samples from well UE-25 WT #17

6.5.4.3 The Empirical-Eh Pu-Solubility Model

Section 6.5.4.1.2, concludes that the theoretical fO_2 model with $fO_2 = 0.2$ bars does not correctly represent Pu behavior in aqueous systems because the model (due to differing oxidation states of plutonium) is sensitive to redox potential. The discussion in Section 6.5.4.2 further suggests that Equation 6.5-5 is a more-realistic upper limit for redox conditions in natural waters and for the repository than Equation 6.5-3, which corresponds to $fO_2 = 0.2$ bars as used in the theoretical fO_2 model previously discussed.

A modified Pu-solubility model (the empirical-Eh model) uses Equation 6.5-5 to set redox conditions for pH values between 3.2 to 12, and Equation 6.5-6 to set redox conditions for pH values between 1.0 to 3.2, while all other conditions are kept the same as described in Section 6.5.2. The controlling phase is still PuO_2(hyd,aged).

Figure 6.5-13 shows the distribution of different oxidation states of Pu species in the empirical-Eh model. Figure 6.5-13 also shows Pu(V) is the dominant oxidation state for pH values between 3 and 9. This matches experimental results very well (Figures 6.5-9 and 6.5-10).

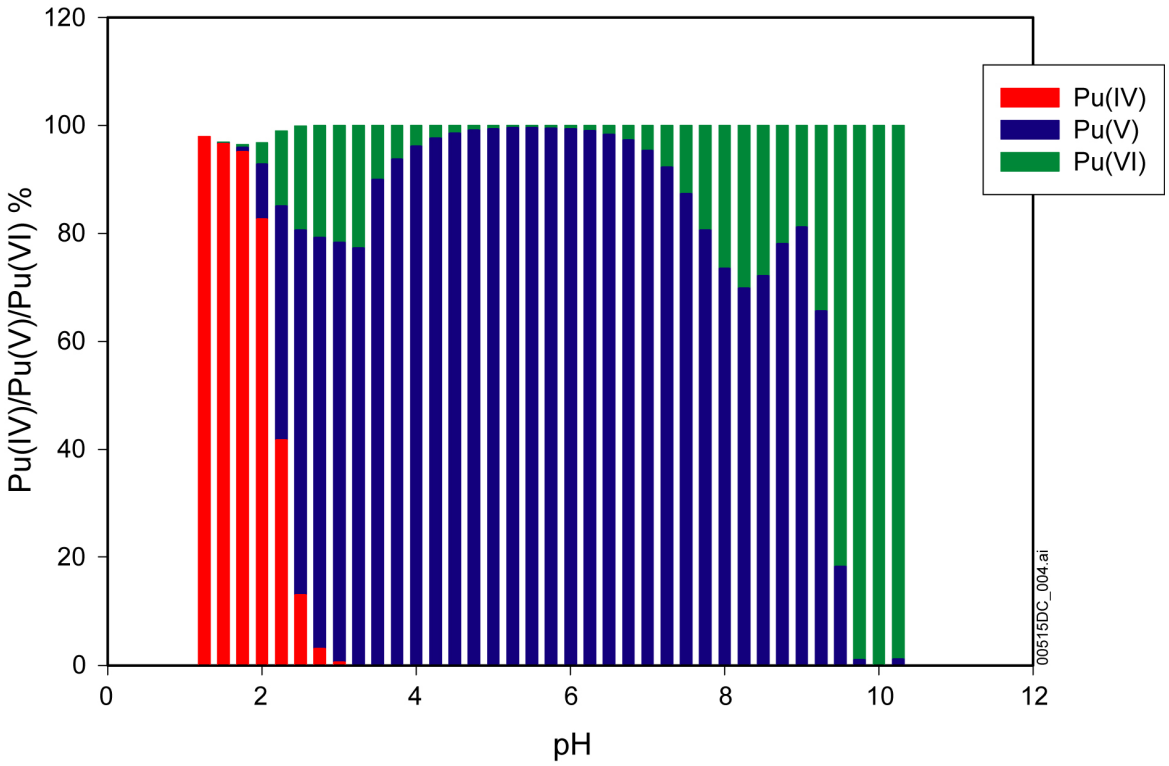

Source: *pu 104 spe dist.jnb* in Appendix I.

NOTE: log fCO_2 = –3.5 bars, Equation 6.5-5 for pH > 3.2, Equation 6.5-6 for pH <3.2. Note that for pH ≤2, the total of Pu(IV), Pu(V), and Pu(VI) is less than 100% because of the existence of Pu(III).

Figure 6.5-13. Pu Oxidation States Distribution Given by the Eh Model

Pu solubility given by the empirical-Eh model is presented in Figure 6.5-14, along with measured Pu solubilities under compatible conditions (Rai 1984 [DIRS 122768]; Nitsche et al. 1993 [DIRS 155218]; Nitsche et al. 1994 [DIRS 144515]; Efurd et al. 1998 [DIRS 108015]; Rai et al. 2001 [DIRS 168392]). These results agree much more closely with the experimental results than those obtained from the fO_2 model and most of the measured Pu solubilities fall within the uncertainty range.

The good match between the modeling results and experimental results in the oxidation state distribution and Pu solubility indicate that the empirical-Eh model better represents Pu solubility.

However, Figure 6.5-14 also shows that although the mean modeled Pu concentration is below most of the experimental results, most are within the upper half of the uncertainty range model. There are several possible explanations for this uneven distribution.

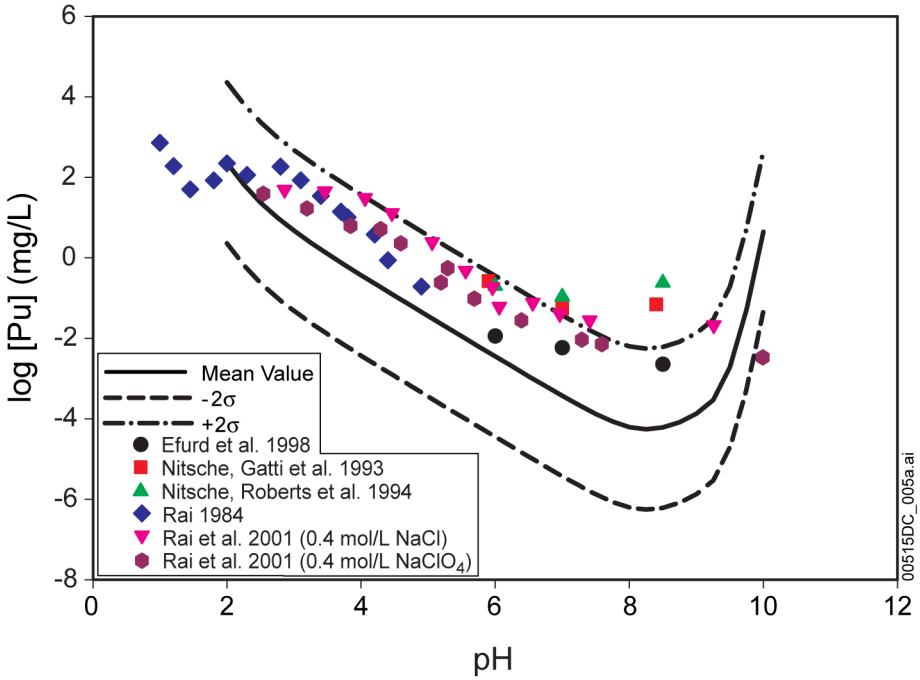

Source: *pu solb 104-3.jnb* in Appendix I.

NOTE: log fCO_2 = –3.5 bars, Equation 6.5-5 for pH > 3.2, Equation 6.5-6 for pH <3.2.

Figure 6.5-14. Pu Solubility Given by the Eh model

The first explanation is that the actual Eh in the experiments does not exactly follow Equations 6.5-5 and 6.5-6. Note that Equations 6.5-5 and 6.5-6 are empirical relations obtained from measurements of natural waters. The Eh measured in individual experiments may have a slightly different value. For example, in Rai's (1984 [DIRS 122768]) experiments, measured Eh values for pH < 4.2 are systematically higher than the values given by Equations 6.5-5 and 6.5-6, as shown in Figure 6.5-14. Moreover, the transition point where Eh becomes horizontal also shifts from pH = 3.2 given by Baas Becking et al. (1960 [DIRS 168371]) to about pH = 2.0 in Rai's (1984 [DIRS 122768]) experiments. For pH between 2 and 3.8, the measured Eh is about 50 to 60 mv higher than the values given by Equation 6.5-6. The measured Eh for pH > 4.25 in Rai's (1984 [DIRS 122768]) experiments is lower than the values given by Equation 6.5-5 by 200 to 300 mv. This was attributed to poor system poise (Rai 1984 [DIRS 122768]).

Adding 60 mv to the calculated Eh value given by Equation 6.5-5, a modified Eh–pH relation is given below:

$$Eh = 1.10 - 0.0592\,pH \qquad \text{(Eq.6.5-7)}$$

Using it for pH ≤ 3, the calculated Pu solubility matches Rai's (1984 [DIRS 122768]) measured Pu solubility very well, as shown in Figure 6.5-15. Moreover, this model also reproduces results found by Efurd et al. (1998 [DIRS 108015]) (Figure 6.5-16).

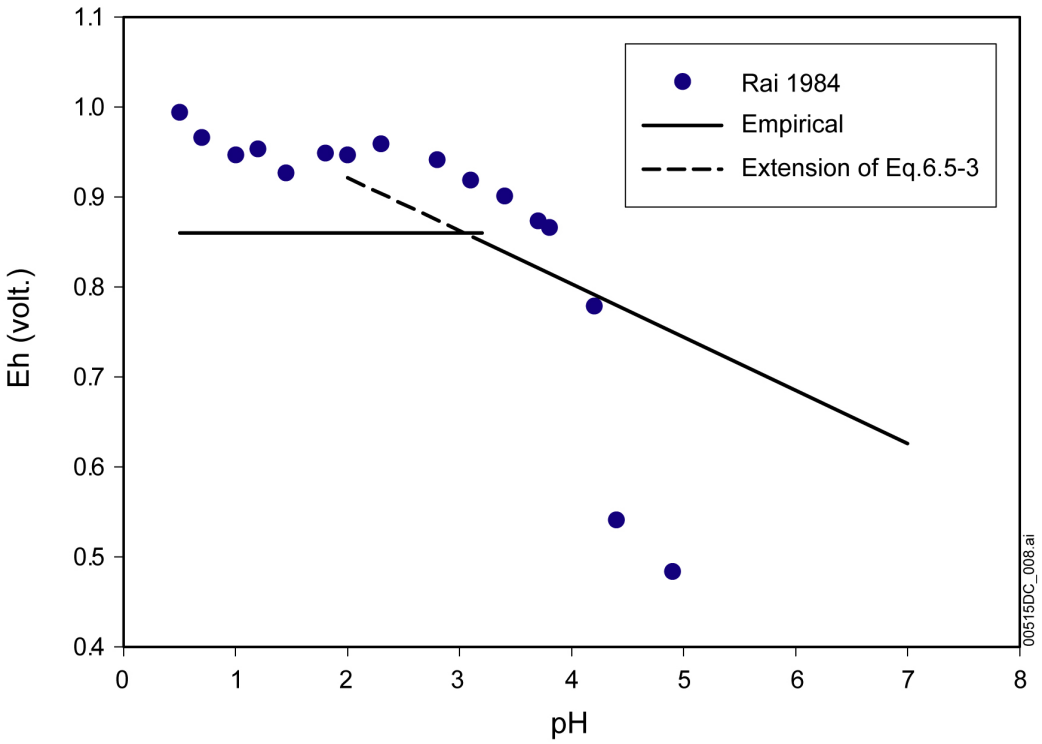

Source: *pu solb 104-3.jnb* in Rai 1984 [DIRS 122768], Appendix I; Baas Becking et al. 1960 [DIRS 168371].

Figure 6.5-15. Measured Eh in Rai Experiments and the Empirical-Eh Relation Given by Baas Becking et al.

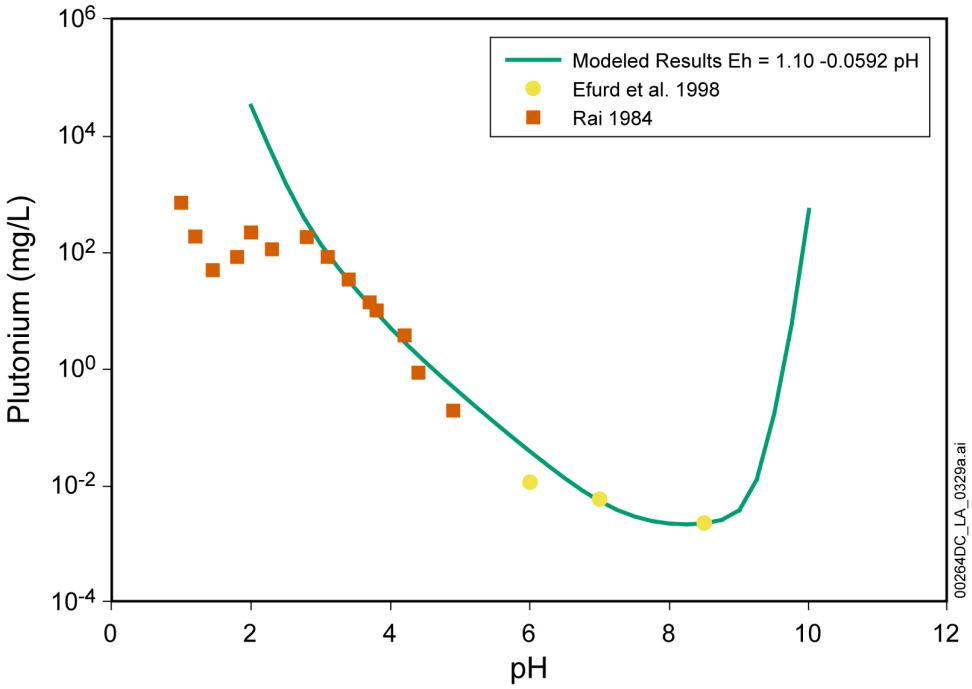

Source: *PuEhAdjModel.jnb* in Appendix I.

Figure 6.5-16. Modeled Results with Adjusted-Eh (Eh = 1.10 – 0.0592 pH) and Experimental Results

The second explanation is that the measured Pu concentrations are not true dissolved Pu, but contain Pu colloids or polymers, or both, which could be smaller than the filter size. For example, Kim and Kanellakopulos (1989 [DIRS 122387]) reported in their experiments that a large percent (80 percent) of Pu is in Pu(IV) colloid form even though the filter size is as small as 1 nm.

The third explanation is that the experimental solutions have a higher ionic strength than that modeled, which yields a higher solubility because of the "salting-in" effect. For example, as discussed in Section 6.5.3.3, in experiments conducted by Rai et al. (2001 [DIRS 168392]), the solutions are 0.402 m NaCl and 0.408 m $NaClO_4$. The ionic strengths of these solutions are about 1 molal.

6.5.5 Effect of Mineral Aging on the Model

The adjusted-Eh model produces results that match experimental results very well. The solubility product of PuO_2(hyd,aged) recommended by the NEA (OECD 2001 [DIRS 159027]) is for Pu(IV) hydrated oxide/hydroxide "aged for several months near room temperature." The experiments used to validate the model were also carried out for only a few months. The aging process of Pu(IV) hydrated oxide/hydroxide actually can go on for several years. For example, Rai and Ryan (1982 [DIRS 112060]) observed continuous aging for a period of 1,266 days, during which the measured Pu solubility continuously decreased.

The OECD (2001 [DIRS 159027], Section 17.2.2.3) notes that radiolysis tends to decrease the stability of PuO_2 solids and that when the crystalline dioxide $^{239}PuO_2$ is in contact with water, it slowly converts to (or becomes coated with) a less-crystalline form. Likewise, Rai and Ryan (1982 [DIRS 112060]) point out that crystalline $^{238}PuO_2$ in contact with water converts to the amorphous solid. Thus, the decreased solubility brought about by aging is balanced by the increased solubility due to radiolysis. For comparison, the solubilities for both minerals (PuO_2(hyd,aged) and PuO_2(c)) are shown in Figure 6.5-17.

The NEA chemical thermodynamic data for PuO_2(hyd,aged) are based on several studies using different experimental approaches and aging times that gave similar results. Their data represent a solid for which the effects of aging are balanced by the effects of radiolysis. Therefore, Pu solubilities calculated using this solid and the adjusted Eh should give realistic Pu concentrations.

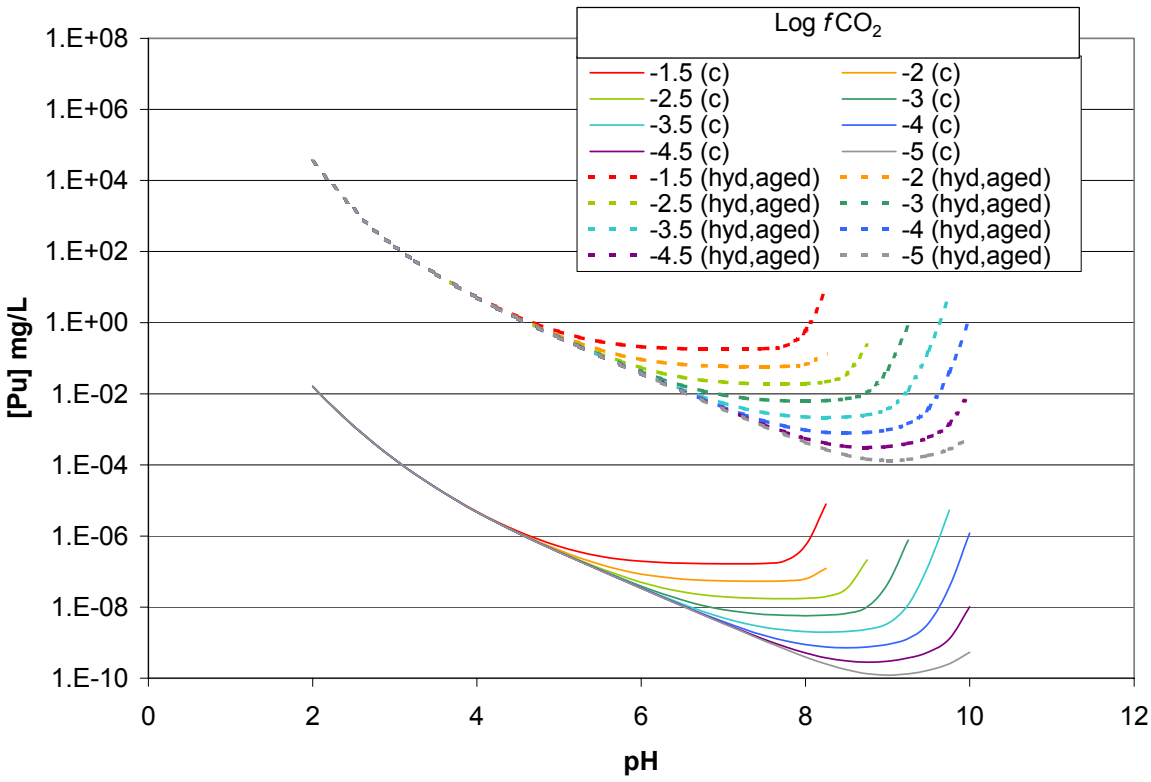

Source: *Pu Alternative.xls* in Appendix I.

Figure 6.5-17. Comparison of Solubilities Between Crystalline PuO_2(c) and PuO_2(hyd,aged)

6.5.6 Relationship of PuO_{2+x} to Plutonium Solubility

Haschke et al. (2000 [DIRS 150367]), Haschke and Oversby (2002 [DIRS 161911]), and Haschke and Allen (2002 [DIRS 162001]) describe a solid with the general formula PuO_{2+x} that forms from PuO_2 in the presence of water vapor at temperatures from 25°C to 350°C. At 300K, free energies of formation of this solid range from –1,033 kJ/mol at x = 0.1 to –1,146 kJ/mol at x = 0.5 (Haschke and Allen 2002 [DIRS 162001]). At 298.15K the free energy of formation of PuO_2(hyd,aged) is –964 kJ/mol (OECD 2001 [DIRS 159027], Table 4.1). This phase was used to calculate the base-case, adjusted-Eh plutonium solubility in Section 6.5.3.

PuO_{2+x} contains both Pu(IV) and Pu(V) in the proportion (1-x):x. Haschke et al. (2000 [DIRS 150367]) attributed the increase in the average oxidation state in PuO_{2+x} to the presence of Pu(VI), and concluded that this would make plutonium more soluble than PuO_2 because Pu(VI) ions are more soluble than Pu(IV) ions. Haschke et al. (2000 [DIRS 150367]) also conclude that because PuO_{2+x} forms from PuO_2 in the presence of O_2, it is more stable. This is borne out by the free energy data from Haschke and Allen (2002 [DIRS 162001]) showing that as 'x' increases, the free energy becomes more negative. However, Haschke and Allen (2002 [DIRS 162001]) also concluded from extended X-ray absorption fine structure (EXAFS) spectra that PuO_{2+x} contains Pu(V) rather than Pu(VI).

The recent update to the NEA compilation of chemical thermodynamic data (Guillaumont et al. 2003 [DIRS 168382], Section 11.2.2.1) includes a review of the results presented by Haschke et al. (2000 [DIRS 150367]) and Haschke and Allen (2002 [DIRS 162001]). The conclusion is that "the evidence for the formation of a thermodynamically stable bulk phase with O/Pu > 2 is far from conclusive."

The dissolution reaction for PuO_{2+x} under the oxidizing conditions used for the calculations described earlier can be written:

$$PuO_{2+x} + H^+ + (0.5 - x)/2\ O_2 = PuO_2^+ + 0.5\ H_2O \qquad \text{(Eq. 6.5-8)}$$

The results of such calculations are given in Table 6.5-7 and show that at equilibrium, PuO_{2+x} solubilities decrease by 24 orders of magnitude as x ranges from 0.0 to 0.5. These calculations were made without considering activity coefficients or the formation of aqueous complexes. To illustrate the magnitude of the errors that may have been introduced by these simplifications, the last column of Table 6.5-7 gives the total plutonium contents calculated by EQ3NR using the adjusted-Eh model at pH = 6 and $fCO_2 = 10^{-5}$ bars for PuO_2(hyd,aged) from Table 6.5-1 The solubility from the simple calculation is within 25 percent of that from the EQ3NR calculation, a considerably smaller difference than the solubility differences due to increasing values of x.

Thus, it can be concluded that the equilibrium solubility of PuO_{2+x} is considerably lower than that of PuO_2(hyd,aged), so choosing solubility control by the latter phase leads to higher calculated-Pu concentrations and is conservative.

Haschke and Bassett (2002 [DIRS 162699]) review whether modeling with solids designated as PuO_2(s) or $Pu(OH)_4$(am) better describes plutonium concentrations reported in a number of laboratory investigations. These phases correspond to the phases designated PuO_2(cr) and PuO_2(hyd,aged) by the OECD (2001 [DIRS 159027], Sections 17.2.1.2 and 17.2.2.3). Haschke and Bassett (2002 [DIRS 162699]) conclude that $Pu(OH)_4$(am) is a better predictor of laboratory results than the PuO_2(s). This is understandable because the properties of the amorphous or poorly crystalline hydrated actinide dioxide solids, of which $Pu(OH)_4$(am) (= PuO_2(hyd,aged) + $2H_2O$) are one example, are derived from laboratory solubility experiments as illustrated by the OECD (2001 [DIRS 159027], Section 17.2.2.3) for plutonium, Hummel et al. (2002 [DIRS 161904], Section 5.21.2) for thorium, and Section 5.23.3.1.3 for uranium.

Haschke and Bassett's (2002 [DIRS 162699]) conclusions are not directly relevant to the solubility calculations in this report for two reasons. First, their calculations were made at lower oxidation potentials than used in this report. Their Eh values range from 0.92 V at pH = 3 to 0.26 V at pH = 8 (Haschke and Bassett 2002 [DIRS 162699], Table 3), while those of the adjusted-Eh model are 0.92 and 0.63 V, respectively. The Eh values used by Haschke and Bassett (2002 [DIRS 162699]) correspond to fO_2 values from 10^{-10} to 10^{-35} bars (Langmuir 1997 [DIRS 100051], Figure 11.2), while the adjusted-Eh model calculations for this report correspond to a fO_2 of $10^{-8.1}$ bars. Second, Haschke and Bassett (2002 [DIRS 162699]) used thermodynamic data for their calculations that predate and are superseded by *Chemical Thermodynamics of Neptunium and Plutonium* (OECD 2001 [DIRS 159027]). The latter data are included in *Data0.ymp.R2* (DTN: MO0302SPATHDYN.000 [DIRS 161756]), the thermodynamic database used for this report. In addition, Haschke and Bassett (2002 [DIRS 162699]) do not include PuO_{2+x} in their review of plutonium-controlling phases.

Table 6.5-7. Data of PuO_{2+x} Stability

X value in PuO_{2+x}	ΔGf kJ/mol	ΔGr kJ/mol	at pH=6 $fO_2 = 10^{-8.1}$ bars log(PuO_2^+)	mg Pu/L	mg Pu/L at $fCO_2 = 10^{-5}$ bars [Pu] Table 6.5-1
0.00	-998.113	26.943	-12.75	4.30E-08	
0.10	-1,032.611	61.441	-18.39	9.88E-14	
0.20	-1,060.958	89.788	-22.95	2.72E-18	
0.30	-1,089.304	118.134	-27.51	7.47E-23	
0.40	-1,117.651	146.481	-32.07	2.05E-27	
0.50	-1,145.998	174.828	-36.63	5.65E-32	
PuO_2(hyd,aged)					
0.00	-963.654	-7.516	-6.71	4.68E-02	3.72E-02

Source: *PuO(2+x)_Calc_REV03.xls* (Appendix I).

NOTE: Free energies of formation, free energy of reaction for Equation 6.5-7, and PuO_2^+ concentrations calculated at $fO_2 = 10^{-8.1}$ bars, corresponding to adjusted-Eh model and pH = 6 for PuO_{2+x} with x ranging from 0.0 to 0.5, and for PuO_2(hyd,aged).The last column gives the total plutonium contents calculated at $fCO_2 = 10^{-5}$ bars for PuO_2(hyd,aged) from Table 6.5-1.

Haschke and Oversby (2002 [DIRS 161911], p. 193) review selected experimental data on plutonium concentrations in laboratory experiments and conclude "that a dissolution model based solely on equilibrium thermodynamics and solubility of PuO_2 and $Pu(OH)_4$(am) is not consistent with the experimental data." Instead, they propose "a kinetically controlled chemical process involving release of Pu(V) from PuO_{2+x} formed by spontaneous reaction of dioxide or hydroxide with water." They propose a sequence of equilibrium and kinetic processes (summarized in their Table 2) that lead to steady-state solution plutonium concentrations similar to the experimental data they review (Haschke and Oversby 2002 [DIRS 161911], Table 3). The initiating reaction they propose is the formation of PuO_{2+x} by reaction with water according to:

$$PuO_2(s) + xH_2O = PuO_{2+x}(s) + xH_2(g) \qquad \text{(Eq. 6.5-9)}$$

Haschke and Oversby (2002 [DIRS 161911]) also note that because this reaction produces hydrogen gas, which leaves the system, their plutonium cycle is not an equilibrium process. There is considerable uncertainty in the steady state concentrations they calculate because of uncertainties in the rate constants required to evaluate the kinetic expressions in their model. In addition, uncertainties exist because of the lack of experimental data to evaluate one of the key factors in their model: the conversion factor between rates expressed in terms of areas and those expressed in terms of volumes (Haschke and Oversby 2002 [DIRS 161911], p. 196).

The results of Haschke and Oversby's (2002 [DIRS 161911]) model are given in their Table 3. For conditions most like those modeled in this report (controlling-phase $Pu(OH)_4$(am), pH 6 to 7, low ionic strength) their modeled concentrations are from –0.1 to –0.9 log[Pu] (in mg/L), and the range of observed concentrations they cite is –0.1 to –2.0 log[Pu]. Both are within the uncertainty range of the adjusted-Eh Pu-solubility model (Fig 6.5-6).

The data of Haschke et al. (2000 [DIRS 150367]) and the model developed to account for them by Haschke and Oversby (2002 [DIRS 161911]) are of considerable interest and possible

importance to the understanding of plutonium chemistry. However, because the steady-state model is only in its first stages of development and in any case leads to concentrations lower than those calculated under the same conditions in this report, the theoretically more-robust thermodynamic equilibrium model is retained here.

6.5.7 Effects of Small Eh Change on Other Elements

The other elements considered in this report that are sensitive to redox conditions are Np and U. As discussed in Section 6.6, Np_2O_5 solubilities were also calculated using the adjusted-Eh values used for Pu and given in Equation 6.5-7. Uranium had previously been modeled with the theoretical fO_2 = 0.2 bars. Published Eh–pH diagrams for U (e.g., Langmuir 1997 [DIRS 100051], Figures 13.8 and 13.9) show all solute species of U are in the U(VI) state with Eh values at least as low as 200mv from pH 0 to 12. Thus, the relatively small reduction in E^0 from 1.22 to 1.10 in going from the theoretical fO_2 model to the adjusted-Eh model (compare Equations 6.5-3 and 6.5-7), although important to the speciation of Pu and Np, does not change U speciation. In addition, the solubility-controlling phases for U all contain U(VI), so no redox reactions are associated with their dissolution. Because the difference between the theoretical fO_2 and adjusted-Eh models would have no effect on U concentrations as modeled here, the U concentrations were calculated with the theoretical fO_2 model.

6.6 NEPTUNIUM SOLUBILITY

6.6.1 Conceptual Models

Several studies concerning neptunium-bearing phase(s) that could form under repository conditions have been conducted. Several types of solubility-controlling phases have been examined. One is pure neptunium phases, consisting primarily of neptunium oxides, hydroxides, and carbonates. The other is neptunium-bearing uranium phases, wherein neptunium constitutes a minor element component in solid solutions.

As discussed in the sections that follow and in Appendix IV, for the base case of TSPA-LA, NpO_2-$NaNpO_2CO_3$ are considered as the controlling phases inside corroding waste packages (Table 6.6-3 and uncertainty terms defined in Table 6.6-5). Additionally, it is recommended that the Np_2O_5-$NaNpO_2CO_3$-solubility model (Table 6.6-9 and uncertainty terms defined in Table 6.6-11) be used for the invert.

Incorporation of neptunium into uranyl minerals is considered an alternative controlling phase (Section 6.6.4). The model enhances the understanding about radionuclide migration and the performance of the repository. However, experimental studies do not provide a solid basis for recommending this as the base-case model for use in the TSPA-LA model. Therefore, it is presented only as an alternative model.

Discussions of testing on the controls of aqueous Np concentrations are located in Appendix V.

6.6.2 Chemical Conditions

Np is known to exist in four oxidation states, but only two (+4 and +5) are important in natural waters (Langmuir 1997 [DIRS 100051], Table 13.8). NpO_2 is modeled with the theoretical fO_2 = 0.2 bars. For $NaNpO_2CO_3$, published Eh–pH diagrams for Np (e.g., Langmuir 1997

[DIRS 100051]) show that the higher oxidation states of Np exist with Eh values as low as 250 mv above a pH of 9 and, thus, are important to the speciation of Np. This shift in species oxidation state is also seen in the EQ3 calculations used to derive the solubilities for Np. Because of this possible change in oxidation state at higher pH values, Np solubilities using $NaNpO_2CO_3$ were calculated using the adjusted-Eh values given in Equation 6.5-7. Using the Eh indicated in Equation 6.5-7 is acceptable as the Eh values derived from this equation are 60 mv higher than the highest Eh measured in natural waters at Yucca Mountain (discussed in Section 6.5.4.2). See Table 6.4-2 for other chemical conditions used for the NpO_2-$NaNpO_2CO_3$ solubility calculations.

6.6.3 Base-Case Neptunium-Solubility Model

6.6.3.1 Selection of Solubility-Controlling Phases for In- and Ex-Package

The following gives an overview of the decisions to use NpO_2 as the solubility-controlling phase in the package and Np_2O_5 as the primary solubility phase in the invert. All references and source documents are in Appendix IV and are not brought forward into this summary. For the full discussion of the solubility-controlling phases and source documentation, see Appendix IV.

The Eh-pH thermodynamic stability fields for neptunium show that NpO_2 is the most thermodynamically stable Np phase over most of the Eh/pH regime of interest. Less thermodynamically stable pure phases such as $Np(OH)_4$ and Np_2O_5 have been shown to preferentially precipitate from solutions in short duration tests at temperatures below 100°C. Although kinetically favored to form from solution, these phases are inappropriate to establish an upper bound for the neptunium dissolved concentrations model because their use as the solubility-controlling phase does not consider processes occurring in a corroding waste package such as reductive nucleation and precipitation of Np species. Additionally, the behavior of Np as the waste form corrodes must also be accounted for.

CSNF has an oxygen potential of approximately -400kJ/mol. Uranium is present primarily in the +4 oxidation state within a fluorite structure. As indicated in EXAFS data, Np in the fuel is in solid solution with the UO_2 comprising the fuel matrix, indicating neptunium is also in the +4 state in the fuel. Upon corrosion of the fuel, reduction of Np(V) is thermodynamically favored as unoxidized U(IV) is oxidized. Additionally, corrosion potentials measured for CSNF are in the range of 300 mV to 620 mV SHE indicating that CSNF corrosion potential may be lower than the potential for anodic dissolution of Np(IV) in the fuel matrix. Therefore, solubility of Np at the fuel surface is controlled by NpO_2 given that oxidation of Np(IV) in the fuel lattice is unlikely.

In CSNF, the uranium in the fuel matrix is present mostly in the U(IV) oxidation state. Np in the CSNF is expected to be present as a solid solution of NpO_2 (an Np(IV) solid) in the UO_2 fluorite structure with which it is compatible. As Np traverses the fuel surface and corrosion rind, some will be oxidized to Np(V) so the rind will contain a mixture of Np(IV) and Np(V). As it traverses through the rind, there is a strong possibility that Np(V) will be incorporated into uranyl phases. Upon entering bulk solution, all of the Np is oxidized to Np(V). Although pure solids are generally used to evaluate radionuclide solubility, it is well recognized that concentrations of most radionuclides, including Np, may not form their own pure phase. Rather,

they are likely to be incorporated into secondary uranium phases as solid solutions. Because of the large availability of uranium in the repository, Np incorporation into secondary uranyl phases is examined in Section 6.6.4.

Natural analogues of UO_2 corrosion/oxidation mineralogy as well as laboratory studies on UO_2 corrosion have yielded a wealth of information on possible uranyl phases that may incorporate Np after it leaves the fuel surface. Additionally, there are a growing number of studies investigating Np incorporation into uranyl phases. To model the complex process of Np incorporation, the following points must be addressed:

- Identities of the most relevant U(VI) solids that are likely to sequester neptunium
- Whether Np is incorporated into the structures of U(VI) corrosion products
- The molar Np:U ratio (or range of Np:U ratios) in Np-bearing U(VI) corrosion products
- The molar Np:U ratio (or range of Np:U ratios) in solutions in contact with Np-bearing U(VI) corrosion products
- The limit of Np concentrations in U(VI) compounds under repository-relevant conditions
- The fate of Np during the alteration of early formed U(VI) corrosion products as they continue to interact with in-package aqueous solutions and Yucca Mountain groundwaters.

Even though data in this area are accumulating quickly, uncertainty in several of the points above would have to be addressed and information deficiencies on many of the points above would need further study to create a validated Np-solubility model based on secondary phase Np incorporation. For example, the primary uranium phases formed in laboratory studies and natural analogues fit under the broad categories of uranium oxides/oxyhydroxides, uranium silicates, and uranium peroxides. However, from these studies, it is apparent that the paragenesis of corroding fuel may be very complex and that unusual phases such as studtite, compreignacite, and Zr-U oxides may be formed.

Many uranyl minerals are known to persist in nature for tens to hundreds of thousands of years. Dissolved concentration modeling of uranium minerals also shows them to be much more resistant than pure phase neptunium minerals. Therefore, the thermodynamically modeled NpO_2 represents a rational conservative upper bound for the control of neptunium dissolved concentrations inside waste packages until more information is available to properly model dissolved concentrations based on neptunium incorporation into uranyl phases.

Reaction paths for Np mineralization in the waste package must also take into account influences of the corroding waste form, corrosion of the waste package materials (primarily steel), and interactions of Np with the products of steel corrosion (primarily reduction of Np by Fe(II) and Cr(III) species). As illustrated earlier, Np(V) species will encounter corroded metals and their corrosion products from waste package internals. These will provide local environments with

lower oxidation potentials than the bulk solution, promoting reductive nucleation and precipitation of Np species by reducing Np(V) to Np(IV).

By assessing the processes occurring along the relevant reaction paths, it can be concluded that the dissolved concentrations of Np are not likely to exceed the solubility of thermodynamically modeled NpO_2 at atmospheric conditions. Also, it is likely that incorporation of either Np into uranyl phases or reductive precipitation onto metal corrosion products, or both, will maintain the dissolved Np concentrations subsaturated with respect to NpO_2. In short, it is appropriate to use the solubility of thermodynamically modeled NpO_2 for the dissolved concentrations of Np inside waste packages.

Once Np(V) leaves the waste package, it is difficult to determine and defend the composition and geometry of any materials it would come into contact with in the invert. Therefore, the use of an NpO_2 model is inappropriate. The Np_2O_5 dissolved concentration model, however, is appropriate for use outside of waste packages.

6.6.3.2 In-Package Neptunium Model: NpO_2-$NaNpO_2CO_3$

Table 6.6-1 gives the calculated neptunium solubility (in units of mg/L) using NpO_2 as the controlling solid.

Figure 6.6-1 shows the calculated solubility using NpO_2 as the controlling solid as a function of pH and fugacity of CO_2. Under the same fCO_2, neptunium solubility increases with pH under alkaline conditions; while under acid conditions, it increases with decrease in pH. Note the insensitivity to fCO_2 on the acid leg, but extreme sensitivity on the basic leg.

Under the modeled conditions, depending on fCO_2, NpO_2 becomes unstable when pH increases. At this point, $NaNpO_2CO_3$ is used as the solubility-controlling phase. Table 6.6-2 lists calculated Np solubility for conditions where NpO_2 is unstable and $NaNpO_2CO_3$ is stable. It clearly shows that the stability field of $NaNpO_2CO_3$ is quite narrow (about a 0.25 to 0.5 pH unit). These solubilities are shown separately from those controlled by NpO_2 because they are the results of different EQ3 calculations.

Table 6.6-1. Calculated NpO_2 Solubility (mg/L)

pH	log fCO_2 (bars)							
	–1.50	–2.00	–2.50	–3.00	–3.50	–4.00	–4.50	–5.00
3.00	1.24E+03	1.24E+03	1.24E+03	1.24E+03	1.24E+03	1.24E+03	1.24E+03	1.24E+03
3.25	6.63E+02	6.63E+02	6.63E+02	6.63E+02	6.63E+02	6.63E+02	6.63E+02	6.63E+02
3.50	3.63E+02	3.63E+02	3.63E+02	3.63E+02	3.63E+02	3.63E+02	3.63E+02	3.63E+02
3.75	2.01E+02	2.01E+02	2.01E+02	2.01E+02	2.01E+02	2.01E+02	2.01E+02	2.01E+02
4.00	1.12E+02	1.12E+02	1.12E+02	1.12E+02	1.12E+02	1.12E+02	1.12E+02	1.12E+02
4.25	6.26E+01	6.26E+01	6.26E+01	6.26E+01	6.26E+01	6.26E+01	6.26E+01	6.26E+01
4.50	3.51E+01	3.51E+01	3.51E+01	3.51E+01	3.51E+01	3.51E+01	3.51E+01	3.51E+01
4.75	1.97E+01	1.97E+01	1.97E+01	1.97E+01	1.97E+01	1.97E+01	1.97E+01	1.97E+01
5.00	1.11E+01	1.11E+01	1.11E+01	1.11E+01	1.11E+01	1.11E+01	1.11E+01	1.11E+01
5.25	6.22E+00	6.22E+00	6.22E+00	6.22E+00	6.22E+00	6.22E+00	6.22E+00	6.22E+00
5.50	3.50E+00	3.50E+00	3.50E+00	3.50E+00	3.50E+00	3.50E+00	3.50E+00	3.50E+00
5.75	1.97E+00	1.97E+00	1.97E+00	1.97E+00	1.97E+00	1.97E+00	1.97E+00	1.97E+00
6.00	1.11E+00	1.11E+00	1.11E+00	1.11E+00	1.11E+00	1.11E+00	1.11E+00	1.11E+00
6.25	6.24E-01	6.22E-01	6.22E-01	6.22E-01	6.22E-01	6.22E-01	6.22E-01	6.22E-01
6.50	3.57E-01	3.51E-01	3.50E-01	3.50E-01	3.50E-01	3.50E-01	3.50E-01	3.50E-01
6.75	2.16E-01	2.01E-01	1.98E-01	1.97E-01	1.97E-01	1.97E-01	1.97E-01	1.97E-01
7.00	1.59E-01	1.19E-01	1.13E-01	1.11E-01	1.11E-01	1.11E-01	1.11E-01	1.11E-01
7.25	1.88E-01	8.17E-02	6.66E-02	6.34E-02	6.26E-02	6.23E-02	6.22E-02	6.22E-02
7.50	4.20E-01	8.19E-02	4.39E-02	3.73E-02	3.57E-02	3.52E-02	3.50E-02	3.50E-02
7.75	1.60E+00	1.47E-01	3.92E-02	2.42E-02	2.10E-02	2.01E-02	1.98E-02	1.97E-02
8.00		4.46E-01	5.84E-02	2.01E-02	1.35E-02	1.18E-02	1.13E-02	1.11E-02
8.25			1.44E-01	2.60E-02	1.08E-02	7.53E-03	6.62E-03	6.35E-03
8.50			6.11E-01	5.33E-02	1.27E-02	5.93E-03	4.22E-03	3.72E-03
8.75				1.76E-01	2.24E-02	6.60E-03	3.28E-03	2.37E-03
9.00				1.25E+00	5.97E-02	1.05E-02	3.54E-03	1.83E-03
9.25				2.16E+01	3.15E-01	2.35E-02	5.32E-03	1.94E-03
9.50					4.40E+00	9.39E-02	1.05E-02	2.81E-03
9.75						1.05E+00	3.29E-02	5.10E-03
10.00							2.87E-01	1.32E-02
10.25								8.84E-02
10.50								2.45E+00

Source: *NpO2.xls* (Appendix I).

NOTE: Some cells have no data because the EQ3NR calculations do not converge (Section 6.4.4).

Table 6.6-2. Calculated Np In-Package Solubility Using $NaNpO_2CO_3$ as the Controlling Phase ([Np] mg/L)

	log fCO_2 (bars)							
pH	**-1.5**	**-2.0**	**-2.5**	**-3.0**	**-3.5**	**-4.0**	**-4.5**	**-5.0**
8.00	1.86E+00							
8.25	3.96E+00	2.49E+00						
8.50	2.66E+01	2.76E+00		**NpO_2 controlled**				
8.75		1.15E+01	2.86E+00					
9.00			6.21E+00					
9.25								
9.50				2.28E+01				
9.75					1.32E+01			
10.00						9.00E+00		
10.25						9.17E+01	7.13E+00	
10.50							5.72E+01	
10.75								4.12E+01

Source: *Np base case-Ehadjusted.xls* in Appendix I.

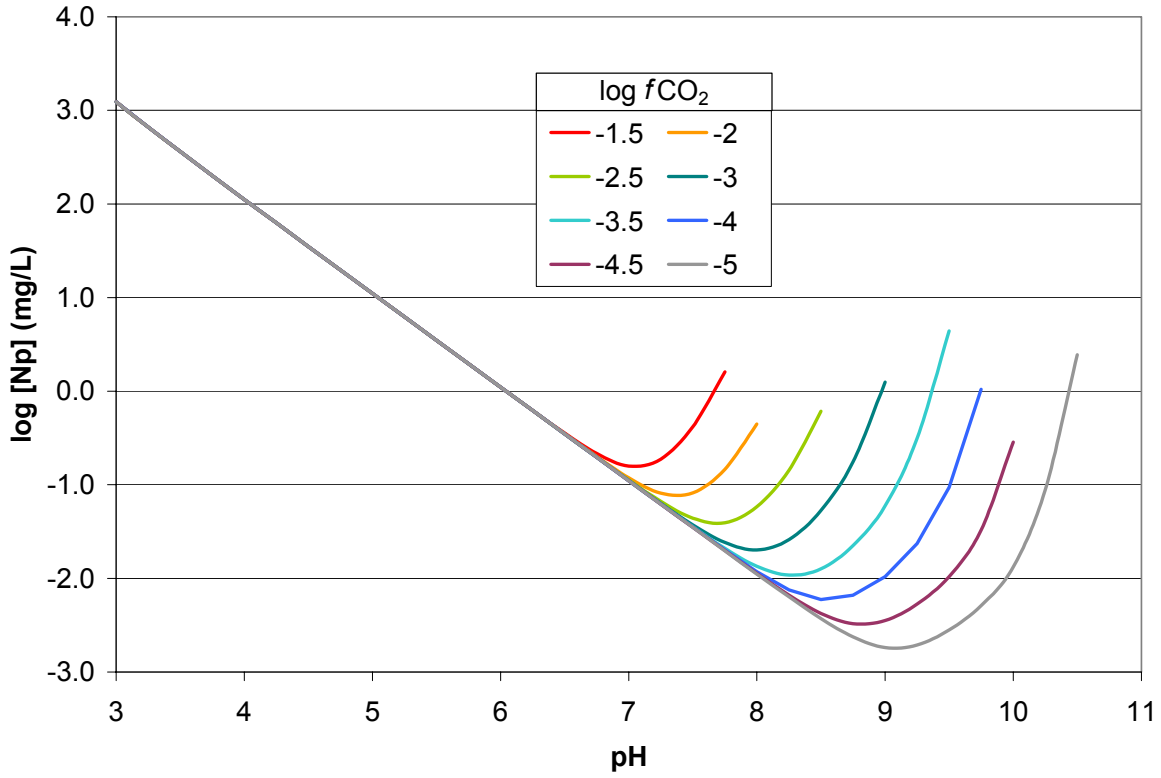

Source: *NpO2.xls* (Appendix I).

Figure 6.6-1. NpO_2 Solubility Modeled as a Function of pH and log fCO_2

6.6.3.2.1 In-Package Neptunium-Solubility Model for Use in TSPA-LA

Combining the calculated-Np solubility using NpO_2 as the controlling phase (Table 6.6-1) and that using $NaNpO_2CO_3$ (Table 6.6-2), Table 6.6-3 is presented for use in TSPA-LA. The logarithm of solubility values is given here to facilitate interpolation that may be needed by the user, because the independent variables of the table are in log scales.

For those calculations that do not converge or are not valid, a large number ("500") is entered to indicate that under such pH and fCO_2 conditions, solubility of neptunium is not defined or the calculation results are outside the valid range of the computing tool. When the flag ("500") is encountered or for conditions between a valid solubility and a flag of "500," concentrations should be calculated according to the dissolution rate of individual waste forms, water volume, and the solubility caps presented in Table 8-3 instead of the flag itself. In addition, for conditions outside of the 3.0 to 11.0 pH range, or the fCO_2 range from $10^{-1.5}$ to $10^{-5.0}$ bars, the concentrations should be calculated according to the dissolution rate of individual waste forms, water volume, and the solubility caps presented in Table 8-3.

Table 6.6-3. Calculated Neptunium Solubility for Inside Waste Packages (Log[Np] (mg/L))

pH	Log fCO_2 (bars)							
	-1.5	-2.0	-2.5	-3.0	-3.5	-4.0	-4.5	-5.0
3.00	3.09E+00	3.09E+00	3.09E+00	3.09E+00	3.09E+00	3.09E+00	3.09E+00	3.09E+00
3.25	2.82E+00	2.82E+00	2.82E+00	2.82E+00	2.82E+00	2.82E+00	2.82E+00	2.82E+00
3.50	2.56E+00	2.56E+00	2.56E+00	2.56E+00	2.56E+00	2.56E+00	2.56E+00	2.56E+00
3.75	2.30E+00	2.30E+00	2.30E+00	2.30E+00	2.30E+00	2.30E+00	2.30E+00	2.30E+00
4.00	2.05E+00	2.05E+00	2.05E+00	2.05E+00	2.05E+00	2.05E+00	2.05E+00	2.05E+00
4.25	1.80E+00	1.80E+00	1.80E+00	1.80E+00	1.80E+00	1.80E+00	1.80E+00	1.80E+00
4.50	1.55E+00	1.55E+00	1.55E+00	1.55E+00	1.55E+00	1.55E+00	1.55E+00	1.55E+00
4.75	1.29E+00	1.29E+00	1.29E+00	1.29E+00	1.29E+00	1.29E+00	1.29E+00	1.29E+00
5.00	1.04E+00	1.04E+00	1.04E+00	1.04E+00	1.04E+00	1.04E+00	1.04E+00	1.04E+00
5.25	7.94E-01	7.94E-01	7.94E-01	7.94E-01	7.94E-01	7.94E-01	7.94E-01	7.94E-01
5.50	5.44E-01	5.44E-01	5.44E-01	5.44E-01	5.44E-01	5.44E-01	5.44E-01	5.44E-01
5.75	2.93E-01	2.94E-01	2.94E-01	2.94E-01	2.94E-01	2.94E-01	2.94E-01	2.94E-01
6.00	4.37E-02	4.36E-02	4.36E-02	4.36E-02	4.36E-02	4.36E-02	4.36E-02	4.36E-02
6.25	-2.05E-01	-2.06E-01	-2.06E-01	-2.06E-01	-2.06E-01	-2.06E-01	-2.06E-01	-2.06E-01
6.50	-4.48E-01	-4.54E-01	-4.56E-01	-4.56E-01	-4.56E-01	-4.56E-01	-4.56E-01	-4.56E-01
6.75	-6.65E-01	-6.98E-01	-7.04E-01	-7.06E-01	-7.06E-01	-7.06E-01	-7.06E-01	-7.06E-01
7.00	-8.00E-01	-9.24E-01	-9.48E-01	-9.54E-01	-9.56E-01	-9.56E-01	-9.56E-01	-9.56E-01
7.25	-7.26E-01	-1.09E+00	-1.18E+00	-1.20E+00	-1.20E+00	-1.21E+00	-1.21E+00	-1.21E+00
7.50	-3.77E-01	-1.09E+00	-1.36E+00	-1.43E+00	-1.45E+00	-1.45E+00	-1.46E+00	-1.46E+00
7.75	2.05E-01	-8.33E-01	-1.41E+00	-1.62E+00	-1.68E+00	-1.70E+00	-1.70E+00	-1.71E+00
8.00	2.70E-01	-3.51E-01	-1.23E+00	-1.70E+00	-1.87E+00	-1.93E+00	-1.95E+00	-1.95E+00
8.25	5.98E-01	3.96E-01	-8.43E-01	-1.59E+00	-1.97E+00	-2.12E+00	-2.18E+00	-2.20E+00

Table 6.6-3. Calculated Neptunium Solubility for Inside Waste Packages (Log[Np] (mg/L)) (Continued)

8.50	1.42E+00	4.41E-01	-2.14E-01	-1.27E+00	-1.90E+00	-2.23E+00	-2.37E+00	-2.43E+00
8.75	500	1.06E+00	4.57E-01	-7.55E-01	-1.65E+00	-2.18E+00	-2.48E+00	-2.63E+00
9.00	500	500	7.93E-01	9.62E-02	-1.22E+00	-1.98E+00	-2.45E+00	-2.74E+00
9.25	500	500	500	1.33E+00	-5.02E-01	-1.63E+00	-2.27E+00	-2.71E+00
9.50	500	500	500	1.36E+00	6.43E-01	-1.03E+00	-1.98E+00	-2.55E+00
9.75	500	500	500	500	1.12E+00	2.13E-02	-1.48E+00	-2.29E+00
10.00	500	500	500	500	500	9.54E-01	-5.42E-01	-1.88E+00
10.25	500	500	500	500	500	1.96E+00	8.53E-01	-1.05E+00
10.50	500	500	500	500	500	500	1.76E+00	3.90E-01
10.75	500	500	500	500	500	500	500	1.61E+00

6.6.3.2.2 Uncertainties in log K Values of Controlling Solid and Aqueous Species

The uncertainty in solubility involves uncertainties in the thermodynamic properties of both the controlling solid and significant dissolved species. The rationale behind the evaluation and combination of these uncertainties is discussed in some detail in Section 6.3.3.1.

The dissolved species accounting for more than 10 percent of the dissolved neptunium were found by examining the EQ3NR output for runs at $\log fCO_2 = -3.0$. They are the same as those for the Np_2O_5 calculations described in Section 6.6.3.3 (Figure 6.6-4).

After an extensive review, OECD (2001 [DIRS 159027]) recommended –1,021.731 ±2.514 kJ/mol for the Gibbs free energy of formation of NpO_2, based on calorimetric studies. Following the procedure outlined in Section 6.3.3.1 leads to log K of 0.81 with a 2σ uncertainty of ±1.1 (at 25°C) for the reaction:

$$NpO_2 + 0.25\ O_2(g) + H^+ = NpO_2^+ + 0.5\ H_2O \qquad \text{(Eq.6.6-1)}$$

The evaluation of reactions from NpO_2 to each of the six dissolved species noted earlier leads to a maximum uncertainty in log K for reaction to $NpO_2(CO_3)_3^{4-}$ of ±1.11. This is a 2σ uncertainty, so the 1σ uncertainty to be applied to log[Np] is ±0.6.

6.6.3.2.3 Uncertainty from Fluoride Concentration

Table 6.6-4 lists the calculated logarithm of NpO_2 solubilities using the fluoride levels indicated in Section 6.3.3.2 (10 times base case for CSNF waste packages and 27 and 95 times for codisposal waste packages and the invert). The fugacity of CO_2 is set to $10^{-3.0}$. The differences between the base-case results and the uncertainty case results vary with pH. The three right-hand columns are the differences between the respective elevated F^- cases and the base case. The maximum difference between the base-case results and the 10× fluoride results expressed as log[Np] is 4.31E-02. The maximum uncertainty for fluoride is for codisposal waste packages (vapor-influx scenario) and the invert; the uncertainty term $\varepsilon_2^{\text{CDSP-vapor influx}}$ expressed as log[Np]

is 5.24E-01. Unlike other actinides (like U and Th), neptunium solubility is not very sensitive to fluoride concentration.

Table 6.6-4. Effects of Variations in Fluoride Concentration on NpO_2 Solubility

	Base Case	CSNF	CDSP – Water-Influx Scenario	CDSP – Vapor-Influx Scenario	CSNF	CDSP – Water-Influx Scenario	CDSP – Vapor-Influx Scenario
pH	**log[Np] mg/L**				**Difference**		
3.00	3.09E+00	3.13E+00	3.20E+00	3.41E+00	3.67E-02	1.11E-01	3.17E-01
3.25	2.82E+00	2.86E+00	2.96E+00	3.22E+00	4.27E-02	1.35E-01	4.00E-01
3.50	2.56E+00	2.60E+00	2.71E+00	3.04E+00	4.31E-02	1.50E-01	4.78E-01
3.75	2.30E+00	2.34E+00	2.45E+00	2.83E+00	3.73E-02	1.46E-01	5.24E-01
4.00	2.05E+00	2.08E+00	2.17E+00	2.56E+00	2.83E-02	1.24E-01	5.16E-01
4.25	1.80E+00	1.82E+00	1.89E+00	2.25E+00	1.98E-02	9.51E-02	4.50E-01
4.50	1.55E+00	1.56E+00	1.62E+00	1.90E+00	1.37E-02	7.00E-02	3.57E-01
4.75	1.29E+00	1.30E+00	1.35E+00	1.56E+00	9.76E-03	5.24E-02	2.67E-01
5.00	1.04E+00	1.05E+00	1.09E+00	1.24E+00	7.39E-03	4.13E-02	1.98E-01
5.25	7.94E-01	8.00E-01	8.28E-01	9.45E-01	6.00E-03	3.47E-02	1.51E-01
5.50	5.44E-01	5.49E-01	5.74E-01	6.65E-01	5.20E-03	3.08E-02	1.21E-01
5.75	2.94E-01	2.98E-01	3.22E-01	3.97E-01	4.75E-03	2.86E-02	1.03E-01
6.00	4.36E-02	4.81E-02	7.09E-02	1.36E-01	4.49E-03	2.73E-02	9.28E-02
6.25	-2.06E-01	-2.02E-01	-1.80E-01	-1.20E-01	4.34E-03	2.66E-02	8.68E-02
6.50	-4.56E-01	-4.52E-01	-4.30E-01	-3.73E-01	4.25E-03	2.62E-02	8.34E-02
6.75	-7.06E-01	-7.01E-01	-6.80E-01	-6.24E-01	4.21E-03	2.60E-02	8.14E-02
7.00	-9.54E-01	-9.50E-01	-9.28E-01	-8.74E-01	4.16E-03	2.58E-02	8.01E-02
7.25	-1.20E+00	-1.19E+00	-1.17E+00	-1.12E+00	4.05E-03	2.56E-02	7.89E-02
7.50	-1.43E+00	-1.42E+00	-1.40E+00	-1.35E+00	3.76E-03	2.50E-02	7.66E-02
7.75	-1.62E+00	-1.61E+00	-1.59E+00	-1.54E+00	2.91E-03	2.36E-02	7.15E-02
8.00	-1.70E+00	-1.69E+00	-1.67E+00	-1.63E+00	5.48E-03	2.17E-02	6.37E-02
8.25	-1.59E+00	-1.58E+00	-1.57E+00	-1.53E+00	7.56E-03	2.02E-02	5.96E-02
8.50	-1.27E+00	-1.26E+00	-1.25E+00	-1.20E+00	8.51E-03	2.33E-02	7.32E-02
8.75	-7.55E-01	-7.42E-01	-7.20E-01	-6.40E-01	1.23E-02	3.46E-02	1.15E-01
9.00	9.62E-02	1.12E-01	1.39E-01	2.41E-01	1.53E-02	4.32E-02	1.45E-01
9.25	1.33E+00	1.35E+00	1.37E+00	1.45E+00	1.20E-02	3.38E-02	1.16E-01
				Maximum:	4.31E-02	1.50E-01	5.24E-01

Source: *NpO2.xls* (Appendix I).

NOTE: $fCO_2 = -3.0$ bars.

6.6.3.2.4 Summary of NpO_2-Solubility Model Uncertainty

The following equation summarizes the NpO_2-solubility model:

$$\log[\mathrm{Np}] = S(pH, \log fCO_2) + \varepsilon_1 + (\varepsilon_2 \times N) \qquad \text{(Eq.6.6-2)}$$

The values for the parameters in this equation depend on the waste package type. Parameter $S\left(pH, \log f_{CO_2}\right)$ is the base solubility and is taken from Table 6.6-3. Parameter ε_1 is associated with the uncertainties in the log K data. Parameter ε_2 is associated with the uncertainties in the fluoride concentrations. Table 6.6-5 gives the values for the parameters ε_1 and ε_2.

Table 6.6-4 shows that the uncertainty terms $\varepsilon_2^{\text{CSNF}}$, $\varepsilon_2^{\text{CDSP- Water Influx}}$, and $\varepsilon_2^{\text{CDSP-Vapor Influx}}$ vary with pH. This pH dependence can be implemented into the TSPA-LA model through the use of a multiplication factor (N) that is a function of pH. Values for N(pH) for both fuel types are given in Table 6.6-6. This modification requires that the $\varepsilon_2^{\text{CSNF}}$, $\varepsilon_2^{\text{CDSP- Water Influx}}$, and $\varepsilon_2^{\text{CDSP-Vapor Influx}}$ values be fixed at the maximum value given in Table 6.6-4. For each realization in the TSPA-LA model, the uncertainty parameters are sampled at the beginning of the realization. This sampled value is then multiplied by N at each timestep to produce a modified ε_2, which is then added to the base solubility value.

Table 6.6-5. Uncertainty Terms of Log[Np] of In-Package Np (NpO_2) Model

Uncertainty Term	Associated With	Distribution Type	Distribution Parameter	Applicable to
ε_1	Uncertainty in log K	Normal Truncated at ±2σ	$\mu = 0, \sigma = 0.6$[a]	All Values in 6.6-1
$\varepsilon_2^{\text{CSNF}}$	Fluoride conc. in CSNF waste package	Triangular	a = b = 0, c = 0.043[b]	CSNF Waste Packages
$\varepsilon_2^{\text{CDSP- Water Influx}}$	Fluoride conc. in CDSP waste package (water-influx scenario)	Triangular	a = b = 0, c = 0.150 [b]	Codisposal waste packages (water-influx-scenario)
$\varepsilon_2^{\text{CDSP-Vapor Influx}}$	Fluoride conc. in CDSP waste package (vapor-influx scenario)	Triangular	a = b = 0, c = 0.524 [b]	Codisposal waste packages (vapor-influx scenario)

NOTE: [a] For ionic strength values between 1 and 3, Log K uncertainty should be treated as a normal distribution truncated at ±2σ with distribution parameters $\mu = 0$, $\sigma = 0.67$.

[b] The pH dependence (N) of the uncertainty term is presented in Table 6.6-6.

Table 6.6-6. Multiplication Factor (N) Used to Modify F^- Uncertainty Terms

	Multiplication Factor for F Uncertainty		
pH	CSNF	CDSP – Water-Influx	CDSP – Vapor Influx
3.00	8.52E-01	7.40E-01	6.06E-01
3.25	9.90E-01	9.00E-01	7.64E-01
3.50	1.00E+00	1.00E+00	9.12E-01
3.75	8.66E-01	9.77E-01	1.00E+00
4.00	6.56E-01	8.29E-01	9.83E-01
4.25	4.60E-01	6.35E-01	8.59E-01
4.50	3.18E-01	4.67E-01	6.80E-01

Table 6.6-6. Multiplication Factor (N) Used to Modify F^- Uncertainty Terms (Continued)

pH	Multiplication Factor for F Uncertainty		
	CSNF	CDSP – Water-Influx	CDSP – Vapor Influx
4.75	**2.27E-01**	**3.50E-01**	**5.10E-01**
5.00	**1.72E-01**	**2.75E-01**	**3.78E-01**
5.25	**1.39E-01**	**2.31E-01**	**2.88E-01**
5.50	**1.21E-01**	**2.05E-01**	**2.31E-01**
5.75	**1.10E-01**	**1.91E-01**	**1.97E-01**
6.00	**1.04E-01**	**1.82E-01**	**1.77E-01**
6.25	**1.01E-01**	**1.78E-01**	**1.66E-01**
6.50	**9.86E-02**	**1.75E-01**	**1.59E-01**
6.75	**9.78E-02**	**1.73E-01**	**1.55E-01**
7.00	**9.65E-02**	**1.72E-01**	**1.53E-01**
7.25	**9.39E-02**	**1.71E-01**	**1.50E-01**
7.50	**8.73E-02**	**1.67E-01**	**1.46E-01**
7.75	**6.76E-02**	**1.57E-01**	**1.36E-01**
8.00	**1.27E-01**	**1.45E-01**	**1.21E-01**
8.25	1.75E-01	1.35E-01	1.14E-01
8.50	1.97E-01	1.56E-01	1.40E-01
8.75	2.86E-01	2.31E-01	2.18E-01
9.00	3.55E-01	2.88E-01	2.76E-01
9.25	2.77E-01	2.26E-01	2.21E-01

Source: *NpO2.xls* (Appendix I)

6.6.3.3 Ex-Package Neptunium Model: Np_2O_5-$NaNpO_2CO_3$

Table 6.6-7 gives the calculated neptunium solubility (in units of mg/L) using Np_2O_5 as the controlling solid.

Figure 6.6-2 shows the calculated solubility using Np_2O_5 as the controlling solid as a function of pH and fugacity of CO_2. Under the same fCO_2, neptunium solubility increases with pH under alkaline conditions; while under acid conditions, it increases with decrease in pH. Note the insensitivity to fCO_2 on the acid leg, but extreme sensitivity on the basic leg.

Table 6.6-7. Calculated Np_2O_5 Solubility (mg/L)

	log fCO_2 (bars)							
pH	**–1.50**	**–2.00**	**–2.50**	**–3.00**	**–3.50**	**–4.00**	**–4.50**	**–5.00**
3.00	2.40E+04	2.40E+04	2.40E+04	2.40E+04	2.40E+04	2.40E+04	2.40E+04	2.40E+04
3.25	1.25E+04	1.25E+04	1.25E+04	1.25E+04	1.25E+04	1.25E+04	1.25E+04	1.25E+04
3.50	6.65E+03	6.65E+03	6.65E+03	6.65E+03	6.65E+03	6.65E+03	6.65E+03	6.65E+03
3.75	3.57E+03	3.57E+03	3.57E+03	3.57E+03	3.57E+03	3.57E+03	3.57E+03	3.57E+03
4.00	1.94E+03	1.94E+03	1.94E+03	1.94E+03	1.94E+03	1.94E+03	1.94E+03	1.94E+03
4.25	1.07E+03	1.07E+03	1.07E+03	1.07E+03	1.07E+03	1.07E+03	1.07E+03	1.07E+03
4.50	5.90E+02	5.90E+02	5.90E+02	5.90E+02	5.90E+02	5.90E+02	5.90E+02	5.90E+02
4.75	3.28E+02	3.29E+02	3.29E+02	3.29E+02	3.29E+02	3.29E+02	3.29E+02	3.29E+02
5.00	1.84E+02	1.84E+02	1.84E+02	1.84E+02	1.84E+02	1.84E+02	1.84E+02	1.84E+02
5.25	1.03E+02	1.03E+02	1.03E+02	1.03E+02	1.03E+02	1.03E+02	1.03E+02	1.03E+02
5.50	5.77E+01	5.77E+01	5.77E+01	5.77E+01	5.77E+01	5.77E+01	5.77E+01	5.77E+01
5.75	3.24E+01	3.24E+01	3.24E+01	3.24E+01	3.24E+01	3.24E+01	3.24E+01	3.24E+01
6.00	1.82E+01	1.82E+01	1.82E+01	1.82E+01	1.82E+01	1.82E+01	1.82E+01	1.82E+01
6.25	1.03E+01	1.02E+01	1.02E+01	1.02E+01	1.02E+01	1.02E+01	1.02E+01	1.02E+01
6.50	5.83E+00	5.78E+00	5.77E+00	5.76E+00	5.76E+00	5.76E+00	5.76E+00	5.76E+00
6.75	3.43E+00	3.29E+00	3.25E+00	3.24E+00	3.24E+00	3.24E+00	3.24E+00	3.24E+00
7.00	2.22E+00	1.92E+00	1.85E+00	1.83E+00	1.82E+00	1.82E+00	1.82E+00	1.82E+00
7.25	1.74E+00	1.23E+00	1.08E+00	1.04E+00	1.03E+00	1.03E+00	1.02E+00	1.02E+00
7.50	1.89E+00	9.56E-01	6.87E-01	6.11E-01	5.87E-01	5.79E-01	5.77E-01	5.76E-01
7.75	2.86E+00	1.02E+00	5.29E-01	3.87E-01	3.44E-01	3.30E-01	3.26E-01	3.24E-01
8.00	3.41E+00	1.48E+00	5.59E-01	2.96E-01	2.18E-01	1.94E-01	1.86E-01	1.83E-01
8.25		2.81E+00	7.96E-01	3.08E-01	1.67E-01	1.23E-01	1.09E-01	1.04E-01
8.50		1.01E+01	1.40E+00	4.35E-01	1.72E-01	9.39E-02	6.91E-02	6.13E-02
8.75			3.45E+00	7.41E-01	2.40E-01	9.70E-02	5.29E-02	3.89E-02
9.00				1.54E+00	4.02E-01	1.33E-01	5.46E-02	2.98E-02
9.25				6.59E+00	7.80E-01	2.22E-01	7.51E-02	3.08E-02
9.50					2.36E+00	4.16E-01	1.23E-01	4.23E-02
9.75						1.05E+00	2.27E-01	6.88E-02
10.00						9.04E+00	5.27E-01	1.26E-01
10.25							3.34E+00	2.80E-01
10.50								1.48E+00

Source: *Np base case-Ehadjusted.xls* (Appendix I).

NOTE: Some cells have no data because the EQ3NR calculations do not converge (Section 6.4.4).

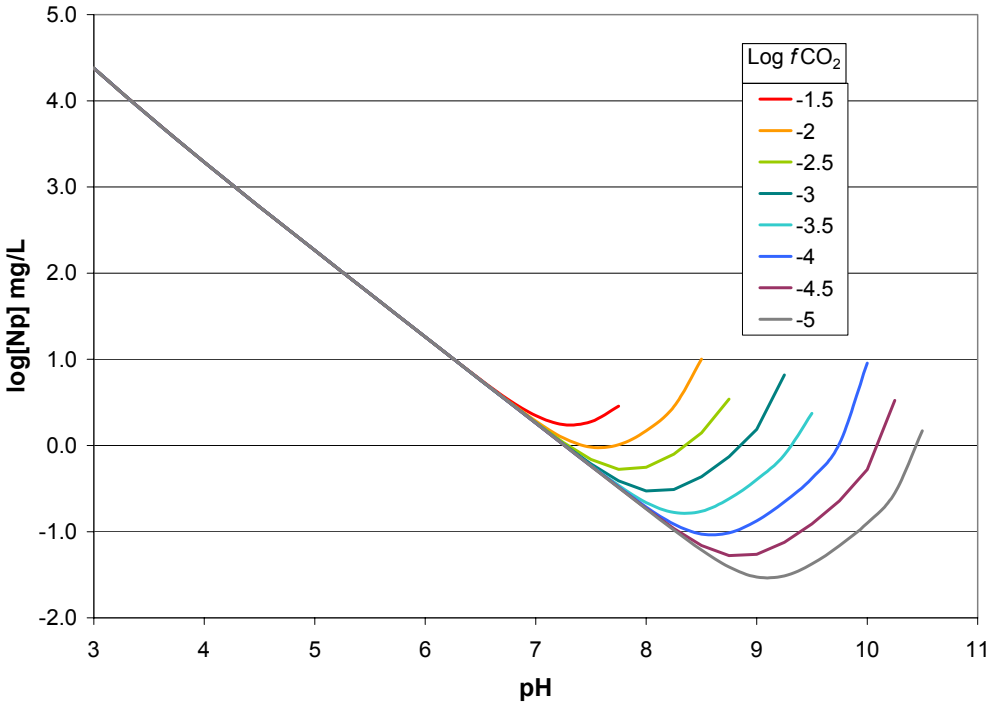

Source: *Np base case-Ehadjusted.xls* (Appendix I).

Figure 6.6-2. Np_2O_5 Solubility Modeled as a Function of pH and log fCO_2

Under the modeled conditions, depending on fCO_2, Np_2O_5 becomes unstable when pH increases and $NaNpO_2CO_3$ becomes a stable phase. Table 6.6-8 lists calculated Np solubility for conditions where Np_2O_5 is unstable and $NaNpO_2CO_3$ is stable. It clearly shows that the stability field of $NaNpO_2CO_3$ is quite narrow (about a 0.25 to 0.5 pH unit). These solubilities are shown separately from those controlled by Np_2O_5 because they are the results of different EQ3 calculations.

Table 6.6-8. Calculated Np Solubility Using $NaNpO_2CO_3$ as the Controlling Phase ([Np] mg/L)

pH	log fCO_2 (bars)						
	-1.5	-2.0	-2.5	-3.0	-3.5	-4.0	-4.5
8.25	3.96E+00						
8.50	2.66E+01						
8.75		1.15E+01					
9.00			6.21E+00				
9.25							
9.50				2.28E+01			
9.75					1.32E+01		
10.00							
10.25						9.17E+01	
10.50							5.72E+01

Np_2O_5 controlled

Source: *Np base case-Ehadjusted.xls* (Appendix I).

Figures 6.6-3 and 6.6-4 show concentrations of total dissolved Np and of aqueous species contributing to that concentration calculated at $fCO_2 = 10^{-3.0}$ bars, expressed as molalities and percent total Np, respectively. The figures span the pH value range from 3 to 10.

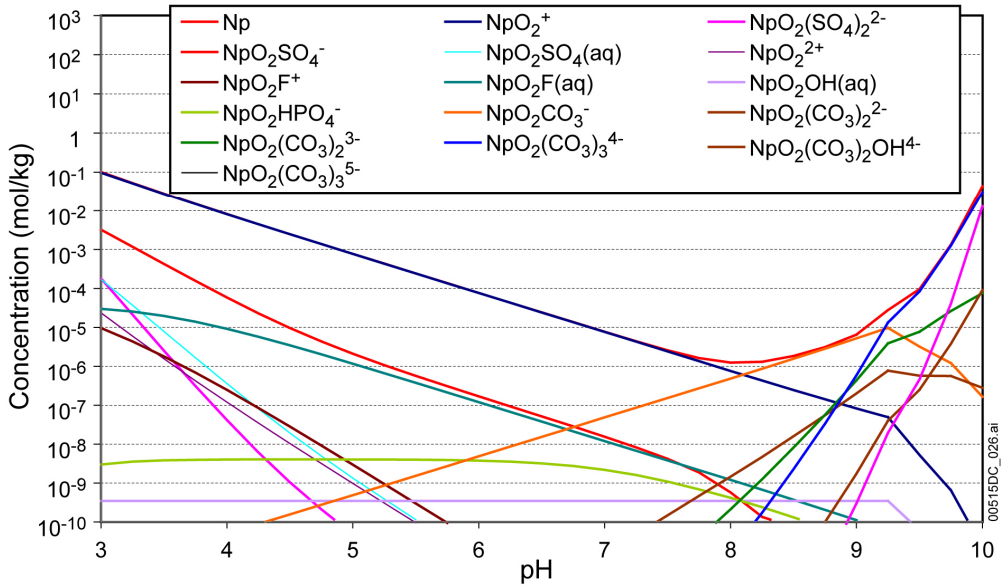

Source: *Np adj Eh species plot.xls* (Appendix I).

Figure 6.6-3. Molal Concentrations of Total Np and of Np Aqueous Complex Species at log fCO_2 (bars) = –3.0 (Ex-Package Model)

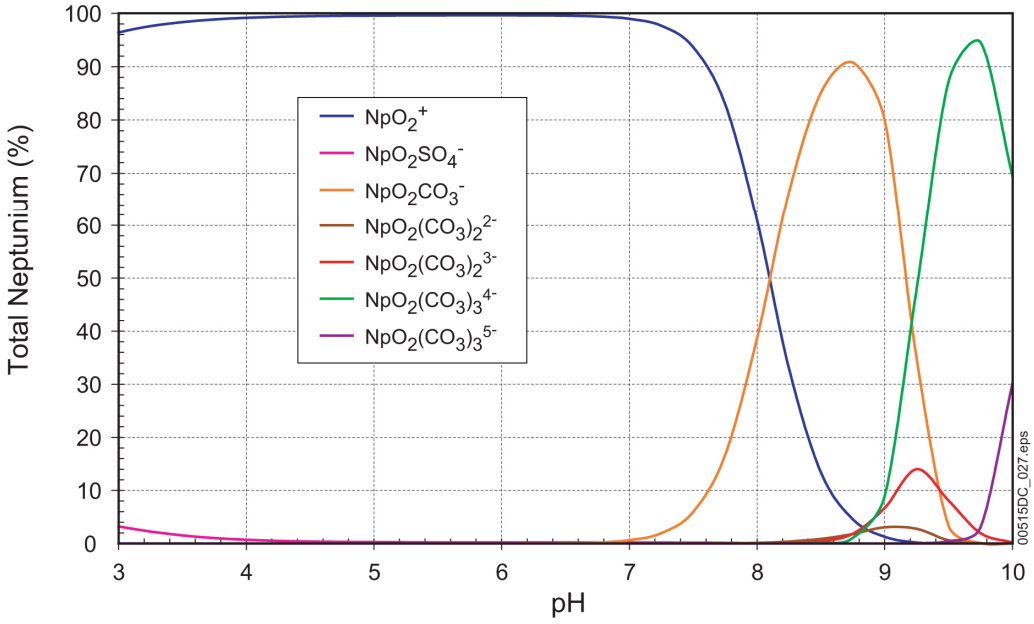

Source: *Np adj Eh species plot.xls* (Appendix I).

Figure 6.6-4. Relative Concentrations of Np Aqueous Complex Species as Percent of Total Dissolved Np at log fCO_2 (bars) = –3.0 (Ex-Package Model)

As Figures 6.6-3 and 6.6-4 show, at fCO_2 equal to 10^{-3}, Np is principally in the Np(V) oxidation state with NpO_2^+ the dominant aqueous species for pH values from 3 to approximately 8. At pH values above 8, virtually all the dissolved Np is present as carbonate complexes including $NpO_2CO_3^-$, $NpO_2(CO_3)_3^{4-}$, $NpO_2(CO_3)_3^{5-}$, $NpO_2(CO_3)_2^{3-}$, $NpO_2(CO_3)_2^{4-}$, and $NpO_2(CO_3)_2OH^{4-}$. Figure 6.6-4 shows that $NpO_2CO_3^-$ is the primary carbonate species between a pH of 8 to 9 and from 9 to 10 is dominated by $NpO_2(CO_3)_3^{4-}$. At a pH of 9, the dominant redox state also shifts from Np(V) to Np(VI) as the principal species become Np(VI) carbonate complexes as indicated by Figure 6.6-4.

6.6.3.3.1 Invert Neptunium Solubility Model for Use in TSPA-LA

Combining the calculated-Np solubility using Np_2O_5 as the controlling phase (Table 6.6-7) and that using $NaNpO_2CO_3$ (Table 6.6-8), Table 6.6-9 is presented for use in TSPA-LA. The logarithm of solubility values is given here to facilitate interpolation that may be needed by the user, because the independent variables of the table are in log scales.

For those calculations that do not converge or are not valid, a large number ("500") is entered to indicate under such pH and fCO_2 conditions, solubility of neptunium is not defined or the calculation results are outside the valid range of the computing tool. When the flag ("500") is encountered or for conditions between a valid solubility and a flag of "500," concentrations should be calculated according to the dissolution rate of individual waste forms, water volume, and the solubility caps presented in Table 8-3 instead of the flag itself. In addition, for conditions outside of the 3.0 to 11.0 pH range, or the fCO_2 range from $10^{-1.5}$ to $10^{-5.0}$ bars, the concentrations should be calculated according to the dissolution rate of individual waste forms, water volume, and the solubility caps presented in Table 8-3.

Table 6.6-9. Np_2O_5-$NaNpO_2CO_3$ Solubility (log[Np], mg/L)

	Log fCO_2 (bars)							
pH	**–1.5**	**–2.0**	**–2.5**	**–3.0**	**–3.5**	**–4.0**	**–4.5**	**–5.0**
3.00	4.38E+00	4.38E+00	4.38E+00	4.38E+00	4.38E+00	4.38E+00	4.38E+00	4.38E+00
3.25	4.10E+00	4.10E+00	4.10E+00	4.10E+00	4.10E+00	4.10E+00	4.10E+00	4.10E+00
3.50	3.82E+00	3.82E+00	3.82E+00	3.82E+00	3.82E+00	3.82E+00	3.82E+00	3.82E+00
3.75	3.55E+00	3.55E+00	3.55E+00	3.55E+00	3.55E+00	3.55E+00	3.55E+00	3.55E+00
4.00	3.29E+00	3.29E+00	3.29E+00	3.29E+00	3.29E+00	3.29E+00	3.29E+00	3.29E+00
4.25	3.03E+00	3.03E+00	3.03E+00	3.03E+00	3.03E+00	3.03E+00	3.03E+00	3.03E+00
4.50	2.77E+00	2.77E+00	2.77E+00	2.77E+00	2.77E+00	2.77E+00	2.77E+00	2.77E+00
4.75	2.52E+00	2.52E+00	2.52E+00	2.52E+00	2.52E+00	2.52E+00	2.52E+00	2.52E+00
5.00	2.26E+00	2.26E+00	2.26E+00	2.26E+00	2.26E+00	2.26E+00	2.26E+00	2.26E+00
5.25	2.01E+00	2.01E+00	2.01E+00	2.01E+00	2.01E+00	2.01E+00	2.01E+00	2.01E+00
5.50	1.76E+00	1.76E+00	1.76E+00	1.76E+00	1.76E+00	1.76E+00	1.76E+00	1.76E+00
5.75	1.51E+00	1.51E+00	1.51E+00	1.51E+00	1.51E+00	1.51E+00	1.51E+00	1.51E+00
6.00	1.26E+00	1.26E+00	1.26E+00	1.26E+00	1.26E+00	1.26E+00	1.26E+00	1.26E+00
6.25	1.01E+00	1.01E+00	1.01E+00	1.01E+00	1.01E+00	1.01E+00	1.01E+00	1.01E+00
6.50	7.66E-01	7.62E-01	7.61E-01	7.60E-01	7.60E-01	7.60E-01	7.60E-01	7.60E-01
6.75	5.35E-01	5.17E-01	5.12E-01	5.11E-01	5.10E-01	5.10E-01	5.10E-01	5.10E-01

Table 6.6-9. Np_2O_5-$NaNpO_2CO_3$ Solubility (log[Np], mg/L) (Continued)

	Log fCO_2 (bars)							
pH	**–1.5**	**–2.0**	**–2.5**	**–3.0**	**–3.5**	**–4.0**	**–4.5**	**–5.0**
7.00	3.46E-01	2.84E-01	2.68E-01	2.63E-01	2.61E-01	2.60E-01	2.60E-01	2.60E-01
7.25	2.41E-01	8.83E-02	3.52E-02	1.83E-02	1.28E-02	1.11E-02	1.05E-02	1.03E-02
7.50	2.76E-01	-1.94E-02	-1.63E-01	-2.14E-01	-2.31E-01	-2.37E-01	-2.39E-01	-2.39E-01
7.75	4.56E-01	8.77E-03	-2.77E-01	-4.12E-01	-4.64E-01	-4.81E-01	-4.87E-01	-4.89E-01
8.00	5.33E-01	1.71E-01	-2.53E-01	-5.29E-01	-6.61E-01	-7.13E-01	-7.31E-01	-7.37E-01
8.25	5.98E-01	4.49E-01	-9.89E-02	-5.11E-01	-7.78E-01	-9.11E-01	-9.63E-01	-9.81E-01
8.50	1.42E+00	1.00E+00	1.47E-01	-3.62E-01	-7.64E-01	-1.03E+00	-1.16E+00	-1.21E+00
8.75	500	1.06E+00	5.38E-01	-1.30E-01	-6.20E-01	-1.01E+00	-1.28E+00	-1.41E+00
9.00	500	500	7.93E-01	1.89E-01	-3.95E-01	-8.75E-01	-1.26E+00	-1.53E+00
9.25	500	500	500	8.19E-01	-1.08E-01	-6.54E-01	-1.12E+00	-1.51E+00
9.50	500	500	500	1.36E+00	3.72E-01	-3.81E-01	-9.10E-01	-1.37E+00
9.75	500	500	500	500	1.12E+00	2.16E-02	-6.44E-01	-1.16E+00
10.00	500	500	500	500	500	9.56E-01	-2.78E-01	-9.00E-01
10.25	500	500	500	500	500	1.96E+00	5.24E-01	-5.52E-01
10.50	500	500	500	500	500	500	1.76E+00	1.72E-01

Source: *Np base case-Ehadjusted.xls* (Appendix I).

NOTE: Some cells have no valid solubility values because the EQ3NR calculations do not converge, and those calculations results are reported as “500” (Section 6.4.4).

6.6.3.3.2 Uncertainties in log K Values of Controlling Solid and Aqueous Species

The uncertainty in solubility involves uncertainties in the thermodynamic properties of both the controlling solid and significant dissolved species. The rationale behind the evaluation and combination of these uncertainties is discussed in some detail in Section 6.3.3.1.

The dissolved species accounting for more than 10 percent of the total dissolved neptunium were found by inspection of Figure 6.6-4. They are NpO_2^+, $NpO_2CO_3^-$, $NpO_2(CO_3)_3^{4-}$, $NpO_2(CO_3)_2^{3-}$, and $NpO_2(CO_3)_3^{5-}$.

After an extensive review, OECD (2001 [DIRS 159027]) recommended −2,031.6 ± 11.2 kJ/mol for the Gibbs free energy of formation of Np_2O_5 based on calorimetric studies. The procedure outlined in Section 6.3.3.1 leads to a log K of 3.7 with a 2σ uncertainty of ±2.8 (at 25°C) for the reaction:

$$Np_2O_5 + 2H^+ = 2NpO_2^+ + H_2O \qquad \text{(Eq. 6.6-3)}$$

This log K value is adopted in *Data0.ymp.R2* (DTN: MO0302SPATHDYN.000 [DIRS 161756]). Efurd et al. (1998 [DIRS 108015]) report a log K value of 5.2 for the reaction presented in Equation 6.6-3 based on solubility experiments using J-13 well water. This higher log K value is attributed to the hydrated nature of the precipitate, which is expected to become a crystalline solid with time due to the aging process. The difference between the log K value adopted in *Data0.ymp.R2* (DTN: MO0302SPATHDYN.000 [DIRS 161756]) and the value

obtained by Efurd et al. (1998 [DIRS 108015]) is 1.5. This is within the calculated 2σ range based on NEA data (± 2.8).

An evaluation of reactions from Np_2O_5 to each of the six dissolved species noted earlier leads to a maximum uncertainty in log K of ±2.83 for reaction of Np_2O_5 to $NpO_2(CO_3)_3^{4-}$. This applies at pH above about 7. For lower pH values, NpO_2^+ prevails with a log K uncertainty of ±2.78. Conservatively, the higher of these is chosen to represent all neptunium solubilities.

The selected Np_2O_5 dissolution reaction discussed in the previous paragraph, which has a 2σ uncertainty in log K of ±3.0 (rounded up from 2.83), produces 2 moles of neptunium in solution per Np_2O_5 formula unit. The uncertainty of the log K of this reaction per mole neptunium is half this value, or ±1.5. This is a 2σ uncertainty, so the 1σ uncertainty to be applied to log[Np] is ±0.8.

The uncertainty of log K for $NaNpO_2CO_3$ dissolution reaction:

$$NaNpO_2CO_3 = Na^+ + NpO_2^+ + CO_3^{2-} \quad \text{(Eq. 6.6-4)}$$

given by the OECD (2001 [DIRS 159027]) is ± 0.501 (2σ), which is much smaller than the uncertainty in log K for Np_2O_5 dissolution reaction. Thus, the uncertainty in log K of $NaNpO_2CO_3$ would not affect the overall uncertainty of the model calculation.

6.6.3.3.3 Uncertainty from Fluoride Concentration

Table 6.6-10 lists the calculated logarithm of Np_2O_5 solubilities using the fluoride levels indicated in Table 6.3-3, (27 and 95 times for the invert). The fugacity of CO_2 is set to $10^{-3.0}$. The differences between the base-case results and the uncertainty case results vary with pH. The two right-hand columns are the differences between the respective elevated F^- cases and the base case. The maximum difference between the base-case results and the 27× fluoride results expressed as log[Np] is 0.026. The maximum uncertainty for fluoride is for codisposal waste packages (vapor-influx scenario, 95× fluoride); the uncertainty term $\varepsilon_2^{\text{CDSP-vapor influx}}$ expressed as log[Np] is 0.079. Unlike uranium, neptunium solubility is not very sensitive to fluoride concentration.

Table 6.6-10. Effects of Variations in Fluoride Concentration on Np Solubility

	Base Case	CDSP – Water-Influx Scenario	CDSP – Vapor-Influx Scenario	CDSP – Water-Influx Scenario	CDSP – Vapor-Influx Scenario
pH	**log[Np] mg/L**			**Difference**	
3.00	4.38E+00	4.39E+00	4.40E+00	6.28E-03	2.26E-02
3.25	4.10E+00	4.11E+00	4.13E+00	9.15E-03	3.33E-02
3.50	3.82E+00	3.84E+00	3.87E+00	1.24E-02	4.53E-02
3.75	3.55E+00	3.57E+00	3.61E+00	1.56E-02	5.65E-02
4.00	3.29E+00	3.31E+00	3.35E+00	1.85E-02	6.49E-02
4.25	3.03E+00	3.05E+00	3.10E+00	2.08E-02	7.03E-02
4.50	2.77E+00	2.79E+00	2.84E+00	2.25E-02	7.36E-02
4.75	2.52E+00	2.54E+00	2.59E+00	2.37E-02	7.57E-02

Table 6.6-10. Effects of Variations in Fluoride Concentration on Np Solubility (Continued)

pH	Base Case	CDSP – Water-Influx Scenario	CDSP – Vapor-Influx Scenario	CDSP – Water-Influx Scenario	CDSP – Vapor-Influx Scenario
	log[Np] mg/L			Difference	
5.00	2.26E+00	2.29E+00	2.34E+00	2.44E-02	7.70E-02
5.25	2.01E+00	2.04E+00	2.09E+00	2.49E-02	7.77E-02
5.50	1.76E+00	1.79E+00	1.84E+00	2.52E-02	7.82E-02
5.75	1.51E+00	1.54E+00	1.59E+00	2.54E-02	7.84E-02
6.00	1.26E+00	1.29E+00	1.34E+00	2.55E-02	7.86E-02
6.25	1.01E+00	1.04E+00	1.09E+00	2.56E-02	7.86E-02
6.50	7.60E-01	7.86E-01	8.39E-01	2.56E-02	7.87E-02
6.75	5.11E-01	5.37E-01	5.90E-01	2.56E-02	7.87E-02
7.00	2.63E-01	2.88E-01	3.41E-01	2.56E-02	7.85E-02
7.25	1.83E-02	4.37E-02	9.62E-02	2.54E-02	7.79E-02
7.50	-2.14E-01	-1.89E-01	-1.38E-01	2.48E-02	7.60E-02
7.75	-4.12E-01	-3.89E-01	-3.41E-01	2.32E-02	7.05E-02
8.00	-5.29E-01	-5.09E-01	-4.70E-01	1.97E-02	5.90E-02
8.25	-5.11E-01	-4.97E-01	-4.69E-01	1.39E-02	4.19E-02
8.50	-3.62E-01	-3.53E-01	-3.34E-01	9.13E-03	2.79E-02
8.75	-1.30E-01	-1.23E-01	-1.07E-01	7.29E-03	2.35E-02
9.00	1.89E-01	1.99E-01	2.26E-01	1.06E-02	3.71E-02
9.25	8.19E-01	8.40E-01	8.92E-01	2.09E-02	7.35E-02
			Maximum	2.6E-02	7.9E-02

6.6.3.3.4 Summary of Np_2O_5–$NaNpO_2CO_3$-Solubility Model Uncertainty

Equation 6.6-5 summarizes the Np_2O_5–$NaNpO_2CO_3$-solubility model:

$$\log[\mathrm{Np}] = S(pH, log f\mathrm{CO}_2) + \varepsilon_1 + (\varepsilon_2 \times N) \qquad \text{(Eq. 6.6-5)}$$

The values for the parameters in this equation depend on the type of waste package. Parameter $S\left(pH, \log f_{CO_2}\right)$ is the base solubility and is taken from Table 6.6-9. Parameter ε_1 is associated with the uncertainties in the log K data. Parameter ε_2 is associated with the uncertainties in the fluoride concentrations. Table 6.6-11 gives the values for parameters ε_1 and ε_2.

Table 6.6-10 shows that the uncertainty terms $\varepsilon_2^{\text{CDSP-water influx}}$ and $\varepsilon_2^{\text{CDSP-vapor influx}}$ vary with pH. This pH dependence can be implemented into the TSPA-LA model through the use of a multiplication factor (N) that is a function of pH. Values for N(pH) for both fuel types are given in Table 6.6-12. This modification requires that the $\varepsilon_2^{\text{CDSP-water influx}}$ and $\varepsilon_2^{\text{CDSP-vapor influx}}$ values be fixed at the maximum value given in Table 6.6-10. For each realization in the TSPA-LA model, the uncertainty parameters are sampled at the beginning of the realization. This sampled

value is then multiplied by N at each timestep to produce a modified ε_2, which is then added to the base solubility value.

Table 6.6-11. Uncertainty Terms of log[Np] of $Np_2O_5/NaNpO_2CO_3$ Model

Uncertainty Term	Associated with	Distribution Type	Distribution Parameter	Applicable to
ε_1	Log K of controlling solid and aqueous species	Normal Truncated at ±2σ	$\mu = 0$, $\sigma = 0.8$[a]	Values in Table 6.6-9
$\varepsilon_2^{\text{CDSP-water influx}}$	Fluoride concentration in codisposal waste packages (water-influx scenario)	Triangular	a = b = 0, c = 0.026	The invert
$\varepsilon_2^{\text{CDSP-vapor influx}}$	Fluoride concentration In CDNR waste package (vapor-influx scenario)	Triangular	a = b = 0, c = 0.079	The invert

NOTE: [a] For ionic strength values between 1 and 3, Log K uncertainty should be treated as a normal distribution truncated at ±2σ with distribution parameters $\mu = 0$, $\sigma = 0.85$ (Section 6.3.3.4, Equation 6.3-7).

Table 6.6-12. Multiplication Factor (N) Used to Modify F^- Uncertainty Term for Neptunium

pH	Multiplication Factor for F^- Uncertainty	
	CDSP – Water-Influx Scenario	CDSP – Vapor-Influx Scenario
3.00	2.45E-01	2.88E-01
3.25	3.57E-01	4.23E-01
3.50	4.84E-01	5.76E-01
3.75	6.10E-01	7.18E-01
4.00	7.21E-01	8.24E-01
4.25	8.10E-01	8.93E-01
4.50	8.78E-01	9.36E-01
4.75	9.25E-01	9.62E-01
5.00	9.54E-01	9.78E-01
5.25	9.74E-01	9.87E-01
5.50	9.85E-01	9.93E-01
5.75	9.92E-01	9.96E-01
6.00	9.95E-01	9.98E-01
6.25	9.98E-01	9.99E-01
6.50	9.99E-01	1.00E+00
6.75	1.00E+00	1.00E+00
7.00	9.98E-01	9.98E-01
7.25	9.91E-01	9.90E-01
7.50	9.69E-01	9.66E-01
7.75	9.05E-01	8.96E-01
8.00	7.69E-01	7.49E-01

Table 6.6-12. Multiplication Factor (N) Used to Modify F^- Uncertainty Term for Neptunium (Continued)

pH	Multiplication Factor for F^- Uncertainty	
	CDSP – Water-Influx Scenario	CDSP – Vapor-Influx Scenario
8.25	5.44E-01	5.32E-01
8.50	3.57E-01	3.54E-01
8.75	2.84E-01	2.99E-01
9.00	4.13E-01	4.71E-01
9.25	8.16E-01	9.34E-01

6.6.4 Alternative Neptunium-Solubility Model: Secondary-Phase Model

6.6.4.1 Laboratory Studies on Np Incorporation

Although, by definition, a solubility-controlling solid may be either a pure solid or a solid solution, pure solids are generally used to evaluate radionuclide solubility for ease of modeling. However, most radionuclides released during the corrosion of spent nuclear fuel may not precipitate as pure phases (Grenthe 1991 [DIRS 161964], pp. 429 to 430; Langmuir 1997 [DIRS 100051], p. 531). Rather, these trace radionuclides may be incorporated into secondary uranium minerals as solid solutions, as uranium will be the most abundant radionuclide released from waste forms in the repository. Many uranyl minerals are known to persist in nature for hundreds of thousands of years (Finch et al. 1996 [DIRS 113056]). This provides a basis for using Np-bearing uranyl compound as long-term Np-limiting solids (> 100,000 years).

Simple mass-balance calculations (Werme and Spahiu 1998 [DIRS 113466]) on the results of spent fuel dissolution experiments as well as neptunium solubility experiments (Werme and Spahiu 1998 [DIRS 113466]; Quinones et al. 1996 [DIRS 161925], p. 42) revealed that the amount of neptunium in the aqueous solution was just a small portion of what should have been released from the dissolved spent nuclear fuel. One explanation for this observation is that released neptunium is included in uranyl solids that form during the degradation process.

Based on an analysis of the crystal-chemical properties of the U–O, Np–O, and Pu–O bonds, Burns et al. (1997 [DIRS 100389], p. 8) predicted "the substitutions Pu^{6+} for U^{6+} and (Np^{5+}, Pu^{5+}) for U^{6+} are likely to occur in most U^{6+} structures."

Recent experiments on humid oxidation of Np-doped U_3O_8 (Np:U=1:8) show formation of NpO_2 in 2 weeks at 150°C and both Np_2O_5 and NpO_2 in 16 weeks at 90°C (Finch 2002 [DIRS 172608]). In these experiments, the starting Np-doped U_3O_8 was demonstrated to be chemically homogeneous, with preliminary X-ray absorption near-edge spectroscopy data indicating that the Np was primarily tetravalent. The Np-doped U_3O_8 was placed inside a crucible within the reaction vessel to prevent direct contact with the added H_2O_2 and water (Finch 2002 [DIRS 172608], p. 641). The vessel was sealed in air and heated. The H_2O_2 was added to the water in order to assure an oxidizing environment in the sealed vessel during the experiment. Oxidation and hydration of the U_3O_8 to dehydrated schoepite was nearly complete at 150°C but only about half way at 90°C. The formation of NpO_2 at 150°C confirms the stability

of that solid at that temperature and suggests that the presence of a redox active solid such as U_3O_8 may catalyze NpO_2 precipitation. At 90°C, it is not clear if both Np_2O_5 and NpO_2 were present either because at that temperature they are equally stable, or if the kinetically favored Np_2O_5 was in the process of converting to NpO_2.

Buck et al. (1998 [DIRS 100388]) examined corrosion products of spent nuclear fuel drip tests by electron energy loss spectroscopy (EELS) analyses in a transmission electron microscope. Their study reported that neptunium was associated with dehydrated schoepite ($UO_3 \cdot 0.8H_2O$) or metaschoepite ($UO_3 \cdot 2H_2O$). Finch et al. (2002 [DIRS 161979]) also reported neptunium association with dehydrated schoepite formed from the reaction of Np-doped U_3O_8 (moles Np:moles U = 1:8, 1:25, 1:80, and 1:160) with water at 90 and 150°C. They estimated that the amount of neptunium associated with dehydrated schoepite may be as high as 2 percent of the host solid based on EELS measurement. These results were later brought into question by Fortner et al. (2003 [DIRS 170980]), who found that plural scattering effects of U interfered with the portion of the EELS spectra of Np used by Buck et al. (1998 [DIRS 100388]) and Finch et al. (2002 [DIRS 161979]). Fortner et al. (2003 [DIRS 170980] found that although they could detect Np in CSNF using X-ray absorption spectroscopy, they could not detect Np in CSNF-alteration products from samples exposed to 100 percent humidity at 90°C for 104 months.

Retention of Np by precipitated uranyl solids has recently been reported by several authors (Buck et al. 2004 [DIRS 172668], Burns et al. 2004 [DIRS 171442]; Friese et al. 2004 [DIRS 172670]; Ebert et al. 2005 [DIRS 173071]). However, the mechanism by which Np was retained in these synthetic uranyl solids (all high surface-area powders) has not yet been identified (e.g., incorporation in the crystal structure, surface sorption, precipitation of amorphous or minor Np-phases).

Burns et al. (2004 [DIRS 171442]) reported the synthesis of uranophane ($Ca(UO_2SiO_3OH)_2 \cdot 5H_2O$) and Na-compreignacite ($Na_2[(UO_2)_3O_2(OH)_3]_2 \cdot 5H_2O$) containing neptunium ranging up to 497 ppm Np. Furthermore, they found that there was a linear relationship between the neptunium content of α-uranophane and Na-compreignacite and the Np^{5+} concentration in their initial synthesis solutions. Burns et al. (2004 [DIRS 171442]) found that only a small amount of Np (a few parts per million) were incorporated in metaschoepite and β-$(UO_2)(OH)_2$. Burns et al. (2004 [DIRS 171442]) attribute this to the lack of suitable low-valence cations in their experiments to provide the charge-balance needed for Np^{5+} incorporation into uranyl (U^{6+}) minerals. Although Burns et al. (2004 [DIRS 171442]) washed their samples to remove any surface sorbed Np, they could not rule out the possibility that a minor/amorphous Np-containing phase, not detectable by X-ray diffraction, could be present in their synthesized samples.

Buck et al. (2004 [DIRS 172668]) coprecipitated Np^{5+} in synthetic studtite. No difference could be found between studtite and Np-doped studtite synthesized under identical conditions (addition of hydrogen peroxide to actinide nitrate solutions) with X-ray diffraction and infrared spectroscopy. Buck et al. (2004 [DIRS 172668]) mention that it is possible that Np may have been incorporated in studtite as Np^{6+} rather than as Np^{5+} under their experimental conditions. Buck et al. (2004 [DIRS 172668]) also analyzed Np-doped uranophane samples that were prepared and then washed to remove adsorbed Np. Using two adjusted EELS techniques that

avoid the U interference encountered by Buck et al. (1998 [DIRS 100388]) and Finch et al. (2002 [DIRS 161979]), Buck et al. (2004 [DIRS 172668]) were able to detect the "high concentration" of Np associated with synthetic studtite and 1,300 and 6,300 ppm of Np associated with samples of synthetic uranophane. Buck et al. (2004 [DIRS 172668]) do not mention washing studtite to remove Np possibly adsorbed on crystal surfaces. None of the analytical techniques used by Buck et al. (2004 [DIRS 172668]) can rule out the presence of an amorphous/trace Np-containing solid phase in their samples.

Friese et al. (2004 [DIRS 172670]) synthesized seven metashoepite samples by adding Np(V) stock solution to uranyl acetate solutions (mol % Np = 0 to 2) and adjusting the pH to values ranging from 4.5 to 10.4. These solutions were allowed to age at room temperature for 2 days and centrifuged for 10 minutes. The liquids were decanted, while the solids were washed with deionized water (3×) and air-dried. Both the decanted liquids and the solids were counted by gamma energy analysis. All solids precipitated were identified as metashoepite or sodium uranium hydroxide hydrate ($Na_2(UO_2)_6(OH)_{14}{\cdot}4H_2O$) by X-ray diffraction analysis. Friese et al. 2004 [DIRS 172670] found that for starting solutions ranging from mol% Np = 0 to 2 aged at pH = 5.5, Np uptake/association with the precipitated solids increased slightly but remained less than 1 percent of the total Np. For starting solutions with mol% Np = 1 but aged with pH values ranging from 6.5 to 10.4, the Np association with the solid increases to 100 percent. Friese et al. (2004 [DIRS 172670]) hypothesized that more Np could be incorporated in metashoepite at high pH since more Na^+ was available to achieve charge balance, but could not rule out the possibility of Np adsorbed on the solids or an amorphous or minor undetected Np solid being responsible for Np uptake.

Ebert et al. (2005 [DIRS 173071], Section 3) have also attempted to coprecipitate Np in U^{6+} solids by adjusting the pH of solutions containing U, Ni, and Np in ratios relevant to a breached waste package with NaOH or tris(hydroxymethyl)aminomethane. These samples were then shaken for 9 days at 90°C. The solids separated from these experiments have not yet been characterized, but the removal of Np from the sample solutions during precipitation is greater than 80 percent for samples titrated with sodium hydroxide to pH values greater than 7. Samples titrated with tris(hydroxymethyl)aminomethane to similar pH values show neptunium uptake of less than 40 percent. This suggests that sodium, which is not present in the tris titrated samples but is available in the NaOH-titrated samples, plays an important role in the neptunium uptake process. Although these Np uptake percentages may also include adsorbed Np, this observation is consistent with the hypothesis that sodium is providing charge compensation that facilitates the incorporation of neptunium into the structure of the precipitating uranyl oxide hydrate.

Recent examination of CSNF specimens that had been subjected to corrosion testing for up to 10 years under unsaturated conditions shows that neptunium and plutonium in CSNF samples remained in proximity to the corroding surface during corrosion and were not retained in the alteration rind (Ebert et al. 2005 [DIRS 173071]). This observation is consistent with the hypothesis that Np is not oxidized to the soluble Np(V) oxidation state as the fuel corrodes because the potential needed to effect this oxidation is higher than the corrosion potential of the CSNF matrix that hosts the neptunium in the Np(IV) oxidation state (Ebert et al. 2005 [DIRS 173071]). This may explain the apparent discrepancy between reported association of neptunium with uranyl phases in the direct synthesis experiments mentioned above and the absence or very low levels of neptunium observed in uranyl alteration phases derived from

corroded CSNF; the CSNF-derived uranyl phases are relatively depleted in neptunium because neptunium has resisted oxidation and is thus unavailable in the solution from which uranyl phases are precipitating (Ebert et al. 2005 [DIRS 173071]).

6.6.4.2 Information Needed to Model Np Incorporation in Uranyl Minerals for TSPA-LA

Although it has been proposed as a model for estimating dissolved Np concentrations (Chen 2003 [DIRS 162709]; Chen et al. 2002 [DIRS 161996]), there is evidence for the incorporation of Np into the structures of only some of the U(VI) corrosion products. Experiments are still needed that can help establish the following (Ebert et al. 2005 [DIRS 173071]):

- Identities of the most relevant U(VI) solids that are likely to sequester neptunium
- Whether Np is incorporated into the structures of U(VI) corrosion products
- The molar Np:U ratio (or range of Np:U ratios) in Np-bearing U(VI) corrosion products
- The molar Np:U ratio (or range of Np:U ratios) in solutions in contact with Np-bearing U(VI) corrosion products
- The limit of Np concentrations in U(VI) compounds under repository-relevant conditions
- The fate of Np during the alteration of early formed U(VI) corrosion products as they continue to interact with in-package aqueous solutions and Yucca Mountain groundwaters.

To model dissolved Np concentrations likely to be controlled by the solubilities of Np-bearing solid corrosion products (if they exist), the following quantitative data are needed of each potentially relevant Np-bearing solid (Ebert et al. 2005 [DIRS 173071]; BSC 2001 [DIRS 154844]):

- The solubilities and thermodynamic stabilities in water chemistries expected in the repository
- Equilibrium partitioning of Np between relevant solids and aqueous solutions (Henry's Law behavior) as a function of solution chemistry, and possibly as a function of solid chemistry as well
- Precipitation and dissolution rates for all relevant Np-bearing solids (kinetic rate laws).

Of the U(VI) minerals precipitated in the experiments above or that are formed during the degradation of CSNF or uraninite, only Na-boltwoodite, schoepite, soddyite, α-uranophane, and Na-weeksite are represented in the thermodynamic database used for geochemical modeling for the Yucca Mountain Repository (BSC 2004 [DIRS 171916]). Therefore, solubility modeling of Np based on Np-U solid solutions will also require the determination of thermodynamic and solubility data for the relevant missing U end members.

6.6.4.3 Concentrating Factor of Neptunium

The experimental data described above show that the neptunium concentrations in solutions degrading spent nuclear fuel are considerably lower than concentrations controlled by pure-neptunium solids. An empirical neptunium solubility limit was developed based on drip test measurements, which does not rely on the identification of neptunium-bearing phases or assumptions about neptunium retention mechanisms (Chen 2001 [DIRS 161997]; Chen et al. 2002 [DIRS 161996]).

The concentrating factor of neptunium in solution is defined as:

$$F_c = \frac{(Np/U)_{soln}}{(Np/U)_{fuel}} \qquad \text{(Eq. 6.6-6)}$$

where $(Np/U)_{soln}$ denotes the ratio of neptunium to uranium in solution and $(Np/U)_{fuel}$ denotes the same ratio in spent nuclear fuel. The concentrating factor (F_c) of neptunium describes the degree of neptunium being concentrated in solution relative to the spent nuclear fuel with which it is in contact.

Rearranging Equation 6.6-6 yields:

$$[Np] = F_c(Np/U)_{fuel}[U] \qquad \text{(Eq. 6.6-7)}$$

where [Np] and [U] denote the concentrations of neptunium and uranium in solution, respectively.

Equation 6.6-7 indicates neptunium concentration is proportional to uranium concentration. The proportionality constant, $(Np/U)_{fuel}$, is a product of a known value of the ratio of neptunium and uranium in the fuel. The uncertain concentrating factor, F_c, is obtained from spent nuclear fuel dissolution experimental data.

6.6.4.3.1 Simple Estimation of F_c of Neptunium Using Data from ANL Drip Tests

Unsaturated spent nuclear fuel dissolution tests developed for the YMP have been described in detail in several journal articles (Finn et al. 1994 [DIRS 100746]; Finn et al. 1997 [DIRS 124142]) and in *Secondary Uranium-Phase Paragenesis and Incorporation of Radionuclides into Secondary Phases* (BSC 2001 [DIRS 154844]). Based on the rates of water added to the spent nuclear fuel samples, those experiments were grouped into three categories: high drip-rate tests, low drip-rate tests, and vapor tests. All other environmental conditions were constant. The tests are designed to simulate the evolution of spent nuclear fuel and the release of radionuclides in the repository. The concentrations of several radionuclides in the leachate were measured and reported (CRWMS M&O 2000 [DIRS 131861]; CRWMS M&O 2000 [DIRS 153105]; DTN: LL991001251021.090 [DIRS 129285]).

Two types of commercial spent nuclear fuel, approved testing material (ATM)-103 with a burn-up of 30 MW-d/kgU and ATM-106 with a burnup of 43 MW-d/kgU (Finn et al. 1994 [DIRS 100746]), were used in the experiments. The calculated $^{237}Np/^{238}U$ ratios in those two

fuels are listed in Table 6.6-13 using the inventory tables given by Guenther et al. (1988 [DIRS 109205]; 1988 [DIRS 109206]), assuming 15 years out of the reactor (Section 5.2).

Table 6.6-13. Calculated Mole Ratio of ^{237}Np to ^{238}U in the Fuels Used in ANL Experiments

	ATM-103	ATM-106
Burnup	30 MW-d/kgU	43 MW-d/kgU
Np-237/U-238	4.20E-04	6.44E-04

Source: *ANL6dripdata.xls* (Appendix I).

There are 46 concentration values of ^{237}Np and ^{238}U available from the high drip-rate and low drip-rate tests (DTN: LL991001251021.090 [DIRS 129285]; CRWMS M&O 2000 [DIRS 153105]). Because isotope fractionation is not expected to significantly change the isotopic ratios of the leachate from that of the fuel, it is concluded that:

$$F_c = \frac{(Np/U)_{soln}}{(Np/U)_{fuel}} = \frac{(Np^{237}/U^{238})_{soln}}{(Np^{237}/U^{238})_{fuel}} \quad \text{(Eq. 6.6-8)}$$

Figure 6.6-5 is a histogram of the log F_c values calculated from the 46 sets of experiments reported. Log F_c has a normal distribution with a mode around 0.0 (i.e., F_c has a mode of 1.0).

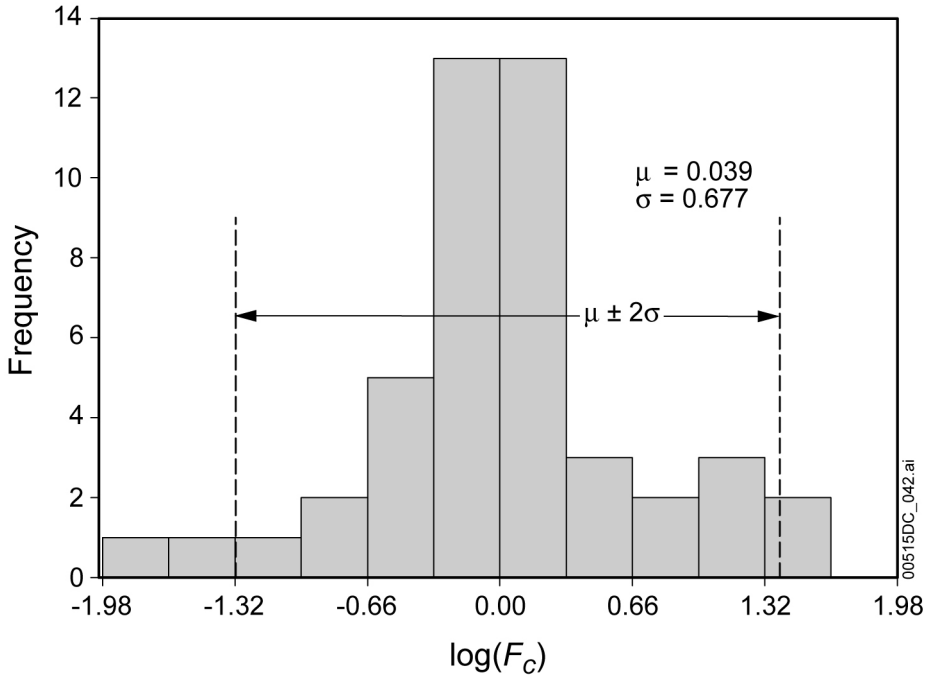

Source: *Fc histogram.jnb* (Appendix I).

Figure 6.6-5. Histogram of F_c on a log Scale

Table 6.6-14 lists the statistical description of F_c for neptunium determined from the ANL high and low drip tests. Of the 46 data points, the geometric mean of F_c is 1.094, which is very close to 1. In other words, the arithmetic mean of log F_c is 0.039, which is very close to 0. The

standard deviation of log F_c is 0.667. With a confidence level of 95 percent, the upper and lower statistical limits ($\mu \pm 2\sigma$) of log F_c are 1.394 and −1.316, respectively. In other words, the probability for log F_c falling between the statistical limits (−1.316, 1.394) is 95.5 percent. Translated back to F_c, the upper and lower limits of F_c are 24.787 and 0.048, respectively. That is the range of uncertainty in F_c of neptunium from ANL high-drip and low-drip tests. It spans less than 3 orders of magnitude.

The fact that the average of log F_c is very close to 0.0 and has a mode of 0.0 strongly suggests that the neptunium–uranium values in the solutions are very close to the neptunium–uranium values in the fuels. In other words, uranium and neptunium are released from the fuel congruently.

In fact, the congruent relation between uranium and neptunium has also been observed in other spent nuclear fuel dissolution experiments. For example, based on PNNL Series 2 and Series 3 steady-state test results, Wilson (1990 [DIRS 100949]; 1990 [DIRS 100793]) states that "the data suggest that Np enters the aqueous phase congruently with uranium as the fuel dissolves." The calculated F_c for Series 2 tests ranges from 0.44 to 2.59, with a geometric mean of 1.13 (*PNL-wilson.xls,* Appendix I). The calculated F_c for Series 3 tests ranges from 3.38 to 11.73, with a geometric mean of 5.90 (*PNL-wilson.xls,* Appendix I).

Table 6.6-14. Statistics of F_c of Neptunium from High and Low Drip Tests

	F_c	log F_c
Number of Samples	46	46
Maximum	30.260	1.481
Minimum	0.015	-1.833
Arithmetic Mean (μ)	3.363	0.039
Geometric Mean	1.094	
Standard Deviation (σ)		0.677
$\mu + 2\sigma$		1.394
$\mu - 2\sigma$		-1.316
Upper Limit (UL) of 95% Confidence Level ($UL = 10^{\mu+2\sigma}$)	24.787	
Lower Limit (LL) of 95% Confidence Level ($LL = 10^{\mu-2\sigma}$)	0.048	
Ratio of Upper to Lower Limit	513.407	

Source: *ANL6dripdata.xls* (Appendix I).

Bruno et al. (1998 [DIRS 101565]) have also observed the congruent relation between neptunium and uranium in spent nuclear fuel dissolution experiments in the Spanish Nuclear Waste Program as shown in Table 6.6-15.

Table 6.6-15. Neptunium–Uranium Ratios in Spent Nuclear Fuel and Its Solution

	Fuel Inventory	Solution
Np/U	4.88E-4	5.25E-4

Source: Bruno et al. 1998 [DIRS 101565].

It is unlikely that the congruent relation between uranium and neptunium is a coincidence. Rather, it reflects the similarity of geochemical behaviors of U(VI) and Np(V). Incorporation of neptunium into uranyl minerals is the most reasonable explanation for this relation.

In summary, based on the simple statistics of ANL drip test data, F_c is a log-normal random variable, with a mean of 1.094. At a confidence level of 95.5 percent, it ranges from 0.048 to 24.787, an uncertainty range of less than three orders of magnitude. However, as explained in Section 6.6.4.3.2, the large departures from F_c ~1 are observed under conditions not relevant to TSPA-LA.

6.6.4.3.2 Trend Analysis of F_c of Neptunium Using Data from ANL Drip Tests

The previous section discussed the conventional statistics of F_c of neptunium. This section further analyzes the variation of F_c in time.

Figure 6.6-6 shows the F_c of neptunium in the ANL high-drip tests as a function of time. The low-drip results are shown in Figure 6.6-7. The solid lines are tests with ATM-103 fuel, while the dashed lines are tests for ATM-106 fuel. They show that in those four tests, F_c of neptunium fluctuates around 1.0. Moreover, in all the tests, the highest F_c occurs in the first sample, and then F_c decreases and reaches the lowest value within two years. In other words, the big variations in F_c occur in the first two years, and decrease with time. This suggests that the coherent relation between neptunium and uranium becomes more obvious as time increases, and the spikes of F_c values observed in the first two years are transient phenomena in the drip tests. The rapid release of neptunium at the early stage of experiments has also been observed in PNNL Series 2 and Series 3 tests (Wilson 1990 [DIRS 100949], Figure 3.5, p. 3.18; Wilson 1990 [DIRS 100793], Figure 3.19, p. 3.39). Early transient phenomena are thought to be due to fuel fines and supersaturation effects. Because this report focuses on long-term performance of the repository, these spikes are not considered to be important. Therefore, it is reasonable to exclude the early data from the ANL drip tests when F_c is estimated.

Excluding those data points measured at time less than two years, subset data (containing 28 data points) of the four drip tests were obtained. Table 6.6-16 presents the statistical results for the subset data. The geometric mean of this reduced data set is still close to 1.0 (1.142), but with a smaller standard deviation. The upper and lower limits of F_c at a confidence level of 95.5 percent now are 10.653 and 0.122, respectively. The data spans less than 2 orders of magnitude.

Table 6.6-16. Statistics of F_c of Neptunium from the Subset of High and Low Drip Tests (t ≥ 2yr.)

Statistic Name	Fc	log Fc
Number of Samples	28	28
Maximum	16.347	1.213
Minimum	0.032	-1.048
Arithmetic Mean (μ)	1.954	0.058
Geometric Mean	1.142	
Standard Deviation (σ)		0.485
μ +2σ		1.027
μ -2σ		-0.912
Upper Limit of 95% Confidence Level (UL = $10^{\mu+2\sigma}$)	10.653	
Lower Limit of 95% Confidence Level (LL = $10^{\mu-2\sigma}$)	0.122	
Ratio of Upper Limit to Lower Limit	86.974	

Source: *ANL6dripdata.xls* (Appendix I).

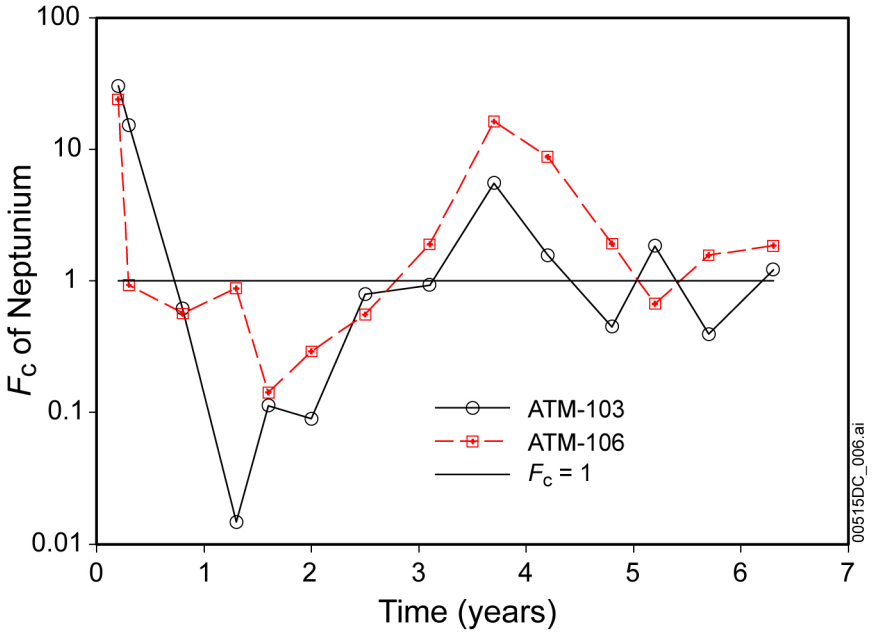

Source: *HighDrip-Fc.jnb* (Appendix I).

NOTE: F_c of neptunium fluctuates around 1 and appears to damp to 1 as time increases.

Figure 6.6-6. F_c Values of Neptunium in the ANL High-Drip Tests as a Function of Time

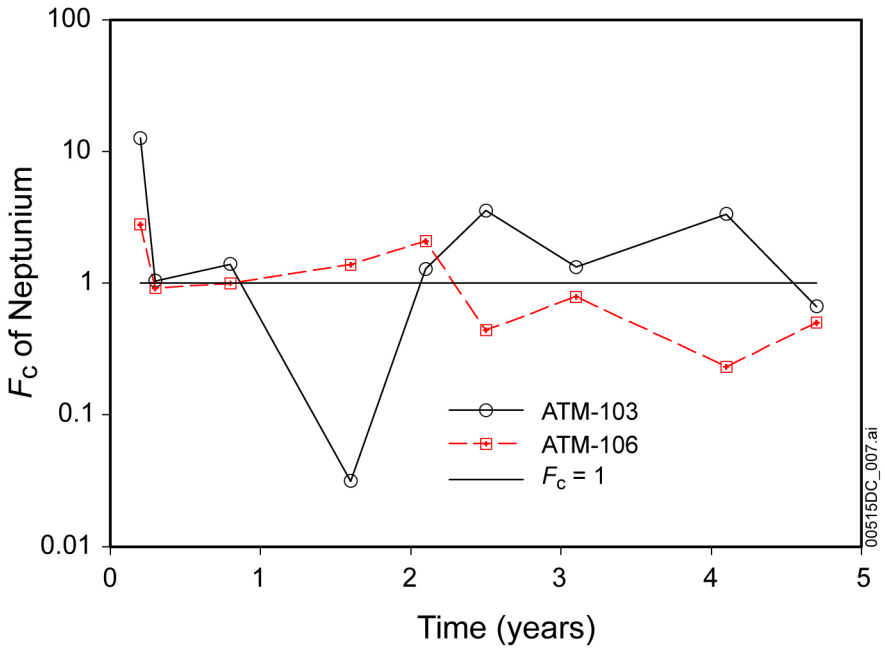

Source: *LowDrip-Fc.jnb* (Appendix I).

NOTE: Similar to Figure 6.6-6, F_c of neptunium fluctuates around 1 and appears to damp to 1 as time increases.

Figure 6.6-7. F_c Values of Neptunium in the ANL Low-Drip Tests as a Function of Time

In summary, excluding the early data points that represent the transient period, F_c was estimated with a geometric mean of 1.142 and ranges from 0.122 to 10.653.

6.7 URANIUM SOLUBILITY

6.7.1 Introduction

Under the oxidizing conditions of the repository, uranium is in the U(VI) (uranyl) oxidation state. To provide U concentrations over the full range of possible environmental conditions, the solubilities of three uranyl (UO_2^{2+}) solids have been modeled: the minerals schoepite ($UO_3 \cdot 2H_2O$) and Na-boltwoodite ($NaUO_2SiO_3OH \cdot 1.5H_2O$), and $Na_4UO_2(CO_3)_3$. The conditions under which each is the controlling solid depend on the ambient water chemistry, pH, and fCO_2. For the case of water found on CSNF following waste package breaching under nominal conditions or by a hypothetical seismic event, U concentrations are controlled by schoepite under all pH and fCO_2 conditions. For codisposal packages under all breach scenarios, CSNF packages breached in the course of an intrusive event and in the invert, all three minerals control the U concentration under various ranges of pH and fCO_2.

Section 6.7.2 discusses the selection of the controlling solids and the conditions under which each is active. Section 6.7.3 describes the chemical conditions for which the calculations were made. The results are given in Section 6.7.4 and include tables of U concentrations for CSNF and codisposal packages at a range of pH and fCO_2 values for various breach scenarios. Section 6.7.5 discusses the uncertainties associated with the U concentrations, while Section 6.7.6 is a concluding summary.

6.7.2 Factors Considered in Selecting Controlling Solids

Following a waste package breach, the exposed waste and other waste package components react with incoming water, either seepage dripping (water-influx scenario) into the failed waste package or water condensed or sorbed (vapor-influx scenario) on waste package internal surfaces (BSC 2004 [DIRS 167621]). The oxidizing state of the repository promotes oxidation of U(IV) to U(VI) and its subsequent dissolution to uranyl ions and other aqueous uranyl species. When the concentration of uranyl and its aqueous species reaches the solubility of uranium solids, precipitation occurs and limits further increases in the total dissolved concentration of uranium. The selection of the uranium-controlling solids was based on three factors: (1) the paragenesis of uranium minerals in laboratory and natural studies, (2) the stability of uranium phases in the possible environments of TSPA-LA, and (3) the availability of thermodynamic data for the phases of interest. If there is no thermodynamic data for a U solid, the phase was eliminated from further consideration as a solubility-controlling phase because it is not possible to determine the solubility of a mineral phase and the resultant aqueous concentration of uranium if there are no thermodynamic data available for that phase. However, this will have no impact, as those phases indicated in the references below that have missing thermodynamic data were not in great abundance or were replaced by other U minerals for which there is thermodynamic data.

Laboratory studies are the basis for the selection of the controlling phases (Finch et al. 1996 [DIRS 113056], Table 1; Murphy 1997 [DIRS 101731]; Wronkiewicz et al. 1992 [DIRS 100493]). A recent and thorough laboratory study (Wronkiewicz et al. 1996 [DIRS 102047]) describes the results of a 10-year study of UO_2 degradation at 90ºC in dripping J-13 type water equilibrated with tuff. The U-bearing alteration phases observed in that study are given in Table 6.7-1. The availability of thermodynamic data for modeling is also shown in the table.

The alteration paragenesis found in the laboratory begins with uranyl-oxide hydrate minerals (principally of the schoepite group) and passes to alkali and alkaline earth uranyl silicate hydrates, ultimately Na-boltwoodite. Uranophane is also an important secondary silicate but it is clear that the final silicate phase is Na-boltwoodite (Wronkiewicz et al. 1996 [DIRS 102047], Section 4.2.1 and Figure 7).

Table 6.7-1. Phases Observed During 10-Year Degradation of UO_2 by Dripping Water of J-13 Composition and Corresponding Phases in the Modeling Database, *Data0.ymp.R2*

Mineral	Phases Formed During Laboratory Degradation of UO_2 and Composition[a]	Composition of Phases for Thermodynamic Data Available in *Data0.ymp.R2*[b]
Uranyl-Oxide Hydrates		
Ianthinite	$UO_2 \cdot 5UO_3 \cdot 10H_2O$	No thermodynamic data available for placement into *Data0.ymp.R2*
Dehydrated Schoepite	$UO_3 \cdot$(0.8 to 1.0 H_2O)	$UO_2(OH)_2$
Schoepite	$UO_3 \cdot nH_2O$ (n<2)	$UO_3 \cdot 2H_2O$
Compreignacite	$K_2[(UO_2)_6O_4(OH)_6] \cdot 8H_2O$	No thermodynamic data available for placement into *Data0.ymp.R2*

Table 6.7-1. Phases Observed During 10-Year Degradation of UO_2 by Dripping Water of J-13 Composition and Corresponding Phases in the Modeling Database, *Data0.ymp.R2* (Continued)

Mineral	Phases Formed During Laboratory Degradation of UO_2 and Composition[a]	Composition of Phases for Thermodynamic Data Available in *Data0.ymp.R2*[b]
Becquerelite	$Ca[(UO_2)_6O_4(OH)_6]\cdot 8H_2O$	No thermodynamic data available for placement into *Data0.ymp.R2*
Uranyl Silicate Hydrate		
Soddyite	$(UO_2)_2SiO_4\cdot 2H_2O$	$(UO_2)_2SiO_4\cdot 2H_2O$
Alkali and Alkaline Earth Uranyl Silicate Hydrates		
Uranophane	$Ca[(UO_2)(SiO_3)(OH)]_2\cdot 5H_2O$[a]	$Ca(UO_2SiO_3OH)_2\cdot 5H_2O$
Sklodowskite	$Mg(UO_2)_2(SiO_4)_2(H_3O)_2\cdot 2H_2O$	No thermodynamic data available for placement into *Data0.ymp.R2*
Weeksite	$K_2(UO_2)_2(Si_2O_5)_3\cdot 4H_2O$	No thermodynamic data available for placement into *Data0.ymp.R2*
Boltwoodite	$K_2(UO_2)_2(SiO_4)_2(H_3O)_2\cdot 2H_2O$	No thermodynamic data available for placement into *Data0.ymp.R2*
Na-boltwoodite	$(Na, K)(UO_2)(SiO_4)(H_3O)\cdot H_2O$	$NaUO_2SiO_3OH\cdot 1.5H_2O$

Source: [a]Wronkiewicz et al. 1996 [DIRS 102047], Table 5.
[b]DTN: MO0302SPATHDYN.000 [DIRS 161756].

NOTE: [a] Brackets missing in Wronkiewicz et al. 1996 [DIRS 102047], Table 5.

As waste packages degrade, the total aqueous U concentration is controlled by the concentration of the complexing ligands (Section 6.4.3) in solution and by the least-soluble uranium phase that is stable for the current fCO_2 and pH conditions. For TSPA-LA, U solubilities must be available for a wide range of possible in-drift–in-package environment pH and fCO_2 values. For conditions of high pH and high fCO_2, there were neither natural analogues nor laboratory studies to provide a framework for selecting a solubility-controlling phase. In these conditions, model runs were executed to simulate the environment in question and determine if a particular mineral phase was stable in that environment. These model runs showed that when the dissolved carbonate reaches a high enough concentration, the solid $Na_4UO_2(CO_3)_3$ forms, limiting further increase in dissolved U.

Data0.yc3.R1 incorporates uranium thermodynamic data compiled by the NEA Thermodynamic Data Project (Grenthe et al. 1992 [DIRS 101671]; Silva and Nitsche 1995 [DIRS 112092]; Guillaumont et al. 2003 [DIRS 168382]). This database was used to calculate uranium solubility and uncertainty terms that account for the effects of temperature and fluoride concentration. Uncertainties in the thermodynamic data themselves were based on values provided in the NEA volumes (Grenthe et al. 1992 [DIRS 101671]; Silva and Nitsche 1995 [DIRS 112092]; Guillaumont et al. 2003 [DIRS 168382]).

Table 6.7-1 shows the uranyl minerals found during laboratory degradation studies for which data are available in *Data0.ymp.R2* (DTN: MO0302SPATHDYN.000 [DIRS 161756]). These are dehydrated schoepite, schoepite, soddyite, uranophane, and Na-boltwoodite. Schoepite, rather than dehydrated schoepite, is selected as one of the controlling phases because laboratory

studies show it to be the dominant early formed phase in UO_2 degradation (Wronkiewicz et al. 1996 [DIRS 102047]). Soddyite and uranophane are found in laboratory degradation studies, but Na-boltwoodite was chosen because it is reported to be the final silicate phase. In the calculations discussed here, the solubility of soddyite is virtually the same as that of schoepite and considerably higher than that of Na-Boltwoodite. Uranophane was not included because it contains calcium. The high carbonate contents of waters with high fCO_2 and pH values leads to low calcium contents because of the limited solubility and rapid formation of calcite ($CaCO_3$) or similar alkaline-earth carbonate minerals. Under these conditions, uranophane would be relatively soluble.

6.7.2.1 Studtite and Metastudtite

Because of the recent plethora of data concerning the minerals studtite and metastudtite that have been made available over the past few years, the following discussion addresses the usefulness of considering these minerals as a solubility-controlling phase for uranium.

Studtite ($UO_4 \cdot 4H_2O$) and metastudite ($UO_4 \cdot 2H_2O$) are the only peroxide minerals known. According to Burns and Hughes (2003 [DIRS 173090], p. 1,165) they have been found in the uranium deposits at Shinkolobwe, Katanga, Democratic Republic of the Congo, and at the Krunkelbach mine, Menzenschwand, Germany. Finch and Ewing (1990 [DIRS 130384]; 1992 [DIRS 113030]) discuss, at length, the uranium mineralization at Shinkolobwe. They describe studtite and metastudtite occurrences in small clusters on the surface of uranyl minerals and suggest they may form in the presence of H_2O_2 generated by radiolysis of water near the surface of the uranium minerals. Neither mineral is described among those identified as products of laboratory tests of spent nuclear fuel degradation (Wronkiewicz et al. 1992 [DIRS 100493]; 1996 [DIRS 102047]).

In the last several years, these minerals have attracted attention because they have been found associated with UO_2 degradation in water subjected to irradiation by alpha particles from a particle accelerator (Sattonnay et al. 2001 [DIRS 173091]) or from spent nuclear fuel (McNamara et al. 2003 [DIRS 172673]). Also, according to McNamara et al. (2003 [DIRS 172673], p. 401) and Sattonnay et al. (2001 [DIRS 173091], p. 17), they have been recognized in other environments with strong radiation fields such as the surface of Chernobyl "lavas" and on the external surfaces of the zircaloy cladding of fuel elements in the Hanford K-east Basin. These minerals appear to form where radiation doses are sufficient to produce peroxide levels high enough to stabilize them, and they must now be considered in any discussion of spent nuclear fuel degradation in a repository environment.

Burns and Hughes (2003 [DIRS 173090]) determined the crystal structure of studtite. Its structural formula is $[(UO_2)(O_2)(H_2O)_2](H_2O)_2$, which is identical to its compositional formula $UO_4 \cdot 4H_2O$. The U(VI) in studtite is at the center of distorted uranyl hexagonal bypyramids. In these, the U(VI) is in linear UO_2^{2+} (uranyl) ions and is additionally bound to four O atoms of peroxide groups and two H_2O groups. The uranyl polyhedra are polymerized into chains by sharing the O atoms of peroxide groups. The chains are linked by hydrogen bonding with interstitial H_2O groups. Metastudtite ($UO_4 \cdot 2H_2O$) is apparently formed by the dehydration of studtite, but its structure has not yet been determined.

Sattonnay et al. (2001 [DIRS 173091]) studied the effects of alpha radiolysis on UO_2 alteration in aerated, deionized water. They did so using a range of fluxes provided by an alpha beam from a cyclotron followed by characterization of the chemistry of both the aqueous solution and the UO_2 surface. Dissolved U (uranyl) and H_2O_2 concentrations increased and pH values decreased with increasing alpha flux. Metastudite was identified on the surface of the UO_2 by X-ray diffraction.

Sattonnay et al. (2001 [DIRS 173091]) point out that the alpha fluxes in their experiments far exceed those to be expected from spent nuclear fuel. However, they also note that if the effects of radiolysis are cumulative with time, accumulated doses from lower flux sources such as spent nuclear fuel or even natural uranium deposits might be sufficient to produce H_2O_2 concentrations high enough to form peroxide minerals. For example, they calculate that a dose equivalent to one hour of radiation at the highest flux they used would accumulate after several years of spent nuclear fuel storage.

McNamara et al. (2003 [DIRS 172673]) examined the phases formed on spent nuclear fuel immersed in small quantities of water for about two years. One-gram samples of fuel were reacted with 8 mL of deionized water in capped vials. Similar tests with unirradiated fuel were run in parallel. Initially samples were held at 60°C, 75°C, and 90°C and fluid samples were drawn weekly. After five weeks the samples were stored in the dark at 28°C. After two years, five of the original 30 sample vials still contained water, although the water volume had been reduced by about half. All vials sampled had schoepite and metaschoepite alteration in the samples taken within the first few weeks and this type of alteration persisted for the two-year period for those samples from which all water had evaporated. The five samples that still contained water had studtite on the fuel surfaces and metastudtite in aggregates accumulated at the air-water interface in the vials. No peroxide measurements were made.

These tests differ from other spent nuclear fuel tests in which studtite formation was not observed (e.g., Wilson 1990 [DIRS 100949] and [DIRS 100793]). The UO_2/water ratios were about the same in both series of tests, but in Wilson's tests fresh water was added to maintain the original volume after sample aliquots were taken, while in the tests of McNamara et al. (2003 [DIRS 172673]) the capped vials were not disturbed during the two-year storage period. McNamara et al. (2003 [DIRS 172673]) reiterate the Sattonnay et al. (2001 [DIRS 173091]) suggestion that a long water-solid contact time is required for peroxide concentrations to reach levels high enough for studtite or metastudtite to form.

McNamara et al. (2004 [DIRS 173085]) present results of radiochemical analyses of the studtite that formed on the solid surfaces and the metastudtite aggregates found at the air-water interfaces of the experiments summarized in the previous paragraphs. These data do not provide additional insight into the conditions leading to the formation of the peroxide phases.

Several groups of experimenters report the formation of studtite and metastudtite from uranyl solution by the direct addition of H_2O_2. Sattonnay et al. (2003 [DIRS 173091], p. 17) refer to several of these and two others will be discussed here.

Kubatko et al. (2003 [DIRS 173070]) determined the enthalpy of formation of the same specimen of mineral studtite for which the structure was determined by Burns and Hughes (2003 [DIRS 173090]). They also studied the reaction:

$$UO_2^{2+} + H_2O_2 + 4H_2O = UO_4 \cdot 4H_2O + 2H^+$$

at UO_2^{2+} concentrations from 2.5×10^{-8} to 2.6×10^{-5} mol, H_2O_2 concentrations from 7.6×10^{-5} to 1×10^{-2} mol. Because of the production of acid by the reaction the final solution pH values ranged from 2.9 to 3.4 at 25ºC. The ion activity product (IAP) of this reaction is:

$$IAP_{studtite} = [UO_2^{2+}] \cdot [H_2O_2] / [H^+]^2$$

Kubatko et al. (2003 [DIRS 173070]) consider that their experiments represent equilibrium so IAP values calculated from their data correspond to studtite solubility products. From their experiments, Kubatko et al. (2003 [DIRS 173070]) obtained a value of$1.34 \pm 0.02 \times 10^{-3}$, which is equivalent to a logK(25ºC) of dissolution of 2.87±0.01. It is of interest that this value is close to a handbook value of 2.826 for this constant quoted by Amme (2002 [DIRS 173088], p. 403) for a solution "of a nearly neutral pH value."

$IAP_{studtite}$ values can also be calculated from the experimental data given by Sattonnay et al. (2001 [DIRS 173091], Table 1). These values (1.3 and 2.7) indicate oversaturation of studtite by 1 or 2×10^3 relative to the solubility product of Kubatko et al. (2003 [DIRS 173070]).

Amme (2002 [DIRS 173088]) describes experiments in which depleted UO_2 pellets were placed in deionized water and groundwater with concentrations of H_2O_2 set from 10^{-5} to 10^{-2} mol by the addition of concentrated H_2O_2. After 1,000 hours of reaction, the solutions were filtered and analyzed, and the surface of the solids was examined by scanning electron microscopy. In 10^{-5} mol H_2O_2 solutions, U concentrations were 5×10^{-5} to 1×10^{-6} mol. U concentrations noticeably decreased to 5×10^{-7} mol in 10^{-2} mol H_2O_2 solutions. The inverse relationship between U and H_2O_2 concentrations would be consistent with studtite precipitation by the reaction given above. $IAP_{studtite}$ values can be calculated from Amme's (2002 [DIRS 173088]) data using solution concentrations read from Figure 1 and pH values from Table 1. The $IAP_{studtite}$ values are from 10^3 to 10^4, far above the solubility product given by Kubatko et al. (2003 [DIRS 173070]). Amme's (2002 [DIRS 173088]) U concentrations, in fact, are closer to those calculated for schoepite saturation (Figure 6.7-1) at low pCO_2 values and pH values around 6.8, which correspond to those at the end of Amme's experiments. Amme did not analyze the H_2O_2 contents of his solutions at the end of his experiments nor make the X-ray diffraction analyses necessary to identify the phase(s) formed during his experiment.

Whether studtite or metastudtite is likely to form in the Yucca Mountain environment appears to depend on the levels of H_2O_2 that develop in the waters in which the waste is degrading. Certainly H_2O_2 will be formed by radiolysis in water contacting the waste, but the question of the concentrations likely to found in that water must be addressed.

Bruno et al. (1999 [DIRS 173089]) report measurements of the concentrations of H_2, O_2, H_2O_2, U and other radioelements that developed when spent nuclear fuel was placed in deaerated solutions of 10 mmol $NaHCO_3$. Four experiments were carried out using the same spent nuclear

fuel sample. In all experiments, H_2 and O_2 concentrations increased with time and reached levels over 10^{-6} mol H_2 and O_2 at about 900 hours (Bruno et al. (1999 [DIRS 173089]), Figures 4-1 to 4-4). The H_2O_2 concentration of all but the first experiment decreased from about 3×10^{-7} to 10×10^{-7} at 100 to 200 hours to about 1.5×10^{-7} to 2×10^{-7} mol at 900 to 1,000 hours (Bruno et al. 1999 [DIRS 173089], Table 8-1). In the first experiment, the H_2O_2 concentration increased from 2.5×10^{-8} at 26 hours to 1.2×10^{-7} mol at 312 hours. The authors attribute the different behavior of their first experiment to the fact that the fuel surface was fresh; whereas, in the other experiments, the fuel had already oxidized.

The inverse relationships between dissolved O_2 and H_2O_2 in these experiments is consistent with the thermodynamic properties of the two substances. H_2O_2 is a stronger oxidant than O_2, but H_2O_2 is also unstable in the presence of O_2. That is, the Gibbs energy of the reaction $H_2O_2 = H_2O + ½\ O_2$ is negative (Stumm and Morgan 1996 [DIRS 125332], p. 673). Furthermore, the dissolved oxygen content of water in contact with the atmosphere at 25ºC is 2.6×10^{-4} mol (Langmuir 1997 [DIRS 100051], p. 420). This is far higher than the O_2 concentrations developed as a result of radiolysis in the experiments of Bruno et al. (1999 [DIRS 173089]). The thermodynamics of the $H_2O_2 - O_2$ reaction supported by the experimental results of Bruno et al. (1999 [DIRS 173089]) indicate that H_2O_2 concentrations in water in contact with the atmosphere should be vanishingly small. This being the case, studtite is not likely to form in the Yucca Mountain environment, in which waste degrades in contact with the atmosphere.

The occurrences of studtite and metastudtite in certain natural environments and in laboratory radiolysis experiments, as discussed above, do not contradict this conclusion. The very rare appearances of these minerals in degrading UO_2 deposits are thought to result from radiolysis occurring in microenvironments with little on no contact with the atmosphere where high concentrations of H_2O_2 could develop over long periods. The laboratory experiments were carried out at far higher fluxes than expected from waste or on solutions that were not in contact with the atmosphere. Neither case is analogous to the conditions at Yucca Mountain.

6.7.3 Chemical Conditions

The chemical conditions for the solubility calculations are given in Table 6.4-2. The range of pH and fCO_2 values within the CSNF and codisposal packages and in the invert is discussed in Sections 6.4.2.3 and 6.4.2.4. For CSNF packages, the minimum pH is 4.5 and the maximum increases from 7.0 at $\log fCO_2 = -1.5$ bars to 8.1 at −5.0 bars. For codisposal packages, the pH range is from 5.0 to 8.4, while waters in the invert may have pH values ranging from 3.5 to 10.5. As discussed in Section 4.1, the composition of the base-case water used for the solubility calculations is that of J-13 well water (Table 4-2). During modeling, Na^+ or SO_4^{--} is added as needed to achieve solution electroneutrality at the pH values specified as discussed in Section 6.4.3.5.

Solubility calculations were carried out for two environments based on those used for modeling the chemistry of in-package fluids (BSC 2004 [DIRS 167621]). The first comprises CSNF packages breached under the nominal or seismic scenarios. In these, the source of the degrading water is water vapor entering the packages, which has low or no initial dissolved Na or silica contents. Although the actual modeling of solubilities in all packages is carried out using the base-case J-13 well water, the mass of silica available is small relative to the mass of U available

because of the small volume of water available in this scenario. Thus, should conditions favoring Na-boltwoodite precipitation occur, precipitation of even small amounts of this mineral forces dissolved silica concentrations to very low values so the effective control of U concentrations under all conditions is schoepite. U solubilities in the first environment were modeled using J-13 well water with U concentrations determined by schoepite solubility for all conditions of pH and fCO_2.

The second environment comprises codisposal packages breached under all scenarios, CSNF packages breached under the intrusion scenario and the invert. In this environment, silica is available to the degrading water from the codisposal glass, surrounding igneous material, and invert construction material, so Na-boltwoodite is included as a U-controlling phase. U concentrations based on this mineral vary inversely with dissolved silica concentrations, so selection of the silica concentration used in the modeling is important.

Table 6.7-2 compares the log K(25°C) values of all the SiO_2 solids in *Data0.ymp.R2* (DTN: MO0302SPATHDYN.000 [DIRS 161756]). The table also gives the dissolved Si and SiO_2(aq) concentrations corresponding to these log K(25°C) values in pure water (water with ionic strength, i = 0, so solute activity = solute molality). For comparison, Table 6.7-2 also gives the Si content of J-13 well water in corresponding units. This concentration corresponds to solubility with a phase intermediate between cristobalite (alpha) and coesite. Because of other sources of silica in the second environment, the silica content of J-13 well water was not used as the silica concentration in the modeling. Instead, dissolved silica is modeled as controlled by the mineral chalcedony, which leads to concentrations within the upper range of silica concentrations in natural groundwater (Section 7.2.4). Choosing chalcedony saturation leads to silica content about one-third that of J-13 well water and to higher, more-conservative modeled U concentrations.

Table 6.7-2. Silica Phases for Which Data Are Provided in Thermodynamic Database, *Data0.ymp.R2*

Phase	log K(25°C)[a] *Data0.ymp.R2*	Si (mol/L at I = 0)[b]	Si (mg/L at I = 0)[b]	SiO_2 (mg/L at I = 0)[b]
Tridymite	-3.82	1.51E-04	4.3	9.1
Quartz	-3.75	1.78E-04	5.0	10.7
Chalcedony	-3.47	3.39E-04	9.5	20.4
Cristobalite(alpha)	-3.19	6.46E-04	18.1	38.8
Coesite	-2.93	1.17E-03	33.0	70.6
Cristobalite(beta)	-2.75	1.78E-03	49.9	106.8
SiO_2(am)	-2.71	1.95E-03	54.8	117.2
	log(Si mol/L)[c]			
J-13 well water	-2.99	1.01E-03	28.5	60.97

Source: [a]log K(25°C) data from DTN: MO0302SPATHDYN.000 [DIRS 161756]
[b]*Silica solids_a.xls* (Appendix I)
[c]J-13 well water data from Table 4-2.

The Na concentration of J-13 well water is ~2 mmol. This increases above pH 8 (at $\log fCO_2 = -3.0$ bars) because Na is added as the charge-balancing cation. The

Si concentration fixed by chalcedony saturation is ~0.35 mmol to pH 8, increasing to ~0.6 mmol at pH 9.

The Na and Si contents of waters predicted by *Engineered Barrier System: Physical and Chemical Environment* (BSC 2004 [DIRS 169860]) and *In-Package Chemistry Abstraction* (BSC 2004 [DIRS 167621]) have been examined for consistency with those used for Na-boltwoodite modeling. The comparisons were made at $\log fCO_2 = -3.0$ bars, as it is the value at which *In-Package Chemistry Abstraction* (BSC 2004 [DIRS 167621]) calculations were made. Calculations in this report and in *In-Package Chemistry Abstraction* (BSC 2004 [DIRS 167621]) were made at 25°C. The closest temperature used in *Engineered Barrier System: Physical and Chemical Environment* (BSC 2004 [DIRS 169860]) was 40°C. Calculations supporting *Engineered Barrier System: Physical and Chemical Environment* (BSC 2004 [DIRS 169860]) reach very high ionic strengths. For consistency with the range of applicability of the results of this report, *Engineered Barrier System: Physical and Chemical Environment* (BSC 2004 [DIRS 169860]) waters with ionic strengths above 3 were not considered (Section 6.3.3.4).

Data used for the comparison were from *checked MOALT r1.xls*, which is included *Engineered Barrier System: Physical and Chemical Environment Model* (BSC 2004 [DIRS 169860], *Attachment_1.zip*). Eight of the more than 5,000 realizations of seepage water chemistry in this file have Na concentrations below 2 mmol, the lowest of which is 1.3 mmol. None of the realizations have Si concentrations below 0.35 mmol. Use of the higher Na and Si contents of *Engineered Barrier System: Physical and Chemical Environment Model* (BSC 2004 [DIRS 169860]) waters would lead to lower U concentrations in equilibrium with Na-boltwoodite. Therefore, the concentrations given in this report are conservative with respect to *Engineered Barrier System: Physical and Chemical Environment* (BSC 2004 [DIRS 169860]) waters.

Data used for the in-package chemistry abstraction were from *In-Package Chemistry Abstraction* (BSC 2004 [DIRS 167621], Appendix F). None of the Na concentrations in the waters emanating from codisposal packages are below 2 mmol. The Si contents of these waters range from ~ 0.1 mmol at lower pH values to as low as ~0.03 mmol at pH values above 7.5. These low Si contents appear to be because of the precipitation of silica-bearing nontronite clays (BSC 2004 [DIRS 167621], Figures 6-9 and 6-10). The comparison with groundwater concentrations described earlier indicates that the selection of chalcedony as the silica-controlling phase for these calculations is appropriate.

6.7.4 Results: Speciation and Solubility

Figures 6.7-3 and 6.7-4 show concentrations of total dissolved uranium and of aqueous species contributing to that total calculated at $fCO_2 = 10^{-3.0}$ bars, expressed as molalities and percents total uranium, respectively.

The inflection points in the line representing total U concentrations in Figure 6.7-3 are where solubility control by one mineral gives way to control by another. As illustrated in Figure 6.7-2, schoepite, the controlling phase at low pH values, is replaced by Na-boltwoodite at a pH of about 7.25, which in turn is replaced by $Na_4UO_2(CO_3)_3$ at a pH of about 9.25. The decrease in

U concentration above pH 9.25 in Figure 6.7-3 is because the Na^+ added to charge balance the solutions at higher pH values decreases the solubility of $Na_4UO_2(CO_3)_3$.

The dominant dissolved species from the highest pH values modeled to about pH 8.1 is $UO_2(CO_3)_3^{3-}$. With decreasing pH, this is succeeded by $UO_2(CO_3)_2^{2-}$ and $(UO_2)_2CO_3(OH)_3^-$. Below about pH 6.6, UO_3(aq) prevails. This species is more commonly written as $UO_2(OH)_2$ (e.g., NEA and NAGRA/PSI databases). Uranyl fluoride complexes, principally UO_2F^+ but with up to more than 10 percent UO_2F_2(aq), prevail from below about pH 6.2 to 4.5. Around pH of 4.5, UO_2^{2+} is an important species and, under conditions more acidic than pH of 4.25, UO_2SO_4(aq) predominates.

Table 6.7-3 and Figure 6.7-1 show the U concentrations calculated for the first environment described in the previous section (CSNF packages breached under nominal conditions or by seismic events). Although values are given for pH values from 3.5 to 7.0 at $fCO_2 = 10^{-1.5}$ bars and to 9.75 at $fCO_2 = 10^{-5.0}$ bars, the actual pH range in this environment is the more narrow region between the heavy lines in the table and the shaded lines in the figure. As discussed, only schoepite controls U solubility in this environment.

Table 6.7-3. Calculated Uranium Solubility as Log [U] (mg/L) Within CSNF Waste Packages Breached Under Nominal Conditions or by Seismic Activity

	log fCO_2 (bars)							
pH	**-1.5**	**-2.0**	**-2.5**	**-3.0**	**-3.5**	**-4.0**	**-4.5**	**-5.0**
3.50	**4.41E+00**	**4.41E+00**	**4.41E+00**	**4.41E+00**	**4.41E+00**	**4.41E+00**	**4.41E+00**	**4.41E+00**
3.75	**3.55E+00**	**3.55E+00**	**3.55E+00**	**3.55E+00**	**3.55E+00**	**3.55E+00**	**3.55E+00**	**3.55E+00**
4.00	**2.87E+00**	**2.87E+00**	**2.87E+00**	**2.87E+00**	**2.87E+00**	**2.87E+00**	**2.87E+00**	**2.87E+00**
4.25	2.33E+00	2.33E+00	2.33E+00	2.33E+00	2.33E+00	2.33E+00	2.33E+00	2.33E+00
4.50	1.93E+00	1.92E+00	1.92E+00	1.92E+00	1.92E+00	1.92E+00	1.92E+00	1.92E+00
4.75	1.62E+00	1.60E+00	1.60E+00	1.59E+00	1.59E+00	1.59E+00	1.59E+00	1.59E+00
5.00	1.35E+00	1.32E+00	1.31E+00	1.31E+00	1.30E+00	1.30E+00	1.30E+00	1.30E+00
5.25	1.10E+00	1.03E+00	1.00E+00	9.95E-01	9.93E-01	9.92E-01	9.92E-01	9.91E-01
5.50	9.31E-01	7.65E-01	6.97E-01	6.74E-01	6.66E-01	6.63E-01	6.63E-01	6.62E-01
5.75	9.05E-01	6.19E-01	4.67E-01	4.07E-01	3.86E-01	3.79E-01	3.77E-01	3.76E-01
6.00	1.03E+00	6.26E-01	3.76E-01	2.51E-01	2.03E-01	1.87E-01	1.82E-01	1.80E-01
6.25	1.25E+00	7.58E-01	4.13E-01	2.07E-01	1.17E-01	8.36E-02	7.27E-02	6.92E-02
6.50	1.52E+00	9.60E-01	5.30E-01	2.48E-01	9.90E-02	3.93E-02	1.87E-02	1.19E-02
6.75	1.86E+00	1.21E+00	7.12E-01	3.53E-01	1.32E-01	3.21E-02	-4.74E-03	-1.71E-02
7.00	2.33E+00	1.51E+00	9.38E-01	5.01E-01	2.11E-01	5.47E-02	-8.42E-03	-3.04E-02
7.25	500	1.89E+00	1.20E+00	6.98E-01	3.34E-01	1.09E-01	6.00E-03	-3.21E-02
7.50	500	2.54E+00	1.52E+00	9.32E-01	4.92E-01	2.00E-01	4.29E-02	-2.10E-02
7.75	500	500	1.98E+00	1.21E+00	6.96E-01	3.26E-01	1.09E-01	7.58E-03
8.00	500	500	500	1.58E+00	9.38E-01	4.97E-01	2.12E-01	6.04E-02
8.25	500	500	500	2.27E+00	1.24E+00	7.07E-01	3.47E-01	1.45E-01

Table 6.7-3. Calculated Uranium Solubility as Log [U] (mg/L) Within CSNF Waste Packages Breached Under Nominal Conditions or by Seismic Activity (Continued)

pH	log fCO_2 (bars)							
	-1.5	-2.0	-2.5	-3.0	-3.5	-4.0	-4.5	-5.0
8.50	500	500	500	500	1.73E+00	9.65E-01	5.26E-01	2.59E-01
8.75	500	500	500	500	500	1.34E+00	7.47E-01	4.16E-01
9.00	500	500	500	500	500	2.11E+00	1.04E+00	6.11E-01
9.25	500	500	500	500	500	500	1.58E+00	8.56E-01
9.50	500	500	500	500	500	500	500	1.24E+00
9.75	500	500	500	500	500	500	500	2.08E+00

Source: *U solubility_dtn.xls*.

NOTE: These concentrations correspond to schoepite saturation.

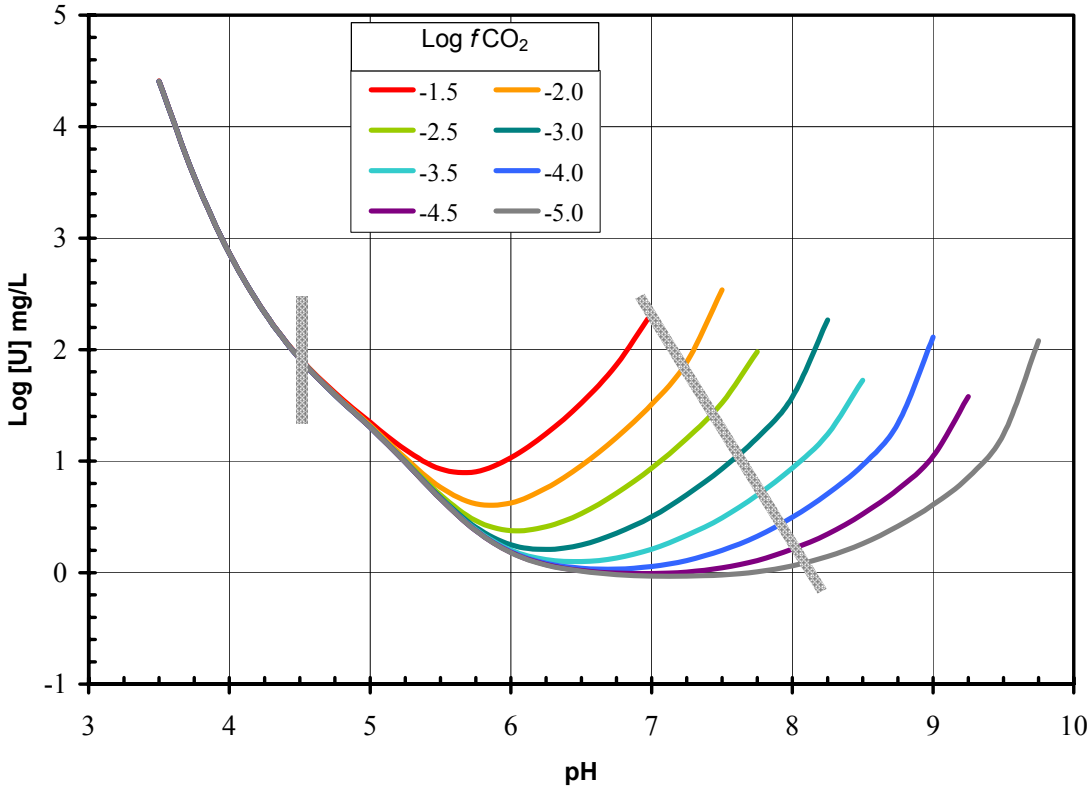

Source: *U solubility plots.xls*.

NOTE: Schoepite is the controlling mineral under all conditions of pH and fCO_2. Shaded bars are boundaries of pH and fCO_2 conditions possible in such packages.

Figure 6.7-1. Uranium Solubility in CSNF Packages Breached Under Nominal and Seismic Scenarios Modeled as a Function of pH and fCO_2

The U concentrations calculated for the second environment (CSNF packages breached by a hypothetical igneous event, all codisposal packages, and water in the invert) are provided in

Tables 6.7-5 and 6.7-6 and illustrated in Figure 6.7-2. In this environment, U concentrations are controlled by schoepite, Na-boltwoodite, or $Na_4UO_2(CO_3)_3$ depending on the pH and fCO_2 as illustrated in the Figure 6.7-2.

At the lower pH values, schoepite is the least soluble phase. At pH values around neutral, there is an inflection in the concentration curves where the solubility curves of Na-Boltwoodite cross those of schoepite, so the controlling mineral phase changes. With increasing pH values, U concentrations increase steeply. The pH values corresponding to this increase vary inversely with fCO_2 being lowest at the highest fCO_2 values. This is due to the increasing carbonate content of the water with increasing pH and fCO_2, which leads to the formation of high concentrations of uranyl carbonate-solution complexes. When the carbonate content reaches sufficiently high values, the uranyl carbonate solid, $Na_4UO_2(CO_3)_3$, becomes stable, thereby limiting further increases in the U concentration.

The pH value at which schoepite control of U concentrations gives way to control by Na-boltwoodite at a given fCO_2 was calculated directly using EQ3NR to solve for the pH at which both minerals were in equilibrium. EQ3NR would not converge when solving for the pH at which Na-boltwoodite and $Na_4UO_2(CO_3)_3$ were in equilibrium because Na^+ is the charge-balancing cation and a constituent of the solubility-controlling phases. Thus, an indirect approach was taken by modeling a reaction path using EQ6. The path began with a solution at a given fCO_2 and pH at equilibrium with an excess of Na-boltwoodite. This solution was titrated with NaOH while maintaining Na-boltwoodite saturation and the initial fCO_2. The pH and U concentration rose with added NaOH until $Na_4UO_2(CO_3)_3$ saturation was reached. At this point, the pH and U concentration remained constant with further NaOH addition as the initial Na-boltwoodite reacted to form $Na_4UO_2(CO_3)_3$. This constant pH is that of the crossover from Na-boltwoodite to $Na_4UO_2(CO_3)_3$. The crossover pH values are given in Table 6.7-4 and shown schematically in Figure 6.7-2.

Table 6.7-4. pH Values at Which Control of Uranium Concentrations Gives Way from Schoepite to Na-boltwoodite and from Na-boltwoodite to $Na_4UO_2(CO_3)_3$ at Various fCO_2 Values

	log fCO_2 (bars)							
Mineral	**-1.5**	**-2.0**	**-2.5**	**-3.0**	**-3.5**	**-4.0**	**-4.5**	**-5.0**
Schoepite - Na-boltwoodite	6.85	7.12	7.18	7.18	7.18	7.18	7.18	7.18
Na-boltwoodite - $Na_4UO_2(CO_3)_3$	7.71	8.21	8.71	9.21	9.71	10.19	10.61	10.91

Source: *U LogK Uncertainty_a.xls* (Appendix I).

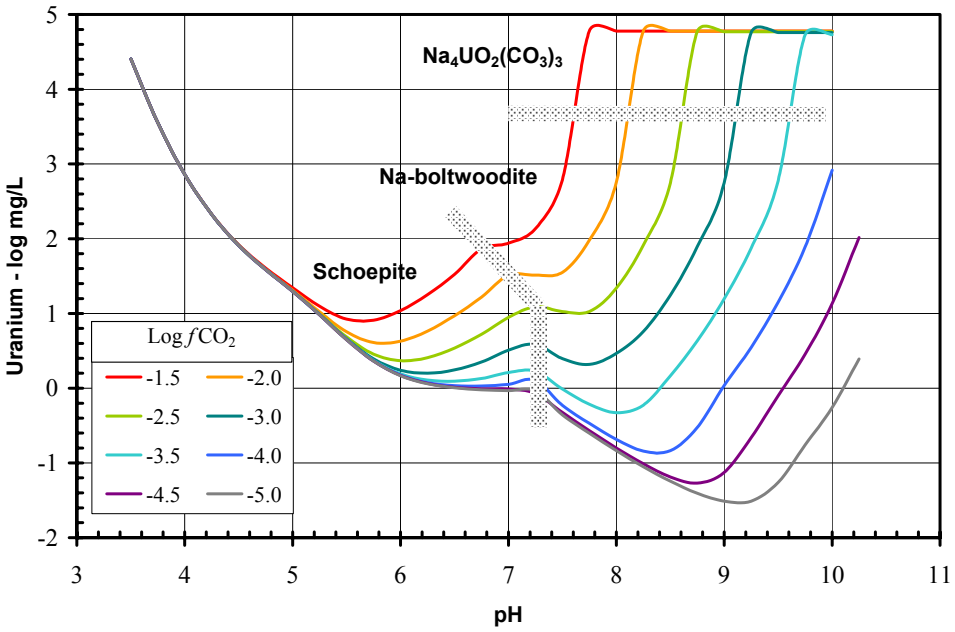

Source: *U solubility plots.xls* (Appendix I).

NOTE: Shaded areas are boundaries between pH–fCO_2 regions controlled by indicated minerals.

Figure 6.7-2. Uranium Solubility in CSNF Packages Breached by a Hypothetical Igneous Event, Codisposal Packages Under Any Breach Scenario and Waters in the Invert Modeled as a Function of pH and fCO_2

The concentrations in Table 6.7-5 represent schoepite solubility and extend over lower pH values where this mineral is the least soluble of the three phases considered. Table 6.7-6 represents solubilities of Na-boltwoodite and $Na_4UO_2(CO_3)_3$ and covers the higher pH ranges. As discussed in Section 6.7.5.1, uncertainties in thermodynamic data lead to a range of pH and log fCO_2 values in which either schoepite or Na-boltwoodite could control the U concentration. This range is indicated by the green shading in Tables 6.7-5 and 6.7-6. In implementing these tables in the TSPA-LA model, for conditions in this range, the U concentration should be sampled from a uniform distribution with bounds based on the values in these tables.

In Table 6.7-6, the value "500" appears as the concentration at pH = 10.25 for log fCO_2 values of –3.5 bars and higher. This is not to be taken literally, but as a flag that the U concentrations are undefined under these conditions. Solutions saturated with $Na_4UO_2(CO_3)_3$ under these conditions have ionic strengths greater than 3 molal, which is taken as the limit of reliability of these calculations (Section 6.3.3.4). The pH and log fCO_2 values at which they appear are beyond the range possible for the environment to which this table is applicable.

Tables 6.7-3 and 6.7-5 give U concentrations based on schoepite saturation for overlapping ranges of pH and fCO_2, yet there are differences of up to 0.13 log mg U/L between them. This difference results from the use of J-13 well water silica concentrations (60.97 mg SiO_2(aq)/L) in the modeling for Table 6.7-3, and chalcedony saturation (~20.4 mg SiO_2(aq)/L; Table 6.7-2) in

the modeling for Table 6.7-5. Higher dissolved silica concentrations give rise to higher U concentrations because of the presence of the $UO_2OSi(OH)_3^+$ solution complex. Higher silica contents lead to higher concentrations of this complex and, in turn, to higher total dissolved U concentrations. The minimum uncertainty in schoepite concentrations is that due to uncertainties in thermodynamic data and equals ±0.5 (ε_1 parameter in Equation 6.7-4; Section 6.7.6). The concentration difference due to the differing silica contents is within this minimum uncertainty. The Pu concentration shown in Figure 6.4-10 has no sensitivity to varying silica contents at these concentrations because the database used for modeling includes no Pu-silicate aqueous complex species analogous to one causing U sensitivity to silica.

Table 6.7-5. Calculated Uranium Solubility (Controlled by Schoepite) as log [U] (mg/L) Within Codisposal Waste Packages Breached Under Any Scenario, CSNF Waste Packages Breached by a Hypothetical Igneous Intrusion and in the Invert

Schoepite								
	log fCO_2 (bars)							
pH	-1.5	-2.0	-2.5	-3.0	-3.5	-4.0	-4.5	-5.0
3.50	4.41E+00	4.41E+00	4.41E+00	4.41E+00	4.41E+00	4.41E+00	4.41E+00	4.41E+00
3.75	3.55E+00	3.55E+00	3.55E+00	3.55E+00	3.55E+00	3.55E+00	3.55E+00	3.55E+00
4.00	2.86E+00	2.86E+00	2.86E+00	2.86E+00	2.86E+00	2.86E+00	2.86E+00	2.86E+00
4.25	2.33E+00	2.33E+00	2.33E+00	2.33E+00	2.33E+00	2.33E+00	2.33E+00	2.33E+00
4.50	1.92E+00	1.91E+00	1.91E+00	1.91E+00	1.91E+00	1.91E+00	1.91E+00	1.91E+00
4.75	1.61E+00	1.59E+00	1.59E+00	1.59E+00	1.59E+00	1.59E+00	1.59E+00	1.59E+00
5.00	1.34E+00	1.31E+00	1.30E+00	1.30E+00	1.30E+00	1.30E+00	1.30E+00	1.30E+00
5.25	1.10E+00	1.02E+00	9.94E-01	9.85E-01	9.83E-01	9.82E-01	9.81E-01	9.81E-01
5.50	9.24E-01	7.55E-01	6.86E-01	6.62E-01	6.54E-01	6.51E-01	6.51E-01	6.50E-01
5.75	9.10E-01	6.11E-01	4.57E-01	3.94E-01	3.73E-01	3.66E-01	3.64E-01	3.63E-01
6.00	1.04E+00	6.30E-01	3.68E-01	2.41E-01	1.92E-01	1.75E-01	1.70E-01	1.68E-01
6.25	1.25E+00	7.66E-01	4.09E-01	2.01E-01	1.09E-01	7.55E-02	6.43E-02	6.08E-02
6.50	1.52E+00	9.70E-01	5.37E-01	2.45E-01	9.45E-02	3.42E-02	1.33E-02	6.55E-03
6.75	1.86E+00	1.22E+00	7.22E-01	3.52E-01	1.30E-01	2.93E-02	-7.88E-03	-2.03E-02
7.00	2.33E+00	1.51E+00	9.48E-01	5.09E-01	2.10E-01	5.32E-02	-1.02E-02	-3.22E-02
7.25		1.89E+00	1.21E+00	7.08E-01	3.34E-01	1.08E-01	5.05E-03	-3.31E-02
7.50		2.54E+00	1.53E+00	9.44E-01	5.01E-01	2.00E-01	4.24E-02	-2.16E-02
7.75			1.98E+00	1.22E+00	7.07E-01	3.33E-01	1.09E-01	7.28E-03
8.00				1.57E+00	9.51E-01	5.06E-01	2.12E-01	6.02E-02

Source: *U solubility_dtn.xls* (Appendix I).

NOTE: These concentrations correspond to schoepite saturation. The green area indicates the region where it is uncertain whether U is controlled by schoepite or Na-boltwoodite saturation.

Table 6.7-6. Calculated Uranium Solubility (Controlled by Na-boltwoodite and $Na_4UO_2(CO_3)_3$) as log [U] (mg/L) Within Codisposal Waste Packages Breached Under Any Scenario, CSNF Waste Packages Breached by a Hypothetical Igneous Intrusion and in the Invert

Na-boltwoodite and $Na_4UO_2(CO_3)_3$								
	log fCO_2 (bars)							
pH	-1.5	-2.0	-2.5	-3.0	-3.5	-4.0	-4.5	-5.0
6.50	2.56E+00							
6.75	2.16E+00	2.00E+00	1.51E+00	1.07E+00	7.46E-01	5.56E-01	4.73E-01	4.43E-01

Table 6.7-6. Calculated Uranium Solubility (Controlled by Na-boltwoodite and $Na_4UO_2(CO_3)_3$) as log [U] (mg/L) Within Codisposal Waste Packages Breached Under Any Scenario, CSNF Waste Packages Breached by a Hypothetical Igneous Intrusion and in the Invert (Continued)

Na-boltwoodite and $Na_4UO_2(CO_3)_3$								
	log fCO_2 (bars)							
pH	-1.5	-2.0	-2.5	-3.0	-3.5	-4.0	-4.5	-5.0
7.00	1.94E+00	1.82E+00	1.28E+00	8.21E-01	4.79E-01	2.77E-01	1.88E-01	1.56E-01
7.25	2.14E+00	1.51E+00	1.09E+00	5.88E-01	2.28E-01	2.04E-02	-7.08E-02	-1.04E-01
7.50	2.79E+00	1.55E+00	1.03E+00	3.97E-01	-9.31E-03	-2.29E-01	-3.23E-01	-3.56E-01
7.75	4.78E+00	1.98E+00	1.03E+00	3.18E-01	-2.14E-01	-4.68E-01	-5.67E-01	-6.01E-01
8.00	4.78E+00	2.76E+00	1.34E+00	4.67E-01	-3.27E-01	-6.84E-01	-8.00E-01	-8.35E-01
8.25	4.78E+00	4.78E+00	1.92E+00	7.59E-01	-2.27E-01	-8.41E-01	-1.01E+00	-1.05E+00
8.50	4.78E+00	4.78E+00	2.75E+00	1.25E+00	1.67E-01	-8.36E-01	-1.19E+00	-1.25E+00
8.75	4.78E+00	4.78E+00	4.77E+00	1.89E+00	6.32E-01	-5.27E-01	-1.27E+00	-1.41E+00
9.00	4.78E+00	4.78E+00	4.77E+00	2.75E+00	1.20E+00	3.81E-02	-1.13E+00	-1.51E+00
9.25	4.78E+00	4.78E+00	4.77E+00	4.76E+00	1.88E+00	5.47E-01	-6.60E-01	-1.51E+00
9.50	4.78E+00	4.78E+00	4.77E+00	4.76E+00	2.78E+00	1.15E+00	-9.89E-02	-1.26E+00
9.75	4.78E+00	4.78E+00	4.77E+00	4.76E+00	4.73E+00	1.89E+00	4.56E-01	-7.58E-01
10.00	4.78E+00	4.78E+00	4.77E+00	4.76E+00	4.73E+00	2.92E+00	1.13E+00	-2.57E-01
10.25	500	500	500	500	500	500	2.02E+00	3.92E-01

Source: *U solubility_dtn.xls* (Appendix I).

NOTE: Values of "500" indicate that no valid solubility data are available because the ionic strengths of the solutions are above 3 molal. See Section 6.3.3.4. These concentrations correspond to Na-boltwoodite and $Na_4UO_2(CO_3)_3$ saturation. The green area indicates the region where it is uncertain whether U is controlled by schoepite or Na-boltwoodite saturation, the blue area where solubility is controlled by $Na_4UO_2(CO_3)_3$.

Figures 6.7-3 and 6.7-4 show concentrations of total dissolved U and of aqueous species contributing to that concentration calculated at $fCO_2 = 10^{-3.0}$ bars, expressed as molalities and percents total U, respectively. The figures span the pH range from 3.5 to 9.5. As discussed in this section, these calculations are based on solubility control by three solids: the minerals schoepite ($UO_3 \cdot 2H_2O$) and Na-boltwoodite ($NaUO_2SiO_3OH \cdot 1.5H_2O$), which prevail at low and intermediate pH values, respectively; and the solid $Na_4UO_2(CO_3)_3$, which is found in laboratory experiments under conditions of high pH and fCO_2. The cusps in the figure(s) represent the point at which solubility control by one solid gives way to control by another.

These figures show that the following species constitute more than 10 percent of the dissolved uranium under the range of conditions modeled: $UO_2(CO_3)_3^{4-}$, $UO_2(CO_3)_2^{2-}$, $(UO_2)_2CO_3(OH)_3^-$, $UO_3(aq)$, UO_2F^+, $UO_2F_2(aq)$, UO_2^{2+}, $UO_2SO_4(aq)$, and $(UO_2)_2(OH)_2^{2+}$.

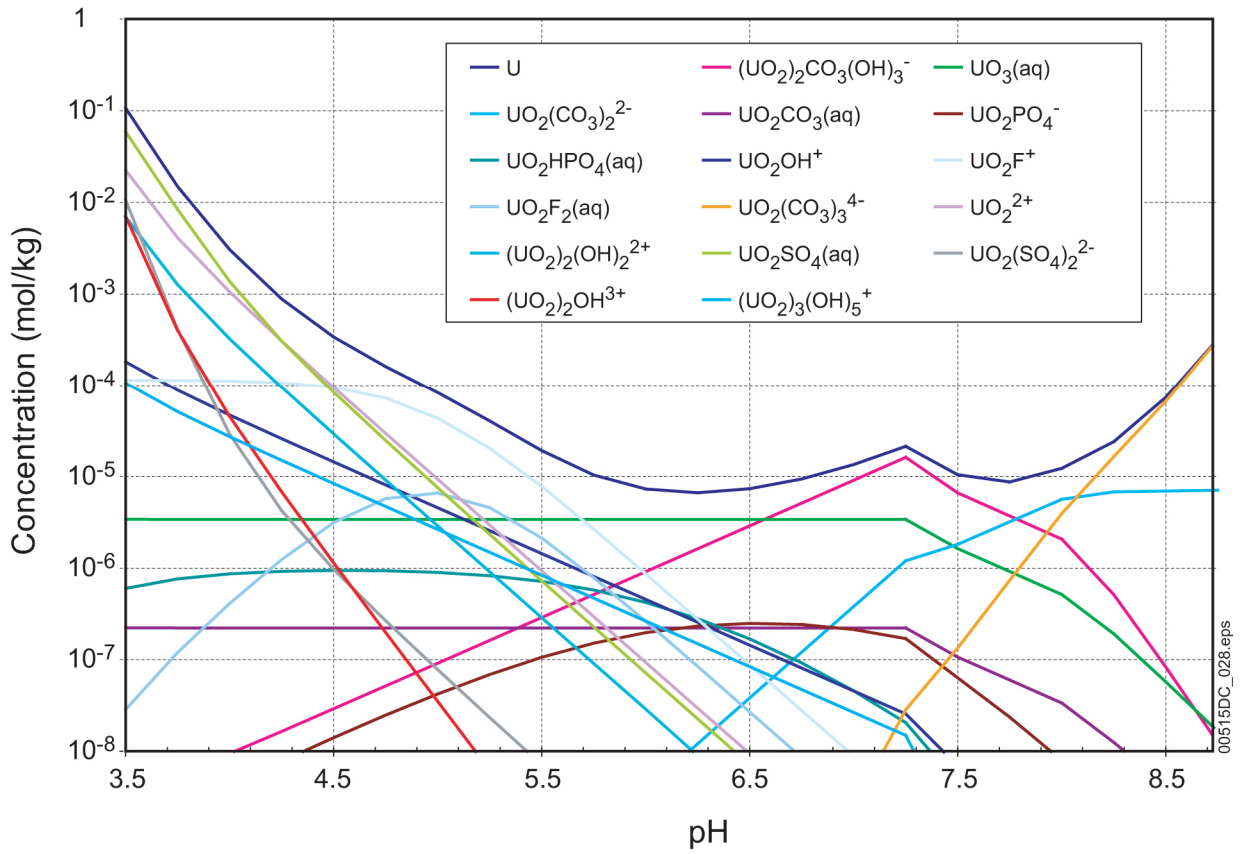

Source: *U species plot.xls* (Appendix I).

NOTE: UO_3(aq) (as indicated in DTN: MO0302SPATHDYN.000 [DIRS 161756]) is the nonconventional equivalent of $UO_2(OH)_2$(aq); the Δ_fG^0 value adopted for UO_3(aq) is consistent with those for $UO_2(OH)_2$(aq).

Figure 6.7-3. Total Uranium Concentration and Speciation Diagram in mol U/kg H_2O Calculated at $fCO_2 = 10^{-3.0}$ bars

Consider the reaction describing the dissolution of the controlling solid, $UO_3 \cdot 2H_2O$, to one of the dominant species, $UO_2(CO_3)_2^{2-}$:

$$UO_3 \cdot 2H_2O + 2\ HCO_3^- = UO_2(CO_3)_2^{2-} + 3\ H_2O \qquad \text{(Eq. 6.7-1)}$$

This reaction is written in terms of HCO_3^- rather than CO_3^{2-} because under the pH range expected, the concentration of bicarbonate exceeds that of carbonate.

The standard state Gibbs free energy of the reaction (Δ_rG^0) is the value needed to calculate its log K using $\Delta_rG^0 = -RTlnK$. This equals:

$$\Delta_rG^0(UO_2(CO_3)_2^{2-}) = \Delta_fG^0(UO_2(CO_3)_2^{2-}) + 3\cdot\Delta_fG^0(H_2O) - \Delta_fG^0(UO_3\cdot 2H_2O) - 2\cdot\Delta_fG^0(HCO_3^-) \qquad \text{(Eq. 6.7-2)}$$

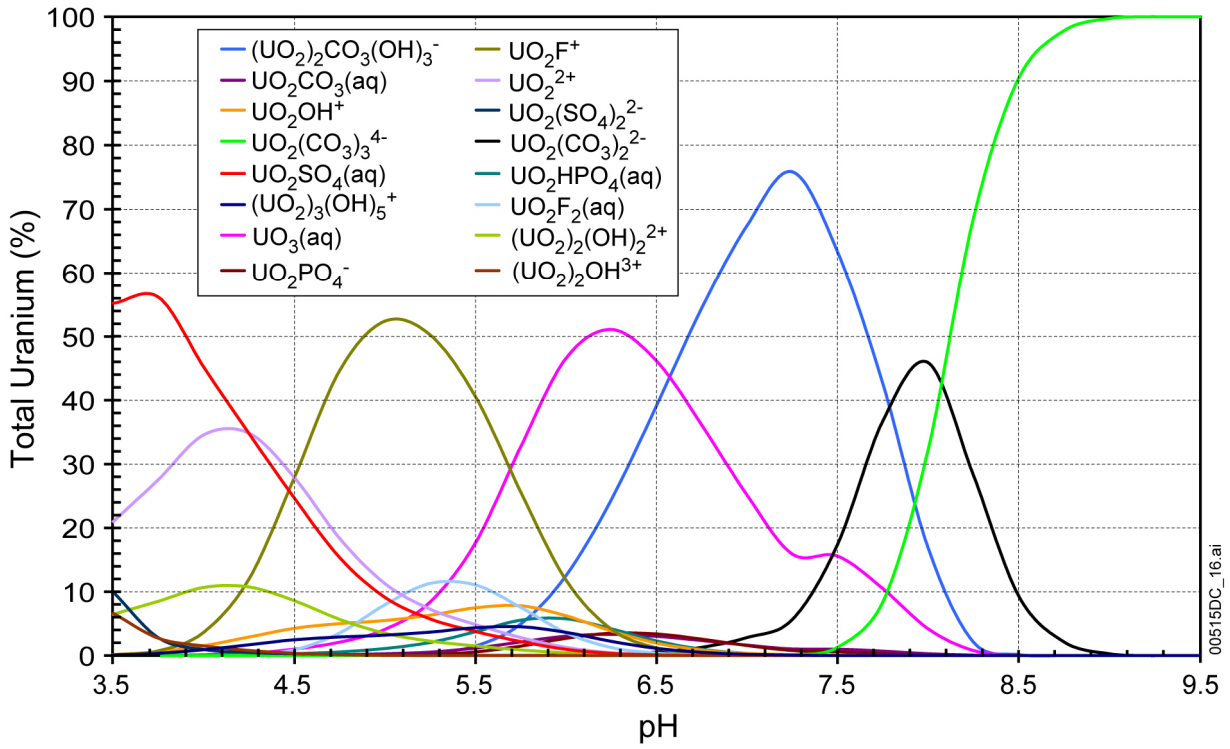

Source: *U species plot.xls* (Appendix I).

NOTE: $UO_3(aq)$ (as indicated in DTN: MO0302SPATHDYN.000 [DIRS 161756]) is the nonconventional equivalent of $UO_2(OH)_2(aq)$; the Δ_fG^0 value adopted for $UO_3(aq)$ is consistent with those for $UO_2(OH)_2(aq)$.

Figure 6.7-4. Uranium-Speciation Diagram in Percent Total Uranium Calculated at $fCO_2 = 10^{-3.0}$ Bars

Because this expression is a simple algebraic sum, the uncertainties of the Δ_fG^0 terms can be combined to give the uncertainty of $\Delta_rG^0(UO_2(CO_3)_2^{2-})$ by the usual square root of the mean (Bevington 1969 [DIRS 146304], Section 4-2). This procedure gives ±2.703 kJ/mol for $2\sigma\Delta_rG^0(UO_2(CO_3)_2^{2-})$. Dividing this by −RTln(10) (= −5.708 kJ/mol at 298.15K) gives $2\sigma \log K = \pm 0.47$ (*log K Uncertainties_040624.xls* in Appendix I). When this procedure is followed for dominant aqueous species, the largest uncertainty is for $(UO_2)_2CO_3(OH)_3^-$ at $2\sigma \log K = \pm 0.99$ for above pH about 6.5 (for $fCO_2 = 10^{-3.0}$ bars as used in the calculation illustrated) where the dominant species are carbonate and hydroxycarbonate complexes. At lower pH values, where fluoride and sulfate complexes and UO_2^{2+} dominate, the largest uncertainties are for the two fluoride complexes, $UO_2F_2(aq)$ and UO_2F^+ at ±0.55 and ±0.48, respectively, and for $UO_2SO_4(aq)$ at ±0.44. The largest $2\sigma \log K$ value of ±0.99 leads to a 1σ standard deviation for the solubility value of ±0.5, which is applied in a normal distribution truncated at ±2σ for all uranium concentrations.

6.7.5 Uncertainty

6.7.5.1 Uncertainty in log K Values of the Controlling Solid and Aqueous Species

This total uncertainty in solubility includes uncertainties in the log K values of the thermodynamic properties of the controlling solid and those for the dissolved species.

The evaluation and combination of these uncertainties are discussed in more detail in Section 6.3.3.1. The total uncertainty applicable to all log [U] values is ±0.99 units. This represents the 2σ limit of a normal distribution with a 1σ uncertainty of ±0.5.

When more than one solubility-controlling solid is used, an additional source of uncertainty is in the pH at which solubility control by one solid gives way to control by another and results from the uncertainties in the log K values of both solids. The uncertainty in crossover pH was evaluated by modeling the pH at which both solids were saturated when the log K values for each are set at the upper and lower limits of their uncertainty ranges.

The uncertainties in the log K values of the solids are not available in *Data0.ymp.R2* (DTN: MO0302SPATHDYN.000 [DIRS 161756]), but are given (or can be derived from) the NEA chemical thermodynamic handbooks (e.g., Guillaumont et al. 2003 [DIRS 168382]) from which the log K values in *Data0.yc3.R1* were themselves derived. The range of log K values and the calculations on which they are based are given in spreadsheet *U-Solids-uncertainty.xls* in Appendix I.

Table 6.7-7 shows the ranges of pH at which schoepite saturation gives way to Na-boltwoodite saturation. This range is based on EQ3 calculations of the pH of solutions at equilibrium with both schoepite and Na-boltwoodite for all combinations of the high and low values of log K (workbook *Raw data*, spreadsheet *U LogK Uncertainty_a.xls,* Appendix I). The difference between the maximum and minimum pH varies from 1.46 pH units at log fCO_2 = –5.0 bars to 0.77 pH units at log fCO_2 = –1.5 bars. This range is shaded green in Tables 6.7-5 and 6.7-6 and solubility values are given for schoepite and Na-boltwoodite. The solubility to be used at a given pH and log fCO_2 is to be chosen randomly from a uniform distribution between the solubilities of the two minerals.

Table 6.7-7. Range of pH Values at Which Schoepite Saturation Gives Way to Na-boltwoodite Saturation Based on Uncertainties in the log K Values of the Solids

log fCO_2 (bars)	pH[a]		
	Maximum	Nominal	Minimum
-5.0	7.77	7.18	6.59
-4.5	7.77	7.18	6.59
-4.0	7.77	7.18	6.59
-3.5	7.77	7.18	6.59
-3.0	7.77	7.18	6.59
-2.5	7.67	7.18	6.59
-2.0	7.41	7.12	6.59
-1.5	7.14	6.85	6.53

Source: *LogK SCHO_NA-BOLT Uncertainty.xls* (Appendix I).

NOTE: [a] pH value at which schoepite saturation equals Na-boltwoodite saturation.

The range of pH values at which Na-boltwoodite saturation gives way to $Na_4UO_2(CO_3)_3$ saturation was not modeled explicitly as was the schoepite–Na-boltwoodite crossover because of the extent of the EQ6 calculations that would have been required. Instead, the uncertainty was calculated directly from the uncertainties to the log K values of the two solids.

The reaction between the two solids can be written:

$$NaUO_2SiO_3OH{:}1.5H_2O + 3Na^+ + 3CO_3^{-2} + 3H^+ = Na_4UO_2(CO_3)_3 + SiO_2(aq) + 3.5H_2O \quad \text{(Eq. 6.7-3)}$$

The uncertainties in the log K values for the solids is ±0.16 for Na-boltwoodite and ±0.25 for $Na_4UO_2(CO_3)_3$. The uncertainty in the equilibrium position of this reaction due to the uncertainties in the log K values of the solids is $(0.16^2 + 0.25^2)^{1/2} = \pm 0.30$ (Section 6.3.3.1). Because there are three H^+ ions in the reaction, the uncertainty per pH unit is 0.30/3 = ±0.10. This is less than the difference between the pH values of adjacent cells in Table 6.7-6, so the crossover uncertainty for these two minerals is not treated explicitly.

6.7.5.2 Uncertainty Addition from High Ionic Strength Solutions

At the high pH and fCO_2 values at which $Na_4UO_2(CO_3)_3$ is the controlling phase, the ionic strength of the solution is above 1 molal and may be as high as 2.5 molal. The nominal range of applicability of the EQ3/6 codes and the *Data0.ymp.R2* (DTN: MO0302SPATHDYN.000 [DIRS 161756]) database is to 1-molal ionic strength. However, as discussed in Section 6.3.3.4, the EQ3/6 codes can be used to an ionic strength of 3 molal if an additional uncertainty of ±0.3 is added by the square root of the mean to the results of calculations with ionic strengths between 1 and 3 molal. This uncertainty can be combined with the ±0.5 uncertainty in the log K values discussed in Section 6.7.5.1 to give a 1σ uncertainty of ±0.6 to be applied uniformly to log [U] for solutions with ionic strengths above 1 molal. These are the solutions shaded blue in Table 6.7-6. Section 6.7.6 already takes this into account in the reported uncertainty values for log K.

6.7.5.3 Uncertainty from Fluoride Concentration

The effects of fluoride uncertainty were evaluated by calculating uranium solubilities at a range of pH values for $fCO_2 = 10^{-3.0}$ bars with fluoride concentrations equal to the highest values expected in each of the three in-package and invert environments. These environments and their fluoride concentrations are described in Section 6.3.3.2 and Table 6.3-3. These results are displayed in Figure 6.7-5 and Table 6.7-8. The values in the tables are the differences between solubilities calculated using the F^- values for sensitivity analyses and the base-case solubility values. As the figure and table show, at the minimum fluoride concentration of 21.8 mg/L (the CSNF environment, 10× the base-case value), the maximum difference from the base-case concentration is +1.03 log[U] (in mg/L) units at a pH of 5.75. At the maximum fluoride concentration of 209 mg/L (the codisposal vapor-influx scenario and invert environment, about 100× the base-case value), the solubility controlled by schoepite is higher by a maximum value of +2.40 log[U] (in mg/L) at a pH of 5.75, and the solubility controlled by Na-boltwoodite is higher by a maximum value of +1.17 log[U] (in mg/L) at the lowest pH modeled for the sensitivity analysis, 6.50.

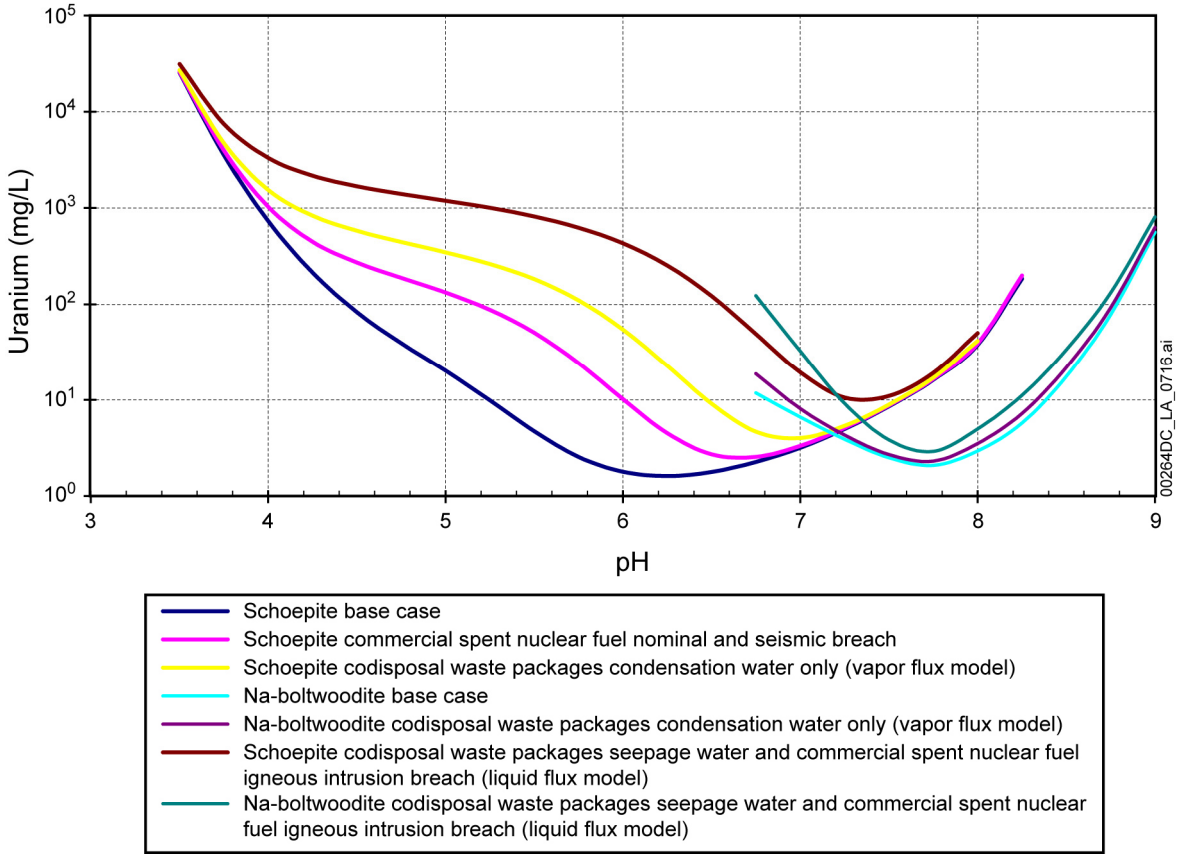

Source: *U-F Sensitivity_a.xls* (Appendix I).

NOTE: See Table 6.7-8 for corresponding F^- concentrations.

Figure 6.7-5. Effect of Fluoride on Solubilities of Schoepite and Na-Boltwoodite at log fCO_2 = –3.0 bars

Table 6.7-8. Increases in Solubilities of Schoepite and Na-boltwoodite with Additional F^- at Various pH Values

F^- Uncertainty for CSNF Waste Packages			**F^- Uncertainty for Water-Influx CDSP Waste Packages**				**F^- Uncertainty for Vapor-Influx CDSP Waste Packages**		
pH	**Schoepite**		**pH**	**Schoepite**	**Boltwoodite-Na**		**pH**	**Schoepite**	**Boltwoodite-Na**
3.50	1.00E-02		3.50	2.80E-02			3.50	9.05E-02	
3.75	4.88E-02		3.75	1.25E-01			3.75	3.23E-01	
4.00	1.48E-01		4.00	3.26E-01			4.00	6.60E-01	
4.25	3.20E-01		4.25	5.95E-01			4.25	1.01E+00	
4.50	5.17E-01		4.50	8.54E-01			4.50	1.32E+00	
4.75	6.81E-01		4.75	1.06E+00			4.75	1.56E+00	
5.00	8.18E-01		5.00	1.24E+00			5.00	1.78E+00	
5.25	9.47E-01		5.25	1.43E+00			5.25	2.02E+00	
5.50	1.03E+00		5.50	1.60E+00			5.50	2.25E+00	
5.75	9.78E-01		5.75	1.65E+00			5.75	2.40E+00	

Table 6.7-8. Increases in Solubilities of Schoepite and Na-boltwoodite with Additional F^- at Various pH Values (Continued)

F^- Uncertainty for CSNF Waste Packages			F^- Uncertainty for Water-Influx CDSP Waste Packages				F^- Uncertainty for Vapor-Influx CDSP Waste Packages		
pH	Schoepite		pH	Schoepite	Boltwoodite-Na		pH	Schoepite	Boltwoodite-Na
6.00	7.58E-01		6.00	1.50E+00			6.00	2.39E+00	
6.25	4.46E-01		6.25	1.16E+00			6.25	2.20E+00	
6.50	1.85E-01		6.50	7.15E-01	3.68E-01		6.50	1.84E+00	1.17E+00
6.75	5.36E-02		6.75	3.17E-01	1.99E-01		6.75	1.34E+00	1.02E+00
7.00	2.03E-02		7.00	9.35E-02	8.88E-02		7.00	7.79E-01	6.90E-01
7.25	1.13E-02		7.25	2.15E-02	4.47E-02		7.25	3.16E-01	3.74E-01
7.50	9.76E-03		7.50	6.88E-03	3.33E-02		7.50	9.76E-02	1.85E-01
7.75	8.78E-03		7.75	9.69E-03	4.28E-02		7.75	5.99E-02	1.46E-01
8.00	1.55E-02		8.00	4.16E-02	7.73E-02		8.00	1.25E-01	2.30E-01
8.25	3.30E-02		8.25		9.97E-02		8.25	2.90E-01	2.88E-01
max	**1.03E+00**		8.50		9.55E-02		8.50		2.82E-01
			8.75		7.37E-02		8.75		2.28E-01
			9.00		4.92E-02		9.00		1.60E-01
			max	**1.65E+00**	**3.68E-01**		**max**	**2.40E+00**	**1.17E+00**

Source: *U-F Sensitivity_a.xls* (Appendix I).

6.7.6 Summary

Uranium solubility is given by the following equation:

$$\log[\mathrm{U}] = S(pH, log f\mathrm{CO_2}) + \varepsilon_1 + (\varepsilon_2 \times N) \qquad \text{(Eq. 6.7-4)}$$

The values for the parameters in this equation depend on the waste package type and breach scenario. Parameter $S\left(pH, \log f_{CO_2}\right)$ is the base-case solubility and is taken from Tables 6.7-3, 6.7-5, or 6.7-6, as described below. Parameter ε_1 is associated with the uncertainties in the log K data. It is normally distributed with mean (μ) and standard deviation (σ) given below. Parameter ε_2 is associated with the uncertainties in the fluoride concentrations. It has a triangular distribution with values of a, b, and c given below.

CSNF Packages Breached Under Nominal Conditions or by Seismic Events:

$S\left(pH, \log f_{CO_2}\right)$: Table 6.7-3
ε_1: $\mu = 0$, $\sigma = 0.5$
ε_2: a = b = 0, c = 1.03
N(pH): Given in Table 6.7-9.

Table 6.7-9. Normalized pH Dependence, N(pH), of c-Parameter of Fluoride Uncertainty Factor ε_2 for CSNF Packages Breached Under Nominal Conditions or by Seismic Events

pH	N(pH)
3.50	9.74E-03
3.75	4.74E-02
4.00	1.44E-01
4.25	3.11E-01
4.50	5.03E-01
4.75	6.62E-01
5.00	7.94E-01
5.25	9.20E-01
5.50	1.00E+00
5.75	9.50E-01
6.00	7.36E-01
6.25	4.34E-01
6.50	1.79E-01
6.75	5.21E-02
7.00	1.97E-02
7.25	1.10E-02
7.50	9.49E-03
7.75	8.53E-03
8.00	1.50E-02
8.25	3.21E-02

Source: Workbook *Normalized F uncertainty*, spreadsheet *U-F Sensitivity_a.xls* (Appendix I).

Codisposal Packages Breached Under Nominal Conditions or by Seismic or Intrusive Events; CSNF Packages Breached by Intrusive Events:

$S\left(pH, \log f_{CO_2}\right)$: Either Table 6.7-5 or 6.7-6, or both:

If pH and log fCO$_2$ fall within unshaded areas of tables, schoepite or Na-boltwoodite is the controlling solid. Select value from appropriate table.

If pH and log fCO$_2$ fall within green-shaded areas of tables, it is uncertain whether schoepite or Na-boltwoodite is the controlling solid. Select a value randomly from a uniform distribution bounded by values from each table.

If pH and log fCO$_2$ fall within blue-shaded areas of tables, $Na_4UO_2(CO_3)_3$ is the controlling solid. Select value from Table 6.7-6.

ε_1: If pH and log fCO$_2$ fall within unshaded areas of tables, $\mu = 0$, $\sigma = 0.5$.

If pH and log fCO$_2$ fall within green-shaded areas of tables, $\mu = 0$, $\sigma = 0.5$.

If pH and log fCO_2 fall within blue-shaded areas of tables, $\mu = 0$, $\sigma = 0.6$ (already takes into account the adjustment to Log K values required at ionic strengths between 1 and 3. Section 6.7.5.2).

ε_2: Depends on the controlling solid and the appropriate in-package chemical abstraction as given in Table 6.7-10 (denoted by "c").

Table 6.7-10. Dependence of ε_2: c Parameter on Solubility-Controlling Solid and Type of Fluid in Waste Package

Solubility-Controlling Solid	Area of Tables	Water Influx: Codisposal and CSNF Packages Breached During Igneous Intrusion	Vapor-Influx: Codisposal Packages
Schoepite	Table 6.7-3, unshaded or green	a = b = 0, c = 1.65	a = b = 0, c = 2.40
Na-boltwoodite	Table 6.7-5, unshaded or green	a = b = 0, c = 0.368	a = b = 0, c = 1.17
$Na_4UO_2(CO_3)_3$	Table 6.7-6, blue shaded	a = b = 0, c = 0	a = b = 0, c = 0

NOTES: c values correspond to "max" values in Table 6.7-9.
N(pH): Depends on water influx or vapor influx in package as shown in Table 6.7-11.

The concentrations of UO_2–F ion pairs at $fCO_2 = 10^{-3}$ and pH 7 that are less than 10^{-8} mol/kg (–2.6 log mgU/L) are decreasing at the rate of two powers of 10 per increasing pH unit (Figure 6.7-3). At this fCO_2, $Na_4UO_2(CO_3)_3$ becomes the controlling phase at pH 9.25. At this pH, the total U is 4.76 log mg/L (Table 6.7-6) while the concentrations of UO_2–F would be less than $-2.6 - 4 = -6.6$ log mg/L (extrapolation from Figure 6.3-1). Thus, UO_2–F complexes make up less than 10^{-11} of the total U when $Na_4UO_2(CO_3)_3$ controls, so there is no need to include F^- sensitivity.

Table 6.7-11. pH Dependence of Fluoride Uncertainty for Codisposal Waste Packages Breached Under Nominal, Seismic, or Hypothetical Igneous Intrusive Scenarios and CSNF Waste Packages Breached by Hypothetical Igneous Intrusive Event

N(pH) for Water Influx: CDSP and CSNF Packages Breached by Igneous Intrusion				N(pH) for Vapor Influx: CDSP Waste Packages		
pH	Schoepite	Boltwoodite-Na		pH	Schoepite	Boltwoodite-Na
3.50	1.70E-02			3.50	3.77E-02	
3.75	7.59E-02			3.75	1.34E-01	
4.00	1.98E-01			4.00	2.75E-01	
4.25	3.61E-01			4.25	4.21E-01	
4.50	5.18E-01			4.50	5.48E-01	
4.75	6.44E-01			4.75	6.49E-01	
5.00	7.54E-01			5.00	7.41E-01	
5.25	8.70E-01			5.25	8.40E-01	
5.50	9.70E-01			5.50	9.37E-01	

Table 6.7-11. pH Dependence of Fluoride Uncertainty for Codisposal Waste Packages Breached Under Nominal, Seismic, or Hypothetical Igneous Intrusive Scenarios and CSNF Waste Packages Breached by Hypothetical Igneous Intrusive Event (Continued)

N(pH) for Water Influx: CDSP and CSNF Packages Breached by Igneous Intrusion				N(pH) for Vapor Influx: CDSP Waste Packages		
pH	Schoepite	Boltwoodite-Na		pH	Schoepite	Boltwoodite-Na
5.75	1.00E+00			5.75	1.00E+00	
6.00	9.08E-01			6.00	9.96E-01	
6.25	7.01E-01			6.25	9.17E-01	
6.50	4.34E-01	1.00E+00		6.50	7.66E-01	1.00E+00
6.75	1.92E-01	5.41E-01		6.75	5.57E-01	8.70E-01
7.00	5.67E-02	2.41E-01		7.00	3.24E-01	5.91E-01
7.25	1.31E-02	1.21E-01		7.25	1.31E-01	3.21E-01
7.50	4.18E-03	9.03E-02		7.50	4.06E-02	1.59E-01
7.75	5.88E-03	1.16E-01		7.75	2.49E-02	1.25E-01
8.00	2.52E-02	2.10E-01		8.00	5.20E-02	1.97E-01
8.25		2.71E-01		8.25	1.21E-01	2.47E-01
8.50		2.59E-01		8.50		2.41E-01
8.75		2.00E-01		8.75		1.95E-01
9.00		1.34E-01		9.00		1.37E-01

Source: *U-F Sensitivity_a.xls* (Appendix I).

6.8 THORIUM SOLUBILITY

6.8.1 Introduction

Data0.ymp.R2 (DTN: MO0302SPATHDYN.000 [DIRS 161756]) includes thorium data from a variety of sources. These have been used with EQ3NR to calculate the thorium concentrations discussed in this section.

6.8.2 Controlling Mineral

ThO_2(am) was chosen as the controlling phase for the full range of pH and fCO_2 values. *Data0.ymp.R2* (DTN: MO0302SPATHDYN.000 [DIRS 161756]) also includes data for the ThO_2 mineral thorianite and for a number of other thorium solids. Thorianite is about 5.5 log units more stable (less soluble) than ThO_2(am). However, as discussed in Section 6.3.2 and, in more detail, by Hummel et al. (2002 [DIRS 161904], Section 5.21.2), solubilities as low as those predicted using thorianite are measured only at pH values below about 5. This is illustrated most clearly by Hummel and Berner (2002 [DIRS 170921]). Figure 2 of that report shows that the solubility calculated from the thermodynamic properties of the high-temperature mineral form of ThO_2 (thorianite) is eight orders of magnitude lower than concentrations measured in laboratory experiments at pH values above about 6. Calculations using ThO_2(am) lead to dissolved thorium concentrations like those commonly measured in solubility studies, as discussed in Section 7.2.5.

Several other solids in *Data0.ymp.R2* (DTN: MO0302SPATHDYN.000 [DIRS 161756]) are less soluble than ThO_2(am) in the nominal reference water under certain conditions of pH and fCO_2. $Th_{0.75}PO_4$ is less soluble under acid conditions. However, because of the amount of uranium available in the waste package environment, phosphate concentrations there are likely to be very low, as discussed in Section 6.4.2.5. Thus, $Th_{0.75}PO_4$ is excluded. $Th(SO_4)_2$, ThF_4, and $ThF_4 \cdot 2.5H_2O$ are also less soluble than ThO_2(am) under acid conditions, with $Th(SO_4)_2$ particularly insoluble at the lowest pH values where SO_4^{2-} concentrations are high because of the use of this anion for charge balance of the modeled solutions. Data for $ThF_4 \cdot 2.5H_2O$ and $Th(SO_4)_2$ are taken from a previous compilation of data (Wagman et al. (1982 [DIRS 159216]). In reviewing the data provided by Wagman et al. 1982 ([DIRS 159216]) and Hummel et al. (2002 [DIRS 161904], Sections 5.21.6 and 7), note that the properties of $ThF_4 \cdot 2.5H_2O$ are based on an estimate and could not determine the original source for the properties of $Th(SO_4)_2$. Thus, these two solids are also excluded from consideration. The relevant F^- concentrations are uncertain, so ThF_4 is also excluded.

Section 6.8.4.2 addresses uncertainty associated with the properties of the controlling phase.

6.8.3 Chemical Conditions

Table 6.4-2 lists the chemical conditions for the thorium calculations.

6.8.4 Thorium-Solubility Model Results

6.8.4.1 Speciation and Solubility

The identity and relative concentrations of the aqueous species that compose the total dissolved Th concentrations modeled are discussed in detail in Section 6.4.2.5.1 and illustrated in Figures 6.4-12 and 6.4-13. That discussion is summarized here.

At $fCO_2 = 10^{-3.0}$, the principal Th species above pH 6 is $Th(OH)_3CO_3^-$, shifting to $Th(CO_3)_5^{6-}$ at pH 9.5. Where the latter species dominates, the Th concentration increases by 10^5 per pH unit. This extreme nonlinearity limits the ability of the EQ3NR program to solve for solutions at higher pH values. At pH values from about 4 to 5.75, the principal species contributing to Th solubility are Th^{4+}–F^- aqueous complexes including ThF_2^{2+}, ThF_3^+, and ThF_4(aq). These species account for the strong increases in dissolved Th concentrations shown in Figure 6.8-2 when F^- concentrations are increased above the value in the base-case (J-13) water. At pH values below about 3.75, $Th(SO_4)^{2+}$ and $Th(SO_4)_2$(aq) are the principal contributors to the total Th concentrations. Because SO_4^{2-} is both the charge-balancing ion and Th^{4+}–SO_4^{2-} complexes make up nearly 95 percent of the total dissolved species of the most acid solutions, EQ3NR is also unable to solve for solution compositions at pH values below pH 3.25 (*th010402.3o* in file *Th Eq3 runs.zip*, Appendix I).

Table 6.8-1 shows the thorium concentrations given in mg/L. Table 6.8-2 and Figure 6.8-1 show the thorium concentrations given in log [Th] (in mg/L) for the reference water calculated using ThO_2(am) as the controlling mineral for pH values from 3.25 to 10.75 and log fCO_2 values from −1.5 to −5.0 bars. Calculations did not converge for conditions outside this range and where

empty cells appear in the table. The pattern of Th solubility exhibited is a result of the speciation of the solutions modeled.

In the high fCO_2 and pH region, increasing CO_3^{2-} concentrations favor the formation of complexes such as $Th(CO_3)_5^{6-}$ and $Th(OH)_3CO_3^-$. This is evident in the sharp increases in the thorium concentrations in the highest pH point of each fCO_2 line in Figure 6.8-1. Even sharper increases at the next pH or fCO_2 step of the modeling prevent EQ3NR from converging.

At pH values below 3.25, the EQ3NR calculations also do not converge. This is due to the rapid increases in total thorium and SO_4 concentrations due to the strength of the $Th(SO_4)_2(aq)$ ion pair and the addition of SO_4^{2-} as the charge-balancing anion (Figures 6.8-2 and 6.8-3). This instability occurs in calculations for other actinides as well, and has a particularly strong effect on the calculations of americium solubilities (Section 6.9.4.1).

Because the independent variables of calculated Th solubility are in log scales and the user of the table may need to interpolate between calculated values, the logarithm of Th solubility is given in Table 6.8-2 for use in the TSPA-LA modeling. The second table includes the value "500" for those ranges of conditions for which no concentrations were given in Table 6.8-1. When the flag ("500") is encountered or for conditions between a valid solubility and a flag of "500," concentrations should be calculated according to the dissolution rate of individual waste forms, water volume, and the solubility caps presented in Table 8-3 instead of the flag itself. In addition, for conditions outside of the 3.25 to 10.75 pH range and the −1.5 to −5.0 fCO_2 range of the table, the concentrations should be calculated according to the dissolution rate of individual waste forms, water volume, and the solubility caps presented in Table 8-3.

Table 6.8-1. Thorium Solubility (mg/L)—ThO_2(am)

	log fCO_2 (bars)							
pH	**-1.50**	**-2.00**	**-2.50**	**-3.00**	**-3.50**	**-4.00**	**-4.50**	**-5.00**
3.25	6.94E+03	6.95E+03	6.95E+03	6.95E+03	6.95E+03	6.95E+03	6.95E+03	6.95E+03
3.50	3.45E+02	3.45E+02	3.45E+02	3.45E+02	3.45E+02	3.45E+02	3.45E+02	3.45E+02
3.75	4.12E+01	4.12E+01	4.12E+01	4.12E+01	4.12E+01	4.12E+01	4.12E+01	4.12E+01
4.00	1.37E+01	1.37E+01	1.37E+01	1.37E+01	1.37E+01	1.37E+01	1.37E+01	1.37E+01
4.25	8.73E+00	8.73E+00	8.73E+00	8.73E+00	8.73E+00	8.73E+00	8.73E+00	8.73E+00
4.50	5.52E+00	5.52E+00	5.52E+00	5.52E+00	5.52E+00	5.52E+00	5.52E+00	5.52E+00
4.75	2.41E+00	2.41E+00	2.41E+00	2.41E+00	2.41E+00	2.41E+00	2.41E+00	2.41E+00
5.00	5.10E-01	5.08E-01	5.07E-01	5.07E-01	5.07E-01	5.07E-01	5.07E-01	5.07E-01
5.25	6.69E-02	6.27E-02	6.14E-02	6.10E-02	6.08E-02	6.08E-02	6.08E-02	6.08E-02
5.50	1.77E-02	1.03E-02	7.93E-03	7.19E-03	6.96E-03	6.89E-03	6.86E-03	6.86E-03
5.75	2.04E-02	7.33E-03	3.18E-03	1.87E-03	1.46E-03	1.32E-03	1.28E-03	1.27E-03
6.00	3.48E-02	1.15E-02	4.10E-03	1.76E-03	1.03E-03	7.92E-04	7.18E-04	6.95E-04
6.25	6.03E-02	1.98E-02	6.69E-03	2.54E-03	1.22E-03	8.09E-04	6.78E-04	6.36E-04
6.50	1.07E-01	3.47E-02	1.14E-02	4.02E-03	1.68E-03	9.46E-04	7.13E-04	6.39E-04
6.75	1.92E-01	6.03E-02	1.98E-02	6.67E-03	2.52E-03	1.21E-03	7.93E-04	6.62E-04

Table 6.8-1. Thorium Solubility (mg/L)—ThO_2(am) (Continued)

	log fCO_2 (bars)							
pH	**-1.50**	**-2.00**	**-2.50**	**-3.00**	**-3.50**	**-4.00**	**-4.50**	**-5.00**
7.00	3.47E-01	1.07E-01	3.47E-02	1.14E-02	4.01E-03	1.68E-03	9.40E-04	7.07E-04
7.25	6.28E-01	1.93E-01	6.03E-02	1.98E-02	6.67E-03	2.52E-03	1.21E-03	7.90E-04
7.50	1.14E+00	3.47E-01	1.07E-01	3.47E-02	1.14E-02	4.01E-03	1.68E-03	9.39E-04
7.75	2.10E+00	6.28E-01	1.93E-01	6.03E-02	1.98E-02	6.67E-03	2.52E-03	1.20E-03
8.00	3.89E+00	1.15E+00	3.47E-01	1.07E-01	3.47E-02	1.14E-02	4.01E-03	1.68E-03
8.25	1.09E+01	2.10E+00	6.29E-01	1.93E-01	6.03E-02	1.98E-02	6.67E-03	2.52E-03
8.50		3.95E+00	1.15E+00	3.47E-01	1.08E-01	3.47E-02	1.14E-02	4.01E-03
8.75		2.56E+01	2.12E+00	6.31E-01	1.93E-01	6.04E-02	1.98E-02	6.66E-03
9.00			4.25E+00	1.16E+00	3.49E-01	1.08E-01	3.41E-02	1.14E-02
9.25			4.17E+02	2.15E+00	6.36E-01	1.94E-01	6.06E-02	1.97E-02
9.50				8.90E+00	1.18E+00	3.53E-01	1.09E-01	3.43E-02
9.75					2.41E+00	6.52E-01	1.96E-01	6.10E-02
10.00						1.25E+00	3.63E-01	1.10E-01
10.25						4.64E+01	6.91E-01	2.03E-01
10.50							4.37E+00	3.86E-01
10.75								1.01E+00

Source: *Th solubility.xls* (Appendix I).

NOTE: Some cells have no data because the EQ3NR calculations do not converge.

Table 6.8-2. Thorium Solubility (log[Th] mg/L)

	log fCO_2 (bars)							
pH	**-1.50**	**-2.00**	**-2.50**	**-3.00**	**-3.50**	**-4.00**	**-4.50**	**-5.00**
3.25	3.84E+00	3.84E+00	3.84E+00	3.84E+00	3.84E+00	3.84E+00	3.84E+00	3.84E+00
3.50	2.54E+00	2.54E+00	2.54E+00	2.54E+00	2.54E+00	2.54E+00	2.54E+00	2.54E+00
3.75	1.61E+00	1.61E+00	1.62E+00	1.62E+00	1.62E+00	1.62E+00	1.62E+00	1.62E+00
4.00	1.14E+00	1.14E+00	1.14E+00	1.14E+00	1.14E+00	1.14E+00	1.14E+00	1.14E+00
4.25	9.41E-01	9.41E-01	9.41E-01	9.41E-01	9.41E-01	9.41E-01	9.41E-01	9.41E-01
4.50	7.42E-01	7.42E-01	7.42E-01	7.42E-01	7.42E-01	7.42E-01	7.42E-01	7.42E-01
4.75	3.82E-01	3.82E-01	3.82E-01	3.82E-01	3.82E-01	3.82E-01	3.82E-01	3.82E-01
5.00	-2.92E-01	-2.94E-01	-2.95E-01	-2.95E-01	-2.95E-01	-2.95E-01	-2.95E-01	-2.95E-01
5.25	-1.17E+00	-1.20E+00	-1.21E+00	-1.21E+00	-1.22E+00	-1.22E+00	-1.22E+00	-1.22E+00
5.50	-1.75E+00	-1.99E+00	-2.10E+00	-2.14E+00	-2.16E+00	-2.16E+00	-2.16E+00	-2.16E+00
5.75	-1.69E+00	-2.13E+00	-2.50E+00	-2.73E+00	-2.84E+00	-2.88E+00	-2.89E+00	-2.90E+00
6.00	-1.46E+00	-1.94E+00	-2.39E+00	-2.75E+00	-2.99E+00	-3.10E+00	-3.14E+00	-3.16E+00
6.25	-1.22E+00	-1.70E+00	-2.17E+00	-2.60E+00	-2.91E+00	-3.09E+00	-3.17E+00	-3.20E+00
6.50	-9.69E-01	-1.46E+00	-1.94E+00	-2.40E+00	-2.77E+00	-3.02E+00	-3.15E+00	-3.19E+00
6.75	-7.16E-01	-1.22E+00	-1.70E+00	-2.18E+00	-2.60E+00	-2.92E+00	-3.10E+00	-3.18E+00

Table 6.8-2. Thorium Solubility (log[Th] mg/L) (Continued)

	log fCO_2 (bars)							
pH	**-1.50**	**-2.00**	**-2.50**	**-3.00**	**-3.50**	**-4.00**	**-4.50**	**-5.00**
7.00	-4.60E-01	-9.69E-01	-1.46E+00	-1.94E+00	-2.40E+00	-2.78E+00	-3.03E+00	-3.15E+00
7.25	-2.02E-01	-7.16E-01	-1.22E+00	-1.70E+00	-2.18E+00	-2.60E+00	-2.92E+00	-3.10E+00
7.50	5.88E-02	-4.60E-01	-9.69E-01	-1.46E+00	-1.94E+00	-2.40E+00	-2.78E+00	-3.03E+00
7.75	3.22E-01	-2.02E-01	-7.15E-01	-1.22E+00	-1.70E+00	-2.18E+00	-2.60E+00	-2.92E+00
8.00	5.90E-01	5.91E-02	-4.60E-01	-9.69E-01	-1.46E+00	-1.94E+00	-2.40E+00	-2.78E+00
8.25	1.04E+00	3.23E-01	-2.01E-01	-7.15E-01	-1.22E+00	-1.70E+00	-2.18E+00	-2.60E+00
8.50	500	5.96E-01	6.01E-02	-4.59E-01	-9.68E-01	-1.46E+00	-1.94E+00	-2.40E+00
8.75	500	1.41E+00	3.25E-01	-2.00E-01	-7.14E-01	-1.22E+00	-1.70E+00	-2.18E+00
9.00	500	500	6.29E-01	6.31E-02	-4.57E-01	-9.67E-01	-1.47E+00	-1.94E+00
9.25	500	500	2.62E+00	3.33E-01	-1.96E-01	-7.12E-01	-1.22E+00	-1.70E+00
9.50	500	500	500	9.49E-01	7.17E-02	-4.53E-01	-9.65E-01	-1.47E+00
9.75	500	500	500	500	3.81E-01	-1.86E-01	-7.07E-01	-1.21E+00
10.00	500	500	500	500	500	9.60E-02	-4.41E-01	-9.58E-01
10.25	500	500	500	500	500	1.67E+00	-1.61E-01	-6.93E-01
10.50	500	500	500	500	500	500	6.41E-01	-4.13E-01
10.75	500	500	500	500	500	500	500	4.71E-03

Source: *Th solubility.xls* (Appendix I).

NOTE: Some cells have no valid data because the EQ3NR calculations do not converge and the results are reported as “500.”

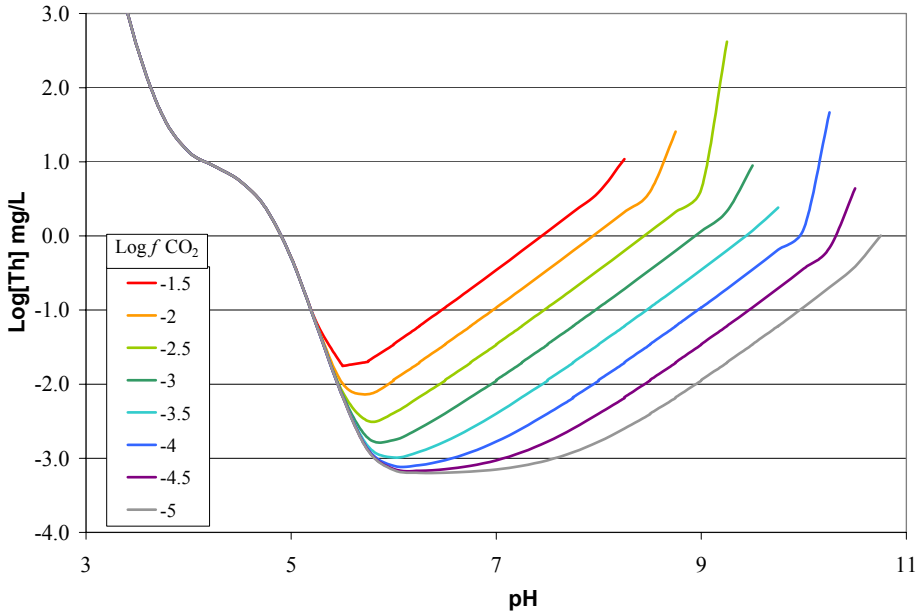

Source: *Th Solubility.xls* (Appendix I).

Figure 6.8-1. ThO_2(am) Solubility Modeled as a Function of fCO_2 and pH

Figures 6.8-2 and 6.8-3 are speciation diagrams for Th values from pH 3.25 to 9.5. The former displays the mol/kg concentration of total Th and its solution complexes; the latter displays the complex concentrations in percent of total Th. The diagrams represent a system at equilibrium with the solid ThO_2(am) at log fCO_2 (bars) = –3.0. The choice of this controlling solid is discussed in Section 6.8.2. Thorium occurs only in the Th(IV) oxidation state in aqueous solution. Therefore, small changes in the Eh of the system do not have any effect on the solubilities shown in Table 6.8-2.

The calculated total Th concentration ranges from nearly 0.1 mol/kg at pH 3.25 to a minimum of less than 10^{-8} mol/kg at pH 6.0 and increases again to nearly 10^{-4} mol/kg at pH 9.5. At the lowest pH, over 90 percent of the total Th consists of the $Th(SO_4)_2$(aq) complex, with the $ThSO_4^{2+}$ complex contributing less than 10 percent of the total. At pH values from below 4.0 to above 5.5, F^--bearing complexes dominate the total Th. The principal complex at pH 4.0 is ThF_2^{2+}, while ThF_3^+ dominates from pH 4.5 to 5.5. From pH 5 to 5.5, ThF_4(aq) also contributes about 15 percent of the total, as does ThF_2^{2+}. At higher pH values, the importance of F^- complexes diminishes and the principal contributors to total Th become the CO_3^{2-} complexes, $Th(OH)_3CO_3^-$ and, at pH 9.5, $Th(CO_3)_5^{6-}$. At around pH 6.0, $Th(OH)_4$(aq) also contributes over 30 percent of the total Th.

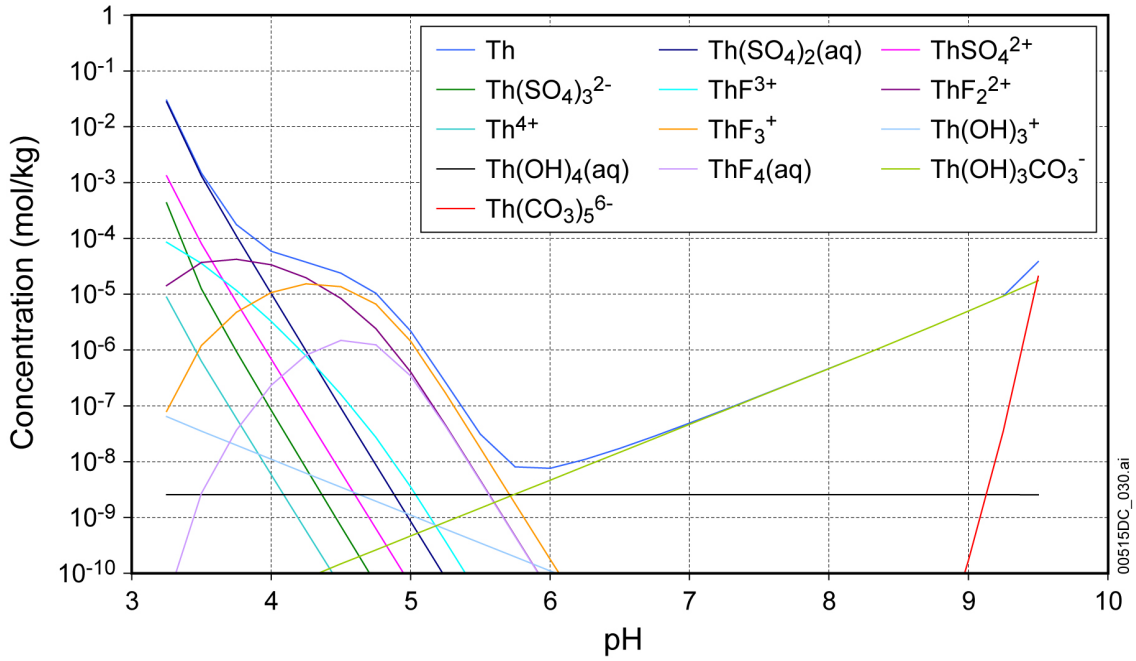

Source: *Th species plot.xls* (Appendix I).

Figure 6.8-2. Total Th Concentration and Speciation Diagram at log fCO_2 (bars) = –3.0 in mol/kg H_2O

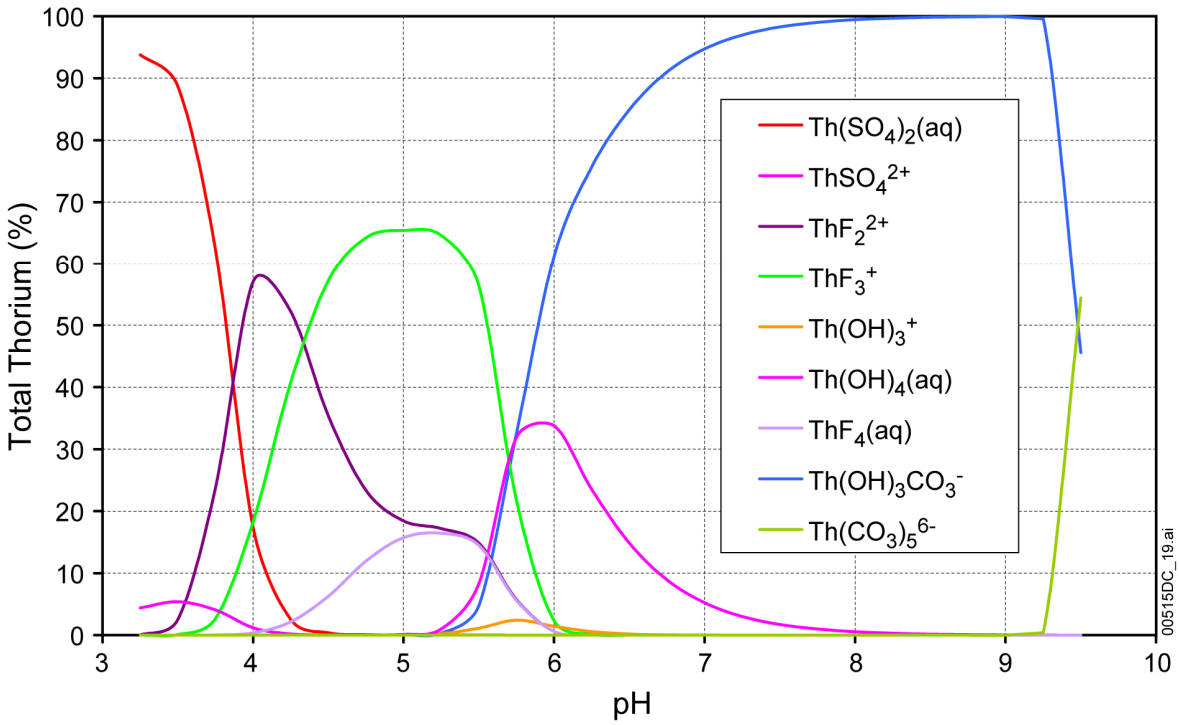

Source: *Th species plot.xls*.

Figure 6.8-3. Th-Speciation Diagram at log fCO_2 (bars) = –3.0 in Percent Total Dissolved Th

$Th(CO_3)_5^{6-}$ is formed by the reaction:

$$Th^{4+} + 5\ HCO_3^- = Th(CO_3)_5^{6-} + 5\ H^+ \qquad \text{(Eq. 6.8-1)}$$

where $Th(CO_3)_5^{6-}$ dominates, the total Th concentration increases by 10^5 for each unit increase in pH. The extreme nonlinearity of the variation of total Th with pH, where this complex dominates, is why the EQ3NR program does not converge in the high pH–high fCO_2 range.

The thermodynamic data for ThO_2(am) in *Data0.ymp.R2* (DTN: MO0302SPATHDYN.000 [DIRS 161756]) are based on solubility studies by Östhols et al. 1994 [DIRS 150834]. Figure 6.8-4 shows the data of Östhols et al. (1994 [DIRS 150834], Tables 2 and 3) plotted along with the model data from Figure 6.8-1. The data from Östhols et al. (1994 [DIRS 150834]) for higher log fCO_2 values indicate higher thorium solubilities than would be expected. Also plotted in Figure 6.8-4 are solubility data measured in 0.1 mol/liter total carbonate solutions. The model is able to predict some of the measured thorium solubilities in 0.1 mol/liter carbonate solutions from Östhols et al. (1994 [DIRS 150834]). However, as mentioned previously, EQ3NR is not able to converge in the high pH–high fCO_2 range. This limitation is discussed further in Section 7.2.5.

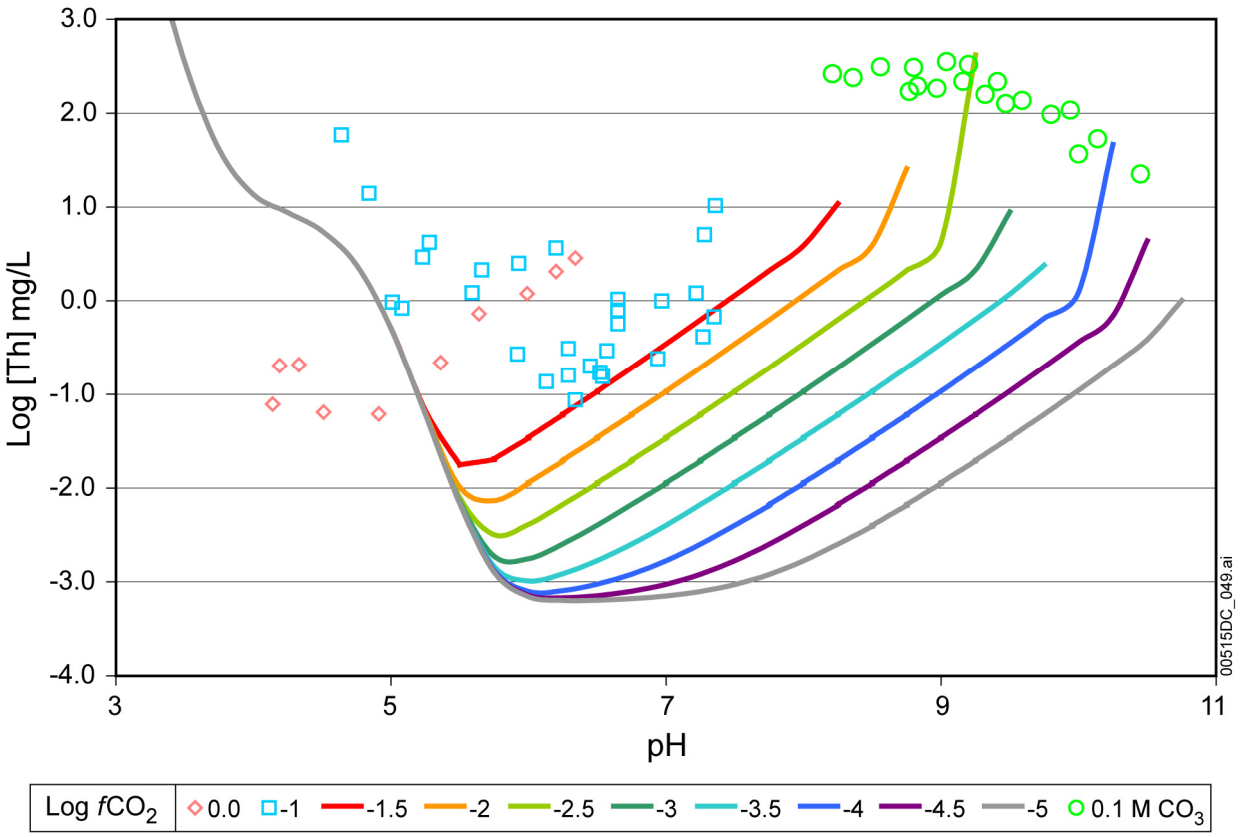

Data Source: Östhols et al. 1994 [DIRS 150834] for thorium solubility data points

Source: *Th Solubility2.xls* (Appendix I).

Figure 6.8-4. ThO_2(am)-Solubility Model with Experimental Solubility Data

Figures 6.8-2 and 6.8-3 show that total Th concentration is sensitive to SO_4^{2-} concentrations at low pH values, to F^- concentrations under moderately acid conditions and to OH^- and CO_3^{2-}concentrations under circumneutral and basic conditions. The OH^- concentrations depend on the pH, and CO_3^{2-} concentrations on pH and fCO_2. The solubilities are tabulated in terms of pH and fCO_2 so the sensitivities to OH^- and CO_3^{2-} variations are considered explicitly. As discussed in Section 6.4.3.5, SO_4^{2-} concentrations are varied in the modeling to maintain charge balance in order to simulate the occurrence of H_2SO_4 in the in-package environment from the oxidation of sulfur during steel degradation. In this way, SO_4^{2-} variations are also considered explicitly. Variations in F^- concentrations are not treated explicitly but rather as uncertainties in the total Th concentrations.

6.8.4.2 Uncertainties

As described in Section 6.3.3, uncertainty in the solubilities has been evaluated considering uncertainties in the thermodynamic data for the solubility-controlling phase and principal aqueous species and uncertainties in the fluoride content of the matrix fluid.

6.8.4.2.1 Uncertainties in Log K

The uncertainty in thorium solubility due to uncertainties in thermodynamic data was calculated as described in Section 6.3.3.1, allowing for uncertainties in log K values of both the controlling solid and the important aqueous thorium species. The total uncertainty applicable to all log [Th] values in Table 6.8-2 is 1.4 units. This represents the 2σ limit of a normal distribution with a 1σ uncertainty of 0.7.

6.8.4.2.2 Uncertainty from Fluoride Concentration

The effects of fluoride uncertainty were evaluated by calculating thorium solubilities at a range of pH values for $fCO_2 = 10^{-3.0}$ bars with fluoride concentrations equal to the highest values expected in each of the in-package and invert environments. These environments and their fluoride concentrations are described in Section 6.3.3.2 and Table 6.3-3. These results are displayed in Figure 6.8-5. Table 6.8-3 gives the calculated concentrations, including those for the base-case fluoride concentration and also shows the differences between the higher-fluoride and base-case solubilities. As the figure and table show, at a fluoride concentration of 2.18 mg/L (the CSNF environment, 10× the base-case value), the maximum difference from the base-case concentration is +3.10 log[Th] (in mg/L) units at a pH of 5.75. At a fluoride concentration of 209 mg/L (the codisposal vapor-influx scenario and invert environment, about 95× the base-case value), the solubility is higher by a maximum value of +5.27 log[Th] (in mg/L) at pH = 6.00.

Increasing fluoride has a stronger effect on thorium solubility than on the solubility of any other actinide examined in this report because Th is the only actinide present in the IV oxidation state under the oxidizing conditions of the repository. Fluoride complexes of actinide(IV) ions are many orders of magnitude more stable than those of corresponding actinide(VI) ions, as can be seen by comparing Tables 3.1.1 and 3.1.3 of *Nagra/PSI Chemical Thermodynamic Data Base 01/01* (Hummel et al. 2002 [DIRS 161904]). The importance of thorium-fluoride complexes even at the lowest base-case fluoride content is also evident from the inflection in the Th-solubility curves in the 4 to 5 pH range (Figure 6.8-1) and in the Th-speciation diagrams (Figures 6.8-2 and 6.8-3) as discussed in Section 6.8.4.1.

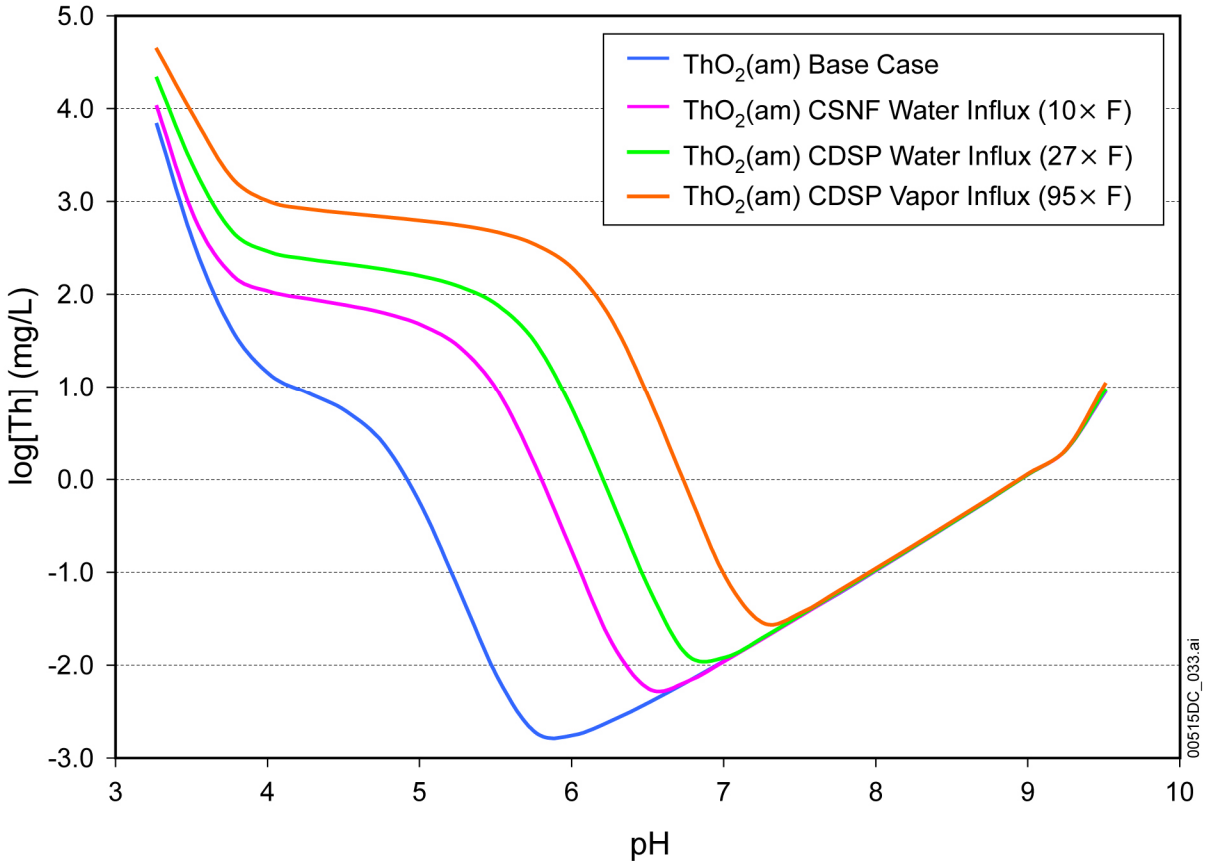

Source: *Th Solubility.xls* and *Th F Sensitivity.xls* (Appendix I)

Figure 6.8-5. ThO_2(am) Solubility at log fCO_2 = –3.0 bars as a Function of pH and F^- Concentrations

Table 6.8-3. Effects in Variation in Fluoride Concentration on Th Solubility

	Base Case	CSNF	CDSP – Water-Influx Scenario	CDSP – Vapor-Influx Scenario	CSNF	CDSP – Water-Influx Scenario	CDSP – Vapor-Influx Scenario
pH	**log[Th] mg/L**				**Difference**		
3.25	3.842	4.035	4.342	4.656	0.193	0.501	0.814
3.50	2.538	2.836	3.363	3.917	0.298	0.825	1.378
3.75	1.615	2.215	2.685	3.260	0.600	1.070	1.644
4.00	1.135	2.038	2.466	3.008	0.902	1.331	1.873
4.25	0.941	1.962	2.392	2.934	1.021	1.451	1.993
4.50	0.742	1.894	2.338	2.889	1.152	1.596	2.147
4.75	0.382	1.808	2.280	2.848	1.426	1.899	2.467
5.00	-0.295	1.675	2.206	2.806	1.970	2.502	3.102

Table 6.8-3. The Effects in Variation in Fluoride Concentration on Th Solubility (Continued)

	Base Case	CSNF	CDSP – Water-Influx Scenario	CDSP – Vapor-Influx Scenario	CSNF	CDSP – Water-Influx Scenario	CDSP – Vapor-Influx Scenario
pH	**log[Th] mg/L**				**Difference**		
5.25	-1.215	1.435	2.094	2.756	2.650	3.309	3.971
5.50	-2.143	0.955	1.891	2.680	3.098	4.034	4.823
5.75	-2.728	0.142	1.480	2.546	2.870	4.208	5.274
6.00	-2.753	-0.824	0.729	2.279	1.930	3.483	5.033
6.25	-2.596	-1.757	-0.224	1.732	0.839	2.372	4.328
6.50	-2.396	-2.259	-1.192	0.865	0.137	1.204	3.261
6.75	-2.176	-2.172	-1.892	-0.113	0.004	0.284	2.063
7.00	-1.943	-1.949	-1.914	-1.052	-0.005	0.030	0.892
7.25	-1.704	-1.709	-1.694	-1.546	-0.005	0.009	0.158
7.50	-1.460	-1.464	-1.452	-1.430	-0.004	0.008	0.030
7.75	-1.220	-1.216	-1.205	-1.192	0.004	0.014	0.028
8.00	-0.969	-0.965	-0.958	-0.944	0.004	0.011	0.024
8.25	-0.715	-0.712	-0.708	-0.695	0.003	0.007	0.021
8.50	-0.459	-0.457	-0.453	-0.442	0.002	0.006	0.017
8.75	-0.200	-0.198	-0.196	-0.186	0.002	0.004	0.014
9.00	0.063	0.064	0.066	0.073	0.001	0.003	0.010
9.25	0.333	0.334	0.335	0.341	0.001	0.002	0.007
9.50	0.949	0.958	0.973	1.038	0.008	0.024	0.089
				Maximum:	3.10	4.21	5.27

Source: *Th Solubility.xls* and *Th F Sensitivity.xls* (Appendix I).

6.8.4.2.3 Summary of Th-Solubility Model Uncertainty

The uncertainties in thorium solubilities are summarized in the following equation:

$$\log[\mathrm{Th}] = S(pH, log f\mathrm{CO_2}) + \varepsilon_1 + (\varepsilon_2 \times N) \qquad \text{(Eq. 6.8-2)}$$

The values for the parameters in this equation depend on the waste package type. Parameter $S\left(pH, \log f_{CO_2}\right)$ is the base solubility and is taken from Table 6.8-2. Parameter ε_1 is associated with the uncertainties in the log K data. Parameter ε_2 is associated with the uncertainties in the fluoride concentrations. Table 6.8-4 gives the values for the parameters ε_1 and ε_2.

Table 6.8-3 shows that the uncertainty terms $\varepsilon_2{}^{\mathrm{CSNF}}$, $\varepsilon_2{}^{\mathrm{CDSP\text{-}water\ influx}}$, and $\varepsilon_2{}^{\mathrm{CDSP\text{-}vapor\ influx}}$ vary with pH. This pH dependence can be implemented through the use of a multiplication factor (N) that is a function of pH. Values for N for both fuel types are given in Table 6.8-5. This modification requires that the $\varepsilon_2{}^{\mathrm{CSNF}}$, $\varepsilon_2{}^{\mathrm{CDSP\text{-}water\ influx}}$, and $\varepsilon_2{}^{\mathrm{CDSP\text{-}vapor\ influx}}$ values be fixed at the

maximum value given in Table 6.8-3. For each realization in the TSPA-LA model the uncertainty parameters are sampled at the beginning of the realization. This sampled value is then multiplied by 'N' at each timestep to produce a modified ε_2, which is then added to the base solubility value.

Table 6.8-4. Uncertainty Terms of log[Th]

Uncertainty Term	Associated with	Distribution Type	Distribution Parameter	Applicability
ε_1	log K of controlling solid and aqueous species	Normal Truncated at ±2σ	μ = 0, σ = 0.7	Values in Table 6.8-2
ε_2^{CSNF}	Fluoride concentration in CSNF waste packages	Triangular	a = b = 0, c = 3.10	CSNF waste packages
$\varepsilon_2^{CDSP\text{-}water\ influx}$	Fluoride concentration in codisposal waste packages (water-influx scenario)	Triangular	a = b = 0, c = 4.21	Codisposal waste packages and the invert
$\varepsilon_2^{CDSP\text{-}vapor\ influx}$	Fluoride concentration In codisposal waste package (vapor-influx scenario)	Triangular	a = b = 0, c = 5.27	Codisposal waste packages and the invert

NOTE: For ionic strength values between 1 and 3, Log K uncertainty should be treated as a normal distribution truncated at ±2σ with distribution parameters μ = 0, σ = 0.76 (Section 6.3.3.4).

Table 6.8-5. Multiplication Factor (N) Used to Modify Alternative F^- Uncertainty Term for Thorium

pH	Multiplication Factor for F^- Uncertainty		
	CSNF	CDSP – Water-Influx Scenario	CDSP – Vapor-Influx Scenario
3.25	6.23E-02	1.19E-01	1.54E-01
3.50	9.62E-02	1.96E-01	2.61E-01
3.75	1.94E-01	2.54E-01	3.12E-01
4.00	2.91E-01	3.16E-01	3.55E-01
4.25	3.30E-01	3.45E-01	3.78E-01
4.50	3.72E-01	3.79E-01	4.07E-01
4.75	4.60E-01	4.51E-01	4.68E-01
5.00	6.36E-01	5.95E-01	5.88E-01
5.25	8.55E-01	7.86E-01	7.53E-01
5.50	1.00E+00	9.59E-01	9.14E-01
5.75	9.26E-01	1.00E+00	1.00E+00
6.00	6.23E-01	8.28E-01	9.54E-01
6.25	2.71E-01	5.64E-01	8.21E-01
6.50	4.42E-02	2.86E-01	6.18E-01
6.75	1.36E-03	6.74E-02	3.91E-01
7.00	-1.70E-03/ 0.00[a]	7.08E-03	1.69E-01
7.25	-1.70E-03/ 0.00[a]	2.20E-03	2.99E-02
7.50	-1.34E-03/ 0.00[a]	1.95E-03	5.73E-03
7.75	1.31E-03	3.45E-03	5.36E-03

Table 6.8-5. Multiplication Factor (N) Used to Modify Alternative F- Uncertainty Term for Thorium (Continued)

pH	Multiplication Factor for F^- Uncertainty		
	CSNF	CDSP – Water-Influx Scenario	CDSP – Vapor-Influx Scenario
8.00	1.14E-03	2.54E-03	4.61E-03
8.25	9.43E-04	1.75E-03	3.92E-03
8.50	7.32E-04	1.40E-03	3.31E-03
8.75	5.30E-04	1.05E-03	2.60E-03
9.00	3.39E-04	7.12E-04	1.85E-03
9.25	2.40E-04	4.97E-04	1.40E-03
9.50	2.72E-03	5.68E-03	1.68E-02

Source: *Th F Sensitivitty.xls* (Appendix I).

NOTE: [a] Negative values set to 0.00, indicating that no normalization is applied.

6.9 AMERICIUM SOLUBILITY

6.9.1 Introduction

Data0.ymp.R2 (DTN: MO0302SPATHDYN.000 [DIRS 161756]) includes americium data from the NEA compilation by Silva et al. (1995 [DIRS 102087]). Only Am(III) is significant under the reference conditions.

The database (*Data0.ymp.R2* (DTN: MO0302SPATHDYN.000 [DIRS 161756])) includes a number of americium solids: oxide and hydroxides AmO_2, $Am(OH)_3$, and $Am(OH)_3$(am); carbonate and hydroxycarbonate $Am_2(CO_3)_2$; and $AmOHCO_3$; fluoride AmF_3 and phosphate, $AmPO_4$(am). Under none of the conditions modeled were $Am_2(CO_3)_2$ or AmF_3 oversaturated, so these can be discounted as solubility-controlling phases. $AmPO_4$(am) was oversaturated under all conditions. However, as discussed in Section 6.4.2.5, because of the amount of uranium available in the waste package environment, the phosphate concentrations in the waste package are very low. In addition, although the log K value for this solid is taken from the NEA data compilation (Silva et al. 1995 [DIRS 102087]), it is excluded from the NAGRA/PSI database because "The solubility constant has been derived at pH < 3." It is not clear whether the same solid is in equilibrium with phosphate containing solutions at neutral or alkaline conditions. In addition, since "only one dihydrogen phosphate complex, $AmH_2PO_4^{2}$" is in the NAGRA database and Data0, "any geochemical model calculation for environmental systems including phosphate at pH > 3 would most probably lead to large errors in dissolved americium concentrations due to the inadequate aqueous speciation model" (Hummel et al. 2002 [DIRS 161904], Section 5.2.6.2). For these reasons, $AmPO_4$(am) is also excluded from consideration here. This is conservative because concentrations would be lower if solubility control by this solid was selected. The solubilities of the oxides and hydroxides increase in the order: $AmO_2 < Am(OH)_3 < Am(OH)_3$(am).

According to Hummel et al. (2002 [DIRS 161904], Section 5.2.3.2), the properties of AmO_2 are based on thermochemical studies and no solubility data are available to assess whether this phase

ever actually controls dissolved Am concentrations under the conditions modeled. Thus it is also excluded as a possible controlling phase. The remaining solids $AmOHCO_3$, $Am(OH)_3$, and $Am(OH)_3$(am) are considered as controlling or alternative controlling phases.

The recent update volume of NEA Chemical Thermodynamics series (Guillaumont et al. 2003 [DIRS 168382]) reports revised values for the log K^0 value for the dissolution reaction of the controlling solid used in the modeling:

$$AmOHCO_3 = Am^{3+} + CO_3^{2-} + OH^- \quad \text{(Eq. 6.11-1)}$$

This was revised from –21.2 ± 1.4 in the original volume (Silva et al. 1995 [DIRS 102087]), which was the source of the modeling data, to –20.2 ± 1.0 in the updated volume (Guillaumont et al. 2003 [DIRS 168382]). This difference corresponds to an increase of an order of magnitude in Am solubility, but with a smaller uncertainty. It is within the uncertainty applied to the solubilities given here (Section 6.9.4.2).

6.9.2 Controlling Phase

$AmOHCO_3$ was chosen as the controlling solid phase in all calculations. The choice of this mineral is based on the studies by Nitsche et al. (1993 [DIRS 155218]; 1994 [DIRS 144515]), which identify $AmOHCO_3$ as the solid phase precipitated from water similar to the J-13 water composition used in these calculations at a pH range from 5.9 to 8.4 and temperatures from 25°C to 90°C. This is the most likely controlling phase under the range of environmental variables of interest to this analysis.

As discussed in Section 6.3.3.1, the uncertainty of the solubility product of this mineral is provided by Silva et al. (1995 [DIRS 102087], Table III.2) as ±1.4 log K units.

6.9.3 Chemical Conditions

Table 6.4-2 lists the chemical conditions for the americium calculations.

6.9.4 Americium-Solubility Model Results

6.9.4.1 Speciation and Solubility

Figures 6.9-1 and 6.9-2 show concentrations of total dissolved Am and of aqueous species contributing to that concentration calculated at $fCO_2 = 10^{-3.0}$ bars, expressed as molalities and percent total Am, respectively. The figures span the pH range from 6 to 10, beyond which EQ3NR was mathematically unable to solve for the solution compositions at this fCO_2.

As these figures illustrate, at pH values above 9, virtually all the dissolved Am is present as $Am(CO_3)_3^{3-}$. Note that at pH 10 the concentration of $Am(CO_3)_5^{6-}$ is increasing rapidly and dominates at higher pH values. The fact that Am concentrations dominated by these complexes increase so rapidly with pH limits the ability of EQ3NR to converge at high pH and fCO_2 values.

As the pH decreases toward 8.5, $Am(CO_3)_2^-$ becomes dominant and is succeeded by $AmCO_3^+$, which dominates to about pH 7. Around pH 7, the three species $AmCO_3^+$, $AmOH^{2+}$, and

$AmSO_4^+$ are of nearly equal importance. At pH values lower than about 6.5, virtually all dissolved Am is $AmSO_4^+$. Results of solubility calculations made at higher fCO_2 values, where calculations were possible at lower pH values, show that with decreasing pH, $Am(SO_4)_2^-$ concentrations become significant (EQ3NR output files in *Am Eq3 runs.zip* in Appendix I). The combination of SO_4^{2-} as the charge balancing species and its presence in the aqueous species dominating the Am concentration limits the ability of EQ3NR to mathematically solve for the solution composition at low pH values. The instability linked to SO_4^{2-} at lower pH and fCO_2 values is specific to americium and thorium. It results from the fact that these elements are present as Am(III) and Th(IV) while the other actinides occur principally in the (V) or higher oxidation states. The SO_4^{2-} complexes of actinide(III) and actinide(IV) species are relatively stronger than those of higher oxidation states (compare Hummel et al. 2002 [DIRS 161904], Tables 3.1.1, 3.1.2, and 3.1.3).

Finally, although Am–F complexes do not dominate under any of the base-case conditions modeled, Figure 6.9-1 shows that at pH values about 7.25, the concentration of AmF^{2+} is within two orders of magnitude of the total Am concentration. Thus, at concentrations of 10× to 95× the base-case F^- concentrations, Am–F complexes are the dominant Am species. This effect is shown by the F^- sensitivity calculations illustrated in Figure 6.9-4.

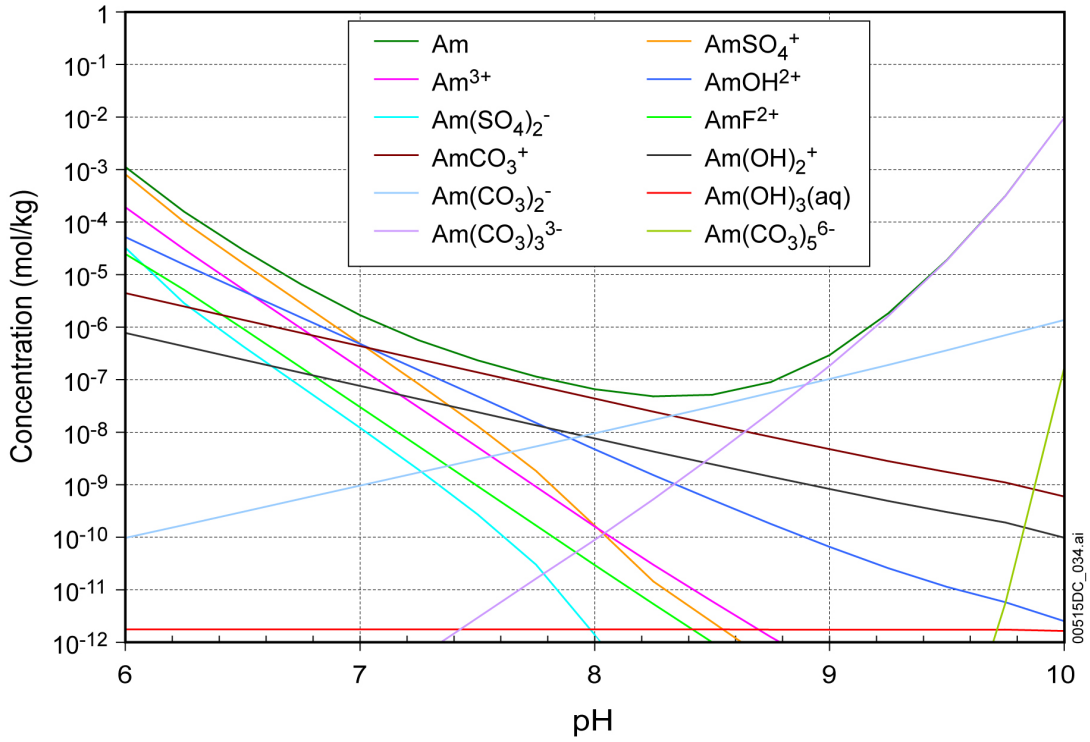

Source: *Am species plot.xls* (Appendix I).

Figure 6.9-1. Total Am Concentration and Speciation Diagram in mol Am/kg H_2O at log fCO_2 (bars) = –3.0

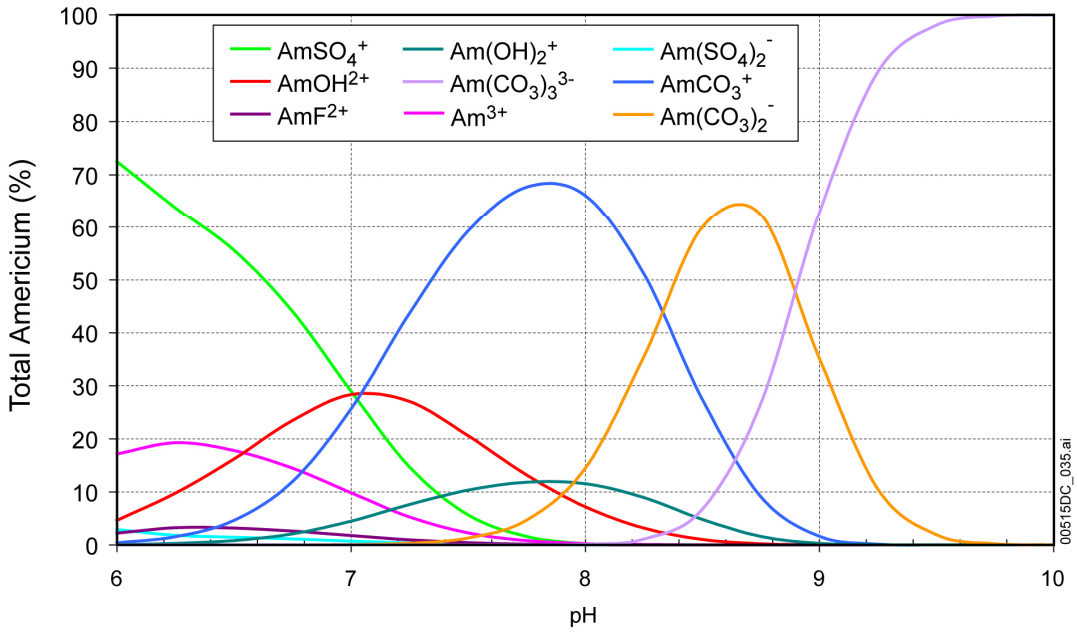

Source: *Am species plot.xls* (Appendix I).

Figure 6.9-2. Am-Speciation Diagram in Percent Total Am at log fCO_2 (bars) = –3.0

Table 6.9-1 and Figure 6.9-3 give the americium concentrations using $AmOHCO_3$ as the controlling mineral for pH values from 5.5 to 10.75, and log fCO_2 values from –1.5 to 5.0. Calculations for conditions outside this range and where empty cells appear in the table either did not converge for the reasons discussed earlier, or led to solution ionic strengths above 1 mol, (outside the range of validity of EQ3NR). At the low pH values, the modeling instability was due to the rapid increases in total americium and SO_4 concentrations due to the strength of the $AmSO_4^+$ ion pair and the addition of SO_4^{2-} as the charge-balancing anion. At high pH and fCO_2 values, the instability was due to rapid increases in total americium and Na^+ concentrations due to the strength of the $Am(CO_3)_3^{3-}$ complexes and the addition of Na^+ as the cation balancing the increasing CO_3^{2-} concentrations at these conditions. Instability from this occurs in calculations of other actinides as well, but the SO_4^{2-}-linked instability at lower pH and fCO_2 values is specific to americium and thorium. It results from the fact that these elements are present as Am(III) and Th(IV) while the other actinides occur principally in the (V) or higher oxidation states. The SO_4^{2-} complexes of M(III) and M(IV) (M stands for metal) species are relatively stronger than those of higher oxidation states.

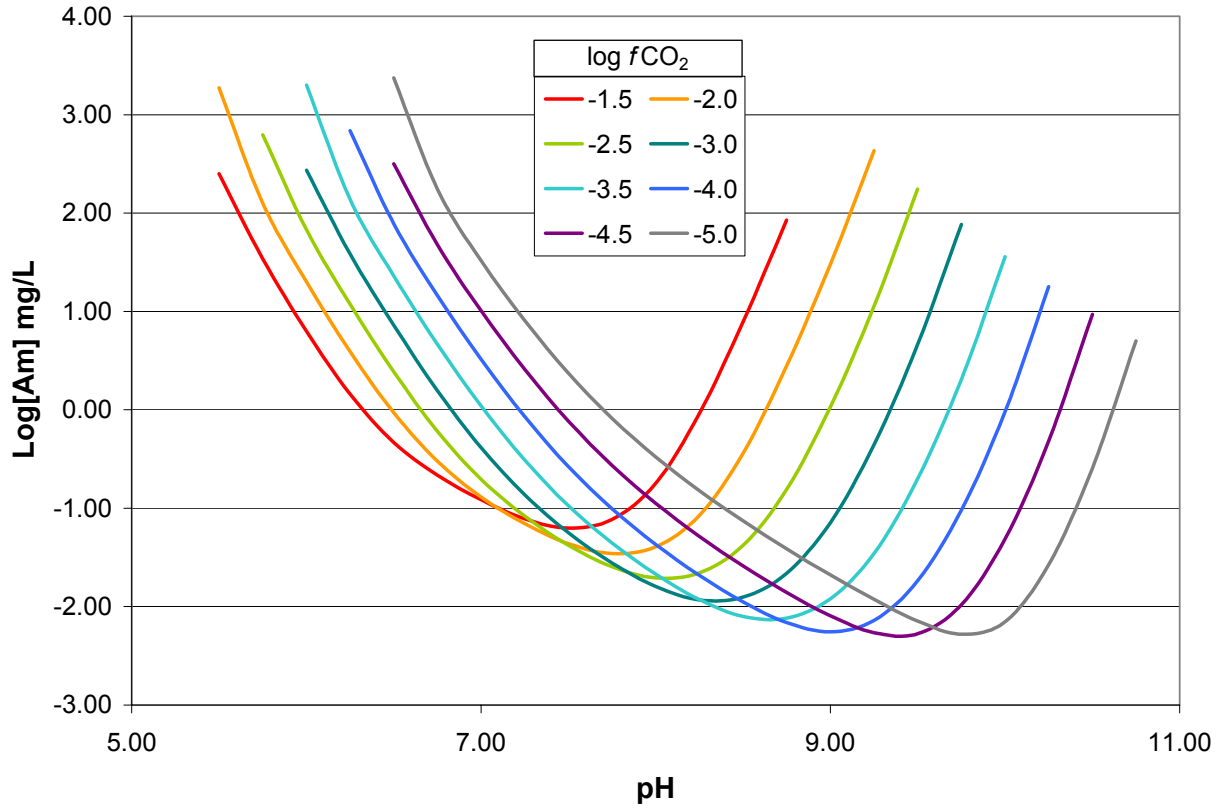

Source: *Am Solubility.xls* (Appendix I).

Figure 6.9-3. $AmOHCO_3$ Solubility Modeled as a Function of fCO_2 and pH

Because the independent variables of calculated Am solubility are in log scales and the user of the table may need to interpolate between calculated values, the logarithm of Am solubility is given in Table 6.9-2 for use in the TSPA-LA modeling.

Table 6.9-2 includes the value "500" for those ranges of conditions for which no concentrations were given in Table 6.9-1. For those calculations that do not converge or are not valid, a large number ("500") is entered to indicate that under such pH and fCO_2 conditions, solubility of americium is not defined or the calculation results are outside the valid range of the computing tool. When the flag ("500") is encountered or for conditions between a valid solubility and a flag of "500," concentrations should be calculated according to the dissolution rate of individual waste forms, water volume, and the solubility caps presented in Table 8-3 instead of the flag itself. In addition, for conditions outside of the 3.0 to 11.0 pH range, or the fCO_2 range from $10^{-1.5}$ to $10^{-5.0}$ bars, the concentrations should be calculated according to the dissolution rate of individual waste forms, water volume, and the solubility caps presented in Table 8-3.

Table 6.9-1. Americium Solubility (mg/L) Calculated with $AmOHCO_3$ as Controlling Solid

	log fCO_2 (bars)							
pH	**–1.50**	**–2.00**	**–2.50**	**–3.00**	**–3.50**	**–4.00**	**–4.50**	**–5.00**
5.50	2.52E+02	1.88E+03	—	—	—	—	—	—
5.75	3.42E+01	1.26E+02	6.25E+02	—	—	—	—	—
6.00	6.30E+00	2.00E+01	6.77E+01	2.72E+02	2.00E+03	—	—	—
6.25	1.45E+00	3.92E+00	1.19E+01	3.84E+01	1.38E+02	6.90E+02	—	—
6.50	4.65E-01	9.38E-01	2.44E+00	7.25E+00	2.29E+01	7.78E+01	3.17E+02	2.37E+03
6.75	2.18E-01	3.02E-01	6.08E-01	1.58E+00	4.67E+00	1.46E+01	4.81E+01	1.76E+02
7.00	1.22E-01	1.30E-01	1.97E-01	4.13E-01	1.10E+00	3.27E+00	1.02E+01	3.30E+01
7.25	7.79E-02	6.98E-02	8.30E-02	1.37E-01	3.08E-01	8.52E-01	2.58E+00	8.07E+00
7.50	6.28E-02	4.38E-02	4.15E-02	5.65E-02	1.06E-01	2.65E-01	7.69E-01	2.36E+00
7.75	7.67E-02	3.46E-02	2.54E-02	2.78E-02	4.43E-02	9.88E-02	2.72E-01	8.21E-01
8.00	1.80E-01	4.06E-02	1.96E-02	1.59E-02	2.14E-02	4.28E-02	1.12E-01	3.31E-01
8.25	9.20E-01	8.42E-02	2.21E-02	1.17E-02	1.18E-02	2.08E-02	5.18E-02	1.51E-01
8.50	7.84E+00	3.62E-01	4.18E-02	1.25E-02	7.90E-03	1.12E-02	2.60E-02	7.44E-02
8.75	8.49E+01	2.80E+00	1.54E-01	2.18E-02	7.63E-03	6.89E-03	1.39E-02	3.88E-02
9.00	—	3.02E+01	1.07E+00	7.10E-02	1.20E-02	5.55E-03	8.05E-03	2.11E-02
9.25	—	4.31E+02	1.14E+01	4.44E-01	3.49E-02	7.25E-03	5.43E-03	1.18E-02
9.50	—	—	1.75E+02	4.62E+00	1.99E-01	1.83E-02	5.29E-03	7.14E-03
9.75	—	—	—	7.66E+01	2.03E+00	9.57E-02	1.04E-02	5.25E-03
10.00	—	—	—	—	3.59E+01	9.62E-01	4.90E-02	7.02E-03
10.25	—	—	—	—	—	1.79E+01	4.84E-01	2.67E-02
10.50	—	—	—	—	—	—	9.33E+00	2.55E-01
10.75	—	—	—	—	—	—	—	5.02E+00

Source: *Am Solubility.xls* (Appendix I).

NOTE: Some cells have no data because the EQ3NR calculations do not converge. Runs with ionic strengths > 1.0 are not reported.

Table 6.9-2. Americium Solubility (log[Am] mg/L)

	log fCO_2 (bars)							
pH	**–1.50**	**–2.00**	**–2.50**	**–3.00**	**–3.50**	**–4.00**	**–4.50**	**–5.00**
5.50	2.40E+00	3.27E+00	500	500	500	500	500	500
5.75	1.53E+00	2.10E+00	2.80E+00	500	500	500	500	500
6.00	7.99E-01	1.30E+00	1.83E+00	2.43E+00	3.30E+00	500	500	500
6.25	1.60E-01	5.93E-01	1.07E+00	1.58E+00	2.14E+00	2.84E+00	500	500
6.50	-3.33E-01	-2.76E-02	3.88E-01	8.60E-01	1.36E+00	1.89E+00	2.50E+00	3.37E+00
6.75	-6.62E-01	-5.20E-01	-2.16E-01	1.98E-01	6.69E-01	1.16E+00	1.68E+00	2.25E+00
7.00	-9.13E-01	-8.85E-01	-7.05E-01	-3.84E-01	3.99E-02	5.14E-01	1.01E+00	1.52E+00
7.25	-1.11E+00	-1.16E+00	-1.08E+00	-8.65E-01	-5.11E-01	-6.96E-02	4.11E-01	9.07E-01
7.50	-1.20E+00	-1.36E+00	-1.38E+00	-1.25E+00	-9.73E-01	-5.76E-01	-1.14E-01	3.74E-01

Table 6.9-2. Americium Solubility (log[Am] mg/L) (Continued)

pH	log fCO_2 (bars)							
	–1.50	**–2.00**	**–2.50**	**–3.00**	**–3.50**	**–4.00**	**–4.50**	**–5.00**
7.75	-1.12E+00	-1.46E+00	-1.60E+00	-1.56E+00	-1.35E+00	-1.01E+00	-5.65E-01	-8.59E-02
8.00	-7.46E-01	-1.39E+00	-1.71E+00	-1.80E+00	-1.67E+00	-1.37E+00	-9.51E-01	-4.80E-01
8.25	-3.64E-02	-1.07E+00	-1.66E+00	-1.93E+00	-1.93E+00	-1.68E+00	-1.29E+00	-8.22E-01
8.50	8.95E-01	-4.41E-01	-1.38E+00	-1.90E+00	-2.10E+00	-1.95E+00	-1.58E+00	-1.13E+00
8.75	1.93E+00	4.47E-01	-8.11E-01	-1.66E+00	-2.12E+00	-2.16E+00	-1.86E+00	-1.41E+00
9.00	500	1.48E+00	3.02E-02	-1.15E+00	-1.92E+00	-2.26E+00	-2.09E+00	-1.68E+00
9.25	500	2.63E+00	1.06E+00	-3.53E-01	-1.46E+00	-2.14E+00	-2.27E+00	-1.93E+00
9.50	500	500	2.24E+00	6.65E-01	-7.01E-01	-1.74E+00	-2.28E+00	-2.15E+00
9.75	500	500	500	1.88E+00	3.08E-01	-1.02E+00	-1.98E+00	-2.28E+00
10.00	500	500	500	500	1.56E+00	-1.70E-02	-1.31E+00	-2.15E+00
10.25	500	500	500	500	500	1.25E+00	-3.16E-01	-1.57E+00
10.50	500	500	500	500	500	500	9.70E-01	-5.94E-01
10.75	500	500	500	500	500	500	500	7.01E-01

Source: *Am Solubility.xls* (Appendix I)

NOTES: Some cells have no valid data because the EQ3NR calculations do not converge and the results are reported as “500.” Runs with ionic strengths >1.0 are also reported as “500.”

6.9.4.2 Uncertainties

6.9.4.2.1 Uncertainty in Log K of the Solubility-Controlling Solid and Aqueous Species

As described in Section 6.3.3, uncertainties in the solubilities have been evaluated considering uncertainties in thermodynamic data and uncertainties in the fluoride content of the matrix fluid. The uncertainty in thermodynamic data was calculated as described in Section 6.3.3.1, allowing for uncertainties in log K values of the controlling solid and the important aqueous americium species.

The principal dissolved americium species accounting for more than 10 percent of the total dissolved americium ($Am(CO_3)_3^{3-}$, $Am(CO_3)_2^{-}$, $AmCO_3^{+}$, $Am(OH)_2^{+}$, $AmOH^{2+}$, $AmSO_4^{+}$, $Am(SO_4)_2^{-}$, and Am^{3+}) are evident in Figure 6.9-2. Uncertainties for log K values of these species found in *Chemical Thermodynamics of Americium* (Silva et al. 1995 [DIRS 102087], Table III.2) range from ±0.03 to ±0.8. Uncertainty in the log K of $AmOHCO_3$, the controlling solid, also reported by Silva et al. (1995 [DIRS 102087], Table III.2), is ±1.4. The largest log K uncertainty was found for the reaction to $Am(CO_3)_3^{3-}$ and equals ±1.94 (*log K concentrations_060424.xls* in Appendix I). This represents a 2σ value. The 1σ uncertainty assigned to the log[Am] values is ±1.0.

6.9.4.2.2 Uncertainty from Fluoride Concentration

The effects of fluoride uncertainty were evaluated by calculating americium solubilities at a range of pH values for $fCO_2 = 10^{-3.0}$ bars with fluoride concentrations equal to the highest values

expected in each of the three in-package and invert environments. These environments and their fluoride concentrations are described in Section 6.3.3.2 and Table 6.3-3. The results are displayed in Figure 6.9-4. Table 6.9-3 gives the calculated concentrations, including those for the base-case fluoride concentration, and also shows the differences between the higher-fluoride and base-case solubilities. As the figure and table show, at a fluoride concentration of 2.18 mg/L (the CSNF environment, 10× the base-case value), the maximum difference from the base-case concentration is +0.06 log[Am] (in mg/L) units at the lowest pH calculated (6.00). At a fluoride concentration of 209 mg/L (the codisposal vapor-influx scenario and invert environment, about 95× the base-case value), the maximum difference from the base-case concentration is +1.00 log[Am] (in mg/L) units at pH 6.50.

Table 6.9-3. Effects of Variations in Fluoride Concentrations on Americium Solubility

	Base Case	CSNF	CDSP – Water-Influx Scenario	CDSP – Vapor-Influx Scenario	CSNF	CDSP – Water-Influx Scenario	CDSP – Vapor-Influx Scenario
pH	**log[Am] mg/L**				**Difference**		
6.00	2.435	2.494	2.799	3.242	0.059	0.364	0.807
6.25	1.584	1.633	1.981	2.551	0.049	0.397	0.967
6.50	0.860	0.902	1.242	1.855	0.042	0.382	0.995
6.75	0.198	0.232	0.533	1.129	0.033	0.335	0.930
7.00	-0.384	-0.362	-0.128	0.407	0.022	0.256	0.791
7.25	-0.865	-0.854	-0.703	-0.280	0.011	0.162	0.585
7.50	-1.248	-1.245	-1.164	-0.891	0.003	0.084	0.357
7.75	-1.556	-1.557	-1.517	-1.377	-0.002	0.039	0.179
8.00	-1.800	-1.793	-1.776	-1.715	0.007	0.024	0.085
8.25	-1.933	-1.928	-1.921	-1.892	0.004	0.012	0.041
8.50	-1.904	-1.900	-1.894	-1.870	0.004	0.011	0.034
8.75	-1.661	-1.656	-1.646	-1.610	0.006	0.016	0.052
9.00	-1.149	-1.141	-1.128	-1.079	0.007	0.021	0.070
9.25	-0.353	-0.346	-0.335	-0.292	0.006	0.018	0.061
9.50	0.665	0.668	0.675	0.700	0.004	0.010	0.035
9.75	1.884	1.885	1.888	1.897	0.001	0.004	0.013
				Maximum	0.059	0.397	0.995

Source: *Am Solubility.xls* and *Am F sensitivity.xls* (Appendix I).

NOTE: $fCO_2 = -3.0$ bars.

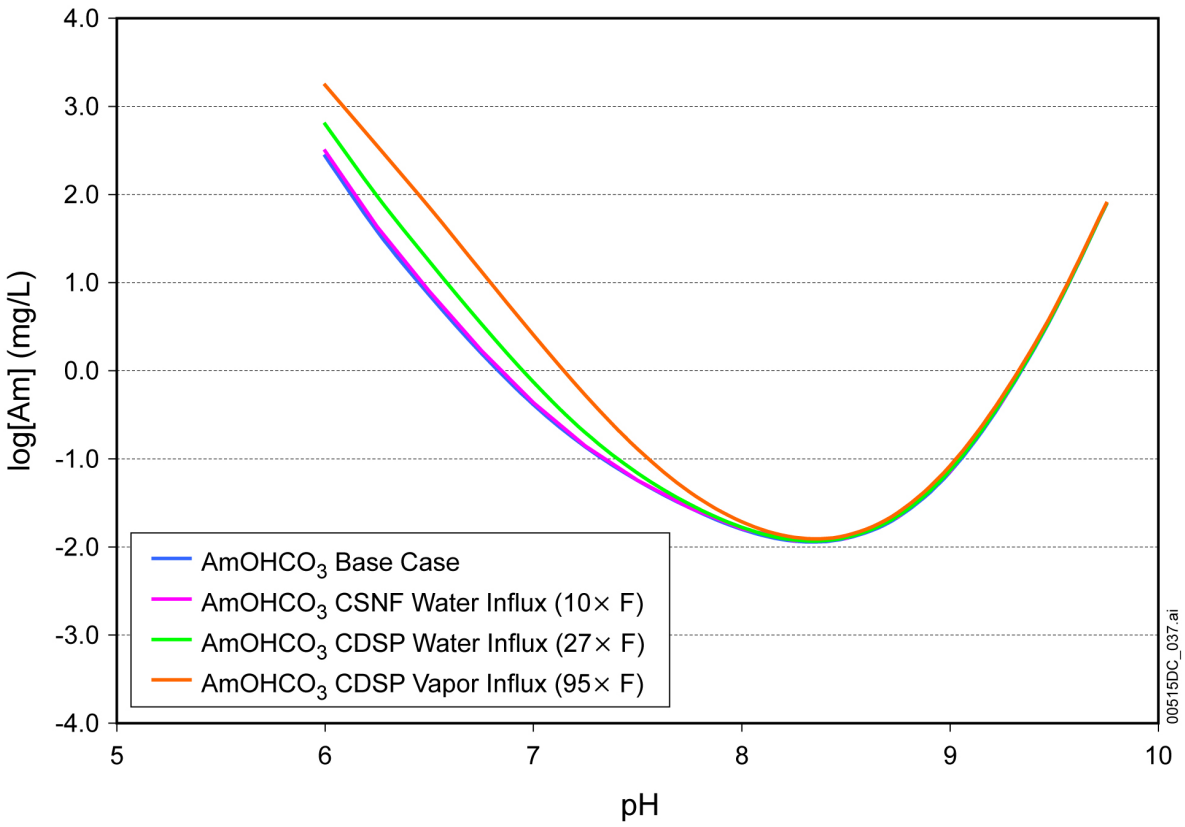

Source: *Am F sensitivity.xls* (Appendix I).

Figure 6.9-4. Sensitivity of Americium Solubility at log fCO_2 = –3.0 bars to Variations of Fluoride Concentrations

6.9.4.2.3 Summary of Am-Solubility Model Uncertainty

The uncertainties in americium solubilities are summarized in the following equation:

$$\log[\mathrm{Am}] = S(pH, \log fCO_2) + \varepsilon_1 + (\varepsilon_2 \times N) \qquad \text{(Eq. 6.9-2)}$$

The values for the parameters in this equation depend on the waste package type. Parameter $S\left(pH, \log f_{CO_2}\right)$ is the base solubility and is taken from Table 6.9-2. Parameter ε_1 is associated with the uncertainties in the log K data. Parameter ε_2 is associated with the uncertainties in the fluoride concentrations. Table 6.9-4 gives the values for the parameters ε_1 and ε_2.

Table 6.9-3 shows that the uncertainty terms $\varepsilon_2^{\text{CSNF}}$, $\varepsilon_2^{\text{CDSP-water influx}}$, and $\varepsilon_2^{\text{CDSP-vapor influx}}$ vary with pH. This pH dependence can be implemented through the use of a multiplication factor (N) that is a function of pH. Values for N for both fuel types are given in Table 6.9-5. This modification requires that the $\varepsilon_2^{\text{CSNF}}$, $\varepsilon_2^{\text{CDSP-water influx}}$, and $\varepsilon_2^{\text{CDSP-vapor influx}}$ values be fixed at the maximum value given in Table 6.9-3. For each realization, the uncertainty parameters are sampled at the beginning of the realization. This sampled value is then multiplied by N at each timestep to produce a modified ε_2 that is then added to the base solubility value.

Table 6.9-4. Uncertainty Terms of log[Am]

Uncertainty Term	Associated With:	Distribution Type	Distribution Parameter	Applicable To:
ε_1	log K of controlling solid and aqueous species	Normal Truncated at $\pm 2\sigma$	$\mu = 0$, $\sigma = 1.0$	Values in Table 6.9-2
ε_2^{CSNF}	Fluoride concentration in CSNF waste packages	Triangular	a = b = 0, c = 5.91E-2	CSNF waste packages
$\varepsilon_2^{CDSP\text{-}water\ influx}$	Fluoride concentration in codisposal waste packages (water-influx scenario)	Triangular	a = b = 0, c = 0.40	Codisposal waste packages and the invert
$\varepsilon_2^{CDSP\text{-}vapor\ influx}$	Fluoride concentration In codisposal waste package (vapor-influx scenario)	Triangular	a = b = 0, c = 0.99	Codisposal waste packages and the invert

NOTES: For ionic strength values between 1 and 3, Log K uncertainty should be treated as a normal distribution truncated at $\pm 2\sigma$ with distribution parameters $\mu = 0$, $\sigma = 1.04$ (Section 6.3.3.4, Equation 6.3-7).

Table 6.9-5. Multiplication Factor (N) Used to Modify F^- Uncertainty Term for Americium

pH	Multiplication Factor for F– Uncertainty		
	CSNF	CDSP – Water-Influx Scenario	CDSP – Vapor-Influx Scenario
6.00	1.00E+00	9.18E-01	8.11E-01
6.25	8.28E-01	1.00E+00	9.72E-01
6.50	7.12E-01	9.62E-01	1.00E+00
6.75	5.64E-01	8.44E-01	9.35E-01
7.00	3.69E-01	6.46E-01	7.96E-01
7.25	1.79E-01	4.07E-01	5.88E-01
7.50	5.37E-02	2.11E-01	3.58E-01
7.75	-2.67E-02/(0.00)[a]	9.93E-02	1.80E-01
8.00	1.18E-01	5.93E-02	8.56E-02
8.25	7.32E-02	2.93E-02	4.10E-02
8.50	6.68E-02	2.65E-02	3.42E-02
8.75	9.63E-02	3.92E-02	5.19E-02
9.00	1.26E-01	5.25E-02	7.05E-02
9.25	1.06E-01	4.44E-02	6.09E-02
9.50	6.00E-02	2.50E-02	3.52E-02
9.75	2.31E-02	9.21E-03	1.32E-02

Source: *Am F sensitivity.xls* (Appendix I).

NOTE: [a] Negative value set to 0.00, indicating that no normalization is applied.

6.9.5 Alternative Conceptual Model

As mentioned in Section 6.9.1, other solids with properties specified in *Data0.ymp.R2* (DTN: MO0302SPATHDYN.000 [DIRS 161756]) are potential controls on americium solubility. Hummel et al. (2002 [DIRS 161904], Section 5.2.3.2) describe experimental observations of solids with properties ranging from those of $Am(OH)_3$ to those of $Am(OH)_3$(am). The less-stable solid appears to form first in many experiments and converts to the more-stable solid with time. However, with additional time, the stable solid becomes less stable once again, presumably as a result of radiation damage. An alternative controlling phase could be chosen conservatively to have properties of $Am(OH)_3$(am).

Examination of the EQ3NR output files shows that $Am(OH)_3$(am) becomes oversaturated under conditions of the lowest fCO_2, but under the remaining conditions modeled it is more soluble than $AmOHCO_3$ (the controlling phase selected). The choice of the controlling solid phase $AmOHCO_3$ in the base-case model is based on the studies by Nitsche et al. (1993 [DIRS 155218]; 1994 [DIRS 144515]), which identify $AmOHCO_3$ as the solid phase precipitated from water similar to the J-13 well water composition used in these calculations at a pH range from 5.9 to 8.4 and temperatures from 25°C to 90°C.

6.10 ACTINIUM SOLUBILITY

6.10.1 Introduction

No thermodynamic data for actinium are included in *Data0.ymp.R2* (DTN: MO0302SPATHDYN.000 [DIRS 161756]), so actinium solubilities have not been calculated. Also, transport of Ac is not modeled in the TSPA-LA model because of its extremely short half-life. Actinium dose is calculated in TSPA-LA by assuming secular equilibrium with ^{231}Pa. Therefore, solubilities of actinium are not investigated in this model.

6.11 PROTACTINIUM SOLUBILITY

6.11.1 Introduction

No thermodynamic data for protactinium are included in *Data0.ymp.R2* (DTN: MO0302SPATHDYN.000 [DIRS 161756]), so protactinium solubilities have not been calculated using EQ3NR. It is generally accepted that properties of elements are consistent with their position in the periodic table. Elements with similar positions in the periodic table of the elements will have similar behaviors due to their similar electronic structure. Thus, corresponding solids of elements of similar positions in the table have similar solubilities.

Properties of elements in solution can be related to their charge (z) and ionic radius (r) (Hummel et al. 2002 [DIRS 161904], Figures 3.1.1 through 3.1.5). Figure 6.11-1 plots z^2/r of selected cations against the log K(25°C) of dissociation of their monohydroxyl solution complexes, for example:

$$MOH^{+(z-1)} + H^+ = M^{+z} + H_2O \qquad \text{(Eq. 6.11-1)}$$

where M represents any metal.

Figure 6.11-1 illustrates the correlation of chemical properties—in this case, solute complexation behavior—with charge and size. The sources of the log K(25°C) values are provided in the figure caption. Figure 6.11-1 also shows what would be expected from inspection of the periodic table, that Pa(IV) behavior is similar to that of Np(IV), Th(IV), and other members of the actinide series.

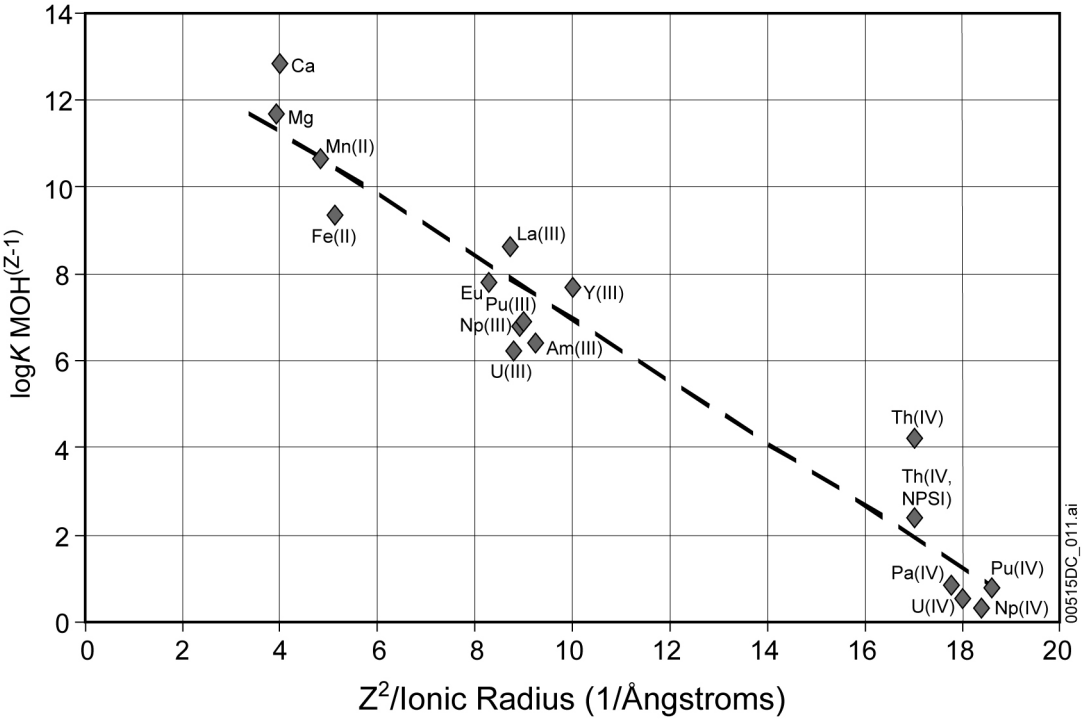

Source: *Fig 6_10-1_2 data and plots.xls* (Appendix I).

Data Sources: Values for r are from Shannon 1976 [DIRS 153587], Table 1. log K(25°C) values are from *Data0.ymp.R2* (DTN: MO0302SPATHDYN.000 [DIRS 161756]), except those for Pa(IV), which are from Baes and Mesmer 1986 [DIRS 100702]; Table 9.1 and Th(IV, NPSI), which is from Hummel et al. 2002 [DIRS 161904], Table 5.21.1.

NOTE: z = charge and r = ionic radius in Ángstroms.
The value for Ac(III) is a maximum value. The arrow in the figure shows the actual value would be lower than the value plotted.

Figure 6.11-1. Correlation Between z^2/r and log K (25°C) for the Formation of the Monohydroxyl Complex of Selected Ions

Thermodynamic data has been extracted from experiments by Baes and Mesmer (1986 [DIRS 100702], Section 9.1), Shibutani et al. (1998 [DIRS 161998]), and Yui et al. (1999 [DIRS 162664]). Protactinium most likely occurs in aqueous solution as Pa(IV) and Pa(V). As Figure 6.11-1 illustrates, the solution properties of Pa(IV) are similar to those of other actinides in their (IV) oxidation state. Thus, if protactinium occurred only as Pa(IV), its solubility would resemble that of Th(IV) (Section 6.8) or Np(IV) (Section 6.6). If protactinium occurred only as Pa(V), its solubility would resemble that of Np(V) (Section 6.6).

Baes and Mesmer (1986 [DIRS 100702], Section 9.1.2) also derive equilibrium constant values for several Pa(V) reactions. These can be compared with data for analogous reactions of Np(V) as follows:

Table 6.11-1. Comparison of Analogous Neptunium and Protactinium Reactions

Reaction	log K - Np(V)[a]	log K - Pa(V)[b]
$MO_2OH(aq) + H^+ = MO_2^+ + H_2O$	11.3	4.5
$M_2O_5 + 2H^+ = 2MO_2^+ + 2H_2O$	3.7	< -4

Sources: [a] *Data0.ymp.R2* (DTN: MO0302SPATHDYN.000 [DIRS 161756]).
[b] Baes and Mesmer 1986 [DIRS 100702], Table 9.1.

The stability of the Pa(V) solid is greater than that of the analogous Np(V) solid while that of the Pa(V) aqueous complex is lower. This indicates that if protactinium occurred only as Pa(V), its solubility would be less than that of neptunium. Baes and Mesmer (1986 [DIRS 100702], Section 9.1.2) describe experimental difficulties in maintaining protactinium in a stable oxidation state in solution, so calculations of the protactinium oxidation state required for solubilities calculation may not be reliable.

6.11.2 Solubility Development

Solubility calculations for Np(IV) and Np(V), as well as Th(IV), have been performed as part of this report. In the absence of data for protactinium in *Data0.ymp.R2* (DTN: MO0302SPATHDYN.000 [DIRS 161756]), protactinium concentrations and related uncertainties are based on those calculated for neptunium and thorium (Sections 6.6 and 6.8). Based on the considerations of chemical analogy, protactinium solubility should range from above that of thorium (Th(IV)) to below that of neptunium (Np(V)). Figure 6.11-2 shows the difference between the solubilities of Np_2O_5 and ThO_2(am). Under the widest range of pH and fCO_2 conditions, Np_2O_5 solubility is greater than that of ThO_2(am). The base-case protactinium solubility is taken equal to that of the ex-package (invert) Np-solubility model (when neptunium is in the Np(V) state) with the difference to the Th solubility accommodated in the uncertainty term (ε_1 term in Table 6.11-4). A conservative approach was taken to use the highest fluoride uncertainty of the two analoques (Np and Th). Therefore, the fluoride uncertainty for protactinium (ε_2 term in Table 6.11-4) is based on thorium.

6.11.3 Chemical Conditions

Because the protactinium solubility is based on the neptunium and thorium calculations, the chemical conditions given in Table 6.4-2 and used for the neptunium and thorium calculations also apply to the protactinium values.

6.11.4 Protactinium-Solubility Model

Table 6.11-2 provides protactinium concentrations in mg/L.

Because the independent variables of calculated Pa solubility are in log scales and the user of the table may need to interpolate between calculated values, the logarithm of Pa solubility is given in Table 6.11-3 for use in the TSPA-LA modeling. The second table includes the value "500" for those ranges of conditions for which no concentrations were provided in Table 6.11-2. The "500" is entered to indicate that under such pH and fCO_2 conditions, solubility of protactinium is not defined or the calculation results are outside the valid range of the computing tool. When the

flag ("500") is encountered or for conditions between a valid solubility and a flag of "500," concentrations should be calculated according to the dissolution rate of individual waste forms, water volume, and the solubility caps presented in Table 8-3 instead of the flag itself. In addition, for conditions outside of the 3.0 to 11.0 pH range, or the fCO_2 range from $10^{-1.5}$ to $10^{-5.0}$ bars, the concentrations should be calculated according to the dissolution rate of individual waste forms, water volume, and the solubility caps presented in Table 8-3.

Table 6.11-2. Base-Case Protactinium Solubility (mg/L)

	log fCO_2 (bars)							
pH	**–1.50**	**–2.00**	**–2.50**	**–3.00**	**–3.50**	**–4.00**	**–4.50**	**–5.00**
3.00	2.40E+04	2.40E+04	2.40E+04	2.40E+04	2.40E+04	2.40E+04	2.40E+04	2.40E+04
3.25	1.25E+04	1.25E+04	1.25E+04	1.25E+04	1.25E+04	1.25E+04	1.25E+04	1.25E+04
3.50	6.65E+03	6.65E+03	6.65E+03	6.65E+03	6.65E+03	6.65E+03	6.65E+03	6.65E+03
3.75	3.57E+03	3.57E+03	3.57E+03	3.57E+03	3.57E+03	3.57E+03	3.57E+03	3.57E+03
4.00	1.94E+03	1.94E+03	1.94E+03	1.94E+03	1.94E+03	1.94E+03	1.94E+03	1.94E+03
4.25	1.07E+03	1.07E+03	1.07E+03	1.07E+03	1.07E+03	1.07E+03	1.07E+03	1.07E+03
4.50	5.90E+02	5.90E+02	5.90E+02	5.90E+02	5.90E+02	5.90E+02	5.90E+02	5.90E+02
4.75	3.28E+02	3.29E+02	3.29E+02	3.29E+02	3.29E+02	3.29E+02	3.29E+02	3.29E+02
5.00	1.84E+02	1.84E+02	1.84E+02	1.84E+02	1.84E+02	1.84E+02	1.84E+02	1.84E+02
5.25	1.03E+02	1.03E+02	1.03E+02	1.03E+02	1.03E+02	1.03E+02	1.03E+02	1.03E+02
5.50	5.77E+01	5.77E+01	5.77E+01	5.77E+01	5.77E+01	5.77E+01	5.77E+01	5.77E+01
5.75	3.24E+01	3.24E+01	3.24E+01	3.24E+01	3.24E+01	3.24E+01	3.24E+01	3.24E+01
6.00	1.82E+01	1.82E+01	1.82E+01	1.82E+01	1.82E+01	1.82E+01	1.82E+01	1.82E+01
6.25	1.03E+01	1.02E+01	1.02E+01	1.02E+01	1.02E+01	1.02E+01	1.02E+01	1.02E+01
6.50	5.83E+00	5.78E+00	5.77E+00	5.76E+00	5.76E+00	5.76E+00	5.76E+00	5.76E+00
6.75	3.43E+00	3.29E+00	3.25E+00	3.24E+00	3.24E+00	3.24E+00	3.24E+00	3.24E+00
7.00	2.22E+00	1.92E+00	1.85E+00	1.83E+00	1.82E+00	1.82E+00	1.82E+00	1.82E+00
7.25	1.74E+00	1.23E+00	1.08E+00	1.04E+00	1.03E+00	1.03E+00	1.02E+00	1.02E+00
7.50	1.89E+00	9.56E-01	6.87E-01	6.11E-01	5.87E-01	5.79E-01	5.77E-01	5.76E-01
7.75	2.86E+00	1.02E+00	5.29E-01	3.87E-01	3.44E-01	3.30E-01	3.26E-01	3.24E-01
8.00	3.41E+00	1.48E+00	5.59E-01	2.96E-01	2.18E-01	1.94E-01	1.86E-01	1.83E-01
8.25		2.81E+00	7.96E-01	3.08E-01	1.67E-01	1.23E-01	1.09E-01	1.04E-01
8.50		1.01E+01	1.40E+00	4.35E-01	1.72E-01	9.39E-02	6.91E-02	6.13E-02
8.75			3.45E+00	7.41E-01	2.40E-01	9.70E-02	5.29E-02	3.89E-02
9.00				1.54E+00	4.02E-01	1.33E-01	5.46E-02	2.98E-02
9.25				6.59E+00	7.80E-01	2.22E-01	7.51E-02	3.08E-02
9.50					2.36E+00	4.16E-01	1.23E-01	4.23E-02
9.75						1.05E+00	2.27E-01	6.88E-02
10.00						9.04E+00	5.27E-01	1.26E-01

Table 6.11-2. Base-Case Protactinium Solubility (mg/L) (Continued)

pH	log fCO_2 (bars)							
	–1.50	**–2.00**	**–2.50**	**–3.00**	**–3.50**	**–4.00**	**–4.50**	**–5.00**
10.25							3.34E+00	2.80E-01
10.50								1.48E+00

Source: *Np base case-Ehadjusted.xls* (Appendix I).

NOTE: Some cells have no data because the EQ3NR calculations do not converge (Section 6.4.4).

Table 6.11-3. Base-Case Protactinium Solubility (log[Pa], mg/L)

pH	log fCO_2 (bars)							
	–1.5	**–2.0**	**–2.5**	**–3.0**	**–3.5**	**–4.0**	**–4.5**	**–5.0**
3.00	4.38E+00	4.38E+00	4.38E+00	4.38E+00	4.38E+00	4.38E+00	4.38E+00	4.38E+00
3.25	4.10E+00	4.10E+00	4.10E+00	4.10E+00	4.10E+00	4.10E+00	4.10E+00	4.10E+00
3.50	3.82E+00	3.82E+00	3.82E+00	3.82E+00	3.82E+00	3.82E+00	3.82E+00	3.82E+00
3.75	3.55E+00	3.55E+00	3.55E+00	3.55E+00	3.55E+00	3.55E+00	3.55E+00	3.55E+00
4.00	3.29E+00	3.29E+00	3.29E+00	3.29E+00	3.29E+00	3.29E+00	3.29E+00	3.29E+00
4.25	3.03E+00	3.03E+00	3.03E+00	3.03E+00	3.03E+00	3.03E+00	3.03E+00	3.03E+00
4.50	2.77E+00	2.77E+00	2.77E+00	2.77E+00	2.77E+00	2.77E+00	2.77E+00	2.77E+00
4.75	2.52E+00	2.52E+00	2.52E+00	2.52E+00	2.52E+00	2.52E+00	2.52E+00	2.52E+00
5.00	2.26E+00	2.26E+00	2.26E+00	2.26E+00	2.26E+00	2.26E+00	2.26E+00	2.26E+00
5.25	2.01E+00	2.01E+00	2.01E+00	2.01E+00	2.01E+00	2.01E+00	2.01E+00	2.01E+00
5.50	1.76E+00	1.76E+00	1.76E+00	1.76E+00	1.76E+00	1.76E+00	1.76E+00	1.76E+00
5.75	1.51E+00	1.51E+00	1.51E+00	1.51E+00	1.51E+00	1.51E+00	1.51E+00	1.51E+00
6.00	1.26E+00	1.26E+00	1.26E+00	1.26E+00	1.26E+00	1.26E+00	1.26E+00	1.26E+00
6.25	1.01E+00	1.01E+00	1.01E+00	1.01E+00	1.01E+00	1.01E+00	1.01E+00	1.01E+00
6.50	7.66E-01	7.62E-01	7.61E-01	7.60E-01	7.60E-01	7.60E-01	7.60E-01	7.60E-01
6.75	5.35E-01	5.17E-01	5.12E-01	5.11E-01	5.10E-01	5.10E-01	5.10E-01	5.10E-01
7.00	3.46E-01	2.84E-01	2.68E-01	2.63E-01	2.61E-01	2.60E-01	2.60E-01	2.60E-01
7.25	2.41E-01	8.83E-02	3.52E-02	1.83E-02	1.28E-02	1.11E-02	1.05E-02	1.03E-02
7.50	2.76E-01	-1.94E-02	-1.63E-01	-2.14E-01	-2.31E-01	-2.37E-01	-2.39E-01	-2.39E-01
7.75	4.56E-01	8.77E-03	-2.77E-01	-4.12E-01	-4.64E-01	-4.81E-01	-4.87E-01	-4.89E-01
8.00	5.33E-01	1.71E-01	-2.53E-01	-5.29E-01	-6.61E-01	-7.13E-01	-7.31E-01	-7.37E-01
8.25	5.98E-01	4.49E-01	-9.89E-02	-5.11E-01	-7.78E-01	-9.11E-01	-9.63E-01	-9.81E-01
8.50	1.42E+00	1.00E+00	1.47E-01	-3.62E-01	-7.64E-01	-1.03E+00	-1.16E+00	-1.21E+00
8.75	500	1.06E+00	5.38E-01	-1.30E-01	-6.20E-01	-1.01E+00	-1.28E+00	-1.41E+00
9.00	500	500	7.93E-01	1.89E-01	-3.95E-01	-8.75E-01	-1.26E+00	-1.53E+00
9.25	500	500	500	8.19E-01	-1.08E-01	-6.54E-01	-1.12E+00	-1.51E+00
9.50	500	500	500	1.36E+00	3.72E-01	-3.81E-01	-9.10E-01	-1.37E+00
9.75	500	500	500	500	1.12E+00	2.16E-02	-6.44E-01	-1.16E+00

Table 6.11-3. Base-Case Protactinium Solubility (log[Pa], mg/L) (Continued)

	log fCO_2 (bars)							
pH	**–1.5**	**–2.0**	**–2.5**	**–3.0**	**–3.5**	**–4.0**	**–4.5**	**–5.0**
10.00	500	500	500	500	500	9.56E-01	-2.78E-01	-9.00E-01
10.25	500	500	500	500	500	1.96E+00	5.24E-01	-5.52E-01
10.50	500	500	500	500	500	500	1.76E+00	1.72E-01

Source: *Np base case-Ehadjusted.xls* (Appendix I).

NOTE: Some cells have no valid solubility values because the EQ3NR calculations do not converge, and those calculations results are reported as "500" (Section 6.4.4).

6.11.5 Uncertainty

It is difficult to assign formal uncertainty to the protactinium solubility because the values are based on chemical analogy, rather than on thermodynamic data, and are supported by only one experimental study made in waters unlike those used for modeling the solubilities of other elements.

The uncertainty range for protactinium solubility is taken as the difference between the solubilities of neptunium and thorium. The uncertainty distribution is taken as a uniform distribution in log[Pa] mg/L ranging from neptunium and thorium solubilities. As Figure 6.11-2 illustrates, these differences range from 0.05 to 4.42 in log mg/L. Because the starting solubility for protactinium is the maximum value possible (by using the neptunium analogue), the uncertainty term should reduce the solubility to account for the lower thorium solubilities, so the uncertainty term is switched to negative values (-0.05 to –4.42).

The uncertainty in protactinium solubilities due to fluoride contents is also unknown. It is taken as the larger of the corresponding uncertainty of the Np_2O_5 or ThO_2(am) solubilities.

The following equation summarizes the protactinium-solubility model:

$$\log[\mathrm{Pa}] = S(pH, \log fCO_2) + \varepsilon_1 + \varepsilon_2 \qquad \text{(Eq 6.11-2)}$$

The values for the parameters in this equation depend on the waste package type. Parameter $S\left(pH, \log f_{CO_2}\right)$ is the base-case solubility and is taken from Table 6.11-3. Parameter ε_1 is associated with the uncertainties in the log K data. Parameter ε_2 is associated with the uncertainties in the fluoride concentrations. Table 6.11-4 gives the values for the parameters ε_1 and ε_2.

The distribution properties of these uncertainty terms are listed in Table 6.11-4.

Table 6.11-4. Uncertainty Terms of log[Pa]

Uncertainty Term	Associated With	Distribution Type	Distribution Parameter	Applicability
ε_1	Analogues	Uniform	Over an interval [–0.05 to –4.42]	Values in Table 6.11-3
ε_2^{CSNF}	Fluoride concentration in CSNF waste packages	Triangular	a = b = 0, c = 3.10	CSNF waste packages
$\varepsilon_2^{CDSP\text{-}water\ influx}$	Fluoride concentration in codisposal waste packages (water-influx scenario)	Triangular	a = b = 0, c = 4.21	Codisposal waste packages and the invert
$\varepsilon_2^{CDSP\text{-}vapor\ influx}$	Fluoride concentration In CDNR waste package (vapor-influx scenario)	Triangular	a = b = 0, c = 5.27	Codisposal waste packages and the invert

Source: ε_1 value from spreadsheet *Pa-Np-Th solubility-new.xls* (Appendix I), ε_2^{CSNF}, $\varepsilon_2^{CDSP\text{-}water\ influx}$, $\varepsilon_2^{CDSP\text{-}vapor\ influx}$ values from Table 6.8-3.

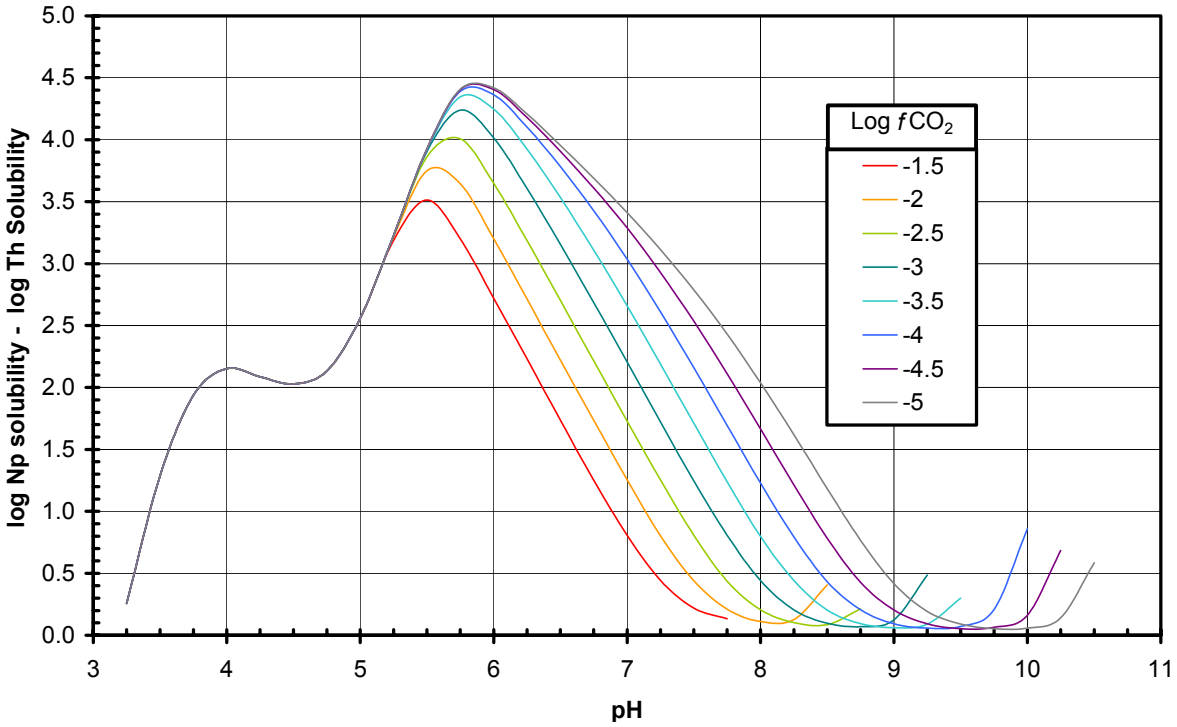

Source: *Pa-Np-Th Solubility-new.xls* (Appendix I).

Figure 6.11-2. Differences Between Np_2O_5 and ThO_2(am) Solubilities (log mg/L) as Functions of pH and fCO_2

6.12 RADIUM SOLUBILITY

Radium is an alkaline earth element with chemical properties similar to barium and exists only in the +2 oxidation state. Because of its nature, radium does not complex easily. Lide (2002 [DIRS 160832], p. 4-81) only reports four radium solids: $RaBr_2$, $RaCl_2$, RaF_2, and $RaSO_4$. Kirby and Salutsky (1964 [DIRS 173080]) divide radium solids into two categories: soluble

salts and insoluble salts. The soluble salts listed are those for radium chloride, bromide, and nitrate. These compounds are very soluble in water and are not expected to form in the repository. The insoluble salts consist of radium sulfate, chromate, carbonate, iodate, beryllium fluoride, and nitrate. Presently, information on the behavior or properties of Ra solids pertinenet to solubilities and thermodynamics is very small. Hummel et al. (2002 [DIRS 161904], Section 5.16) describe only two radium solids in the NAGRA/PSI thermodynamic database. These are $RaSO_4$(cr) and $RaCO_3$(cr).

Radium solubility has been studied briefly in *Pure Phase Solubility Limits – LANL* (CRWMS M&O 2001 [DIRS 154629], Section 6.3.7). EQ3NR runs (EQ3NR output files in *Ra Eq3 files.zip* of Appendix I) at log $fCO_2 = -3.0$ bars indicate that the solubility-controlling phase, if solid solutions with $BaSO_4$ or $SrSO_4$ are not taken into account, is $RaSO_4$. Accordingly, the solubility depends primarily on the concentration of free SO_4^{2-} in the solution (free means not combined with other elements in complexes or ion pairs). The free SO_4^{2-} is expected to vary over a wide range for two reasons. First, acid conditions may arise from the oxidation of sulfur to SO_4^{2-} during the corrosion of steel (Section 6.4.3.5). Such an increase in SO_4^{2-} represses the solubility of Ra^{2+}. Second, under alkaline conditions ion pairs, such as $NaSO_4^-$ or $CaSO_4$(aq) should form, thereby limiting the reducing free SO_4^{2-} and enhancing solubility.

For slightly alkaline (J-13 well water) and acidified Yucca Mountain waters, the calculated radium solubility ranges from 9.1E-03 to 1.9E-02 mg/L. A constant solubility of 2.0E-02 mg/L is recommended for radium for pH 7.75 or less. Under more alkaline conditions, pH values from 8.0 to 9.75, the calculated solubility ranges from 7.1E-02 to 1.2 mg/L. For this pH range a constant value of 1.2 mg/L is recommended. These values are recommended for both CSNF and codisposal waste packages.

At pH at or above 10, the rate of release of radium from the waste must be used. A higher pH cannot be achieved at equilibrium with the specified values of fCO_2 because any attempt to do so (e.g., adding NaOH to the solution) simply results in the precipitation of sodium bicarbonate or carbonate. Similarly, the addition of any other cation, such as Ca^{2+}, would result in the supersaturation and precipitation of the corresponding carbonate, or an oxide or hydroxide. The EQ3NR runs show that the solution becomes supersaturated in a sodium-calcium carbonate (gaylussite) and several calcium or magnesium carbonates, or both, at pH 7.75. The recommended radium solubility limits are summarized in Table 6.12-1.

Table 6.12-1. Radium Solubility Values

pH Range	Radium Solubility (mg/L)	log [Ra] (mg/L)
3.0 to 7.75	2.0E-2	-1.7
7.75 to 9.75	1.2	0.0792
> 9.75	500 (not controlled by solubility)	500 (not controlled by solubility)

6.13 LEAD SOLUBILITY

Lead is one of the least mobile of the heavy metals as it forms a number of sparingly soluble mineral phases and sorbs strongly to many mineral surfaces. Surface waters containing 1 ppb

lead are reasonably common. Waters with lead loads greater than 100 ppb are found in areas subject to substantial air pollution (such as heavily industrialized areas). However, reported concentrations of 10 ppb indicate that most of the lead was in particulate, mineral-associated form, as opposed to dissolved lead (Hem 1985 [DIRS 115670], p. 144).

The formation of $Pb_3(CO_3)_2(OH)_2$ can limit dissolved lead levels to 50 ppb or less under neutral to alkaline conditions (Hem 1985 [DIRS 115670], p. 144). Lead sulfate forms under sulfate-rich, acidic conditions,. Low-solubility lead-phosphate formation limits dissolved lead levels in some soils. Lead ion (Pb^{2+}) forms complexes with carbonate, hydroxyls, and sulfate. It also interacts strongly with a number of organic acids and coprecipitates with MnO_2 (Hem 1985 [DIRS 115670]).

Rickard and Nriagu (1978 [DIRS 154847]) report that freshwaters contain about 10^{-8} M (approximately 2 ppb) dissolved lead. Carbonate complexes are usually strong, and in the vast majority of freshwater systems lead carbonate complexes will dominate the inorganic chemistry of dissolved lead.

Carroll et al. (1998 [DIRS 144731]) studied concentrations of lead in waters from the Tri-State Mining District (Kansas-Missouri-Oklahoma), which consists of Mississippi Valley-type ore deposits characterized by zinc and lead sulfide mineralization in a chert and carbonate host rock. Even though the quantities of lead in this region should far exceed the levels produced in the repository, the majority of measured aqueous lead concentrations are quite low, less than 0.05 ppm (2.41E-07 M).

Gibson (1961 [DIRS 173470]) reports lead solids can be insoluble to only slightly soluble in water. For example, the solubility of lead carbonate is 0.00011g/100ml (approximately 5.3E-08) Gibson (1961 [DIRS 173470]) also indicates the ability of lead to coprecipitate with a number of different elements, which would further limit its solubility.

Peacey (2002 [DIRS 173073]) studied the concentration of lead in waters from a uranium mine. Surface waters have an average concentration of 0.00412 mg/L (approximately 2E-08 M or 4 ppb), while porewater within the first meter of mine tailings exhibited an average concentration of 0.121 mg/L (approximately 5.84E-07 M or 121 ppb). The higher concentrations of lead in the tailings are most likely due to upward diffusion of Pb in the tailings pile, artificially increasing the lead concentrations to unrealistic high levels. This is further corroborated by the decrease in Pb concentrations in the porewater between 0.15 meters and 1 meter below the tailings surface.

Because in-package fluids are expected to be either low-pH sulfate-rich waters or neutral-to-alkaline carbonate-rich waters, or some combination of the two, there is a strong likelihood that dissolved lead levels are limited by either lead sulfate or lead hydroxycarbonate formation. Uptake by corrosion products is also substantial. Because the lead sinks in the waste package environment are similar to a number of those that control lead in the environment, it is reasonable to expect dissolved lead levels to roughly reflect natural distributions (i.e., levels between 1 and 100 ppb). This corresponds to a range of 4.8E-9 to 4.8E-7 M. Therefore, it is recommended that TSPA-LA use a log-uniform distribution, with a minimum of 4.8E-9 mol/L and a maximum of 4.8E-7 mol/L to constrain lead solubility.

6.14 TECHNETIUM SOLUBILITY

Under the repository conditions, no solubility-controlling solid exists for technetium. Therefore, technetium solubility is undefined and flagged by the default value of "500." In TSPA-LA modeling, the release of technetium is controlled by the dissolution rate of waste forms rather than by solubility.

6.15 CARBON SOLUBILITY

Although under neutral or high-pH conditions, calcite may control the solubility of carbon; under pH as low as 3.6, calcite is not stable (Langmuir 1997 [DIRS 100051], Figure 6.6, p. 202). Therefore, carbon solubility is undefined and it is flagged by the default value of "500." In TSPA-LA modeling, the release of carbon is controlled by the dissolution rate of waste forms rather than by solubility.

6.16 IODINE SOLUBILITY

Under repository conditions, no solubility-controlling solid exists for iodine. Therefore, iodine solubility is undefined and it is flagged by the default value of "500." In TSPA-LA modeling, the release of iodine is controlled by the dissolution rate of waste forms rather than by solubility.

6.17 CESIUM SOLUBILITY

Under the repository conditions, no solubility-controlling solid exists for cesium. Therefore, cesium solubility is undefined and it is flagged by the default value of "500." In TSPA-LA modeling, the release of cesium is controlled by the dissolution rate of waste forms rather than by solubility.

6.18 STRONTIUM SOLUBILITY

Strontium is quite soluble. The most likely solids to precipitate under the repository conditions are carbonate (strontianite, $SrCO_3$) or sulfate (celestite, $SrSO_4$). It is conservatively assumed that no solubility-controlling solid exists for strontium. Therefore, strontium solubility is undefined and flagged by the default value of "500." In TSPA-LA modeling, the release of strontium is controlled by the dissolution rate of waste forms rather than by solubility. Strontium solubility can be developed using strontianite or celestite as its solubility-controlling solid.

6.19 CONSIDERATION OF ALTERNATIVE CONCEPTUAL MODELS

Alternative conceptual models are considered in developing the solubility models reported for many of the elements included in this report. These alternative models were described explicitly or implicitly in the discussions of each element. Some elements are assigned arbitrarily high solubilities so the control on their concentrations is release rates from the waste form rather than solubility control. No alternative conceptual models are considered for these elements.

The alternative conceptual models considered are summarized in Table 6.19-1.

Table 6.19-1. Summary of Alternative Conceptual Models

Element	Alternative Conceptual Model	Model Bases	Screening Assessment and Basis
Pu	Theoretical fO_2 model	fO_2 = 0.2 bars (Section 5.1).	Model results differ significantly from experimental measurements
	Empirical Eh model	Eh = 1.04 – 0.0592pH	Model results are lower than experimental results
Np	Neptunium incorporation into uranyl secondary phases	Neptunium concentration controlled by solid solution rather than by pure phases	Experimental studies on whether secondary uranyl phase can incorporate neptunium and immobilize it during spent nuclear fuel corrosion do not provide a solid basis for recommending this model to be used in the TSPA-LA model.
Th	Solubility control by other Th phases including ThO_2 (thorianite), $Th_{0.75}PO_4$, $Th(SO_4)_2$, ThF_4, $ThF_4 \cdot 2H_2O$	Solubility of thermodynamically most-stable phase controls concentrations	Solubilities calculated with ThO_2(am) are consistent with measured Th solubility in pure water. Other phases may be less soluble under only certain conditions or may be based on questionable data.
Am	Solubility control by phase with properties between $Am(OH)_3$(am) to $Am(OH)_3$.	Initially formed $Am(OH)_3$(am) inverts to more-stable $Am(OH)_3$ with time. $Am(OH)_3$ stability decreases with time from self-irradiation.	$AmOHCO_3$ is formed in americium solubility experiments under Yucca Mountain conditions. Under some conditions, $Am(OH)_3$ may be less soluble, but choosing $AmOHCO_3$ is, generally, conservative.
Ac	N/A (Section 6.10)	N/A (Section 6.10)	N/A (Section 6.10)
Pa	Solubility is same as that of ThO_2(am)	Thorium is also a good analogue to protactinium and was modeled in this report	Solubility of Np_2O_5 was chosen because it is higher than that of ThO_2(am) under conditions modeled, so its choice is conservative
Ra	None	N/A	Chemistry of in-package and invert waters are not so far outside the normal range of natural waters to cause different radium solubilities
Pb	None	N/A	Chemistry of in-package and invert are not so far outside the normal range of natural waters to cause different lead solubilities
Tc	None	N/A	No solubility was defined and inventory release should be in control
C	None	N/A	No solubility was defined and inventory release is in control
I	None	N/A	No solubility was defined and inventory release is in control
Cs	None	N/A	No solubility was defined and inventory release is in control
Sr	Solubility controlled by $SrCO_3$ or $SrSO_4$	N/A	No solubility was defined and inventory release is in control. This is a conservative approach.

INTENTIONALLY LEFT BLANK

7. VALIDATION

The purpose of this report is to develop models to evaluate solubility limits of elements with radioactive isotopes. The models are based on geochemical modeling calculations using geochemical modeling tools, thermodynamic databases, and measurements collected from laboratory experiments and fieldwork.

The scope of this modeling activity is the development of solubility limits as tabulated functions with pH and log fCO_2 as independent variables, distributions, or constants for elements with radioactive isotopes transported outside breached waste packages identified by *Radionuclide Screening* (BSC 2002 [DIRS 160059]). Fourteen elements with radioactive isotopes are identified by *Radionuclide Screening* (BSC 2002 [DIRS 160059]) as important to dose for the time period from 10^2 to 2×10^4 years: actinium, americium, carbon, cesium, iodine, lead, neptunium, plutonium, protactinium, radium, strontium, technetium, thorium, and uranium. TSPA-LA uses the results of this report to constrain the release of these elements. Even though selection of an appropriate set of radionuclides documented in *Radionuclide Screening* (BSC 2002 [DIRS 160059]) includes actinium, transport of Ac is not modeled in TSPA-LA model because of its extremely short half-life. Actinium dose is calculated in TSPA-LA by assuming secular equilibrium with ^{231}Pa (Section 6.10); therefore, Ac is not analyzed in this report.

As described in Section 6.3, development of solubility models for use in TSPA-LA has several components including: (1) a thermodynamic database and modeling tool, (2) the environmental conditions of concern, (3) the construction of the conceptual model, and (4) the calculation of solubility limits using a geochemical modeling tool based on the conceptual model. Because the thermodynamic database used in this report and the EQ3/6 code are controlled products and are used within their valid ranges, the first and fourth components need no validation. The second component is represented by inputs to the model and also needs no validation. Therefore, model validation discussed in this report focuses on the third component, the conceptual model (e.g., the solubility-controlling mechanism).

Alternative solubility models described in this document are not recommended for the TSPA-LA base-case analyses. Therefore, they have no impact on the estimate of mean annual dose.

7.1 CONFIDENCE BUILDING DURING MODEL DEVELOPMENT TO ESTABLISH SCIENTIFIC BASIS AND ACCURACY FOR INTENDED USE

Sections 2.1 and 2.2 of *Technical Work Plan for Postclosure Waste Form Modeling* (BSC 2005 [DIRS 173246]) specify that each model contains documentation of decisions and activities implemented during the model development process to build confidence and verify a reasonable, credible, technical approach using scientific and engineering principles.

The decisions or activities required for confidence building in all models, regardless of the level of confidence, as specified in LP-SIII.10Q-BSC (Section 5.3.2(b)) and LP-2.29Q-BSC (Attachment 3), are as follows:

1. *Selection of input parameters and/or input data, and a discussion of how the selection process builds confidence in the model* (LP-SIII.10Q-BSC, Section 5.3.2(c)(1); LP-2.29Q-BSC, Attachment 3, Level I (a)).

The selection of the solubility-controlling solid phases, as documented in Section 6, is based on laboratory observations and corroborated by Project-specific laboratory results where feasible and reasonable (Pu, Np, and Am). Other corroborative information includes natural analogue data (U), data published in peer-reviewed literature (U, Th, Pa), and demonstration of conservatism (Pu, Np, U, Am, Pa, Ra). As determined through analyses (Sections 6.14 through 6.18), aqueous concentrations of technetium, carbon, iodine, cesium, and strontium are not controlled by solubility-controlling phases; rather they are controlled by waste form dissolution rates, no solubility models are developed for these elements and, therefore, no validation is required. Lead aqueous concentrations are derived from analysis of values in peer-reviewed literature and professional judgment and no validation is required.

2. *Description of calibration activities, and/or initial boundary condition runs, and/or run convergences, and a discussion of how the activity or activities build confidence in the model. Inclusion of a discussion of impacts of any non-convergence runs. Documentation of activities to ensure that simulation conditions are set up to span the range of intended use and avoid inconsistent outputs* (LP-SIII.10Q-BSC, Section 5.3.2(b)(2); LP-2.29Q-BSC, Attachment 3, Level I (e)).

Discussion of the chemical system (temperature, oxidation potential, pH, fugacity of CO_2, water chemistry, etc) used in model runs is described in Sections 6.3 and 6.4. Dissolved concentrations of elements with radioactive isotopes are discussed in modeling sections (Sections 6.5 through 6.9, 6.11, and 6.12). The solubilities span the range of intended use conditions for each of the factors that influence the dissolved concentrations of important elements with radioactive isotopes (Pu, Np, U, Th, Am, Pa, and Ra) (Sections 6.3 and 6.4). Run nonconvergences are discussed in Section 6.4.

3. *Discussion of the impacts of uncertainties to the model results including how the model results represent the range of possible outcomes consistent with important uncertainties* (LP-SIII.10Q-BSC, Section 5.3.2(b)(3); LP-2.29Q-BSC, Attachment 3, Level 1 (d) and (f)).

The uncertainty associated with the selection of solubility-controlling phases is discussed in Section 6.3.2. Uncertainty in the selection of the solubility-controlling solid for U is discussed in Section 6.7.2. Uncertainties associated with thermodynamic data (log K) are added to model outputs as indicated in Section 8.1 (ε_1 in Equations 8.1 and 8.2) and Table 8-2. Uncertainties associated with fluoride content are added to model outputs as indicated in Section 8.1 (ε_2 in Equations 8.1 and 8.2) and Table 8-2.

4. *Formulation of defensible assumptions and simplifications*. (LP-2.29Q-BSC, Attachment 3, Level I (b)).

Discussions of assumptions and their rationale are provided in Section 5.

5. *Consistency with physical principles, such as conservation of mass, energy, and momentum* (LP-2.29Q-BSC, Attachment 3 Level I (c)).

Section 6 discusses the choice of solubility-controlling phases. All choices are consistent with physical principles.

7.2 CONFIDENCE-BUILDING AFTER MODEL DEVELOPMENT TO SUPPORT THE SCIENTIFIC BASIS OF THE MODEL

Post-model development validation is required by LP-SIII.10Q-BSC. As mentioned in Section 1, Np and Pu require Level II validation. The rest of the solubility models (for U, Th, Am, Pa, and Ra) require Level I validation. For confidence building after model development, Tables 2-1 and 2-3 of *Technical Work Plan for Postclosure Waste Form Modeling* (BSC 2005 [DIRS 173246]) specify the following validation activities and criteria for Pu, Np, U, Th, Am, Pa, and Ra (validation activities (VA) are described in the technical work plan (BSC 2005 [DIRS 173246]):

1. Are the solubility-controlling phases selected in the model consistent with experimental or literature data? (VA 1, VA 3, or both)

2. Are the solubilities calculated in the model consistent with experimental or literature data? (VA 1, VA 3, or both)

3. To increase confidence for elements with little or no experimental data, is the model reasonable and acceptable given the level of validation required (low)? (VA N/A)

Validation metric/criteria for validation activities/criteria 1 through 3 requires that corroborating data match qualitatively or are bounded by model predictions

In addition to the above, the following validation activity and criteria applies to Pu and Np.

4. The solubility model will be validated by an independent technical review, and the review will answer the following questions: (VA 5)

   - Do the treatments of the kinetics and thermodynamic factors adequately capture the behavior of the radionuclides over geologic timeframes?

   - Is the value for Eh implemented in the model consistent with conditions expected in the repository over geologic timeframes?

   - Is the model adequate and appropriate for its intended use?

Validation metric/criteria for validation activities/criteria 4 indicates independent technical review: assessment of the validation activities will be qualitative, and considered successful if deemed defendable by the independent technical reviewer.

The following elements are investigated in the report through analyses and are not models: Pb, Tc, C, I, Cs, and Sr; therefore, validation is not applicable. Additionally, TSPA-LA does not require solubility data for Ac (Section 6.10). Therefore, no model was created in this report negating the need for validation on this element (Section 7.2.7) (BSC 2005 [DIRS 173246], Table 2-3).

In Sections 7.2.2 and 7.2.3, the postdevelopment activities for Pu and Np (Level II) are described. Sections 7.2.4 through 7.2.6 and 7.2.8 through 7.2.9 describe postdevelopment activities for U, Th, Am, Pa, and Ra (Level I). Corroborative data used to validate solubility models are summarized in Table 7-1.

Table 2-1 of *Technical Work Plan for Postclosure Waste Form Modeling* (BSC 2005 [DIRS 173246]) also indicates the following validation activity:

> *Technical review planned in the applicable TWP, by reviewers independent of the development, checking, and review of the model documentation* (LP-SIII.10Q-BSC, Section 5.3.2 (c) (5)).

Section 7.2.1 and Appendix III contain the independent technical review of the Pu and Np models. The validation of the Pu- and Np-solubility models introduces additional challenges due to the new analytical approach of Eh-adjustment that is used in the model. Additionally, these models are important to dose calculations for the TSPA-LA. As a result, the use of an independent technical review by an individual with appropriate expertise was deemed to be the most appropriate method of validation for the Np and Pu solubility limits models and does not apply to the validation of Level I models. The use of an independent technical review as a post model development activity, and the rationale provided above, satisfy a Level II validation for the Pu and Np solubility models.

Additionally, to ensure the look-up tables for actinide solubility provide a fine enough grid to adequately describe the solubility models for Pu, Np, U, Th, and Am (i.e., there are no unexpected "spikes"), several EQ3NR runs were performed between the normal pH and fCO_2 values shown in the look-up tables. Note this activity was not done for Pa since the solubility tables are based on the Np model (see Section 6.11). This activity is not required by *Technical Work Plan for Postclosure Waste Form Modeling* (BSC 2005 [DIRS 173246]); however, it is included to provide additional confidence in the models.

Table 7-1. Corroborative Data Used for Model Validation

Model	Source	Note
Plutonium Solubility	Wilson 1990 [DIRS 100949][a]	Plutonium concentrations measured at spent nuclear fuel corrosion experiments
	Wilson 1990 [DIRS 100793][a]	
	CRWMS M&O 2000 [DIRS 131861][b] and CRWMS M&O 2000 [DIRS 153105][b] for ANL high- and low-drip tests	
Base-Case NpO_2 and Np_2O_5 Solubility	Wilson 1990 [DIRS 100949][a]	Neptunium concentrations measured at spent nuclear fuel corrosion experiments
	Wilson 1990 [DIRS 100793][a]	
	CRWMS M&O 2000 [DIRS 131861][b], CRWMS M&O 2000 [DIRS 153105][b], and Thomas 2004 [DIRS 163048] for ANL high- and low-drip tests	
Uranium Solubility	Pearcy et al. 1994 [DIRS 100486][c]	Natural analogue corroboration of phases used to control U solubility
	Wilson 1990 [DIRS 100949][a]	Uranium concentrations measured at spent nuclear fuel corrosion experiments
	Wilson 1990 [DIRS 100793][a]	
	CRWMS M&O 2000 [DIRS 131861][b], CRWMS M&O 2000 [DIRS 153105][b], and Thomas 2004 [DIRS 163048] for ANL high- and low-drip tests	
Thorium Solubility	Felmy et al. 1991 [DIRS 173044] Rai et al. 2000 [DIRS 173045] Bitea et al. 2003 [DIRS 173041] Neck et al. 2002 [DIRS 168259] Altmaier et al. 2004 [DIRS 173049]	Thorium solubilities
	Bundschuh et al. 2000 [DIRS 173047] Neck and Kim 2001 [DIRS 168258]	Aqueous thorium concentrations
	Felmy et al. 1997 [DIRS 173046] Neck and Kim 2000 [DIRS 173043]	Modeling approach for carbonate species
	Ryan and Rai 1987 [DIRS 173042]	Colloidal effects on measured thorium concentrations
	Altmaier 2005 [DIRS 173048]	Thorium solubility versus carbonate concentration
Americium Solubility	Wilson 1990 [DIRS 100949][a]	Americium concentrations measured at spent nuclear fuel corrosion experiments
	Wilson 1990 [DIRS 100793][a]	
	CRWMS M&O 2000 [DIRS 131861][b] and CRWMS M&O 2000 [DIRS 153105][b] for ANL high- and low-drip tests	
Protactinium Solubility	Berry et al. 1989 [DIRS 144728]	Protactinium solubility
	Berner 2002 [DIRS 162000][d]	
	Martinez-Estaban et al. 2002 [DIRS 172755]	

Table 7-1. Corroborative Data Used for Model Validation (Continued)

Model	Source	Note
Radium Solubility	Martinez-Estaban et al. 2002 [DIRS 172755] Langmuir 1997 [DIRS 100051][e] Kirby and Salutsky 1964 [DIRS 173080][f] Berner and Curti 2002 [DIRS 173083]	Radium solubility as a function of solubility-controlling phases
	Peacey et al. 2002 [DIRS 173073]	Radium concentration in uranium mine tailings
	Laul and Maiti 1990 [DIRS 173072] Evans et al. 1982 [DIRS 173074]	Radium concentrations in natural waters
	Langmuir and Reise 1985 [DIRS 106457]	Control of radium concentrations by coprecipitation and solid solution

NOTES: [a] References were used in Section 6.6 as part of the alternative conceptual model for neptunium incorporation into uranyl phases. It was not used for the base case neptunium solubility models. Additionally, the references were cited in Section 6.7 for mineralization during spent fuel corrosion. The aqueous actinide concentrations from spent fuel dissolution used for Pu, Np, U, and Am validation were not used in the development of these models. Series 2 experiments were carried out at 25°C. Series 3 experiments were carried out at 25°C and 85°C.

[b] References were used in Section 6.6 as part of the alternative conceptual model for neptunium incorporation into uranyl phases. It was not used for the base-case neptunium solubility models. The aqueous actinide concentrations from spent fuel dissolution used for Pu, Np, U, and Am validation were not used in the development of these models. Experiments were carried out at 90°C.

[c] Reference used in Appendix IV in the discussion of neptunium incorporation into uranyl phases. It was not used in the development of the U solubility model, so it is acceptable for use in Section 7 for uranium validation.

[d] Reference used in Section 6.3.3 for discussion of completeness of thermodynamic database for actinide(III) species (Np^{+3}, Pu^{+3}, and Am^{+3}) and actinide(IV) species (Th^{+4}, U^{+4}, Np^{+4}, and Pu^{+4}). It was not used in the development of the protactinium model, so it is acceptable for use in Section 7 for protactinium validation

[e] Reference used for multiple modeling purposes including dissolved oxygen content in Section 6.7.2.1, Np oxidation states in Section 6.6.2, activity coefficient discussion in Section 6.3 and 6.5, carbon solubility in Section 6.15 and secondary U phases in Section 6.6.4.1. It was not used, however, in the development of the radium model, so it is acceptable for use in Section 7 for radium validation.

[f] Reference was used in Section 6.12 in a discussion of radium minerals. However, the choice of solubility controlling phase did not use this reference. Additionally, the solubility data from this reference was not used in the development of the radium model, so it is acceptable for use in Section 7 for radium validation.

7.2.1 Pu and Np Independent Technical Review

A technical review of the solubility models for Pu and Np was conducted. Dr. Gregory Choppin, Department of Chemistry and Biogeochemistry of Florida State University, a recognized expert in the field of actinide and lanthanide geochemistry, was selected to review and report on the models for Np and Pu. Dr. Choppin's independent review was conducted on REV 03 of this document. Since the plutonium model has not changed, Dr. Choppin's review of the Pu model is still valid and carried over to this revision. The results are reported in Appendix III. Since this review was also performed under a different technical work plan, deviations from the most current technical work plan (BSC 2005 [DIRS 173246]) are also outlined in Appendix III. The

reviewer, Dr. Greg Choppin, who was independent of the development and checking of the document, concluded:

> I agree with your answers to my questions and the changes you made in the document. The new paragraph is a very good response to my concerns and should be adequate to inform the readers of the colloid situation in connection with the truly dissolved concentration.

Significant changes to the neptunium-solubility model require this model to undergo a new technical review. The requirements for this review per *Technical Work Plan for Postclosure Waste Form Modeling* (BSC 2005 [DIRS 173246]) are listed in Section 7.2. This review considered the Pu-solubility model, as well as the two Np-solubility models.

Dr. William Downs, who is independent of the development and checking of the document, conducted a technical review of the solubility models for Pu and Np. Dr. Downs is a Ph.D. geochemist with over 30 years of experience in the field of aqueous environmental geochemistry. He has held positions as: 1) senior geochemist on the Uranium Mill Tailings Remedial Action Project, 2) consulting geochemist on the Weldon Spring Remedial Action Project, 3) consulting geochemist on the Paducah Gaseous Diffusion Plant Remediation Project, and 4) consulting geochemist on the Hanford Reservation T-106 Radionuclide Fate and Transport Project. These projects required the geochemical characterization of nuclear wastes and the environment, and numerical simulation of the fate and transport of radionuclides and toxic metals and metalloids. In his review, Dr. Downs found the Pu and Np models to be adequate and appropriate for their intended use (Appendix III).

The independent technical review for the Pu and Np models has deemed them defensible. Therefore, the Pu and Np dissolved concentrations models have been validated by means of a technical review.

7.2.2 Validation of the Plutonium-Solubility Model

The bases for the adjusted-Eh Pu-solubility model are experimental observations consisting of (1) the solubility-controlling phase PuO_2(hyd,aged), (2) solubility measurements, and (3) Eh measurements of natural waters at Yucca Mountain. The selection of the solubility-controlling phase for this model is consistent with laboratory experiments conducted as discussed in Section 6.5.3.1.

Figure 7-1 presents the adjusted-Eh Pu-solubility model for $\log f\mathrm{CO_2} = -3.5$ bars. The solid line represents the mean values of log[Pu]; the dotted and dashed lines represent upper and lower thermodynamic uncertainty ranges at 95 percent confidence interval, respectively. Four sets of experimental data used for model validation are also plotted in Figure 7-1. Most of the data points from these four sets of experiments fall within the uncertainty range of the model. More importantly, no data points fall above the upper bound of the model.

Data sets plotted in Figure 7-1 are plutonium concentrations measured in spent nuclear fuel leaching experiments by Wilson (1990 [DIRS 100949]; 1990 [DIRS 100793]) and ANL high- and low-drip tests (CRWMS M&O 2000 [DIRS 131861]; CRWMS M&O 2000 [DIRS 153105]).

These data sets are not solubility measurements, but are Pu concentrations measured in spent nuclear fuel dissolution experiments. They may be a more-realistic benchmark for Pu released from spent nuclear fuel, as spent nuclear fuel was used in these experiments as the source of Pu. As most of these data fall in the lower half of the uncertainty range suggests the model may be conservative when it is used to predict Pu release from spent nuclear fuel.

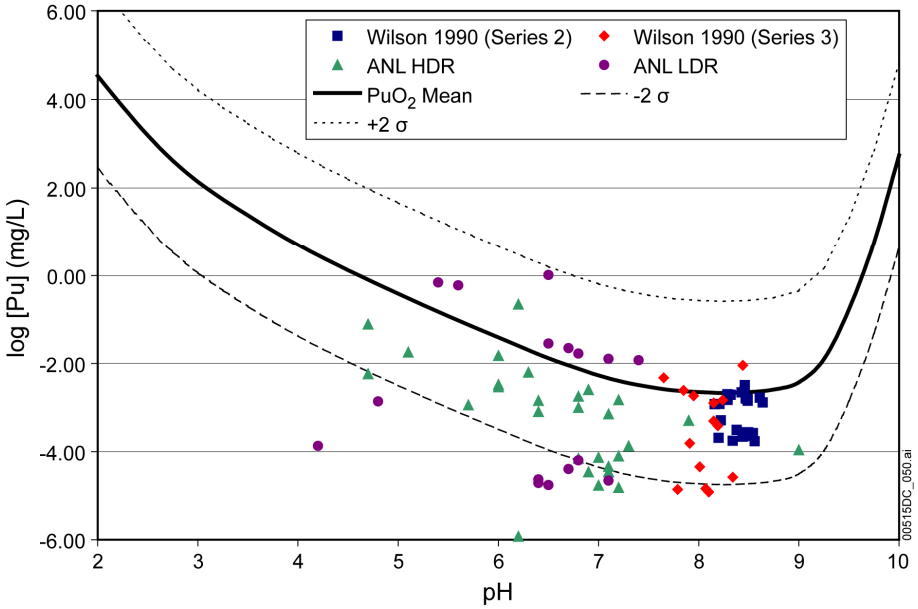

Data Source: Wilson 1990 [DIRS 100949]; Wilson 1990 [DIRS 100793] (Series 2 and Series 3 tests, respectively); CRWMS M&O 2000 [DIRS 131861] and CRWMS M&O 2000 [DIRS 153105] for ANL high-drip (HDR) and low-drip (LDR) tests.

Source: *Wilson-ANL.xls* (Appendix I).

Figure 7-1. Comparison of Experimental Data with the Predictions of Plutonium-Solubility Model at log fCO_2 = -3.5

The favorable comparison between the model results and experimental results, which were not used in the choice of the solubility-controlling phase, strongly indicates that the proposed plutonium-solubility model is representative of literature studies and slightly conservative when compared against the dissolution of commercial spent nuclear fuel and, thus, is valid. The independent technical reviews of the Pu-solubility model (Section 7.2.1 and Appendix III) also indicate the model is adequate and justified for its intended use. Therefore, the required level of confidence (Level II) is obtained.

Additionally, to check that the look-up table for Pu solubility provides a fine enough grid to adequately describe the Pu model (i.e., there are no unexpected "spikes"), several EQ3NR runs were performed between the normal pH and fCO_2 values shown in Table 6.5-1. The results are shown in Table 7-2.

Table 7-2. Check of Effects of the Use of Finer Increments of pH and fCO_2 on Plutonium Look-Up Table

Solubility (mg/L) when pH is changed						
Log fCO_2	**pH = 5.00**	**pH = 5.05**	**pH = 5.10**	**pH = 5.15**	**pH = 5.20**	**pH = 5.25**
-3.00	3.869E-01	3.434E-01	3.049E-01	2.710E-01	2.410E-01	2.162E-01
Solubility (mg/L) when fCO_2 is changed						
pH	**Log fCO_2 = -3.0**	**Log fCO_2 = -3.1**	**Log fCO_2 = -3.2**	**Log fCO_2 = -3.2**	**Log fCO_2 = -3.4**	**Log fCO_2 = -3.5**
5.00	3.869E-01	3.857E-01	3.848E-01	3.841E-01	3.835E-01	3.831E-01

Source: EQ3 files in Appendix I.

Table 7-2 shows that the grid chosen for the Pu look-up table is sufficiently small to adequately describe the model without the worry of the appearance of "spikes". This result is consistent with basic thermodynamic principles. The various pH and CO_2 concentration-dependent solubility curves were developed from the thermodynamic database *Data0.ymp.R2* (DTN: MO0302SPATHDYN.000 [DIRS 161756]). The basic thermodynamic principles exclude the possibility of "solubility spikes" because there is no commensurate thermodynamic data spike. Significant changes in between the defined values on the solubility table could only occur if significant changes in pH, CO_2, Eh, etc. would occur; however, the data is already given as a function of these parameters and, therefore, solubility "spikes" in this report are a thermodynamic impossibility.

Experimental data on individual solubility investigations and the reviews of similar waste disposal reports of other countries also shows this absence of "spikes" in solubility curves for all relevant or evaluated compounds.

Differences in the solubility data have been observed when the controlling solid is in a crystalline versus amorphous form; however, the data is consistent in that only smooth solubility curves are created.

7.2.3 Validation of Neptunium-Solubility Models

The basis for the in-package Np-solubility model is the use of NpO_2 for the solubility-controlling phase under low-pH conditions, and $NaNpO_2CO_3$ for the solubility-controlling phase under high-pH conditions. The basis for the ex-package (invert) Np-solubility model is the use of Np_2O_5 for the solubility-controlling phase under low-pH conditions, and $NaNpO_2CO_3$ for the solubility-controlling phase under high-pH conditions. The selection of these solubility-controlling solids is based on an argument outlined in Appendix IV (for NpO_2) and laboratory observations (for Np_2O_5).

Figure 7-2 presents the NpO_2-solubility model at fCO_2 of $10^{-3.5}$ bars and the Np_2O_5-solubility model at fCO_2 of $10^{-3.5}$ bars. Figure 7-2 also presents measured neptunium concentrations in several spent nuclear fuel corrosion experiments. These experiments were conducted at PNNL (Wilson 1990 [DIRS 100949]; Wilson 1990 [DIRS 100793]) and at ANL (CRWMS M&O 2000 [DIRS 131861]; CRWMS M&O 2000 [DIRS 153105]; Thomas 2004 [DIRS 163048]). This comparison shows that the neptunium-solubility models developed in this report are conservative and, thus, are adequate for TSPA-LA use. The fact that

the measured neptunium concentrations in spent nuclear fuel corrosion experiments are four to six orders of magnitude lower than the modeled pure neptunium phase solubility indicates that neptunium may be controlled by different mechanism(s) than by pure-phase solubility (Section 6.6).

Data sets plotted in Figure 7-2 are neptunium concentrations measured in spent nuclear fuel leaching experiments by Wilson (1990 [DIRS 100949]; 1990 [DIRS 100793] and ANL high-drip and low-drip tests (CRWMS M&O 2000 [DIRS 131861]; CRWMS M&O 2000 [DIRS 153105]; Thomas 2004 [DIRS 163048]). These data sets are not solubility measurements, but are Np concentrations measured in spent nuclear fuel dissolution experiments. They may be a more-realistic benchmark for Np released from spent nuclear fuel, as spent nuclear fuel was used in these experiments as the source of Np. The fact that all data fall in the lower half of the uncertainty range suggests the model is conservative when it is used to predict Np release from spent nuclear fuel.

In summary, comparison between the model results and experimental results, which were not used in the choice of the solubility-controlling phase, strongly indicates that the proposed neptunium-solubility models are conservative when compared against the dissolution of commercial spent nuclear fuel and, thus, are valid. The independent technical review of the Np-solubility model (Section 7.2.1 and Appendix III) also indicates that the models are adequate and justified for their intended use. Therefore, the required level of confidence (Level II) is obtained.

To ensure the look-up table for Np solubility provides a fine enough grid to adequately describe the Np model (i.e., there are no unexpected "spikes"), several EQ3NR runs were performed between the normal pH and fCO_2 values shown in Tables 6.6-3 and 6.6-9. The results are shown in Tables 7-3 and 7-4.

Tables 7-3 and 7-4 show that the grid chosen for the Np look-up tables is sufficiently small to adequately describe the models without the worry of the appearance of "spikes." This result is consistent with basic thermodynamic principles as discussed in Section 7.2.2.

Table 7-3. Check of Effects of the Use of Finer Increments of pH and fCO_2 on the In-Package Neptunium Look-Up Table

Solubility (mg/L) when pH is changed						
Log fCO_2	**pH = 5.00**	**pH = 5.05**	**pH = 5.10**	**pH = 5.15**	**pH = 5.20**	**pH = 5.25**
-3.00	1.107E+01	9.863E+00	8.789E+00	7.832E+00	6.980E+00	6.220E+00
Solubility (mg/L) when fCO_2 is changed						
pH	**Log fCO_2 = -3.0**	**Log fCO_2 = -3.1**	**Log fCO_2 = -3.2**	**Log fCO_2 = -3.3**	**Log fCO_2 = -3.4**	**Log fCO_2 = -3.5**
5.00	1.107E+01	1.107E+01	1.107E+01	1.107E+01	1.107E+01	1.107E+01

Source: EQ3 files in Appendix I.

Table 7-4. Check of Effects of the Use of Finer Increments of pH and fCO_2 on the Ex-Package Neptunium Look-Up Table

Solubility (mg/L) When pH is Changed						
Log fCO_2	**pH = 5.00**	**pH = 5.05**	**pH = 5.10**	**pH = 5.15**	**pH = 5.20**	**pH = 5.25**
-3.00	1.84E+02	1.63E+02	1.46E+02	1.30E+02	1.15E+02	1.03E+02
Solubility (mg/L) When fCO_2 is Changed						
pH	**Log fCO_2 = -3.0**	**Log fCO_2 = -3.1**	**Log fCO_2 = -3.2**	**Log fCO_2 = -3.3**	**Log fCO_2 = -3.4**	**Log fCO_2 = -3.5**
5.00	1.84E+02	1.84E+02	1.84E+02	1.84E+02	1.84E+02	1.84E+02

Source: EQ3 files in Appendix I.

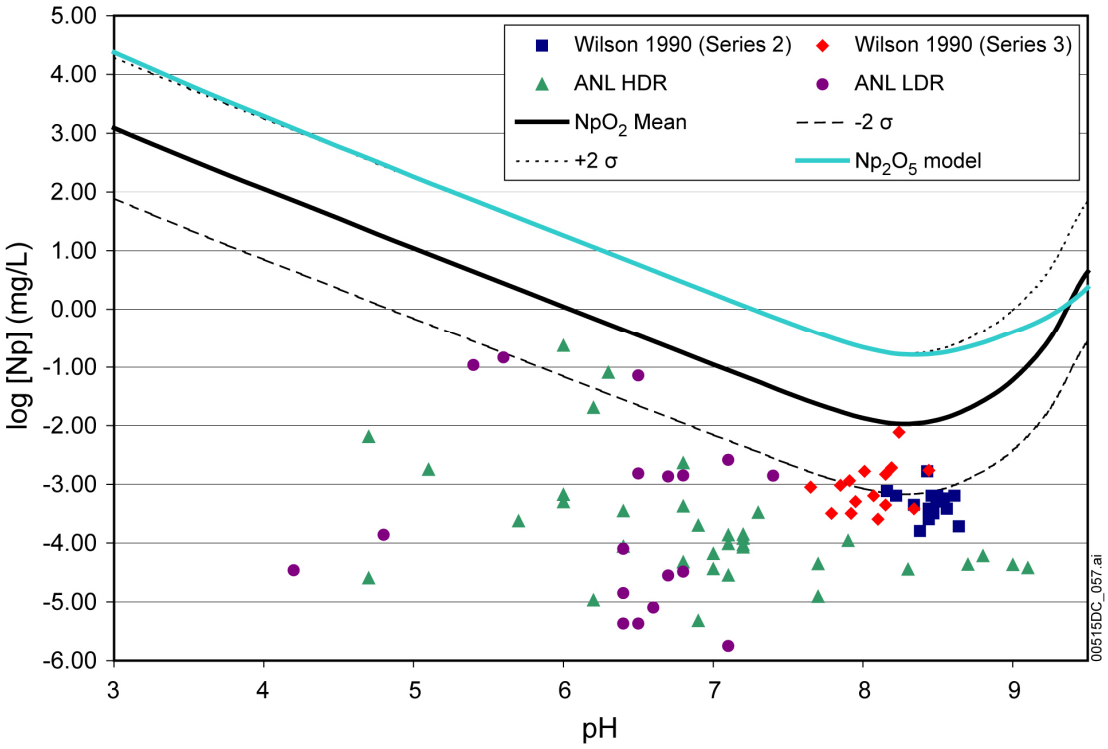

Data Source: Wilson 1990 [DIRS 100949]; Wilson 1990 [DIRS 100793] (Series 2 and Series 3 tests, respectively); and CRWMS M&O 2000 [DIRS 131861]; CRWMS M&O 2000 [DIRS 153105]; and Thomas 2004 [DIRS 163048] for ANL high-drip and low-drip tests.

Source: *Wilson-ANL.xls* (Appendix I).

NOTE: In-package (NpO_2) and Ex-package (Np_2O_5) models are shown here. For discussion of models, see Section 6.6 and Appendix IV. The NpO_2 model and Np_2O_5 models include $NaNpO_2CO_3$ at high-pH values (see Sections 6.6.3.2 and 6.6.3.3).

Figure 7-2. Comparison of Neptunium-Solubility Models at log fCO_2 = -3.5 with PNNL and ANL Measurements

7.2.4 Validation of Uranium-Solubility Model

The uranium-solubility model is based on three U-bearing solubility-controlling phases. These are schoepite ($UO_3 \cdot 2H_2O$), the controlling mineral at low to moderate pH and fCO_2 values;

Na-boltwoodite ($NaUO_2SiO_3OH \cdot 1.5H_2O$), the controlling solid at moderate to high pH and fCO_2 values; and the solid $Na_4UO_2(CO_3)_3$, the controlling solid at high pH and fCO_2 values. The solubility calculations are carried out for a range of pH and fCO_2 values in water the composition of J-13 well water, modified by the addition of Na^+ or SO_4, as required for solution electroneutrality, and with dissolved silica fixed by saturation with the silica phase chalcedony. The selection of these U-controlling phases and the silica-controlling phase is validated in this section with evidence from a natural analogue. Further, the calculated solubilities are corroborated by comparing them with U concentrations measured during fuel degradation experiments.

The selection of the solids used to model U concentrations is based on laboratory studies (Section 6.7.2). The data presented by Pearcy et al. (1994 [DIRS 100486]) are used to corroborate the model. Pearcy et al. (1994 [DIRS 100486]) describe a natural analogue study of uraninite alteration in the Nopal I deposit at Peña Blanca, Mexico (an environment similar in most respects to that of Yucca Mountain). The principal silicate alteration product is uranophane. Weeksite and boltwoodite are also found, but they occur further from the uraninite deposit and tend to form over earlier-formed phases. Pearcy et al. (1994 [DIRS 100486], p. 726) conclude, "the specific uranyl silicate formed in a given area depended on the local geochemical conditions rather than on the broad evolution of the oxidizing system." The paragenesis of alteration products in the natural analogue study is entirely consistent with that of the laboratory study. The differences that are evident are related to the chemistry of the alteration water in the two situations. Table 7-5 lists the U-bearing alteration phases observed in both studies.

Table 7-5. Comparison of Phases Observed in Natural UO_2 Alteration in a Geologic Environment Similar to Yucca Mountain

Mineral	Principal Natural Analogue Phases and Composition (Pearcy et al. 1994 [DIRS 100486])	Composition of Phases for Available Thermodynamic Data (*Data0.ymp.R2*)
Uranyl-Oxide Hydrates		
Ianthinite	$U^{+4}(U^{+6}O_2)_5(OH)_{14} \cdot 3H_2O$	
Schoepite	$UO_3 \cdot 2H_2O$	$UO_3 \cdot 2H_2O$
Uranyl Silicate Hydrate		
Soddyite	$(UO_2)_2SiO_4 \cdot 2H_2O$	$(UO_2)_2SiO_4 \cdot 2H_2O$
Alkali and Alkaline Earth Uranyl Silicate Hydrates		
Uranophane	$Ca(UO_2)_2Si_2O_7 \cdot 6H_2O$	$Ca(UO_2SiO_3OH)_2 \cdot 5H_2O$
Boltwoodite	$HK(UO_2)SiO_4 \cdot 1.5H_2O$	Na equivalent in database ($NaUO_2SiO_3OH \cdot 1.5H_2O$)

NOTE: Phases observed in natural UO_2 alteration in a geologic environment closely similar to Yucca Mountain (Pearcy et al. 1994 [DIRS 100486]). Corresponding phases for which thermodynamic data are available in modeling database, *Data0.ymp.R2* (DTN: MO0302SPATHDYN.000 [DIRS 161756]) are also shown. Database (*Data0.ymp.R2*) comparison is for information purposes only and not used for validation.

Figure 7-3 shows the uranium solubility calculated at log fCO_2 = -3.5. This figure also presents measured uranium concentrations in several spent nuclear fuel corrosion experiments. These experiments were conducted at PNNL and ANL using artificial J-13 water exposed to the atmosphere (Wilson 1990 [DIRS 100949] and Wilson 1990 [DIRS 100793], for Series 2 and

Series 3 tests, respectively; CRWMS M&O 2000 [DIRS 131861]; CRWMS M&O 2000 [DIRS 153105]; Thomas 2004 [DIRS 163048] for ANL high-drip and low-drip tests; *Wilson-U Validation.xls* in Appendix I). Most of the measured values (with the exception of 1 point) fit within or are below the uncertainty bands for calculated uranium solubilities using schoepite and Na-boltwoodite as the solubility-controlling phases. This corroborates the realism of the calculated concentrations.

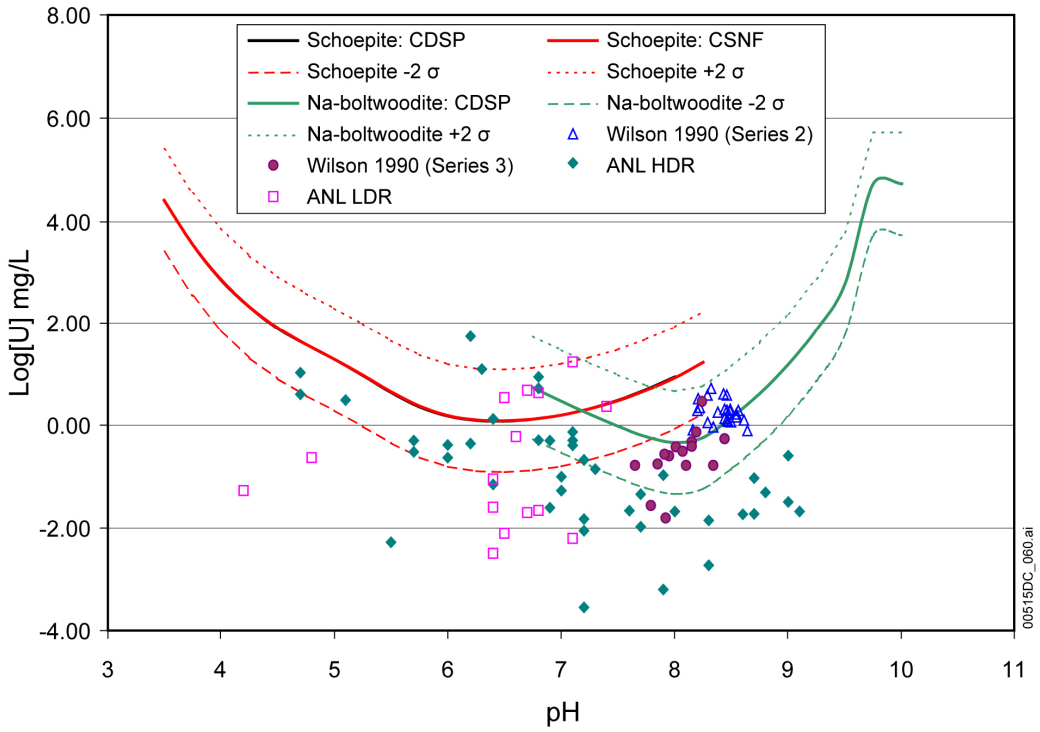

Data Source: Calculated solubility curves from Tables 7.6-3 (Schoepite CSNF), 6.7-5 (Schoepite CDSP), and 6.7-6 (Na-boltwodite CDSP). Experimental data is from Wilson 1990 [DIRS 100949]; Wilson 1990 [DIRS 100793] (Series 2 and Series 3 tests, respectively); and CRWMS M&O 2000 [DIRS 131861], CRWMS M&O 2000 [DIRS 153105], and Thomas 2004 [DIRS 163048] for ANL high-drip and low-drip tests.

Source: *Wilson-U Validation.xls Sheet: U Validation Plot* (Appendix I).

Figure 7-3. Comparison of Uranium-Solubility Model at log fCO_2 = -3.5 with PNNL Measurements

In summary, the choice of U-controlling phases is corroborated by comparison with phases reported in the reviewed literature from a natural analogue site to Yucca Mountain. Additionally, postdevelopment model validation shows uranium-solubility model results are corroborated by Project-specific experimental data, and that the model is conservative and adequate for TSPA-LA use.

To ensure the look-up table for uranium solubility provides a fine enough grid to adequately describe the uranium model (i.e., there are no unexpected "spikes"), several EQ3NR runs were performed between the normal pH and fCO_2 values shown in Tables 6.7-3 and 6.7-6. The results are shown in Tables 7-6 and 7-7.

Tables 7-6 and 7-7 show that the grid chosen for the uranium look-up tables is sufficiently small to adequately describe the model without the worry of the appearance of "spikes." This result is consistent with basic thermodynamic principles as discussed in Section 7.2.2.

Table 7-6. Check of Effects of the Use of Finer Increments of pH and fCO_2 on the Uranium Look-Up Table for CSNF Waste Packages (Schoepite)

Solubility (mg/L) When pH is Changed						
Log fCO_2	**pH = 5.00**	**pH = 5.05**	**pH = 5.10**	**pH = 5.15**	**pH = 5.20**	**pH = 5.25**
-3.00	2.02E+01	1.76E+01	1.53E+01	1.33E+01	1.15E+01	9.89E+00
Solubility (mg/L) When fCO_2 is Changed						
pH	**Log fCO_2 = -3.0**	**Log fCO_2 = -3.1**	**Log fCO_2 = -3.2**	**Log fCO_2 = -3.3**	**Log fCO_2 = -3.4**	**Log fCO_2 = -3.5**
5.00	2.02E+01	2.02E+01	2.02E+01	2.02E+01	2.02E+01	2.02E+01

Source: EQ3 files in Appendix I.

Table 7-7. Check of Effects of the Use of Finer Increments of pH and fCO_2 on the Uranium Look-Up Table for Codisposal Waste Packages (Boltwoodite-Na)

Solubility (mg/L) When pH is Changed						
Log fCO_2	**pH = 7.00**	**pH = 7.05**	**pH = 7.10**	**pH = 7.15**	**pH = 7.20**	**pH = 7.25**
-3.00	6.62E+00	5.92E+00	5.31E+00	4.77E+00	4.29E+00	3.87E+00
Solubility (mg/L) When fCO_2 is Changed						
pH	**Log fCO_2 = -3.0**	**Log fCO_2 = -3.1**	**Log fCO_2 = -3.2**	**Log fCO_2 = -3.3**	**Log fCO_2 = -3.4**	**Log fCO_2 = -3.5**
7.00	6.62E+00	5.52E+00	4.66E+00	3.97E+00	3.44E+00	3.01E+00

Source: EQ3 files in Appendix I.

7.2.5 Validation of Thorium-Solubility Model

The basis of the thorium model is the use of ThO_2(am) as the solubility-controlling phase, as described in Section 6.8. This is based on several considerations, including the fact that ThO_2(am) is generally more soluble than thorianite (ThO_2). The choice of ThO_2(am) is corroborated by the observation that use of ThO_2(am) in solubility calculations leads to dissolved thorium concentrations similar to those commonly measured in solubility studies .

Recent Th-solubility studies using laser-induced breakdown detection of thorium colloid formation indicates earlier solubility studies may not have adequately removed Th colloids by filtration or centrifugation (Bundschuh et al. 2000 [DIRS 173047]; Neck et al. 2002 [DIRS 168259]; Bitea et al. 2003 [DIRS 173041]). This would lead to an overestimation of ThO_2 or ThO_2(am) solubility, since the large surface area of colloidal particles increases their solubility over that of a crystalline or amorphous solid phase. This may be especially true of studies for which ThO_2(am) was synthesized, washed with water, and then used as a suspension without drying (Ryan and Rai 1987 [DIRS 173042]; Felmy et al. 1991 [DIRS 173044]; Rai et al. 2000 [DIRS 173045]). Figure 7-4 compares the Th-solubility model with data from several ThO_2(am)-solubility studies. Table 7-8 lists the experimental conditions for these studies.

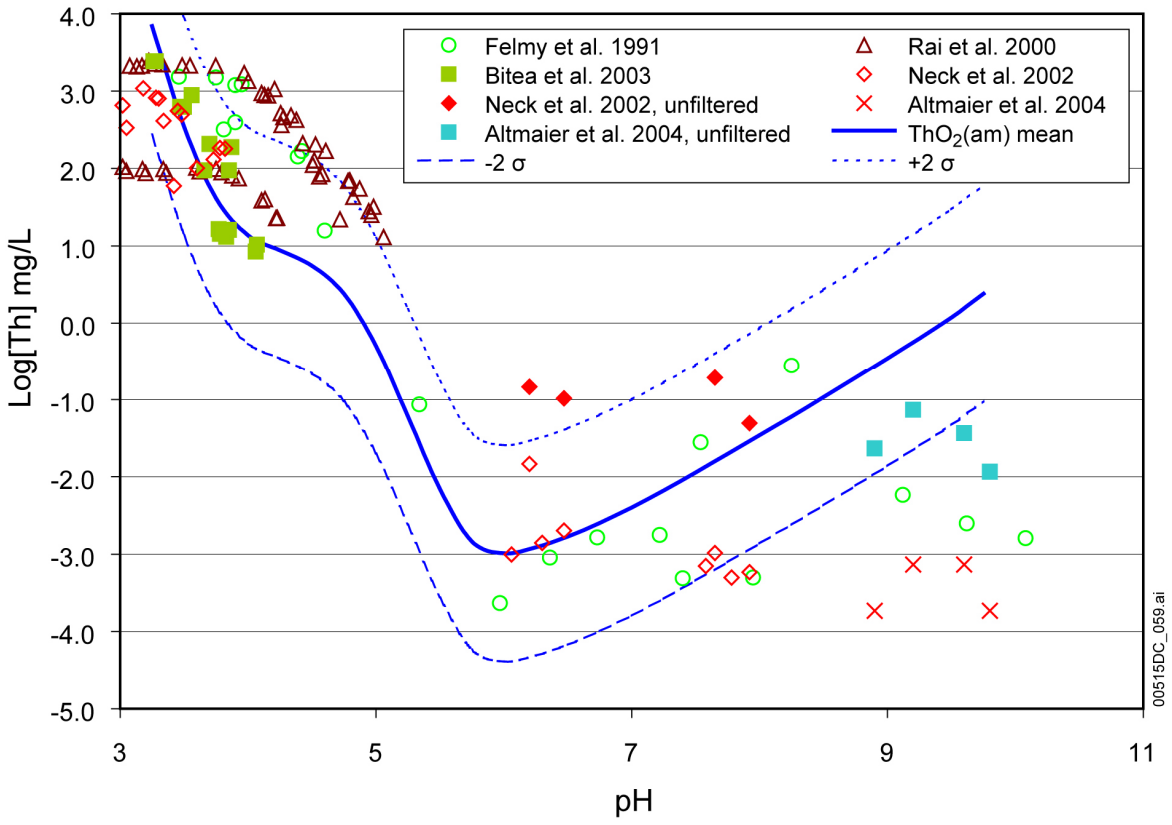

Data Source: Felmy et al. 1991 [DIRS 173044]; Rai et al. 2000 [DIRS 173045]; Bitea et al. 2003 [DIRS 173041]; Neck et al. 2002 [DIRS 168259]; and Altmaier et al. 2004 [DIRS 173049] for Th-solubility data.

Source: *Th solubilty2.xls* (Appendix I).

Figure 7-4. Comparison of Experimental Data with the Predictions of Th-Solubility Model at log fCO_2 = -3.5

Table 7-8. Experimental Conditions for Solubility Data in Figure 7-4

Data Source	Experimental Conditions
Felmy et al. 1991 [DIRS 173044]	0.6 M NaCl or KCl, argon atmosphere (CO_2-free), 7 to 98 days, 1.8-nm pore-size membrane filter
Rai et al. 2000 [DIRS 173045]	0.1 M NaCl, 23+/-2°C, 5 to 22 days, centrifuged 5,000 rpm 10 to 15 minutes
Bitea et al. 2003 [DIRS 173041]	0.5 M NaCl, 22+/-2°C, up to 400 days, 1.2-nm pore-size ultrafiltration
Neck et al. 2002 [DIRS 168259]	0.5 M NaCl, 25°C, 71 to 112 days, argon atmosphere (CO_2-free), 1.4-nm pore-size ultrafiltration for acid samples, ultracentrifugation at 60,000 rpm for 60 minutes for neutral to alkaline samples
Altmaier et al. 2004 [DIRS 173049]	0.5 M NaCl or 0.25 M $MgCl_2$, 22+/-2°C, 15 to 373 days, CO_2-free, ultracentrifugation at 60,000 rpm for 60 minutes

Figure 7-4 indicates the model underestimates or matches the thorium-solubility values from experiments by Felmy et al. (1991 [DIRS 173044]) and Rai et al. (2000 [DIRS 173045]), which

may have been reporting the solubility of a mixture of ThO_2(am) and colloids. The model also matches data from unfiltered solubility samples from experiments by Neck et al. (2002 [DIRS 168259]) and Altmaier et al. (2004 [DIRS 173049]), which contained colloids. The model matches quite closely the data collected by Bitea et al. (2003 [DIRS 173041]). As Table 7-8 shows, the solubility data in Figure 7-4 were collected under CO_2-free conditions or were conducted at acid pH where carbonate formation from CO_2(g) is insignificant. As the model is calculating thorium solubility as a function of fCO_2, it would be expected to overestimate the thorium solubility data from these experiments at high pH. This is illustrated by the model overestimation of the data presented by Felmy et al. (1991 [DIRS 173044]), Neck et al. (2002 [DIRS 168259]), and Altmaier et al. (2004 [DIRS 173049]) above pH 7.

The minimum thorium concentration modeled is 6.36×10^{-4} mg/L (2.7×10^{-9} mol/L) at a fCO_2 of 10^{-5} bars and a pH of 6.25. At this pH and low fCO_2 the impact of Thorium–F^-, SO_4^{2-}, and CO_3^{2-} complexes is minimal and the hydroxyl complex $Th(OH)_4$(aq) dominates. This solubility should, therefore, represent the experimental solubility of thorium dioxide in pure water at moderate-to-high pH values. Neck and Kim (2001 [DIRS 168258]) used the results of a number of aqueous thorium solubility studies to calculate thorium solubility in pure water. They calculated that at pH values above 6, the log[Th] is −8.5±0.6 mol/L (Neck and Kim 2001 [DIRS 168258], Section 3.1). The minimum thorium concentration modeled in this report is 6.36×10^{-4} mg/L (2.7×10^{-9} mol/L). This is equal to log[Th] = −8.6 mol/L, close to the value of Neck and Kim (2001 [DIRS 168258], Section 3.1]) and well within the uncertainty of the measured values.

In summary, it is demonstrated that the thorium-solubility model is corroborated by data published in the peer-reviewed literature.

The thermodynamic data for ThO_2(am) in *Data0.ymp.R2* (used to model thorium solubility) are based on solubility studies by Östhols et al. (1994 [DIRS 150834]) (see Section 6.8). Neck et al. (2002 [DIRS 168259]) found the data reported by Östhols et al. (1994 [DIRS 150834]) was similar to their solubility data for ThO_2(am) determined using laser-induced breakdown detection. They hypothesized that this may be related to air drying of the ThO_2(am) used in the solubility studies by Östhols et al. (1994 [DIRS 150834]) and formation of fewer Th colloids due to low Th concentrations used in their study.

In the high fCO_2 and pH region, increasing CO_3^{2-} concentrations favor the formation of complexes such as $Th(CO_3)_5^{6-}$ and $Th(OH)_3CO_3^-$. This is evident in the sharp increases in the thorium concentrations in the highest pH point of each fCO_2 line in Figure 7-3. Where $Th(CO_3)_5^{6-}$ dominates, the total Th concentration increases by 10^5 for each unit increase in pH. The extreme nonlinearity of the variation of total Th with pH, where this complex dominates, is why the EQ3NR program does not converge in the high pH–high fCO_2 range. As shown in Figure 6.8-4, the thorium-solubility model was not able to match all of the Th-solubility data from Östhols et al. (1994 [DIRS 150834]) in 0.1 molar total carbonate.

Thorium solubility does increase with increasing carbonate concentration. Altmaier et al. (2005 [DIRS 173048]) measured the solubility of ThO_2(am) in solutions with an ionic strength of 0.5 molar (Na_2CO_3-$NaHCO_3$-NaCl or Na_2CO_3-NaOH-NaCl). They found that increasing the total carbonate concentration from 0 to 0.1 molar increased the Th solubilities measured at pH values from 8 to 10 up to 5 orders of magnitude (Altmaier et al. 2005 [DIRS 173048], Figure 2) and that $Th(CO_3)_5^{6-}$ is expected to dominate in concentrated carbonate solutions at pH values

from 7 to 10 (Altmaier et al. 2005 [DIRS 173048]). Felmy et al. (1997 [DIRS 173046]) have confirmed the presence of $Th(CO_3)_5^{6-}$ in concentrated bicarbonate and carbonate solutions with extended X-ray absorption fine structure (EXAFS) spectroscopy.

The accurate thermodynamic modeling of actinide carbonate complexes, especially highly charged species like $Th(CO_3)_5^{6-}$, is difficult. The methods used to determine the activity coefficients for calculating thermodynamic equilibrium constants may lead to different values. Felmy et al. (1997 [DIRS 173046]) used a Pitzer approach to modeling Th solubility and were able to reproduce the data of Östhols et al. (1994 [DIRS 150834]). However, very large ion interaction parameters and large mixing terms were required to model $Th(CO_3)_5^{6-}$. Neck and Kim (2000 [DIRS 173043]) have proposed an approach based on electrostatic interaction to model highly charged actinide carbonate complexes. More recently, Altmaier et al. (2005 [DIRS 173048]) used specific ion interaction theory (SIT) to evaluate formation constants for ternary thorium hydroxide-carbonate complexes. Their approach determined, for modeling experimental data at I = 0.5 molar, that $Th(OH)(CO_3)_4^{5-}$ and $Th(OH)_2(CO_3)_2^{2-}$ may be important and several other ternary complexes also make contributions to Th solubility besides $Th(CO_3)_5^{6-}$ and $Th(OH)_3CO_3^-$. Altmaier et al. (2005 [DIRS 173048]) also were able to successfully model the data of Östhols et al. (1994 [DIRS 150834]) by using this approach. However, there is no spectroscopic data available to confirm the existence of the ternary complexes included in the model by Altmaier et al. (2005 [DIRS 173048]).

Although EQ3NR can use a Pitzer approach to modeling solubility, no qualified EQ3/6 Pitzer database that includes data for actinides yet exists and inclusion of SIT parameters in an EQ3/6 database has not been done to date. Since these other modeling methods are not available at this time, our modeling of thorium solubility in high pH-high fCO_2/carbonate solutions is limited as mentioned.

To ensure the look-up table for thorium solubility provides a fine enough grid to adequately describe the thorium model (i.e., there are no unexpected "spikes"), several EQ3NR runs were performed between the normal pH and fCO_2 values shown in Table 6.8-2. The results are shown in Table 7-9.

Table 7-9 shows that the grid chosen for the thorium look-up tables is sufficiently small to adequately describe the model without the worry of the appearance of "spikes." This result is consistent with basic thermodynamic principles as discussed in Section 7.2.2.

Table 7-9. Check of Effects of the Use of Finer Increments of pH and fCO_2 on the Thorium Look-Up Table.

Solubility (mg/L) When pH is Changed						
Log fCO_2	**pH = 5.00**	**pH = 5.05**	**pH = 5.10**	**pH = 5.15**	**pH = 5.20**	**pH = 5.25**
-3.00	5.07E-01	3.41E-01	2.25E-01	1.47E-01	9.47E-02	6.10E-02
Solubility (mg/L) When fCO_2 is Changed						
pH	**Log fCO_2 = -3.0**	**Log fCO_2 = -3.1**	**Log fCO_2 = -3.2**	**Log fCO_2 = -3.3**	**Log fCO_2 = -3.4**	**Log fCO_2 = -3.5**
5.00	5.07E-01	5.07E-01	5.07E-01	5.07E-01	5.07E-01	5.07E-01

Source: EQ3 files in Appendix I.

7.2.6 Validation of Americium-Solubility Model

The basis for the americium-solubility model is the solubility-controlling phase $AmOHCO_3$.

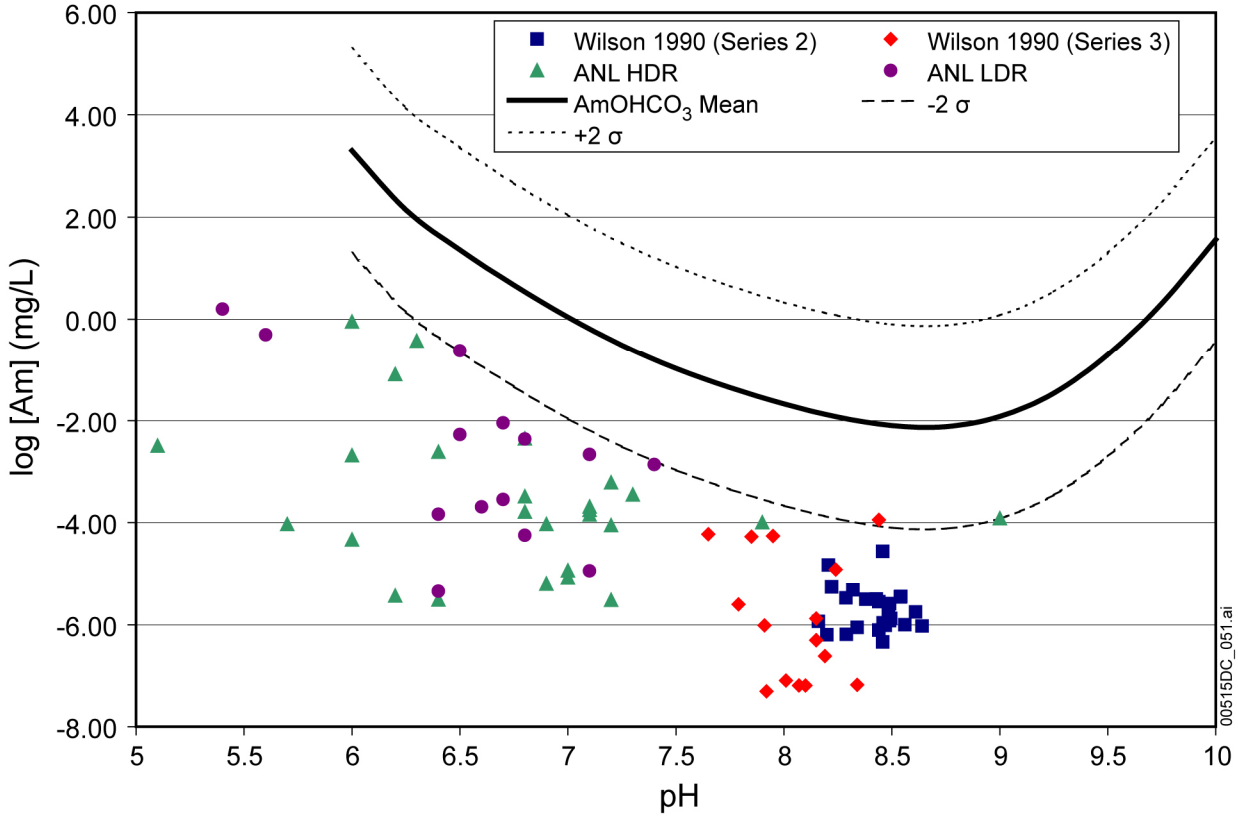

Data Source: Wilson 1990 [DIRS 100949]; Wilson 1990 [DIRS 100793] (Series 2 and Series 3, respectively); and CRWMS M&O 2000 [DIRS 131861] and CRWMS M&O 2000 [DIRS 153105] for ANL high-drip and low-drip tests.

Source: *Wilson-ANL.xls* (Appendix I).

Figure 7-5. Comparison of Americium-Solubility Model at log fCO_2 = -3.5 with PNNL and ANL Measurements

Data sets plotted in Figure 7-5 are americium concentrations measured in spent nuclear fuel leaching experiments by Wilson (1990 [DIRS 100949]; 1990 [DIRS 100793) and ANL high-drip and low-drip tests (CRWMS M&O 2000 [DIRS 131861]; CRWMS M&O 2000 [DIRS 153105]). These data sets are not solubility measurements, but are americium concentrations measured in spent nuclear fuel dissolution experiments. They may be a more-realistic benchmark for americium released from spent nuclear fuel, as spent nuclear fuel was used in these experiments as the source of americium. The fact that all data fall below the lowest half of the uncertainty range suggests the model is conservative when used to predict americium release from spent nuclear fuel.

In summary, postdevelopment model validation shows americium-solubility models results are corroborated by Project-specific experimental data, and the model is conservative and adequate for TSPA-LA use.

To ensure the look-up table for americium solubility provides a fine enough grid to adequately describe the americium model (i.e., there are no unexpected "spikes"), several EQ3NR runs were performed between the normal pH and fCO_2 values shown in Table 6.9-2. The results are shown in Table 7-10.

Table 7-10 shows that the grid chosen for the americium look-up tables is sufficiently small to adequately describe the model without the worry of the appearance of "spikes." This result is consistent with basic thermodynamic principles as discussed in Section 7.2.2.

Table 7-10. Check of Effects of the Use of Finer Increments of pH and fCO_2 on the Americium Look-Up Table.

Solubility (mg/L) When pH is Changed						
Log fCO_2	**pH = 6.00**	**pH = 6.05**	**pH = 6.10**	**pH = 6.15**	**pH = 6.20**	**pH = 6.25**
-3.00	2.72E+02	1.75E+02	1.16E+02	7.93E+01	5.48E+01	3.84E+01
Solubility (mg/L) When fCO_2 is Changed						
pH	**Log fCO_2 = -3.0**	**Log fCO_2 = -3.1**	**Log fCO_2 = -3.2**	**Log fCO_2 = -3.3**	**Log fCO_2 = -3.4**	**Log fCO_2 = -3.5**
6.00	2.72E+02	3.77E+02	5.37E+02	7.92E+02	1.22E+03	2.00E+03

Source: EQ3 files in Appendix I.

7.2.7 Validation of Actinium-Solubility Model

As indicated in Section 6.10, TSPA-LA calculations do not use actinium in transport models so its solubility is not modeled in this report. Therefore, no validation was conducted.

7.2.8 Validation of Protactinium-Solubility Model

Since there are no thermodynamic data for protactinium in the database (*Data0.ymp.R2*), protactinium is treated as an analogue of neptunium (as discussed in Section 6.11). Experimental data indicate Pa(V) solubility should be less than that of Np(V) (Section 6.11). In the protactinium-solubility model, protactinium (Pa_2O_5) solubility is set equal to the solubility of Np_2O_5, which is conservative according to the cited experimental data.

Berner (2002 [DIRS 162000], Section 4.7) discusses protactinium in terms of Pa_2O_5 as the solubility-limiting solid and $PaO(OH)_3(aq)$ as the dominant complex in solution. Berner (2002 [DIRS 162000]) notes a "sensible" estimate could be on the order of 10^{-8} mol/L (corresponding to roughly 3×10^{-3} mg/L). Table 6.11-2 lists protactinium solubilities (based on Np_2O_5 analogue) for a range of pH and fCO_2 conditions; every calculated value is higher than Berner's (2002 [DIRS 162000]) estimate, supporting the conservative calculated values.

Berry et al. (1989 [DIRS 144728]) describe experiments on protactinium behavior in solutions of several types at a range of pH values. The protactinium behavior is dominated by sorption, but the authors were able to develop a solubility limit of 10^{-10} mol/L (2.3×10^{-5} mg/L) at high pH values in waters typical of those emanating from cements. This is two orders of magnitude lower than the lowest solubility calculated for thorium(IV) (Figure 6.8-1) and four orders of magnitude lower than the lowest neptunium(V) solubility (Figure 6.6-2). Although the experiments were carried out for reducing aqueous conditions, the oxidation state of the protactinium was unaffected. The relative solubilities of protactinium and neptunium corroborate the basis of the protactinium-solubility model (i.e., Pa_2O_5 solubility is lower than the solubility of Np_2O_5, and setting Pa_2O_5 solubility equal to Np_2O_5 solubility is, therefore, conservative).

When using Pa_2O_5 as the solubility-controlling phase for Pa, Martinez-Esteban et al. (2002 [DIRS 172755]) report Pa concentrations of 2E-08 mol/L (approximately 4.6E-04 mg/L). This value is also much lower than the modeled concentrations given for Pa, indicating that the Pa model is conservative.

As shown in Section 7.2.3, the grid chosen for the neptunium solubility look-up table is sufficiently small to adequately describe the model without the worry of the appearance of "spikes." This result is consistent with basic thermodynamic principles as discussed in Section 7.2.2. Therefore, since the protactinium model is based on neptunium (through analogy), the model is considered adequate.

7.2.9 Validation of Radium-Solubility Model

The radium-solubility model uses a single solubility-controlling phase ($RaSO_4$) to model the dissolved concentrations of radium in the waste package and invert. However, radium is known to be readily incorporated into various sulfate minerals and it is more probable that radium concentrations will be limited by coprecipitation or solid solution with sulfate minerals (such as $SrCO_4$, $BaSO_4$, and $CaSO_4$) (Langmuir and Riese 1985 [DIRS 106457]; Langmuir 1997 [DIRS 100051]; Berner and Curti 2002 [DIRS 173083]). The solubility of $RaSO_4$ from several different sources as well as dissolved concentrations taking into account coprecipitation and solid solution are listed below (Table 7-11) and compared to this report's modeled radium concentrations. Table 7-11 shows good comparison among models that use $RaSO_4$ as the solubility-controlling phase. Additionally, the table also shows that the use of $RaSO_4$ as the sole solubility-controlling phase is conservative as solubility controlled by coprecipitation and solid solution are much lower.

Table 7-11. Comparison of Dissolved Concentrations Derived from Several Different Modeling Techniques

Reference		Controlling Phase	Modeled Solubility (in reference)	Solubility (mg/L)
This report	pH range 3.0 to 7.75	$RaSO_4$	2.0E-2 mg/L	2.0E-2 mg/L
	pH range 7.75 to 9.75		1.2 mg/L	1.2 mg/L
	pH > 9.75		500 (not controlled by solubility)	500 (not controlled by solubility)
Martinez-Esteban et al. 2002 [DIRS 172755]		$RaSO_4$	On the order of 1E-4 to 1E-6 mol/L	0.226 to 22.6 mg/L
		Coprecipitation Model	1E-14 mol/L (but conservatively use the concentration common in groundwater – approx 1E-12)	2.26E-07 mg/L (conservative high)
Langmuir 1997 [DIRS 100051]		Coprecipitation with Ca model	(assumed range) 10^{-9} to 10^{-5} M	2.26 to 2.26E-04 mg/L
			Probable 10^{-7} M	2.26E-02 mg/L
Kirby and Salutsky 1964 [DIRS 173080]		$RaSO_4$	2.1E-4 g/100mL	2.14E-02
Berner and Curti 2002 [DIRS 173083]		$RaSO_4$	4.8E-8 mol/L	1.08E-02
		Solid solution (Ra-Ba-Sr-Ca-SO_4)	8.6E-12 mol/kg	1.94E-06

NOTE: All conversions to mg/L were performed in *Ra waters.xls* in Appendix I.

Field studies have shown radium concentrations in natural waters are orders of magnitude below levels corresponding to $RaSO_4$ saturation (Table 7-12). Additionally, an analogue of water associated with uranium mine tailings shows, although above the concentrations found in natural waters, the radium being leached from the uranium deposit (Table 7-13) is still much lower than the concentrations due solely to $RaSO_4$ saturation.

Table 7-12. Concentration of Radium in Several Natural Waters

Reference	Water Type	Concentration (mg/L)
Laul and Maiti 1990 [DIRS 173072]	J-13 well water	4.60E-09
Evans et al. 1982 [DIRS 173074]	Lake water	5.95E-08
	Stream/River water	9.88E-08
	Well water	7.19E-07

NOTE: All conversions to mg/L were performed in *Ra waters.xls* in Appendix I.

Table 7-13. Concentration of Radium in Uranium Mine Tailings

Reference	Water Type	Minimum Conc. (mg/L)	Maximum Conc. (mg/L)
Peacey et al. 2002 [DIRS 173073].	Porewater of mine tailings	5.94E-06	1.07E-04
	Surface water on mine tailings	4.15E-05	4.65E-05

NOTE: All conversions to mg/L were performed in *Ra waters.xls* in Appendix I.

Based on the above data, a radium concentration based on pure $RaSO_4$ solubility is conservative and adequate for TSPA-LA use.

7.3 VALIDATION SUMMARY

The solubility models have been validated by applying acceptance criteria based on an evaluation of the model's relative importance to the potential performance of the repository system. All validation requirements defined in Section 2 of *Technical Work Plan for Postclosure Waste Form Modeling* (BSC 2005 [DIRS 173246]) have been fulfilled, including corroboration of model results with experimental data, publications of refereed journals, and independent technical review. Activities required for confidence building during model development have been satisfied. The model development activities and postdevelopment validation activities described establish the scientific basis for the solubility models. Based on this, the solubility models summarized in Section 8 are considered to be sufficiently accurate and adequate for their intended purpose. The level of confidence required by the model's relative importance to the performance of the repository system has been met.

8. CONCLUSIONS

The scope of this modeling activity is to predict dissolved concentrations or solubility limits as functions of environmental conditions (in the form of look-up tables, as distributions, or single values) for all elements with radioactive isotopes transported outside breached waste packages important to the performance of the repository. Solubility models and analyses have been developed based on geochemical modeling calculations using geochemical modeling tools, thermodynamic databases, and measurements made in laboratory experiments and field work. For the 14 elements with radioactive isotopes, seven base-case models (for plutonium, neptunium, uranium, thorium, americium, protactinium, and radium) and six analyses (for lead, technetium, carbon, iodine, cesium, and strontium) were performed. TSPA-LA does not require solubility data for Ac; therefore, no model was created in this report. One alternative conceptual model for neptunium is also discussed in Section 6.6.

The output from this model can be found archived in output DTN: MO0501SPADISCN.000.

8.1 MODEL OUTPUT

The base-case model output is summarized in Table 8-1. The output for plutonium, neptunium, uranium, thorium, americium, and protactinium solubilities are tabulated as functions of pH and log fCO_2. These tables are located in Section 6 and are not repeated in this section. There are two base case neptunium-solubility models. One is for inside the waste packages (in-package), and the other is for the invert (ex-package). There are two base-case uranium-solubility models. One is for CSNF waste packages in nominal and seismic scenarios, and the other is for CDSP waste packages in all scenarios and for CSNF packages breached during an igneous intrusion and for the invert. For some very soluble elements, there is no adequate basis to specify a solubility-controlling solid, so they are modeled as highly soluble, and their releases are considered to be controlled by the dissolution rate of waste forms. Elements in this category are technetium, carbon, iodine, cesium, and strontium.

Table 8-1. Summary of Base-Case Solubility Models

Element	Value	Note
Pu	Table 6.5-1 (log of solubility in mg/L)	
Np	Table 6.6-3 (log of solubility in mg/L)	For in-package
	Table 6.6-9 (log of solubility in mg/L)	For ex-package (invert)
U	Table 6.7-3 (log of solubility in mg/L)	For CSNF waste packages in nominal and seismic scenarios
	Tables 6.7-5 and 6.7-6 (log of solubility in mg/L)	For CDSP waste packages, for CSNF waste packages breached during an igneous intrusion, and for the invert
Th	Table 6.8-2 (log of solubility in mg/L)	
Am	Table 6.9-2 (log of solubility in mg/L)	
Ac	N/A	
Pa	Table 6.11-3 (log of solubility in mg/L)	

Table 8-1. Summary of Base-Case Solubility Models (Continued)

Element	Value	Note
Ra	8.8E-8 mol/L (2.0E-2 mg/L) for pH range of 3.0 to 7.75 5.3E-6 mol/L (1.2 mg/L) for pH range of 7.75 to 9.75 500 for pH > 9.75	Constants for two intervals
Pb	4.8E-9 to 4.8E-7 mol/L (1.0E-3 to 1.0E-1 mg/L)	log uniform distribution
Tc	500	Controlled by dissolution rate of waste form
C	500	Controlled by dissolution rate of waste form
I	500	Controlled by dissolution rate of waste form
Cs	500	Controlled by dissolution rate of waste form
Sr	500	Controlled by dissolution rate of waste form

8.2 OUTPUT UNCERTAINTY

Uncertainties from various sources are addressed in this report. They consist of (1) uncertainty in selection of the solubility-controlling phase (for uranium-solubility model only), (2) uncertainty in log K of the solubility-controlling phase, (3) uncertainty associated with temperature variations, (4) uncertainty associated with variations in fluoride concentrations, and (5) additional uncertainty in solubility values in solutions with ionic strengths from 1 to 3 molal.

The output uncertainty for the base-case models is summarized in Table 8-2. For Pu, Np, U, Th, and Am, uncertainty is added to the solubilities presented in Table 6.5-1 (for Pu); Table 6.6-3 (for Np in-package); Table 6.6-9 (for Np in the invert); Tables 6.7-3, 6.7-5, and 6.7-6 (for U); Table 6.8-2 (for Th); and Table 6.9-2 (for Am) by the following equation:

$$\log[\text{Pu, Np, U, Am, or Th}] = S(\text{pH},\log fCO_2) + \varepsilon_1 + (\varepsilon_2 \times N) \qquad \text{(Eq. 8.1)}$$

Uncertainty for Pa is added to the solubility values presented in Table 6.11-3 (for Pa) by the following equation:

$$\log[\text{Pa}] = S(\text{pH},\log fCO_2) + \varepsilon_1 + \varepsilon_2 \qquad \text{(Eq. 8.2)}$$

where:

$S(pH, \log f_{CO_2})$ is log of the actinide concentration (see Table 8-1) as a function of pH and $\log f_{CO2}$

ε_1 is the uncertainty term associated with uncertainty in log K values. This term has a normal distribution truncated at 2σ. The value used during a given run is chosen from within this distribution by the TSPA-LA model.

ε_2 is the uncertainty term associated with variations in fluoride concentration. The range of fluoride uncertainty for a given TSPA-LA run depends on the type of waste package being considered and the pH. This term has a right-angled triangular distribution with the

minimum (indicated by "a"), most probable values (indicated by "b") equal to one another (i.e., a = b), and the maximum value (indicated by "c") corresponding to the maximum value uncertainty.

N is the factor by which the maximum fluoride uncertainty (ε_2) is normalized for pH.

Table 8-2. Summary of Uncertainty for Base-Case Solubility Models

Element	Sources of Uncertainty		Uncertainty Distribution	Characteristic Values	Notes
Plutonium solubility	log K		Normal Truncated at ±2σ	μ = 0, σ = 1.0 (1.04)[a]	Table 6.5-5
	F^- (for CSNF waste packages – Water-Influx Scenario)		Triangular	a = b = 0, c = 0.50 (pH dependence of c indicated in Table 6.5-4)	
	F^- (for codisposal waste package and invert)	Water-Influx Scenario	Triangular	a = b = 0, c = 0.96 (pH dependence of c indicated in Table 6.5-4)	
		Vapor-Influx Scenario	Triangular	a = b = 0, c = 1.69 (pH dependence of c indicated in Table 6.5-4)	
Neptunium solubility (in-package)	log K		Normal Truncated at ±2σ	μ = 0, σ = 0.60 (0.67) [a]	Table 6.6-5
	F^- (for CSNF waste packages – Water-Influx Scenario)		Triangular	a = b = 0, c = 0.043 (pH dependence of c indicated in Table 6.6-6)	
	F^- (for codisposal waste package)	Water-Influx Scenario	Triangular	a = b = 0, c = 0.150 (pH dependence of c indicated in Table 6.6-6)	
		Vapor-Influx Scenario	Triangular	a = b = 0, c = 0.524 (pH dependence of c indicated in Table 6.6-6)	
Neptunium solubility (invert)	log K		Normal Truncated at ±2σ	μ = 0, σ = 0.80 (0.85) [a]	Table 6.6-11
	F^- (for invert)	Water-Influx Scenario	Triangular	a = b = 0, c = 0.026 (pH dependence of c indicated in Table 6.6-12)	
		Vapor-Influx Scenario	Triangular	a = b = 0, c = 0.079 (pH dependence of c indicated in Table 6.6-12)	
Uranium solubility: CSNF packages for nominal and seismic breach scenarios	log K - schoepite		Normal Truncated at ±2σ	μ = 0, σ = 0.50 (0.60)[a]	Section 6.7.6
	F^- (for CSNF waste packages – Water-Influx Scenario)		Triangular	a = b = 0, c = 1.03 (pH dependence of c indicated in Table 6.7-9)	

Table 8-2. Summary of Uncertainty for Base-Case Solubility Models (Continued)

Element	Sources of Uncertainty		Uncertainty Distribution	Characteristic Values	Notes
Uranium solubility: Codisposal packages, CSNF packages breached during an igneous intrusion, and invert	Schoepite	log K	Normal Truncated at ±2σ	μ = 0, σ = 0.50 (0.60) [a]	Section 6.7.6
		F^- - (Water-Influx CDSP and CSNF packages breached during an igneous intrusion)	Triangular	a = b = 0, c = 1.65 (pH dependence of c indicated in Table 6.7-11)	Table 6.7-10
		F^- - (Vapor-Influx CDSP Waste Packages and Invert)	Triangular	a = b = 0, c = 2.40 (pH dependence of c indicated in Table 6.7-11)	
	Na-boltwoodite	log K	Normal Truncated at ±2σ	μ = 0, σ = 0.50 (0.60) [a]	Section 6.7.6
		F^- – (Water-Influx CDSP and CSNF packages breached during an igneous intrusion)	Triangular	a = b = 0, c = 0.368 (pH dependence of c indicated in Table 6.7-11)	Table 6.7-10
		F^- – (Vapor-Influx CDSP Waste Packages and invert)	Triangular	a = b = 0, c = 1.17 (pH dependence of c indicated in Table 6.7-11)	Table 6.7-10
	$Na_4UO_2(CO_3)_3$	log K	Normal Truncated at ±2σ	μ = 0, σ = 0.6 [b]	Section 6.7.6
		F^- – (CDSP and CSNF packages breached during an igneous intrusion, and invert)	Triangular	a = b = 0, c = 0	Table 6.7-10
		F^- – (Vapor-Influx CDSP Waste Packages and invert)	Triangular	a = b = 0, c = 0	Table 6.7-10
Thorium solubility	log K		Normal Truncated at ±2σ	μ = 0, σ = 0.7 (0.76)[a]	Table 6.8-4
	F^- (for CSNF waste packages – Water-Influx Scenario)		Triangular	a = b = 0, c = 3.10 (pH dependence of c indicated in Table 6.8-4)	
	F^- (for codisposal waste package and invert)	Water-Influx Scenario	Triangular	a = b = 0, c = 4.21 (pH dependence of c indicated in Table 6.8-4)	
		Vapor-Influx Scenario	Triangular	a = b = 0, c = 5.27 (pH dependence of c indicated in Table 6.8-4)	

Table 8-2. Summary of Uncertainty for Base-Case Solubility Models (Continued)

Element	Sources of Uncertainty		Uncertainty Distribution	Characteristic Values	Notes
Americium solubility	log K		Normal Truncated at ±2σ	μ = 0, σ = 1.0 (1.04)[a]	Table 6.9-4
	F^- (for CSNF waste packages – Water-Influx Scenario)		Triangular	a = b = 0, c = 5.91E-2 (pH dependence of c indicated in Table 6.9-5)	
	F^- (for codisposal waste package and invert)	Water-Influx Scenario	Triangular	a = b = 0, c = 0.40 (pH dependence of c indicated in Table 6.9-5)	
		Vapor-Influx Scenario	Triangular	a = b = 0, c = 0.99 (pH dependence of c indicated in Table 6.9-5)	
Protactinium solubility	Analogues		Uniform	Over an interval of [-0.05 to –4.42]	Table 6.11-4
	F^- (for CSNF waste packages – Water-Influx Scenario)		Triangular	a = b = 0, c = 3.10	
	F^- (for codisposal waste package and invert)	Water-Influx Scenario	Triangular	a = b = 0, c = 4.21	
		Vapor-Influx Scenario	Triangular	a = b = 0, c = 5.27	
Radium solubility	N/A		N/A	Distribution	N/A
Lead solubility	N/A		N/A	Distribution	N/A
Technetium solubility	N/A		N/A	Constant	N/A
Carbon solubility	N/A		N/A	Constant	N/A
Iodine solubility	N/A		N/A	Constant	N/A
Cesium solubility	N/A		N/A	Constant	N/A
Strontium Solubility	N/A		N/A	Constant	N/A

NOTES: [a] When used with solutions having an ionic strength from 1 to 3 molal, log K uncertainty is the number indicated in parentheses.
[b] EQ3NR runs show ionic strength of solutions are usually above 1 when $Na_4UO_2(CO_3)_3$ is the dominant U phase,. Therefore, the log K uncertainty term already accounts for the square root of the mean addition of ±0.3 to the uncertainty term.

The look-up tables for radionuclide solubilities (summarized in Table 8-1) include a flag of "500," which indicates no solubility can be calculated within the valid range of the model. Constraining the dissolved concentrations is necessary for use in TSPA-LA calculations for cases in which solubility is undefined, such as when "500" flags are indicated or conditions are outside of the range of validity of the dissolved concentrations model (e.g., ionic strength above 3). As an example, because of the instantaneous release rate attributed to codisposed spent nuclear fuel, it is possible to release the entire inventory in one TSPA time step. Setting caps on the solubilities will prevent unconstrained concentrations of actinides entering solution.

The "500" flag indicates that release rates, rather than concentration limits, should be selected for these physicochemical conditions in the TSPA-LA modeling. To obtain aqueous concentrations where solubility is undefined, the inventory concentrations will be calculated using the dissolution rate of individual waste forms and water volume. These concentrations based on water volume and waste form dissolution rate are capped at (can not exceed) the metal densities presented in Table 8-3. This method is to be used when:

- A "500" flag is indicated in the solubility look-up tables or for conditions between a valid solubility and a "500" flag
- Conditions are outside of the range of validity for the dissolved concentrations model (see Table 8-4 for range of applicable conditions).

Note that inventories for Tc, Ra, Pb, C, I, Cs, and Sr are low enough that they do not require solubility caps. Therefore caps for these elements are not presented in Table 8-3.

Table 8-3. Density of Actinides at 25°C

	Pu	Np	U	Th	Am	Pa
Density (g/cm^3)	19.7	20.2	19.1	11.7	12.0	15.4
Density (mg/L)	1.97E+07	2.02E+07	1.91E+07	1.17E+07	1.20E+07	1.54E+07

Source: Lide 2002 [DIRS 160832].

8.3 YUCCA MOUNTAIN REVIEW PLAN ACCEPTANCE CRITERIA

Yucca Mountain Review Plan, Final Report (NRC 2003 [DIRS 163274]) contains Acceptance Criteria intended to establish the basis for the review of the material contained in the License Application. As this report serves, in part, as the basis for the license application, it is important to show how the information contained herein addresses each of the applicable Acceptance Criteria.

The Acceptance Criteria applicable to this report are identified in *Technical Work Plan for Postclosure Waste Form Modeling* (BSC 2005 [DIRS 173246], Table 3-1). For each applicable criterion, the criterion is quoted in italics, followed by pointers to where within the report the information addressing the criterion can be found. In some cases, the criterion is only partially addressed in this report. A demonstration of full compliance requires a review of multiple reports.

Radionuclide Release Rates and Solubility Limits (NRC 2003 [DIRS 163274], Section 2.2.1.3.4.3)

Acceptance Criterion 1—System Description and Model Integration Are Adequate

(1) Total system performance assessment adequately incorporates important design features, physical phenomena, and couplings, and uses consistent and appropriate assumptions throughout the radionuclide release rates and solubility limits abstraction process.

Sections 6.3 and 6.4 addresse the chemical conditions expected in the repository. Assumptions are listed in Section 5. As indicated in Section 1, the TSPA-LA model uses the solubility models generated by this report in conjunction with *In-Package Chemistry Abstraction* (BSC 2004 [DIRS 167621])' *Dike/Drift Interactions* (BSC 2004 [DIRS 170028])' and *Engineered Barrier System: Physical and Chemical Environment* (BSC 2004 [DIRS 169860]). This report and *Dike/Drift Interactions* (BSC 2004 [DIRS 170028]) correlate well with one another. Both reports use dilute solutions for the base-case scenarios, and calculations are made at 25°C. *In-Package Chemistry Abstraction* (BSC 2004 [DIRS 167621]) feeds TSPA-LA pH values good for temperatures from 25°C to 100°C. Section 6 of the model indicates the lowest pH values (approximately 4.5 to 5.5) are derived from higher-temperature cases of waste package corrosion. However, even at these low pH values, TSPA-LA uses the conservative 25°C dissolved concentrations values described in this report. *Engineered Barrier System: Physical and Chemical Environment* (BSC 2004 [DIRS 169860]) provides TSPA-LA with a number of look-up tables for possible water compositions in the drift. These waters are at various stages of evaporation depending on the conditions in the drift. Most of these waters contain constituent concentrations that fit within those studied in Section 6.4.2.5 of this report. However, several possible drift waters provided by *Engineered Barrier System: Physical and Chemical Environment* (BSC 2004 [DIRS 169860]) are quite concentrated. These waters were not evaluated in this report as they are usually of very limited volume.

> *(2) The abstraction of radionuclide release rates and solubility limits uses assumptions, technical bases, data, and models that are appropriate and consistent with other related U.S. Department of Energy abstractions. For example, the assumptions used for this model abstraction are consistent with the abstractions of "Degradation of Engineered Barriers" (Section 2.2.1.3.1); "Mechanical Disruption of Waste Packages" (Section 2.2.1.3.2); "Quantity and Chemistry of Water Contacting Waste Packages and Waste Forms" (Section 2.2.1.3.3); "Climate and Infiltration" (Section 2.2.1.3.5); and "Flow Paths in the Unsaturated Zone" (Section 2.2.1.3.6). The descriptions and technical bases provide transparent and traceable support for the abstraction of radionuclide release rates and solubility limits;*

The range of chemical conditions expected in the repository (Sections 6.3 and 6.4) and the assumptions (Section 5) are consistent with other models, such as *In-Package Chemistry Abstraction* (BSC 2004 [DIRS 167621]), *Dike/Drift Interactions* (BSC 2004 [DIRS 170028]), and *Engineered Barrier System: Physical and Chemical Environment* (BSC 2004 [DIRS 169860]) (see comment above for differences in models).

> *(3) The abstraction of radionuclide release rates and solubility limits provides sufficient, consistent design information on waste packages and engineered barrier systems. For example, inventory calculations and selected radionuclides are based on the detailed information provided on the distribution (both spatially and by compositional phase) of the radionuclide inventory, within the various types of high-level radioactive waste;*

Section 1 indicates the radionuclides selected to be included in this report are based on the radiation dose a person located near the repository might receive.

(4) The U.S. Department of Energy reasonably accounts for the range of environmental conditions expected inside breached waste packages and in the engineered barrier environment surrounding the waste package. For example, the U.S. Department of Energy should provide a description and sufficient technical bases for its abstraction of changes in hydrologic properties in the near field, caused by coupled thermal-hydrologic-mechanical-chemical processes;

The solubility models account for the range of environmental conditions (pH, temperature, and carbonate) expected, as described in Sections 6.3 and 6.4.

(5) The description of process-level conceptual and mathematical models is sufficiently complete, with respect to thermal-hydrologic processes affecting radionuclide release from the emplacement drifts. For example, if the U.S. Department of Energy uncouples coupled processes, the demonstration that uncoupled model results bound predictions of fully coupled results is adequate;

The influence of temperature on the solubilities is discussed in Section 6.3.3.3.

(6) Technical bases for inclusion of any thermal-hydrologic-mechanical-chemical couplings and features, events, and processes in the radionuclide release rates and solubility limits model abstraction are adequate. For example, technical bases may include activities, such as independent modeling, laboratory or field data, or sensitivity studies;

As discussed in Section 6, the selections of the solubility-controlling solid phases were based on laboratory or field observations and corroborated by Project-specific laboratory results.

(7)…

Not Applicable (applies to criticality).

(8) Guidance in NUREG-1297 and NUREG-1298 or other acceptable approaches for peer reviews and data qualification is followed.

Section 4.1 addresses data inputs to the model and qualification of data.

Acceptance Criterion 2—Data Are Sufficient for Model Justification

(1) Geological, hydrological, and geochemical values used in the license application are adequately justified. Adequate description of how the data were used, interpreted, and appropriately synthesized into the parameters is provided;

The thermodynamic database and other inputs are discussed in Section 4.1. As discussed in Section 6, the selections of the solubility-controlling solid phases were based on laboratory or field observations and corroborated by Project-specific laboratory results.

(2) Sufficient data have been collected on the characteristics of the natural system and engineered materials to establish initial and boundary conditions for conceptual models and simulations of thermal-hydrologic-chemical coupled processes. For example, sufficient data should be provided on design features, such as the type, quantity, and reactivity of materials, that may affect radionuclide release for this abstraction;

Experimental data used to establish controlling phase and uncertainties are listed in Sections 4.1, 6, and 6.1. Chemistry of the water is discussed in Section 6.4.

(3) Where the U.S. Department of Energy uses data supplemented by models to support abstraction of solubility limits, the anticipated range of proportions and compositions of phases under the various physicochemical conditions expected are supported by experimental data;

Laboratory experiments and observations of natural systems supporting the choice of solubility-controlling solids are discussed in Sections 6, 6.3.2, and 7.

(4) The corrosion and radionuclide release testing program for high-level radioactive waste forms intended for disposal provides consistent, sufficient, and suitable data for the in-package and in-drift chemistry used in the abstraction of radionuclide release rates and solubility limits. For expected environmental conditions, the U.S. Department of Energy provides sufficient justification for the use of test results, not specifically collected from the Yucca Mountain site, for engineered barrier components, such as high-level radioactive waste forms, drip shield, and backfill.

Results from testing used to validate the solubility models are discussed in Section 7.

Acceptance Criterion 3—Data Uncertainty Is Characterized and Propagated Through the Model Abstraction

(1) Models use parameter values, assumed ranges, probability distributions, and bounding assumptions that are technically defensible, reasonably account for uncertainties and variabilities, and do not result in an under-representation of the risk estimate;

Uncertainty is discussed in Sections 6.3.3, 6.5 through 6.11, and 8.2.

(2) Parameter values, assumed ranges, probability distributions, and bounding assumptions used in the abstractions of radionuclide release rates and solubility limits in the total system performance assessment are technically defensible and reasonable based on data from the Yucca Mountain region, laboratory tests, and natural analogs. For example, parameter values, assumed ranges, probability distributions, and bounding assumptions adequately reflect the range of environmental conditions expected inside breached waste packages;

Parameter values and uncertainty are discussed in Sections 4.1, 6.3, and 6.4.

(3)…

Not applicable (applies to release, rather than solubility).

(4) Uncertainty is adequately represented in parameter development for conceptual models, process models, and alternative conceptual models considered in developing the abstraction of radionuclide release rates and solubility limits, either through sensitivity analyses or use of bounding analyses;

Uncertainty is addressed throughout the document, such as Sections 6.3.3, 6.5 through 6.11, and 8.2.

(5-6)…

Not Applicable (applies to water flow and criticality).

(7) The U.S. Department of Energy uses as appropriate range of time-history of temperature, humidity, and dripping to constrain the probability for microbial effects, such as production of organic by-products that act as complexing ligands for actinides and microbially enhanced dissolution of the high-level radioactive waste glass form;

The complexing ligands important to solubility are discussed in Section 6.4.1. Organic complexing ligands are not expected to be present in significant concentrations in the repository (BSC 2004 [DIRS 170020], Section 6.2.25).

(8) The U.S. Department of Energy adequately considers the uncertainties, in the characteristics of the natural system and engineered materials, such as the type, quantity, and reactivity of material, in establishing initial and boundary conditions for conceptual models and simulations of thermal-hydrologic-chemical coupled processes that affect radionuclide release; and

Uncertainty is addressed throughout the document, such as in Sections 6.3.3, 6.5 through 6.11, and 8.2.

(9)…

Not Applicable (applies only when insufficient data exists).

Acceptance Criterion 4—Model Uncertainty Is Characterized and Propagated Through the Model Abstraction

(1) Alternative modeling approaches of features, events, and processes are considered and are consistent with available data and current scientific

understanding, and the results and limitations are appropriately considered in the abstraction;

Alternative modeling approaches are discussed in Section 6.19.

(2) In considering alternative conceptual models for radionuclide release rates and solubility limits, the U.S. Department of Energy uses appropriate models, tests, and analyses that are sensitive to the processes modeled for both natural and engineering systems. Conceptual model uncertainties are adequately defined and documented, and effects on conclusions regarding performance are properly assessed. For example, in modeling flow and radionuclide release from the drifts, the U.S. Department of Energy represents significant discrete features, such as fault zones, separately, or demonstrates that their inclusion in the equivalent continuum model produces a conservative effect on calculated performance; and

Alternative models and their effects on solubility are discussed in Sections 6.3.3 and 6.19.

(3) Consideration of conceptual model uncertainty is consistent with available site characterization data, laboratory experiments, field measurements, natural analog information and process-level modeling studies; and the treatment of conceptual model uncertainty does not result in an under-representation of the risk estimate; and

Alternative models and their effects on solubility are discussed in Section 6.19.

(4) …

Not applicable (refers to radionuclide release rather than solubility).

Acceptance Criterion 5—Model Abstraction Output Is Supported by Objective Comparisons

(1) The models implemented in this total system performance assessment abstraction provide results consistent with output from detailed process-level models and/or empirical observations (laboratory and field testing and/or natural analogs);

As discussed in Section 6, the selections of the solubility-controlling solid phases were based on laboratory or field observations and corroborated by Project-specific laboratory results.

(2) ...

Not Applicable (applies to thermal hydrologic models).

(3) …

Not applicable (applies to radionuclide release rather than solubility).

(4)…

Not Applicable (applies to the performance confirmation program).

8.4 RESTRICTIONS

As discussed in Section 6.4, the solubility models developed in this report are valid for broad ranges of water composition, as listed in Table 8-4. They may be applied inside and outside waste packages.

Table 8-4. Valid Range of the Solubility Models Reported in This Report

Variable	Value or Range
pH	3.0 to 11.0
log fCO_2	–5.0 to –1.5 bars
Temperature	25 °C to 100°C
F^- concentration	For Pu, Np, U, Th, Am, and Pa models: 1 to 10 times the base-case value for CSNF packages; 1 to 27 times the base-case value for water-influx codisposal packages; 1 to 95 times the base-case value for vapor-influx codisposal packages and invert .
Ionic Strength	Less than 1 molal: With σ values for log K uncertainties given in Table 8-2 for all controlling solids. From 1 to 3 molal: With σ values for log K uncertainties equal to $(\sigma^2 + 0.3^2)^{1/2}$ where σ is the log K uncertainty value given in Table 8-2 for all controlling solids except $Na_4UO_2(CO_3)_3$. For $Na_4UO_2(CO_3)_3$ as controlling solid use log K uncertainty value given in Table 8-2.

9. INPUTS AND REFERENCES

9.1 DOCUMENTS CITED

159352 Ahn, T.M. and Leslie, B.W. 1998. *Corrosion Products of Steels in High-Level Waste Management at the Proposed Yucca Mountain Repository.* Washington, D.C.: U.S. Nuclear Regulatory Commission. TIC: 242152.

159372 Allen, B.L. and Hajek, B.F. 1995. "Mineral Occurrence in Soil Environments." Chapter 5 of *Minerals in Soil Environments.* 2nd Edition. Dixon, J.B. and Weed, S.B., eds. Soil Science Society of America Book Series, no. 1. Madison, Wisconsin: Soil Science Society of America. TIC: 237222.

173049 Altmaier, M.; Neck, V.; and Fanghanel, Th. 2004. "Solubility and Colloid Formation of Th(IV) in Concentrated NaCl and $MgCl_2$ Solution." *Radiochimica Acta, 92,* 537-543. München, Germany: Oldenbourg Wissenschaftsverlag. TIC: 257090.

173048 Altmaier, M.; Neck, V.; Müller, R.; and Fanghänel, Th. 2005. "Solubility of $ThO_2 \cdot xH_2O$(am) in Carbonate Solution and the Formation of Ternary Th(IV) Hydroxide-Carbonate Complexes." *Radiochimica Acta, 93,* 83-92. München, Germany: Oldenbourg Wissenschaftsverlag. TIC: 257060.

173088 Amme, M. 2002. "Contrary Effects of the Water Radiolysis Product H_2O_2 Upon the Dissolution of Nuclear Fuel in Natural Groundwater and Deionized Water." *Radiochimica Acta, 90*, pp. 399-406. München, Germany: Oldenbourg Wissenschaftsverlag. TIC: 256822.

159378 Apps, J.A.; Neil, J.M.; and Jun, C.-H. 1989. *Thermochemical Properties of Gibbsite, Bayerite, Boehmite, Diaspore, and the Aluminate Ion Between 0 and 350°C.* NUREG/CR-5271. Washington, D.C.: U.S. Nuclear Regulatory Commission. TIC: 234405.

134303 Atkins, P.W. 1994. *Physical Chemistry.* 5th Edition. New York, New York: W.H. Freeman and Company. TIC: 246986.

168371 Baas Becking, L.G.M.; Kaplan, I.R.; and Moore, D. 1960. "Limits of the Natural Environment in Terms of pH and Oxidation-Reduction Potentials." *Journal of Geology*, 68, (3), 243-284. Chicago, Illinois: University of Chicago Press. TIC: 255394.

100702 Baes, C.F., Jr. and Mesmer, R.E. 1986. *The Hydrolysis of Cations.* Malabar, Florida: Krieger Publishing Company. TIC: 223481.

172677 Beall, G.W.; Allard, B.; Krajewski, T.; and O'Kelly, G.D. 1980. "Chemical Reactions in the Bedrock-Groundwater System of Importance for the Sorption of Actinides." *Scientific Basis for Nuclear Waste Management,* Proceedings of the International Symposium, Boston, Massachusetts, November 27-30, 1979. Northrup, C.J.M. Jr. ed. *2,* p. 625-631. New York, New York: Plenum Press. TIC: 248272.

162000 Berner, U. 2002. *Project Opalinus Clay: Radionuclide Concentration Limits in the Near-Field of a Repository for Spent Fuel and Vitrified High-Level Waste.* PSI Bericht 02-22. Villigen, Switzerland: Paul Scherrer Institut. TIC: 253856.

173083 Berner, U. and Curti, E. 2002. *Radium Solubilities from SF/HLW Wastes Using Solid Solution and Co-Precipitation Models.* TM-44-02-04. Villigen, Switzerland: Paul Shrerrer Institut. TIC: 257100.

144728 Berry, J.A.; Hobley, J.; Lane, S.A.; Littleboy, A.K.; Nash, M.J.; Oliver, P.; Smith-Briggs, J.L.; and Williams, S.J. 1989. "Solubility and Sorption of Protactinium in the Near-Field and Far-Field Environments of a Radioactive Waste Repository." *Analyst, 114,* 339-347. Cambridge, England: Royal Society of Chemistry. TIC: 247004.

146304 Bevington, P.R. 1969. *Data Reduction and Error Analysis for the Physical Sciences.* New York, New York: McGraw-Hill. TIC: 244912.

159330 Birch, W.D.; Pring, A.; Reller, A.; and Schmalle, H. 1992. "Bernalite: A New Ferric Hydroxide with Perovskite Structure." *Naturwissenschaften, 79,* (11), 509-511. New York, New York: Springer-Verlag. TIC: 252810.

159387 Birch, W.D.; Pring, A.; Reller, A.; and Schmalle, H.W. 1993. "Bernalite, $Fe(OH)_3$, a New Mineral from Broken Hill, New South Wales: Description and Structure." *American Mineralogist, 78,* (7-8), 827-834. Washington, D.C.: Mineralogical Society of America. TIC: 252812.

173041 Bitea, C.; Müller, R.; Neck, V.; Walther, C.; and Kim, J.I. 2003. "Study of the Generation and Stability of Thorium(IV) Colloids by LIBD Combined with Ultrafiltration." *Colloids and Surfaces A: Physicochemical and Engineering Aspects*, 217, 63-70. New York, New York: Elsevier. TIC: 257099.

159331 Booth, G.H.; Cooper, A.W.; and Tiller, A.K. 1967. "Corrosion of Mild Steel in the Tidal Water of the Thames Estuary. III. Results of 3 and 5 Years' Immersion." *British Corrosion Journal, 2,* (6), 222-228. London, England: British Joint Corrosion Group. TIC: 252628.

159332 Booth, G.H.; Cooper, A.W.; and Tiller, A.K. 1967. "Corrosion of Mild Steel in the Tidal Waters of the Afon Dyfi and a Comparison With the River Thames." *British Corrosion Journal, 2,* (1), 21-24. London, England: British Joint Corrosion Group. TIC: 252627.

111794 Bruno, J.; Cera, E.; de Pablo, J.; Duro, L.; Jordana, S.; and Savage, D. 1997. *Determination of* Radionuclide *Solubility Limits to be Used in SR 97 - Uncertainties Associated to Calculated Solubilities.* SKB TR-97-33. Stockholm, Sweden: Svensk Kärnbränsleförsörjning A.B. TIC: 239307.

101565 Bruno, J.; Cera, E.; Eklund, U.B.; Eriksen, T.E.; and Grive, M. 1998. *Some Preliminary Modeling Results of Long Term Radiolytic Mass Balance Experiments.*

Presentation at the Spent Fuel Workshop 1998, Las Vegas, Nevada, May 18-20, 1998. Barcelona, Spain: Quantisci. TIC: 240716.

173089 Bruno, J.; Cera, E.; Grive, M.; Eklund, U.; and Eriksen, T. 1999. *Experimental Determination and Chemical Modelling of Radiolytic Processes at the Spent Fuel/Water Interface.* SKB TR-99-26. Stockholm, Sweden: Swedish Nuclear Fuel and Waste Management. TIC: 246955.

159355 Brush, E.G. and Pearl, W.L. 1972. "Corrosion and Corrosion Product Release in Neutral Feedwater." *Corrosion, 28,* (4), 129-136. Houston, Texas: National Association of Corrosion Engineers. TIC: 252684.

154844 BSC (Bechtel SAIC Company) 2001. *Secondary Uranium-Phase Paragenesis and Incorporation of Radionuclides into Secondary Phases.* ANL-EBS-MD-000019 REV 00 ICN 01. Las Vegas, Nevada: Bechtel SAIC Company. ACC: MOL.20010625.0306.

160059 BSC 2002. *Radionuclide Screening.* ANL-WIS-MD-000006 REV 01. Las Vegas, Nevada: Bechtel SAIC Company. ACC: MOL.20020923.0177.

169982 BSC 2004. *Aqueous Corrosion Rates for Waste Package Materials.* ANL-DSD-MD-000001 REV 01. Las Vegas, Nevada: Bechtel SAIC Company. ACC: DOC.20041012.0003.

169987 BSC 2004. *CSNF Waste Form Degradation: Summary Abstraction.* ANL-EBS-MD-000015 REV 02. Las Vegas, Nevada: Bechtel SAIC Company. ACC: DOC.20040908.0001.

170028 BSC 2004. *Dike/Drift Interactions*. MDL-MGR-GS-000005 REV 01. Las Vegas, Nevada: Bechtel SAIC Company. ACC: DOC.20041124.0002.

169860 BSC 2004. *Engineered Barrier System: Physical and Chemical Environment.* ANL-EBS-MD-000033 REV 03. Las Vegas, Nevada: Bechtel SAIC Company. ACC: DOC.20041201.0001.

170022 BSC 2004. *Initial Radionuclide Inventories.* ANL-WIS-MD-000020 REV 01. Las Vegas, Nevada: Bechtel SAIC Company. ACC: DOC.20040921.0003.

167621 BSC 2004. *In-Package Chemistry Abstraction*. ANL-EBS-MD-000037 REV 03, ACN 01. Las Vegas, Nevada: Bechtel SAIC Company. ACC: DOC.20041109.0007; DOC.20050330.0002.

171916 BSC 2004. *Qualification of Thermodynamic Data for Geochemical Modeling of Mineral-Water Interactions in Dilute Systems.* ANL-WIS-GS-000003 REV 00. Las Vegas, Nevada: Bechtel SAIC Company. ACC: DOC.20041129.0006.

171583 BSC 2004. *Technical Work Plan For: Regulatory Integration Modeling and Analysis of the Waste Form and Waste Package*. TWP-WIS-MD-000009 REV 00 ICN 01. Las Vegas, Nevada: Bechtel SAIC Company. ACC: DOC.20040910.0001.

170025 BSC 2004. *Waste Form and In-Drift Colloids-Associated Radionuclide Concentrations: Abstraction and Summary.* MDL-EBS-PA-000004 REV 01. Las Vegas, Nevada: Bechtel SAIC Company. ACC: DOC.20041028.0007.

170020 BSC 2004. *Waste-Form Features, Events, and Processes*. ANL-WIS-MD-000009 REV 02. Las Vegas, Nevada: Bechtel SAIC Company. ACC: DOC.20041028.0006.

171190 BSC 2005. *Q-List*. 000-30R-MGR0-00500-000-001. Las Vegas, Nevada: Bechtel SAIC Company. ACC: ENG.20050217.0010.

173246 BSC 2005. *Technical Work Plan for Postclosure Waste Form Modeling*. TWP-WIS-MD-000014 REV 01. Las Vegas, Nevada: Bechtel SAIC Company. ACC: DOC.20050407.0008.

172684 BSC 2005. *Technical Work Plan for Postclosure Waste Form Testing*. TWP-WIS-MD-000012 REV 00. Las Vegas, Nevada: Bechtel SAIC Company. ACC: DOC.20050125.0006.

100388 Buck, E.C.; Finch, R.J.; Finn, P.A.; and Bates, J.K. 1998. "Retention of Neptunium in Uranyl Alteration Phases Formed During Spent Fuel Corrosion." *Scientific Basis for Nuclear Waste Management XXI, Symposium held September 28-October 3, 1997, Davos, Switzerland.* McKinley, I.G. and McCombie, C., eds. *506,* 87-94. Warrendale, Pennsylvania: Materials Research Society. TIC: 240702.

172668 Buck, E.C.; Hanson, B.D.; Mcnamara, B.K. 2004. "The Geochemical Behavior of Tc, Np, and Pu in Spent Nuclear Fuel in an Oxidizing Environment." *Energy, Waste, and the Environment: A Geochemical Perspective.* eds. Giere, R. and Stille, P.. Geological Society of London Special Publication, 236. pp. 65-88. London, England: The Geological Society of London. TIC: 256910.

173047 Bundschuh, T.; Knopp, R.; Muller, R.; Kim, J.I.; Neck, V.; and Fanghanel, Th. 2000. "Application of LIBD to the Determination of the Solubility Product of Thorium(IV)-Colloids." *Radiochimica Acta, 88,* 625-629. München, Germany: Oldenbourg Wissenschaftsverlag. TIC: 257058.

173090 Burns, P.C. and Hughes, K.A. 2003. "Studtite, $[UO_2)(O_2)(H_2O)_2](H_2O)_2$: The First Structure of a Peroxide Mineral." *American Mineralogist, 88,* 1165-1168. Washington, D.C.: Mineralogical Society of America. TIC: 256823

171442 Burns, P.C.; Deely, K.M.; and Skanthakumar, S. 2004. "Neptunium Incorporation into Uranyl Compounds that Form as Alteration Products of Spent Nuclear Fuel: Implications for Geologic Repository Performance." *Radiochimica Acta, 92,* 151-159. München, Germany: Oldenbourg Wissenschaftsverlag. TIC: 256456.

100389 Burns, P.C.; Ewing, R.C.; and Miller, M.L. 1997. "Incorporation Mechanisms of Actinide Elements into the Structures of U^{6+} Phases Formed During the Oxidation of Spent Nuclear Fuel." *Journal of Nuclear Materials, 245,* (1), 1-9. Amsterdam, The Netherlands: North-Holland. TIC: 235501.

166275 Canori, G.F. and Leitner, M.M. 2003. *Project Requirements Document.* TER-MGR-MD-000001 REV 02. Las Vegas, Nevada: Bechtel SAIC Company. ACC: DOC.20031222.0006.

144731 Carroll, S.A.; O'Day, P.A.; and Piechowski, M. 1998. "Rock-Water Interactions Controlling Zinc, Cadmium, and Lead Concentrations in Surface Waters and Sediments, U.S. Tri-State Mining District. 2. Geochemical Interpretation." *Environmental Science & Technology*, 32, (7), 956-965. Washington, D.C.: American Chemical Society. TIC: 247008.

161997 Chen, Y. 2001. "An Empirical Np Solubility Model Based on Spent Fuel Dissolution Experiments." *Back to the Future - Managing the Back End of the Nuclear Fuel Cycle to Create a More Secure Energy Future," Proceedings of the 9th International High-Level Radioactive Waste Management Conference (IHLRWM), Las Vegas, Nevada, April 29-May 3, 2001.* La Grange Park, Illinois: American Nuclear Society. TIC: 247873.

162709 Chen, Y. 2003. "Using Reactive Transport Modeling to Evaluate the Source Term at Yucca Mountain." *Computers & Geosciences, 29*, (3), 385-397. New York, New York: Pergamon. TIC: 254363.

161996 Chen, Y.; Loch, A.R.; Wolery, T.J.; Steinborn, T.L.; Brady, P.V.; and Stockman, C.T. 2002. "Solubility Evaluation for Yucca Mountain TSPA-SR." *Scientific Basis for Nuclear Waste Management XXV, Symposium held November 26-29, 2001, Boston, Massachusetts.* McGrail, B.P. and Cragnolino, G.A., eds. *713,* 775-782. Warrendale, Pennsylvania: Materials Research Society. TIC: 248663.

168395 Choppin, G.R. 1983. "Aspects of Plutonium Solution Chemistry." Chapter 14 of Plutonium Chemistry. Carnall, W.T. and Choppin, G.R., eds. ACS Symposium Series 216. Washington, D.C.: American Chemical Society. TIC: 219103.

168308 Choppin, G.R. 2003. "Actinide Speciation in the Environment." *Radiochimica Acta, 91*, (11), 645-649. München, Germany: Oldenbourg Wissenschaftsverlag. TIC: 255776.

168379 Choppin, G.R. and Stout, B.E. 1989. "Actinide Behavior in Natural Waters." *Science of the Total Environmental, 83,* (3), 203-216. Amsterdam, The Netherlands: Elsevier. TIC: 255706.

168377 Choppin, G.R.; Roberts, R.A.; and Morse, J.W. 1986. "Effects of Humic Substances on Plutonium Speciation in Marine Systems." *Organic Marine Geochemistry.* Sohn, M.L., ed. ACS Symposium Series 305. Pages 382-388. Washington, D.C.: American Chemical Society. TIC: 255705.

100222 CRWMS M&O 1997. *Degraded Mode Criticality Analysis of Immobilized Plutonium Waste Forms in a Geologic Repository.* Predecisional Document. A00000000-01717-5705-00014 REV 01. Las Vegas, Nevada: CRWMS M&O. ACC: MOL.19980422.0911.

100348 CRWMS M&O 1998. *Constraints on Solubility-Limited Neptunium Concentrations for Use in Performance Assessment Analyses.* B00000000-01717-2200-00191 REV 00. Las Vegas, Nevada: CRWMS M&O. ACC: MOL.19980213.0484.

131861 CRWMS M&O 2000. *Commercial Spent Nuclear Fuel Degradation in Unsaturated Drip Tests.* Input Transmittal WP-WP-99432.T. Las Vegas, Nevada: CRWMS M&O. ACC: MOL.20000107.0209.

152507 CRWMS M&O 2000. *Data Qualification Report: Composition of J-13 Well Water for Use on the Yucca Mountain Project, Revision 0.* TDR-NBS-HS-000003 REV 00. Las Vegas, Nevada: CRWMS M&O. ACC: MOL.20000724.0463.

135790 CRWMS M&O 2000. *In-Drift Accumulation of Fissile Material from Waste Packages Containing Plutonium Disposition Waste Forms.* CAL-EDC-GS-000001 REV 00. Las Vegas, Nevada: CRWMS M&O. ACC: MOL.20001016.0008.

153105 CRWMS M&O 2000. *Measured Solubilities, Argonne National Lab High Drip Rate Tests.* Input Transmittal 00333.T. Las Vegas, Nevada: CRWMS M&O. ACC: MOL.20000919.0019.

154629 CRWMS M&O 2001. *Pure Phase Solubility Limits - LANL.* ANL-EBS-MD-000017 REV 00 ICN 01. Las Vegas, Nevada: CRWMS M&O. ACC: MOL.20010126.0005.

172669 Cui, D. and Eriksen, T.E. 1996. *Reduction of Tc(VII) and Np(V) in Solution by Ferrous Iron, A Laboratory Study of Homogenous and Heterogeneous Redox Processes.* SKB-TR-96-03. Stockholm, Sweden: Swedish Nuclear Fuel and Waste Management Company. TIC: 225225.

164037 Dehaudt, P. 2001. "State of the Art of the Oxidation of Spent Nuclear Fuel." Section 7.2 of *Synthesis on the Long Term Behavior of the Spent Nuclear Fuel*. Poinssot, C., ed. CEA-R-5958(E). Volume II. Paris, France: Commissariat à l'Énergie Atomique. TIC: 253976.

105778 Deng, Y.; Stjernstrom, M.; and Banwart S. 1996. "Accumulation and Remobilization of Aqueous Chromium (VI) at Iron Oxide Surfaces: Application of a Thin-film Continuous Flow-through Reactor." *Journal of Contaminant Hydrology, 21,* 141-151. Amsterdam, The Netherlands: Elsevier. TIC: 243062.

159374 Dixon, J.B. 1995. "Kaolin and Serpentine Group Minerals." Chapter 10 of *Minerals in Soil Environments.* 2nd Edition. Dixon, J.B. and Weed, S.B., eds. Soil Science Society of America Book Series, no. 1. Madison, Wisconsin: Soil Science Society of America. TIC: 237222.

166268 DOE (U.S. Department of Energy) 2003. *Review of DOE Spent Nuclear Fuel Release Rate Test Results.* DOE/SNF/REP-073, Rev. 0. Idaho Falls, Idaho: U.S. Department of Energy, Idaho Operations Office. ACC: DOC.20030905.0010.

105788 Eary, L.E. and Rai, D. 1989. "Kinetics of Chromate Reduction by Ferrous Ions Derived from Hematite and Biotite at 25C." *American Journal of Science*, 289, 180-213. New Haven, Connecticut: Yale University. TIC: 243614.

173071 Ebert, W.L.; Fortner, J.A.; Finch, R.J.; Jerden, J.L.; and Cunnane, J.C. 2005. *Yucca Mountain Project FY 2004 Annual Report for Waste Form Testing Activities.* ANL-05/08. Argonne, IL: Argonne National Laboratory. ACC: MOL.20050502.0239.

108015 Efurd, D.W.; Runde, W.; Banar, J.C.; Janecky, D.R.; Kaszuba, J.P.; Palmer, P.D.; Roensch, F.R.; and Tait, C.D. 1998. "Neptunium and Plutonium Solubilities in a Yucca Mountain Groundwater." *Environmental Science & Technology, 32,* (24), 3893-3900. Easton, Pennsylvania: American Chemical Society. TIC: 243857.

173074 Evans, S.; Lampe, S.; and Sundblad, B. 1982. *Natural Levels of Uranium and Radium in Four Potential Areas for the Final Storage of Spent Nuclear Fuel.* KBS TR 82-22. Nyköping, Sweden: Studsvik Energiteknik AB. TIC: 205891.

168170 Fanghänel, Th. and Neck, V. 2002. "Aquatic Chemistry and Solubility Phenomena of Actinide Oxides/Hyrodxides." *Pure and Applied Chemistry, 74,* (10), 1895-1907. Oxford, England: Blackwell Science. TIC: 255767.

173044 Felmy, A.R.; Rai, D.; and Mason, M.J. 1991. "The Solubility of Hydrous Thorium(IV) Oxide in Chloride Media: Development of an Aqueous Ion-Interaction Model." *Radiochimica Acta, 55,* 177-185. München, Germany: Oldenbourg Wissenschaftsverlag. TIC: 257139.

173046 Felmy, A.R.; Rai, D.; Sterner, S.M.; Mason, M.J.; Hess, N.J.; and Conradson, S.D. 1997. "Thermodynamic Models for Highly Charged Aqueous Species: Solubility of Th(IV) Hydrous Oxide in Concentrated $NaHCO_3$ and Na_2CO_3 Solutions." *Journal of Solution Chemistry, 26,* (3), 233-248. New York, New York: Plenum Publishing Corporation. TIC: 255458.

130384 Finch, R. and Ewing, R. 1990. *Uraninite Alteration in an Oxidizing Environment and Its Relevance to the Disposal of Spent Nuclear Fuel*. SKB TR-91-15. Stockholm, Sweden: Svensk Kärnbränsleförsörjning A.B. TIC: 208641.

172608 Finch, R.J. 2002. "Precipitation of Crystalline NpO_2 During Oxidative Corrosion of Neptunium-Bearing Uranium Oxides." *Scientific Basis for Nuclear Waste Management XXV, Symposium held November 26-29, 2001, Boston, Massachusetts.* McGrail, B.P. and Cragnolino, G.A., eds. *713,* 639-646. Warrendale, Pennsylvania: Materials Research Society. TIC: 248663.

113030 Finch, R.J. and Ewing, R.C. 1992. "The Corrosion of Uraninite Under Oxidizing Conditions." *Journal of Nuclear Materials*, 190, 133-156. Amsterdam, The Netherlands: Elsevier. TIC: 246369.

127332 Finch, R.J.; Buck, E.C.; Finn, P.A.; and Bates, J.K. 1999. "Oxidative Corrosion of Spent UO_2 Fuel in Vapor and Dripping Groundwater at 90°C." *Scientific Basis for Nuclear Waste Management XXII, Symposium held November 30-December 4, 1998, Boston, Massachusetts, U.S.A.* Wronkiewicz, D.J. and Lee, J.H., eds. *556,* 431-438. Warrendale, Pennsylvania: Materials Research Society. TIC: 246426.

161979 Finch, R.J.; Fortner, J.A.; Buck, E.C.; and Wolf, S.F. 2002. "Neptunium Incorporation into Uranium(VI) Compounds Formed During Aqueous Corrosion of Neptunium-Bearing Uranium Oxides." *Scientific Basis for Nuclear Waste Management XXV, Symposium held November 26-29, 2001, Boston, Massachusetts.* McGrail, B.P. and Cragnolino, G.A., eds. *713,* 647-654. Warrendale, Pennsylvania: Materials Research Society. TIC: 248663.

113056 Finch, R.J.; Suksi, J.; Rasilainen, K.; and Ewing, R.C. 1996. "Uranium Series Ages of Secondary Uranium Minerals, with Applications to the Long-Term Storage of Spent Nuclear Fuel." *Scientific Basis for Nuclear Waste Management XIX, Symposium held November 27-December 1, 1995, Boston, Massachusetts.* Murphy, W.M. and Knecht, D.A., eds. *412,* 823-830. Pittsburgh, Pennsylvania: Materials Research Society. TIC: 233877.

100746 Finn, P.A.; Buck, E.C.; Gong, M.; Hoh, J.C.; Emery, J.W.; Hafenrichter, L.D.; and Bates, J.K. 1994. "Colloidal Products and Actinide Species in Leachate from Spent Nuclear Fuel." *Radiochimica Acta, 66/67,* 197-203. München, Germany: R. Oldenbourg Verlag. TIC: 238493.

124142 Finn, P.A.; Hoh, J.C.; Wolf, S.F.; Surchik, M.T.; Buck, E.C.; and Bates, J.K. 1997. "Spent Fuel Reaction: The Behavior of the Epsilon-Phase Over 3.1 Years." *Scientific Basis for Nuclear Waste Management XX, Symposium held December 2-6, 1996, Boston, Massachusetts.* Gray, W.J. and Triay, I.R., eds. *465,* 527-534. Pittsburgh, Pennsylvania: Materials Research Society. TIC: 238884.

172671 Fortner, J. A.; Mertz, C. J.; Goldberg, M. M.; and Shelton-Davis, C. V. 2001. "Corrosive Alteration of N-reactor Fuel Exposed to Unsaturated Conditions Using Simulated Groundwater." *Back to the Future - Managing the Back End of the Nuclear Fuel Cycle to Create a More Secure Energy Future," Proceedings of the 9th International High-Level Radioactive Waste Management Conference (IHLRWM), Las Vegas, Nevada, April 29–May 3, 2001.* La Grange Park, Illinois: American Nuclear Society. TIC: 247873.

170980 Fortner, J.A.; Finch, R.J.; Kropf, A.J.; and Cunnane, J.C. 2003. "Re-Evaluating Neptunium in Uranyl Phases Derived from Corroded Spent Fuel." *Proceedings of the 10th International High-Level Radioactive Waste Management Conference*

(IHLRWM), March 30-April 2, 2003, Las Vegas, Nevada. Pages 764-771. La Grange Park, Illinois: American Nuclear Society. TIC: 254559.

172670 Friese, J.I.; Douglas, M.; Clark, S.B.; Buck, E. C.; and Hanson, B.D 2004. "Neptunium(V) Incorporation/Sorption with Uranium(VI) Alteration Products." Scientific Basis for Nuclear Waste Management XXVIII, Symposium held April 13-16, 2004, San Francisco, California, U.S.A. Hanchar, J.M.; Stroes-Gascoyne, S. and Browning, L.; eds. 824, 127-132. Warrendale, Pennsylvania: Materials Research Society. TIC: 256855.

144877 Garrels, R.M. and Christ, C.L. 1990. *Solutions, Minerals, and Equilibria.* Boston, Massachusetts: Jones and Bartlett Publishers. TIC: 223483.

173470 Gibson, W.M. 1961. *The Radiochemistry of Lead*. NAS-NS-3040. Washington, D.C.: National Academy of Science, National Research Council. TIC: 228855.

158382 Goldberg, S.; Forster, H.S.; and Godfrey, C.L. 1996. "Molybdenum Adsorption on Oxides, Clay Minerals, and Soils." *Soil Science Society of America Journal, 60,* 425-432. Madison, Wisconsin: Soil Science Society of America. TIC: 252573.

162391 Grambow, B.; Loida, A.; Martinez-Esparza, A.; Diaz-Arocas, P.; de Pablo, J.; Paul, J.L.; Marx, G.; Glatz, J.P.; Lemmens, K.; Ollila, K.; and Christensen, H. 2000. "Long-Term Safety of Radioactive Waste Disposal: Source Term for Performance Assessment of Spent Fuel as a Waste Form, Final Report." *Forchungszentrum Karlsruhe, Technik und Umwelk, FZKA 6420*. Karlsruhe, Germany: Forschungszentrum Karlsruhe GmbH. TIC: 254058.

161964 Grenthe, I. 1991. "Thermodynamics in Migration Chemistry." *Radiochimica Acta, 52/53,* (Part II), 425-432. München, Germany: R. Oldenbourg Verlag. TIC: 250613.

101671 Grenthe, I.; Fuger, J.; Konings, R.J.M.; Lemire, R.J.; Muller, A.B.; Nguyen-Trung, C.; and Wanner, H. 1992. *Chemical Thermodynamics of Uranium.* Volume 1 of *Chemical Thermodynamics.* Wanner, H. and Forest, I., eds. Amsterdam, The Netherlands: North-Holland Publishing Company. TIC: 224074.

109205 Guenther, R.J.; Blahnik, D.E.; Campbell, T.K.; Jenquin, U.P.; Mendel, J.E.; Thomas, L.E.; and Thornhill, C.K. 1988. *Characterization of Spent Fuel Approved Testing Material ATM–103.* PNL-5109-103. Richland, Washington: Pacific Northwest Laboratory. ACC: NNA.19911017.0104.

109206 Guenther, R.J.; Blahnik, D.E.; Campbell, T.K.; Jenquin, U.P.; Mendel, J.E.; and Thornhill, C.K. 1988. *Characterization of Spent Fuel Approved Testing Material–ATM-106.* PNL-5109-106. Richland, Washington: Pacific Northwest Laboratory. ACC: NNA.19911017.0105.

168382 Guillaumont, R.; Fanghänel, T.; Fuger, J.; Grenthe, I.; Neck, V.; Palmer, D.A.; and Rand, M.H. 2003. *Update on the Chemical Thermodynamics of Uranium, Neptunium,*

Plutonium, Americium and Technetium. Mompean, F.J.; Illemassene, M.; Domenech-Orti, C.; and Ben Said, K., eds. Chemical Thermodynamics 5. Amsterdam, The Netherlands: Elsevier. TIC: 255230.

100814 Harrar, J.E.; Carley, J.F.; Isherwood, W.F.; and Raber, E. 1990. *Report of the Committee to Review the Use of J-13 Well Water in Nevada Nuclear Waste Storage Investigations.* UCID-21867. Livermore, California: Lawrence Livermore National Laboratory. ACC: NNA.19910131.0274.

162001 Haschke, J.M. and Allen, T.H. 2002. "Equilibrium and Thermodynamic Properties of the PuO_{2+x} Solid Solution." *Journal of Alloys and Compounds, 336,* (1-2), 124-131. New York, New York: Elsevier. TIC: 253947.

162699 Haschke, J.M. and Bassett, R.L. 2002. "Control of Plutonium Dioxide Solubility by Amorphous Tetrahydroxide: A Critical Review of the Model." *Radiochimica Acta, 90*, (9-11), 505-509. München, Germany: Oldenbourg Verlag. TIC: 252601.

161911 Haschke, J.M. and Oversby, V.M. 2002. "Plutonium Chemistry: A Synthesis of Experimental Data and a Quantitative Model for Plutonium Oxide Solubility." *Journal of Nuclear Materials, 305,* (2-3), 187-201. New York, New York: Elsevier. TIC: 253028.

150367 Haschke, J.M.; Allen, T.H.; and Morales, L.A. 2000. "Reaction of Plutonium Dioxide with Water: Formation and Properties of PuO_{2+x}." *Science, 287,* [5451] 285-287. Washington, D.C: American Association for the Advancement of Science. TIC: 248119.

115670 Hem, J.D. 1985. *Study and Interpretation of the Chemical Characteristics of Natural Water. 3rd Edition*. U.S. Geological Survey Water-Supply Paper 2254. 3rd Edition. Washington, D.C.: U.S. Government Printing Office. ACC: NNA.19940427.0181.

105875 Hsu, P.H. 1995. "Aluminum Hydroxides and Oxyhydroxides." Chapter 7 of *Minerals in Soil Environments.* 2nd Edition. Dixon, J.B. and Weed, S.B., eds. SSSA Book Series, No. 1. Madison, Wisconsin: Soil Science Society of America. TIC: 237222.

170921 Hummel, W. and Berner, U. 2002. *Application of the Nagra/PSI TDB 01/01: Solubility of Th, U, Np, and Pu.* Nagra Technical Report 02-12. Wettingen, Switzerland: National Cooperative for the Disposal of Radioactive Waste. TIC: 256305.

161904 Hummel, W.; Berner, U.; Curti, E.; Pearson, F.J.; and Thoenen, T. 2002. *Nagra/PSI Chemical Thermodynamic Data Base 01/01.* Parkland, Florida: Universal Publishers. TIC: 253421.

159328 Jobe, D.J.; Lemire, R.J.; and Taylor, P. 1997. *Iron Oxide Redox Chemistry and Nuclear Fuel Disposal*. AECL-11667. Pinawa, Manitoba, Canada: Whiteshell Laboratories. TIC: 236264.

151237 Kielland, J. 1937. "Individual Activity Coefficients of Ions in Aqueous Solutions." *Journal of the American Chemical Society, 59,* (9), 1675-1678. Easton, Pennsylvania: The American Chemical Society. TIC: 248309.

122387 Kim J.I. and Kanellakopulos B. 1989. "Solubility Products of Plutonium(IV) Oxide and Hydroxide." *Radiochimica Acta, 48,* 145-150. Munich, Germany: R. Oldenbourg Verlag. TIC: 246360.

173080 Kirby, H.W. and Salutsky, M.L. 1964. *The Radiochemistry of Radium.* NAS-NS 3057. Washington, D.C.: National Academy of Science National Research Council. TIC: 228982.

172672 Kohler, M.; Honeyman, B.D.; and Leckie, J.O. 1999. "Neptunium (V) Sorption on Hematite (Alpha- Fe_2O_3) in Aqueous Suspension: The Effect of CO_2." *Radiochimica Acta, 85,* pp. 33-48. München, Germany: Oldenbourg Wissenschaftsverlag. TIC: 256909.

101702 Krauskopf, K.B. and Bird, D.K. 1995. *Introduction to Geochemistry.* 3rd Edition. New York, New York: McGraw-Hill. TIC: 239316.

173092 Kropf, A.J.; Finch, R.J.; Fortner, J.A.; Aase, S.; Karanfil, C.; Serge, C.U.; Terry, J.; Bunker, G.; and Chapman, L.D. 2003. "Bent Silicon Crystal in the Laue Geometry to Resolve X-Ray Fluorescenece for X-Ray Absorption Spectroscopy." *Review of Scientific Instruments, 74,* (11), 4696-4702. Philadelphia, Pennsylvania: American Institute of Physics. TIC: 256872.

173070 Kubato, K.A.H.; Helean, K.B.; Navrotsky, A.; and Burns, P.C. 2003. "Stability of Peroxide-Containing Uranyl Phases." *Science, 302,* pp. 1,191-1,193. Washington, D.C.: American Association for the Advancement of Science. TIC: 257044.

100051 Langmuir, D. 1997. *Aqueous Environmental Geochemistry.* Upper Saddle River, New Jersey: Prentice Hall. TIC: 237107.

106457 Langmuir, D. and Riese, A.C. 1985. "The Thermodynamic Properties of Radium." *Geochimica et Cosmochimica Acta, 49,* 1593-1601. New York, New York: Pergamon Press. TIC: 241035.

173072 Laul, J.C. and Maiti, T.C. 1990. "Natural Radionuclides in Groundwater from J-13 Well at the Nevada Test Site." High Level Radioactive Waste Management, Proceedings of the International Topical Meeting, Las Vegas, Nevada, April 8-12, 1990. 1,137-142. La Grange Park, IL: American Nuclear Society. TIC: 228982.

101706 Lemire, R.J. 1984. *An Assessment of the Thermodynamic Behaviour of Neptunium in Water and Model Groundwaters from 25 to 150°C.* AECL-7817. Pinawa, Manitoba, Canada: Atomic Energy of Canada Limited. TIC: 238910.

101876 Lide, D.R., ed. 1995. *CRC Handbook of Chemistry and Physics.* 76th Edition. Boca Raton, Florida: CRC Press. TIC: 216194.

160832 Lide, D.R., ed. 2002. *CRC Handbook of Chemistry and Physics.* 83rd Edition. Boca Raton, Florida: CRC Press. TIC: 253582.

100917 Marsh, G.P. and Taylor, K.J. 1988. "An Assessment of Carbon Steel Containers for Radioactive Waste Disposal." *Corrosion Science, 28,* (3), 289-320. Oxford, England: Pergamon Press. TIC: 223393.

172755 Martínez-Esteban, A.; Esteban, J.A.; Quiñones, J.; de Pablo, J.; Casas, I.; Giménez, J.; Clarens, F.; Rovira, M.; Merino, J.; Cera, E.; Bruno, J.; and Ripoll, S. 2002. "Modelling Spent Fuel and HLW Behaviour in Repository Conditions." *Workshop of Spent Fuel Behavior Modelling, 5th Euratom Framework Programme*. SFS Project, Avila. June 2002. Madrid, Spain: Empresa Naciaonal de Residuas Radiactivos, S.A.. TIC: 256908.

172673 McNamara, B.; Buck, E.; and Hanson, B. 2003. "Observation of Studtite and MetaStudtite on Spent Fuel." *Scientific Basis for Nuclear Waste Management XXVI, Symposium held December 2-5, 2002, Boston, Massachusetts.* Finch, R.J. and Bullen D.B. eds.. *757,* pp. 401-406. Warrendale, Pennsylvania: Materials Research Society. TIC: 254940.

173085 McNamara, B.; Hanson, B.; Buck, E.; and Soderquist, C. 2004. "A Radiochemical Analyses of Metastudtite and Leachates from Spent Fuel." *Scientific Basis for Nuclear Waste Management XXVIII, Symposium held April 13-16, 2004, San Francisco, California U.S.A.* Hanchar, J.M.; Stroes-Gascoyne, S. and Browning, L.; eds. *824,*. Warrendale, Pennsylvania: Materials Research Society. TIC: 256855.

159327 Misawa, T.; Hashimoto, K.; and Shimodaira, S. 1974. "The Mechanism of Formation of Iron Oxide and Oxyhydroxides in Aqueous Solutions at Room Temperature." *Corrosion Science, 14,* 131-149. New York, New York: Pergamon Press. TIC: 212539.

100469 Murphy, W.M. 1995. "Natural Analogs for Yucca Mountain." *Radwaste Magazine, 2*, (6), 44-50. La Grange Park, Illinois: American Nuclear Society. TIC: 237929.

101731 Murphy, W.M. 1997. "Retrograde Solubilities of Source Term Phases." *Scientific Basis for Nuclear Waste Management XX, Symposium held December 2-6, 1996, Boston, Massachusetts.* Gray, W.J. and Triay, I.R., eds. *465,* 713-720. Pittsburgh, Pennsylvania: Materials Research Society. TIC: 238884.

168433 Murphy, W.M. and Shock, E.L. 1999. "Environmental Aqueous Geochemistry of Actinides." Chapter 5 of *Uranium: Mineralogy, Geochemistry and the Environment.* Burns, P.C. and Finch, R.J., eds. Reviews in Mineralogy Volume 38. Washington, D.C.: Mineralogical Society of America. TIC: 247121.

170922 NAGRA (National Cooperative for the Disposal of Radioactive Waste) 2002. *Project Opalinus Clay, Safety Report, Demonstration of Disposal Feasibility for Spent Fuel, Vitrified High-Level Waste and Long-Lived Intermediate-Level Waste*

(Entsorgungsnachweis). NAGRA NTB 02-05. Wettingen, Switzerland: National Cooperative for the Disposal of Radioactive Waste. TIC: 254437.

172674 Nakata, K.; Nagasaki, S.; Tanaka, S.; Sakamoto, Y.; Tanaka, T.; and Ogawa, H. 2002. "Sorption and Reduction of Neptunium(V) on the Surfaces of Iron Oxides." *Radiochimica Acta, 90,* pp. 665-669. München, Germany: Oldenbourg Wissenschaftsverlag. TIC: 252601.

172675 Nakata, K.; Nagasaki, S.; Tanaka, S.; Sakamoto, Y.; Tanaka, T.; and Ogawa, H. 2004. "Reduction Rate of Neptunium(V) in Heterogenous Solution with Magnetite." *Radiochimica Acta, 92,* pp. 145-149. München, Germany: Oldenbourg Wissenschaftsverlag. TIC: 252601.

172676 Nakayama, S. and Sakamoto, Y. 1991. "Sorption of Neptunium on Naturally-Occurring Iron-Containing Minerals." *Radiochimica Acta, 52/53,*. 153-157. München, Germany: Oldenbourg Wissenschaftsverlag. TIC: 238750.

168258 Neck, V. and Kim, J.I. 2001. "Solubility and Hydrolysis of Tetravalent Actinides." *Radiochimica Acta, 89,* (1), 1-16. München, Germany: Oldenbourg Wissenschaftsverlag. TIC: 250728.

173043 Neck, V.; Kim, J.I. 2000. "An Electrostatic Approach for the Prediction of Actinide Complexation Constants with Inorganic LigandsApplication to Carbonate Complexes." *Radiochimica Acta, 88*, 815-822. München, Germany: Oldenbourg Wissenschaftsverlag. TIC: 257059.

168259 Neck, V.; Müller, R.; Bouby, M.; Altmaier, M.; Rothe, J.; Denecke, M.A.; and Kim, J.I. 2002. "Solubility of Amorphous Th(IV) Hydroxide – Application of LIBD to Determine the Solubility Product and EXAFS for Aqueous Speciation." *Radiochimica Acta, 90,* (09/11), 485-494. München, Germany: Oldenbourg Wissenchaftsverlag. TIC: 255812.

155218 Nitsche, H.; Gatti, R.C.; Standifer, E.M.; Lee, S.C.; Müller, A.; Prussin, T.; Deinhammer, R.S.; Maurer, H.; Becraft, K.; Leung, S.; and Carpenter, S.A. 1993. *Measured Solubilities and Speciations of Neptunium, Plutonium, and Americium in a Typical Groundwater (J-13) from the Yucca Mountain Region*. LA-12562-MS. Los Alamos, New Mexico: Los Alamos National Laboratory. ACC: NNA.19930507.0136.

144515 Nitsche, H.; Roberts, K.; Prussin, T.; Muller, A.; Becraft, K.; Keeney, D.; Carpenter, S.A.; and Gatti, R.C. 1994. *Measured Solubilities and Speciations from Oversaturation Experiments of Neptunium, Plutonium, and Americium in UE-25P #1 Well Water from the Yucca Mountain Region Milestone Report 3329-WBS1.2.3.4.1.3.1.* LA-12563-MS. Los Alamos, New Mexico: Los Alamos National Laboratory. TIC: 210589.

153965 Nordstrom, D. K. and Munoz, J. L. 1986. *Geochemical Thermodynamics*. Palo Alto, CA. Blackwell Scientific. TIC: 208228.

163274 NRC (U.S. Nuclear Regulatory Commission) 2003. *Yucca Mountain Review Plan, Final Report.* NUREG-1804, Rev. 2. Washington, D.C.: U.S. Nuclear Regulatory Commission, Office of Nuclear Material Safety and Safeguards. TIC: 254568.

159027 OECD (Organisation for Economic Co-operation and Development, Nuclear Energy Agency) 2001. *Chemical Thermodynamics of Neptunium and Plutonium. Volume 4 of Chemical Thermodynamics*. New York, New York: Elsevier. TIC: 209037.

150834 Osthols, E.; Bruno, J.; and Grenthe, I. 1994. "On the Influence of Carbonate on Mineral Dissolution: III. The Solubility of Microcrystalline ThO_2 in CO_2-H_2O Media." *Geochimica et Cosmochimica Acta, 58,* (2), 613-623. New York, New York: Pergamon. TIC: 245115.

159511 Parkhurst, D.L. and Appelo, C.A.J. 1999. *User's Guide to PHREEQC (Version 2)—A Computer Program for Speciation, Batch-Reaction, One-Dimensional Transport, and Inverse Geochemical Calculations.* Water-Resources Investigations Report 99-4259. Denver, Colorado: U.S. Geological Survey. TIC: 253046.

173073 Peacey, V.; Yanful, E.K.; and Payne, R. 2002. "Field Study of Geochemistry and Solute Fluxes in Flooded Uranium Mine Tailings." Canadian Geotechnical Journal, 39, 357-376. Ottawa, Ontario, Canada: National Research Council of Canada. TIC: 257054.

130197 Pearcy, E.C. and Murphy, W.M. 1991. *Geochemical Natural Analogs Literature Review*. CNWR 90-008. San Antonio, Texas: Center for Nuclear Waste Regulatory Analyses. TIC: 213164.

100486 Pearcy, E.C.; Prikryl, J.D.; Murphy, W.M.; and Leslie, B.W. 1994. "Alteration of Uraninite from the Nopal I Deposit, Pena Blanca District, Chihuahua, Mexico, Compared to Degradation of Spent Nuclear Fuel in the Proposed U.S. High-Level Nuclear Waste Repository at Yucca Mountain, Nevada." *Applied Geochemistry, 9,* 713-732. New York, New York: Elsevier. TIC: 236934.

159329 Pednekar, S.P. 1987. *Final Report on Corrosion of Carbon Steel in Aqueous Environments at Temperatures Below Boiling - A Literature Review to Electric Power Research Institute, February 24, 1987*. Columbus, Ohio: Battelle, Columbus Division. TIC: 224492.

161925 Quinones, J.; Grambow, B.; Loida, A.; and Geckeis, H. 1996. "Coprecipitation Phenomena During Spent Fuel Dissolution. Part 1: Experimental Procedure and Initial Results on Trivalent Ion Behaviour." *Journal of Nuclear Materials, 238*, (1), 38-43. Amsterdam, The Netherlands: Elsevier. TIC: 252663.

122768 Rai, D 1984. "Solubility Product of Pu(IV) Hydrous Oxide and Equilibrium Constants of Pu(IV)/Pu(V), Pu(IV)/Pu(VI), and Pu(V)/Pu(VI) Couples." *Radiochimica Acta, 35,* 97-106. Munchen, German: Oldenbourg Verlag. TIC: 219109.

112060 Rai, D. and Ryan, J.L. 1982. "Crystallinity and Solubility of Pu(IV) Oxide and Hydrous Oxide in Aged Aqueous Suspensions." *Radiochimica Acta, 30,* 213-216. München, Germany: R. Oldenbourg Verlag. TIC: 219107.

144599 Rai, D. and Swanson, J.L. 1981. "Properties of Plutonium(IV) Polymer of Environmental Importance." *Nuclear Technology, 54,* (1), 107-112. La Grange Park, Illinois: American Nuclear Society. TIC: 221390.

168392 Rai, D.; Moore, D.A.; Felmy, A.R.; Choppin, G.R.; and Moore, R.C. 2001. "Thermodynamics of the PuO_2^+-Na^+-OH^--Cl^--ClO_4^--H_2O System: Use of NpO_2^+ Pitzer Parameters for PuO_2^+." *Radiochimica Acta, 89,* (8), 491-498. München, Germany: Oldenbourg Wissenschaftsverlag. TIC: 255398.

173045 Rai, D.; Moore, D.A.; Oakes, C.S.; and Yui, M. 2000. "Thermodynamic Model for the Solubility of Thorium Dioxide in the Na^+-$Cl^-OH^-H_2O$ System at 23°C and 90°C." *Radiochimica Acta, 88,* 297-306. München, Germany: Oldenbourg Wissenschaftsverlag. TIC: 257055.

144598 Rai, D.; Strickert, R.G.; and McVay, G.L. 1982. "Neptunium Concentrations in Solutions Contacting Actinide-Doped Glass." *Nuclear Technology*, 58, 69-76. La Grange Park, Illinois: American Nuclear Society. TIC: 248048.

159354 Raman, A. and Nasrazadani, S. 1990. "Packing Corrosion in Bridge Structures." *Corrosion, 46,* (7), 601-605. Houston, Texas: National Association of Corrosion Engineers. TIC: 235061.

154847 Rickard, D.T. and Nriagu, J.O. 1978. "Aqueous Environmental Chemistry of Lead." Chapter 8 of *The Biogeochemistry of Lead in the Environment*. Nriagu, J.O., ed. New York, New York: Elsevier. TIC: 248543.

162536 Roberts, K.E.; Wolery, T.J.; Atkins-Duffin, C.E.; Prussin, T.G.; Allen, P.G.; Bucher, J.J.; Shuh, D.K.; Finch, R.J.; and Prussin, S.G. 2003. "Precipitation of Crystalline Neptunium Dioxide from Near-Neutral Aqueous Solution." *Radiochimica Acta, 91*, (2), 87-92. München, Germany: Oldenbourg Wissenschaftsverlag. TIC: 254035.

107105 Roberts, W.L.; Campbell, T.J.; and Rapp, G.R., Jr. 1990. *Encyclopedia of Minerals.* 2nd Edition. New York, New York: Van Nostrand Reinhold. TIC: 242976.

108567 Robinson, R.A. and Stokes, R.H. 1965. *Electrolyte Solutions, The Measurement and Interpretation of Conductance, Chemical Potential and Diffusion in Solutions of Simple Electrolytes*. 2nd Edition (Revised). Washington, D.C.: Butterworth. TIC: 242575.

168432 Runde, W.; Conradson, S.D.; Efurd, D.W.; Lu, N.P.; VanPelt, C.E.; and Tait, C.D. 2002. "Solubility and Sorption of Redox-Sensitive Radionuclides (Np, Pu) in J-13 Water from the Yucca Mountain Site: Comparison between Experiment and Theory." *Applied Geochemistry, 17,* (6), 837-853. New York, New York: Pergamon. TIC: 254046.

173042 Ryan, J.L.; Rai, D. 1987. "Thorium(IV) Hydrous Oxide Solubility." *Inorganic Chemistry*, 26, (24), 4140-4142. Washington, D.C.: American Chemical Society: TIC: 257043.

173091 Sattonnay, G.; Ardois, C.; Lucchini, J.F.; Barthe, M.F.; Garrido, F.; and Gosset 2001. "Alpha-Radiolysis Effects on UO_2 Alteration in Water." Journal of Nuclear Materials, 288, pp. 11-19. Amsterdam, Netherlands: North-Holland. TIC: 256824.

144629 Schwertmann, U. and Cornell, R.M. 1991. *Iron Oxides in the Laboratory: Preparation and Characterization.* New York, New York: VCH Publishers. TIC: 237942.

105959 Schwertmann, U. and Taylor, R.M. 1995. "Iron Oxides." Chapter 8 of *Minerals in Soil Environments.* 2nd Edition. Dixon, J.B. and Weed, S.B., eds. SSSA Book Series, No. 1. Madison, Wisconsin: Soil Science Society of America. TIC: 237222.

153587 Shannon, R.D. 1976. "Revised Effective Ionic Radii and Systematic Studies of Interatomic Distances in Halides and Chalcogenides." *Acta Crystallographica, A32,* (5), 751-767. Copenhagen, Denmark: Munksgaard International Publishers. TIC: 240561.

161998 Shibutani, T.; Shibutani, S.; and Yui, M. 1998. *Database Development of Chemical Thermodynamics of Protactinium for Performance Assessment of HLW Geological Disposal System*. Tokyo, Japan: Tokai Works, Power Reactor and Nuclear Fuel Development Corporation. TIC: 251126.

162405 Shoesmith, D.W. 2000. "Fuel Corrosion Processes under Waste Disposal Conditions." *Journal of Nuclear Materials, 282,* (1), 1-31. Amsterdam, The Netherlands: North-Holland. TIC: 254043.

112092 Silva, R.J. and Nitsche, H. 1995. "Actinide Environmental Chemistry." *Radiochimica Acta, 70/71,* 377-396. München, Germany: R. Oldenbourg Verlag. TIC: 243223.

102087 Silva, R.J.; Bidoglio, G.; Rand, M.H.; Robouch, P.B.; Wanner, H.; and Puigdomenech, I. 1995. *Chemical Thermodynamics of Americium.* Volume 2 of *Chemical Thermodynamics.* Amsterdam, The Netherlands: Elsevier. TIC: 237106.

161956 Steinborn, T.L.; Wolery, T.J.; Alcorn, S.R.; Arthur, S.E.; Bernot, P.A.; Brady, P.V.; Chen, Y.; Domski, P.S.; Jolley, D.M.; Metcalf, R.C.; and Thomas, E. 2003. *Data Qualification: Update and Revision of the Geochemical Thermodynamic Database, Data0.ymp*. TDR-EBS-MD-000022 REV 00. Las Vegas, Nevada: Bechtel SAIC Company. ACC: DOC.20030331.0003.

111047 Stout, R.B. and Leider, H.R. 1998. *Waste Form Characteristics Report, CD-ROM Version*. UCRL-ID-132375. Livermore, California: Lawrence Livermore National Laboratory. TIC: 246106.

125332 Stumm, W. and Morgan, J.J. 1996. *Aquatic Chemistry, Chemical Equilibria and Rates in Natural Waters.* 3rd Edition. New York, New York: John Wiley & Sons. TIC: 246296.

163048 Thomas, E. 2003. "Transmittal of Unsaturated Testing of Bare Spent UO_2 Fuel Fragments: Data Report, Argonne National Laboratory." Interoffice memorandum from E. Thomas (BSC) to J.C. Cunnane, July 2, 2003, 0702037939, with attachment. ACC: MOL.20030702.0116; MOL.20030311.0097.

144644 Tochiyama, O.; Endo, S.; and Inoue, Y. 1995. "Sorption of Neptunium(V) on Various Iron Oxides and Hydrous Iron Oxides." *Radiochimica Acta, 68,* (2), 105-111. München, Germany: R. Oldenbourg Verlag. TIC: 238248.

168394 Toth, L.M.; Friedman, H.A.; and Osborne, M.M. 1983. "Aspects of Plutonium(IV) Hydrous Polymer Chemistry." Chapter 15 of *Plutonium Chemistry.* Carnall, W.T. and Choppin, G.R., eds. ACS Symposium Series 216. Washington, D.C.: American Chemical Society. TIC: 219103.

170136 Truesdell, A.H. and Jones, B.F. 1974. "WATEQ, A Computer Program for Calculating Chemical Equilibria of Natural Waters." *Journal of Research of the U.S. Geological Survey, 3,* (2), 233-248. Menlo Park, California: U.S. Geological Survey. TIC: 224163.

159216 Wagman, D.D.; Evans, W.H.; Parker, V.B.; Schumm, R.H.; Halow, I.; Bailey, S.M.; Churney, K.L.; and Nuttall, R.L. 1982. "The NBS Tables of Chemical Thermodynamic Properties, Selected Values for Inorganic and C_1 and C_2 Organic Substances in SI Units." *Journal of Physical and Chemical Reference Data, 11,* (Supplement No. 2), Pages 2-276 and 2-282. Washington, D.C.: American Chemical Society. TIC: 239715.

113466 Werme, L.O. and Spahiu, K. 1998. "Direct Disposal of Spent Nuclear Fuel: Comparison Between Experimental and Modelled Actinide Solubilities in Natural Waters." *Journal of Alloys and Compounds, 271-273,* 194-200. Lausanne, Switzerland: Elsevier. TIC: 243085.

100949 Wilson, C.N. 1990. *Results from NNWSI Series 2 Bare Fuel Dissolution Tests.* PNL-7169. Richland, Washington: Pacific Northwest Laboratory. ACC: NNA.19900814.0048.

100793 Wilson, C.N. 1990. *Results from NNWSI Series 3 Spent Fuel Dissolution Tests.* PNL-7170. Richland, Washington: Pacific Northwest Laboratory. ACC: NNA.19900329.0142.

100836 Wolery, T.J. 1992. *EQ3NR, A Computer Program for Geochemical Aqueous Speciation-Solubility Calculations: Theoretical Manual, User's Guide, and Related Documentation (Version 7.0).* UCRL-MA-110662 PT III. Livermore, California: Lawrence Livermore National Laboratory. ACC: MOL.19980717.0626.

163350 Wronkiewicz, D.J.; Bates, J.K.; Buck, E.C.; Hoh, J.C.; Emery, J.W.; and Wang, L.M. 1997. *Radiation Effects in Moist-Air Systems and the Influence of Radiolytic Product Formation on Nuclear Waste Glass Corrosion.* ANL-97/15. Argonne, Illinois: Argonne National Laboratory. TIC: 234821.

100493 Wronkiewicz, D.J.; Bates, J.K.; Gerding, T.J.; Veleckis, E.; and Tani, B.S. 1992. "Uranium Release and Secondary Phase Formation During Unsaturated Testing of UO_2 at 90°C." *Journal of Nuclear Materials, 190,* 107-127. Amsterdam, The Netherlands: North-Holland Publishing Company. TIC: 236558.

102047 Wronkiewicz, D.J.; Bates, J.K.; Wolf, S.F.; and Buck, E.C. 1996. "Ten-Year Results from Unsaturated Drip Tests with UO_2 at 90°C: Implications for the Corrosion of Spent Nuclear Fuel." *Journal of Nuclear Materials, 238,* (1), 78-95. Amsterdam, The Netherlands: North-Holland Publishing Company. TIC: 243361.

162664 Yui, M.; Azuma, J.; and Shibata, M. 1999. *JNC Thermodynamic Database for Performance Assessment of High-Level Radioactive Waste Disposal System*. JNC TN8400 99-070. Tokyo, Japan: Tokai Works, Japan Nuclear Cycle Development Institute. TIC: 251129.

171238 Zarrabi, K.; McMillan, S.; Elkonz, S.; and Cizdziel, J. 2003. *Corrosion and Mass Transport Processes in Carbon Steel Miniature Waste Packages.* Document TR-03-003, Rev. 0. Task 34. Las Vegas, Nevada: University of Nevada, Las Vegas. ACC: MOL.20040202.0079.

9.2 CODES, STANDARDS, REGULATIONS, AND PROCEDURES

173164 10 CFR 63. 2004 Energy: Disposal of High-Level Radioactive Wastes in a Geologic Repository at Yucca Mountain, Nevada. ACC: MOL.20050323.0071.

AP-2.22Q, Rev. 1, ICN 1. *Classification Analyses and Maintenance of the Q-List.* Washington, D.C.: U.S. Department of Energy, Office of Civilian Radioactive Waste Management. ACC: DOC.20040714.0002.

LP-2.29Q-BSC, Rev. 0, ICN 0. *Planning for Science Activities*. Washington, D.C.: U.S. Department of Energy, Office of Civilian Radioactive Waste Management. ACC: DOC.20050114.0001.

LP-SI.11Q-BSC, Rev. 0, ICN 1. *Software Management*. Washington, D.C.: U.S. Department of Energy, Office of Civilian Radioactive Waste Management. ACC: DOC.20041005.0008.

LP-SIII.10Q-BSC, Rev. 0, ICN 01. *Models*. Washington, D.C.: U.S. Department of Energy, Office of Civilian Radioactive Waste Management. ACC: DOC.20050623.0001.

105725 ASTM C 1174-97. 1998. *Standard Practice for Prediction of the Long-Term Behavior of Materials, Including Waste Forms, Used in Engineered Barrier Systems*

(EBS) for Geological Disposal of High-Level Radioactive Waste. West Conshohocken, Pennsylvania: American Society for Testing and Materials. TIC: 246015.

165003 ASTM A 240/A 240M-03b. 2003. *Standard Specification for Chromium and Chromium-Nickel Stainless Steel Plate, Sheet, and Strip for Pressure Vessels and for General Applications*. West Conshohocken, Pennsylvania: American Society for Testing and Materials. TIC: 254845.

162723 ASTM A 516/A 516M-01. 2001. *Standard Specification for Pressure Vessel Plates, Carbon Steel, for Moderate- and Lower-Temperature Service.* West Conshohocken, Pennsylvania: American Society for Testing and Materials. TIC: 253997.

144744 ASTM B 209–96. 1996. *Standard Specification for Aluminum and Aluminum-Alloy Sheet and Plate.* West Conshohocken, Pennsylvania: American Society for Testing and Materials. TIC: 247078.

168403 ASTM B 932-04. 2004. *Standard Specification for Low-Carbon Nickel-Chromium-Molybdenum-Gadolinium Alloy Plate, Sheet, and Strip.* West Conshohocken, Pennsylvania: American Society for Testing and Materials. TIC: 255846.

9.3 SOURCE AND CORROBORATIVE DATA, LISTED BY DATA TRACKING NUMBER

160899 GS020408312272.003. Collection and Analysis of Pore Water Samples for the Period from April 2001 to February 2002. Submittal date: 04/24/2002.

149202 LA0004AM831234.001. Flow-Through Cell Measurements for NC-EWDP-01S, 22-Feb-99 and 23-Feb-99. Submittal date: 04/17/2000.

149213 LA0004AM831234.002. Downhole Probe Measurements for NC-EWDP-03S, 23-Feb-99. Submittal date: 04/17/2000.

160051 LA0206AM831234.001. Eh-pH Field Measurements on Nye County EWDP Wells. Submittal date: 06/21/2002.

149196 LA9907AM831234.003. Downhole Eh and pH Measurements for NC-EWDP-01D, 11-Jan-99. Submittal date: 01/27/2000.

149209 LA9907AM831234.009. Flow-through Cell Measurements for NC-EWDP-01S, NC-EWDP-03S, NC-EWDP-09SX, 5/17/99, 5/18/99, 5/19/99, 5/20/99. Submittal date: 01/27/2000.

149210 LA9907AM831234.010. Flow-Through Cell Measurements for SD6-ST1, 2-Jun-99 and 8-Jun-99. Submittal date: 01/27/2000.

168347 LAAM831311AQ98.003. Downhole Eh and pH Measurements for UE-25 WT#17. Submittal date: 09/14/1998.

168346 LAAM831311AQ98.004. Downhole Eh and pH Measurements for UE-25 WT#3. Submittal date: 09/14/1998.

149181 LAAM831311AQ98.005. Geochemical Field Measurements for UE-25 WT#17, 27-Jan-98. Submittal date: 09/14/1998.

149520 LAAM831311AQ98.007. Flow-Thru Cell and Static Measurements at UE-25 WT#3, 22-Jun-98. Submittal date: 09/14/1998.

149521 LAAM831311AQ98.008. Analysis of Bailed Sample for UE-25 WT#17, 04 Jun 98. Submittal date: 09/14/1998.

168348 LAAM831311AQ98.009. Flow through Cell Measurements for UE-25 WT#17, 01-Jul-98. Submittal date: 09/14/1998.

129285 LL991001251021.090. Draft - CSNF Waste Form Degradation: Unsaturated Drip Tests - G2020 Analysis and Modeling Report. Submittal date: 10/04/1999.

151029 MO0006J13WTRCM.000. Recommended Mean Values of Major Constituents in J-13 Well Water. Submittal date: 06/07/2000.

161756 MO0302SPATHDYN.000. Thermodynamic Data Input Files - Data0.YMP.R2. Submittal date: 02/05/2003.

170760 MO0407SEPFEPLA.000. LA FEP List. Submittal date: 07/20/2004.

172759 SN0410T0510404.001. Corrections to Errors in the DATA0.YMP.R2 Thermodynamic Database. Submittal date: 11/01/2004.

9.4 OUTPUT DATA, LISTED BY DATA TRACKING NUMBER

MO0501SPADISCN.000. Dissolved Concentration Limits of Elements with Radioactive Isotopes. Submittal Date: 01/26/2005.

9.5 SOFTWARE CODES

173680 *Software Code: GetEQData*. V. 1.0.1. PC w/Windows 2000. 10809-1.0.1-00.

153964 *Software Code: EQ3/6.* V7.2b. UCRL-MA-110662 (LSCR198).

155520 *Software Routine: BUILDEQ3.BAS.* V1.0. PC, Windows NT 4.0. 10365-1.00-00.

159731 *Software Code: EQ6*, Version 7.2bLV. PC. 10075-7.2bLV-02. Windows NT, 2000.

APPENDIX I
CD-ROM

INTENTIONALLY LEFT BLANK

APPENDIX II
LIST OF COMPUTER FILES

INTENTIONALLY LEFT BLANK

II. LIST OF COMPUTER FILES

This appendix contains the name and size of the .zip file placed on the electronic media (Appendix I). Winzip 8.1 was used to compress the files.

```
Directory of D:\

03/22/2005  04:40p      <DIR>          Am
06/20/2005  08:11a      <DIR>          general
03/22/2005  04:40p      <DIR>          Np
03/22/2005  04:41p      <DIR>          Pa
03/22/2005  04:41p      <DIR>          Pu
03/22/2005  04:41p      <DIR>          Ra
03/22/2005  04:41p      <DIR>          Sensitivities
03/22/2005  04:42p      <DIR>          sigma plots
03/22/2005  04:42p      <DIR>          Th
03/22/2005  04:42p      <DIR>          U
06/28/2005  04:21p      <DIR>          validation

Directory of D:\Am

03/22/2005  02:42p          12,998,434 Am EQ3 runs.zip
03/22/2005  02:42p             718,815 Am spreadsheets.zip
               2 File(s)     13,717,249 bytes

Directory of D:\general

06/20/2005  08:11a             174,149 general.zip
               1 File(s)        174,149 bytes

Directory of D:\Np

05/17/2005  09:17a          55,431,896 Np EQ3 runs.zip
05/17/2005  09:20a           2,339,078 Np spreadsheets.zip
               2 File(s)     57,770,974 bytes

Directory of D:\Pa

03/22/2005  03:00p          27,913,677 Pa EQ3 runs.zip
03/22/2005  03:02p             594,128 Pa spreadsheets.zip
               2 File(s)     28,507,805 bytes

Directory of D:\Pu

03/22/2005  03:14p          70,220,155 Pu EQ3 runs.zip
05/17/2005  09:21a           1,675,139 Pu spreadsheets.zip
               2 File(s)     71,895,294 bytes

Directory of D:\Ra

03/22/2005  03:17p           1,582,088 Ra EQ3 files.zip
```

```
03/22/2005  03:18p             154,857 Ra spreadsheets.zip
               2 File(s)      1,736,945 bytes

Directory of D:\Sensitivities

03/22/2005  03:28p          46,547,857 sens EQ3 files.zip
03/22/2005  03:28p             420,167 sens Spreadsheets.zip
               2 File(s)     46,968,024 bytes

Directory of D:\sigma plots

03/22/2005  03:29p             211,801 sigmaplots.zip
               1 File(s)        211,801 bytes

Directory of D:\Th

03/22/2005  03:31p          12,840,090 Th EQ3 runs.zip
05/17/2005  09:21a             820,876 Th spreadsheets.zip
               2 File(s)     13,660,966 bytes

Directory of D:\U

03/22/2005  03:49p         204,160,281 U Eq3-6 runs.zip
05/17/2005  09:22a           4,365,780 U spreadsheets.zip
               2 File(s)    208,526,061 bytes

Directory of D:\validation

06/28/2005  04:21p           1,329,902 validation.zip
               1 File(s)      1,329,902 bytes

     Total Files Listed:
              19 File(s) 444,499,170 bytes
```

The zip files contain files of various types:

Excel files (extensions = xls)

EQ3 input files (extension = 3i)

EQ6 input files (extension = 6i)

ASCII text file: provides input parameters for EQ3

EQ3 output files (extension = 3o)

EQ6 output files (extension = 6o)

ASCII text file: provides detailed information about the system at each print point, which is specified by the user in the input file

EQ3/6 text data files used for the calculations, *Data0.ymp.R2* and *Data0.yc3.R1*

Winzip files (extension = zip).

INTENTIONALLY LEFT BLANK

APPENDIX III
EVALUATION OF DISSOLVED CONCENTRATION LIMITS OF NEPTUNIUM AND PLUTONIUM

INTENTIONALLY LEFT BLANK

III. EVALUATION OF DISSOLVED CONCENTRATION LIMITS OF NEPTUNIUM AND PLUTONIUM

The following evaluation was performed by Dr. Greg Choppin (GC) on 8/20/2004 under direction from *Technical Work Plan for: Regulatory Integration Modeling and Analysis of the Waste Form and Waste Package* (BSC 2004 [DIRS 171583]). Since this review was done, the TWP was updated to *Technical Work Plan for Postclosure Waste Form Modeling* (BSC 2005 [DIRS 173246]). However, since the Pu model has not changed since this update, this review is still used as part of the independent technical review for the Pu-solubility model. The questions required by the TWP (BSC 2005 [DIRS 173246]) for the independent technical review include the two questions below, as well as "Is the model adequate and appropriate for its intended use" (Section 7.2). Dr. Choppin's review does not answer this question, which is a deviation from the current TWP (BSC 2005 [DIRS 173246]).

The evaluation by Dr. Choppin (GC) raised several questions that were answered by Patricia A. Bernot (PAB) below:

This is a review of Sections 6.5 (Plutonium Solubility).

To answer the two principle questions:

1. Do the treatments of the kinetic and thermodynamic factors adequately capture the behavior of the radionuclides over geologic timeframes?

   - (GC) The treatment of the thermodynamic and with kinetic factors is somewhat brief, especially if geologic times are considered. The text associated for Sections 6.5 and 6.6 speak of the effects of CO_3^{2-}, OH^-, F^- complexation but do not cite the stability constants and the ionic strength associated with these, in the modeling. Earlier, I had reviewed some of the reports and publications used in some of the model calculations for Pu but did not have time today to check these. To allow validation of these reports for the NRC, some better documentation of the values used in modeling seems necessary. Also, in this report there is no evaluation of the effect of ionic strength or temperature on these modeling parameters – both in the thermodynamics and the kinetics. If the evaluation is to be for time spans of millennia, this seems very necessary. The treatment of the thermodynamic modeling for solubility and speciation is probably acceptable for 298°C (where most complexation constants have been measured) but questionable if YMT is a "hot repository." Similarly, the solubility, redox, complexation, etc.kinetics are very temperature dependent. Whenever kinetics are discussed for speciation or solubility modeling, or both, the temperature must be cited and the effects of temperature change over time should be included in the calculations.

   - (PAB) Actinide solubility is recognized as very complex and dependent upon temperature, pH, fugacity of CO_2 and O_2, etc. The effects of these parameters on solubility limits of elements with radioactive isotopes are only given a brief overview in Chapters 6.5 and 6.6, since they are covered elsewhere in the report. Sections 6.3 and 6.4 provide discussions on the effects different conditions have on

solubilities. These include temperature, oxidation potential, pH, CO_2 fugacity, and water composition. Fugacity of CO_2 and pH are already taken into account in model outputs, which present solubility limits as a function of pH and CO_2 fugacity. Justification for solubility modeling at atmospheric oxygen levels and ambient temperatures are outlined in Sections 6.4.2.1 and 6.4.2.2, respectively. The effects of water chemistry are studied in depth in a sensitivity analysis presented in Section 6.4.2.5. Any ions (such as fluoride) shown to have a large effect on solubilities are included as an uncertainty term in the model as indicated in Section 6.4.3.6. Time also plays a crucial factor in determining solubility limits. It is impossible to know for what time periods a kinetic system will dominate over a thermodynamically stable system in a repository over geologic time scales. For this reason, modeling uses conservative bases to choose solubility-controlling phases and aqueous species.

2. Is the value for Eh implemented in the model consistent with conditions expected in the repository over geologic timeframes?

   - (GC) Evaluation of E_h effects is difficult. In natural systems, the measured E_h for the aquatic media is often irrelevant for modeling of the behavior of metal ion systems due to localized conditions. Sorbed materials (e.g., humic material, biota etc.) can induce redox behaviors not related to the gross E_h of the solution. As a result, it is difficult to predict redox behavior in environmental systems. This would become more of a problem over time as the repository ages and conditions change. The E_h effect in homogenous true solutions (no colloids or suspended material) is usually predictable but the abnormal redox occurs on surfaces of colloids, etc. Since, in a repository, colloids and suspended material is most likely, calculations of speciation, etc. based on E_h values for true solutions is to be treated with caution. If E_h is accepted in the YMT systems, the calculations in Sections 6.5 and 6.6 seem well done. Nevertheless, the reliability of such calculations in this case should be discussed.

   - (PAB) As indicated in Section 6.4.2.1, the repository is designed so the waste is under atmospheric conditions except in isolated local situations. Thus, oxidizing conditions are assumed as indicated in Section 5.1. Additionally, solubility limits of elements with radioactive isotopes are known to be less soluble in reduced conditions than in fully oxidized systems. Therefore, the treatment of solubilities in a fully oxidized system is conservative and is indicated as such in the report.

At a later time, Dr. Choppin also brought up a concern related to the clarity of what the report defines as colloidal and dissolved Pu. This was answered by addition of text to the second paragraph of Section 6.5.1.

Concurrence with the text changes and answers to concerns is located in Section 7.2.1.

An independent technical review was conducted on the new Np-solubility model and the Pu-solubility model by Dr. William Downs. The independent technical review was performed to the current TWP criteria (BSC 2005 [DIRS 173246]) without deviations.

The evaluation by Dr. Downs (WD) answered the three questions posed in *Technical Work Plan for Postclosure Waste Form Modeling* (BSC 2005 [DIRS 173246])

1) Do the treatments of the kinetics and thermodynamic factors adequately capture the behavior of the radionuclides over geologic timeframes?

    - (WD) Yes. The repository is being simulated for a minimum of 10,000 years. Thus, any reactions that are predicted to occur will have come to equilibrium over this timeframe (i.e., reactions will not be rate limited). The solubility modeling is an equilibrium thermodynamic simulation that does not use reaction rate data. Once the solutions and solubility-controlling phases come to equilibrium, the concentrations of radionuclides in solution will not change without a change in the physicochemical environment.

2) Is the value for Eh implemented in the model consistent with conditions expected in the repository over geologic timeframes?

    - (WD) Yes. The simulations have assumed that the system is open to the atmosphere and have modeled a range of fCO_2 conditions that include the current atmospheric value and two orders of magnitude higher as well as lower concentrations. There is no geologic evidence that the earth has had this range of fCO_2 variation since the evolution of plants over 1,000 Ma ago.

3) Is the model adequate and appropriate for its intended use?

    - (WD) Yes. The model uses either realistic or conservative solubility-controlling phases, assumes that the system is open to the atmosphere for maximum actinide solubility, and varies the fCO_2-controlling the carbonate species activities - over a range of greater than 2 orders of magnitude. In addition, the model is based on the assumption of attainment of equilibrium within the system. This will provide conservative estimates of the concentrations of radionuclides within the system.

INTENTIONALLY LEFT BANK

APPENDIX IV
IDENTIFYING THE SOLID PHASE(S) CONTROLLING DISSOLVED CONCENTRATIONS OF NEPTUNIUM IN WASTE PACKAGES AND THE INVERT

INTENTIONALLY LEFT BLANK

IV. IDENTIFYING THE SOLID PHASE(S) CONTROLLING DISSOLVED CONCENTRATIONS OF NEPTUNIUM IN WASTE PACKAGES AND THE INVERT

Dissolved concentrations are based on thermodynamic equilibrium calculations of solubilities of pure phases in Yucca Mountain J-13 reference water. Prerequisite to such modeling is the selection of the controlling phase and the availability of thermodynamic data.

Thermodynamic data on actinide solids are derived from laboratory solubility measurements and from direct thermochemical measurements such as calorimetry (Nordstrom and Munoz 1986 [DIRS 153965], Chapter 11). The thermodynamic properties of the minerals uraninite (UO_2), thorianite (ThO_2), and the analogous high-temperature phases (NpO_2 and PuO_2) have been well defined using direct thermochemical techniques. Room temperature solubility studies of actinide dioxides, using over- and under-saturation tests at pH values above the threshold of hydrolysis indicate dissolved actinide concentrations are not controlled by high-temperature crystalline phases, but by either solids such as hydrated or amorphous phases that are considerably more soluble, or both (Grenthe et al. 1992 [DIRS 101671], Section v3.2.3.3; Guillaumont et al. 2003 [DIRS 168382], Section 9.3.2.2; Hummel et al. 2002 [DIRS 161904]; Neck and Kim 2001 [DIRS 168258], Fanghänel and Neck 2002 [DIRS 168170]). Hummel et al. (2002 [DIRS 161904], Figure 3.2.2) show the solubility calculated from the thermodynamic properties of the mineral form of ThO_2 is nine orders of magnitude lower than concentrations measured in room temperature laboratory experiments at pH values above about 6. Similarly, that report (Hummel et al. 2002 [DIRS 161904], Figure 3.2.3) shows the calculated solubility of the mineral form of UO_2 to be six orders of magnitude lower than concentrations measured in room-temperature laboratory experiments at pH values above about 3. Fanghänel and Neck (2002 [DIRS 168170], Figure 8) show similar comparisons for Th, U, and Pu.

The more soluble phases leading to the higher, laboratory-measured concentrations are not well defined crystallographically. However, their solubility values are reproducible and these solubility values do not change over the usual time scale of laboratory experiments (weeks to months). Thus, critically compiled thermodynamic databases such as those maintained by the Nuclear Energy Agency (NEA) (Grenthe et al. 1992 [DIRS 101671]; Silva et al. 1995 [DIRS 102087]; OECD 2001 [DIRS 159027]; Guillaumont et al. 2003 [DIRS 168382]) and the National Cooperative for the Disposal of Radioactive Waste (NAGRA) / Paul Scherrer Institute (PSI) (Hummel et al. 2002 [DIRS 161904]) include several actinide dioxide solids for Th, U, Np, and Pu. One is the crystalline variety and is designated by its mineral name or as NpO_2 or NpO_2(cr) (cr = crystalline)), for example. The others are solids controlling room-temperature laboratory solubilities and are written as NpO_2 (am,hyd) (am = amorphous, hyd = hydrated).

From the viewpoint of thermodynamics, the most-stable solid would be selected as the controlling phase because thermodynamically less-stable phases would be ultimately replaced by the most stable phase. However, unless it can be demonstrated that the thermodynamically most-stable solid appears during the regulatory period under the expected repository conditions, for conservatism, solids known to form under short duration laboratory conditions are chosen as the solubility controlling phase.

This precept was followed in the previous revision of this report in the selection of Np_2O_5 as the controlling phase for Np. At the conditions relevant to solubility limits in the repository (oxidizing conditions and temperatures from 25°C to 100°C), the observed precipitates in solubility experiments are $Np_2O_5 \cdot xH_2O$, Np_2O_5, and $NaNpO_2CO_3 \cdot xH_2O$ (Efurd et al. 1998 [DIRS 108015]; Nitsche et al. 1993 [DIRS 155218], p. 37). At the upper end of the temperature range and at higher temperatures NpO_2 is also found and becomes dominant over Np_2O_5 as temperature increases. The base-case model from REV 03 uses Np_2O_5 and $NaNpO_2CO_3$ (for high-pH end only) as the solubility-controlling phases for dissolved neptunium concentrations.

The calculated concentrations were validated as conservative by comparisons with concentrations measured in various fuel degradation tests carried out at PNNL and ANL (BSC 2004 [DIRS 169425], Section 7.2.3, Figure 7-2). As pointed out in that section:

> The fact that the measured neptunium concentrations in spent nuclear fuel corrosion experiments are four to six orders of magnitude lower than the modeled pure neptunium phase solubility indicates that neptunium may be controlled by different mechanism(s) than by pure-phase [Np_2O_5] solubility.

This report revision reexamines possible controls on Np concentrations to select a model that is a more realistic representation of experimental fuel degradation data. Consideration of the electrochemical mechanisms of waste form degradation and of additional laboratory studies of the behavior of pure Np solutions during long-term and high-temperature testing indicates a model based on NpO_2 should be adopted as the preferred, base-case model for use in TSPA. Comparison of this model with the results of waste-form degradation tests validates its use as a reasonably conservative basis for modeling Np concentrations.

The solubility of an element is defined in Section 6.3.1. The solubility of a pure phase of any element can be confidently used as an upper bound on the dissolved concentration of that element in an aqueous solution contacting that phase when it can be shown either:

- The forward (dissolution) reactions (producing the dissolved species) will not produce supersaturated solutions in the system of interest, or
- The backward (precipitation) reactions leading to the pure phase are fast enough to ensure that solutions that are supersaturated with respect to the pure phase will not persist for significant time periods, or both.

The thermodynamically most-stable pure phase for Np (NpO_2) is a special case of interest because its solubility represents a reasonable pure-phase upper bound on the dissolved concentration. The solubility of less-thermodynamically stable pure phases (i.e., metastable phases) establishes unreasonable upper bounds on the dissolved concentration unless the metastable phases are unreactive for time periods approaching the time of regulatory compliance.

The Eh–pH thermodynamic stability fields for pure-neptunium phases have been estimated (Kaszuba and Runde 1999 [DIRS 122379]; Lemire 1984 [DIRS 101706]). These results show NpO_2 is the most thermodynamically stable Np phase over most of the Eh–pH regime of interest. However, $Np(OH)_4$ and Np_2O_5 may be kinetically favored for more-reducing and higher-pH

conditions, respectively (Kaszuba and Runde 1999 [DIRS 122379]). Data from short term oversaturation experiments (Nitsche et al. 1993 [DIRS 155218], Efurd et al. 1998 [DIRS 108015]) indicate that these and other phases precipitate preferentially from solutions that are supersaturated with respect to NpO_2, even under conditions where NpO_2 is expected to be the most-stable phase.

NpO_2 has been observed to precipitate homogenously only at 200°C (Roberts et al. 2003 [DIRS 162536]). It has been observed to precipitate at 150°C (and perhaps also at 90°C) in a heterogeneous system containing some U(IV) that may have catalyzed the reduction steps involved in the NpO_2 nucleation and precipitation (Finch 2002 [DIRS 172608]). These observations probably indicate that metastable Np(V) phases are precipitated in preference to NpO_2 because their nucleation and precipitation are kinetically favored over the reductive nucleation and precipitation of NpO_2. This behavior is not surprising given that Np(V) is the predominant oxidation state for the aqueous species in air-saturated water (Kaszuba and Runde 1999 [DIRS 122379]; Lemire 1984 [DIRS 101706]); homogenous precipitation of Np(IV) solids from such solutions is a reductive nucleation and precipitation process of the aqueous Np(V) species. This could occur either by reduction of Np(V) to Np(IV), nucleation of NpO_2, reductive precipitation of NpO_2, or by nucleation and precipitation of a metastable Np(V) solid (if the solution is supersaturated with respect to such a solid phase) followed by reductive aging of this metastable solid to form NpO_2. Because the rate of transformation of these metastable Np(V) phases to the more-thermodynamically stable NpO_2 could be very slow, they can define slow reaction paths for NpO_2 precipitation from some supersaturated solutions and their solubility could, therefore, effectively control the dissolved-Np concentration if these were the only NpO_2-formation paths available for the nominal and disruptive scenarios in the CSNF and codisposal waste packages.

The reaction paths available for NpO_2 formation in the heterogeneous waste package systems are influenced by the corrosion of the waste form, the corrosion of the waste package materials, and the interactions with the corrosion product materials. Because Np is a trace element in the presence of much larger amounts of other materials (specifically U, Fe, and their corrosion products), processes that can cause dissolved Np species to be associated with a precipitating phases of U and Fe (e.g., “sorption,” ion exchange, incorporation into the lattice structure of the precipitating host phase) may control the dissolved concentrations at levels even lower than the solubility of the most-stable (thermodynamically) pure phase. Although the scope of this document involves consideration of these processes, it does so only with the limited objective of showing that they are likely to control the dissolved-Np concentrations at levels lower than the NpO_2 solubility; it does not address the question of what these lower levels are or the possible conceptual model required to predict these more complex processes.

Based on the above background, the content of this appendix is intended to show:

- The waste form dissolution reaction paths are not likely to lead to Np-dissolved concentrations that are supersaturated with respect to pure Np(V) phases that are metastable compared to NpO_2 and that may serve as "Np traps" that could inhibit rapid formation of NpO_2.

- Heterogeneous interactions inside the waste packages are likely to promote the reductive precipitation of NpO_2 or other reactions that will inhibit formation of solutions that are supersaturated with respect to metastable Np(V) phases that could control the dissolved Np concentration at values higher than the NpO_2 solubility.

Each of these points is assessed for the relevant conditions expected to occur inside the CSNF and codisposal waste packages in the nominal, igneous intrusion, and seismic scenarios. Sections IV.2.1.1 and IV.2.1.2 outline the following arguments for in-package controls on Np-dissolved concentrations and use of NpO_2 as the conservative bound:

- **CSNF Nominal and Seismic Scenario**—Solubility-controlling phase at the fuel surface will be NpO_2. Elsewhere in the package, NpO_2 and Np incorporation into uranyl-silicates or oxides will control Np solubility. The rationale for this is as follows: Neptunium is initially present in the fuel as Np(IV). Np(IV) in the presence of UO_2 at fuel surface will not oxidize to Np(V). Np(V) in bulk solution inside the waste package will be reduced to NpO_2 by metallic components of the waste package. NpO_2 is the most stable Np phase and will form sufficiently quickly in the waste package to control dissolved Np. Coprecipitated solids should have Np solubilities lower than NpO_2.

- **CSNF Igneous Intrusion Scenario**—Solubility-controlling phase at the fuel surface will be NpO_2. Elsewhere in the package, NpO_2 and Np incorporation into uranyl-silicates or oxides will control Np solubility. The rationale for this is as follows: NpO_2 is most stable Np phase and will form sufficiently quickly in the waste package to control dissolved Np. Coprecipitated solids should have Np solubilities lower than NpO_2.

- **Codisposal Waste Packages (Including Fuel/Waste Forms and HLW Glass)**—Solubility-controlling phase at the fuel surface will be NpO_2. Elsewhere in the package, NpO_2 and Np incorporation into uranyl-silicates or oxides will control Np solubility. The rationale for this is as follows: U-metal fuels will rapidly oxidize to UO_2 and uranyl oxi-hydroxides. Al-based fuels will oxidize to UO_2 and uranyl oxi-hydroxides. MOX fuels are UO_2 and PuO_2 and should behave like CSNF. Np(V) in solution will be reduced to NpO_2 by metallic components of the waste package. NpO_2 is the most stable Np phase and will form sufficiently quickly in the waste package to control dissolved Np. Coprecipitated solids should have Np solubilities lower than NpO_2.

Since aqueous neptunium in a solution in contact with the atmosphere will be in the five oxidation state, the neptunium leaving the waste package is expected to be Np(V). Once Np(V) leaves the waste package, it is difficult to determine and defend the composition and geometry of

any materials it would come into contact with in the invert. Therefore, the use of an incorporation model or taking credit for reductive precipitation is inappropriate. The ex-package (invert) dissolved concentration model is based on the Np(V) minerals Np_2O_5 and $NaNpO_2CO_3$, and appropriate for use outside of waste packages. Section IV.1 discusses aqueous Np and Np solids formed from Np(V) solutions.

IV.1 NEPTUNIUM CHEMISTRY IN AQUEOUS SYSTEMS

Published Eh–pH diagrams for Np at 25°C (e.g., Langmuir 1997 [DIRS 100051], Figures 13.27 through 13.29) show two oxidation states (Np(V) and Np(IV)) dominate Np chemistry in natural waters. In solution, Np(V) species dominate the upper half of the stability field of water (higher Eh values) while Np(IV) species dominate the lower half (lower Eh values). The predominant solid is NpO_2 even in oxidizing carbonate waters. The OECD (2001 [DIRS 159027], Table 3.1, p. 41) gives the free energy of formation ($\Delta_f G^0$) of NpO_2 as –1,021.731 kJ/mol, while $\Delta_f G^0$ of Np_2O_5 is –2,031.574 kJ/mol. Given these data, then, NpO_2 is more stable than Np_2O_5 at 298.15 K, because of the following reaction:

$$Np_2O_5 = 2\ NpO_2 + \frac{1}{2} O_2(g)$$

$$\Delta_r G^0 = 2 \times \Delta_f G^o_{NpO2} - \Delta_f G^o_{Np2O5} = 2 \times (-1{,}021.731) - (-2{,}031.574) = -11.888\ (\text{kJ})$$

If kinetic barriers do not prevent NpO_2 from precipitating, it should control neptunium-equilibrium solubility under most conditions, even those with atmospheric fO_2.

In neptunium solubility experiments, NpO_2 is only found at higher temperatures, suggesting kinetic inhibition of formation of NpO_2 from a Np(V) solution. For example Roberts et al. (2003 [DIRS 162536]) produced crystalline NpO_2 from a Np(V) solution after about 100 days at 200°C. Several pure-neptunium phases have been identified in neptunium solubility experiments, including $Np_2O_5 \cdot xH_2O$, Np_2O_5, $NaNpO_2CO_3 \cdot xH_2O$, and NpO_2 (Efurd et al. 1998 [DIRS 108015]; Nitsche et al. 1993 [DIRS 155218]; Roberts et al. 2003 [DIRS 162536]), at various temperatures and solution compositions. At conditions more relevant to solubility limits in the repository (oxidizing conditions and temperatures from 25°C to 100°C), the observed precipitates in solubility experiments are $Np_2O_5 \cdot xH_2O$, Np_2O_5, and $NaNpO_2CO_3 \cdot xH_2O$ (Efurd et al. 1998 [DIRS 108015]; Nitsche et al. 1993 [DIRS 155218], p. 37).

$NaNpO_2CO_3 \cdot xH_2O$ was observed in neptunium solubility experiments using J-13 well water (Nitsche et al. 1993 [DIRS 155218], p. 37). However, a detailed analysis by Runde in *Pure Phase Solubility Limits–LANL* (CRWMS M&O 2001 [DIRS 154629]) found $NaNpO_2CO_3 \cdot xH_2O$ to be stable only when $[Na^+]$ is greater than 0.05 molar at neutral pH. Based on the X-ray diffraction data and by further analyzing the stability field for Np(V) solid phases (Np_2O_5, $NpO_2(OH)$, and $NaNpO_2CO_3 \cdot xH_2O$), Runde (CRWMS M&O 2001 [DIRS 154629]) concluded that Np_2O_5 is the most stable pentavalent neptunium phase in J-13 well water under oxidizing conditions (CRWMS M&O 2001 [DIRS 154629], p. 21). In work by the OECD (2001 [DIRS 159027]), equilibrium solubility product constants for both $NaNpO_2CO_3$ and $NaNpO_2CO_3 \cdot 3.5H_2O$ were given. The anhydrous phase is considered as the aging product of the

hydrated solid. Given that this difference between their log K is only 0.5 units, which is within the uncertainty ranges for each constant, and this difference is well within the uncertainty range of the model, these solids are considered to be the same thermochemically.

Efurd et al. (1998 [DIRS 108015]) conducted neptunium solubility experiments using J-13 well water at pH values of about 6.0, 7.0, and 8.5 at temperatures of 25°C, 60°C, and 90°C. These studies were conducted from both oversaturation and undersaturation to demonstrate that the steady-state concentrations attained represented equilibrium with the solid phases formed (even if these were metastable equilibrium conditions). They identified the neptunium-controlling solid using X-ray diffraction as $Np_2O_5 \cdot xH_2O$ and noted that the crystallinity of the solid, as shown by the sharpness of the diffraction patterns, increased with increasing temperature. These laboratory experiments were conducted over a period of about one year. Because the more-crystalline form of the solid was produced in these laboratory tests at temperatures of 90°C after about 1 year, and (in general) reaction rates double for each 10-degree-rise in temperature, this transformation would require about 100 years at ambient temperature. For the 10,000-year regulatory period for the postclosure system, this increased crystallinity would be expected to occur even sooner than 100 years because the temperature of the waste form will be elevated well above ambient temperatures in most cases. As a typical TSPA-LA time step is approximately 100 years or more (with the smallest time step being 10 years), it is expected that within one (or two) TSPA-LA timesteps, the crystalline phase would form and control the dissolved-neptunium concentrations.

The NEA thermochemical database handbook review volume on neptunium (OECD 2001 [DIRS 159027]) recommended −2,031.6 ± 11.2 kJ/mol for the Gibbs free energy of formation of crystalline Np_2O_5 based on calorimetric studies (equivalent to −1,015.8+/-5.6kJ/mol for $NpO_{2.5}$). For the solubility product reaction of Np_2O_5, the procedure outlined in Section 6.3.3.1 leads to a log K of 3.7 with a 2σ uncertainty of ±2.8 (at 25°C). Efurd et al. (1998 [DIRS 108015]) report a log K value of 5.2 with an uncertainty of ±2.8 for the solubility product reaction of $Np_2O_5 \cdot xH_2O$. This higher log K value is attributed to the hydrated nature of the precipitate, which is expected to convert to crystalline Np_2O_5 solid with time due to the aging process (Efurd et al. 1998 [DIRS 108015]). This conversion would effectively lower the log K value from that reported in Efurd et al. 1998 (DIRS 108015) to that given by the OECD (2001 [DIRS 159027]). The OECD (2001 [DIRS 159027]) value has been adopted in the Project's thermodynamic database (*Data0.ymp.R2*) and differs from the value obtained by Efurd et al. (1998 [DIRS 108015]) for the hydrated, amorphous phase by 1.5 units. This means that the value for the $Np_2O_5 \cdot xH_2O$ falls within the calculated 2σ range for the OECD (2001 [DIRS 159027]) value, which is based on the critically reviewed NEA data (± 2.8), which is within the model uncertainty.

It is recognized that the determination of the Np-solubility-controlling phase is very complex and depends upon a number of parameters, such as temperature, time, redox controls, and solution composition. However, there are numerous reasons to conclude that the Np-solubility model based on the pentavalent neptunium (Np(V)) solids described above (Np_2O_5 and $NaNpO_2CO_3$) is a very conservative representation of the possible controls on dissolved-neptunium concentrations over geologic time, further justifying the use of the more crystalline solids.

Figures IV-1 through IV-3 show concentrations of total dissolved Np and of aqueous species contributing to that concentration calculated at $fO_2 = 10^{-0.7}$ bars and fCO_2 values of $10^{-3.0}$ bars

and 10^{-10} bars, expressed as molalities and percent total Np, respectively. The figures span the pH range from 3 to 9.5 with minor species equal to that in J-13 well water. As can be seen in Figures IV-2 and IV-3, F^- and SO_4^{2-} at J-13 well water concentrations have negligible influence on Np solubility. Carbonate species, however, dominate at pH values above 8 at log fCO_2 = -3. The dominant Np solution species are pentavalent up to pH 9, where the hexavalent $NpO_2(CO_3)_2^{2-}$ and $NpO_2(CO_3)_3^{4-}$ dominates, while the stable-solid phase is tetravalent. Comparison of the different model results at $fCO_2 = 10^{-3.0}$ bars and $fCO_2 = 10^{-10}$ bars in Figure IV-1 shows the profound effect carbonate has on the solubility and oxidation state of Np in alkaline solutions.

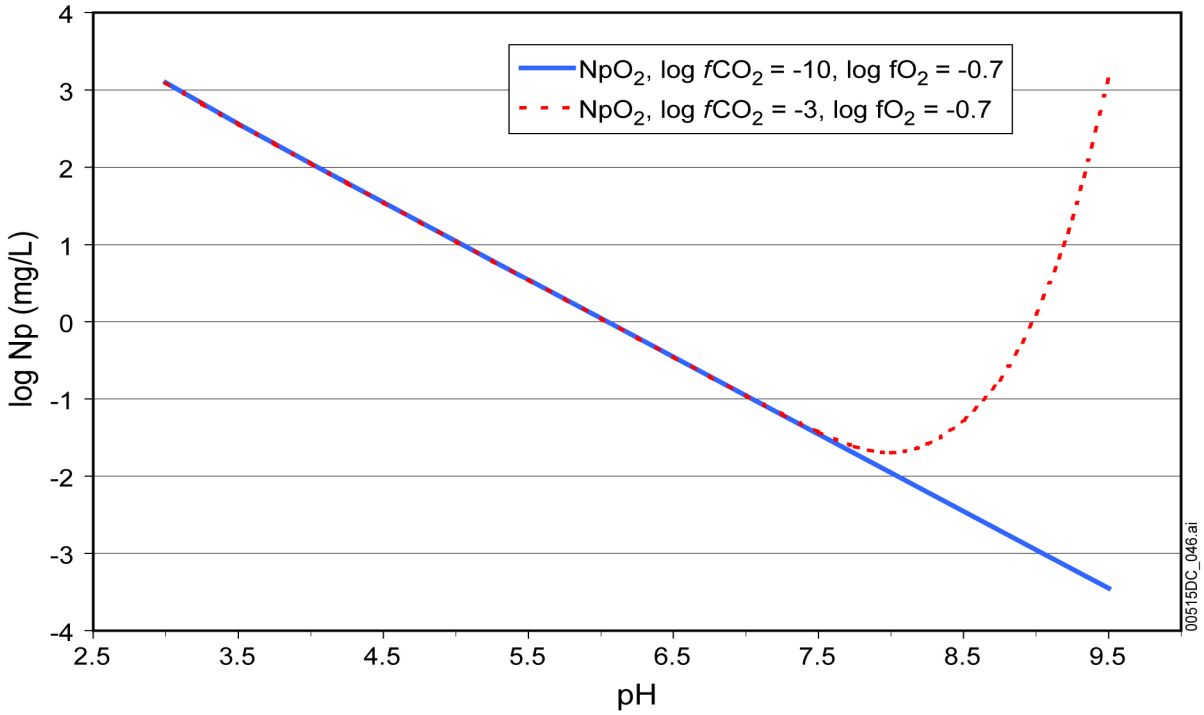

Source: *NpO2 sensitivities.xls* (Appendix I).

Figure IV-1. NpO_2 Model Showing the Effects of CO_2 on Dissolved Concentrations

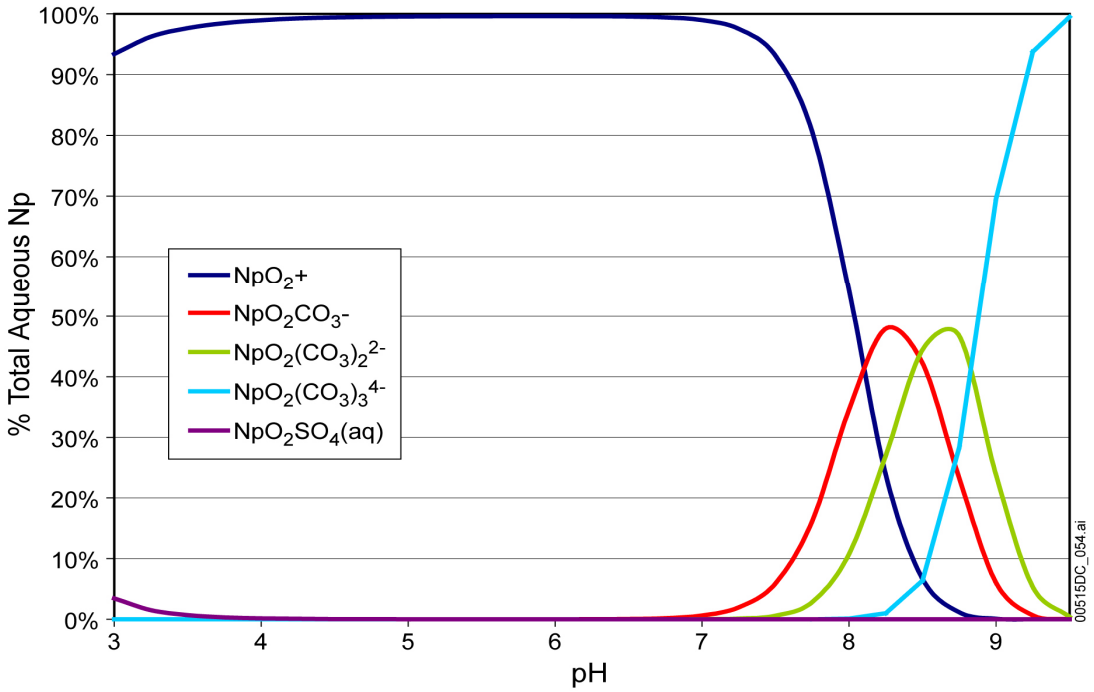

Source: *NpO2 sensitivity speciation.xls* (Appendix I).

Figure IV-2. Primary Aqueous Species at Atmospheric O_2 and log fCO_2 = -3 bars

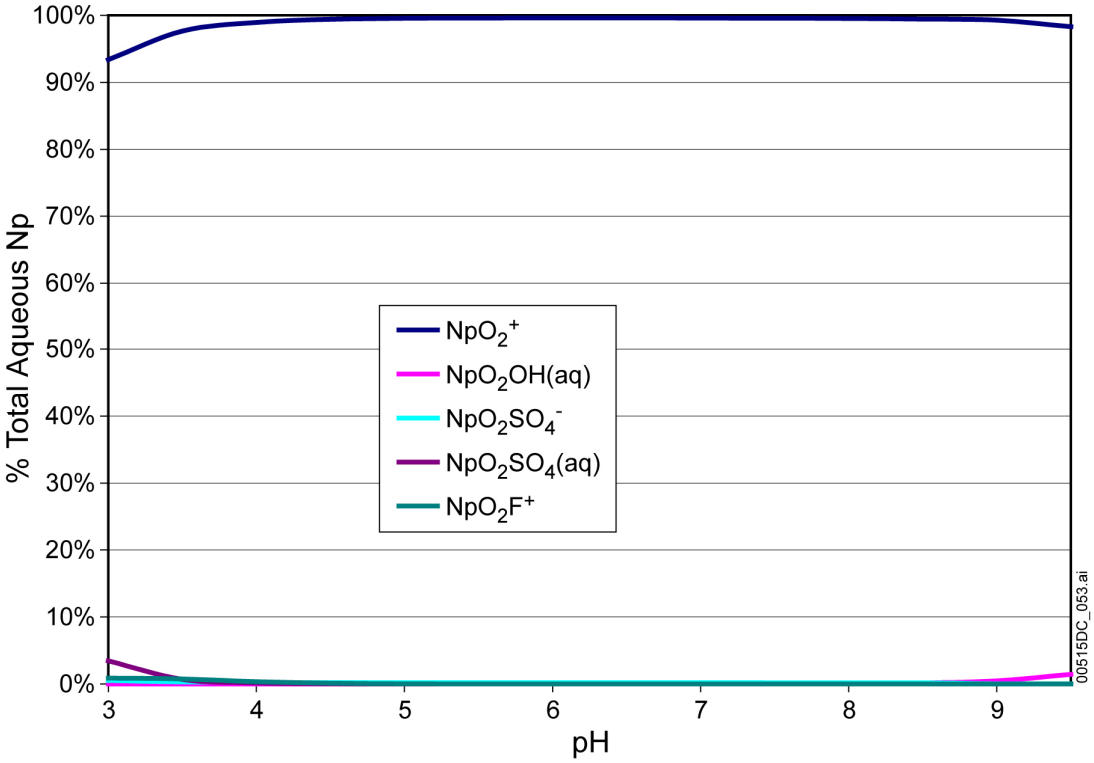

Source: *NpO2 sensitivity speciation.xls* (Appendix I).

Figure IV-3. Primary Aqueous Species at Atmospheric O_2 log fCO_2 = -10 bars

Figure IV-4 shows the Np concentrations under reducing conditions (log fO_2 = -60). It shows Np concentrations over ten orders of magnitude lower than under oxidizing conditions as shown in Figure IV-1. Figure IV-5 shows the reduced importance of the pentavalent NpO_2^+, which only dominates between pH 4 and 5.5. Tetravalent species dominate over the rest of the pH range, with minor J-13 water species like fluoride showing increased importance at lower pH values.

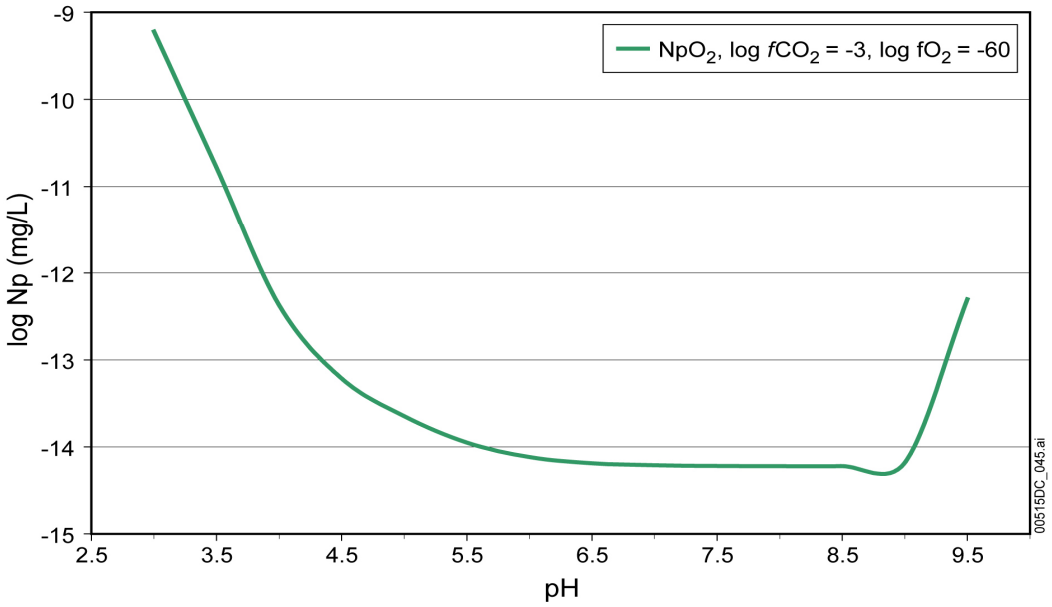

Source: *NpO2 sensitivities.xls* (Appendix I).

Figure IV-4. NpO_2 Model Showing Lower Dissolved Concentrations Under Reducing Conditions

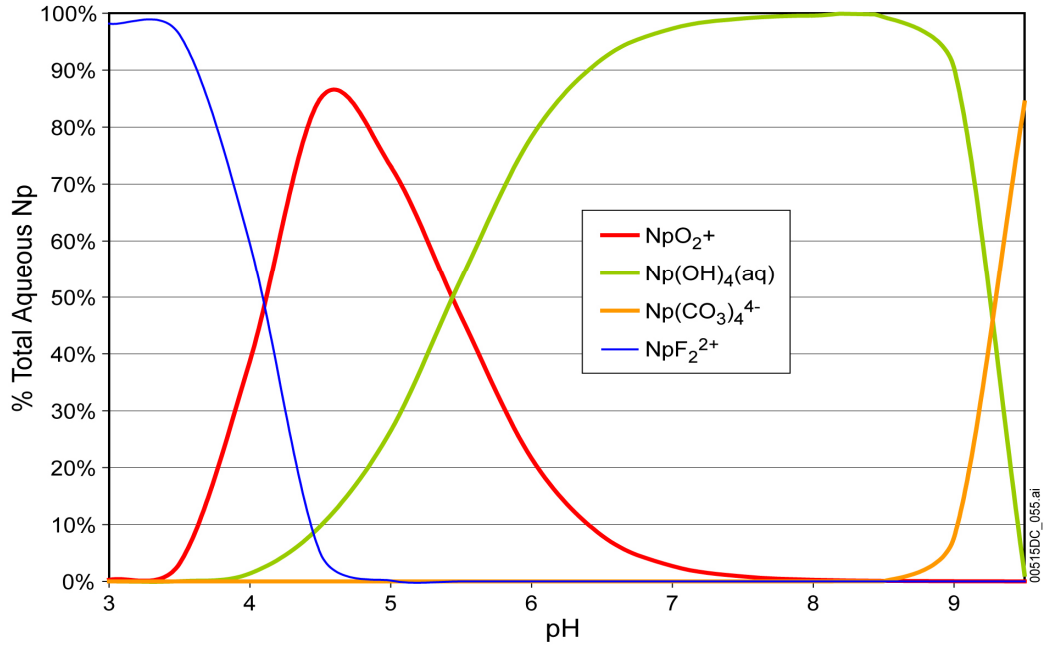

Source: *NpO2 sensitivity speciation.xls* (Appendix I).

Figure IV-5. Primary Aqueous Species Under Reducing Conditions

IV.2 NEPTUNIUM IN WASTE FORMS

CSNF packages comprise the bulk (~ 67 percent; 7,472 out of 11,184 packages) of the spent nuclear fuel packages to be stored (BSC 2004 [DIRS 170022], Table 6-3). CSNF packages also contain much greater content of Np per package than codisposal waste packages. Of the many codisposed spent nuclear fuel types, the top three chosen for study according to the need for laboratory data based on mass, fissile content, fission product content, expected release rates, uniqueness, and availability, were U-metal, Al-based, and MOX (DOE 2003 [DIRS 166268], p. 2-4). The testing focused mainly on dissolution rates using the flow-through method but some of the tests shed light on Np behavior in repository-like conditions, most notably the drip tests.

To identify the reaction paths and solid phases that may control the dissolved Np concentration inside the waste package, it is instructive to consider the initial state of the Np in the waste forms and the processes or chemical reactions that can lead to dissolution and reprecipitation of this Np as the waste form corrodes (i.e., it is instructive to consider the evolution of the reaction paths and how they are expected to influence the controls that are effective for the dissolved Np concentration). This involves assessing the form of Np in the host waste form solids, the waste form degradation-corrosion reactions, and the likely behavior (including dissolution and re-precipitation behavior) of Np as the host solid corrodes. It also involves considering how the dissolved Np that is released during the waste form corrosion will interact with the waste form corrosion products and the corroding metals and their corrosion products inside the CSNF and codisposal waste packages.

Figure IV-6 illustrates the general conceptualization of salient features and processes that are considered here for the waste form corrosion and metal corrosion reaction paths. It is intended to illustrate the fact that the relevant Np reaction paths start in the waste forms and progress through the waste form alteration rind, the bulk solution, and the metal corrosion products and corroding metal. Figure IV-6 also qualitatively illustrates the relevant potentials Np will "see" for reactions (as identified in five sections) occurring: (1) at the surface of the waste form, (2) in the waste form corrosion rind, (3) in the bulk solution, (4) in the corrosion product layer on metal surfaces, and (5) at the surface of a corroding metal.

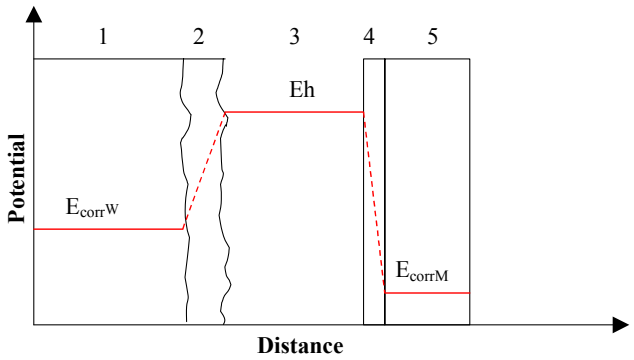

NOTE: $E_{corr}w$ = Corrosion potential of the waste; Eh is the Eh of the bulk solution; $E_{corr}M$ = corrosion potential of the waste package metals. The numbers at the top of the figure correspond to and are called out in discussions within the body of this report.

Figure IV-6. General Conceptualization for the Waste Form Corrosion and Metal Corrosion Reaction Paths

IV.2.1 Corrosion of Waste Form Materials and Neptunium Behavior

IV.2.1.1 CSNF

Nominal and Seismic Scenarios

In CSNF the oxygen potential is less than about –400 kJ/mol (Dehaudt 2001 [DIRS 164037], Section 5.2.6.5). Under these conditions, the uranium in the fuel matrix is present mostly in the U(IV) oxidation state. Np in the CSNF is expected to be present as a solid solution of NpO_2 in the UO_2 fluorite structure with which it is compatible (Dehaudt 2001 [DIRS 164037], Section 5.2.6.5). Recent X-ray absorption near-edge spectroscopy data indicate that the oxidation state of Np in the CSNF matrix is Np(IV) and extended X-ray absorption fine structure (EXAFS) data indicate that the Np(IV) is present in a UO_2-like phase, which is consistent with it being in solid solution in the fuel's UO_2 fluorite lattice structure (Kropf et al. 2004 [DIRS 173092]).

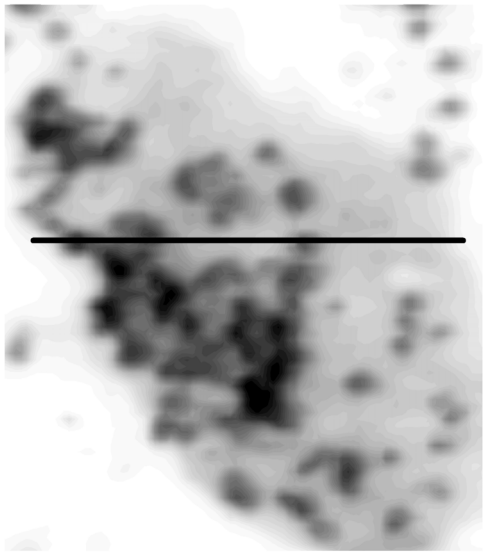

Source Ebert et al. 2005 [DIRS 173071], Figure 2-18

Figure IV-7. Uranium X-Ray Absorption Spectrometer (XAS) Map of the S62J-104 Specimen

The darker areas in Figure IV-7 are fuel grains, while the lighter, gray areas are uranyl alteration phases. The black horizontal line denotes the location of the line scan of uranium and neptunium shown in Figure IV-8. The field of view of the image is approximately 340 microns × 340 microns.

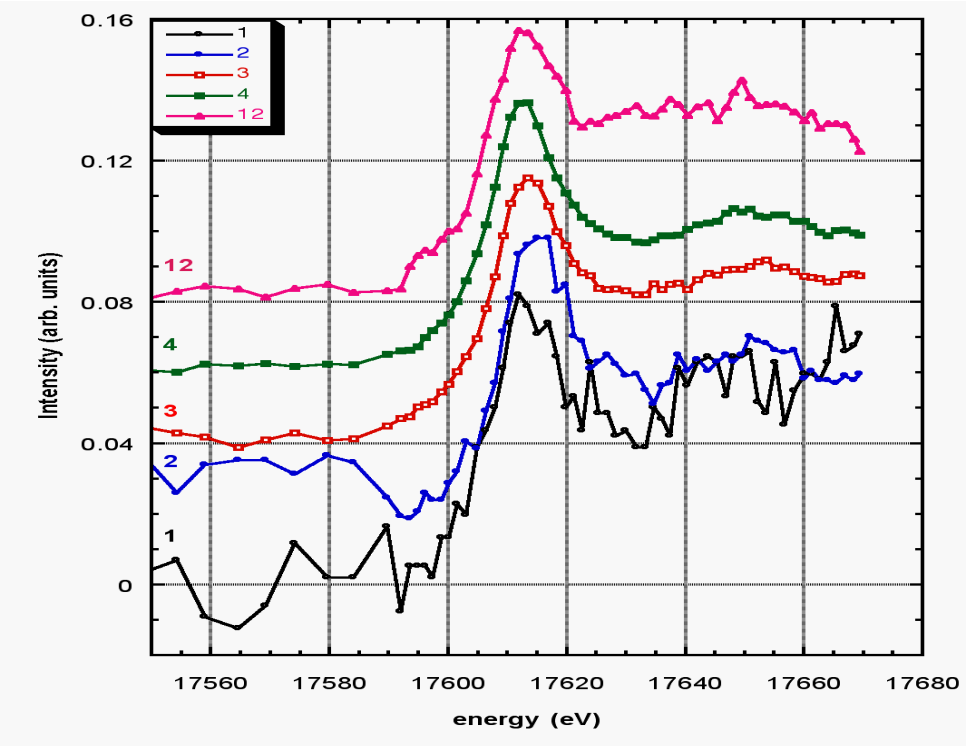

Source Ebert et al. 2005 [DIRS 173071], Figure 2-19b

Figure IV-8. Normalized Np XAS Spectra from Selected Points in the Line Scan

Figure IV-8 shows normalized Np XAS spectra from selected points in the line scan, (labeled in order as 1, 2, 3, 4, and 12). These spectra are consistent with Np(IV), with the possible exception of spectrum 12, which may indicate a mixed valence (Kropf et al. 2004 [DIRS 173092]).

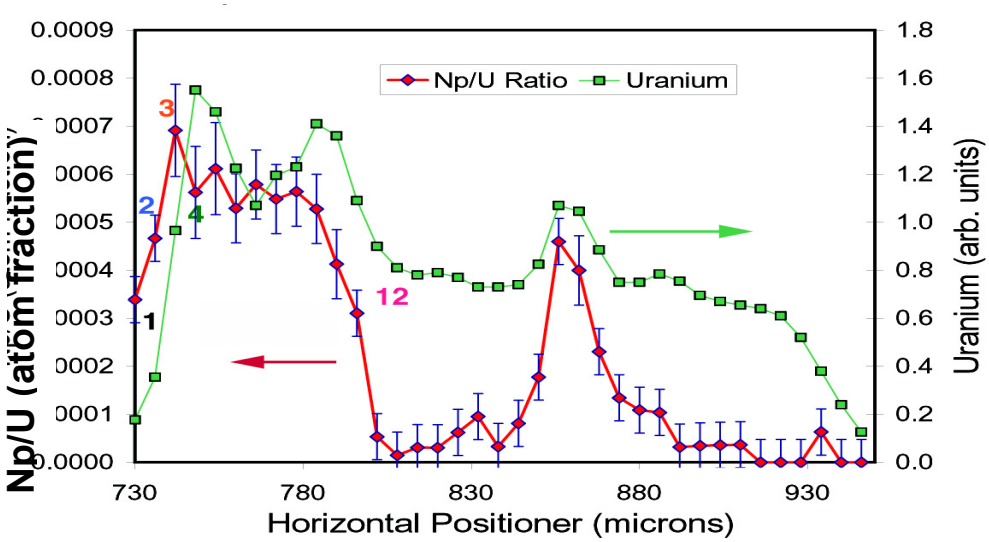

Source Ebert et al. 2005 [DIRS 173071], Figure 2-19a

Figure IV-9. Line Scans for Total Uranium Intensity and the Ratio of Neptunium to Uranium

Figure IV-9 includes line scans showing total uranium intensity and the ratio of neptunium to uranium signal. The more intense uranium signals coincide with fuel grains, while intermediate levels are uranyl alteration phases. The neptunium appears to remain localized in or near the unaltered fuel, with a suggestion of enrichment above the nominal Np/U level of 0.00047 toward the left edge of the figure at position "3." A weak Np signal (Np/U ~ 0.0001) appears to coincide with a uranyl phase near the positioner setting of 880 microns. The true length scale of the line scan is given by multiplying the indicated scale by the square root of 2 (e.g., the line scan spans 300 microns).

Np can be released from the CSNF matrix when the matrix degrades by oxidative dissolution. To assess the likely behavior of Np as the host CSNF matrix undergoes oxidative dissolution, it is instructive to consider the electrochemical interactions between U(IV) and Np(IV). Available data indicate that the standard potential for the UO_2^{2+}/U^{4+} is significantly lower than the standard potential for the NpO_2^{+}/Np^{4+} couple and indicate that reduction of Np(V) by unoxidized U(IV) as the fuel corrodes is thermodynamically favored as shown by the following reaction (Finch 2002 [DIRS 172608]):

$$2NpO_2^{+} + U^{4+} + 4H^{+} = 2\ Np^{4+} + UO_2^{2+} + 2\ H_2O \qquad E^o = 0.405 \text{ to } 0.469V$$

This indicates that while the CSNF is corroding it is capable of reducing dissolved Np(V) to Np(IV) at the surface of the residual CSNF.

Although the above arguments indicate reduction of Np(V) by U(IV) is favored thermodynamically, it is instructive to assess if Np(IV) is likely to be oxidized under the corrosion conditions at the corroding fuel surface. This can be done by comparing the standard potential for the anodic dissolution of Np(IV) to the CSNF corrosion potential.

Standard potentials for Np(IV) and U(IV) anodic dissolution half reactions are (Finch 2002 [DIRS 172608]):

$$NpO_2^{+} + e^{-} + 4H^{+} = Np^{4+} + 2H_2O \qquad E^o = 0.739V$$

$$UO_2^{2+} + 2e^{-} + 4H^{+} = U^{4+} + 2H_2O \qquad E^o = 0.27 \text{ to } 0.334V$$

Measured corrosion potentials (E_{corr}) for CSNF in aerated near-neutral pH solutions depend on many factors but are generally in the range of about 300 mV to 600 mV SHE (Shoesmith 2000 [DIRS 162405], Figure 33). Corrosion potentials in the range of 510 mV to 620 mV SHE were also measured for UO_2 in 95 percent saturated NaCl solutions when 0.1M H_2O_2 was added to simulate the influence of radiolysis products (Grambow et al. 2000 [DIRS 162391], p. 123). These data indicate that the CSNF corrosion potential (Figure IV-6) may be lower than the standard potential for the anodic dissolution of Np(IV) in the fuel matrix. This indicates that oxidation of Np(IV) in the fuel's lattice is unlikely to occur under the pertinent potential conditions at the fuel's surface. When the solubility of NpO_2 is reached at the corroding CSNF surface, it is likely that NpO_2 will precipitate onto, or be incorporated into, the corroding UO_2 fluorite lattice structure with which it is compatible. This indicates that the dissolved concentration of Np at the corroding CSNF surface is likely to be controlled by the solubility of NpO_2. Preliminary X-ray absorption data supports these hypotheses (Ebert et al. 2005 [DIRS 173071], Figures 2-18 and 2-19b, reproduced in this report as Figures IV-7 and IV-8).

As Figure IV-6 illustrates, any Np(IV) that does diffuse away from the corroding CSNF will encounter increasing oxidizing conditions as it diffuses through the CSNF rind and into the bulk solution. It is, therefore, likely that some of the aqueous Np(IV) will be oxidized to Np(V) species as it traverses the CSNF's corrosion product rind. However, there is a strong possibility that the Np(V) will then be incorporated into the uranyl phases of the rind (Section 6.6.4).

Figure IV-6 also illustrates aqueous Np(V) species in the bulk solution will encounter corroding metals and their corrosion products from the waste package internals. These corrosion products will provide local environments with lower oxidizing potentials than the bulk Eh and may, therefore, be effective in promoting reductive precipitation of NpO_2 by reducing aqueous Np(V) to Np(IV) species (see Section IV.4.3 for further explanation).

Igneous Intrusion Scenario

For the igneous intrusion scenario, CSNF is assumed to be oxidized when the fuel may be exposed to hot and humid air (a few years following the event). In this case, the Np(IV) in the fuel's matrix is likely to be oxidized to Np(V). For the conceptual picture shown in Figure IV-6, this indicates that the dissolution of the oxidized fuel would occur at the Eh potential (i.e., unlike the unoxidized CSNF), the Np in the oxidized CSNF would not experience the fuel's redox buffering effects discussed above. However, the Np-reaction path is expected to include the effects of coprecipitation into the uranyl alteration phases that are formed when the oxidized fuel is exposed to water. Also, the discussion of the reductive precipitation onto the corroding metallic waste package internals and the corrosion products apply to the Np behavior for the igneous intrusion scenario.

It is likely that incorporation of Np into either uranyl alteration phases or reductive precipitation onto metal corrosion products, or both will maintain the dissolved Np concentrations subsaturated with respect to NpO_2 (see Sections 6.6.4 and IV.4.3 for further explanation). In short, it is appropriate to use the solubility of NpO_2 to model the dissolved concentration of Np in the CSNF waste packages for the igneous intrusion scenarios

IV.2.1.2 Codisposed Spent Nuclear Fuels/Waste Forms

The codisposal waste packages contain two broad categories of waste material (i.e., spent fuel and DHLW). The initial state of Np in the codisposed spent nuclear fuels is principally as Np metal given that the majority of the uranium inventory of codisposed spent nuclear fuel is unoxidized N-reactor fuel. In the context of Figure IV-6, the corrosion potential of the N-reactor fuel is probably much lower (less oxidizing) than CSNF. Also, available experimental evidence indicates that the corrosion of this metal fuel proceeds by initially forming UO_2 (Fortner et al. 2001 [DIRS 172671]). If the Np in the fuel is oxidized to Np(IV) and incorporated into this intermediate UO_2, then the above discussion of the Np behavior for the CSNF reaction path also applies here. For codisposed spent nuclear fuel, the Np reaction path is expected to include the effects of coprecipitation into the uranyl alteration phases that are formed when the UO_2 is further oxidized to U(VI) and precipitated as uranyl alteration phases. Also, the discussions of reductive precipitation onto the corroding metallic waste package internals and corrosion products apply to the Np behavior for the igneous intrusion scenario (see Sections 6.6.4 and IV.4.3 for further explanation).

U-Metal—Drip tests on 0.5g of declad irradiated N-reactor fuel showed rapid corrosion (DOE 2003 [DIRS 166268], pp. 3-35 to 3-39). At 1 month, there was a large amount of a corrosion product sludge consisting of black 10 nm UO_2 particles with some yellow particles of metaschoepite. Filtration of the leachate showed the released U was 10 percent colloidal and 55 percent particulate (> 0.45 microns). At 4 months, the fuel was completely corroded and the sludge showed increasing agglomeration. At 8.5 months, X-ray diffraction (XRD) indicated the reaction products were a mixture of uranium oxyhydroxides, primarily U_4O_9. At that time, the released U was 85 percent particulate and 15 percent dissolved and the released Np was 100 percent dissolved at 6 ppb (2.5×10^{-8} molar). At 11 months the percent dissolved U and Np had declined to 10 percent and 70 percent with the Np concentration dropping to 2 ppb (8×10^{-9} molar). The authors note that Np may have been incorporated in the growing particulate phase and may have been retained in the corrosion products.

Al-based—The aluminum-based fuel consists of particles of UAl alloy, UAl_x, U_3Si_2, or U_3O_8 dispersed in an aluminum phase. Drip tests on an unirradiated UAl alloy fuel showed formation of a hydrogel layer of boehmite ($Al_2O_3 \cdot H_2O$) containing silicon and calcium covering the sample surface (DOE 2003 [DIRS 166268], pp. 4-24 to 4-29). Uranium leached from the UAl alloy particles formed spherical uranium-rich patches throughout the hydrogel layer. These patches were identified as uranyl oxyhydroxides with aluminum, silicon, and calcium present. After drying, these patches crystallized to platelets of schoepite and becquerelite 1 micron to 5 microns on a side. Another unknown uranium-bearing needle-shaped phase formed later in the experiments.

MOX—MOX fuel is similar to light water reactor (LWR) UO_2 spent nuclear fuel except MOX fuel has two phases (PuO_2 and the UO_2) and can have higher burnup. Flow-through tests showed the PuO_2 phase reacting slower than the UO_2 phase, which is slower than LWR UO_2 spent nuclear fuel (DOE 2003 [DIRS 166268], p 5-17), but the drip tests showed the release rates from MOX to be faster than for LWR UO_2 spent nuclear fuel for all radionuclides except ^{99}Tc (DOE 2003 [DIRS 166268], p. 5-26). In the drip tests, the smallest measured radionuclide releases were of ^{239}Pu and ^{237}Np.

Glass—The other waste form source of Np in the codisposal packages is the DHLW. Because the DHLW is expected to have very little electronic conductivity, the oxidizing potential at the corroding glass surface is likely to "float" to the bulk solution Eh. For the conceptual picture shown in Figure IV-6, this indicates that the dissolution of the DHLW is likely to occur at the Eh potential (i.e., unlike the unoxidized codisposed spent nuclear fuel), the Np in the DHLW would not experience redox buffering effects at the corroding glass surface or in the glass alteration rind. However, the Np reaction path is expected to include the effects of coprecipitation into the uranyl alteration phases that are formed by the codisposed spent nuclear fuel. Also, the earlier discussions of the reductive precipitation onto the corroding metallic waste package internals and the corrosion products apply to the DHLW Np behavior (see Sections 6.6.4 and IV.4.3 for further explanation).

Rai et al. (1981 [DIRS 144598]) investigated the behavior of Np during degradation of actinide-doped glass. The redox of the solution was controlled by the quinone-hyroquinone buffer to pe + pH = 11.8. They measured log Np (M) from –5.41 to -5.80 at pH values from 4.45 to 6.55, which was consistent with their measured solubility of crystalline NpO_2 under those conditions.

Solvent extraction techniques were used to determine that the neptunium in solution was oxidized, which is consistent with the current thermodynamic database and would predict NpO_2^+ as the dominant aqueous species. The experiments showed no kinetic barrier to precipitation of the solubility-controlling solid. Rai et al. (1981 [DIRS 144598]) cited a similar study conducted under atmospheric conditions without the redox buffer giving consistent results. Rai et al. (1981 [DIRS 144598]) concluded NpO_2 could be used to predict the maximum concentrations of Np that can be leached from glass.

It is likely that incorporation of Np into uranyl alteration phases or reductive precipitation onto metal corrosion products or a combination of the two will maintain the dissolved Np concentrations subsaturated with respect to NpO_2. In short, it is appropriate to use NpO_2 solubility to model the dissolved concentration of Np in the codisposal waste packages (see Sections 6.6.4 and IV.4.3 for further explanation).

IV.3 NEPTUNIUM INCORPORATION INTO URANYL PHASES

Although by definition, solubility-controlling solids can be either a pure solid or a solid solution, in practice, pure solids are generally used to evaluate radionuclide solubility. Using pure-phase control is acceptable for TSPA-LA calculations because it is conservative. However, it is well recognized that the concentration of most radionuclides released during the corrosion of spent nuclear fuel is likely to be very low (except for uranium and thorium) and that the radionuclides may not form their own pure phases (Grenthe 1991 [DIRS 161964], pp. 429 and 430; Langmuir 1997 [DIRS 100051], p. 531). Rather, they may be incorporated into secondary uranium minerals as solid solutions because of the large availability of uranium in the repository.

Neptunium concentrations in solution at 25°C to 90°C have been measured in a number of spent nuclear fuel degradation experiments (Finn et al. 1994 [DIRS 100746]; Finn et al. 1997 [DIRS 124142]; CRWMS M&O 2000 [DIRS 131861]; Wilson 1990 [DIRS 100949]; Wilson 1990 [DIRS 100793]). Neptunium concentrations based on Np_2O_5 and NpO_2 solubilities calculated at 25°C are several orders of magnitude higher than the neptunium concentrations measured in the degradation experiments. This suggests that neptunium concentrations resulting from fuel degradation in a repository may be lower than the concentrations predicted by pure-phase solubility modeled at 25°C.

There is also the possibility of Np incorporation into uranyl phases as a solubility control of neptunium in waste packages. Section 6.6.4 provides a more in depth discussion on Np incorporation into uranyl phases. This section will focus primarily on the U phases that are possible on the surface of the corroded fuel (rind composition).

IV.3.1 Uranium Mineralization

IV.3.1.1 Uranium Mineralization in the Rind

Buck et al. (2004 [DIRS 172668], Table 2) and Friese et al. (2004 [DIRS 172670], Table 1.1) give exhaustive lists of U minerals of "potential" interest to spent nuclear fuel in a repository. Table IV-1 indicates the phases reported to form in fuel corrosion experiments carried out for up to 10 years. The tests on UO_2 degradation performed by Wronkiewicz et al. (1996 [DIRS 102047]) included unsaturated tests (drip tests) on zircaloy-clad fuel segments inside

Stainless Steel Type 304 reaction vessels at 90°C. Those tests performed by Finch et al. (1999 [DIRS 127332]) were drip tests with fuel fragments held in Zircaloy-4 fuel holders inside a Stainless Steel Type 304 reaction vessel at 90°C. McNamara et al. (2003 [DIRS 172673]) carried out fuel corrosion tests on low burn-up fuel particles submerged in deionized water in capped vials at 90°C for 6 weeks. The vials were then stored at approximately 28°C for 2 years. Table IV-1 also shows the uranyl minerals found during laboratory degradation studies for which data are available in *Data0.ymp.R2* (DTN: MO0302SPATHDYN.000 [DIRS 161756]) are schoepite, soddyite, uranophane, and Na-boltwoodite.

Table IV-1. Phases Observed During Degradation of UO_2

Mineral	Formula (Roberts et al. 1990 [DIRS 107105])	Phases Reported for Laboratory Degradation of UO_2			*Data0.ymp.R2*
		Wronkiewicz et al. 1996 [DIRS 102047], Table 5	Finch et al. 1999 [DIRS 127332], Table I[b]	McNamara et al. 2003 [DIRS 172673]	DTN: MO0302SPATHDYN.000 [DIRS 161756]
Uranyl-Oxide Hydrates					
Ianthinite	$UO_2 \cdot 5UO_3 \cdot 10H_2O$	√			
Metaschoepite	$UO_3 \cdot 1\text{-}2H_2O$		√	√ (90°C)	
Dehydrated Schoepite	[a]$UO_2(OH)_2$	√	√		
Schoepite	$UO_3 \cdot 2H_2O$	√		√ (90°C)	√
Compreignacite	$K_2(UO_2)_6O_4(OH)_6] \cdot 8H_2O$	√			
Becquerelite	$Ca[(UO_2)_6O_4(OH)_6] \cdot 8H_2O$	√			
Uranyl Silicate Hydrate					
Soddyite	$(UO_2)_2SiO_4 \cdot 2H_2O$	√	√		√
Alkali and Alkaline Earth Uranyl Silicate Hydrates					
Uranophane	$Ca(UO_2)(SiO_3)(OH)_2 \cdot 5H_2O$	√	√		√
Sklodowskite	$(H_3O)_2Mg(UO_2)_2(SiO_4)_2 \cdot 2H_2O$	√			
Weeksite	$K_2(UO_2)_2(Si_2O_5)_3 \cdot 4H_2O$	√			
Boltwoodite	$(H_2O)K(UO_2)(SiO_4)$	√			
Na-boltwoodite	[a]$NaUO_2SiO_3OH \cdot 1.5H_2O$	√	√		√
Uranyl Peroxides					
Studite	$UO_4 \cdot 4H_2O$			√ (28°C)	
Metastudite	$UO_4 \cdot 2H_2O$			√ (28°C)	

NOTES: [a] Composition from *Data0.ymp.R2* (DTN: MO0302SPATHDYN.000 [DIRS 161756])
[b] Reference also reports $[(Na,K)_2[(UO_2)_3O_2(OH)_3]_2(H_2O)_7]$ and $[(Cs,Ba)(UO_2)_5(MoO_6)(OH)_6(H_2O)n]$, as well as a Zr-U oxide and Zr-U-Pu oxide

Wilson (1990b [DIRS 100793], Series 3) also show UO_2 and uranophane with possible haiweeite [$Ca(UO_2)_2Si_6O_{15}\cdot 5H_2O$] and soddyite.

Drip tests at 1 month on 0.5g of declad, irradiated N-reactor fuel showed a large amount of a corrosion product sludge consisting of black 10-nm UO_2 particles with some yellow particles of metaschoepite. At 8.5 months, XRD indicated the reaction products were a mixture of uranium oxyhydroxides (primarily U_4O_9).

Drip tests on an unirradiated UAl alloy fuel showed formation of a hydrogel layer of boehmite ($Al_2O_3\cdot H_2O$) containing silicon and calcium covering the sample surface (DOE 2003 [DIRS 166268], pp. 4-24 to 4-29). Uranium leached from the UAl alloy particles formed spherical uranium-rich patches throughout the hydrogel layer. These patches were identified as uranyl oxyhydroxides with aluminum, silicon, and calcium present. After drying, these patches crystallized to platelets of schoepite and becquerelite 1 to 5 microns on a side. Another unidentified uranium-bearing needle-shaped phase formed later in the experiments.

MOX fuel is similar to LWR UO_2 spent nuclear fuel except MOX fuel has two phases, the PuO_2 and the UO_2 phases. The mineralization for MOX fuel is considered the same as for UO_2 (CSNF).

Wronkiewicz et al. (1997 [DIRS 163350], pp. 177, 183, and 191) show the alteration mineral paragenetic sequences for a number of high-level waste glasses. Depending on the glass, the minerals formed include: amorphous iron minerals, apatite, boltwoodite, clays, and zeolites with the uranium minerals haiweeite, soddyite, and weeksite.

IV.3.1.2 Natural Analogue Studies

CSNF Waste Form Degradation: Summary Abstraction (BSC 2004 [DIRS 169987], Section 7.3) discusses natural analogues for spent nuclear fuel (SNF) degradation. Most of the material below is from that discussion.

CSNF consists of uranium dioxide (UO_2) with a cubic fluorite-crystalline structure. Uranium dioxide occurs in nature as the mineral uraninite, also exhibiting a fluorite structure. Many geologic sites contain uraninite, and studies of natural uraninite alteration cover a wide range of geologic conditions. Of the several extensively studied sites, only Nopal I, the uranium-mining site at Pena Blanca, Mexico, has geologic, geochemical, and hydrogeologic characteristics similar to those at Yucca Mountain (Murphy 1995 [DIRS 100469]). The volcanic (tuffaceous) host rock at Nopal I, the youngest of the studied sites, has been exposed to oxygen for tens of thousands of years. Uraninite, containing U(IV), was originally formed several million years ago. Pearcy and Murphy (1991 [DIRS 130197]) discuss in some detail other natural analogue sites around the world (Koongarra in Australia, Pocos de Caldas in Brazil, the Shinkolobwe mine in the Congo, and the Krunkelbach mine in Germany). These sites are either somewhat reducing or hydrologically saturated, or the mineralogy of the uraninite alteration is significantly affected by the presence of chemical elements not found at Yucca Mountain (e.g., lead, phosphorus, or vanadium).

The process of uranium mineral formation and subsequent uranium transport at Nopal I have been extensively studied. Because the sites are geologically similar, it is anticipated that the uranium compound alteration and transport processes will be comparable to those that would occur at the repository at Yucca Mountain.

Table IV-2 lists the uranium minerals found at Nopal I with a qualitative illustration of their relative time sequence of formation and relative abundance. The compounds found are limited compared to other sites because of the simple chemistry of the Pena Blanca system.

Table IV-2. Paragenesis of Uranium Minerals at Nopal I

Mineral Group	Mineral	Time	Nominal Chemical Formula
Oxide	Uraninite	…….	UO_{2+x}
Oxyhydroxides	Ianthinite	—	$U^{4+}(U^{6+}O_2)_5(OH)_{14}\cdot 3H_2O$
	Schoepite	—·····	$UO_3\cdot 2H_2O$
	Dehydrated Schoepite		$UO_3\cdot nH_2O(n<2)$
	Becquerelite	—····	$Ca(UO_2)_6O_4(OH)_6\cdot 8H_2O$
	Billietite(?)	·····	$Ba(UO_2)_6O_4(OH)_6\cdot nH_2O(n=4\text{-}8)$
	Abernathyite(?)		$K(UO_2)(AsO_4)\cdot 4H_2O$
Silicates	Soddyite	—	$(UO_2)_2SiO_4\cdot 2H_2O$
	Weeksite and	·····	$K_2(UO_2)_2Si_6O_{15}\cdot 4H_2O$
	Boltwoodite		$KH(UO_2)SiO_4\cdot 1.5H_2O$
	Uranophane: β-Uranophane	———————	$Ca(UO_2)_2Si_2O_7\cdot 6H_2O$

Source: BSC 2004 [DIRS 169987], Table 7-15; Pearcy et al. 1994 [DIRS 100486]

NOTES: ····· minor
—····· abundant, then minor
— abundant
—— very abundant
? indicates tentative identification

IV.3.2 Comparison of Laboratory Corrosion Products to Nopal Minerals

The sequence of uraninite alteration at Nopal I is similar to that of CSNF and UO_2 in laboratory tests (Stout and Leider 1998 [DIRS 111047], pp. 2-250 and 2-261, Section 2.1.3.5). Uraninite is already partially oxidized (Pearcy et al. 1994 [DIRS 100486]). Spent nuclear fuel and UO_2 must first undergo surface oxidation to approach uraninite. The corrosion products observed in laboratory CSNF and UO_2 tests conform to the mineral phases seen at Nopal I. The general sequence is oxidation of the solid surface followed by hydration and the formation of uranyl-oxide hydrates. Silicate in the groundwater is incorporated as soddyite. The silicate, in combination with alkali ions (e.g., calcium and sodium), forms various alkaline uranyl silicate hydrates, such as Na-boltwoodite and β-uranophane. The exact sequence and timing of formation depends significantly on local chemical environment, water flows, and time in the laboratory tests and at the Nopal I site. Simultaneous precipitation is indicated in laboratory and field tests. Some alteration phases, such as sklodowskite and compreignacite, are found in the laboratory tests but not at Nopal I. This may simply be a result of the small number of samples in all studies. Also, some phases, such as ianthanite, seen at the Nopal I site have not been

reported in the laboratory tests. The fact that ianthanite was not observed does not preclude its possible presence in the tests. Ianthanite is an interesting phase, containing a mixture of U(VI) and U(IV) sites. The conditions under which it forms, thus, may reflect local redox conditions present in the natural system at Nopal, but not reproduced in the drip tests.

The Nopal I groundwater is richer in calcium than J-13 well water (Pearcy et al. 1994 [DIRS 100486]), but poorer in sodium and potassium. This could explain the dominance of β-uranophane at the natural site, as well as the limited soddyite and weeksite occurrence. There is substantial calcite at Yucca Mountain. In time, this may make repository-alteration products conform more to the Nopal I sequence, which produces β-uranophane at long times, than that seen in the laboratory.

IV.3.3 Incorporation of Np in Uranyl Corrosion Products of Spent Nuclear Fuel

See Section 6.6.4.

IV.4 NEPTUNIUM IN CONTACT WITH WASTE PACKAGE MATERIALS (EXCLUDING FUEL)

Reaction paths for Np mineralization in the waste package must also take into account influences of corrosion of the waste package materials (primarily steel), and interactions of the corrosion products of steel corrosion (primarily Fe(II) and Cr(III) species). Np(V) species will encounter corroded metals and their corrosion products from waste package internals. As discussed below, these will provide local environments with lower oxidation potentials than the bulk solution promoting reductive nucleation and precipitation of Np species by reducing Np(V) to Np(IV). To show this, this section first establishes which metals are in the waste packages, their compositions, and their corrosion rates. This lays the groundwork for determination of the reductants that will be present and the time frames for their release, establishing what will control the system over geologic time frames. After laying this groundwork, a discussion of Np reduction by products of steel and alloy corrosion is presented.

IV.4.1 Waste Packages Materials

Waste packages come in a variety of different forms built with varied materials. The primary materials composing waste packages (nonfuel components) are aluminum alloys, carbon steel, stainless steel, nickel alloys, and zircaloys (BSC 2004 [DIRS 169982], Table 4-1). These materials corrode at different rates, affecting or controlling the chemistry inside the package at different times during corrosion of canisters in the repository. The degradation rates for these materials are found in Table IV-3.

Table IV-3. Examples of Possible Corrosion Rates of Waste Package Materials

Material	Aluminum Alloy[a]	Carbon Steel Type A516[a]	Stainless Steel Type 316[a]	Nickel Alloy (Ni-Gd)[a]	Zircaloy[b]
Minimum rate	0.40	29.53	0.0007	0.002	0.3 mils per million years
Mean rate	12.95	51.80	0.0083	0.053	
Maximum rate	36.93	88.68	0.0475	0.077	

Source: [a]BSC 2004 [DIRS 169982], Table 7-1 (units are in μm/year)

[b]BSC 2004 [DIRS 169982], Section 6.2.5

From these rates it can be seen that carbon steel and aluminum alloy will control the system early in waste package corrosion, with stainless steel and the Ni alloy having greater effect over longer periods. Zircaloy degrades so slowly that it should have minimal effect on the chemistry inside the waste package. This is further justified by *In-Package Chemistry Abstraction* (BSC 2004 [DIRS 167621]), which provides plots of materials degradation (assuming constant degradation rate) over time for CSNF and CDSP waste packages. Figures IV-10 and IV-11 present the lifetime of waste package materials.

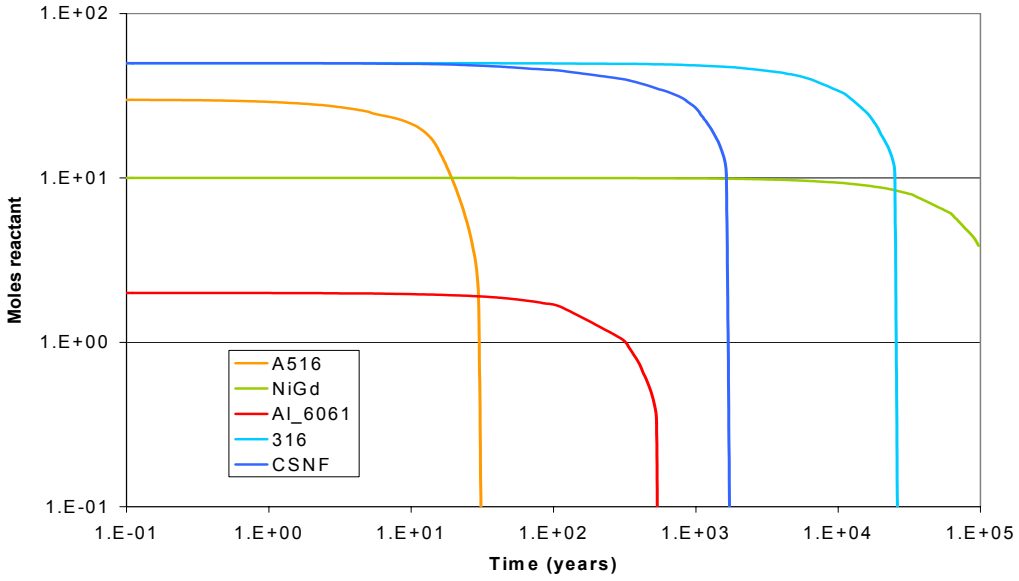

Source: BSC 2004 [DIRS 167621], Appendix F.

Figure IV-10. Lifetime of CSNF Waste Package Materials

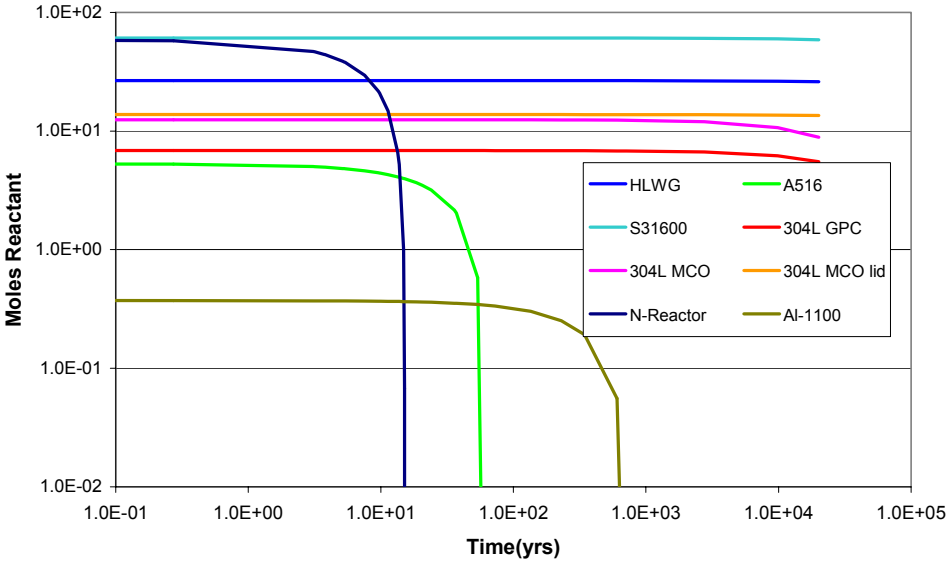

Source: BSC 2004 [DIRS 167621], Appendix F.

Figure IV-11. Lifetime of CDSP Waste Package Materials

Table IV-4 provides compositions for the major alloys and steels affecting water chemistry. These are the main components available for reaction in the waste packages.

Table IV-4. Major Element Composition of Steels and Alloys

Element	Carbon Steel Type A516 (wt %)[a]	Aluminum Alloy 6061 (wt %)[b]	Stainless Steel Type 316 (wt %)[c]	Aluminum Alloy 1100 (wt %)[b]	Stainless Steel Type 304L (wt %)[c]	NiGd Alloy (wt %)[d]
Mn	0.85 to 1.2	0.15	2.00	0.05	2.00	0.5
Cr	—	0.04 to 0.35	16.0 to 18.0	—	18.0 to 20.0	14.5 to 17.1
Ni	—	—	10.0 to 14.0	—	8.0 to 12.0	64.035
Co	—	—	—	—	—	2
Mo	—	—	2.00 to 3.00	—	—	13.1 to 16.0
Fe	98.3	0.7	65.495	0.95 (Si+Fe)	68.045	1
Mg	—	0.8 to 1.2	—	—	—	—
Al	—	96.68	—	99.85	—	—
Gd	—	—	—	—	—	1.9 to 2.1

Source: [a]ASTM A 516/A 516M-01 2001 [DIRS 162723], Table 1, grade 70, 1/2" to 2" thickness
[b]ASTM B 209-96 1996 [DIRS 144744], Table 1, p. 7
[c]ASTM A 240/A 240M-03b 2003 [DIRS 165003], Table 1, p. 4
[d]ASTM B 932-04. 2004 [DIRS 168403]

NOTE: Major elemental composition of alloys and steels. Any element not comprising at least 1 wt% of any waste package component is not presented in this table.

IV.4.2 Minerals and Aqueous Species

The major components of the metals in waste packages are Fe, Al, Cr, Mo, and Ni. The major minerals formed inside the packages from these elements are as follows:

Iron Minerals—Most of the information on the major iron minerals in this section comes from Schwertmann and Cornell (1991 [DIRS 144629]) and Schwertmann and Taylor (1995 [DIRS 105959]). Any material not from these two sources will have an accompanying reference as to its source.

Goethite (α-FeOOH) and hematite (α-Fe_2O_3) are the two most-thermodynamically stable Fe minerals under aerobic conditions. This makes them the most widespread Fe minerals. Goethite is found in almost all soils and in other areas such as lakes and streams. Hematite, on the other hand, is usually found in tropical and subtropical regions where higher temperatures and lower water activities aid in its formation. It is generally accepted that goethite forms through precipitation directly from solution. Hematite needs a precursor, such as ferrihydrite, from which it forms through dehydration and rearrangement. Under surface conditions, simple transformation of goethite to hematite has not yet been observed, though it may occur after sediment burial.

In addition to hematite and goethite, other Fe minerals are found in the natural environment. Even though less-thermodynamically stable, they may be kinetically more favorable for formation depending on the environment. Over time, these minerals would be expected to change or transform into either the more-thermodynamically stable hematite or goethite, or both. The exact process depends on time, temperature, chemical environment, etc., and so far there is no exact model. A simplified diagram showing some of these transformations and the required conditions is presented in Figure IV-12 The "rust flow chart" comes from a compilation of information primarily from Schwertmann and Cornell 1991 [DIRS 144629], Schwertmann and Taylor 1995 [DIRS 105959], and Misawa et al. 1974 [DIRS 159327]. Minor contributions were made by Jobe et al. 1997 [DIRS 159328] and Pednekar 1987 [DIRS 159329]. This diagram does not present all of the processes possible, but the ones that are well understood and occur frequently.

Lepidocrocite (γ-FeOOH) forms from the oxidation of Fe^{2+}. The formation of lepidocrocite is usually kinetically favored over that of goethite and its transformation to goethite is extremely slow, so it may exist on the time scale of several thousand years. However, in carbonate-rich solutions and those containing Al, goethite is more favored to form than lepidocrocite from Fe^{2+}. On the other hand, Cl and Si favor lepidocrocite formation, and Si also helps to stabilize the structure of the mineral so its transformation to goethite is stunted.

When iron corrodes in aerated solutions of neutral pH, the overall reaction can be written:

$$2Fe + 2H_2O + O_2 \rightarrow 2Fe^{2+} + 4OH^- \rightarrow 2Fe(OH)_2$$

However, in oxygen rich environments, this Fe hydroxide is unstable and is oxidized to lepidocrocite, which in time changes to magnetite, maghemite, or hematite (Pednekar 1987 [DIRS 159329]).

Maghemite (γ-Fe_2O_3) occurs primarily in the soils of tropical and subtropical regions, but has been found in temperate regions. In addition to oxidation of magnetite and dehydration of lepidocrocite, maghemite can be formed from other Fe oxides, such as goethite. However, an essential prerequisite for this is the presence of organic matter and heat. In temperate zones, bush or forest fires usually provide the heat.

Magnetite (Fe_3O_4) is usually found on the protected side of any "rust deposit." That is, it forms directly against the metal and below any other oxide/hydroxide that may have formed. It is common in low-oxygen and higher-temperature conditions.

Only a few occurrences of feroxyhyte (δ'-FeOOH) have been reported. Rapid oxidation is presumed to be required for its formation.

Green rusts are not oxides or hydroxides in a strict sense, but contain anions as an essential structural component. Forms with chloride, sulfate, and carbonate are known. The name is derived from the bluish-green color of the compounds and their occurrence as anoxic products of steel corrosion. They usually occur as an intermediate form between Fe^{2+} solutions and FeOOH. Green rusts are very sensitive to oxidation from which they quickly transform to other more stable iron oxide/hydroxides.

Ferrihydrite ($Fe_5HO_8 \cdot 4H_2O$) is limited to situations where fast hydrolysis occurs and where organic matter, phosphates, and silicates inhibit crystallization of more stable minerals. These inhibitors also retard its formation to stable minerals, such as hematite. Because of its high solubility and unstable crystalline structure, ferrihydrite may only last on the order of days to a few years.

Akaganeite (β-FeOOH) requires the presence of high chloride concentrations and elevated temperatures ($\cong 60°C$).

Wüstite (FeO) forms from the dehydration of $Fe(OH)_2$ at higher temperatures in nonoxygenated atmospheres. At lower temperatures, wüstite decomposes into Fe_3O_4 and Fe.

$Fe(OH)_3$ is actually representative of amorphous or poorly crystalized Fe hydroxides such as ferrihydrite, with a general chemical formula of $Fe(OH)_3$ (am). True crystalline $Fe(OH)_3$ is called bernalite. It was accepted as a mineral name only in 1992 (Birch et al. 1992 [DIRS 159330]; Birch et al. 1993 [DIRS159387]). This crystalline form of $Fe(OH)_3$ is very rare and occurs in very limited quantities, so is not expected to form in the waste package.

In the presence of sulfides or sulfate-reducing bacteria, FeS and $FeSO_4$ are also recorded as corrosion products of steels. This is shown by Booth et al. (1967a [DIRS 159331]; 1967b [DIRS 159332]), and in the literature review by Pednekar (1987 [DIRS 159329]). Siderite ($FeCO_3$) is also a common mineral in carbonate rich waters.

The Fe^{3+} in the octahedral position may be partially replaced by other trivalent metal cations of similar size such as Al^{3+}, Mn^{3+}, and Cr^{3+} without modifying the structure. Chromium and molybdenum may, however, replace some of the Fe in the structure of the Fe minerals due to the very similar ionic radii of the ions (Fe^{3+} = 0.064 and Cr^{3+} = 0.061, Schwertman and Cornell 1991

[DIRS 144629], Table 1-2). Chromium replacement of iron is known to occur in goethite and lepidocrocite (Schwertman and Cornell 1991 [DIRS 144629]; Eary and Rai 1989 [DIRS 105788]; Deng et al. 1996 [DIRS 105778]). Molybdenum replacement of Fe in Fe oxides is highly dependent on pH of the system. Molybdenum adsorption reaches a maximum between pH values 4 and 5 and then decreases as pH increases until, at pH of 8, very little sorption occurs (Goldberg et al. 1996 [DIRS 158382]).

From the discussion above, the most prevalent forms of iron in the waste packages are magnetite, goethite, lepidocrocite, and hematite. This also agrees with what has been observed in experiments on the corrosion of miniature waste packages corroded under two different configurations (flow-through and "bathtub"). XRD analysis on materials collected from the effluent leaving these packages consisted of poorly crystalline materials containing magnetite, goethite, and lepidocrocite (Zarrabi et al. 2003 [DIRS 171238]. Maghemite and iron oxide hydrate ($Fe_2O_3 \cdot H_2O$) were also reported once. Glass-walled miniature waste packages (at 25°C) with carbon steel internals showed the formation of reddish brown, green, and black (magnetic) corrosion products likely goethite, green rusts and magnetite. As duration of the experiments increased, the black magnetite increased in abundance. These tests show the prevalence of Fe(II) minerals within the corrosion products. Additionally, at higher temperatures, a higher concentration of the magnetite would be expected due to lower available oxygen. The results of these experiments with the miniature waste packages also agrees with the general literature, which also shows a good mix of Fe(II) and Fe(III) mineral species (Table IV-5).

Table IV-5. Sampling of Iron Minerals Reported from Different Corrosive Environments

References	Year	Test	Corrosion products
Ahn and Leslie [DIRS 159352]	1998	Literature review (aqueous corrosion)	γ-FeOOH, Fe_3O_4, and $Fe(OH)_2$
Raman and Nasrazadani [DIRS 159354]	1990	Analysis of Bridge packing Materials (atm)	Exposed surface = α + γ-FeOOH Unexposed surface = Fe_3O_4 and α-FeOOH
Marsh and Taylor [DIRS 100917]	1988	Submerged granite and bentonite covered steel coupons	Fe_3O_4
Pednekar [DIRS 159329]	1987	Literature review of mild and carbon steels in varied environments	Atmosphere = α +γ-FeOOH and Fe_3O_4
			Fresh water = α +γ-FeOOH, Fe_3O_4, and α +γ- Fe_2O_3
			Saltwater = = α +γ-FeOOH, Fe_3O_4, and γ- Fe_2O_3
			Bacteria influenced = α,γ, and δ-FeOOH, Fe_3O_4, α +γ-Fe_2O_3, FeS, and $FeSO_4$
Brush and Pearl [DIRS 159355]	1972	Submerged steel coupons	Fe_3O_4 and α-FeOOH with some α-Fe_2O_3 at the water-oxide interface

As discussed in Section IV.4.3, Fe(II) species can reduce Np(V) to Np(IV) and will be responsible for most of the reductive nucleation and precipitation of Np species by waste package materials.

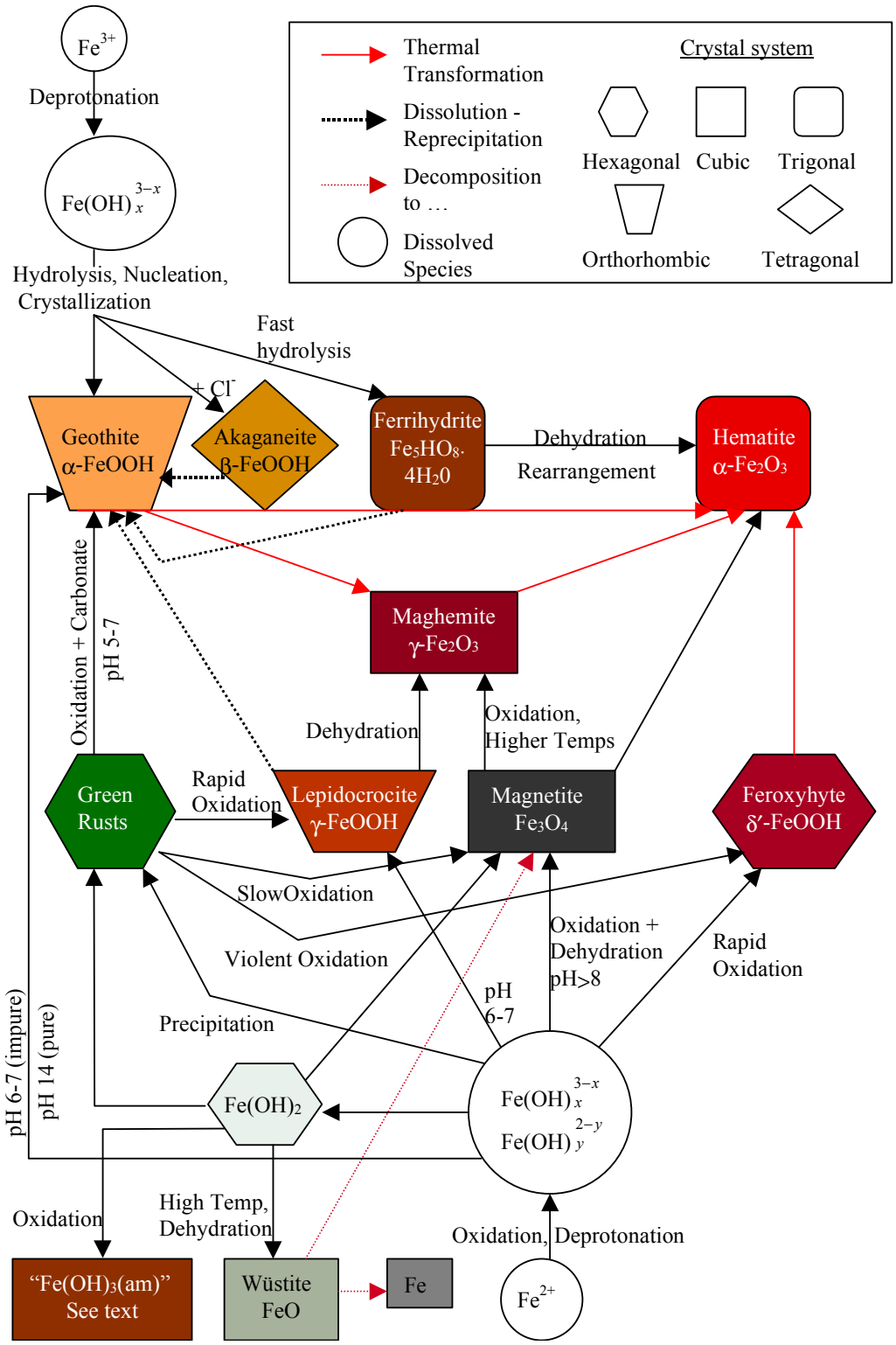

Figure IV-12. Simplified Diagram of Interactions Between Fe Oxides, Hydroxides, and Oxyhydroxides

Aluminum Minerals—Like iron, aluminum forms a number of different minerals and a mixture of these is expected to form in the waste packages. However, unlike the iron minerals where

usually only one mineral forms in the simulation of waste package degradation, a primary mineral (an oxide, hydroxide, or oxyhydroxide) will form (gibbsite in the EQ6 cases), along with a host of clay minerals including smectites, kaolins, and zeolites. A more in-depth discussion follows.

Crystalline $Al(OH)_3$ exists as four polymorphs: gibbsite, nordstrandite, doyleite, and bayerite, of which gibbsite is the most common. Most naturally occuring $Al(OH)_3$ polymorphs are very finely crystalline and usually admixed with each other and other Al minerals. Gibbsite is the most abundant of these polymorphs (Hsu 1995 [DIRS 105875]). Bayerite can be most readily synthesized but is rarely seen in nature, while norstrandite is the most frequently occurring, after gibbsite, in the natural environment (Apps et al. 1989 [DIRS 159378]).

Aluminum oxyhydroxides (AlO(OH) – boehmite and diaspore) are rarer than the hydroxides and are known to exist in many bauxite deposits. They are, thus, regarded as the ultimate product of intensive weathering of primary Al silicates in soils (Allen and Hajek 1995 [DIRS 159372]).

Smectites are any monoclinic layer silicates of the general formula $X_{0.33}Y_{2to3}Z_4O_{10}(OH,F)_2 \cdot nH_2O$, where X = Ca, Li, or Na; Y = Al, Cr^{+3}, Fe^{+2}, Fe^{+3}, Li, Mg, Ni, or Zn; and Z = Al, Si (Roberts et al. 1990 [DIRS 107105]). The three most common forms of smectite are nontronite, montmorillinite, and beidellite. Smectites are common soil minerals in temperate and cold climates. They do not form where leaching is intense due to either a loss of bases or silica, or both. They form through alteration of other phyllosilicates and synthesis. Where weathering and leaching are extensive, smectites usually alter to kaolinite.

Minerals in the kaolinite-serpentine group are silicates of the general formula $M_{2to3}Z_2O_5(OH)_4 \cdot nH_2O$, where M = Al, Fe^{+2}, Fe^{+3}, Mg, Mn^{+2}, Ni, or Zn; and Z = Al, Fe^{+3}, or Si (Roberts et al. 1990 [DIRS 107105]). The most common are kaolinite and halloysite (Dixon 1995 [DIRS 159374]).

Zeolites are hydrous aluminosilicates of alkali and alkali earth elements characterized by the ratio (Al+Si):O = 1:2, and the reversible loss of water (Roberts et al. 1990 [DIRS 107105]). The most commonly reported zeolites in sedimentary environments are analcime, chabazite, clinoptilolite, erionite, heulandite, laumontite, mordenite, and phillipsite with clinoptilolite being the most abundant.

Although aluminum solids will be very abundant in the waste packages, the form of Np control they provide is by sorption and will not be responsible for the reductive nucleation and precipitation of Np species. Therefore, they are not discussed in any greater detail for neptunium retardation.

Chromium Minerals—The following is taken from *Engineered Barrier System: Physical and Chemical Environment* (BSC 2004 [DIRS 169860]):

Chromium exists in many oxidation states; however, only the +6 and +3 oxidation states are common.

Cr(VI) exists in solution as $H_2CrO_4°$, bichromate ($HCrO_4^-$), chromate (CrO_4^{2-}), or dichromate ($Cr_2O_7^{2-}$) with the relative concentration of these species dependent on the pH and total Cr(VI) concentration. Below a pH of 6.5, $Cr_2O_7^{2-}$ dominates when Cr(VI) concentrations are above 1 mM (and possibly as low as 30 mM) and $HCrO_4^-$ dominates when Cr(VI) concentrations are <30 mM. Above a pH of 6.5, CrO_4^{2-} is the dominant species.

Cr(III) exists in solution primarily as Cr^{3+} below a pH of 3.5. Increasing hydrolysis with increasing pH values yields $Cr(OH)^{2+}$, $Cr(OH)_2^+$, $Cr(OH)_3°$, and $Cr(OH)_4^-$. Cr(III) can precipitate as amorphous $Cr(OH)_3$, which can subsequently crystallize to $Cr(OH)_3 \cdot 3H_2O$ or eskolaite (Cr_2O_3). In groundwaters with pH greater than 4, Cr(III) and Fe(III) can precipitate in a solid solution with a general formula of $Cr_xFe_{1-x}(OH)_3$.

There is evidence that the chromium in the waste packages will be in the form of Cr(III). Chromium speciation during the corrosion of 316L stainless steel showed a predominance of Cr(III) species and that oxidation of Cr(III) to Cr(VI) was negligible at room temperature. Reaction with stainless steel or oxalic acid caused much greater reduction of Cr(VI) than the oxidation of the Cr(III). Reduction of Cr(VI) in the presence of hematite (Fe_2O_3) is attributable to the small amount of an FeO component in the hematite. Oxidation experiments exposing Cr(III) species to dissolved oxygen at near ambient conditions over a pH range of 4.0 to 12.5 did not detect Cr(VI) within 24 days. Additionally, Langmuir (1997 [DIRS 100051], Figure 11.5) shows observed disequilibrium of dissolved oxygen in water corresponds to the much more rapidly reacting O_2-H_2O_2 couple. In the pH range of 6 to 9, the Eh values for this couple (approximately 0.4 to 0.6 volts) corresponds to the Cr(III) field in *Engineered Barrier System: Physical and Chemical Environment* (BSC 2004 [DIRS 169860], Figure 6.8-3).

As discussed in Section IV.4.3, Cr(II) species can reduce Np(V) to Np(IV) and will be responsible for some of the reductive nucleation and precipitation of Np species by waste package materials.

Molybdenum Minerals—Molybdenum solids will not be very prevalent in the waste packages since Mo is only a minor constituent of waste package materials Additionally, the form of Np control they provide is by sorption and not be will be responsible for the reductive nucleation and precipitation of Np species. Therefore, they are not discussed in any greater detail for neptunium retardation.

Nickel Minerals—The following is an excerpt from *Engineered Barrier System: Physical and Chemical Environment* (BSC 2004 [DIRS 169860], Section 6.8.1.2):

Only Ni(II) occurs at ambient environmental conditions. The higher oxidation states occur rarely and, even in those cases, it is not clear whether the ligand rather than the metal atom oxidizes. No other oxidation state would be expected under repository environmental conditions once Ni is released by oxidation of the metal alloys.

Once the Ni is released into an aqueous environment under oxidizing conditions, nickel hydroxides [$Ni(OH)_2$] are stable in a pH range between 8 and 12. Otherwise, either the Ni^{2+} ion or the $HNiO_2^-$ ions are in solution, indicating that the Ni is relatively soluble under neutral-acidic conditions and under relatively alkaline conditions.

Nickel tends to substitute for iron and manganese in solid phases, and tends to be coprecipitated as $Ni(OH)_2$ with both iron oxides and manganese oxides. Nickel will also adsorb to clays, iron and manganese oxides, and organic matter.

Although Ni solids will be very abundant in the waste packages, the form of Np control they provide is by sorption and will not be responsible for the reductive nucleation and precipitation of Np species. Therefore, they are not discussed in any greater detail for neptunium retardation.

As indicated in Section IV.4.1, carbon steel will control the system early in waste package corrosion, with stainless steel having greater effect over longer periods. Therefore, iron species will be of great importance in the reduction of Np(V) to Np(IV) in short and long time frames, whereas chromium from stainless steel corrosion will only be instrumental over long time frames.

IV.4.3 Reduction of Np by Corrosion Products and Reduced Species

Sorption of Np(V) and subsequent reduction to Np(IV) is another suggested mechanism for the creation of NpO_2 inside waste packages. Several experiments show Np(V) is readily sorbed to iron corrosion products (Nakayama and Sakamoto 1991 [DIRS 172676], Kohler et al. 1999 [DIRS 172672]; Tochiyama et al. 1995 [DIRS 144644]). However, Nakata et al. (2002 [DIRS 172674]); Nakata et al. (2004 [DIRS 172675]) show that neptunium sorbed to Fe(II) inside mineral phases reduces Np(V) to Np(IV). Specifically, experiments on neptunium sorption on magnetite show a very fast uptake of neptunium in the first hour, which is attributed to this reduction of neptunium to the +4 oxidation state. This is also suggested by Beall et al. (1980 [DIRS 172677]), who also report this quick uptake of Np by Fe(II) minerals. Although reported only for magnetite, it is also reasonable that there could be reduction of Np(V) by the FeO component of impure phases of hematite, goethite, and lepidocrocite in the package. Like Fe(II), Cr(III) will also reduce Np from Np(V) to Np(IV).

As shown in several experiments, Np reduction by aqueous Fe species is not reported (Nakata et al. 2004 [DIRS 172675] and Cui and Eriksen 1996 [DIRS 172669]). This may be due to the fact that iron forms very insoluble corrosion products so the aqueous concentrations of iron are very low. This is corroborated by Hem (1985 [DIRS 115670]), who indicated that natural waters are very low in Fe content because of the durability of iron-containing minerals.

APPENDIX V
SUMMARY OF NEPTUNIUM TESTING

INTENTIONALLY LEFT BLANK

V. SUMMARY OF NEPTUNIUM TESTING

The scientific basis for modeling the redox and dissolution behavior of Np associated with the corrosion of waste forms in the Yucca Mountain repository is described in Section 6.6 and Appendix IV.

When the reaction paths for Np release from CSNF are considered, it is apparent that Np(IV) in the fuel's matrix may not be effectively oxidized to Np(V) at the corrosion potentials of uranium dioxide spent nuclear fuel in air-saturated aqueous solutions. Also, the fuel's UO_2 matrix may facilitate reductive precipitation of any aqueous Np(V) species that are formed. The behavior of Np under the redox conditions at and near the corroding surface and how the crystal lattice structures at the corroding surface promote/enhance nucleation of NpO_2 and Np_2O_5 are, therefore, addressed by the testing program. The general objectives of the testing are to obtain data that can address the following questions:

- Are the waste form dissolution reaction paths likely to lead to oxidative dissolution of Np(IV) at the corroding fuel surface or does the Np remain in the Np(IV) oxidation state and become enriched at the corroding $U_{(1-x)}Np_xO_2$ surface?

- What is the temperature dependence (specifically the activation energy) for the homogenous precipitation of NpO_2 from Np(V) solutions? Also, do heterogeneous interactions with the corroding fuel matrix promote the reduction and/or nucleation steps involved in the reductive precipitation of NpO_2?

The fiscal year 2005 testing program, which is conducted under work package AWFTA3 (BSC 2005 [DIRS 172684]), addresses these questions by conducting two experimental activities to:

- Examine the form and distribution of Np at and near the interface between corroded fuel and the alteration phase rind layer, and

- Examine the kinetics of NpO_2 precipitation from supersaturated Np(V) solutions.

Activity One:

The objectives of this activity are to examine corroded CSNF from the Argonne National Laboratory unsaturated tests to assess neptunium accumulation at or near the interface between the corroding fuel and the alteration rind and to assess the extent to which neptunium is incorporated into the rind's uranyl alteration phases. Other radionuclides, including technetium, will also be examined, with the objective of determining the extent to which the five-metal epsilon-ruthenium phase particles, which contain a substantial amount of the technetium in CSNF, have corroded.

Specimens will be prepared from corroded fuel pellet fragments in such a manner to provide cross sectional views of the interface between the corroding fuel and the rind of alteration products. These specimens will be prepared by mounting selected fuel fragments in epoxy, and cutting or microcoring, or both, to provide a cross-sectional view of the fuel-corrosion rind interface. The cross-sectional specimens may then be further cut, polished, thin-sectioned, or

otherwise altered as needed for removal from the hot cells for further processing and examination. After sufficient size reduction has been completed, the samples will be mounted in sample holders suitable for X-ray Absorption (XAS) and other studies. The planned XAS studies involve scanning an incident X-ray beam across the fuel and alteration rind interface region while detecting fluorescent X-rays from Np and other radionuclides (including Tc). X-ray absorption spectroscopy (using a bent Laue analyzer as needed to select trace Np fluorescence in the presence of U) will be used to characterize the oxidation state and structure of Np phases.

Activity Two:

The objectives of this activity are to examine the homogenous precipitation behavior of dissolved Np(V) and the effects of heterogeneous interactions with metal and UO_2 substrates on the precipitation kinetics.

Homogenous precipitation of Np(IV) solids from air-saturated solutions is a reductive nucleation and precipitation process involving both reduction and precipitation of the aqueous Np(V) species. This could occur either by reduction of Np(V) to Np(IV), nucleation of NpO_2, and reductive precipitation of NpO_2 or by nucleation and precipitation of a metastable Np(V) solid (if the solution is supersaturated with respect to such a solid phase) followed by reductive ageing of this metastable solid to form NpO_2. Because the rate of transformation of these metastable Np(V) phases to the more-thermodynamically stable NpO_2 could be very slow, they can define slow reaction paths for NpO_2 precipitation from some supersaturated solutions. However, the nucleation and precipitation behavior may be quite different in the heterogeneous environment near the corroding fuel surface. Based on the isostructural relationship between UO_2 and NpO_2 (and perhaps between U_3O_8 and Np_2O_5) the spent fuel matrix may act as a structural template that facilitates the precipitation of pure-phase neptunium solids (i.e., it may counteract nucleation energy barriers by acting as a substrate for epitaxial growth).

The scope of this activity involves examination of the precipitation kinetics of NpO_2(cr) from NpO_2^+ aqueous solution at various temperatures under expected Yucca Mountain conditions. It will also include assessing the effects of nucleation by investigating the effect of NpO_2 seed crystals on the precipitation kinetics. Potential effects of the waste package internal components (e.g., stainless steel and CSNF) on the reduction and nucleation steps involved will also be investigated. Solid phases obtained in the course of the experiments will be analyzed using electron microscopy, X-ray absorption spectroscopy, and X-ray diffraction.